

AD-A077 688

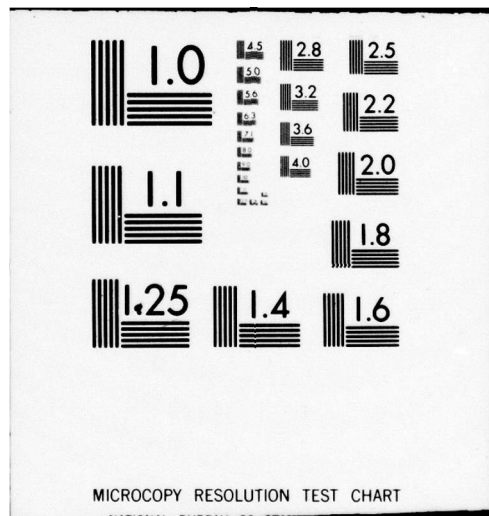
LOCKHEED-GEORGIA CO MARIETTA
AERODYNAMIC INVESTIGATION OF C-141 LEADING EDGE MODIFICATION
JUN 79 W T BLACKERBY, P R SMITH
LG78ER0233-VOL-2

F/G 1/3
F09603-77-A-0204
AFFDL-TR-79-3059-VOL-2
NL

UNCLASSIFIED

1 OF 4
ADA
077688





AD A 077688

AFFDL-TR-79-3059
Volume II

2

LEVEL

A076610

VOL I

**AERODYNAMIC INVESTIGATION OF C-141
LEADING EDGE MODIFICATION FOR
CRUISE DRAG REDUCTION**

n.s.d.

W. T. BLACKERBY
P. R. SMITH
LOCKHEED-GEORGIA COMPANY
86 SOUTH COBB DRIVE
MARIETTA, GEORGIA 30063

JUNE 1979

TECHNICAL REPORT AFFDL-TR-79-3059 Volume II
Final Report June 1977 to September 1978

DDC
RECEIVED
DEC 6 1979
RECEIVED
A

Approved for public release; distribution unlimited.

DDC FILE COPY

AIR FORCE FLIGHT DYNAMICS LABORATORY
AIR FORCE SYSTEMS COMMAND
WRIGHT-PATTERSON AIR FORCE BASE, OHIO 45433

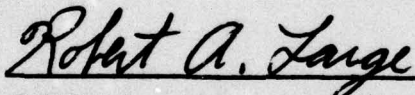
79 22 5 001

NOTICE

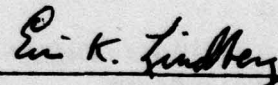
When Government drawings, specifications, or other data are used for any purpose other than in connection with a definitely related Government procurement operation, the United States Government thereby incurs no responsibility nor any obligation whatsoever; and the fact that the government may have formulated, furnished, or in any way supplied the said drawings, specifications, or other data, is not to be regarded by implication or otherwise as in any manner licensing the holder or any other person or corporation, or conveying any rights or permission to manufacture, use, or sell any patented invention that may in any way be related thereto.

This report has been reviewed and cleared for open publication and/or public release by the appropriate Office of Information (OI), in accordance with AFR 190-17 and DODD 5230.9. There is no objection to unlimited distribution of this report to the public at large, or by DDC to the National Technical Information Service.

This technical report has been reviewed and is approved for publication.

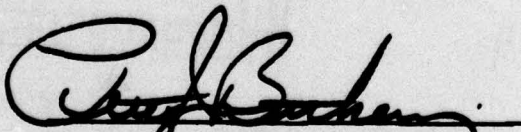


ROBERT A. LARGE, Capt, USAF
Project Engineer/Technical Monitor



ERIC K. LINDBERG, Maj, USAF
Chief, Aerodynamics & Airframe Branch

FOR THE COMMANDER:



PETER J. BUTKEWICZ, Col, USAF
Chief, Aeromechanics Division
Air Force Flight Dynamics Laboratory

(18) AFFDL

(19) TR-79-3059-VOL-2

SECURITY CLASSIFICATION OF THIS PAGE (When Data Entered)

REPORT DOCUMENTATION PAGE		READ INSTRUCTIONS BEFORE COMPLETING FORM
1. REPORT NUMBER AFFDL-TR-79-3059 Vol. II	2. GOVT ACCESSION NO.	3. RECIPIENT'S CATALOG NUMBER
4. TITLE (and Subtitle) AERODYNAMIC INVESTIGATION OF C-141 LEADING EDGE MODIFICATION FOR CRUISE DRAG REDUCTION Volume II.	5. TYPE OF REPORT & PERIOD COVERED Technical - Final June 1977 - September 1978	
7. AUTHOR(s) W. T. Blackerby P. R. Smith	6. PERFORMING ORG. REPORT NUMBER LG78ER0233-VOL-2	
9. PERFORMING ORGANIZATION NAME AND ADDRESS Lockheed-Georgia Company 86 South Cobb Drive Marietta, Georgia 30063	14. CONTRACT OR GRANT NUMBER(s) F09603-77-A-0204-0010	
11. CONTROLLING OFFICE NAME AND ADDRESS Air Force Flight Dynamics Laboratory (FXM) Wright Patterson AFB, Ohio 45433	10. PROGRAM ELEMENT, PROJECT, TASK AREA & WORK UNIT NUMBERS 2404-10-02	
14. MONITORING AGENCY NAME & ADDRESS (if different from Controlling Office) 12/319	12. REPORT DATE June 1979	
	13. NUMBER OF PAGES 318	
	15. SECURITY CLASS. (of this report) Unclassified	
16. DISTRIBUTION STATEMENT (of this Report) Approved for public release; distribution unlimited 9 Final rept. Jun 77-Sep 78,		
17. DISTRIBUTION STATEMENT (of the abstract entered in Block 20, if different from Report) 6220 IF		
18. SUPPLEMENTARY NOTES		
19. KEY WORDS (Continue on reverse side if necessary and identify by block number) C-141, Drag Reduction, Fuel Savings, Leading Edge Modification, Wing Design, Transonic, Wing Modification, Wing Drag Rise, Airfoil Drag Rise, Wing Pressure Distributions.		
20. ABSTRACT (Continue on reverse side if necessary and identify by block number) A study of the aerodynamic design and high speed wind tunnel investigation of wing leading edge modifications for cruise drag reduction on the C-141 aircraft has been completed. Also investigated were the effects of a wing swept tip extension and trail- ing edge anti-drag bodies. These modifications were tested in the AEDC 16-Foot Transonic Facility, using a 0.044 scale C-141B model, to determine the effects on C-141 cruise aerodynamic characteristics and wing chordwise pressure distributions. Design of the leading edge modifications was based on the use of transonic wing → next page		

DD FORM 1 JAN 73 1473 EDITION OF 1 NOV 65 IS OBSOLETE

SECURITY CLASSIFICATION OF THIS PAGE (When Data Entered)

210 065

JOB

cont.

theory, transonic airfoil theory and experience previously gained with a two-dimensional airfoil leading edge modification program. Force data results were analyzed to determine the effects on C-141 cruise drag, drag rise characteristics and cruise performance. Correlations were made with transonic theory using the measured chordwise pressure distributions. A fuel and cost savings evaluation was made of the selected leading edge configuration based on measured and predicted cruise performance improvements.

K

Accession For	
NTIS GRA&I	<input checked="" type="checkbox"/>
DDC TAB	<input type="checkbox"/>
Unannounced	<input type="checkbox"/>
Justification	
By	
Distribution/	
Availability Codes	
Dist.	Avail and/or special
A	

FOREWORD

This is the final report on the aerodynamic design, test and analysis of modified wing leading edges for cruise drag reduction on the C-141 aircraft. This work was performed by the Lockheed-Georgia Company, Marietta, Georgia, under Contract No. F09603-77-A-0204-0010 for the Air Force Flight Dynamics Laboratory. The studies and wind tunnel testing were accomplished between June 1977 and September 1978.

This report is published in two volumes. Volume I covers the aerodynamic design approach for modifying an existing 0.044 scale C-141B model for high speed tests at the AEDC 16-Foot Transonic Facility, the analysis and correlation of the wind tunnel results and a fuel and cost savings evaluation of the performance improvements due to the selected leading edge modification. Volume II contains the details of the wind tunnel model, the test program and plotted wind tunnel test results.

Mr. J. D. Wallace was the Program Manager and W. T. Blackerby was the Technical Leader. The wing leading edge modification design was accomplished by P. R. Smith and M. E. Carlton. The technology base for this program, in the form of transonic analysis and numerical optimization methods for wings and airfoils, was developed by the Advanced Flight Sciences Department at Lockheed-Georgia.

The authors wish to thank J. P. Perdue for assistance in conducting the wind tunnel test and W. F. LaBozzetta for assisting with the analysis of the wind tunnel results and preparation of the final report.

Technical direction for this program was provided by Mr. J. K. Johnson of the Air Force Flight Dynamics Laboratory/FXM.

This report is also identified as LG78ER0233 for Lockheed Corporation's internal control purposes.

TABLE OF CONTENTS

SECTION	PAGE
I	1
INTRODUCTION	1
II	2
WIND TUNNEL TEST	2
1. TEST FACILITY	2
2. MODEL AND INSTRUMENTATION	2
3. TEST CONDITIONS AND SCHEDULE	5
4. DATA REDUCTION	5
III	8
BASIC AERODYNAMIC DATA	8
Sketch of the Swept Wing Tip	8
Photograph of the Swept Tip Installation	7
Lift, Drag and Pitching Moment Characteristics for	8
Baseline Loading Edge, Free Transition	8
Lift, Drag and Pitching Moment Characteristics for	9
Baseline Loading Edge, Free Transition, Report	9
Lift, Drag and Pitching Moment Characteristics for	10
Baseline Loading Edge, Free Transition, Grit Code B	10
Same as Figure 10, Grit Code C	11
Same as Figure 10, Grit Code B	12
Same as Figure 10, Grit Code C, Tail-On	13
Same as Figure 10, Grit Code C, $M_\infty = 2.5 \times 10^5/\text{ft}^2$	14

LIST OF ILLUSTRATIONS

FIGURE		PAGE
1	Photograph of the 0.044 Scale C-141B Model Installed at AEDC 16T	23
2	Three-View Sketch of the 0.044 Scale C-141B Model	24
3	Sketch Comparison of the Basic and Modified Leading Edges	27
4	Location of Anti-Drag Bodies	28
5	Photograph of the Anti-Drag Bodies Installed on the Model	29
6	Sketch of the Swept Wing Tip	30
7	Photograph of the Swept Tip Installation	31
8	Lift, Drag and Pitching Moment Characteristics for Baseline Leading Edge, Free Transition	32
9	Lift, Drag and Pitching Moment Characteristics for Baseline Leading Edge, Free Transition, Repeat	34
10	Lift, Drag and Pitching Moment Characteristics for Baseline Leading Edge, Fixed Transition, Grit Code B	36
11	Same as Figure 10, Grit Code C	38
12	Same as Figure 10, Grit Code D	40
13	Same as Figure 10, Grit Code C, Tail-On	42
14	Same as Figure 10, Grit Code C, $R_N = 2.5 \times 10^6/MAC$	44

LIST OF ILLUSTRATIONS (CONT'D)

FIGURE		PAGE
15	Same as Figure 14, $R_N = 5.4 \times 10^6/\text{MAC}$	46
16	Lift, Drag and Pitching Moment Characteristics for w^{35} Leading Edge Modification, Free Transition	48
17	Lift, Drag and Pitching Moment Characteristics for w^{35} Leading Edge Modification, Fixed Transition, Grit Code B	50
18	Same as Figure 17, Grit Code D	52
19	Lift, Drag and Pitching Moment Characteristics for w^{36} Leading Edge Modification, Free Transition	54
20	Lift, Drag and Pitching Moment Characteristics for w^{36} Leading Edge Modification, Fixed Transition, Grit Code B	56
21	Same as Figure 20, Grit Code C	58
22	Lift, Drag and Pitching Moment Characteristics for Baseline Leading Edge, Fixed Transition, Grit Code C, Pylon/Nacelles Off	60
23	Same as Figure 22, Grit Code D, Pylon/Nacelles Off	62
24	Lift, Drag and Pitching Moment Characteristics for w^{35} Leading Edge Modification, Fixed Transition, Grit Code D, Pylon/Nacelles Off	64
25	Lift, Drag and Pitching Moment Characteristics for Baseline Leading Edge, Fixed Transition, Grit Code D, Eight Anti-Drag Bodies	66

LIST OF ILLUSTRATIONS (CONT'D)

FIGURE		PAGE
26	Lift, Drag and Pitching Moment Characteristics for W ³⁵ Leading Edge Modification, Free Transition, Four Anti-Drag Bodies	68
27	Lift, Drag and Pitching Moment Characteristics for Baseline Leading Edge, Fixed Transition, Grit Code C, One Swept Tip	70
28	Same as Figure 27, Both Swept Tips	72
29	Chordwise Pressure Distributions for Various Angles of Attack. Baseline Leading Edge, Free Transition, M = 0.7	74
30	Same as Figure 29, M = 0.75	78
31	Same as Figure 29, M = 0.77	82
32	Same as Figure 29, M = 0.79	86
33	Same as Figure 29, M = 0.81	90
34	Chordwise Pressure Distributions for Various Angles of Attack. Baseline Leading Edge, Fixed Transition, Grit Code C, M = 0.7	94
35	Same as Figure 34, M = 0.75	98
36	Same as Figure 34, M = 0.77	102
37	Same as Figure 34, M = 0.79	106

LIST OF ILLUSTRATIONS (CONT'D)

FIGURE		PAGE
38	Same as Figure 34, $M = 0.81$	110
39	Chordwise Pressure Distributions for Various Angles of Attack. Baseline Leading Edge, Fixed Transition, Grit Code D, $M = 0.7$	114
40	Same as Figure 39, $M = 0.75$	118
41	Same as Figure 39, $M = 0.77$	122
42	Same as Figure 39, $M = 0.79$	126
43	Same as Figure 39, $M = 0.81$	130
44	Chordwise Pressure Distributions for Various Angles of Attack. W^{35} Leading Edge Modification, Free Transition, $M = 0.7$	134
45	Same as Figure 44, $M = 0.75$	138
46	Same as Figure 44, $M = 0.77$	142
47	Same as Figure 44, $M = 0.79$	146
48	Same as Figure 44, $M = 0.81$	150
49	Chordwise Pressure Distributions for Various Angles of Attack. W^{35} Leading Edge Modification, Fixed Transition, Grit Code D, $M = 0.7$	154
50	Same as Figure 49, $M = 0.75$	158

LIST OF ILLUSTRATIONS (CONT'D)

FIGURE		PAGE
51	Same as Figure 49, $M = 0.77$	162
52	Same as Figure 49, $M = 0.79$	166
53	Same as Figure 49, $M = 0.81$	170
54	Chordwise Pressure Distributions for Various Angles of Attack. W^{36} Leading Edge Modification, Fixed Transition, Grit Code B, $M = 0.7$	174
55	Same as Figure 54, $M = 0.75$	178
56	Same as Figure 54, $M = 0.77$	182
57	Same as Figure 54, $M = 0.79$	186
58	Same as Figure 54, $M = 0.81$	190
59	Chordwise Pressure Distributions for Various Angles of Attack. Baseline Leading Edge, Fixed Transition, Grit Code D, Pylon/Nacelle Off, $M = 0.7$	194
60	Same as Figure 59, $M = 0.75$	198
61	Same as Figure 59, $M = 0.77$	202
62	Same as Figure 59, $M = 0.79$	206
63	Chordwise Pressure Distributions for Various Angles of Attack. W^{35} Leading Edge Modification, Fixed Transition, Grit Code D, Pylon/Nacelle Off, $M = 0.7$	210

LIST OF ILLUSTRATIONS (CONT'D)

FIGURE		PAGE
64	Same as Figure 63, $M = 0.75$	214
65	Same as Figure 63, $M = 0.77$	218
66	Same as Figure 63, $M = 0.79$	222
67	Chordwise Pressure Distributions for Various Angles of Attack. Baseline Leading Edge, Fixed Transition, Grit Code D, Eight Anti-Drag Bodies, $M = 0.7$	226
68	Same as Figure 67, $M = 0.75$	230
69	Same as Figure 67, $M = 0.77$	254
70	Same as Figure 67, $M = 0.79$	238
71	Same as Figure 67, $M = 0.81$	242
72	Chordwise Pressure Distributions for Various Angles of Attack. W ³⁵ Leading Edge Modification, Free Transition Four Anti-Drag Bodies, $M = 0.7$	246
73	Same as Figure 72, $M = 0.75$	250
74	Same as Figure 72, $M = 0.77$	254
75	Same as Figure 72, $M = 0.79$	258
76	Same as Figure 72, $M = 0.81$	262

LIST OF ILLUSTRATIONS (CONT'D)

FIGURE		PAGE
77	Chordwise Pressure Distributions for Various Angles of Attack. Baseline Leading Edge, Fixed Transition, Grit Code C, One Swept Tip, $M = 0.7$	266
78	Same as Figure 77, $M = 0.75$	270
79	Same as Figure 77, $M = 0.77$	274
80	Same as Figure 77, $M = 0.79$	278
81	Same as Figure 77, $M = 0.81$	282
82	Chordwise Pressure Distributions for Various Angles of Attack. Baseline Leading Edge, Fixed Transition, Grit Code C, Both Swept Tips, $M = 0.7$	286
83	Same as Figure 82, $M = 0.75$	290
84	Same as Figure 82, $M = 0.77$	294
85	Same as Figure 82, $M = 0.79$	298
86	Same as Figure 82, $M = 0.81$	302

LIST OF TABLES

TABLE		PAGE
1	Configuration Symbols	9
2	Model Dimensional Data	11
3	Wing Pressure Orifice Location	16
4	Test Program Summary	17
5	Plot Schedule for Force Data	21
6	Plot Schedule for Pressure Data	22

SECTION I INTRODUCTION

This volume contains information on the wind tunnel test program and results for the C-141 wing leading edge modification studies described in Volume I. The Lockheed-Georgia Company was contracted to prepare an existing C-141B high-speed wind tunnel model for installation and test in the AEDC 16-Foot Transonic Facility for the purpose of evaluating two modified wing leading edges. The wind tunnel test was designated AEDC TF-481 and was conducted during April 1978.

1. WIND TUNNEL TEST PROGRAM

The 0.044 scale C-141B model was used in this test. The model has been used previously for tests for speed and transonic wing buffet testing. The wing was equipped with instrumentation of 1400 static and dynamic pressure taps. Other model components are the fuselage, tail, and landing gear. A list of the model components with identification symbols and reference drawings is given in Table 1. A three-view sketch of the model is shown in Figure 1.

The C-141B configuration was used throughout the wind tunnel investigation. This is the basic C-141B production configuration with

SECTION II

WIND TUNNEL TEST

1. TEST FACILITY

The test was conducted in the Arnold Engineering Development Center 16-foot Propulsion Transonic Wind Tunnel located at Arnold Air Force Station, Tennessee. This is a continuous flow, closed circuit tunnel with a Mach number operating range from 0.20 to 1.60. Total pressure and Reynolds number range capability are from approximately 200 to 3400 psfa and 0.5 to 5.5 million per foot, respectively, depending on the Mach number.

Test section Cart 2 used in this test is 16 feet square and 40 feet long, with all four walls perforated. The perforated walls allow part of the main flow to be removed into the evacuated surrounding plenum chamber, unchoking the test section near sonic speeds and alleviating blockage and wall effects. A photograph of the model installed in the Cart 2 test section is shown in Figure 1.

2. MODEL AND INSTRUMENTATION

The 0.044 scale C-141 model was used in this test. The model has been used numerous times for both low speed and transonic wind tunnel testing. The wing and empennage are constructed of 4340 steel and the fuselage is made of aluminum. Other model components are made from combinations of metal, plastic, and fiberglass. A list of the model components with identification symbols and reference drawing numbers is shown in Table 1, and model dimensional data for each component is given in Table 2. A three-view sketch of the model is shown in Figure 2.

The C-141B configuration was used throughout the wind tunnel investigation. This is the basic C-141A production configuration with

the 12.320 inch (280 inch full scale) stretched fuselage (B¹²) and the inflight refueling pod (P⁴).

The forward 12% of the wing, full span, is removable. Three leading edge configurations were investigated; basic C-141 (W^{12C}), 3-D CONMIN (W³⁵), and a leading edge based on tailoring a previously tested C-141 2-D airfoil leading edge modification to fit the wing (W³⁶).

A sketch of the comparison of these leading edges is shown in Figure 3. Anti-drag bodies (Z^{fl}) installed on the wing trailing edge and a swept tip (Z^{t6}) were also investigated. Location details and installation on the wing are shown in Figures 4 through 7.

The right hand wing contains 118 static pressure orifices located at four spanwise stations, upper and lower surfaces. All the orifices were connected to and recorded from a four module 48 SGM Scanivalve unit located in the fuselage nose. In addition, internal cavity pressure and differential across the balance was measured from two single orifices located fore and aft in the blade cavity and a single orifice located aft of the balance. Tabulation of the wing pressure orifice locations is shown in Table 3.

The model was mounted on a Task 3500-B MK-I-3.5 inch internal balance supported by a blade-sting system. The balance was installed in the model in a rolled and yawed attitude of 180 degrees direction from conventional installation. The balance attached to a blade adapter in the forward fuselage section and was pinned to the model on the right side of the model. The swept blade entered the fuselage along the forward lower centerline and attached to the balance adapter. The forward blade support minimizes support interference effects on the aft fuselage. The blade lower section was attached to a sting adapter and the AEDC PWT 16T "A" sting (S-5.533M-143.29-9.125M).

An AEDC Angular Position Indicator, PWT #9, used as a model angle-of-attack back-up system was mounted in the balance chamber of the fuselage, immediately aft of the balance.

Transition was fixed on the model by means of sparse distributions of Ballotini glass beads applied in strips. Free transition sublimation runs were made for the three wing configurations at the beginning of the test to determine strip location and bead size. The primary transition strip pattern (identified as grid code D) is defined below:

<u>Component</u>	<u>Location</u> (Inches from <u>Leading Edge</u>)	<u>Width</u> (Inches)	<u>Bead Dia.</u> (Inches)
Wing (Upper Surface & Lower Surface)	0.70	0.05	0.0024
		0.05	0.0031
Fuselage	0.90	0.10	0.0045
Horizontal Stabilizer (Upper & Lower Surfaces)	0.60	0.05	0.0038
Vertical Stabilizer (Both Sides)	0.65	0.05	0.0038
Pylons (Inboard and Outboard Surfaces)	0.20	0.05	0.0038
Nacelles (External)	0.80	0.05	0.0038

Above measurements were in a streamwise direction.

Additional tests were completed with the transition strip re-located and larger bead diameter on the upper surface of the wing as shown in the test program summary of Table 4.

3. TEST CONDITIONS AND SCHEDULE

All configurations were run at a Reynolds number of 4.8 million per foot (4.69 million based on model wing MAC) and a nominal free-stream Mach number range from $M = 0.600$ to 0.830 . Wing W^{12C} and W^{36} configurations were also run at Reynolds numbers of 2.5 and 5.5 million per foot (2.44 and 5.37 million based on model wing MAC) for scale effects. Six-component force and wing pressure measurements were obtained at zero yaw over an angle-of-attack range from -4° to $+6^\circ$. Flow visualization photos of fluorene/sublimation and oil flow patterns were obtained for selected configurations as part of the wing transition investigation.

A summary of the test program showing the test conditions, type of data obtained and the corresponding test part numbers are presented in Table 4.

4. DATA REDUCTION

a. Force Data

Six-component force and moment data were recorded from the Task 3500-B internal balance, reduced to coefficient form and transferred to the stability axis system coincident with the reference moment center. Data reduction was based on the following model dimensions:

Wing area, ft^2	6.247
Mean aero. chord (MAC), in/ft	11.724/0.977
Span, in/ft	84.302/7.025

Ref. Moment Center	FS 40.605*
	WL 10.428
	BL 0.00

Balance Center	FS 40.605
	WL 8.800
	BL 0.00

*Model MAC FS = Ref. Mom. Ctr. FS = 24.1% Full Scale MAC

The balance output data were reduced to coefficient form based on incompressible dynamic pressure, $q = \frac{\gamma}{2} \rho M^2$ and a balance calibration conducted by the AEDC personnel prior to the test. Balance outputs were also monitored for model-balance dynamics during the test. Blockage and tunnel wall effects were assumed to be negligible due to the small model-tunnel ratio and porous walls of the test section. No corrections for effects of blade-sting tare and interference, nacelle internal drag or flow angularity were applied, as the objective of this test was to identify drag increments between the basic and modified configurations.

Sting indicated pitch and roll angles were determined from output of a strut, internally-mounted, synchro-transmitters. An angular position indicator was mounted in the model aft of the balance as a back-up pitch indicator.

b. Pressure Data

Pressure data were recorded from the ± 12.5 psid transducers contained in the 48SQM Scanivalve module unit and reduced to coefficient form

$$C_p = \frac{P_M - P_S}{q}$$

where

C_p = pressure coefficient

P_M = model pressure

P_S = freestream or reference static pressure

q = freestream dynamic pressure

During the acquisition of pressure data, computer evaluation of the pressure rate-of-change was used and the transducer output was not acquired for computational purposes until either the rate of change was within acceptable limits or a maximum time delay was reached.

SECTION III

BASIC AERODYNAMIC DATA

The wind tunnel data from AEDC TF-481 is presented in two major sets, force data and chordwise pressure distributions. All the force data is presented first as plots of lift coefficient vs. angle of attack, pitching moment coefficient vs. lift coefficient, and drag vs. lift coefficient. For each configuration, all Mach numbers are included on each figure with the lift and pitching moment plots placed together on a single page as part (a) of the figure and the drag polar plotted separately as part (b). Table 5 is a schedule of configurations and figure numbers for the force data plots. The baseline leading edge data is presented in Figures 8 through 15. Figures 8 and 9 are free transition repeat runs. Figures 10 through 12 present the baseline force data for the three types of transition fixing used during the test. Figures 13 through 15 contain tail-on results and data for alternate Reynolds numbers. Force data for modified leading edge W^{35} are presented in Figures 16 through 18 for free transition and two transition methods. W^{36} data is presented in Figures 19 through 21. A limited amount of data was obtained with the pylons and nacelles removed from the wing. These results are shown in Figures 22 and 23 for the baseline and Figure 24 for W^{35} . Force data for the anti-drag body configurations tested is presented in Figures 25 and 26 and the swept tip results are presented in Figures 27 and 28.

Chordwise pressure distribution plots begin with Figure 29 and are presented for selected configurations and conditions. Each figure contains data for a particular Mach number and varying angles of attack for all four pressure measuring stations. Data for each station is plotted on a separate page as parts (a), (b), (c), and (d) of the figure. The symbol list on each plot is interpreted as follows: the three columns after each symbol contain the AEDC Part Number, Point and Angle of Attack, respectively; a different symbol is used for the lower surface pressures, thus the double entry for each angle of attack. Table 6 contains a schedule of the configurations plotted showing figure numbers for each.

TABLE 1
CONFIGURATION SYMBOLS

<u>SYMBOLS</u>	<u>COMPONENT</u>	<u>DRAWING NOS.</u>
B ¹²	<u>FUSELAGE</u> - C-141B Base; Basic C-141A Fuselage with 280 inch Full Scale Extensions	07-C141-0167-201A 07-C141-0167-202A
b ⁸	<u>BULLET FAIRING</u> - Empennage; Vert.- Horiz. Stab. Intersection	07-C141-0108-409
D ⁴	<u>DORSAL</u>	07-C141-0108-405
H ⁸	<u>HORIZONTAL STABILIZER</u>	07-C141-0108-400
K ¹⁹	<u>PYLONS</u> - Engine Nacelles	07-C141-0108-301 07-C141-0394-300
N ⁸	<u>NACELLES</u> - Flow Through, with Inlet Spinners	07-C141-0108-305 07-C141-0394-300
P ⁴	<u>AERIAL REFUELING POD</u> - Prototype Production	07-C141-0380-201 Loft 3R12100
V ⁶	<u>VERTICAL STABILIZER</u>	07-C141-0108-401
W ^{12C}	<u>WING</u> - Basic High/Low Speed W ¹² Steel Wing with Removable Leading Edges (Forward 12% C _W). 3 Panels L.E. Each Semi-Span	07-C141-0108-003 07-C141-0108-100 07-C141-0108-101 07-C141-0394-100 07-C-141-0110-900
W ³⁵	<u>WING</u> - W ^{12C} With 3-D CONMIN Leading Edge	07-C141-0394-900 07-C141-0394-100

TABLE 1 (CONT'D)

<u>SYMBOLS</u>	<u>COMPONENT</u>	<u>DRAWING NO.</u>
w ³⁶	<u>WING</u> - w ^{12C} With 2-D Test Airfoil (LE6) Tailored to Fit 3-D Wing	07-C141-0394-901 07-C141-0394-100
z ^{a2}	<u>ANTENNA FAIRING</u> - Located Top of Fuselage, Aft of Wing	07-C141-0108-901
z ^{f1}	<u>ANTI-DRAG BODIES</u> - Flap Track Fairing Type, Wing Trailing Edge; 8 per Semi-Span	07-C141-0394 07-C141-0394
z ^{f2}	<u>ANTI-DRAG BODIES</u> - 4 Per Semi-Span	
z ^{G21}	<u>WHEEL WELL FAIRING</u>	07-C141-0108-602
z ^{t6}	<u>WING TIP</u> - Swept; Chord/Span Ratio = 1.33/1	07-C141-0394-101
z ^{W7A}	<u>WING-FUSELAGE FILLET</u> - C-141A Pro- duction Fillets	07-C141-0108-101
s ¹	B ¹² K ¹⁹ N ⁸ P ⁴ z ^{a2} z ^{G21} z ^{W7}	
s ²	s ¹ WITHOUT K ¹⁹ N ⁸	

TABLE 2
MODEL DIMENSIONAL DATA

FUSELAGE - B¹²

Length, Inches	82.350
Max. Frontal Area, Ft ²	0.305
Max. Equiv. Diameter, Inches	7.480
Fineness Ratio (L/D)	11.009
Nose Location, FS	3.098
Fuselage Reference Line (FRL), WL	8.800

EMPENNAGE BULLET FAIRING - b⁸

Length, Inches	13.394
Max. Frontal Area, In ²	2.920
Nose Location, FS	78.723

DORSAL - D⁴

Location Root Chord L.E., FS	66.007
------------------------------	--------

HORIZONTAL STABILIZER - H⁸

Airfoil Section	Root: NACA 64A(010)010.5
	Tip: NACA 64A(010)010.5
Area, Ft ²	0.935
Span, Inches	26.487
Aspect Ratio	5.210
Taper Ratio	0.370
Sweep of 25% Chord, Degrees	25.0
Twist, Degrees	0.0
Dihedral, Degrees	0.0
Root Chord, Inches	7.422
Mean Aerodynamic Chord, Inches	5.442
Tip Chord, Inches	2.746
Location 25% MAC, FS	85.349
WL	24.581
BL	5.607

TABLE 2 (CONT'D)

Tail Length, Inches	43.477	
Tail Volume Coefficient	0.555	
Incidence Settings, Degrees	0, <u>+1</u> , <u>+2</u>	
<u>PYLONS</u> - K ¹⁹		
	<u>INBOARD</u>	<u>OUTBOARD</u>
Area, Ft ²	0.090	0.093
Span, Inches	1.453	1.517
MAC, Inches	8.800	8.800
Thickness, Streamwise, % Chord	8.000	8.000
Sweep of Leading Edge, Degrees	73.000	73.000
<u>NACELLES</u> - N ⁸		
Area, Side per Nacelle, Ft ²		0.168
Length, Inches		8.256
Max. External Diameter, Inches		2.900
Internal Diameter, Inches - Inlet		2.244
- Exit		1.940
Internal Area, In ² - Inlet		3.954
- Exit		2.956
Fineness Ratio, (L/D) Ext.		2.843
Toe-In, Degrees - Inboard		2.0
- Outboard		1.0
Location of Inlet ϕ - INBOARD, FS		29.104
	WL	8.479
	BL	12.272
- OUTBOARD FS		32.709
	WL	8.163
	BL	20.103
<u>AERIAL REFUELING POD</u> - P ⁴		
Length, Inches		8.83
Max. Width, Inches		1.48
Max. Height, Inches		0.88
Leading Edge Location, FS		8.93

TABLE 2 (CONT'D)

VERTICAL STABILIZER - V^6

Airfoil Section	Root: NACA 64A(012)013
	Tip: NACA 64A(012)013
Area, Ft^2	0.770
Span, Inches	11.577
Mean Aerodynamic Chord, Inches	9.763
Aspect Ratio	1.208
Taper Ratio	0.617
Sweep of 25% Chord, Degrees	35.0
Root Chord, Inches	11.852
Tip Chord, Inches	7.317
Location 25% Mac, FS	80.283
WL	18.336
BL	0.000
Tail Length, Inches	38.962
Tail Volume Coefficient	0.057

WING* - W^{12C}

Airfoil Section	
Root (BL 0.000)	NACA 0013.0-1.10-40/1.575(MOD.), MEAN LINE $a_o = 0.8(\text{MOD.})$ DESIGN LIFT COEFFICIENT $c_{li} =$ 0.153
Inboard Break (BL 17.804)	NACA 0011.2-1.10-40/1.575(MOD.), MEAN LINE $a_o = 0.8(\text{MOD.})$ DESIGN LIFT COEFFICIENT $c_{li} =$ 0.194
Outboard Break (BL 18.778)	NACA 0011.0 - 1.10 - 40/1.575 (MOD.) MEAN LINE $a_o = 0.8 (\text{MOD.})$ DESIGN LIFT COEFFICIENT $c_{li} =$ 0.201

TABLE 2 (CONT'D)

TIP	NACA 0010.0 - 2.20 - 40/1.575
	MEAN LINE 1/2 (NACA 66 @ c_{li} =
	1.0 + NACA 230 @ c_{li} = 1.0) ⁱ
	DESIGN LIFT COEFFICIENT c_{li} =
	0.452
Area, Ft^2 (S)	6.247
Span (Equiv.), Inches/Ft(b)	84.302/7.025
Aspect Ratio (A)	7.9
Taper Ratio (λ)	0.373
Thickness Ratio (t/c) - Root (BL 0.00)	0.130
- Inboard Break (BL 17.804)	0.112
- Outboard Break (BL 18.778)	0.110
- Tip	0.100
- Mean	0.113
Sweep of 25% chord, Degrees ($\Lambda_{0.25c}$) - Inboard	23.734
- Outboard	25.025
Sweep of Leading Edge, Degrees ($\Lambda_{L.E.}$)	
- Inboard	28.253
- Outboard	27.285
Dihedral, Degrees (Γ) - Inboard	-0.941
- Outboard	-1.195
Incidence, Degrees from FRL @ BL 0.00 (i)	4.891
Twist, Degrees (θ) - Root (BL 0.00)	0.00
Inboard Break (BL 17.804)	-2.201
Outboard Break (BL 18.778)	-2.279
Tip (BL 42.151)	-5.584
Chord Lengths (Projected), in.- Root(c_r)BL 0.0	17.547
MAC (\bar{c})BL 17.309	11.724
Inbd. Brk. BL 17.804	10.591
Outbd. Brk. BL 18.778	10.379
Tip (c_t) BL 42.151	5.803
Chord Locations - Root (L.E.) FS	28.545
WL	13.045

TABLE 2 (CONT'D)

BL	0.00
(MAC (25%) FS	40.605
WL	11.629
BL	17.309
TIP(L.E.) FS	50.531
WL	10.219
BL	42.151

***NOTE:** Wind Tunnel data based on projected wing planform with root chord @ 0° incidence and aero L.E. and 100% chord T.E.
 Aero data analysis based on area measured from L.E. to T.E., and 25% MAC location referenced to wing reference plane.
 W.T. Data 25% MAC location = 24.1% MAC Aero Analysis Data.

ANTENNA FAIRING - za2

Length, inches	11.616
Width, inches	2.68
Leading Edge Location, FS	41.931
Trailing Edge Location, FS	53.547

WHEEL WELL FAIRINGS - zG21

Length, Inches	17.776
Max. Frontal Area Per Side, Inches	7.480
Max. Equiv. Diameter, Inches	3.086
Fineness Ratio	5.760
Leading Edge Location, FS	34.936

TABLE 3
WING PRESSURE ORIFICE LOCATIONS

BL 8.127	BL 17.634	BL 26.825	BL 33.437
<u>$\eta = 0.193$</u>	<u>$\eta = 0.418$</u>	<u>$\eta = 0.637$</u>	<u>$\eta = 0.793$</u>

(X/C's FOR ORIFICE LOCATIONS)

<u>UPPER</u>	<u>LOWER</u>	<u>UPPER</u>	<u>LOWER</u>	<u>UPPER</u>	<u>LOWER</u>	<u>UPPER</u>	<u>LOWER</u>
0.0	0.02	0.0	0.02	0.0	0.02	0.0	0.02
0.015	0.05	0.015	0.05	0.015	0.05	0.015	0.05
0.03	0.10	0.03	0.10	0.03	0.10	0.03	0.10
0.05	0.20	0.05	0.15	0.05	0.15	0.05	0.15
0.07	0.30	0.07	0.20	0.07	0.20	0.07	0.20
0.09	0.40	0.09	0.30	0.09	0.30	0.09	0.30
0.11	0.50	0.11	0.40	0.11	0.40	0.11	0.40
0.20	0.63	0.15	0.50	0.15	0.50	0.15	0.50
0.30	0.80	0.20	0.65	0.20	0.65	0.20	0.65
0.40	0.95	0.25	0.85	0.25	0.85	0.25	0.85
0.50		0.30		0.30		0.30	
0.63		0.37		0.35		0.35	
0.80		0.40		0.40		0.40	
0.95		0.45		0.45		0.45	
1.0		0.50		0.50		0.50	
		0.60		0.60		0.60	
		0.70		0.70		0.70	
		0.80		0.80		0.80	
		0.90		0.90		0.90	
		0.95		0.95		0.95	
		1.00		1.00		1.00	

TABLE 4
TEST PROGRAM SUMMARY
AEDC TF-481

DESCRIPTION & CONFIGURATION	GRIT CODE	$R_N \times 10^{-6}$ PER FT	PWT PN @ INDICTED MACH NUMBER								
			.600	.700	.750	.770	.780	790	.800	.810	.830
I. SUBLIMATION											
1. Free Transition											
$S_{W1.12C}$ ↓	A	4.8 ↓				109 193					
$S_{W1.35}$ ↓	A	4.8 ↓				161 204 207					
$S_{W1.36}$	A	4.8				137					
2. Fixed Transition											
$S_{W1.12C}$ ↓	B C D	4.8 4.8 4.8				190 105 245					
$S_{W1.35}$ ↓	D	4.8				264					
$S_{W1.36}$	B	4.8				134					

TABLE 4 (CONT'D)

DESCRIPTION & CONFIGURATION	GRIT CODE	$R_N \times 10^{-6}$ PER FT	PWT PN @ INDICATED MACH NUMBER								
			.600	.700	.750	.770	.780	.790	.800	.810	.830
II. BASE WING (w12C)											
1. Transition Grit Var.											
$S_W^{1,12C}$	A	4.8	30	31	33	37		38		39	
↓		↓	196	197	36 198	199		200		201	
	B		180	181	182	183		184			
	C		46	47	49	50	51	52	53	54	55
↓	D	↓	213	214	215	216		217		218	
2. Reynolds No. Var.											
$S_W^{1,12C}$	C	2.5		61	62	63		64		65	
↓	C	5.5		48 60	59	58		57		56	
3. Tail On											
$S_W^{1,12C} D V H_O^{4,6,8,8}$	C	4.8	88	89	90	91		92		93	
4. Swept Tips											
$S_W^{1,12C} Z^{t6}_{RH}$	C	4.8		68	69	70		71		72	
$S_W^{1,12C} Z^{t6}$	C	4.8		75	76	77		78		79	
5. Pylons-Nacelles Off											
$S_W^{2,12C}$	C	4.8	97	98	99	100		101		102	
↓	D	4.8		224	222	221		223			
6. Anti-Drag Bodies (8)											
$S_W^{1,12C} Z^{f1}$	D	4.8	230	232	233	234		235		236	
		4.8	242	241	240	239		238		237	

TABLE 4 (CONT'D)

DESCRIPTION & CONFIGURATION	GRIT CODE	$R_N \times 10^{-6}$ PER FT	PWT PN @ INDICATED MACH NUMBER								
			.600	.700	.750	.770	.780	.790	.800	.810	.830
III. 3-D WING (w^{35})											
1. Transition Grit Var.											
slw^{35}	A	4.8	151	152	153	154		155		156	
↓	B	↓	140	141	142	143	144	145	146	147	148
↓	D	↓	248	249	250	251		252		253	
2. Pylons-Nacelles Off											
s^2w^{35}	D	4.8		256	257	258		259			
3. Anti-Drag Bodies (4)											
$slw^{35}zf2$	D	4.8	267	268	269	270	272	271		273	
IV. 2-D WING (w^{36})											
1. Transition Grit Var.											
slw^{36}	A	4.8	172	173	174	175		176		177	
↓	B	↓	112	113	114	115	116	117	118	119	120
↓	C	↓	164	165	166	167		168		169	
2. Reynolds No. Var.											
slw^{36}	B	2.5		125	126	127		128			
	B	5.5		124	123	122		121			

TABLE 4 (CONT'D)

WING TRANSITION GRIT CODE:

<u>CODE</u>	<u>DESCRIPTION</u>	<u>STRIP LOCATION</u>	<u>GRIT SIZE (In. Dia.)</u>
A	Free Transition		
B	Heavy Density Grit	4% c Upper Surface	0.0031
		7 1/2% c Lower Surface	0.0031
C	Light Density Grit	4% c Upper Surface	0.0031
		7 1/2% c Lower Surface	0.0031
D	Light Density Grit	0.7 In. from L.E., Upper & Lower Surfaces	0.0024 (Upper) 0.0031 (Lower)

TABLE 5
PLOT SCHEDULE FOR FORCE DATA

DESCRIPTION AND CONFIGURATION	GRIT CODE	$R_N \times 10^{-6}/FT$	FIGURE NUMBER
1. Baseline Leading Edge (W ^{12C})			
slw ^{12C}	A	4.8	8
Repeat	A	4.8	9
	B	4.8	10
	C	4.8	11
	D	4.8	12
Tail-on	C	4.8	13
	C	2.5	14
	C	5.5	15
2. Modified Leading Edge (W ³⁵)			
slw ³⁵	A	4.8	16
	B	4.8	17
	D	4.8	18
3. Modified Leading Edge (W ³⁶)			
slw ³⁶	A	4.8	19
	B	4.8	20
	C	4.8	21
4. Pylons & Nacelles Off			
s ² w ^{12C}	C	4.8	22
s ² w ^{12C}	D	4.8	23
s ² w ³⁵	D	4.8	24
5. Anti-Drag Bodies			
slw ^{12C} _z f1	D	4.8	25
slw ³⁵ _z f2	A	4.8	26
Swept Tip			
slw ^{12C} _z t6 (R.H.)	C	4.8	27
slw ^{12C} _z t6	C	4.8	28

TABLE 6
PLOT SCHEDULE FOR PRESSURE DATA

DESCRIPTION AND CONFIGURATION	GRIT CODE	$R_N \times 10^{-6}/FT$	FIGURE NO. AT INDICATED MACH NO.				
			.70	.75	.77	.79	.81
1. Baseline Leading Edge (w^{12C})							
slw^{12C}	A	4.8	29	30	31	32	33
slw^{12C}	C	4.8	34	35	36	37	38
slw^{12C}	D	4.8	39	40	41	42	43
2. Modified Leading Edge (w^{35})							
slw^{35}	A	4.8	44	45	46	47	48
slw^{35}	D	4.8	49	50	51	52	53
3. Modified Leading Edge (w^{36})							
slw^{36}	B	4.8	54	55	56	57	58
4. Pylons and Nacelles Off							
$s2w^{12C}$	D	4.8	59	60	61	62	
$s2w^{35}$	D	4.8	63	64	65	66	
5. Anti-Drag Bodies							
$slw^{12C}z^{f1}$	D	4.8	67	68	69	70	71
$slw^{35}z^{f2}$	A	4.8	72	73	74	75	76
6. Swept Tip							
$slw^{12C}z^{t1}$ (one side only)	C	4.8	77	78	79	80	81
$slw^{12C}z^{t2}$	C	4.8	82	83	84	85	86

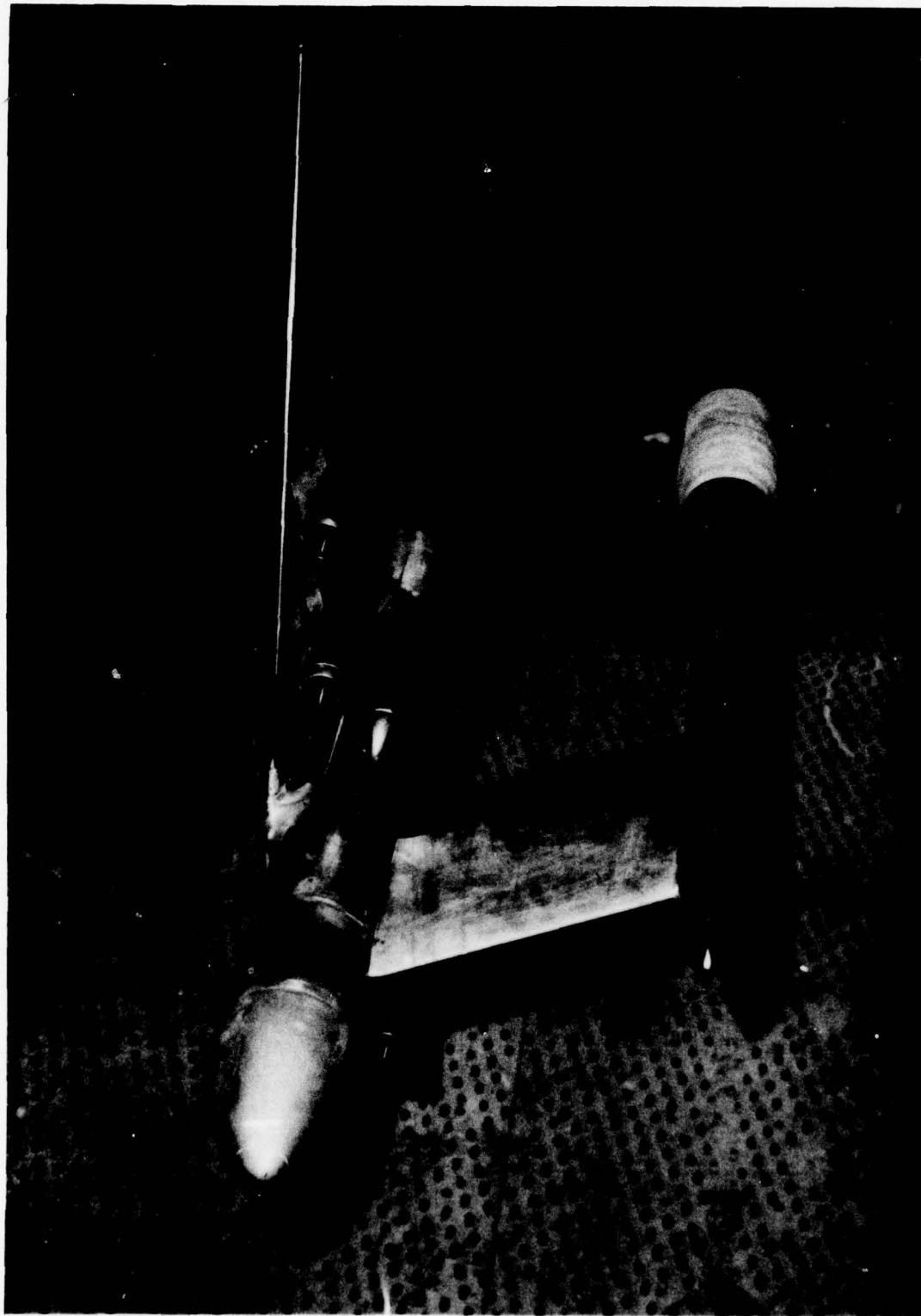
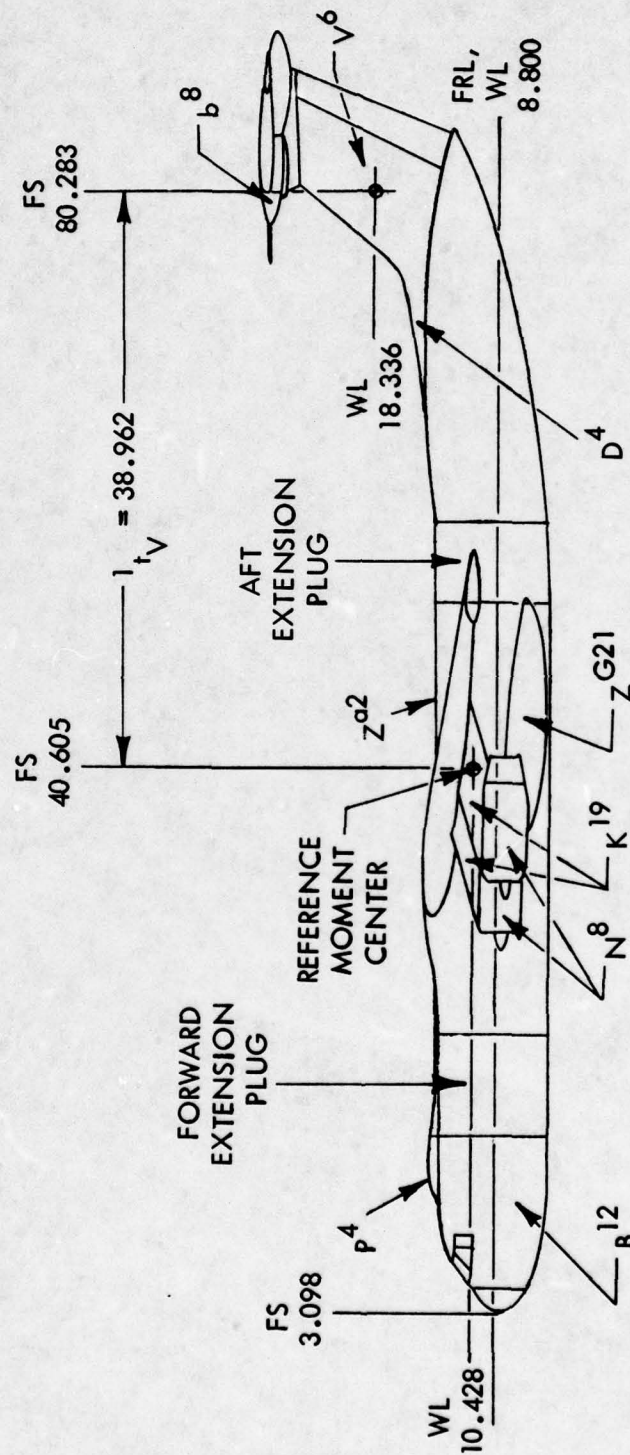
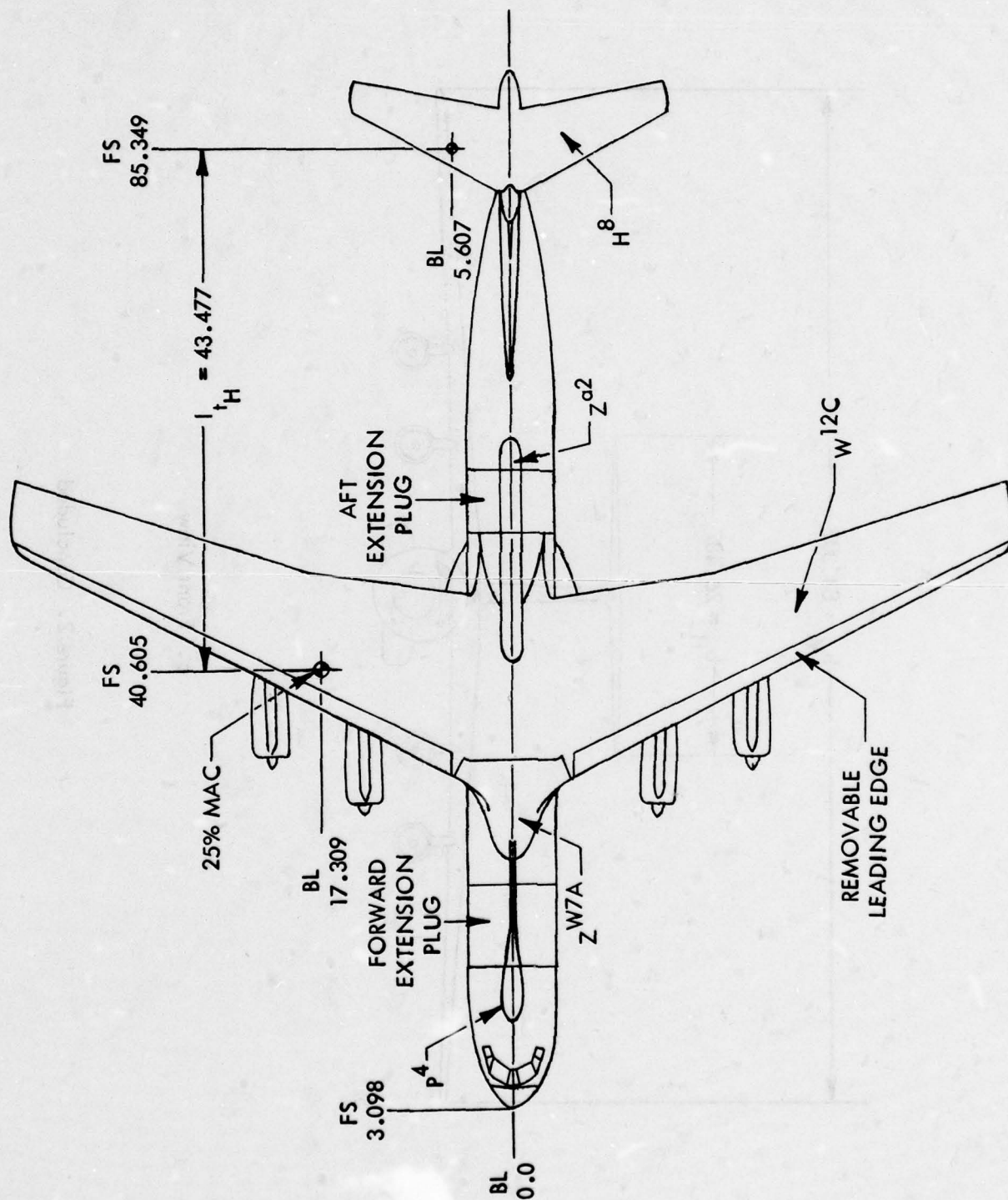


Figure 1. Photograph of the 0.044 Scale C-141B Model Installed at AEDC 16T

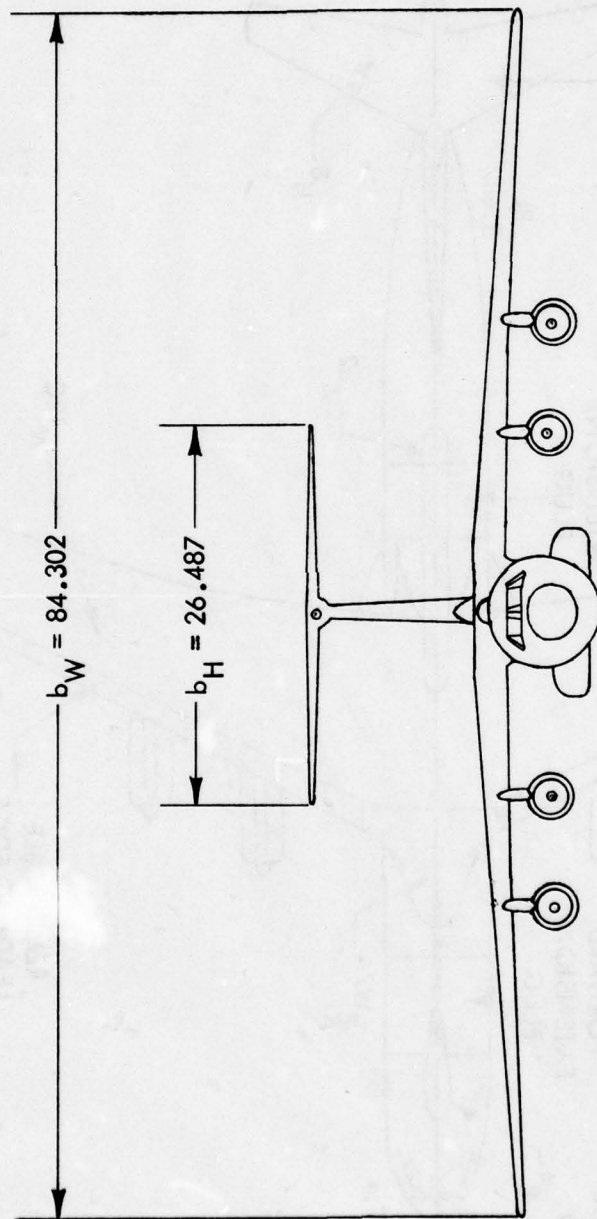


a. Side View

Figure 2. Three-View Sketch of the 0.044 Scale C-141B Model



b. Plan View
Figure 2. Continued



c. Front View

Figure 2. Concluded

$$\eta = 0.793$$

— W^{12C} (BASIC)
 — W^{35}
 - - - W^{36}

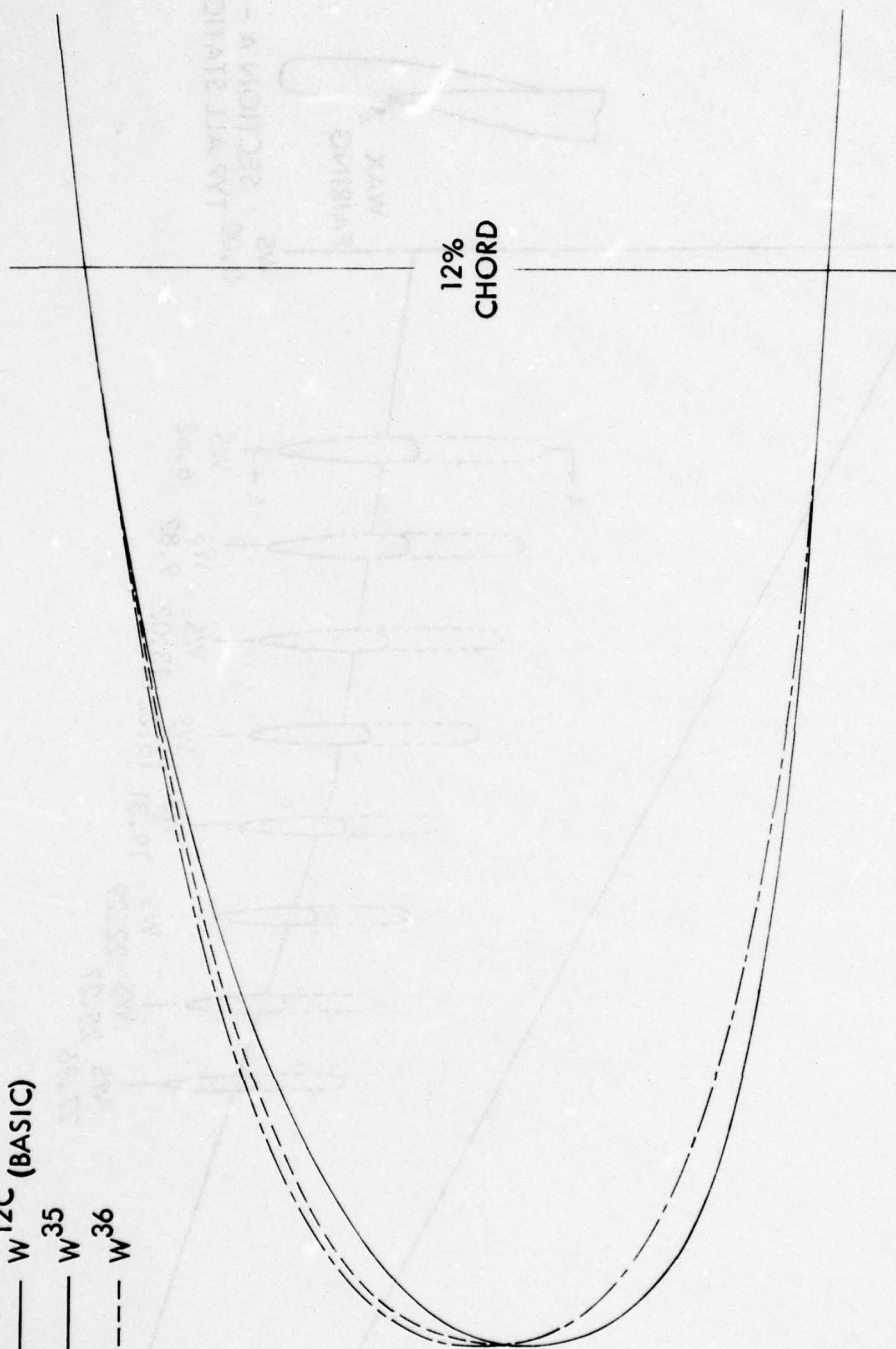


Figure 3. Sketch Comparison of the Basic and Modified Leading Edges

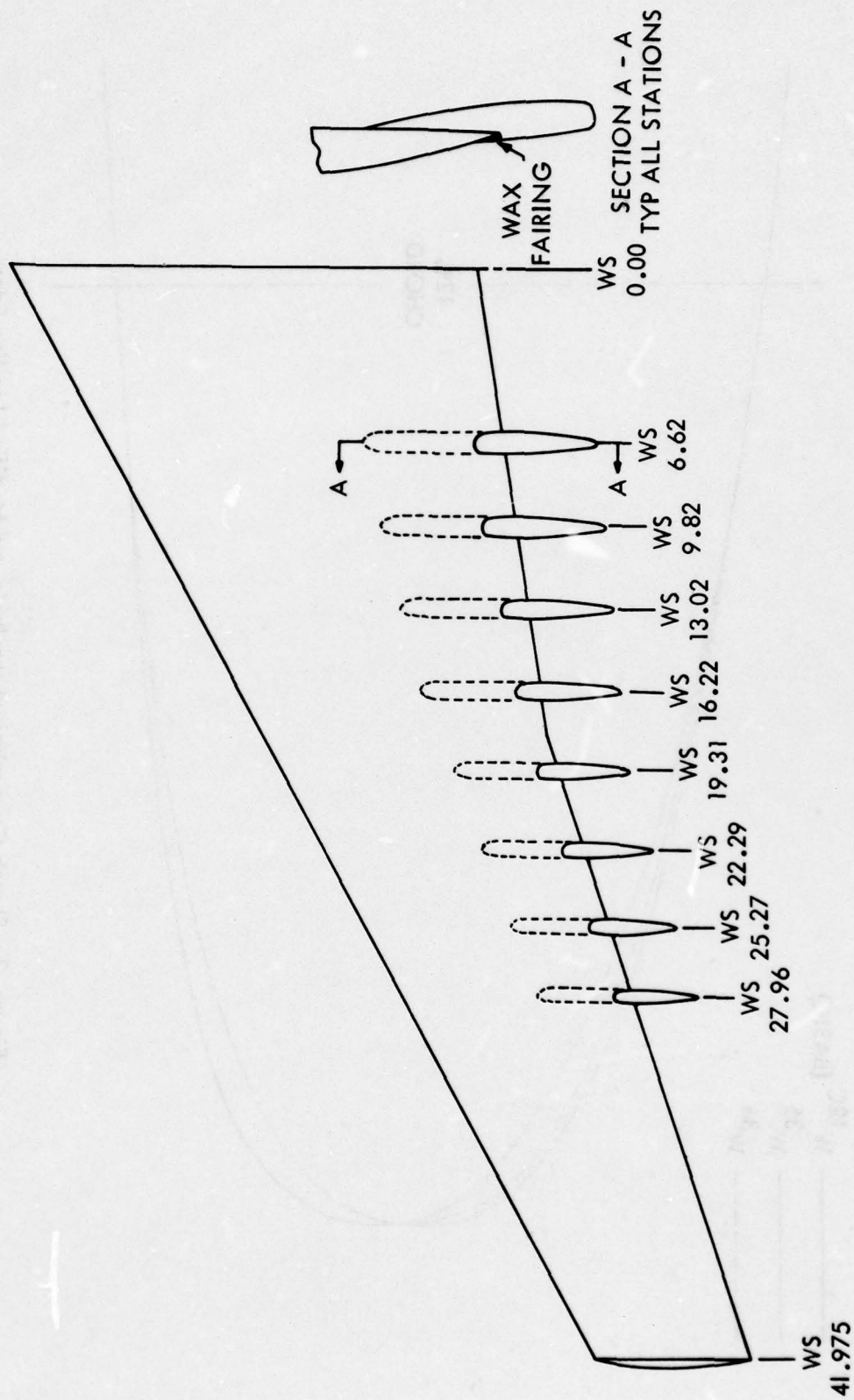


Figure 4. Location of Anti-Drag Bodies



Figure 5. Photograph of the Anti-Drag Bodies Installed on the Model

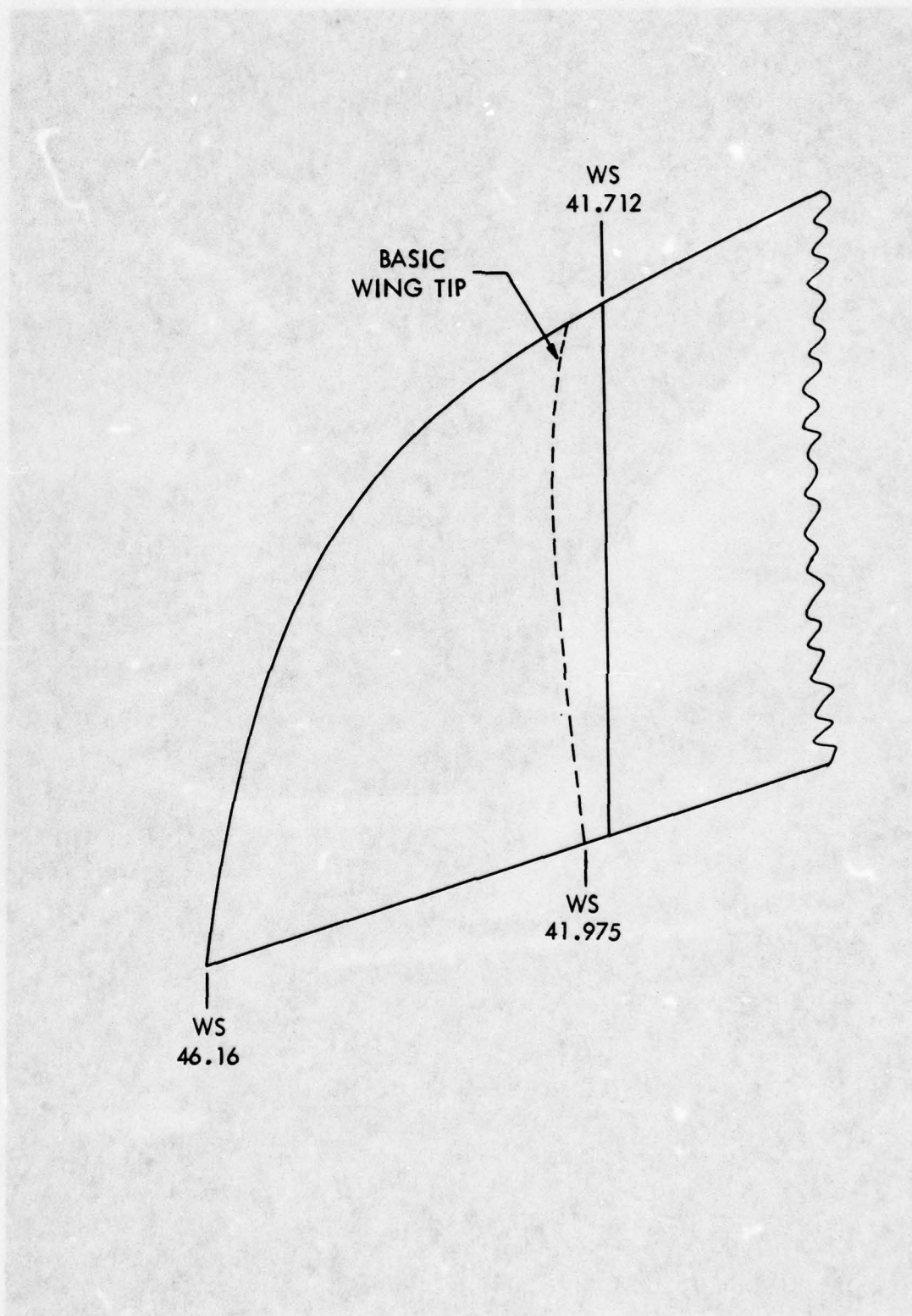


Figure 6. Sketch of Swept Wing Tip

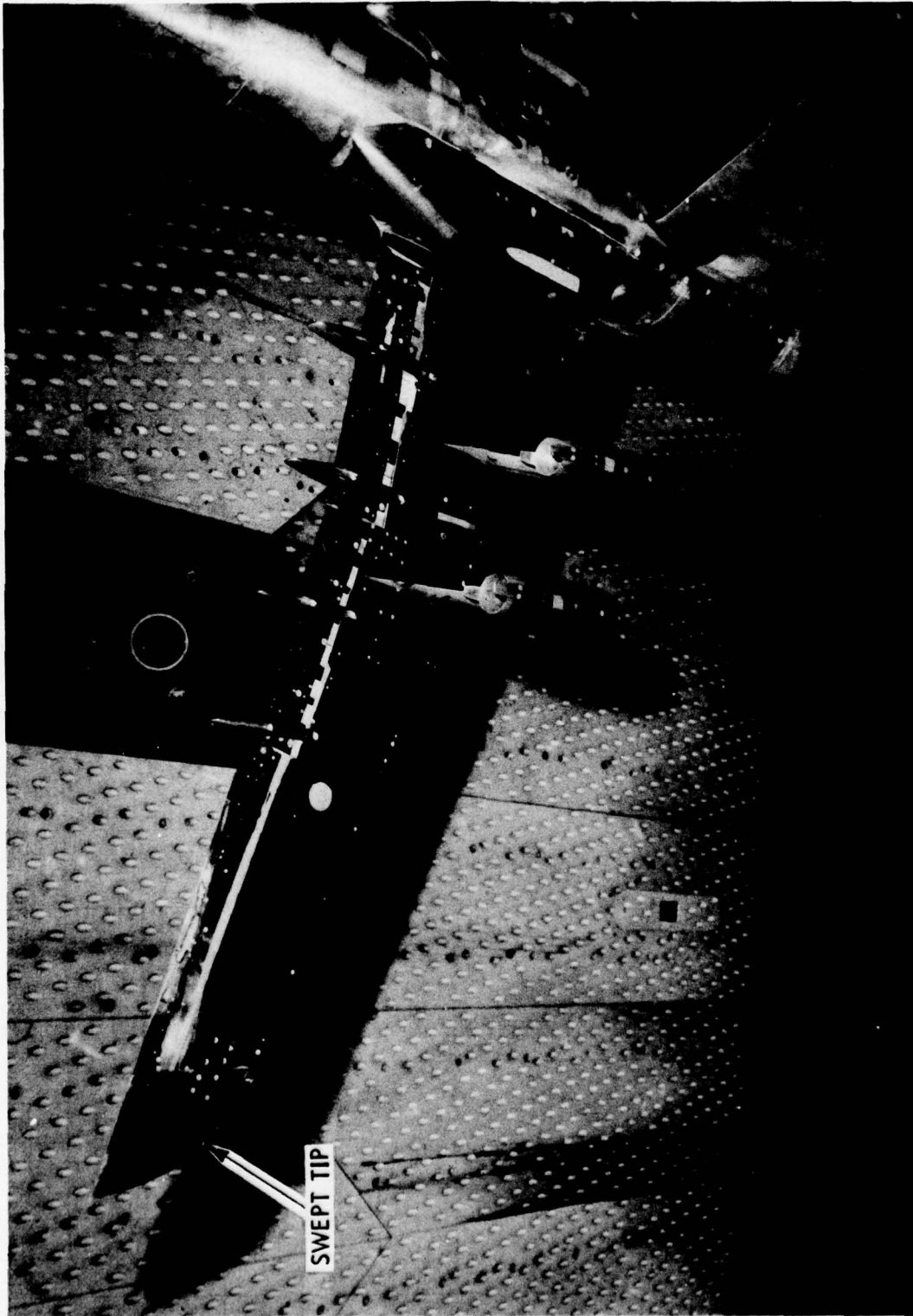
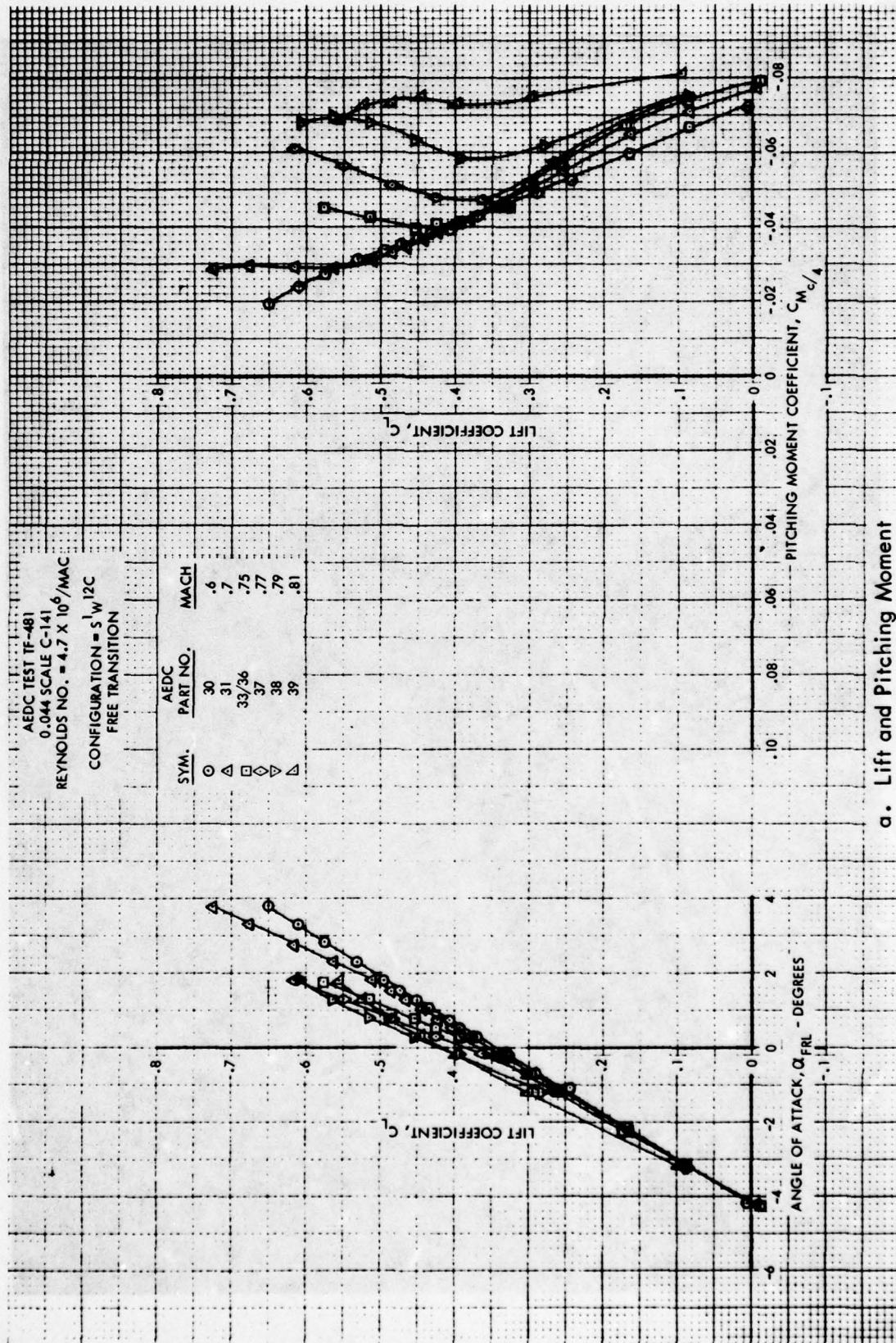
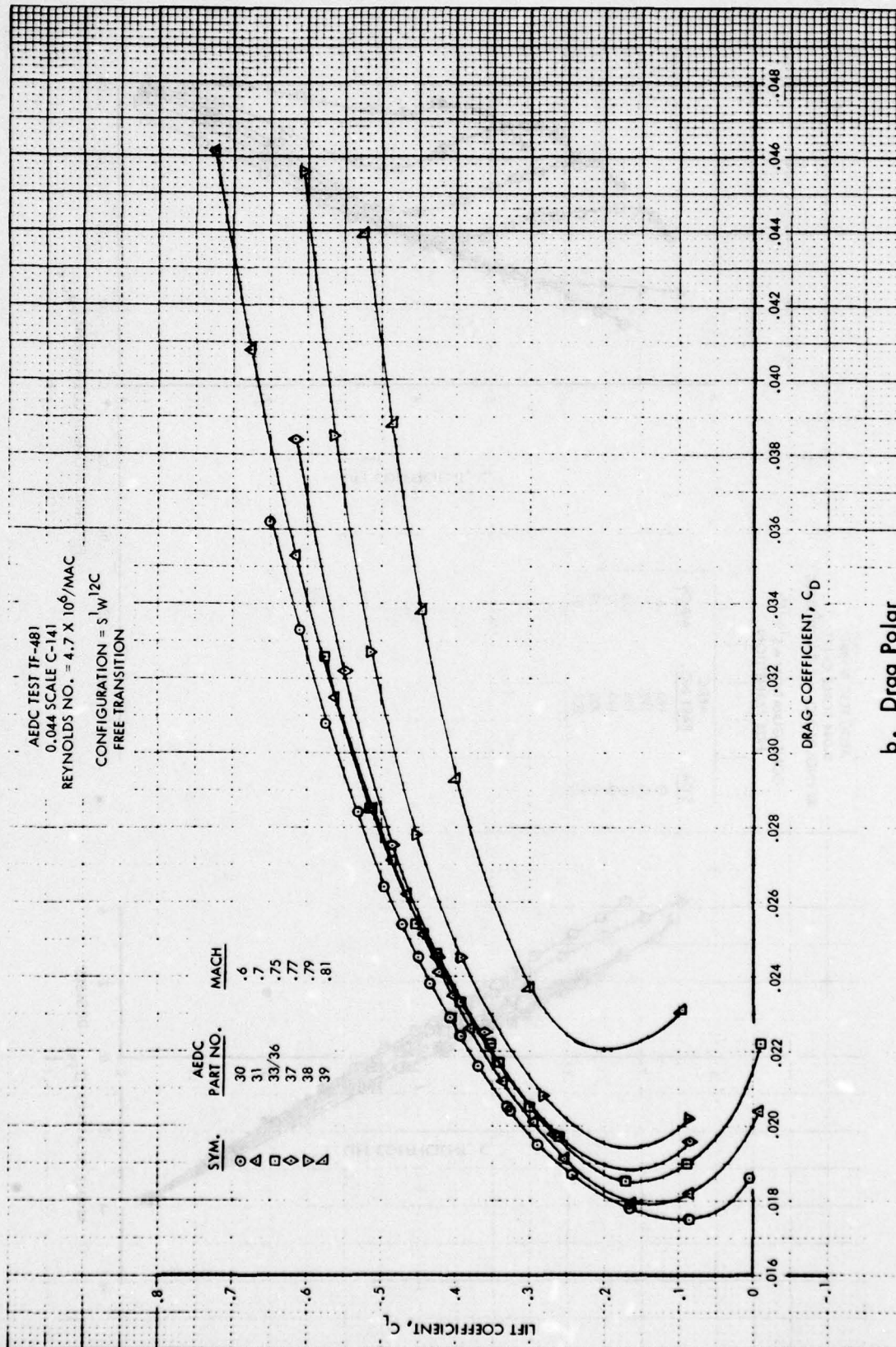


Figure 7. Photograph of the Swept Tip Installation.

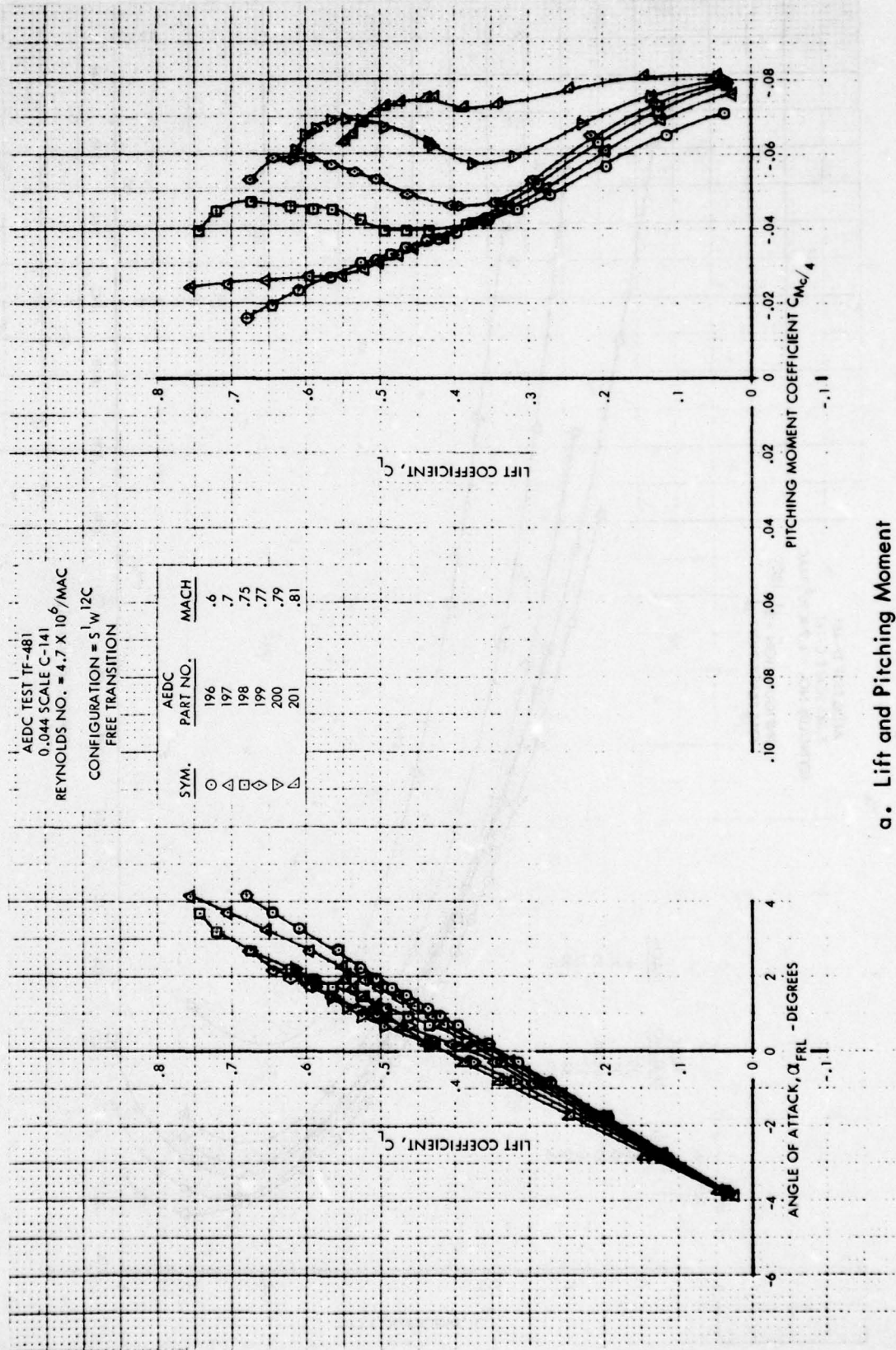


a. Lift and Pitching Moment

Figure 8. Lift, Drag and Pitching Moment Characteristics for Baseline Leading Edge, Free Transition

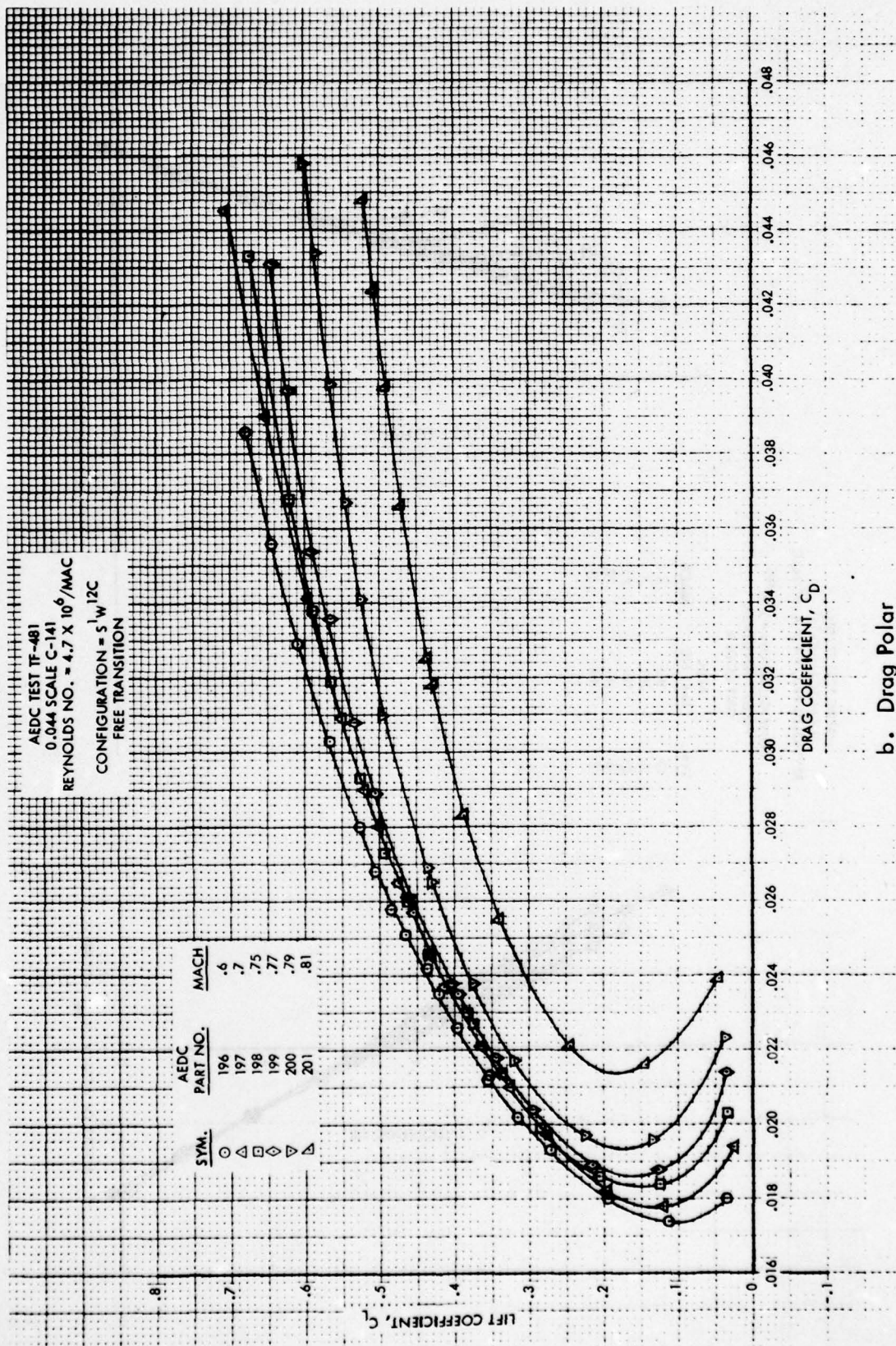


b. Drag Polar
Figure 8. Concluded

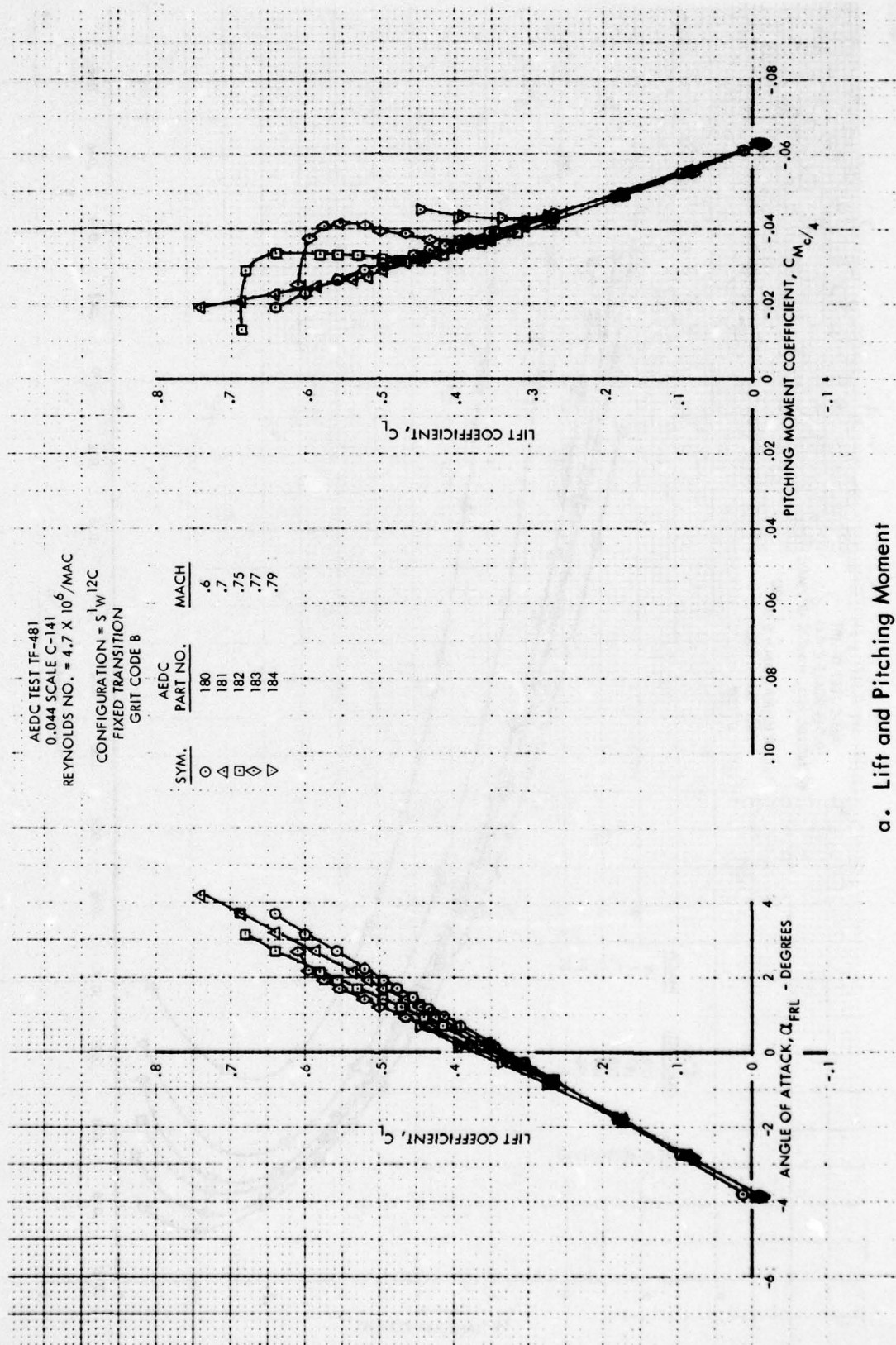


a. Lift and Pitching Moment

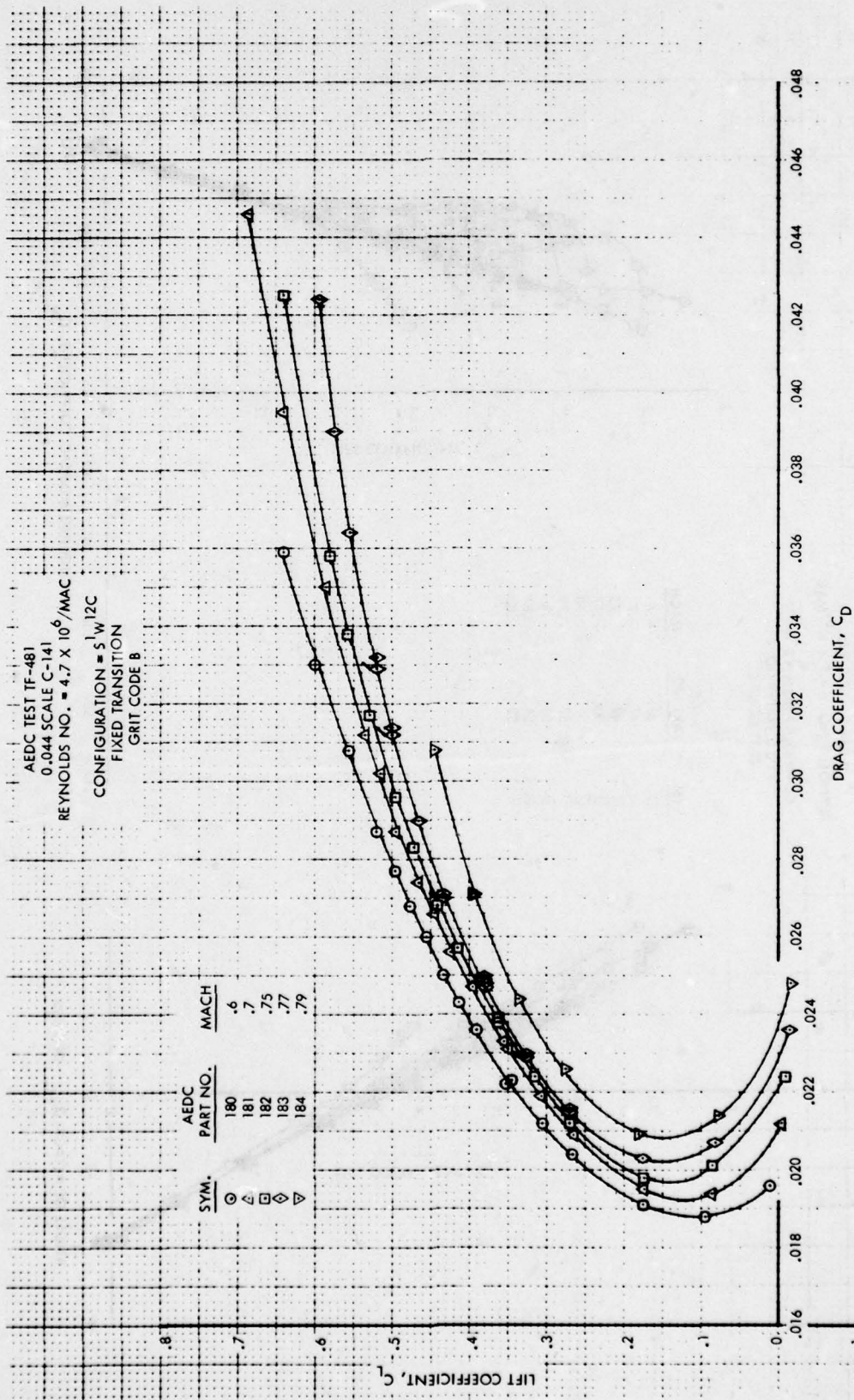
Figure 9. Lift, Drag and Pitching Moment Characteristics for Baseline Leading Edge, Free Transition, Repeat



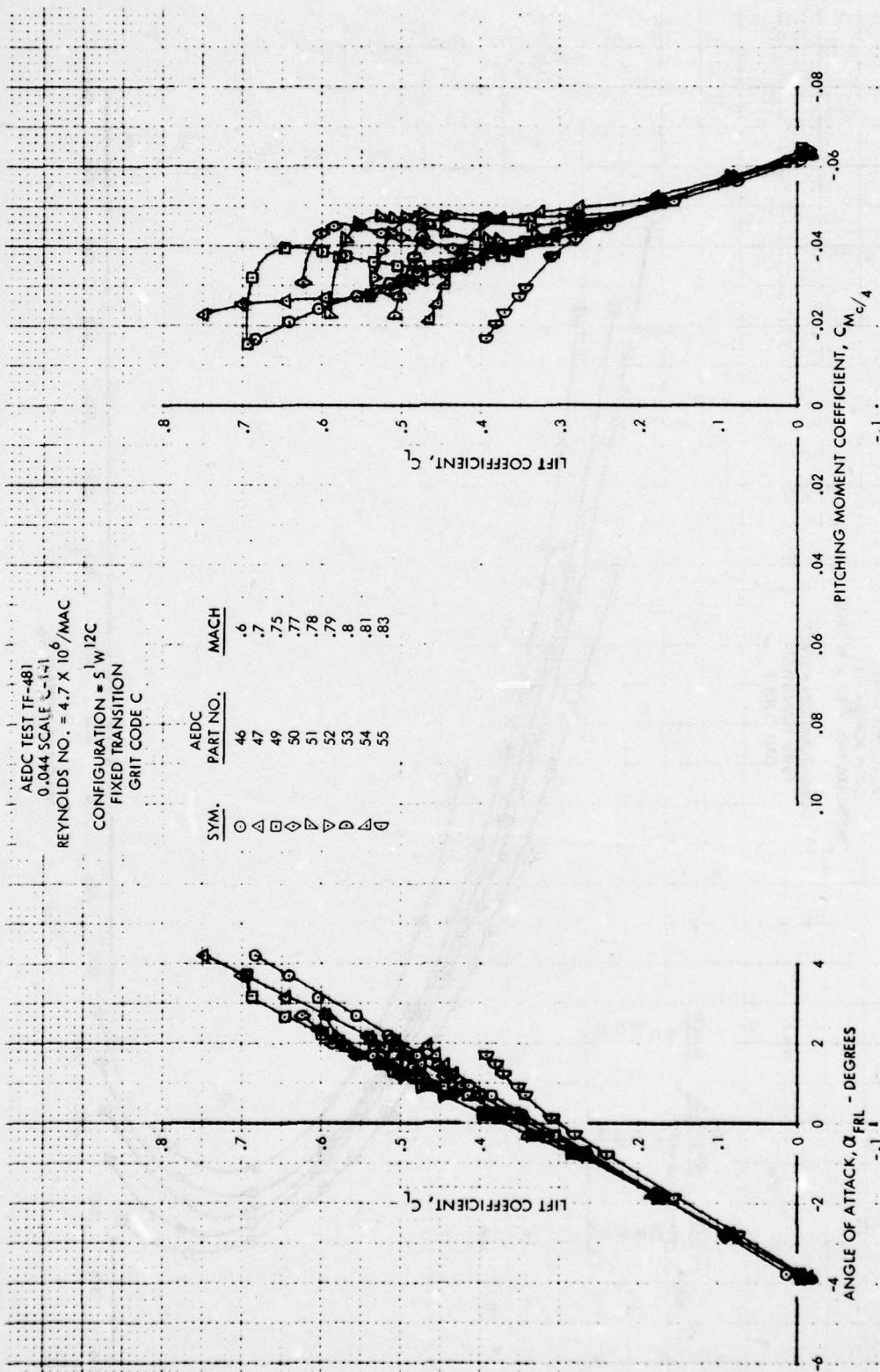
b. Drag Polar
Figure 9. Concluded



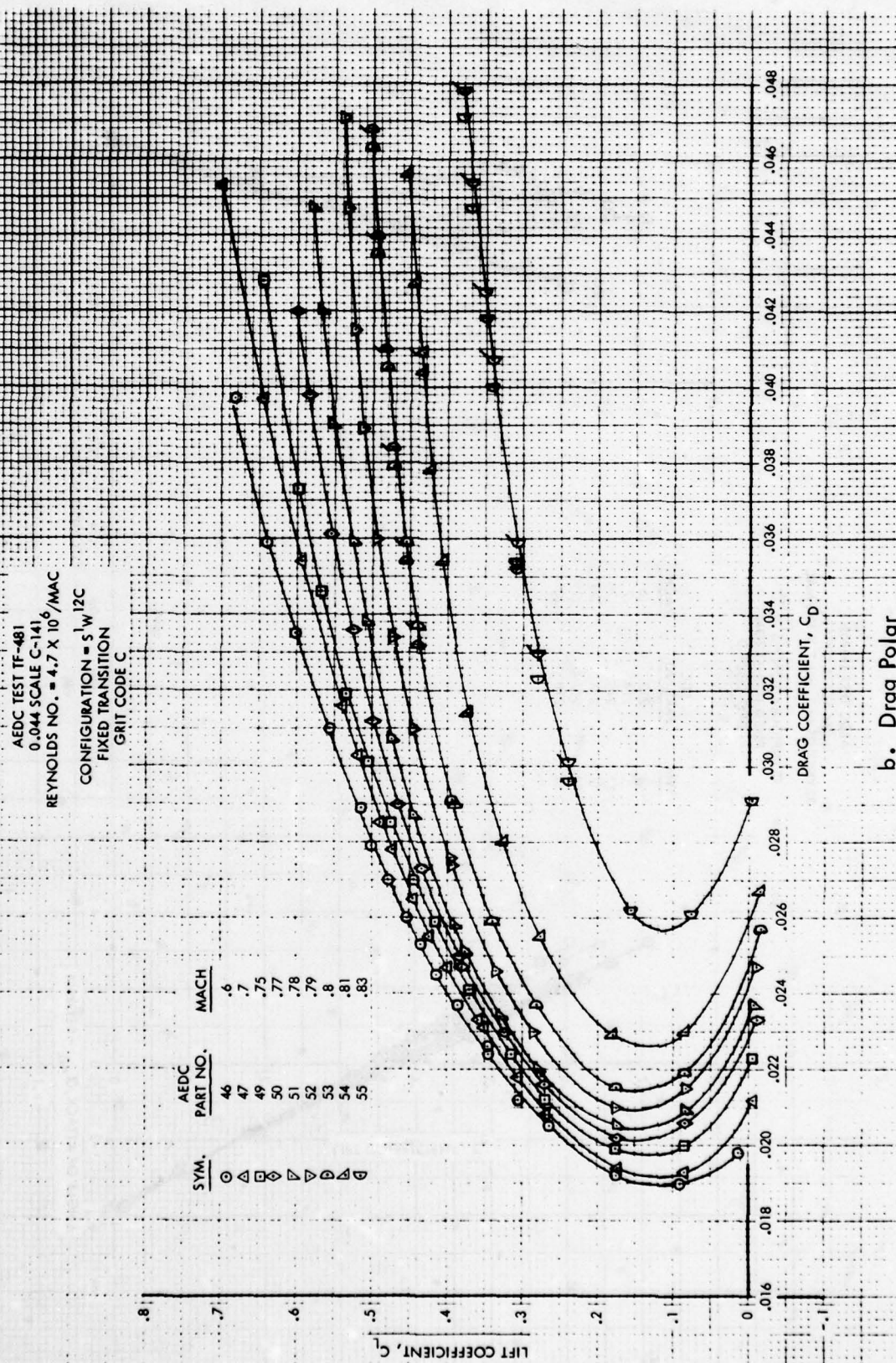
a. Lift and Pitching Moment
 Figure 10. Lift, Drag and Pitching Moment Characteristics for Baseline Leading Edge,
 Fixed Transition, Grit Code B



b. Drag Polar
Figure 10. Concluded



a. Lift and Pitching Moment
Figure 11. Lift, Drag and Pitching Moment Characteristics for Baseline Leading Edge,
Fixed Transition, Grit Code C



b. Drag Polar
 Figure 11. Concluded

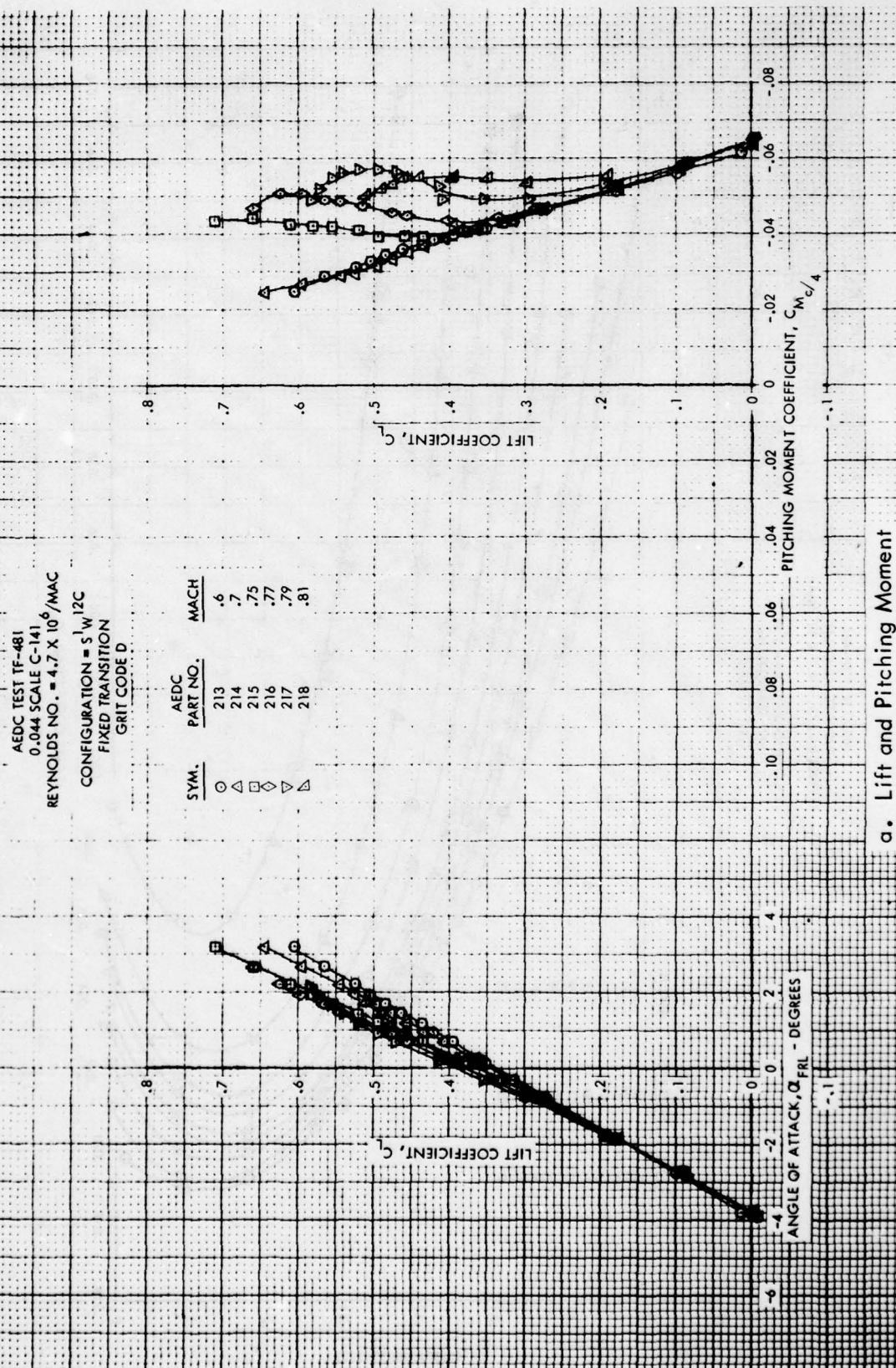
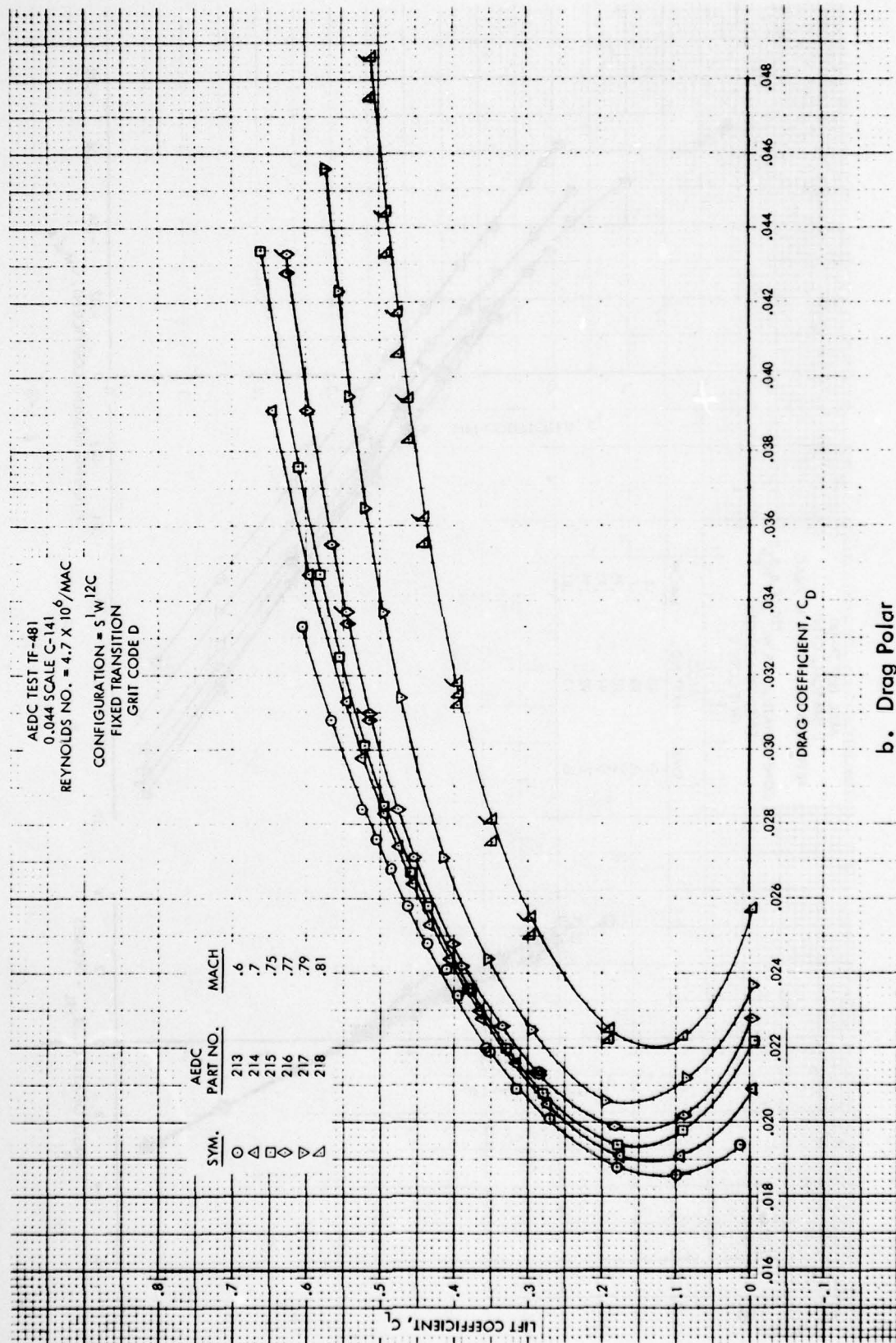
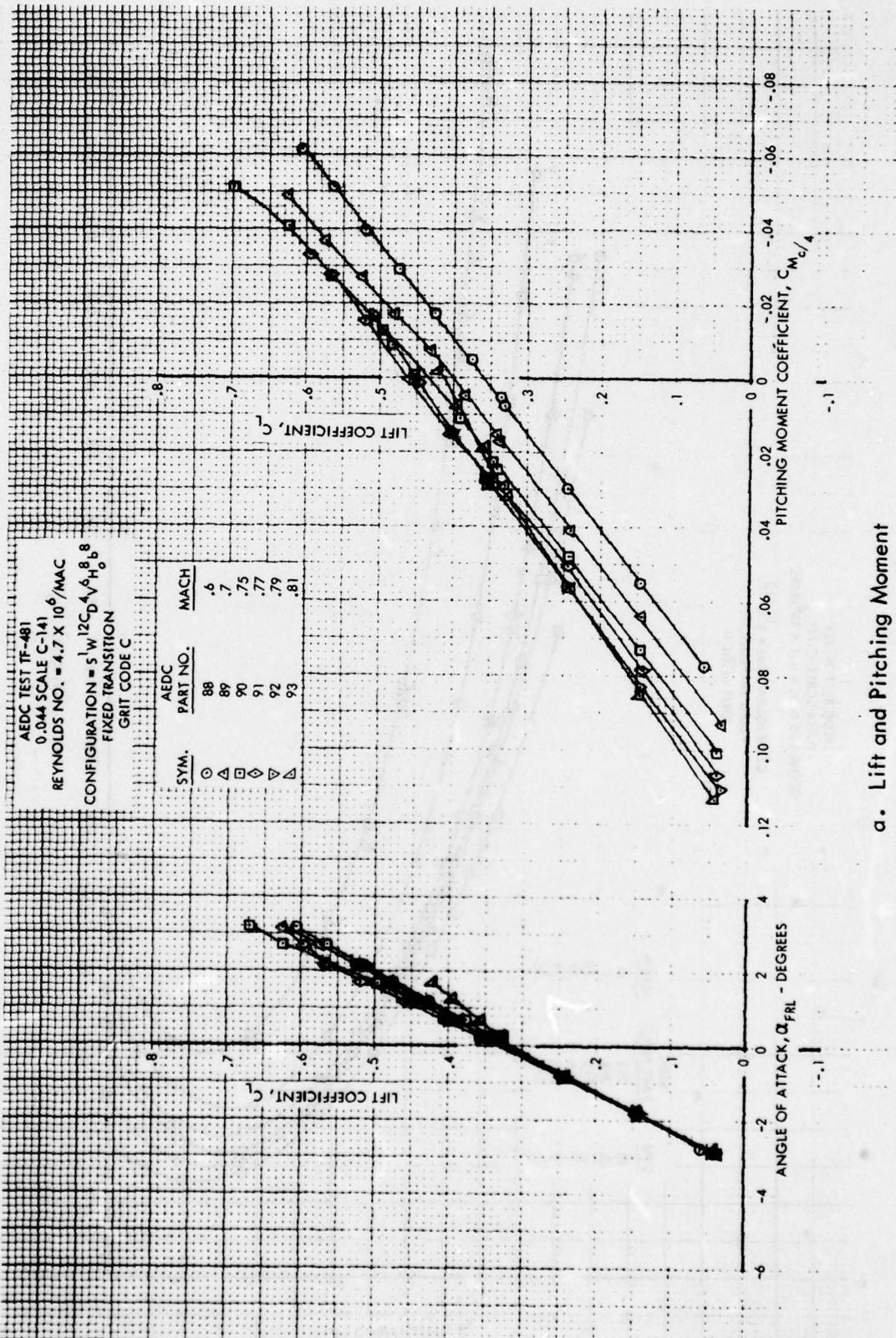


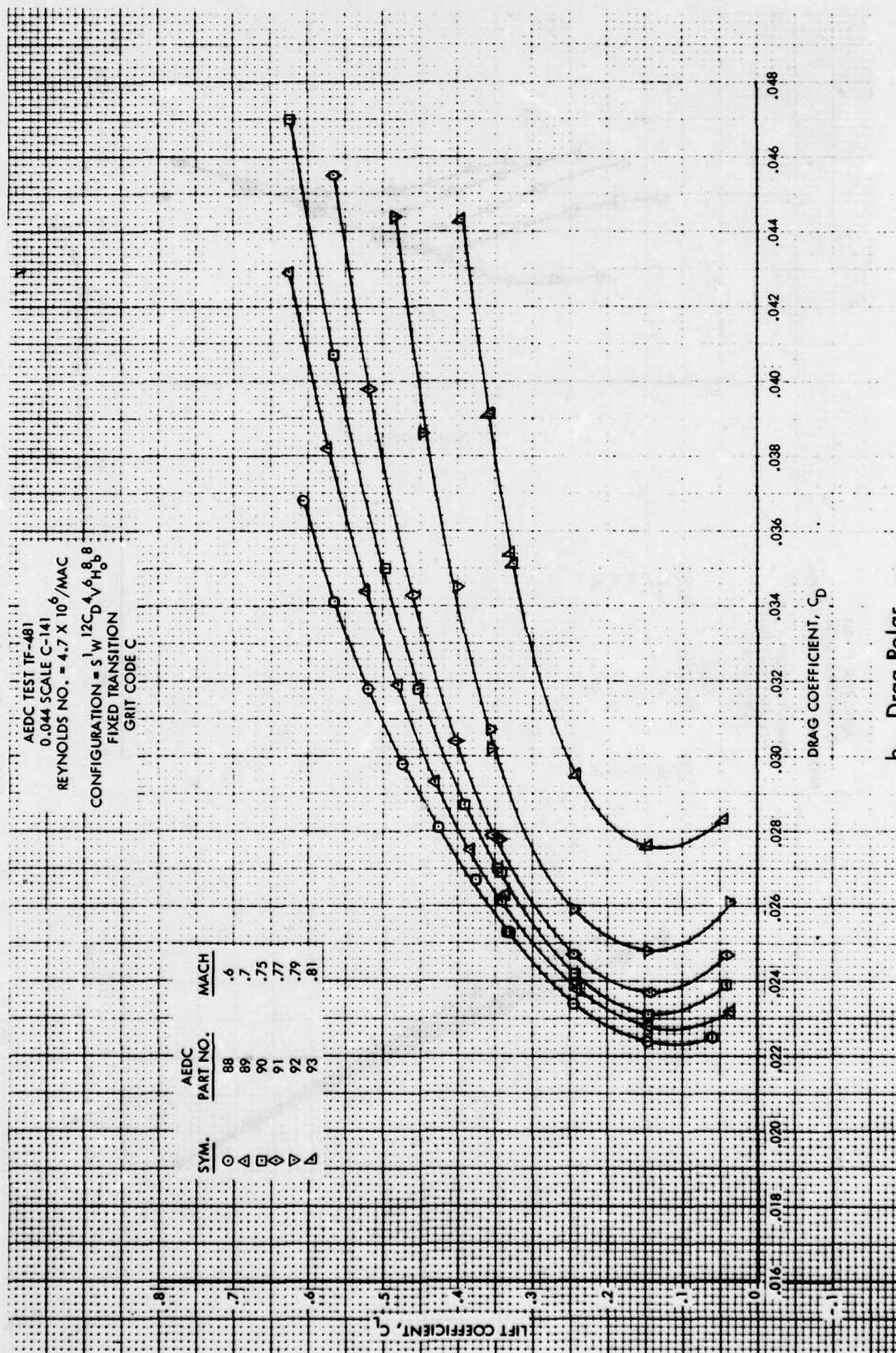
Figure 12. Lift, Drag and Pitching Moment Characteristics for Baseline Leading Edge, Fixed Transition, Grit Code D



b. Drag Polar
Figure 12. Concluded



a. Lift and Pitching Moment
 Figure 13. Lift, Drag and Pitching Moment Characteristics for Baseline Leading Edge, Fixed Transition, Grit Code C, Tail-On



b. Drag Polar
Figure 13. Concluded

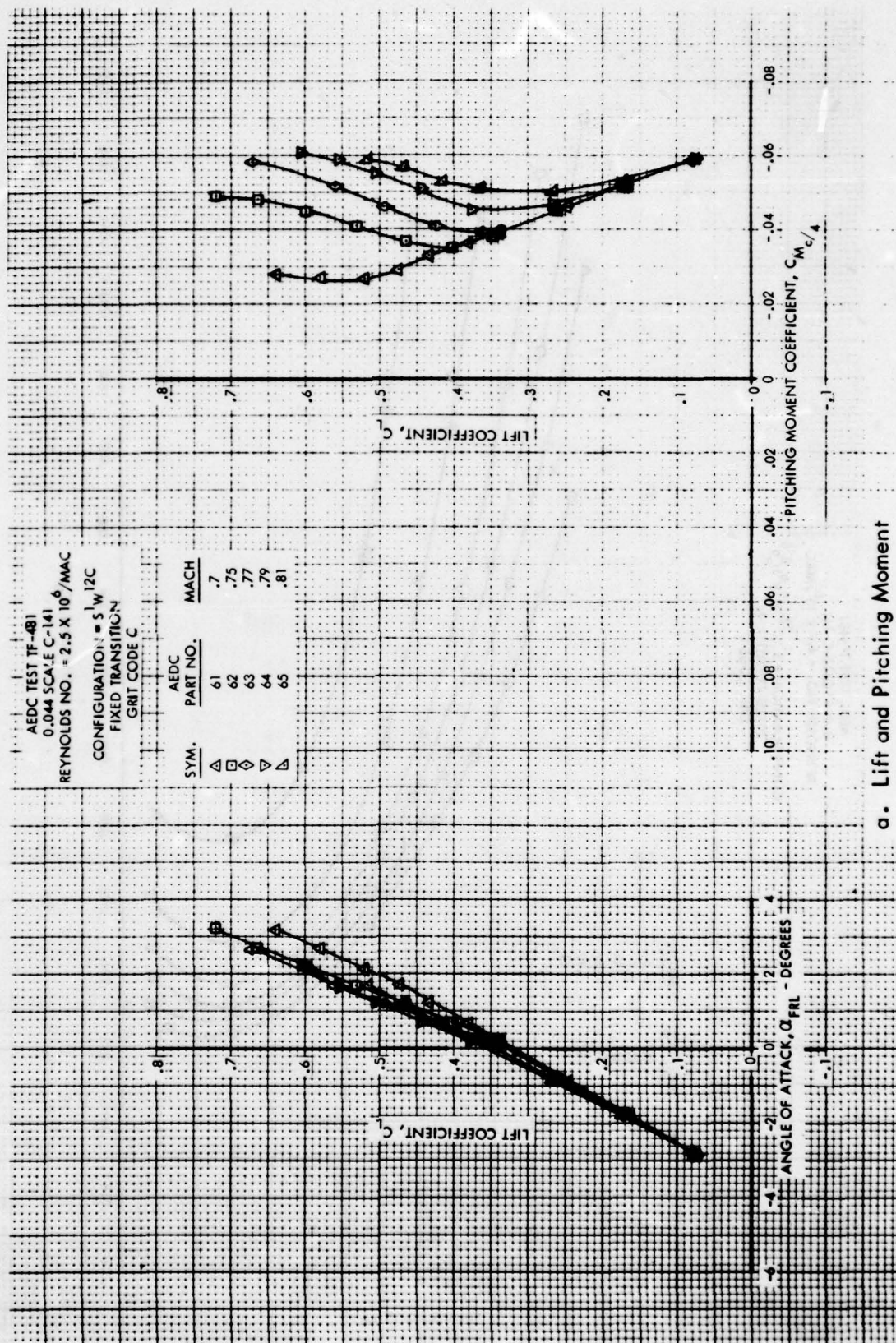
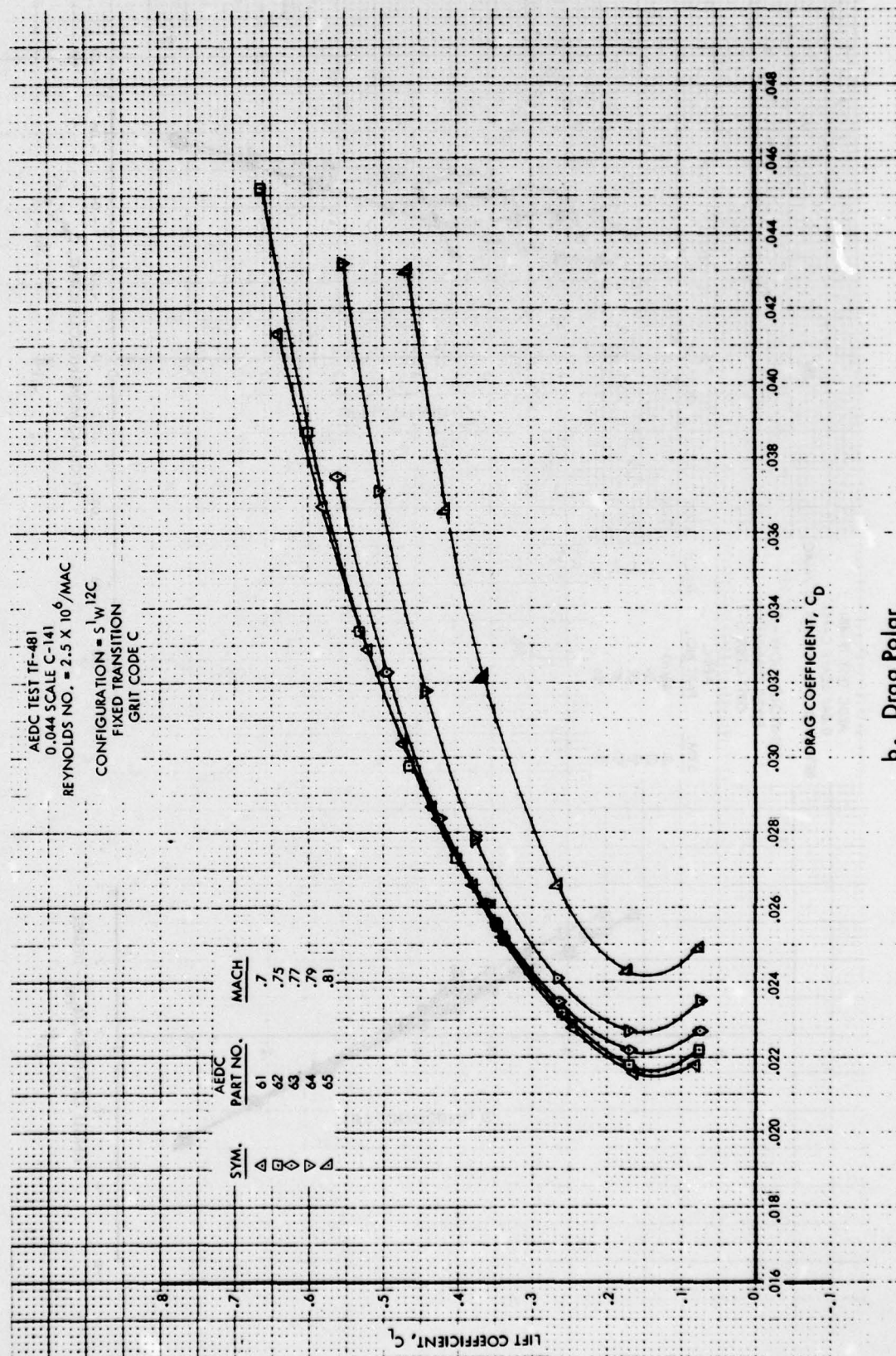
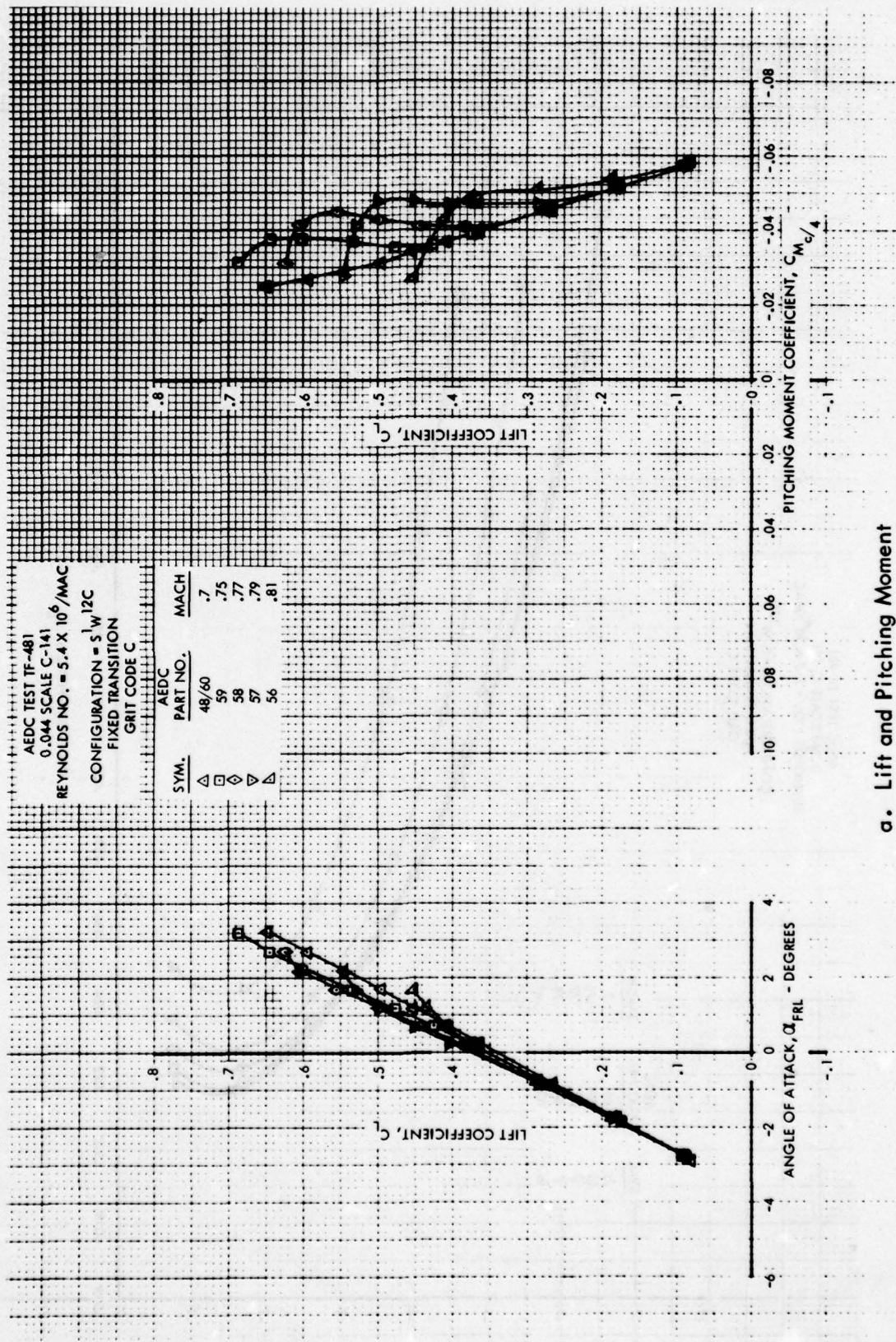


Figure 14. Lift, Drag and Pitching Moment Characteristics for Baseline Leading Edge, Fixed Transition, Grit Code C, $R_N = 2.5 \times 10^6$ /MAC

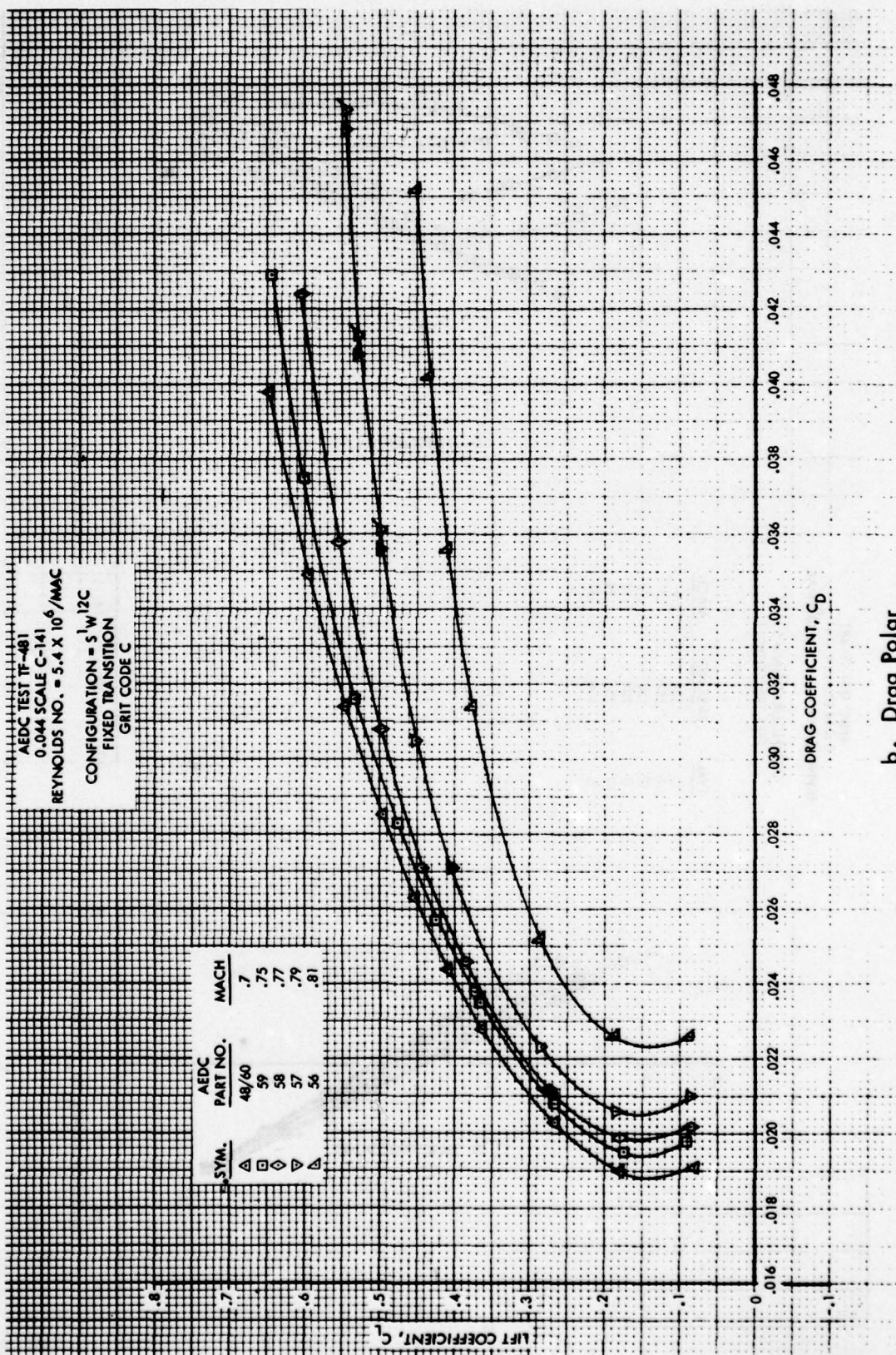


b. Drag Polar
 Figure 14. Concluded



a. Lift and Pitching Moment

Figure 15. Lift, Drag and Pitching Moment Characteristics for Baseline Leading Edge, Fixed Transition, Grit Code C, $R_N = 5.4 \times 10^6 / MAC$



b. Drag Polar
 Figure 15. Concluded

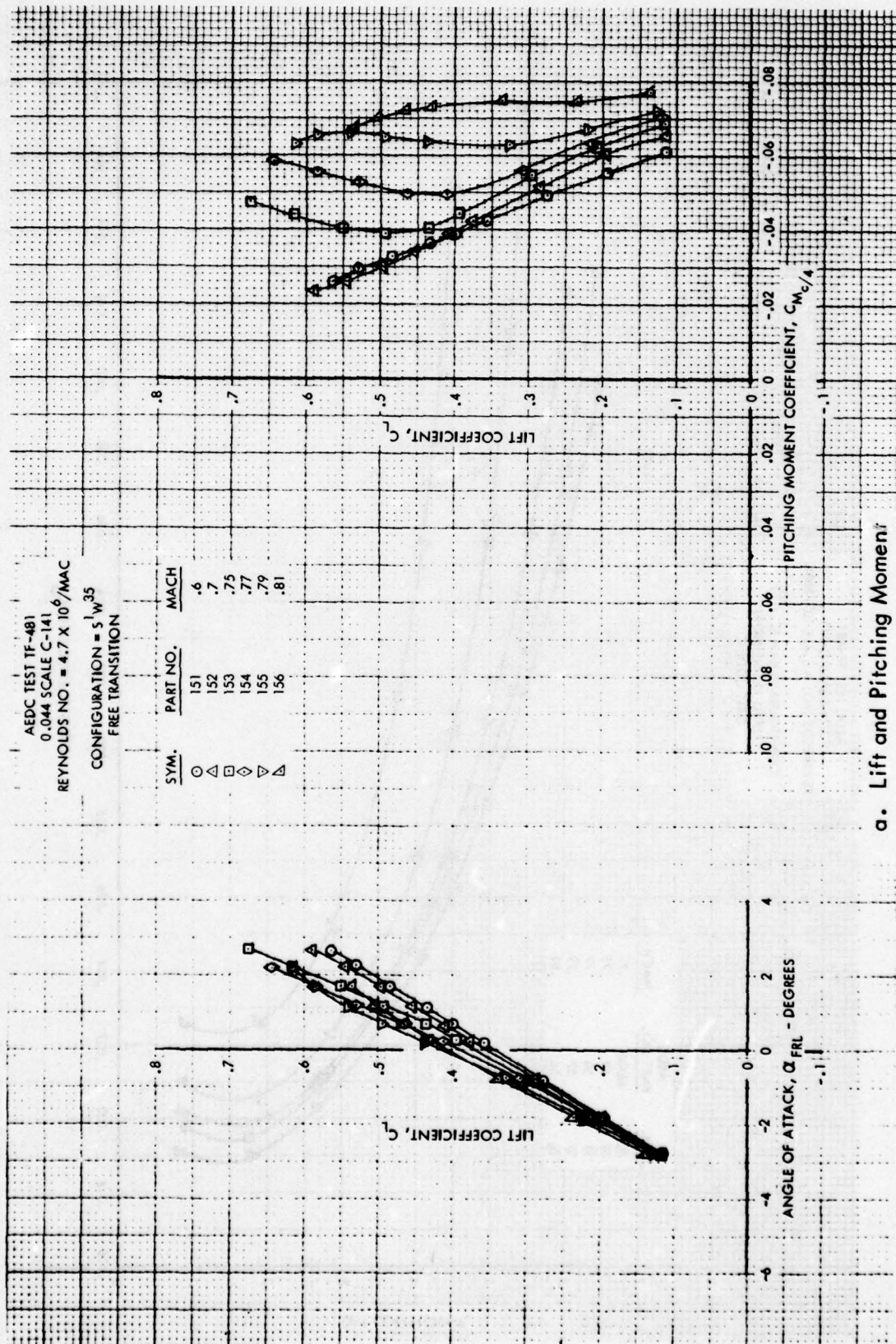
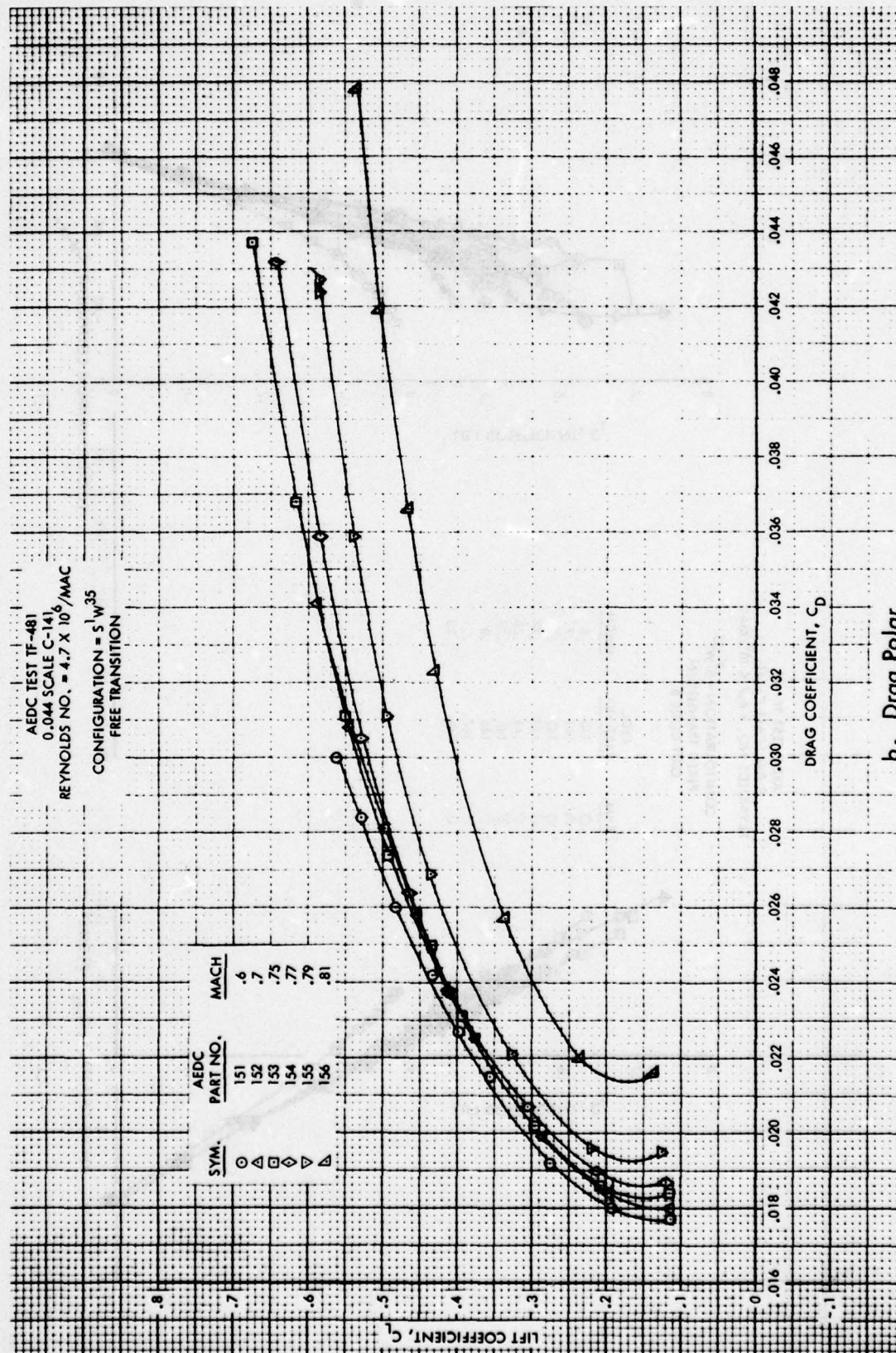
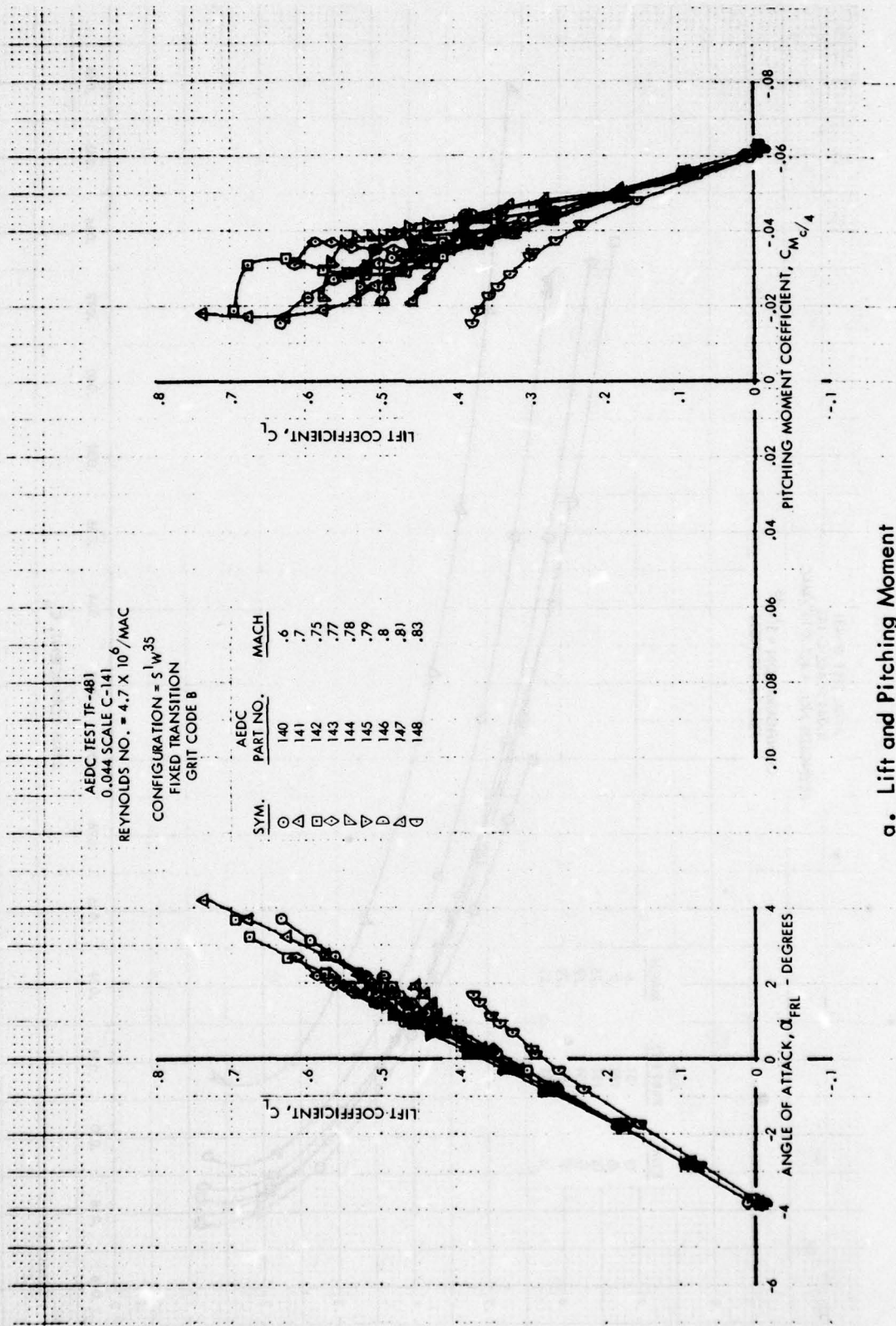


Figure 16. Lift, Drag and Pitching Moment Characteristics for $W^{.35}$ Leading Edge Modification, Free Transition

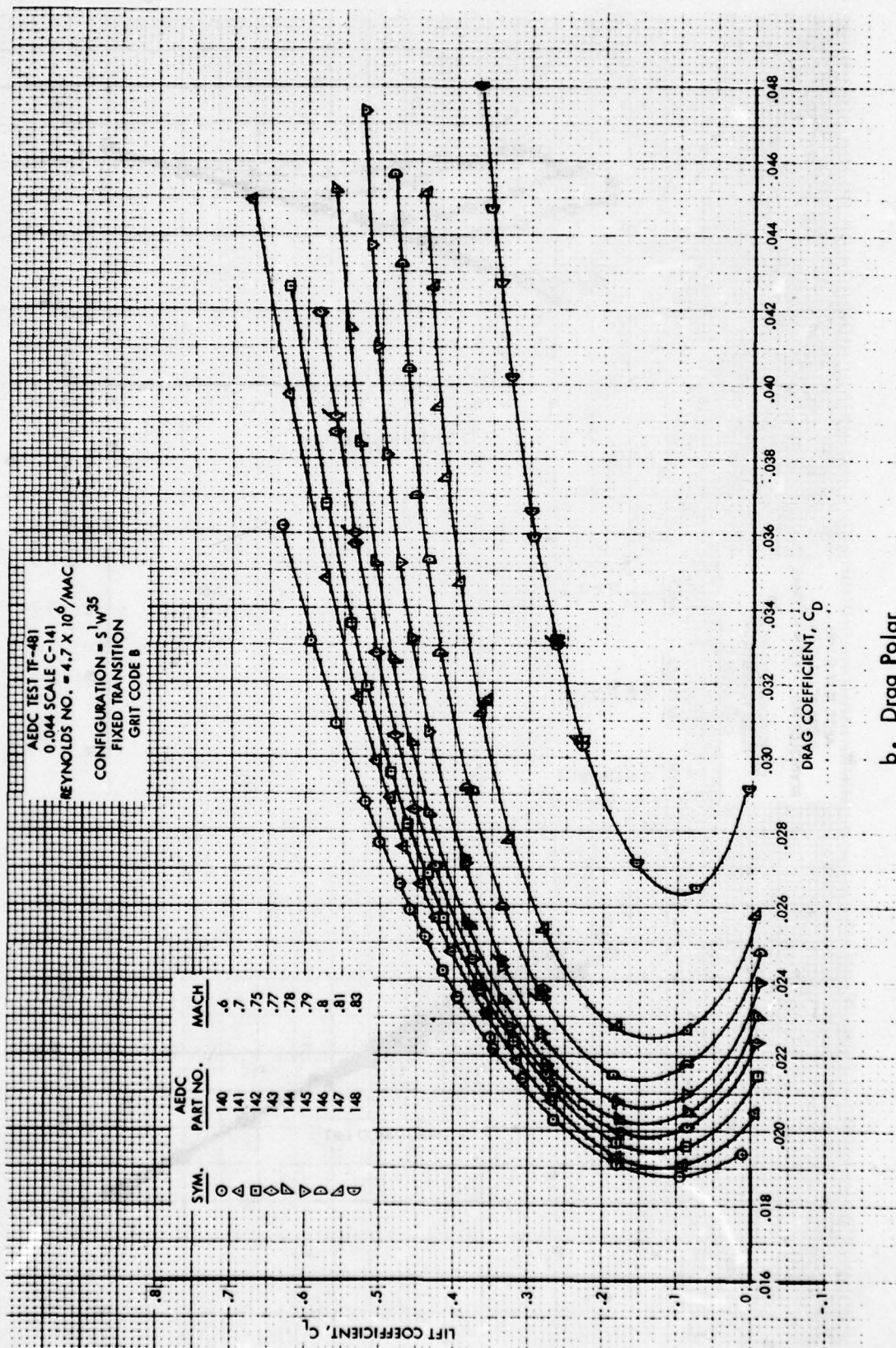


b. Drag Polar
Figure 16. Concluded

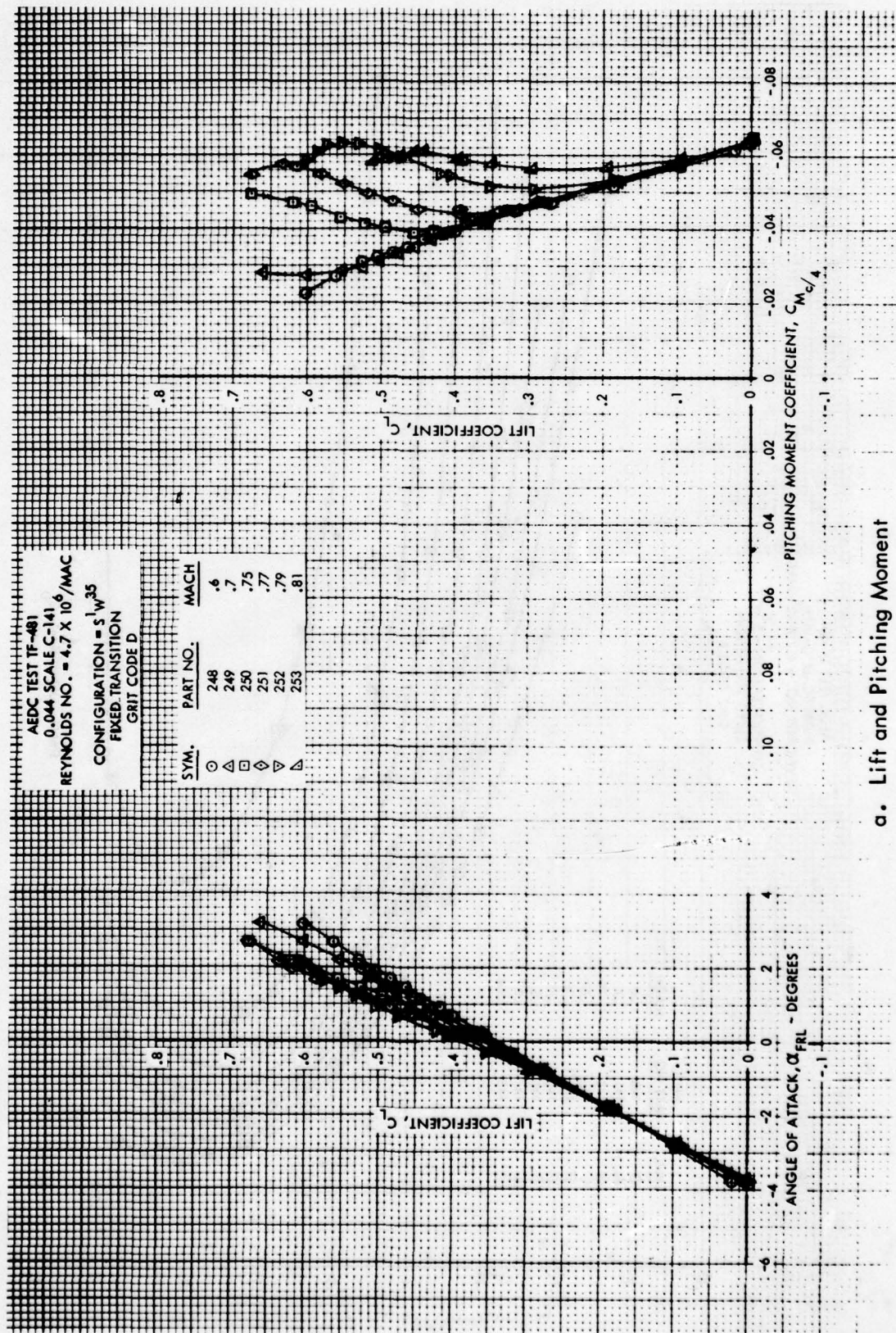


a. Lift and Pitching Moment

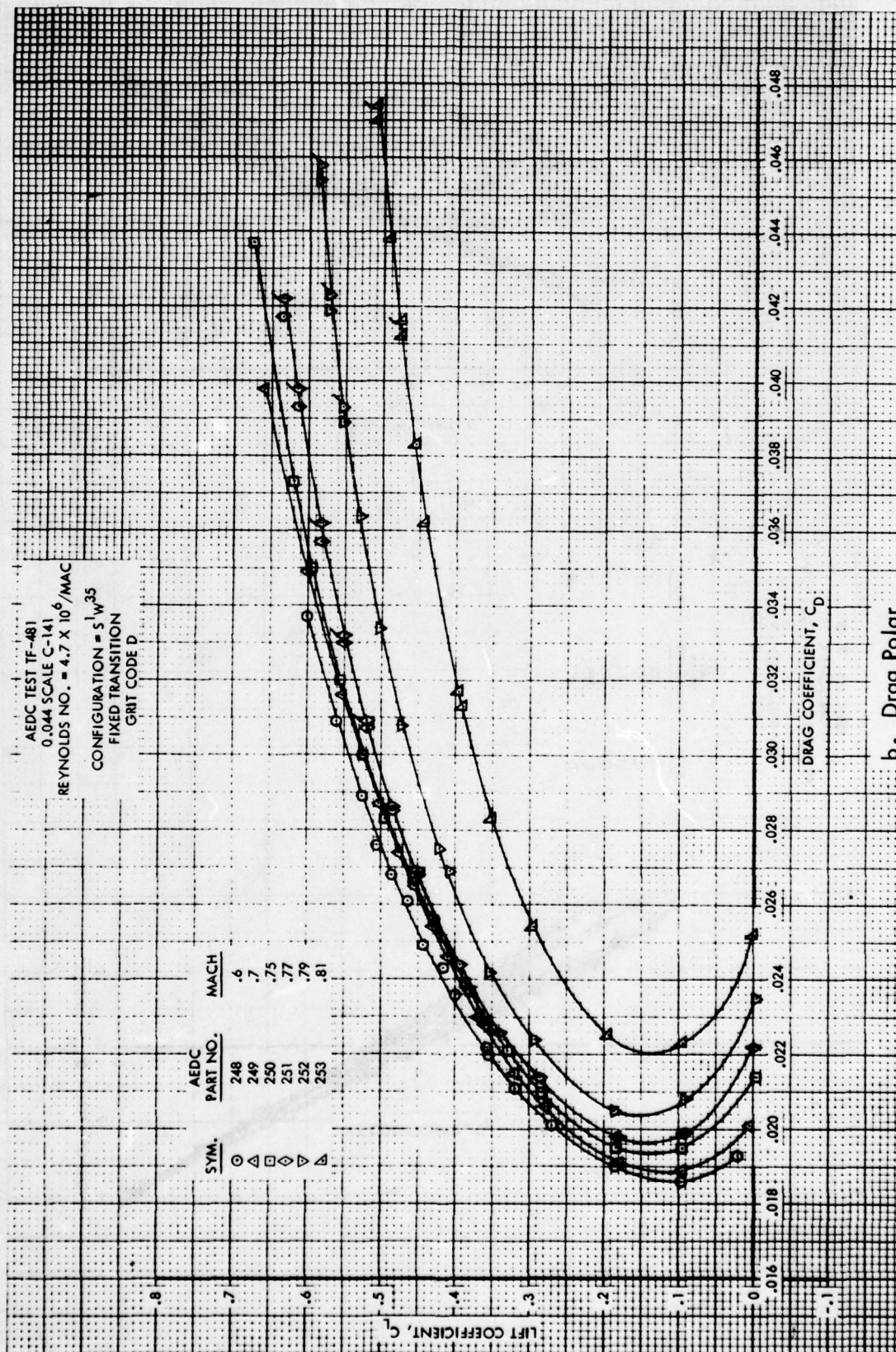
Figure 17. Lift, Drag and Pitching Moment Characteristics for W³⁵ Leading Edge Modification, Fixed Transition, Grit Code B



b. Drag Polar
 Figure 17. Concluded



a. Lift and Pitching Moment Characteristics for $W^{.35}$ Leading Edge Modification, Fixed Transition, Grit Code D



b. Drag Polar
Figure 18. Concluded

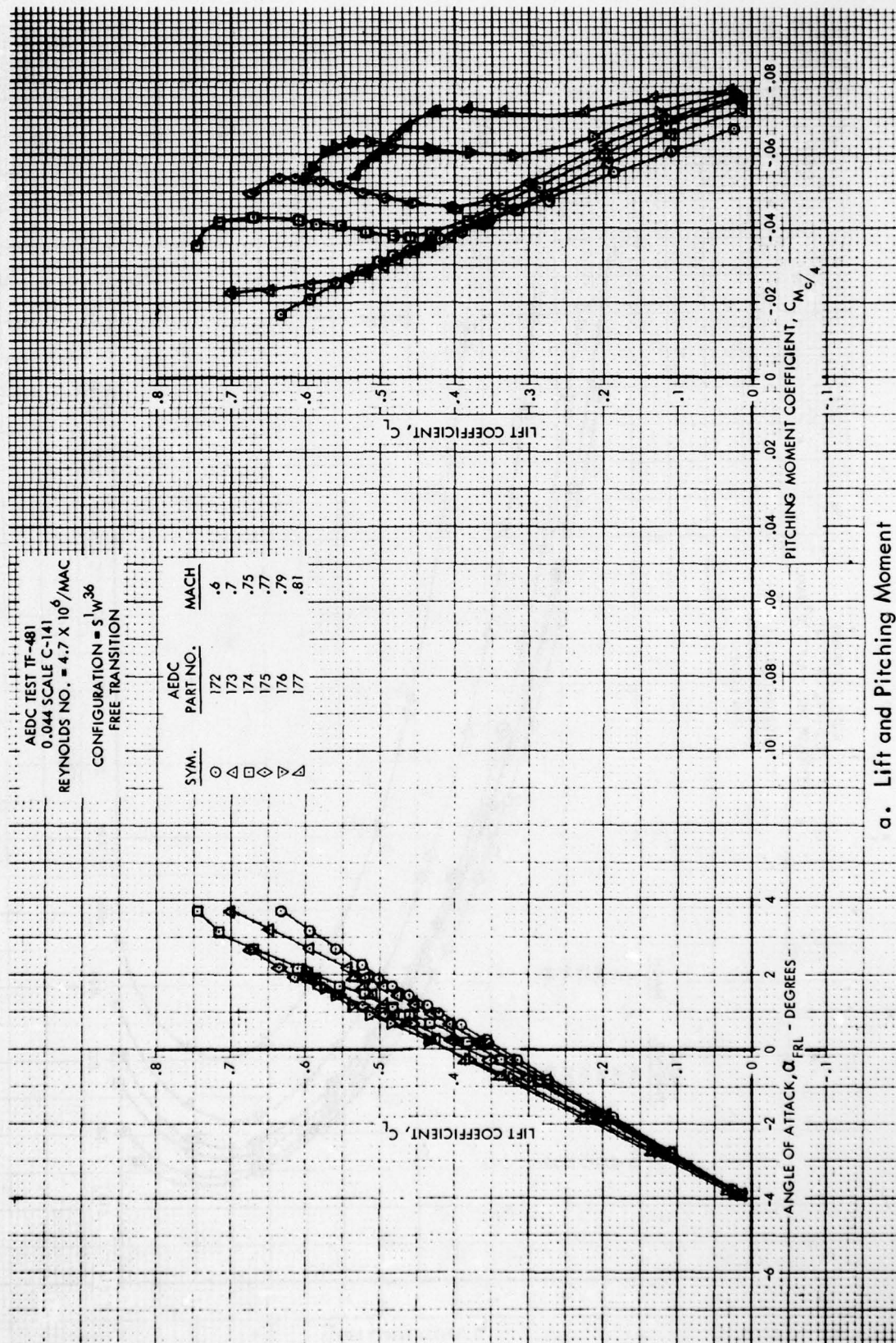
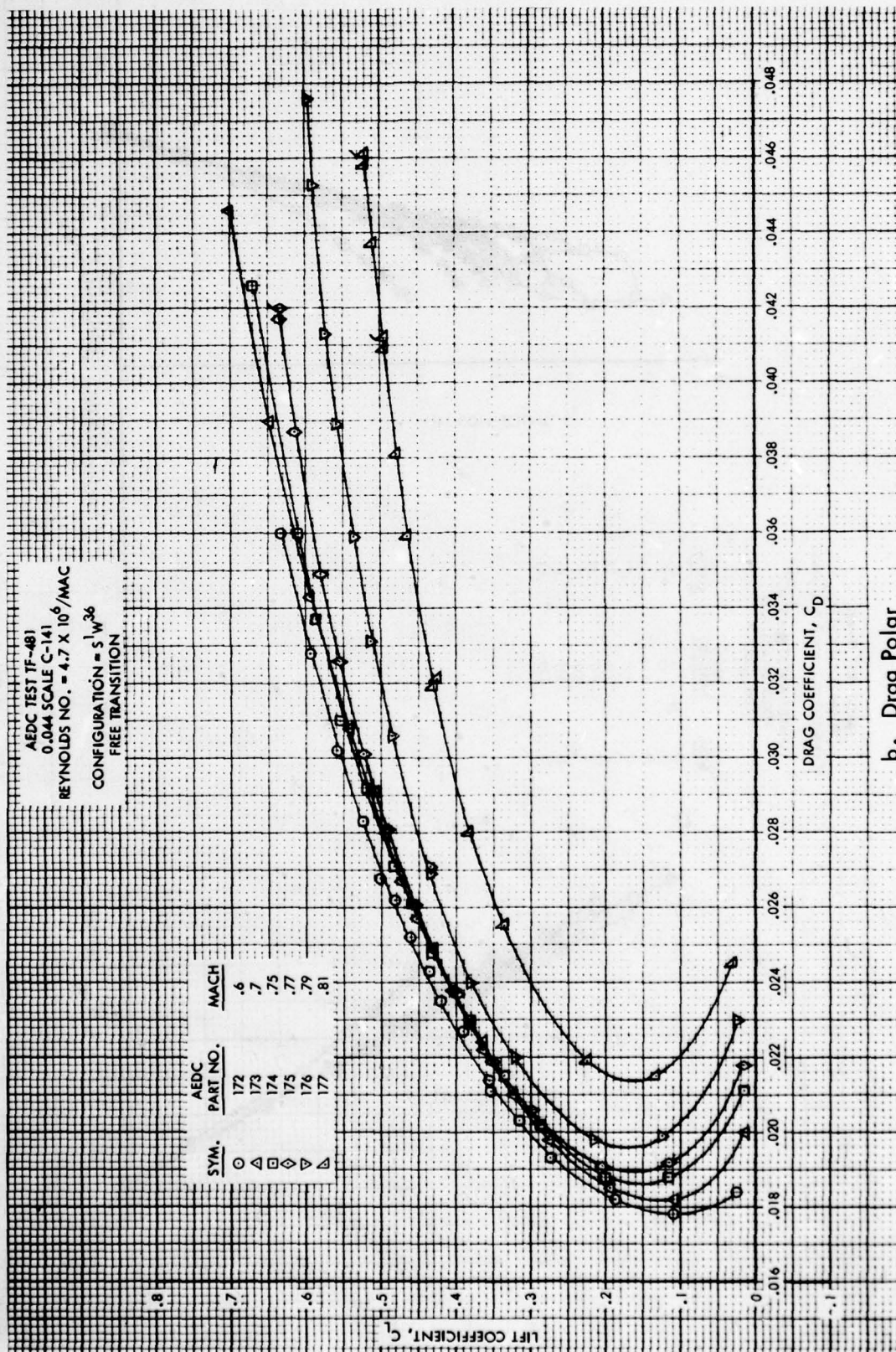
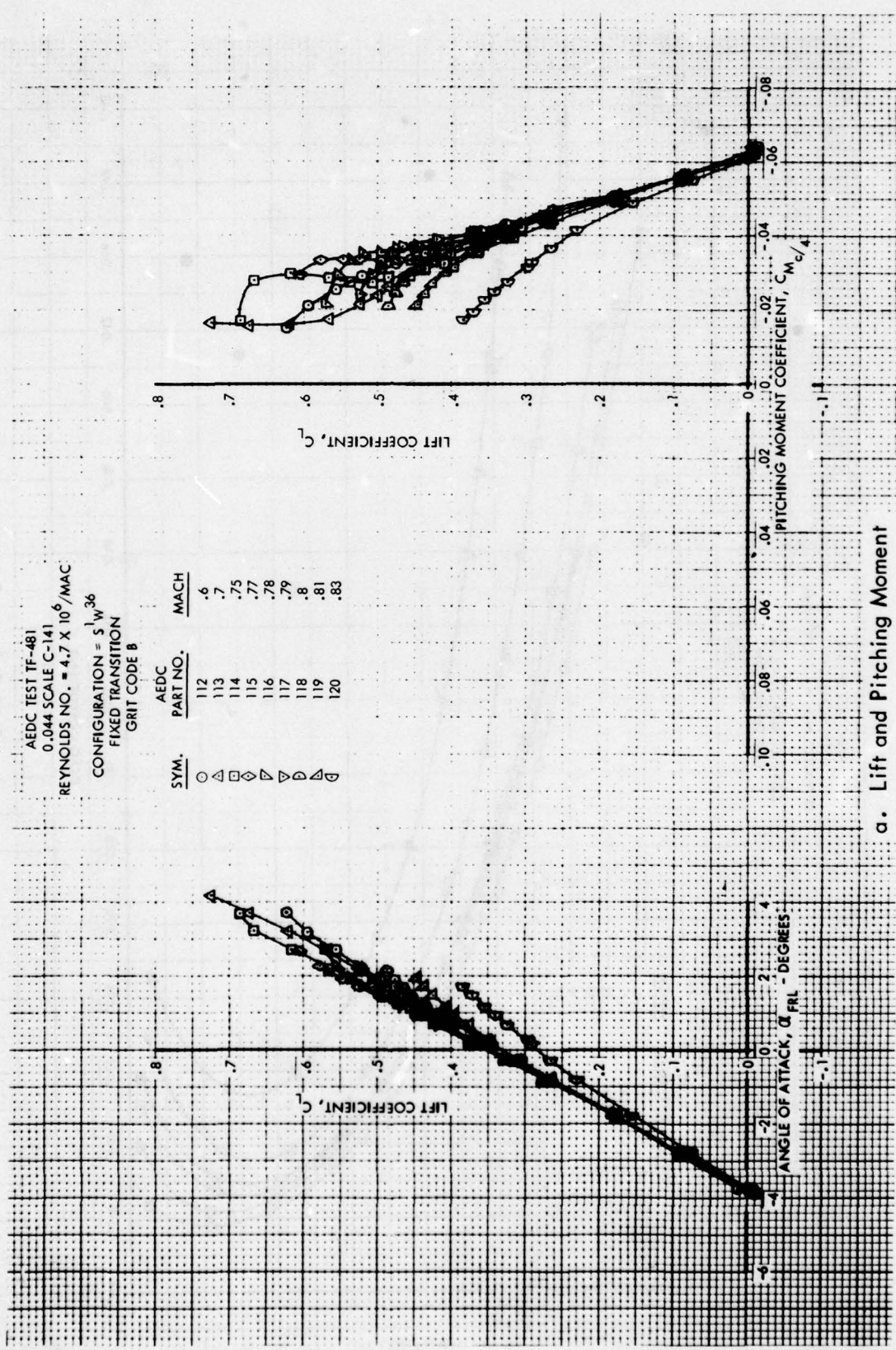


Figure 19. Lift, Drag and Pitching Moment Characteristics for W^{36} Leading Edge Modification, Free Transition

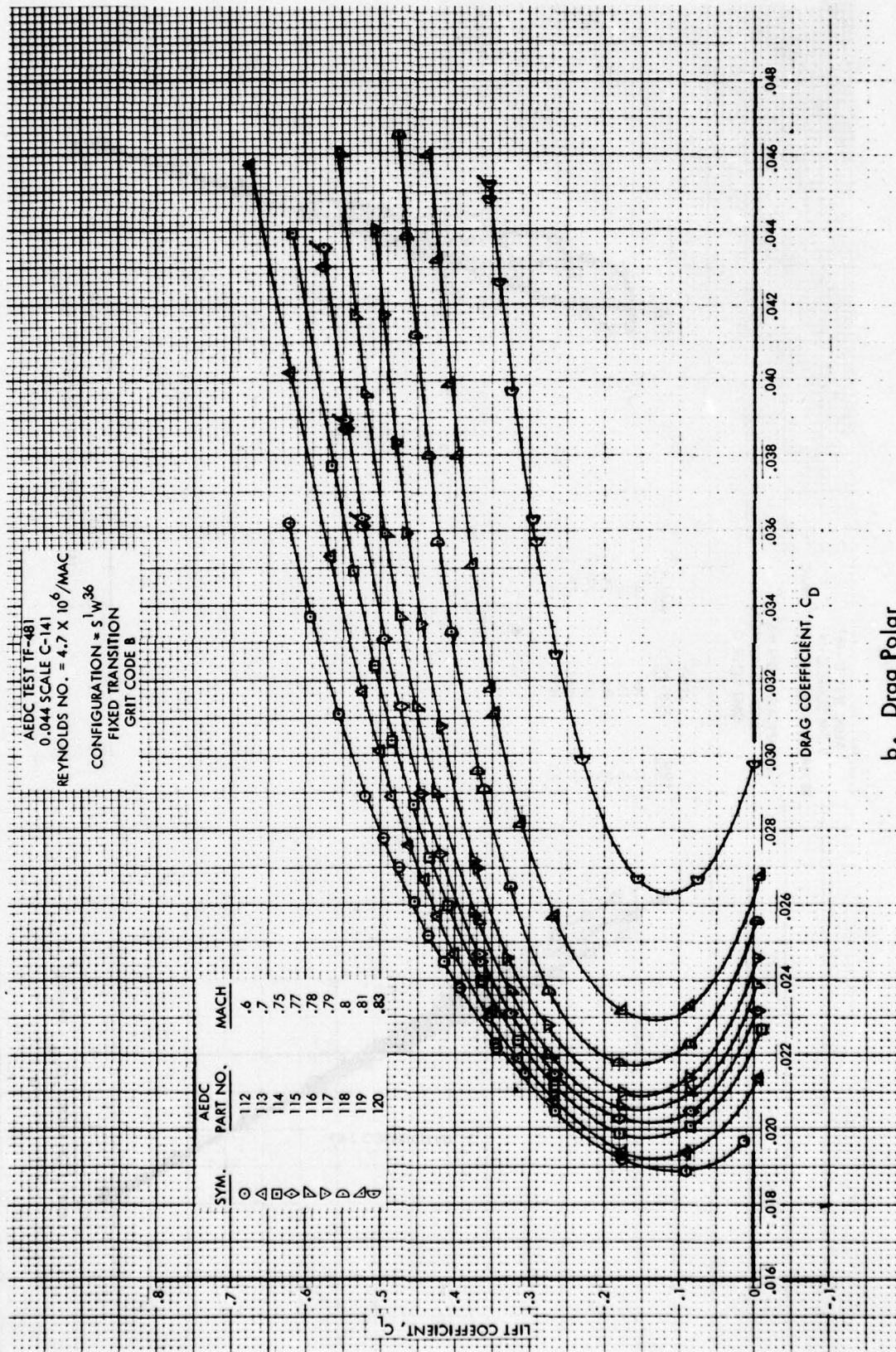


b. Drag Polar
 Figure 19. Concluded



a. Lift and Pitching Moment

Figure 20. Lift, Drag and Pitching Moment Characteristics for W^{36} Leading Edge Modification, Fixed Transition, Grit Code B



b. Drag Polar
 Figure 20. Concluded

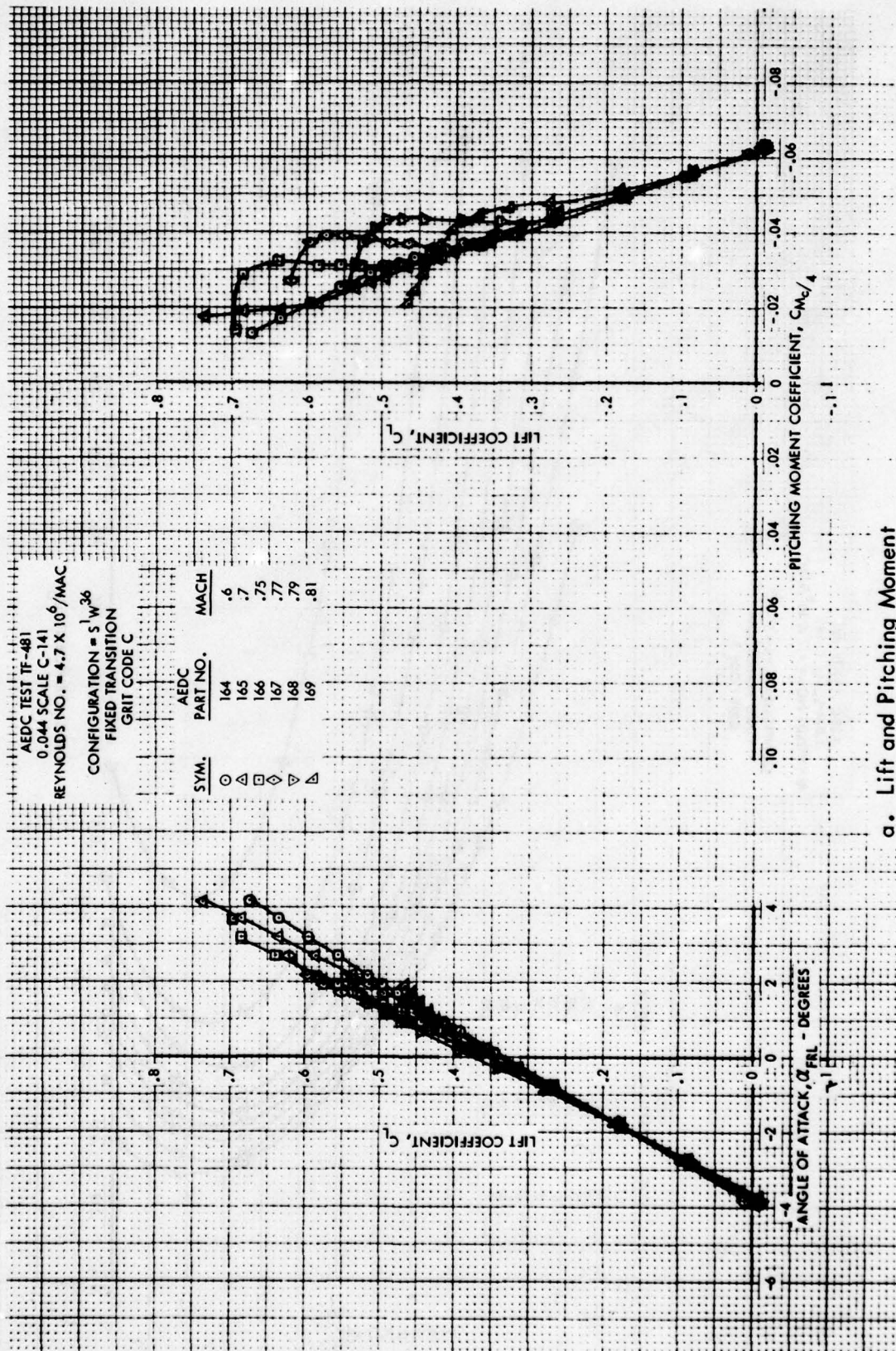
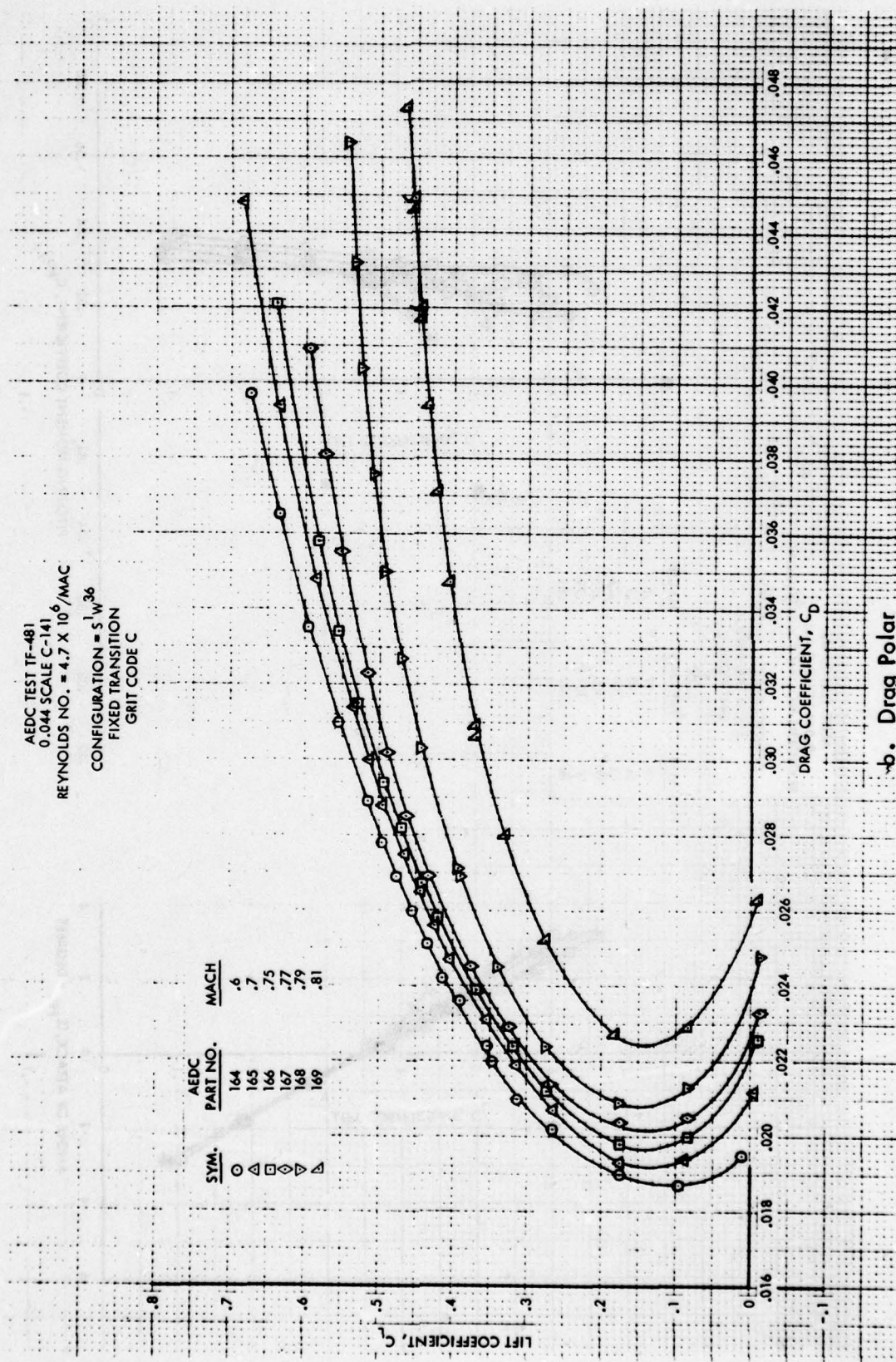
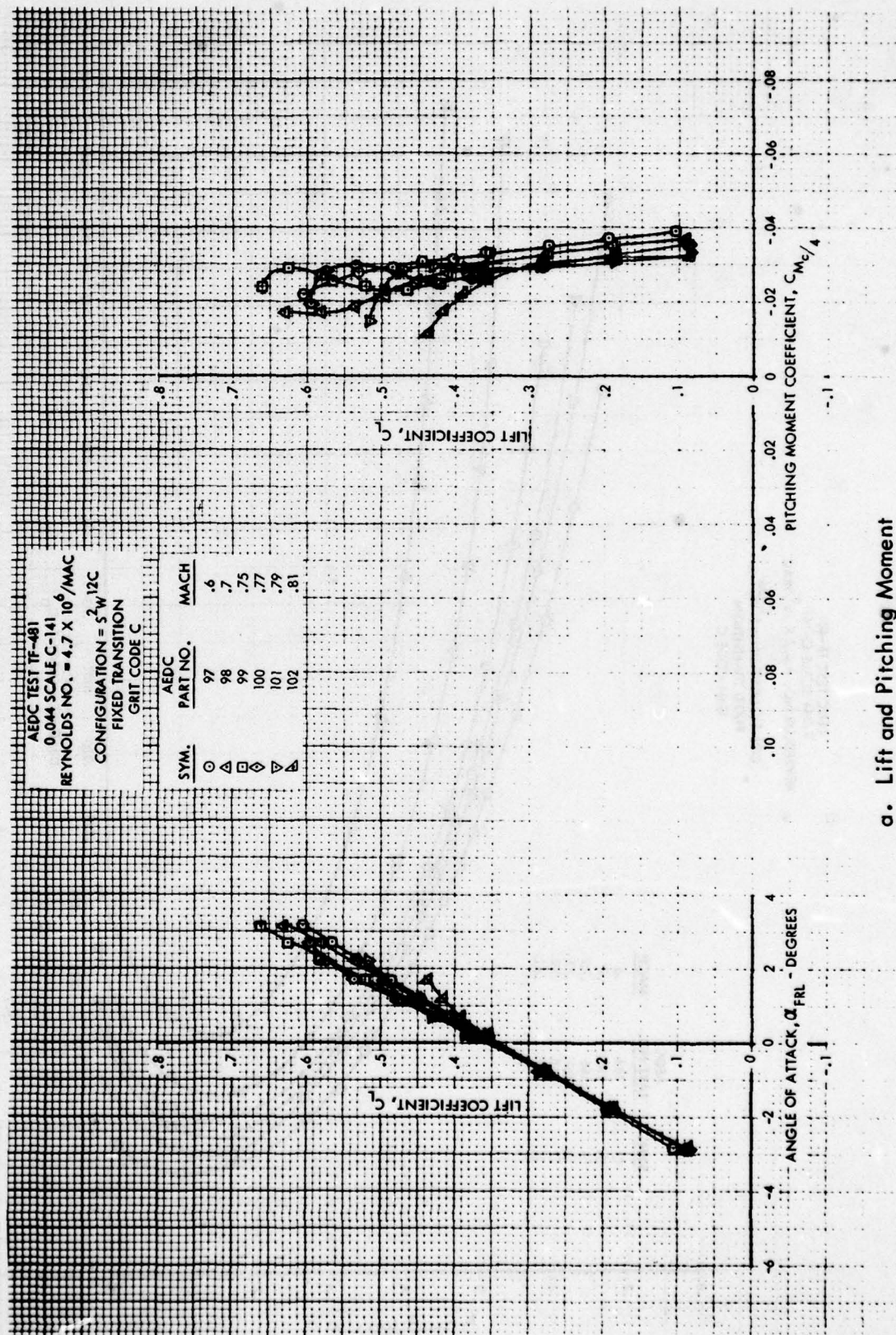


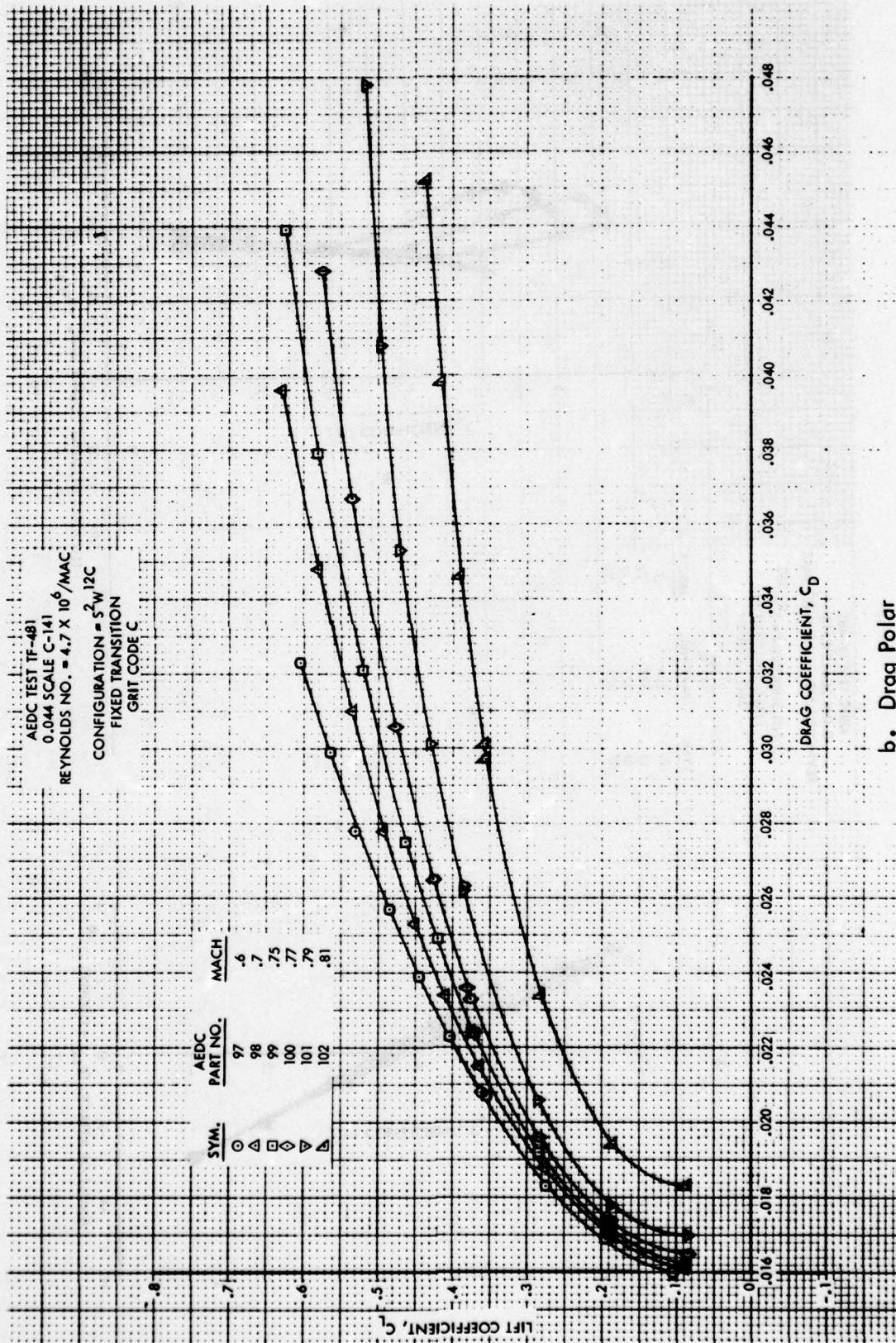
Figure 21. Lift, Drag and Pitching Moment Characteristics for W^{36} Leading Edge Modification, Fixed Transition, Grit Code C



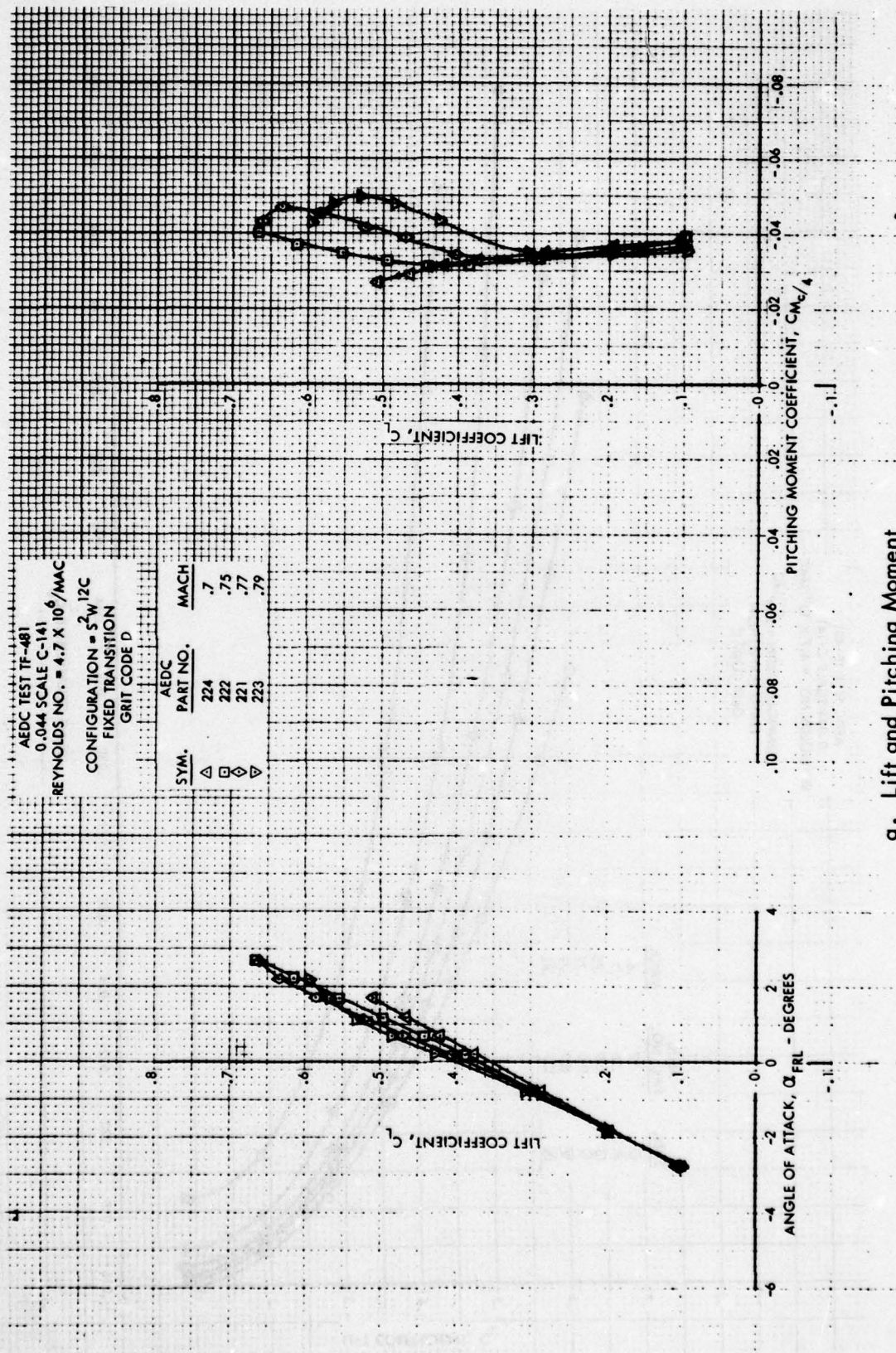
b. Drag Polar
Figure 21. Concluded



a. Lift and Pitching Moment
Figure 22. Lift, Drag and Pitching Moment Characteristics for Baseline Leading Edge, Fixed Transition, Grit Code C, Pylon/Nacelles Off

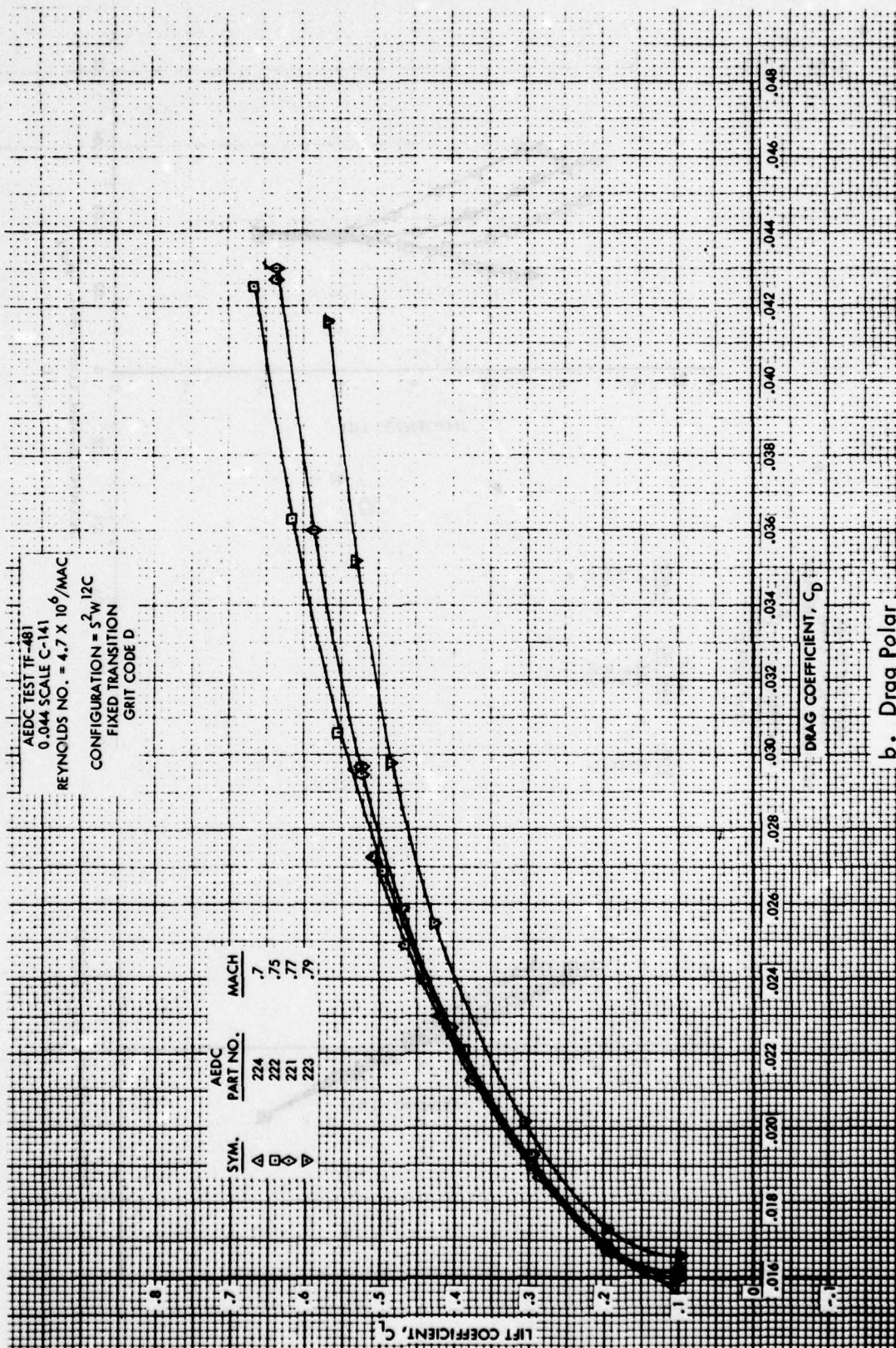


b. Drag Polar
 Figure 22. Concluded

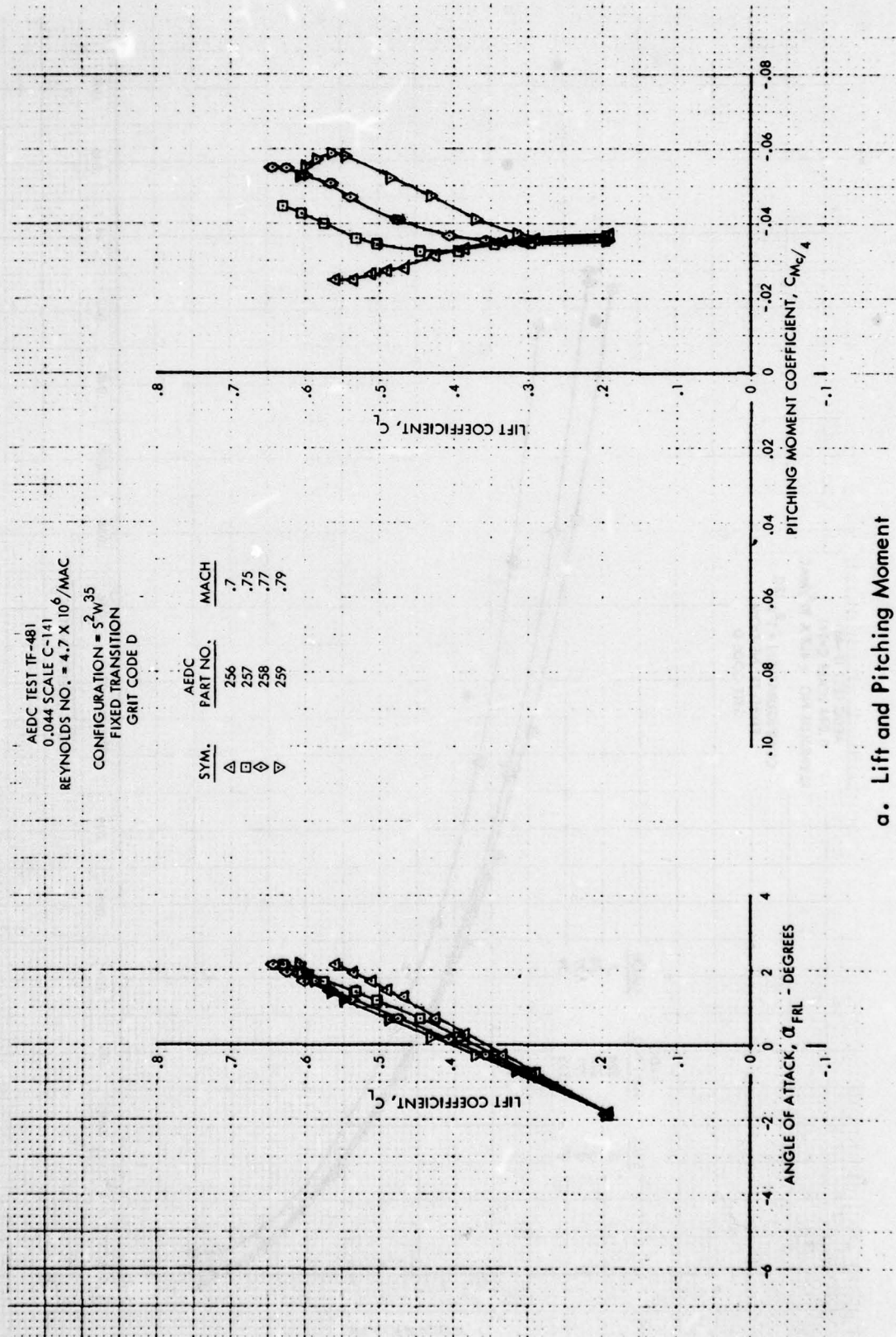


a. Lift and Pitching Moment

Figure 23. Lift, Drag and Pitching Moment Characteristics for Baseline Leading Edge, Fixed Transition, Grit Code D, Pylon/Nacelles Off

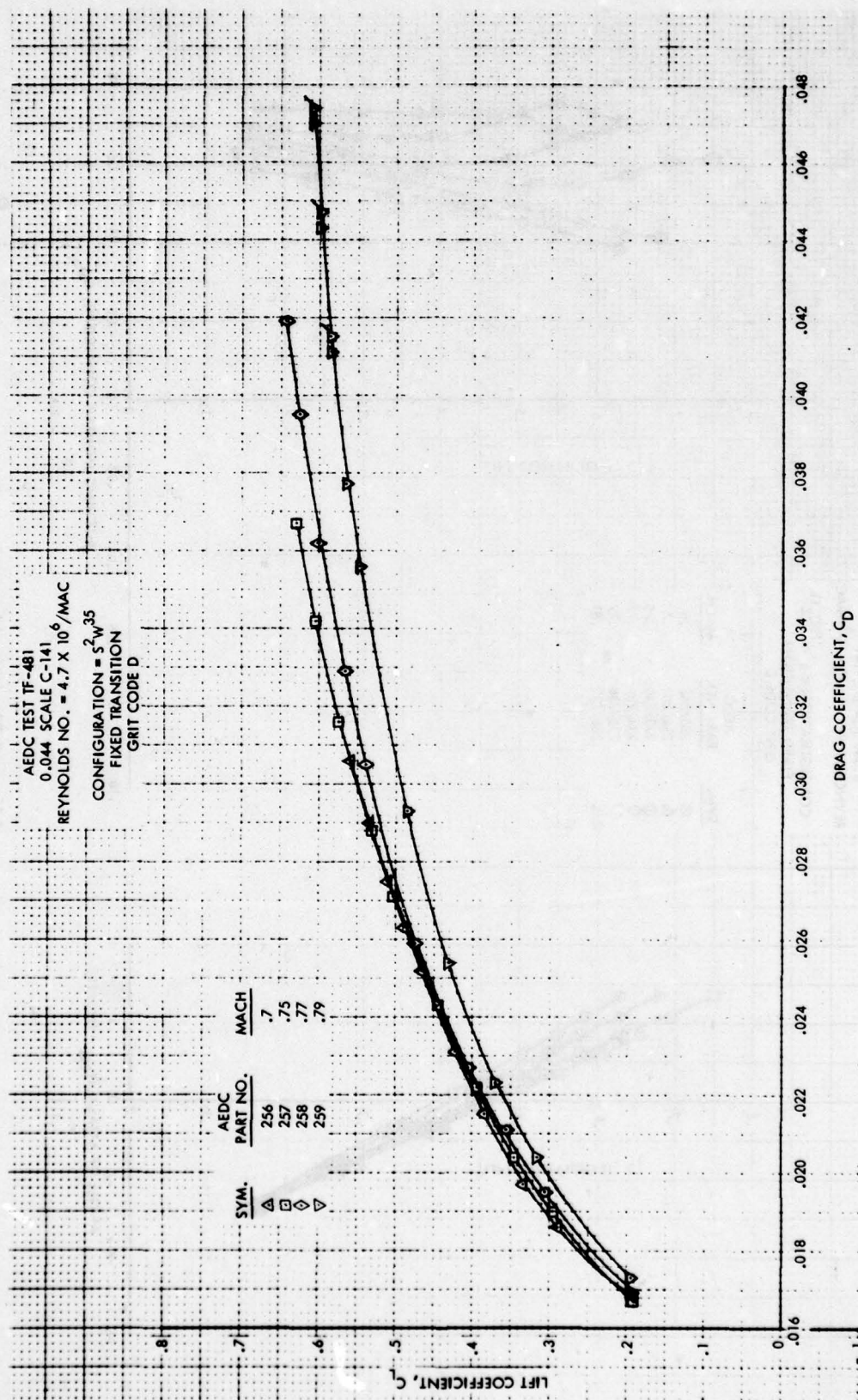


b. Drag Polar
Figure 23. Concluded

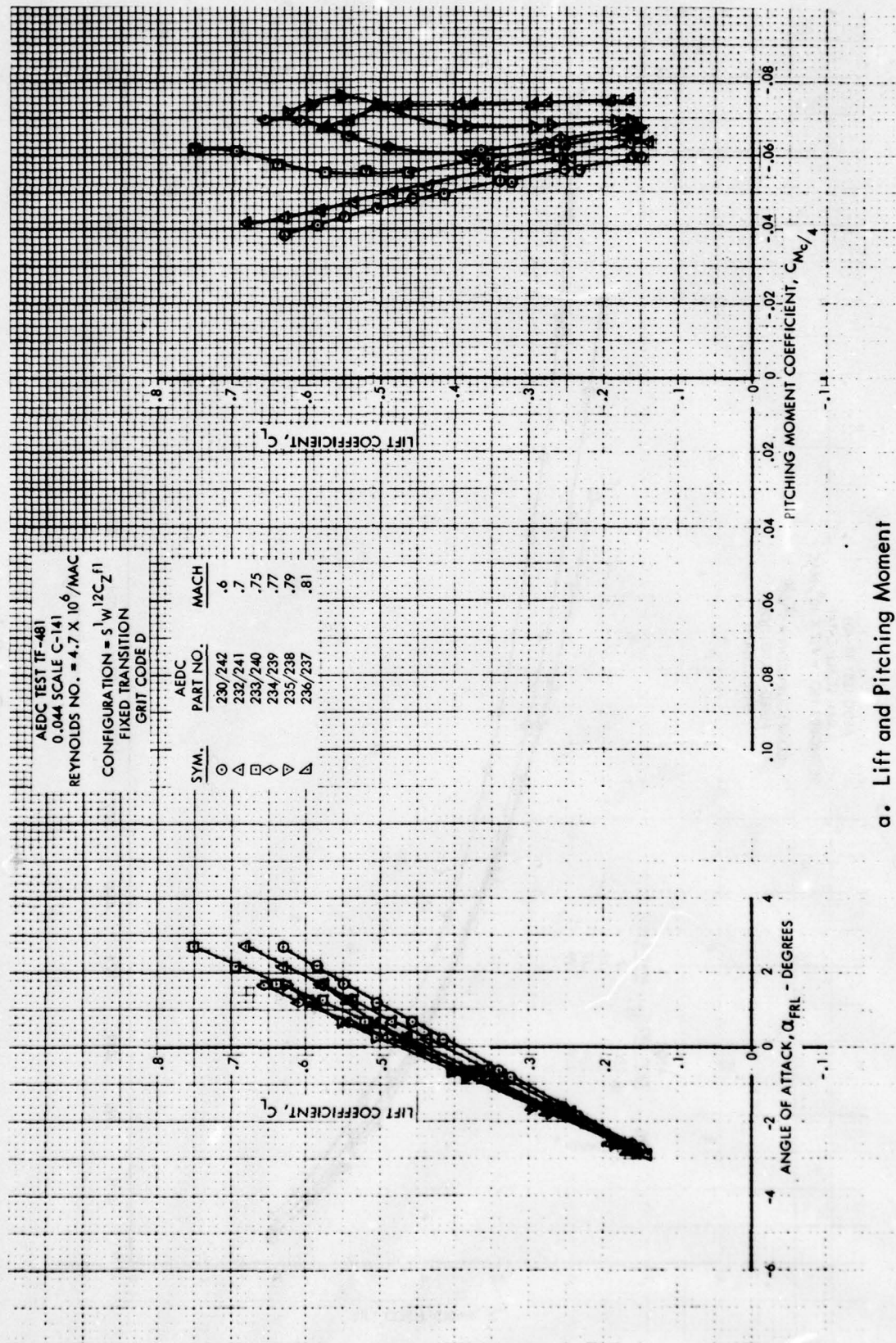


a. Lift and Pitching Moment

Figure 24. Lift, Drag and Pitching Moment Characteristics for W^{35} Leading Edge Modification, Fixed Transition, Grit Code D, Pylon/Nacelles Off

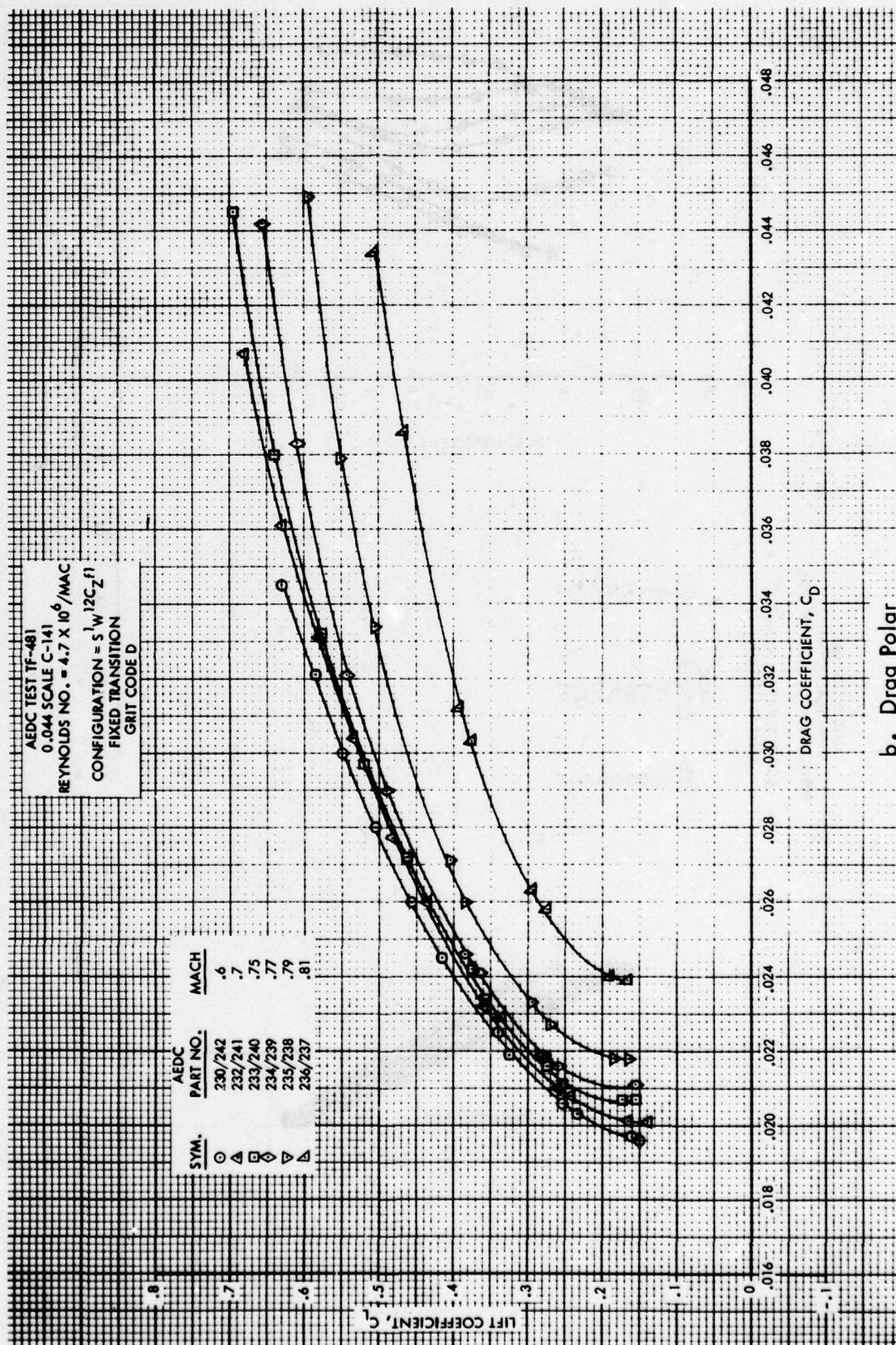


b. Drag Polar
Figure 24. Concluded

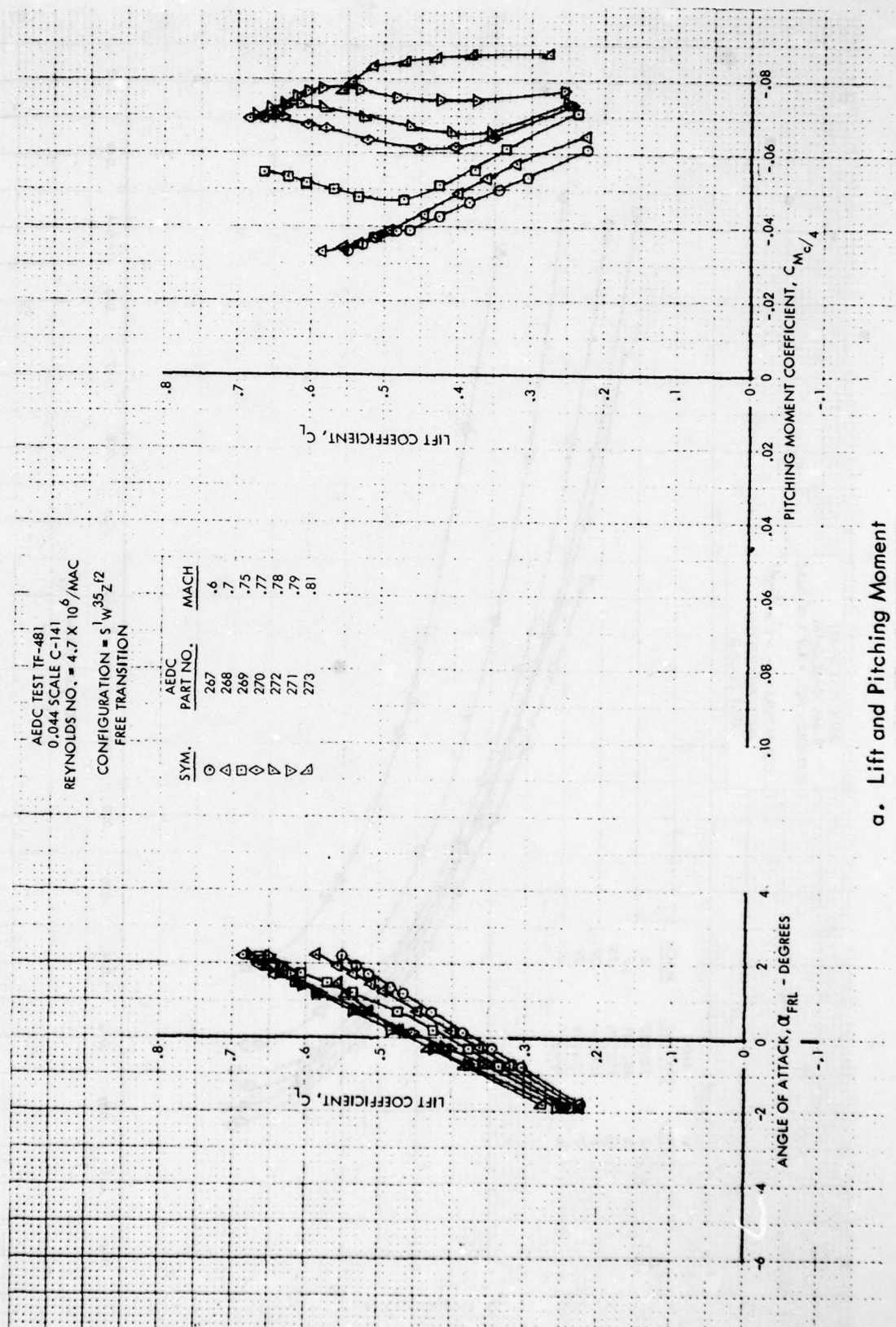


a. Lift and Pitching Moment

Figure 25. Lift, Drag and Pitching Moment Characteristics for Baseline Leading Edge, Fixed Transition, Grit Code D, Eight Anti-Drag Bodies

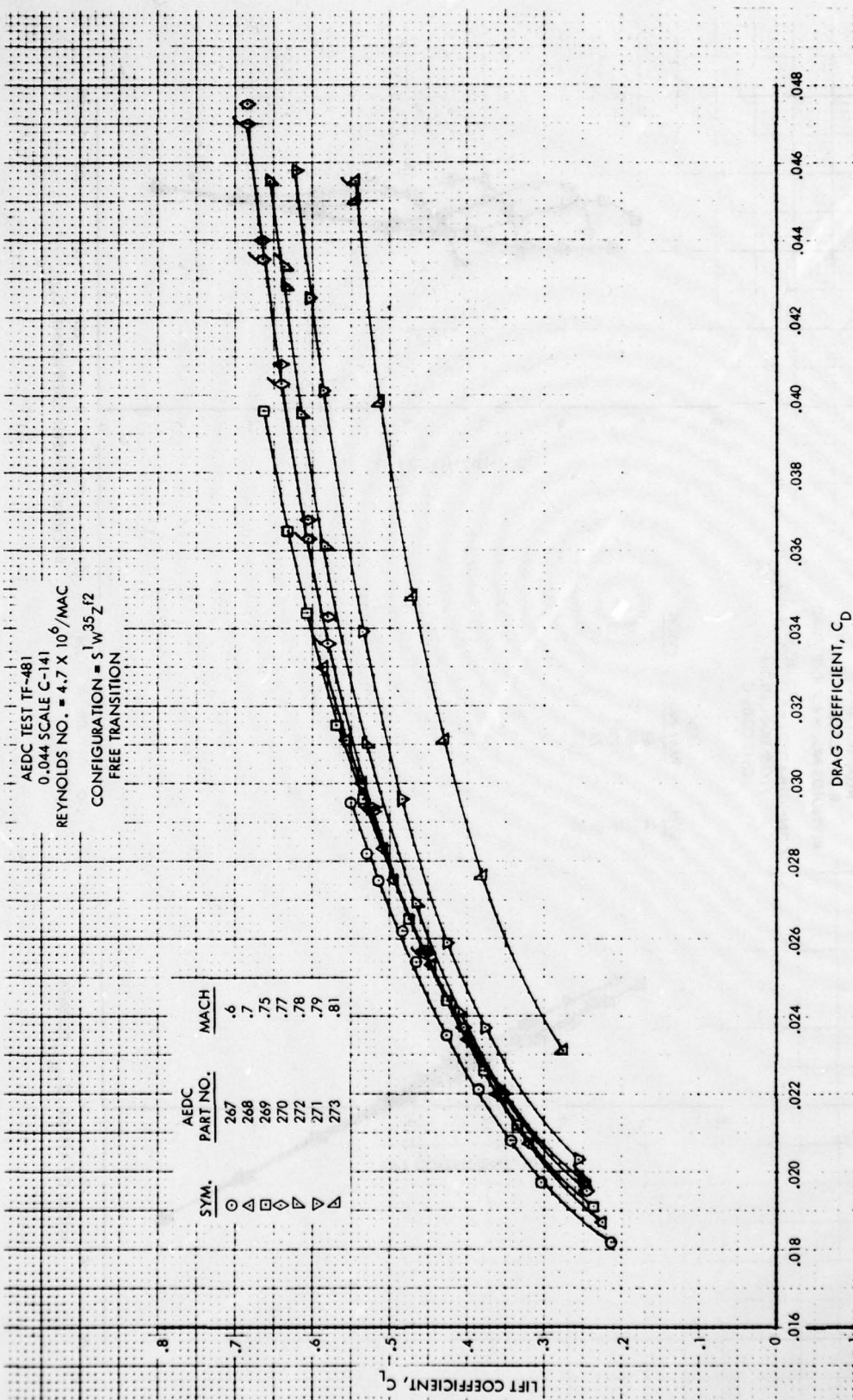


b. Drag Polar
Figure 25. Concluded

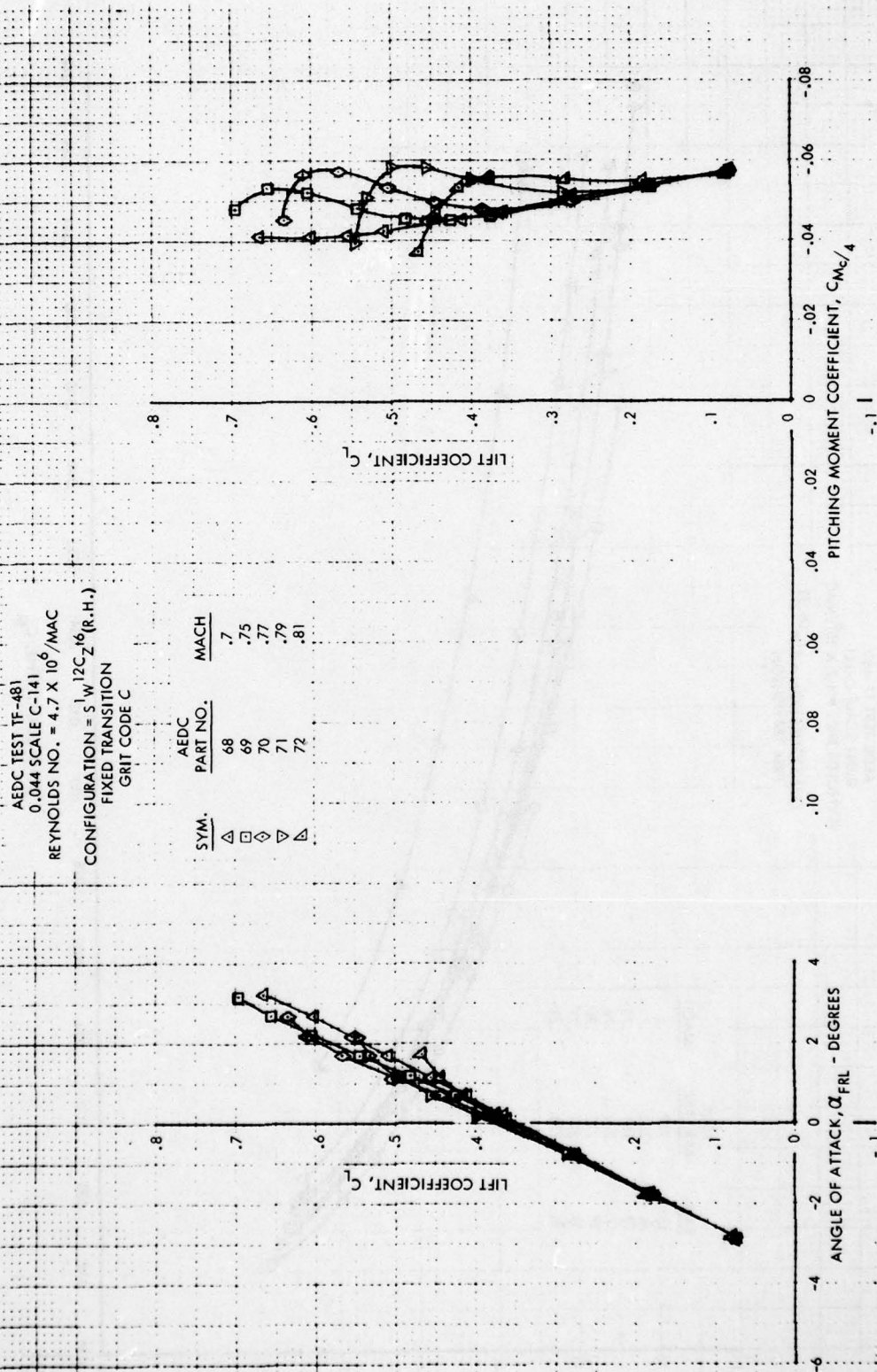


a. Lift and Pitching Moment

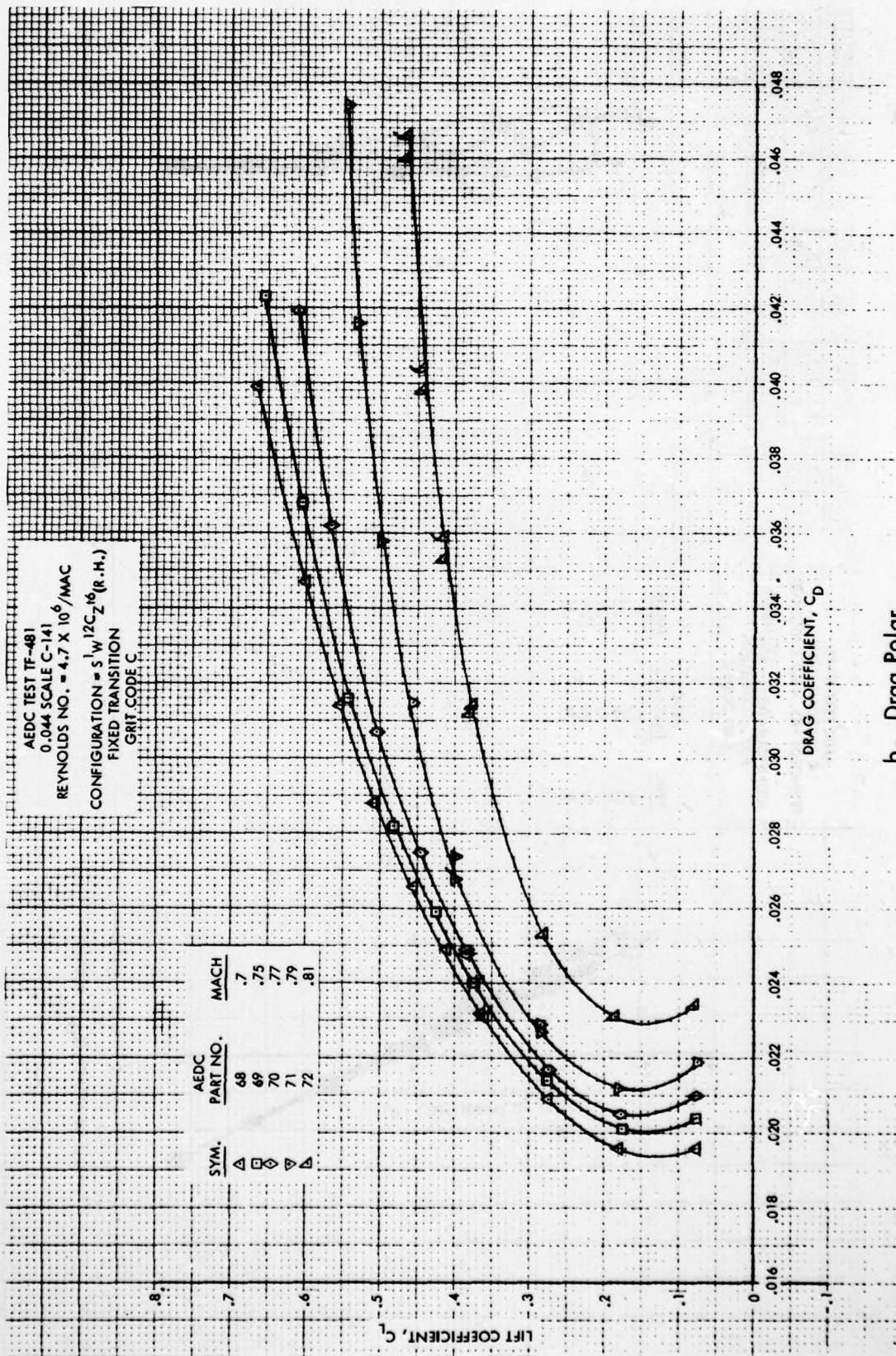
Figure 26. Lift, Drag and Pitching Moment Characteristics for W^{35} Leading Edge Modification, Free Transition, Four Anti-Drag Bodies



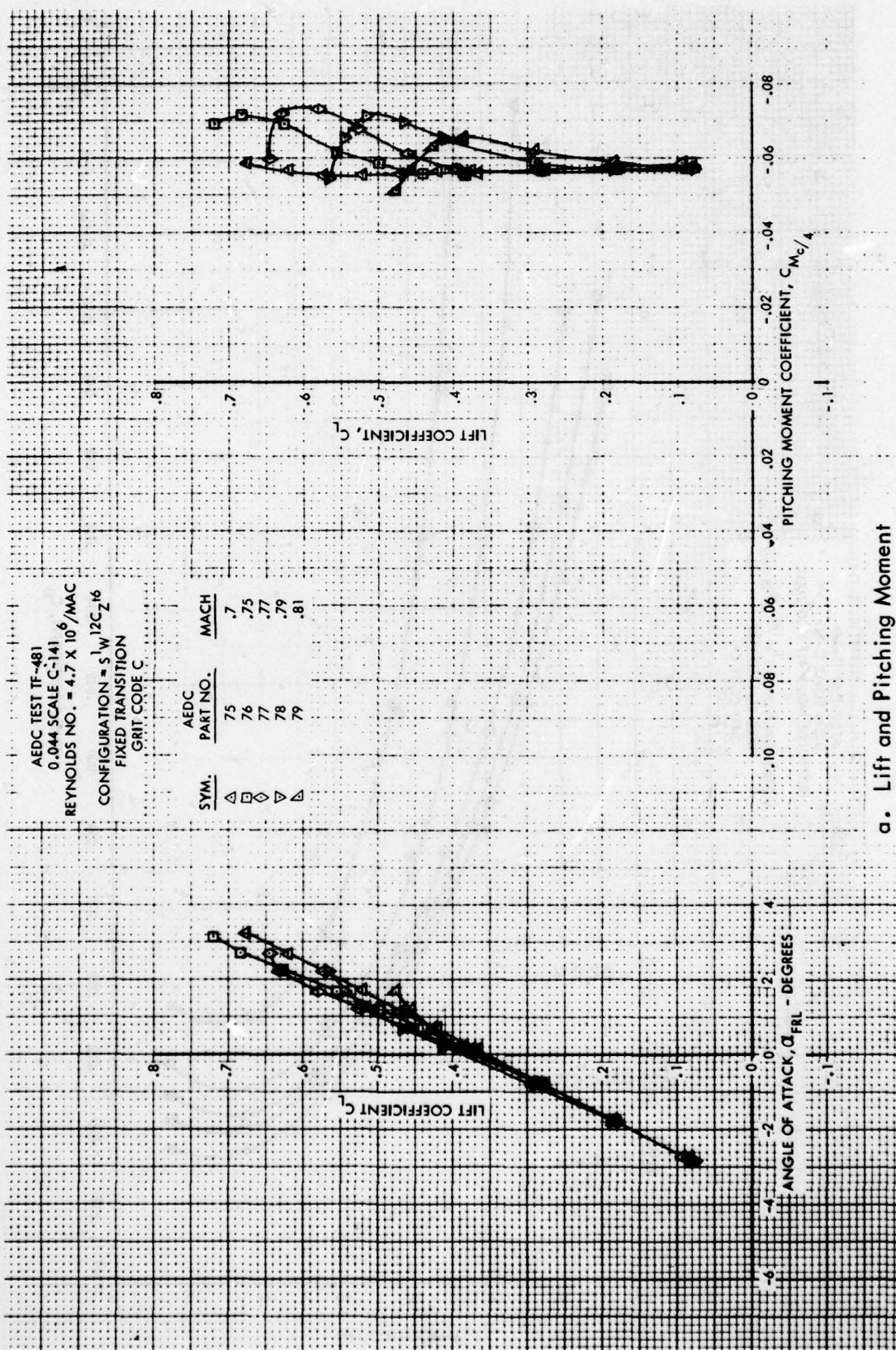
b. Drag Polar
Figure 26. Concluded



a. Lift and Pitching Moment
 Figure 27. Lift, Drag and Pitching Moment Characteristics for Baseline Leading Edge,
 Fixed Transition, Grit Code C, One Swept Tip

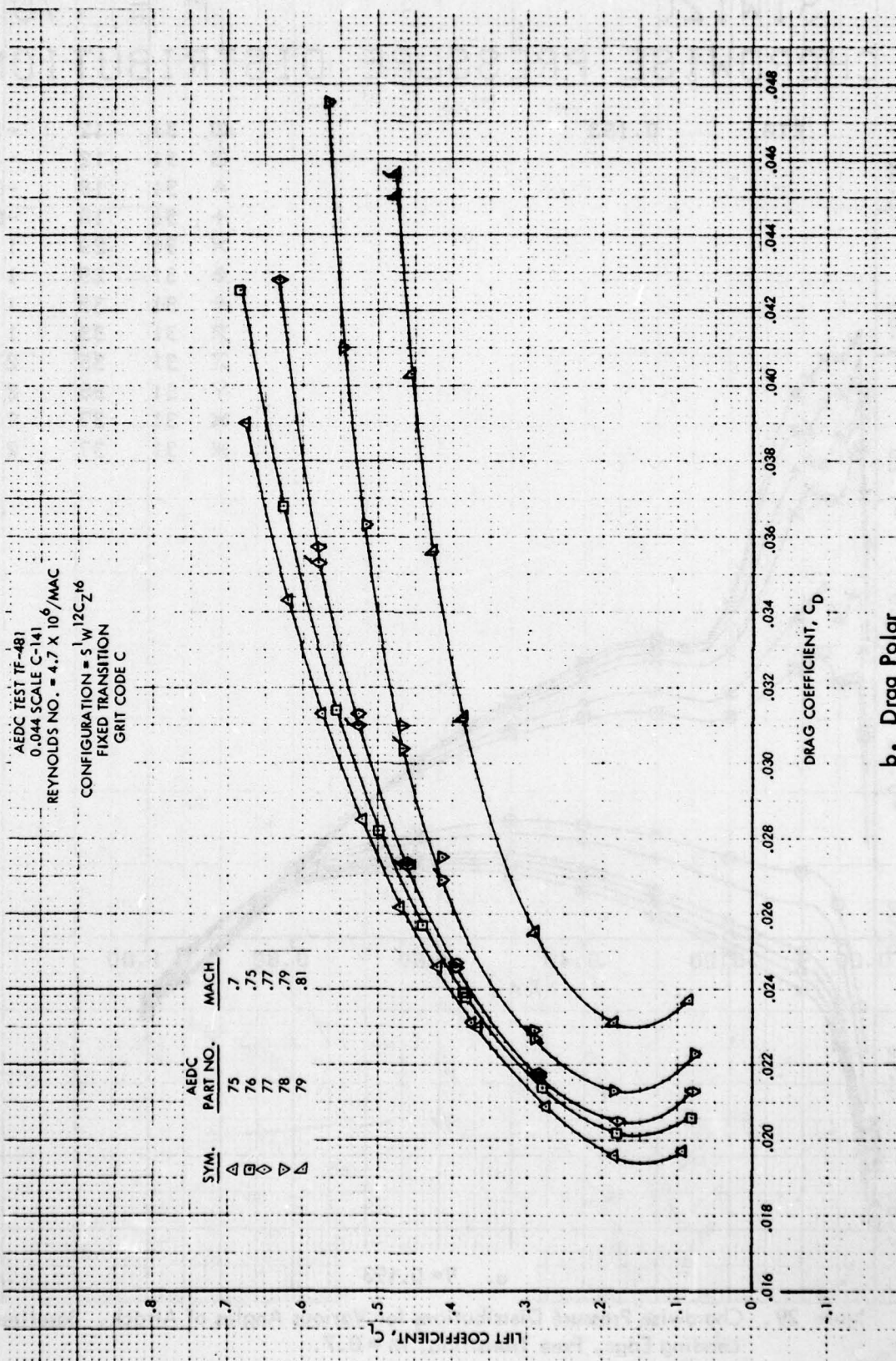


b. Drag Polar
Figure 27. Concluded



a. Lift and Pitching Moment

Figure 28. Lift, Drag and Pitching Moment Characteristics for Baseline Leading Edge, Fixed Transition, Grit Code C, Both Swept Tips



b. Drag Polar
Figure 28. Concluded

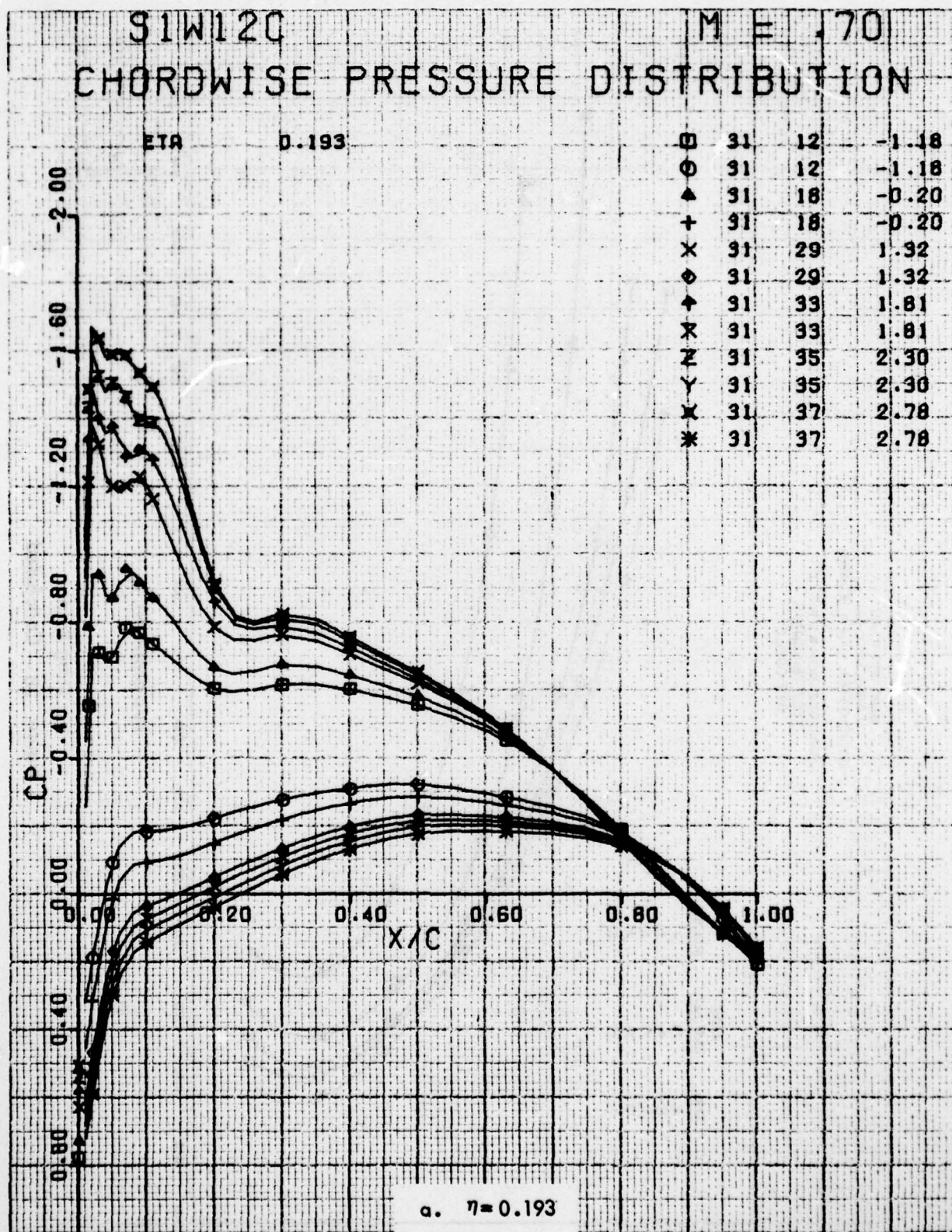


Figure 29. Chordwise Pressure Distributions for Various Angles of Attack. Baseline Leading Edge, Free Transition, $M = 0.7$.

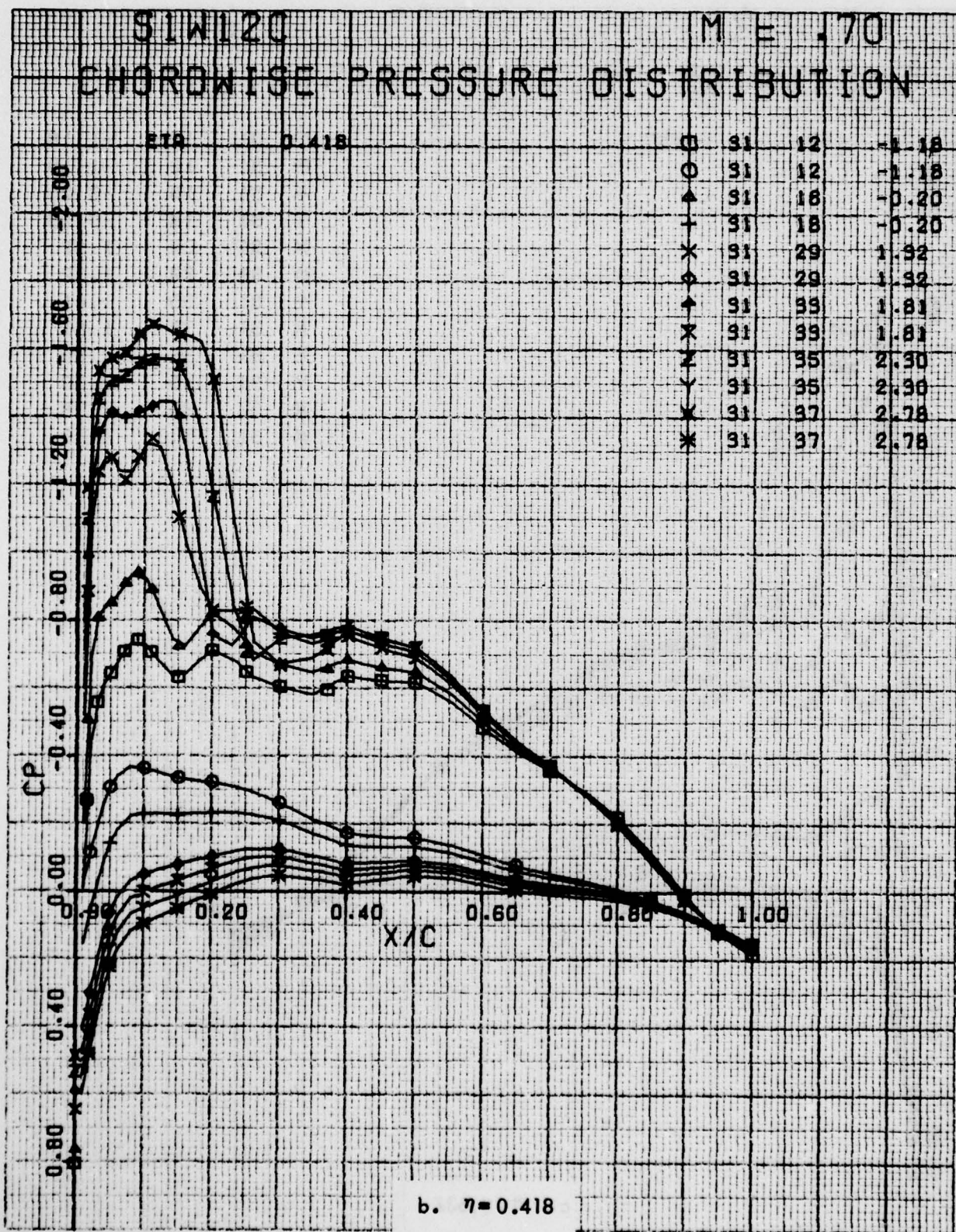


Figure 29. Continued

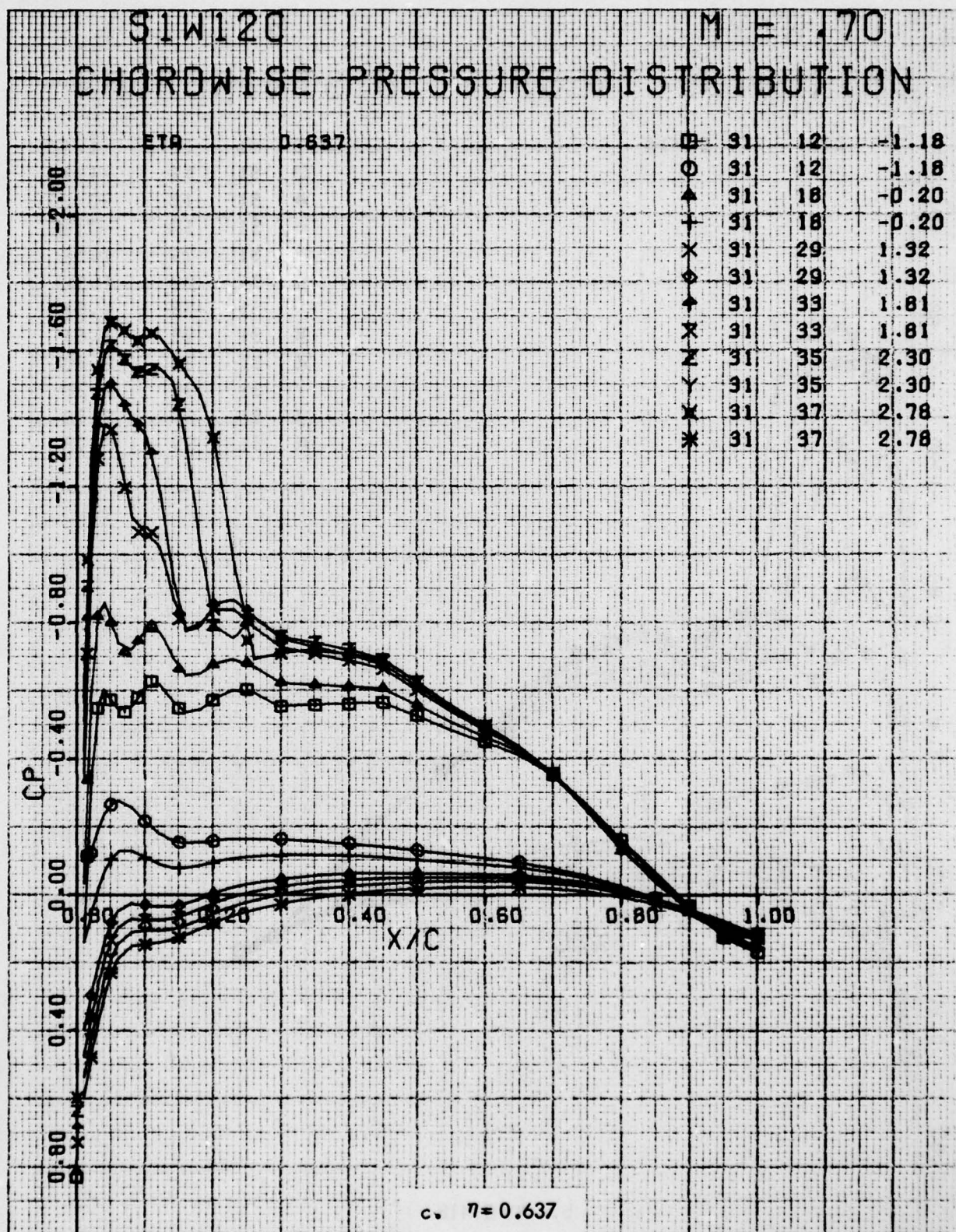


Figure 29. Continued

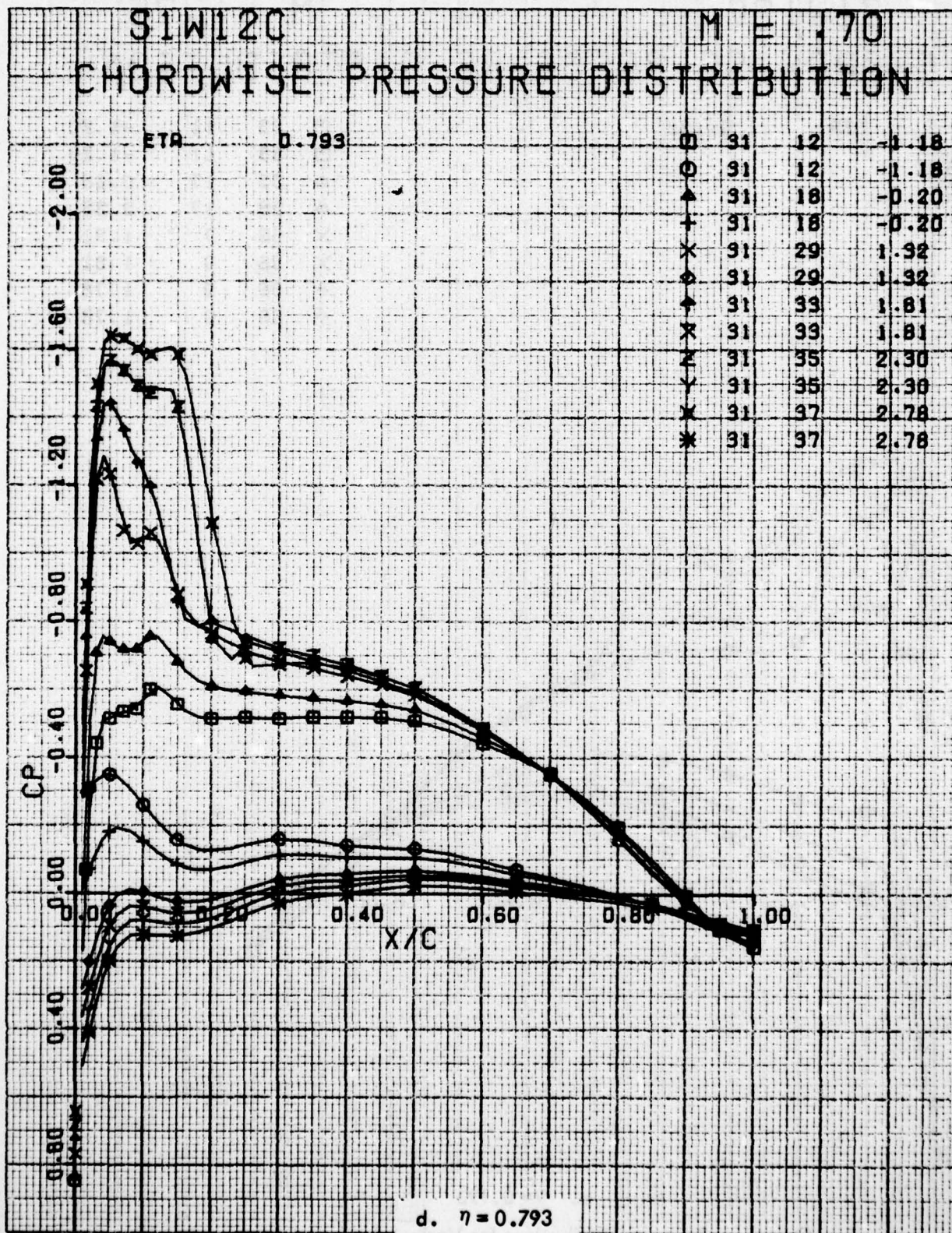


Figure 29. Concluded

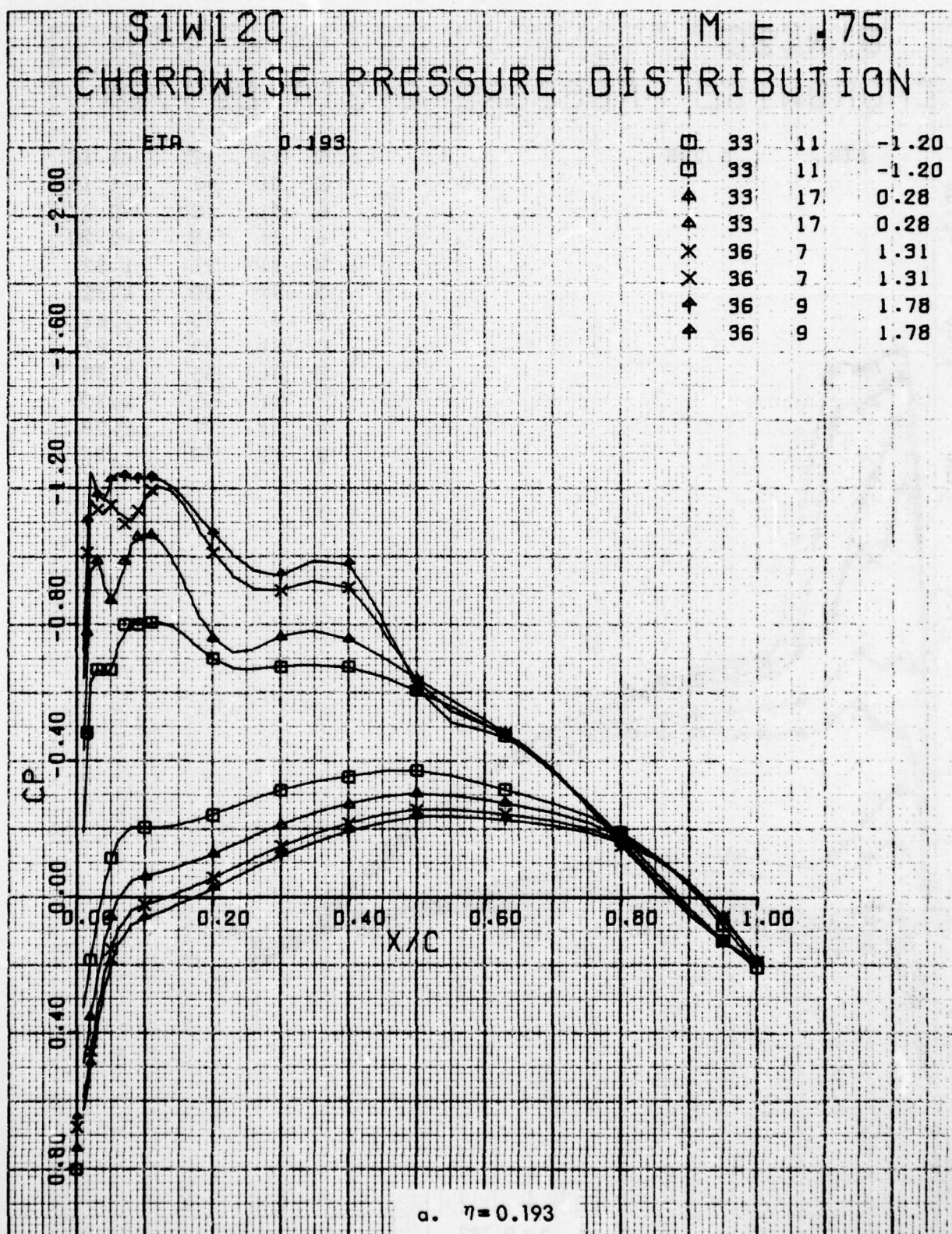


Figure 30 . Chordwise Pressure Distributions for Various Angles of Attack. Baseline Leading Edge, Free Transition, $M = 0.75$.

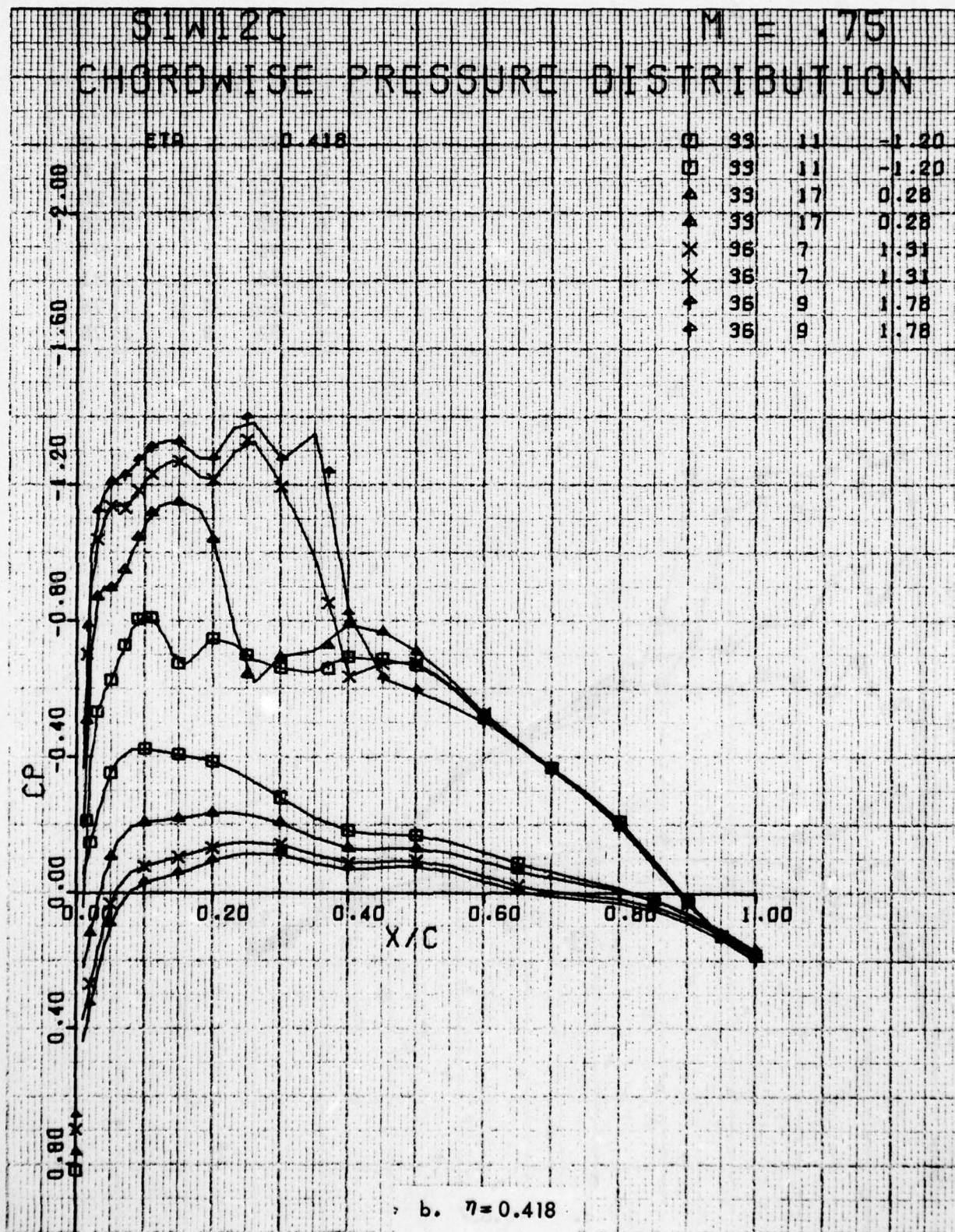


Figure 30 . Continued

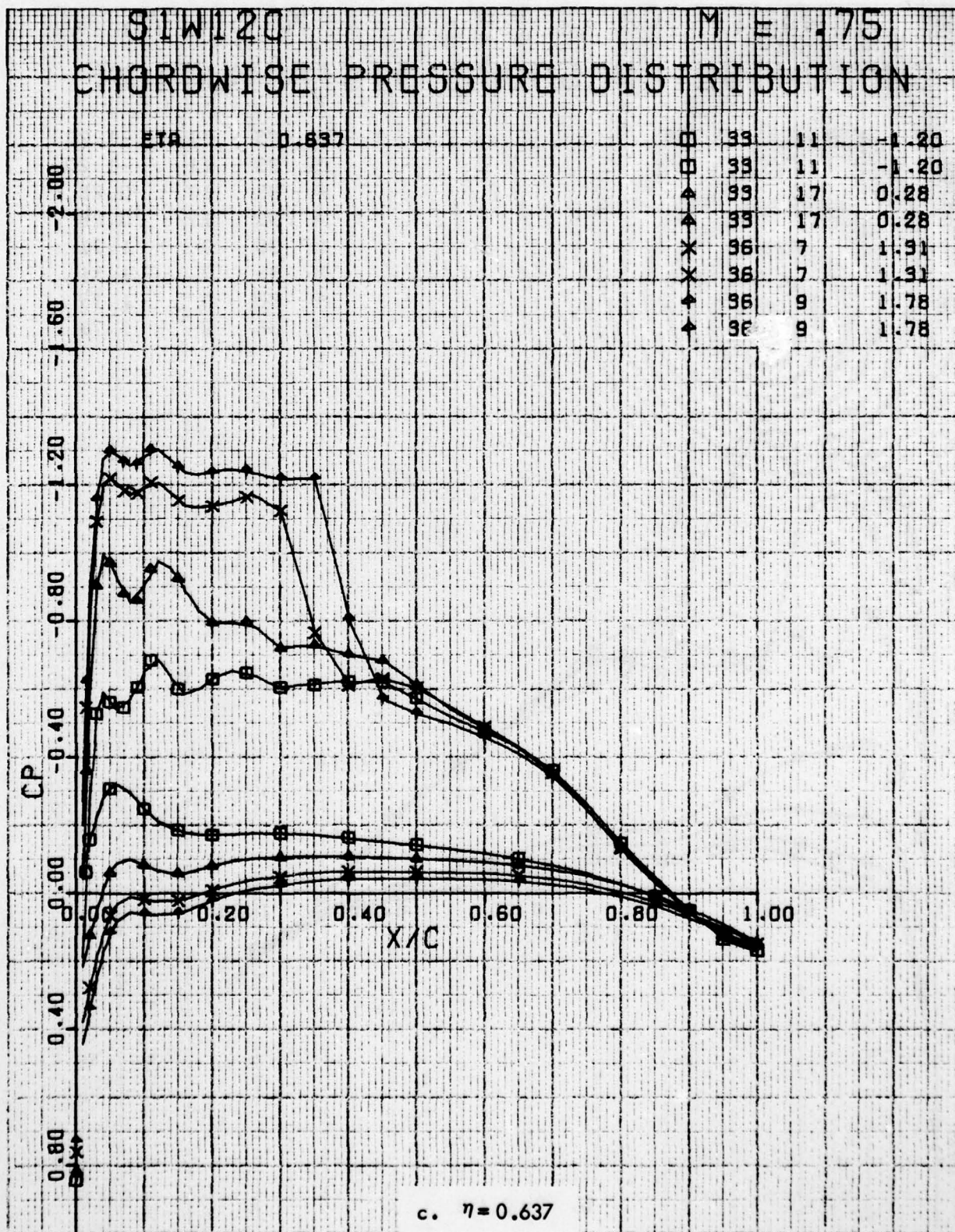


Figure 30. Continued

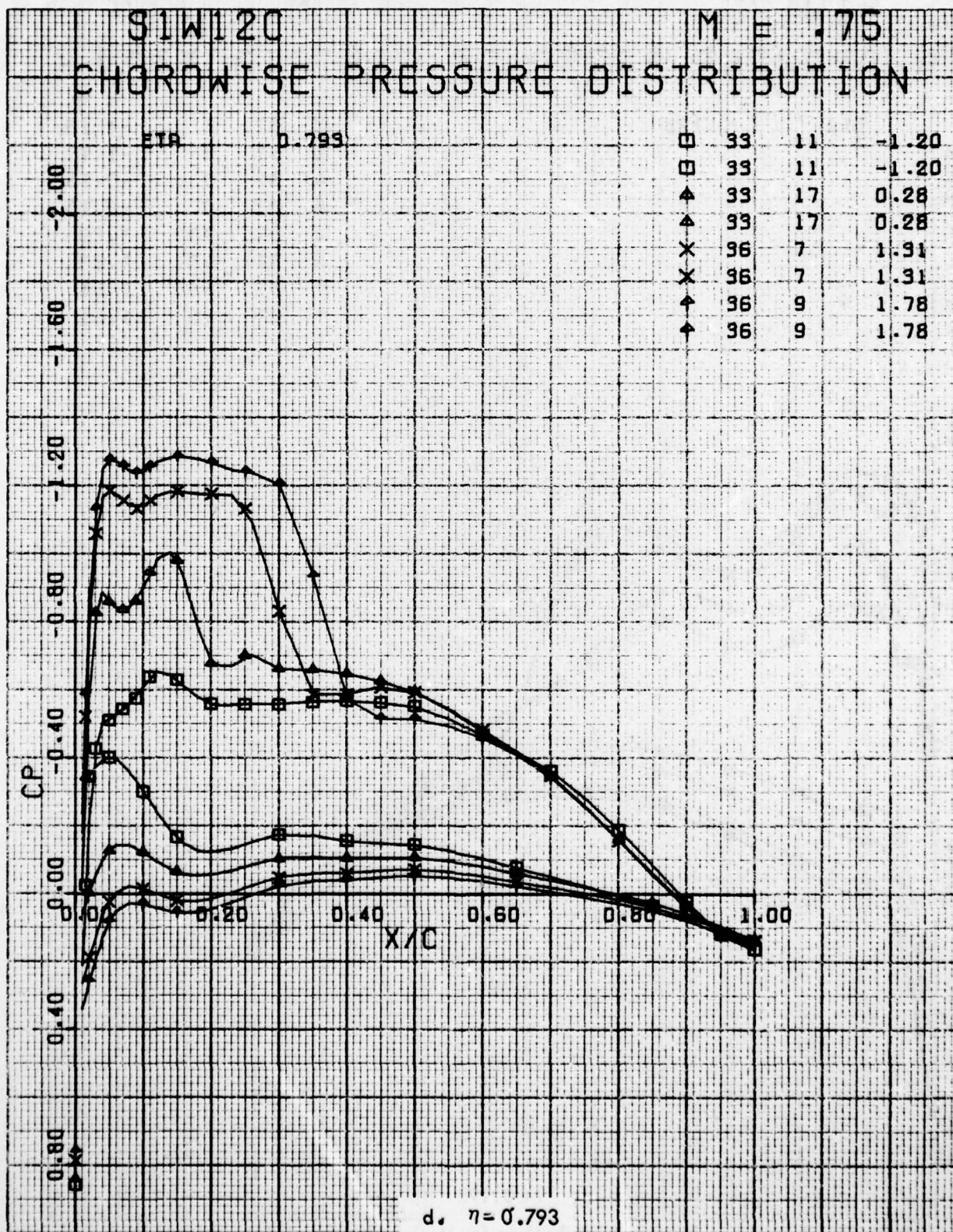


Figure 30. Concluded

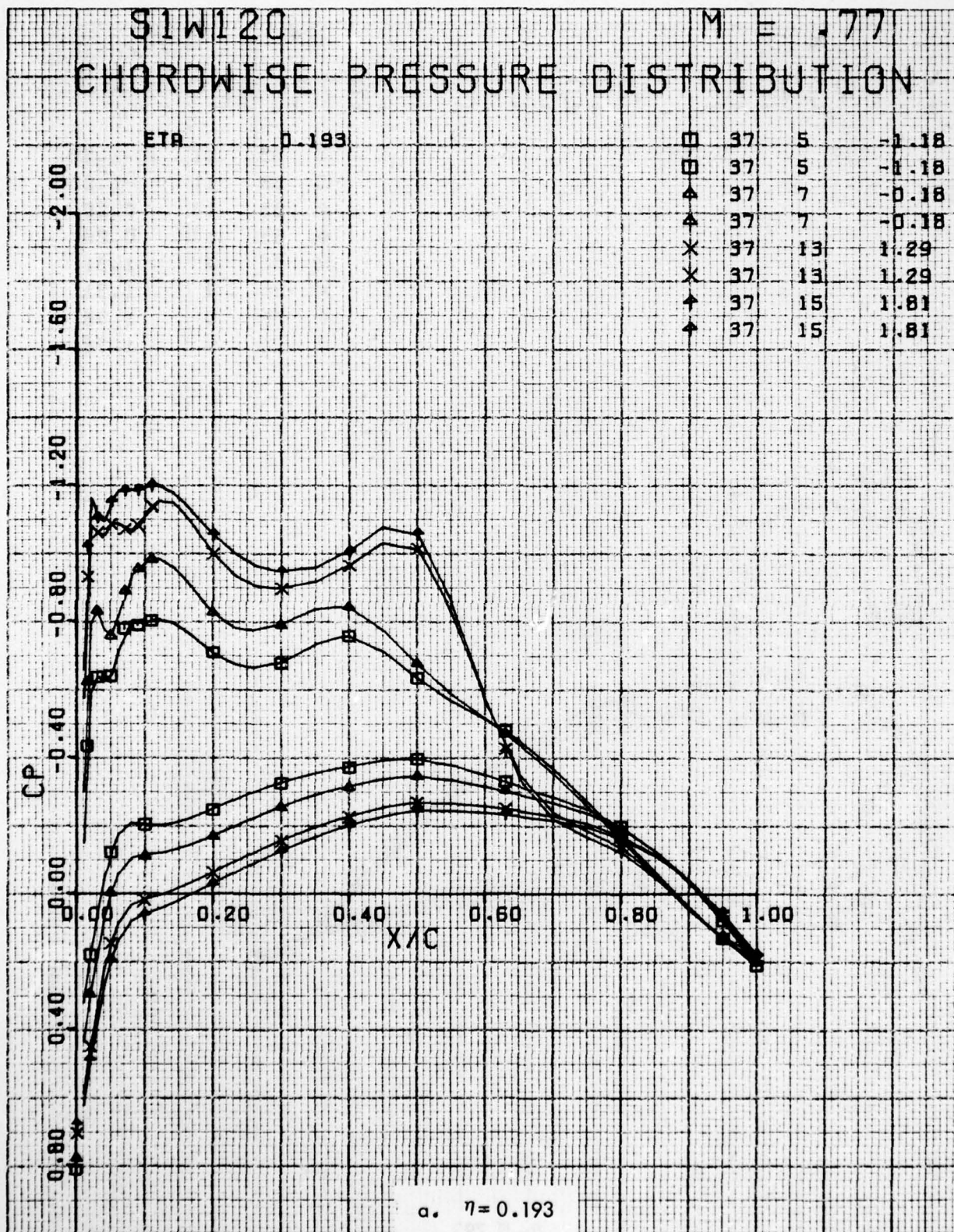


Figure 31. Chordwise Pressure Distributions for Various Angles of Attack. Baseline Leading Edge, Free Transition, $M = 0.77$.

AD-A077 688

LOCKHEED-GEORGIA CO MARIETTA

F/G 1/3

AERODYNAMIC INVESTIGATION OF C-141 LEADING EDGE MODIFICATION F0--ETC(U)

JUN 79 W T BLACKERBY , P R SMITH

F09603-77-A-0204

UNCLASSIFIED

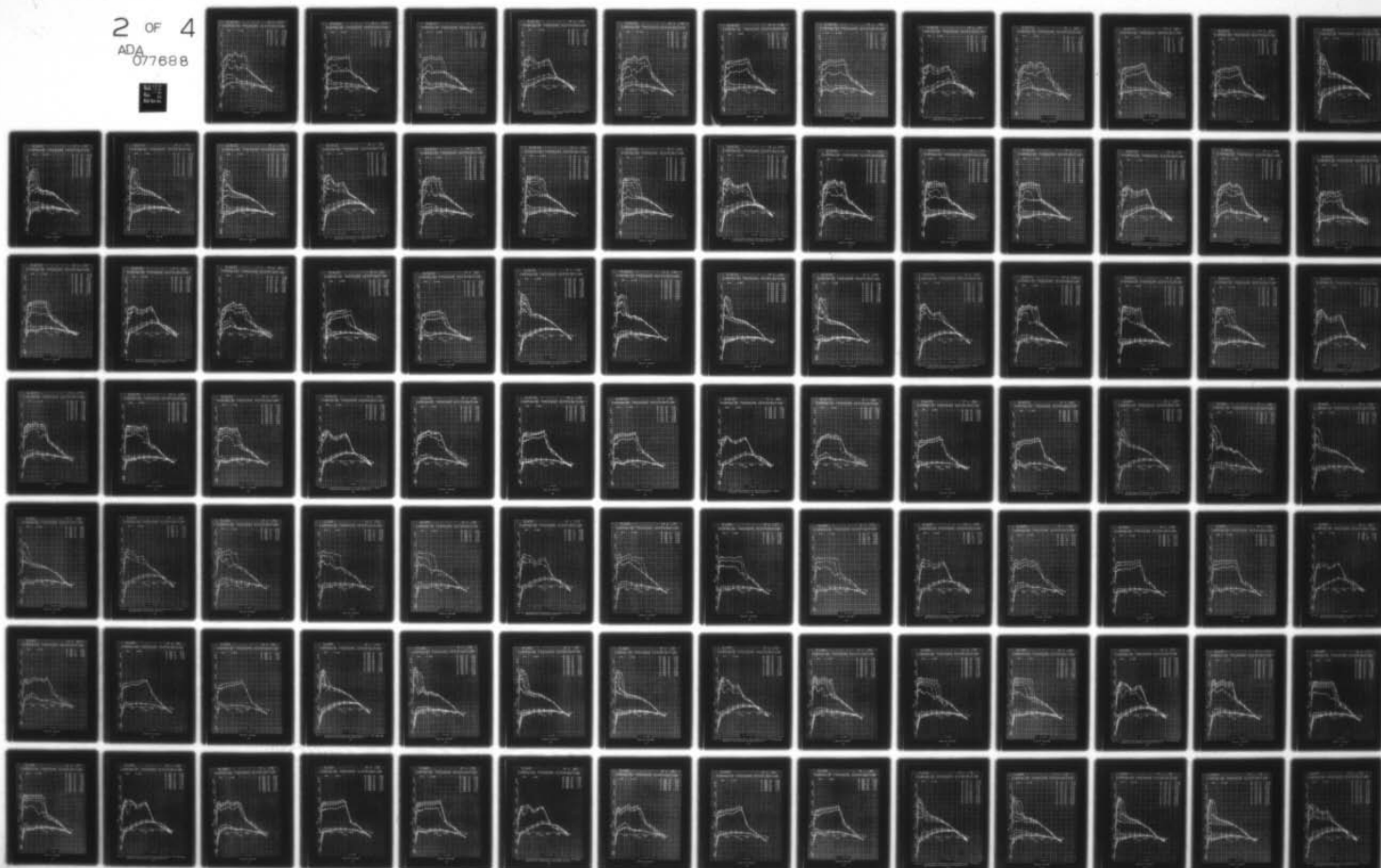
LG78ER0233-VOL-2

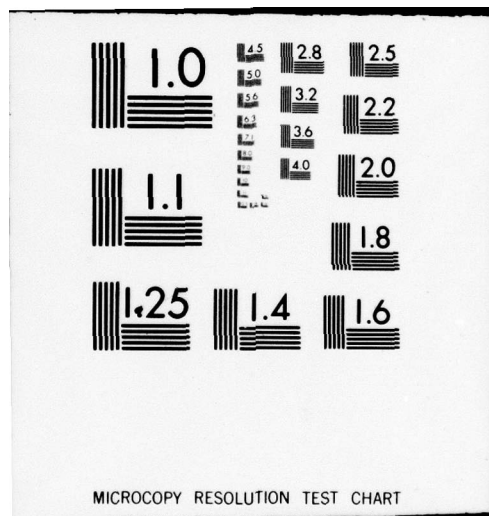
AFFDL-TR-79-3059-VOL-2

NL

2 OF 4

ADA
077688





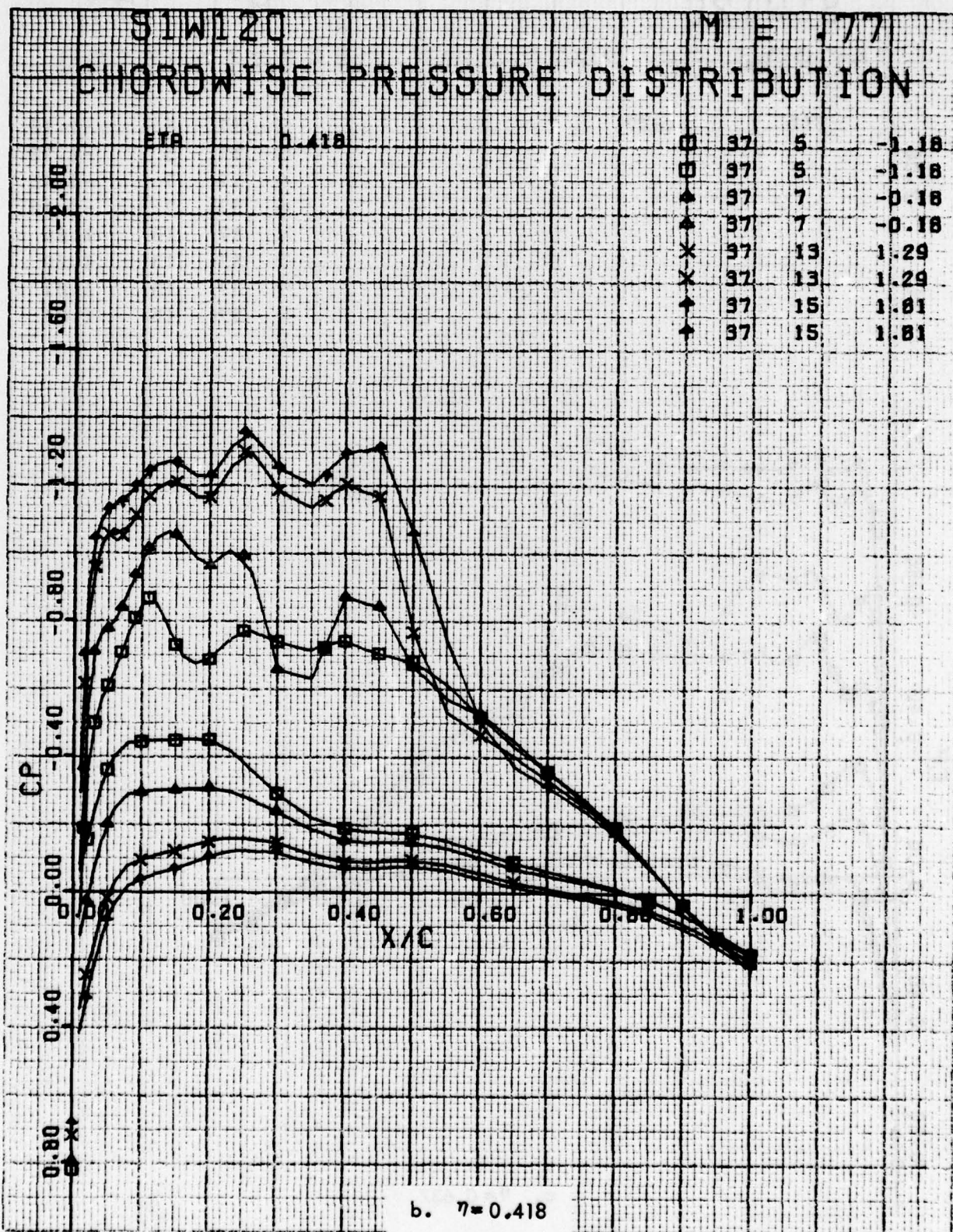


Figure 31. Continued

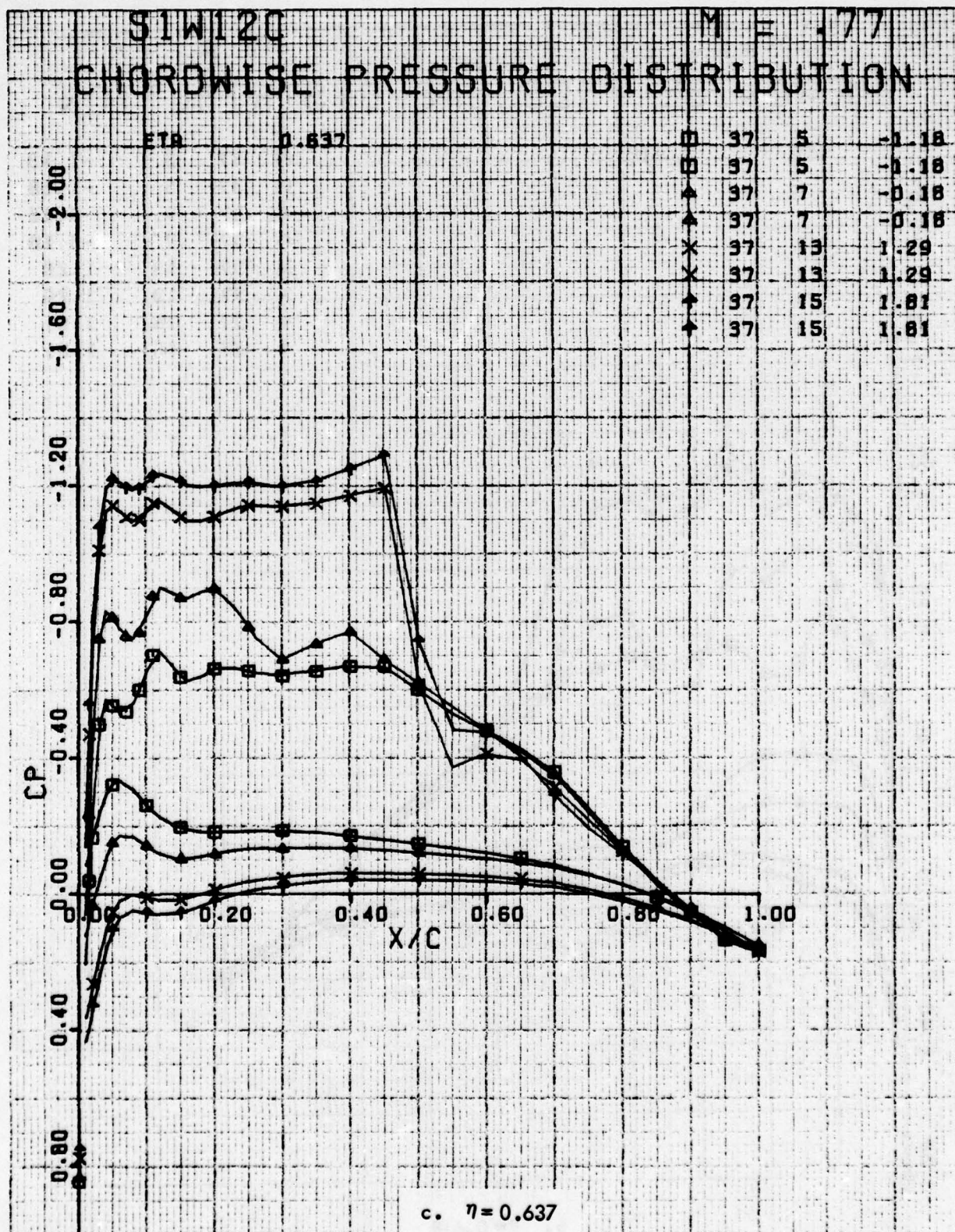


Figure 31. Continued

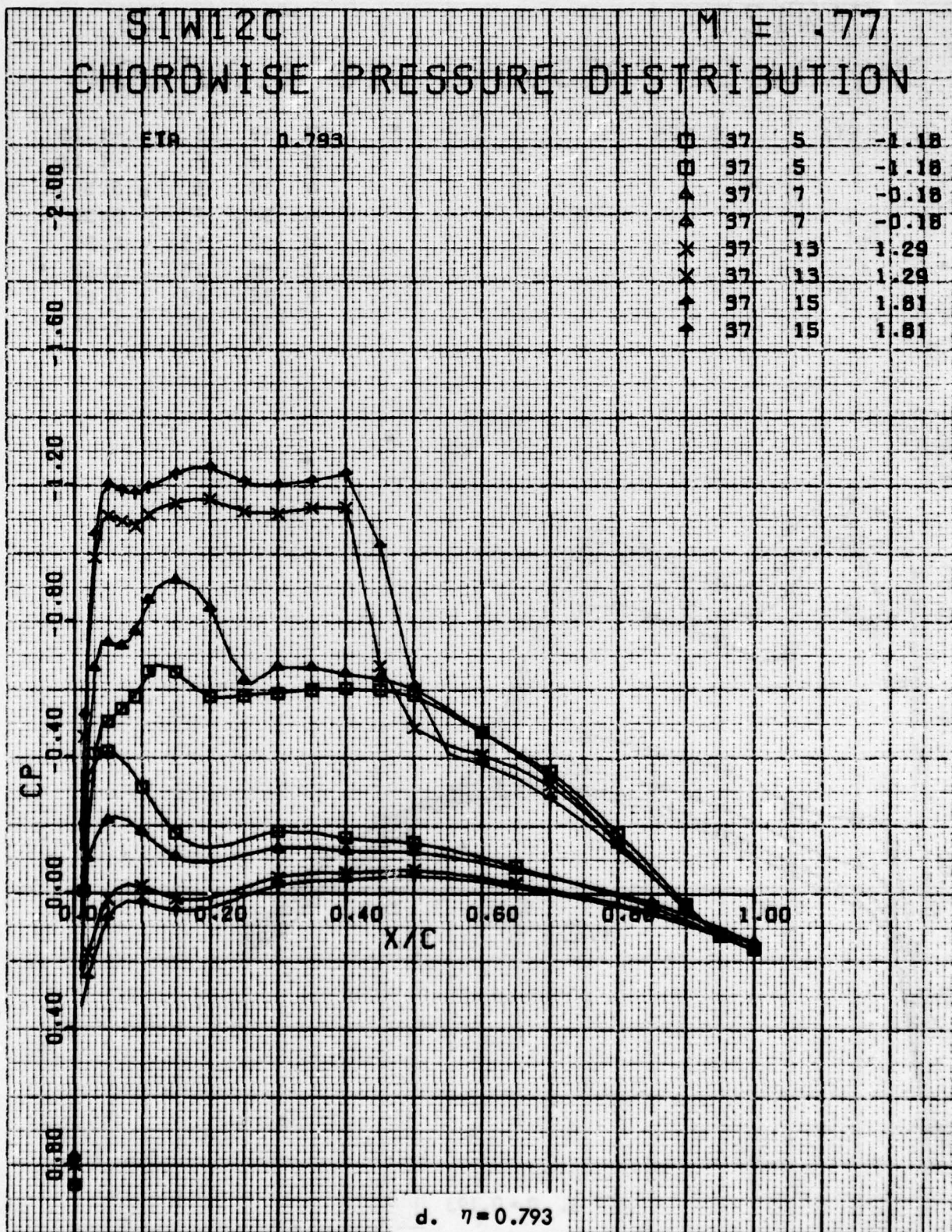


Figure 31. Concluded

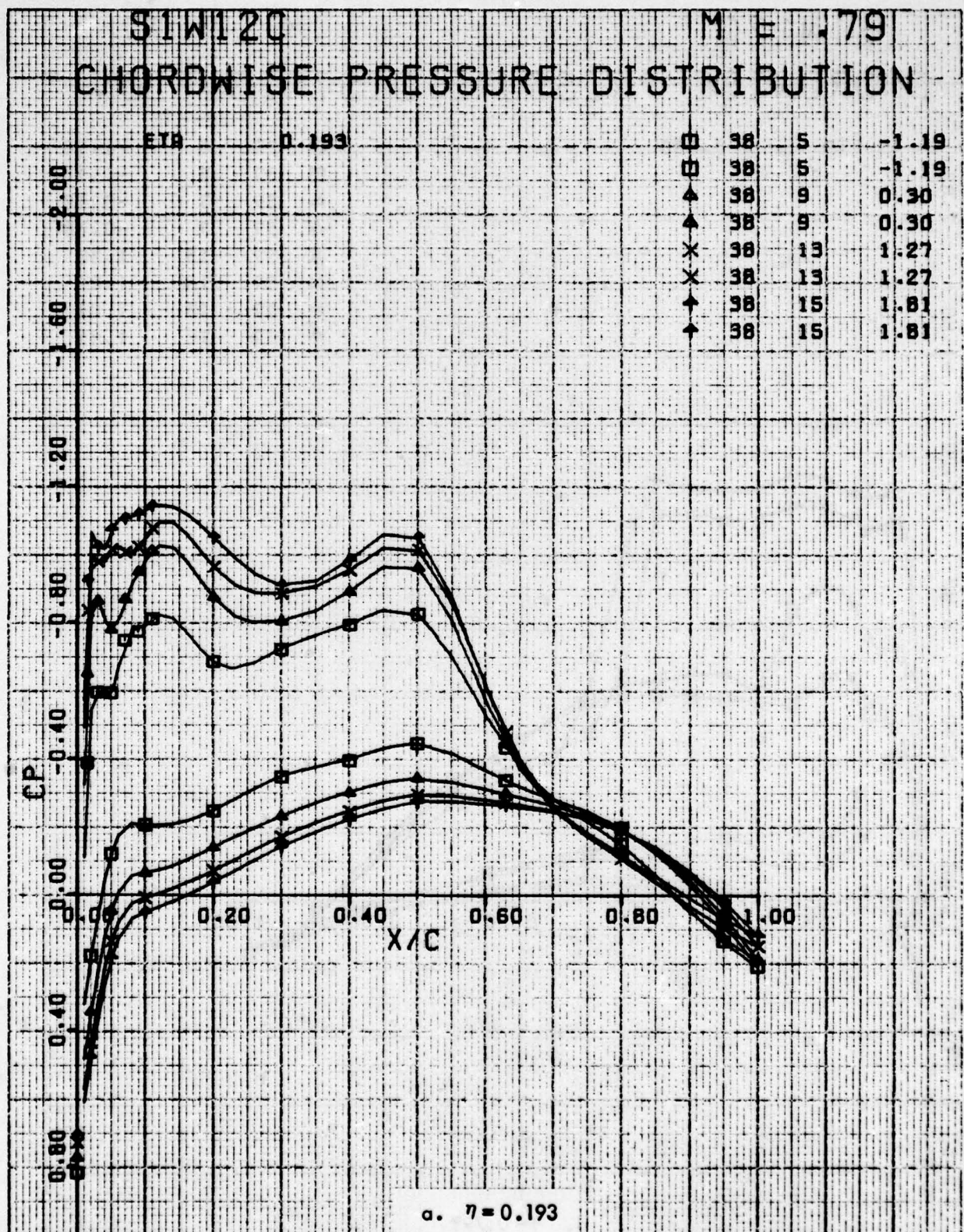


Figure 32. Chordwise Pressure Distributions for Various Angles of Attack. Baseline Leading Edge, Free Transition, $M = 0.79$.

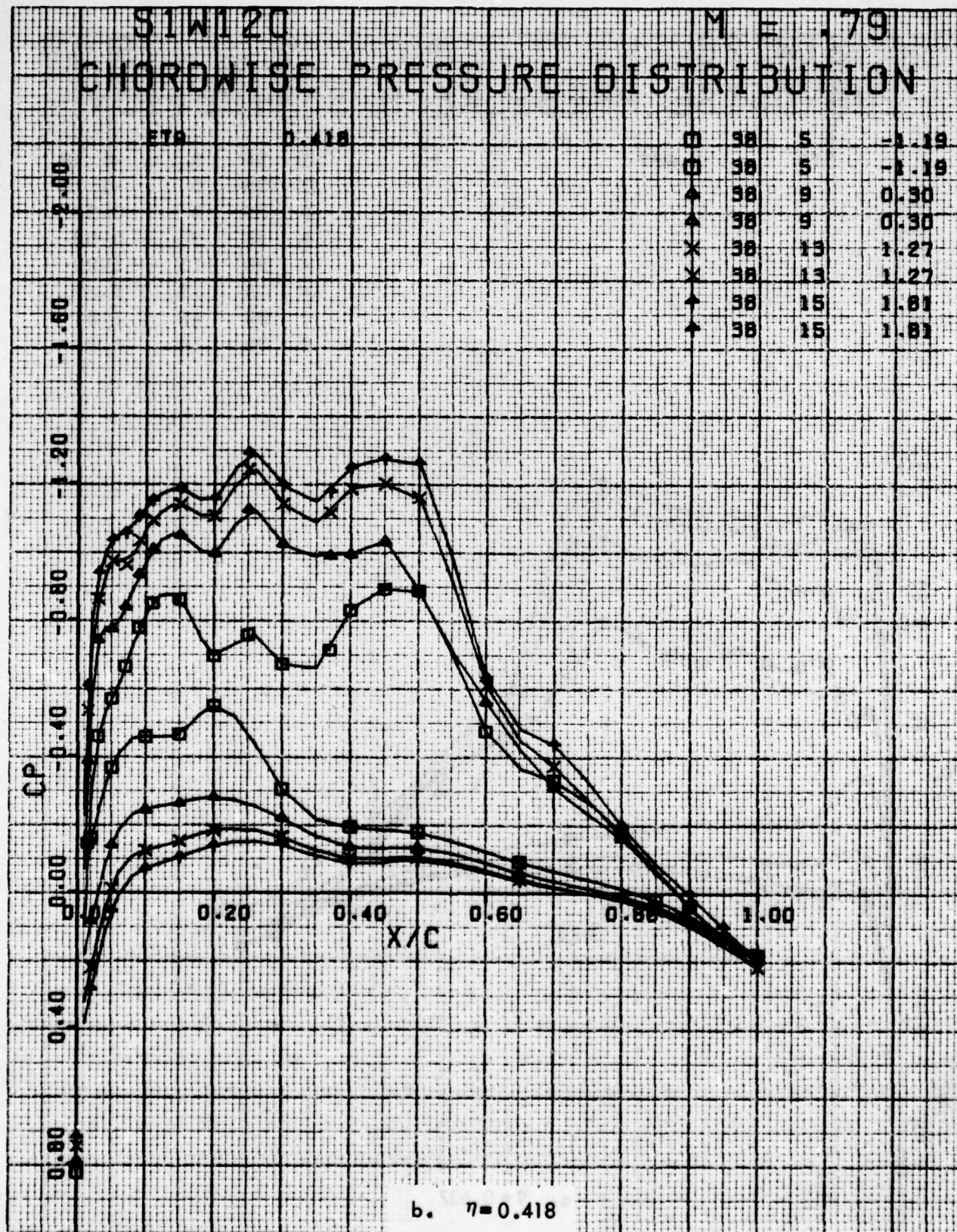


Figure 32. Continued

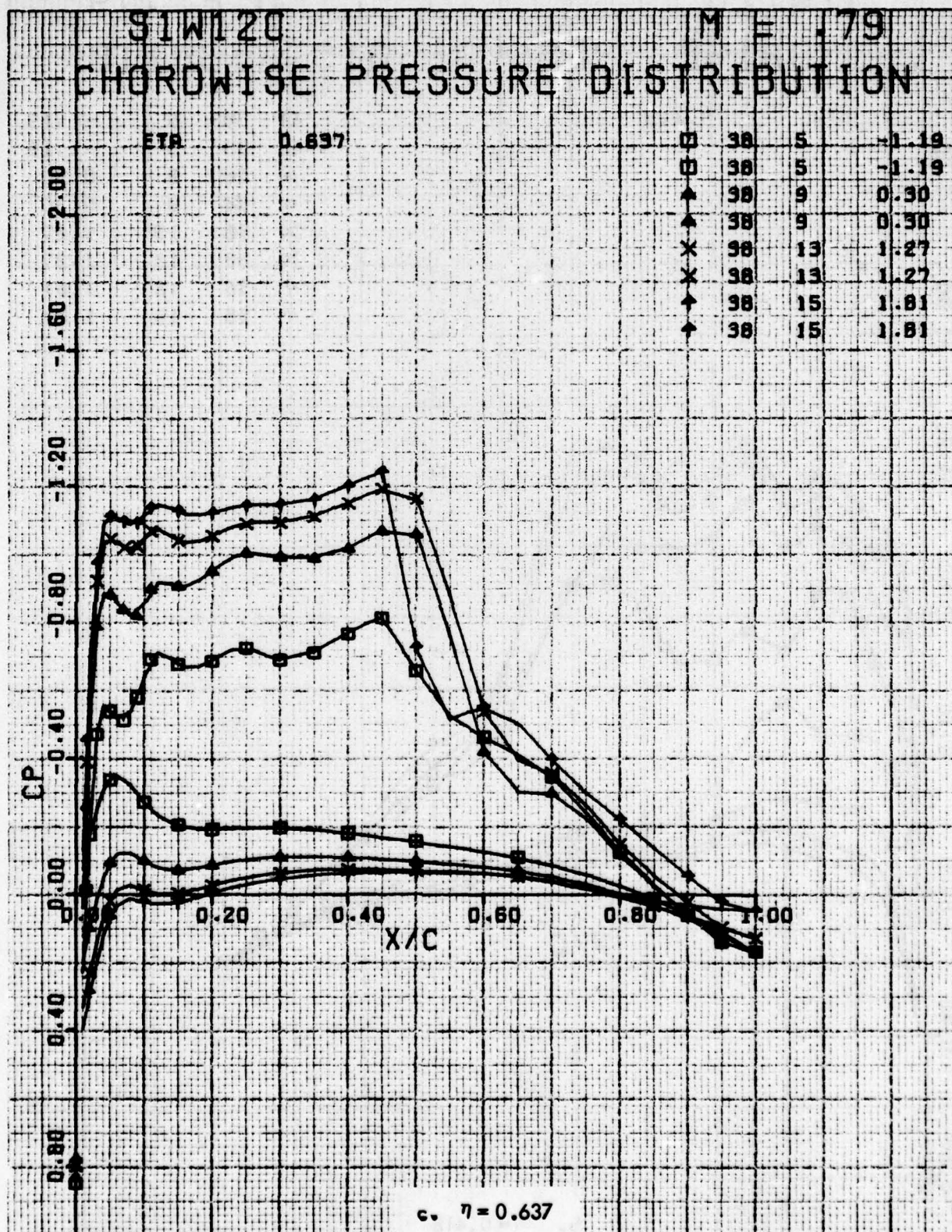


Figure 32. Continued

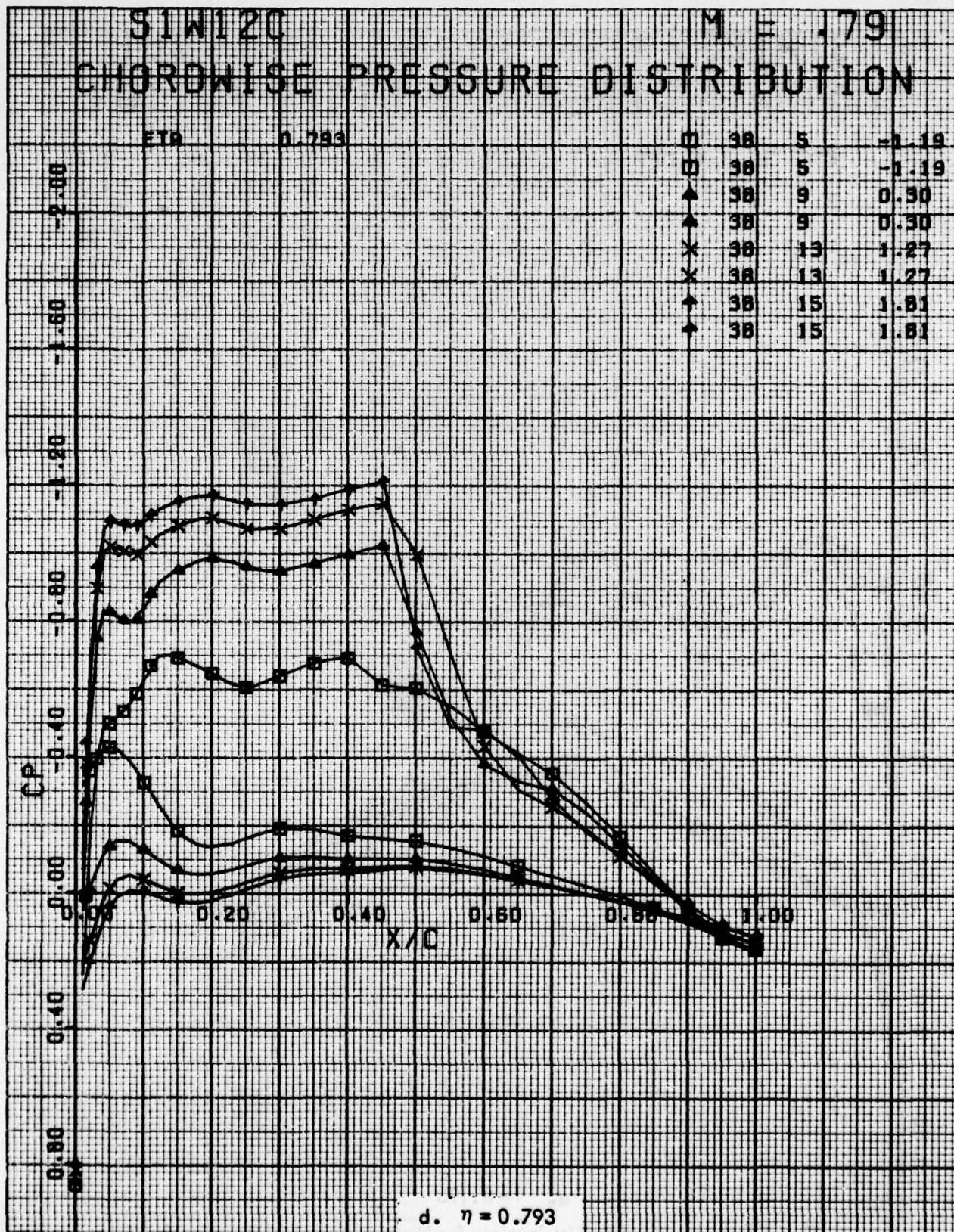


Figure 32. Concluded

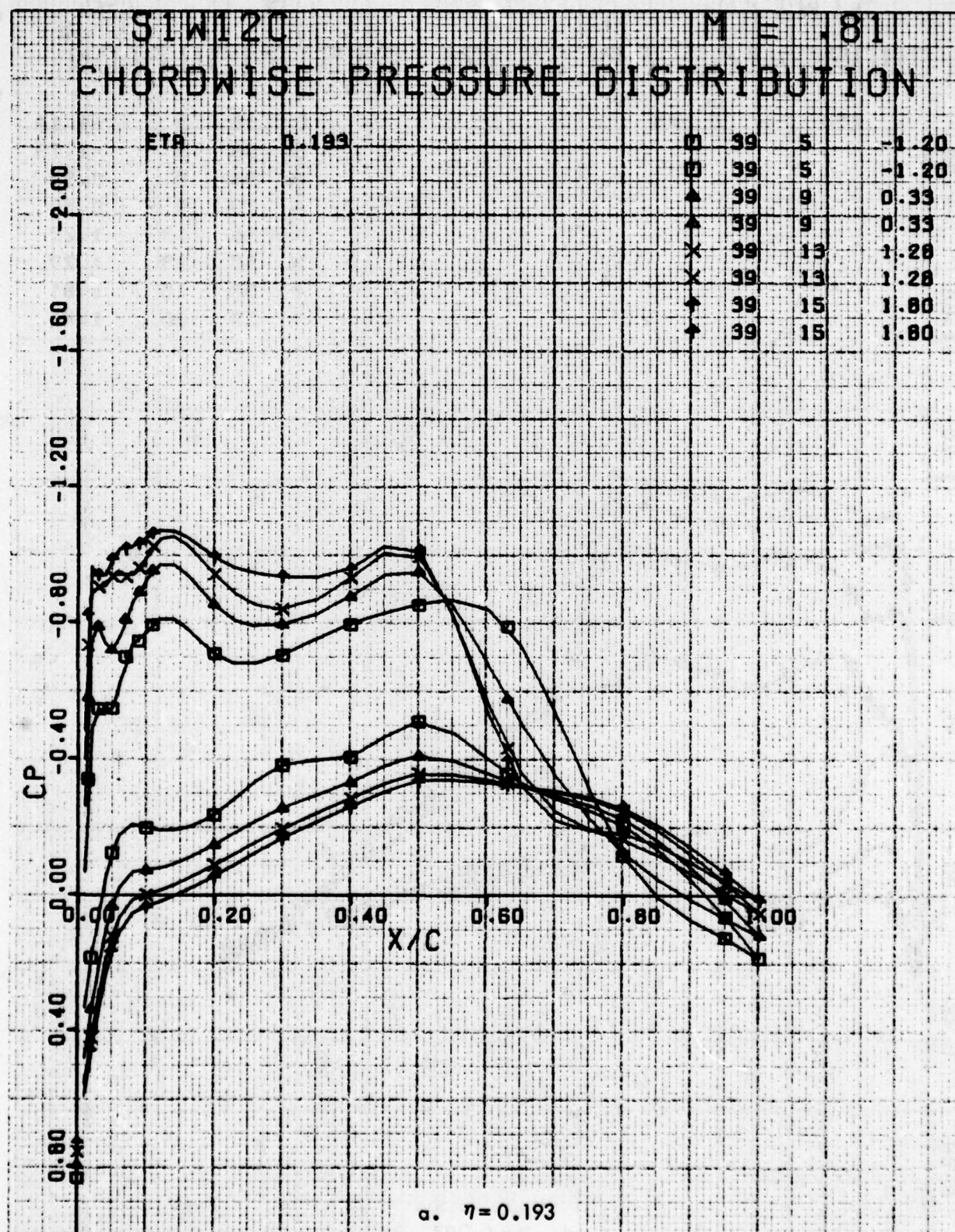


Figure 33. Chordwise Pressure Distributions for Various Angles of Attack. Baseline Leading Edge, Free Transition, $M = 0.81$.

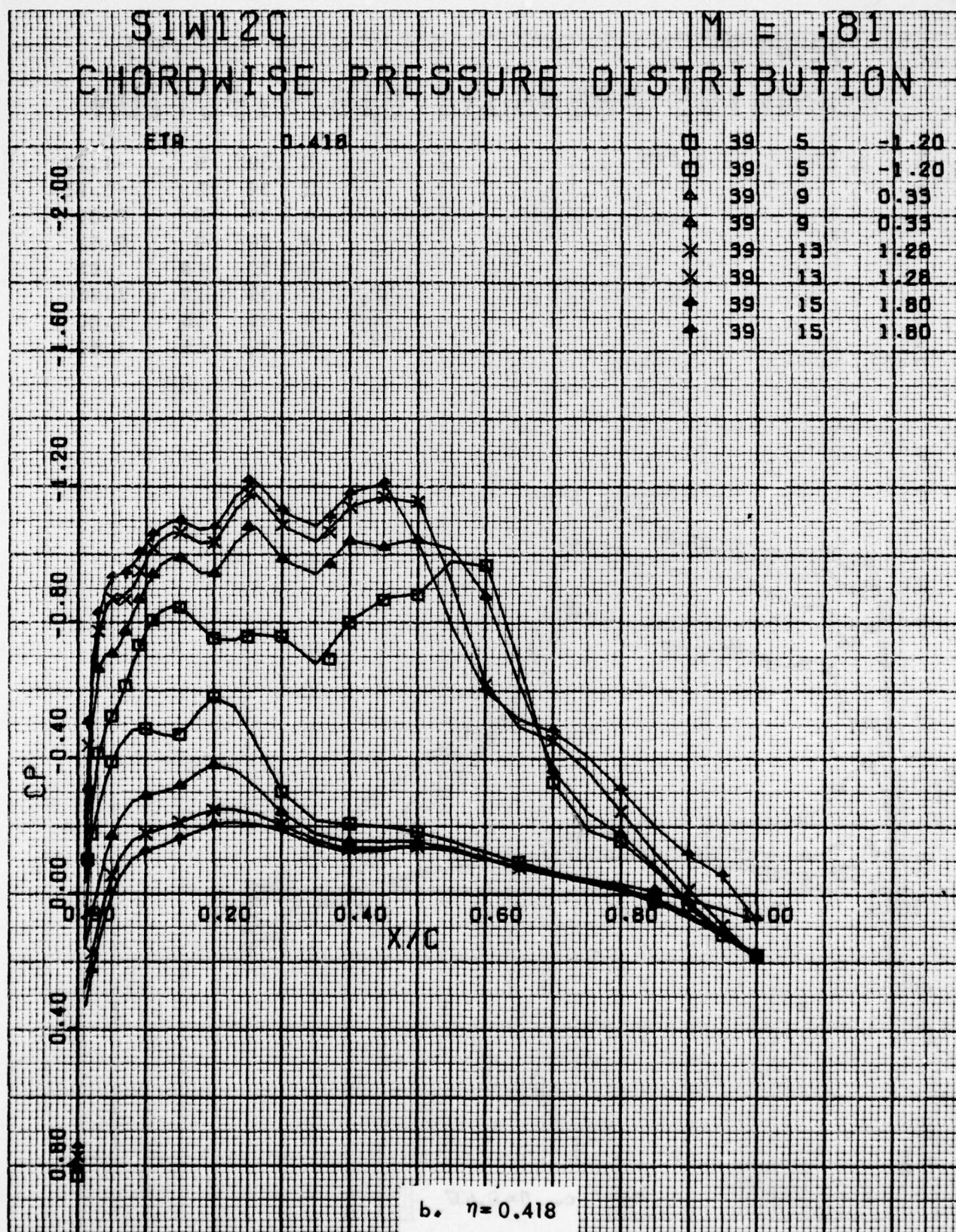


Figure 33. Continued

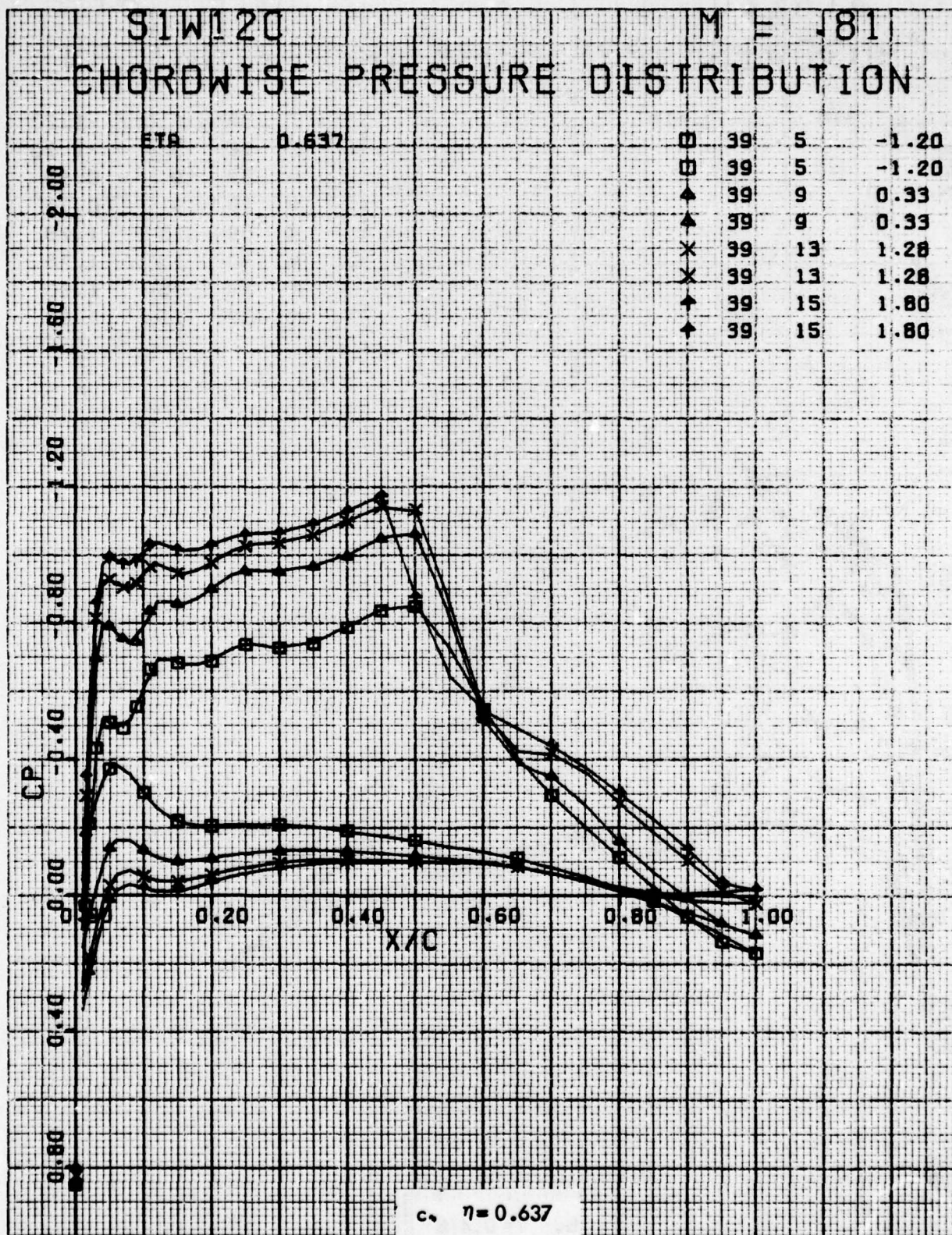


Figure 33. Continued

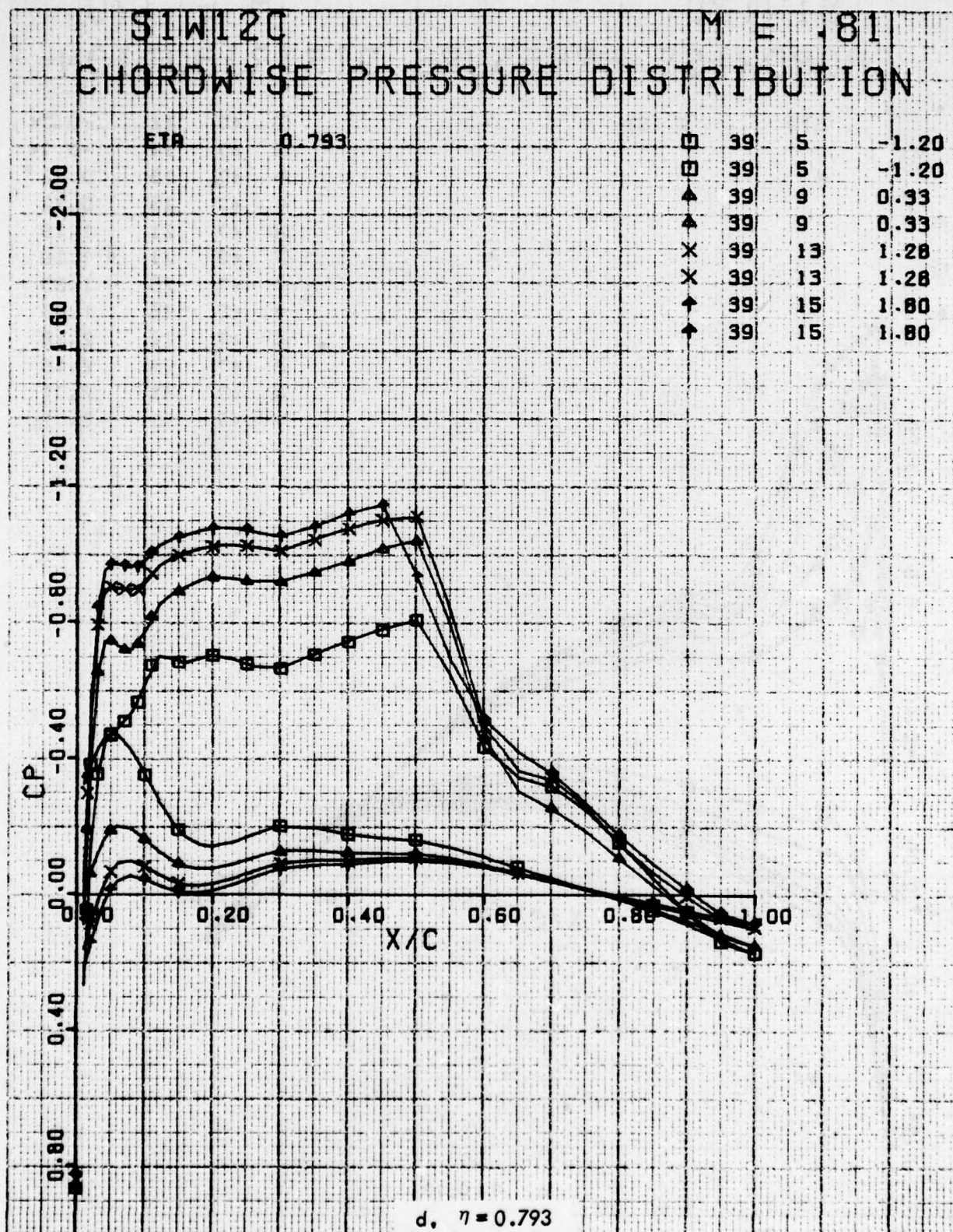


Figure 33. Concluded

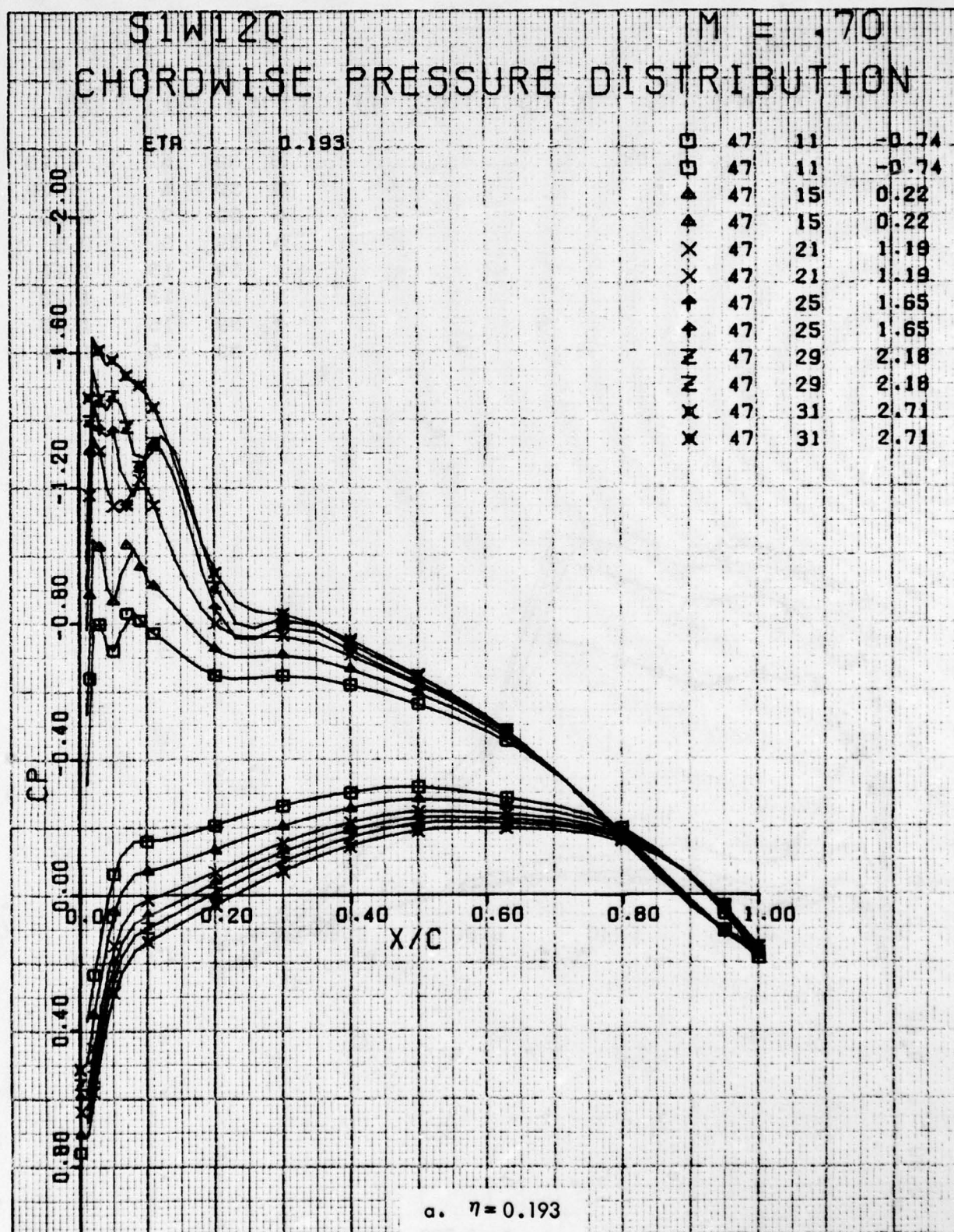


Figure 34 . Chordwise Pressure Distributions for Various Angles of Attack. Baseline Leading Edge, Fixed Transition, Grit Code C, M = 0.7.

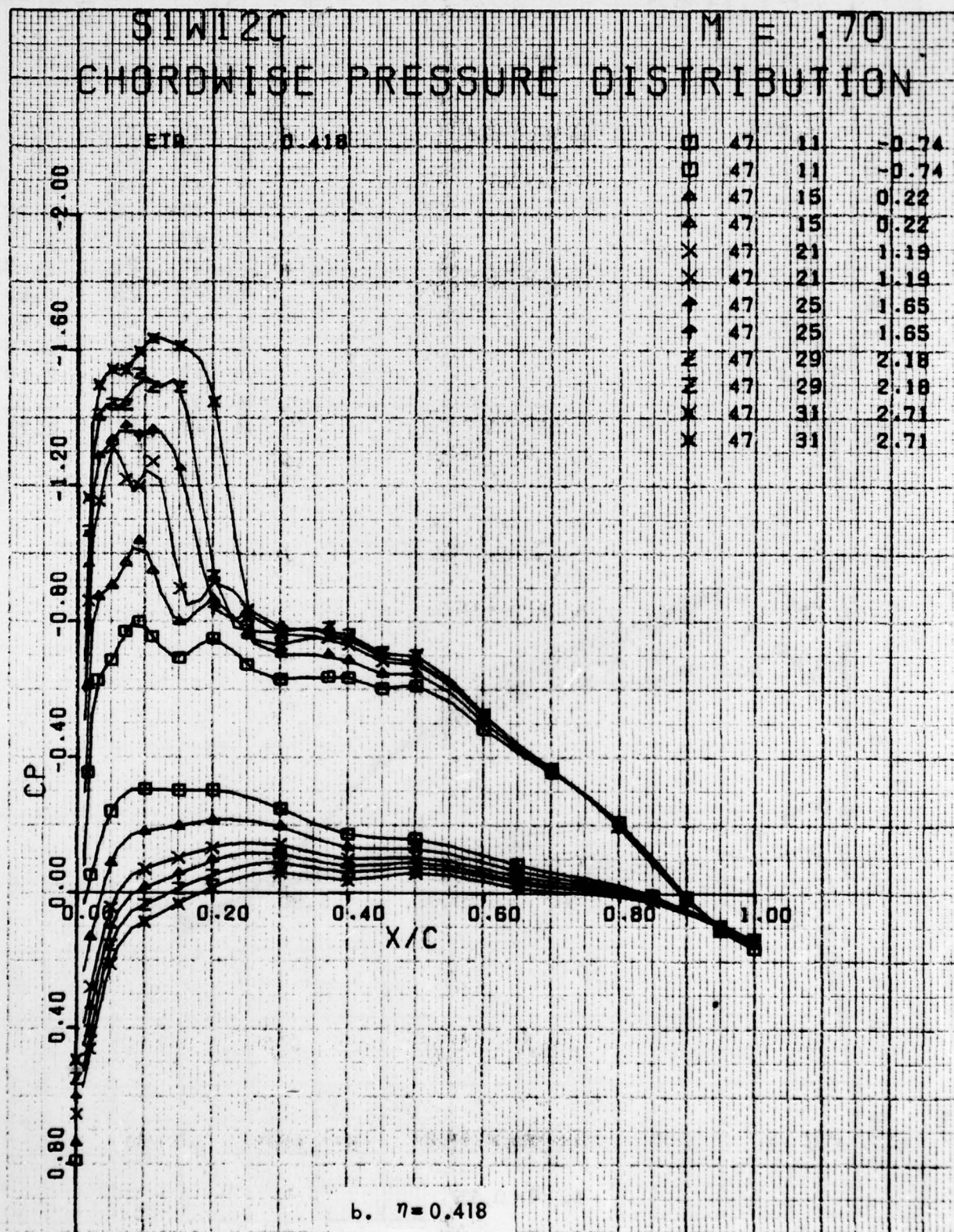


Figure 34. Continued

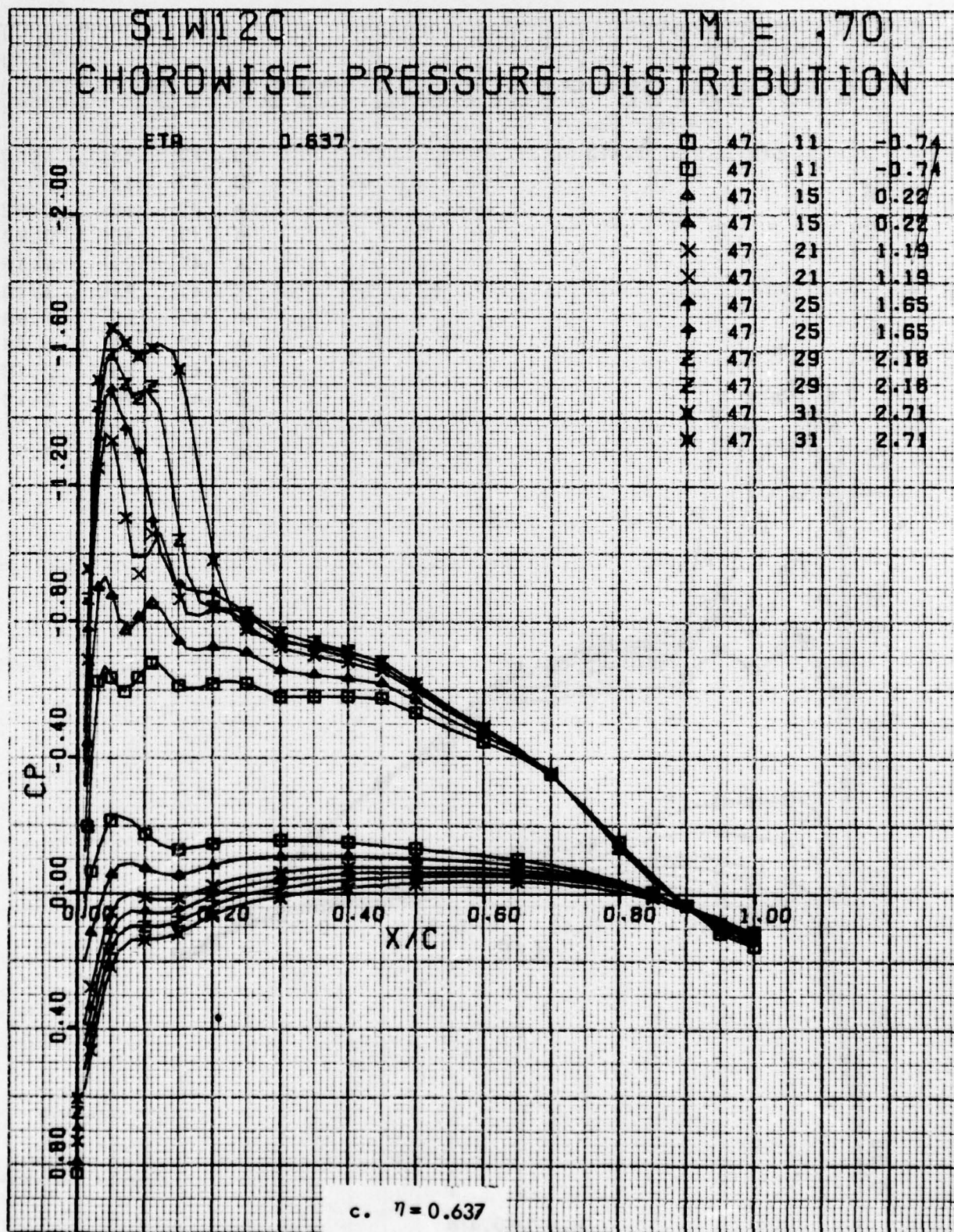


Figure 34. Continued

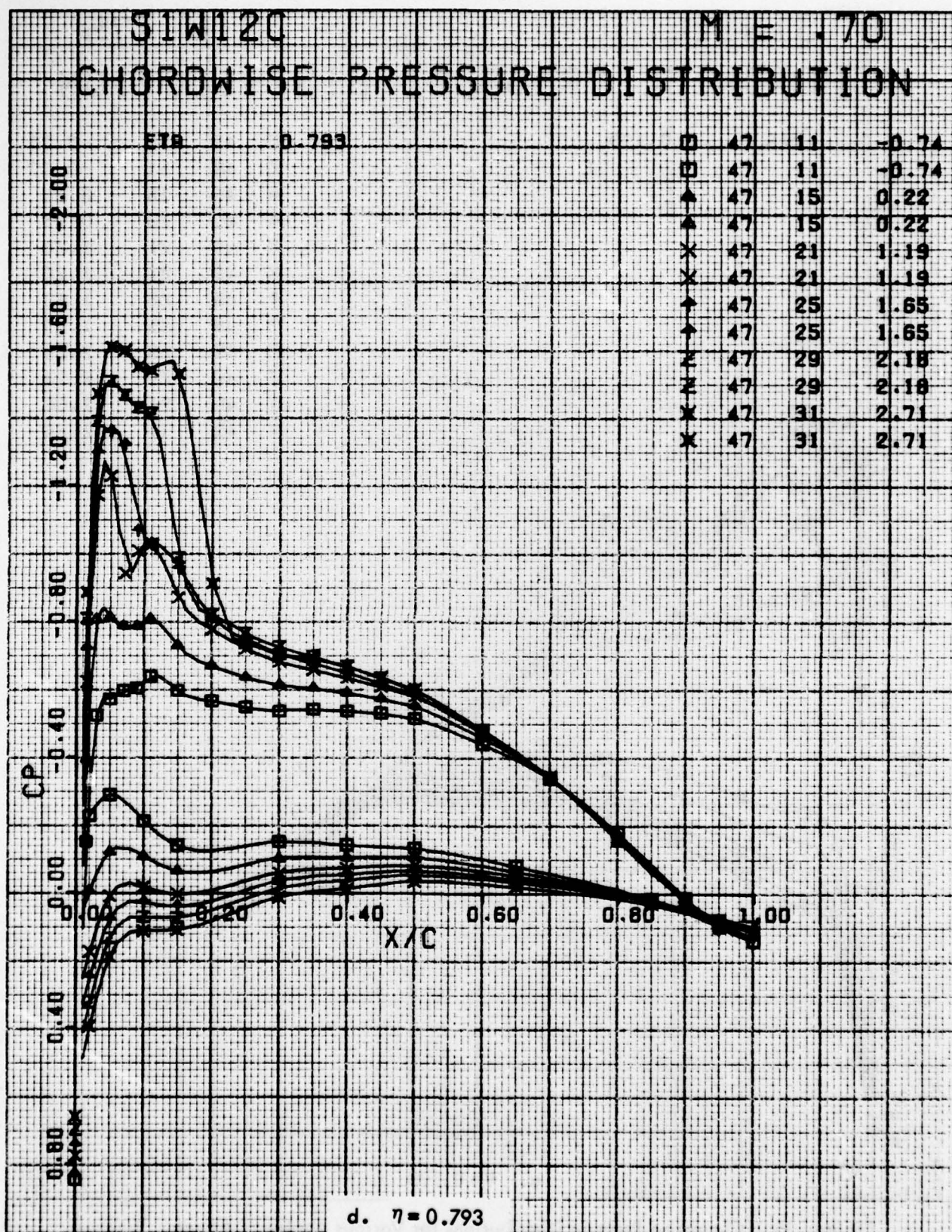


Figure 34. Concluded

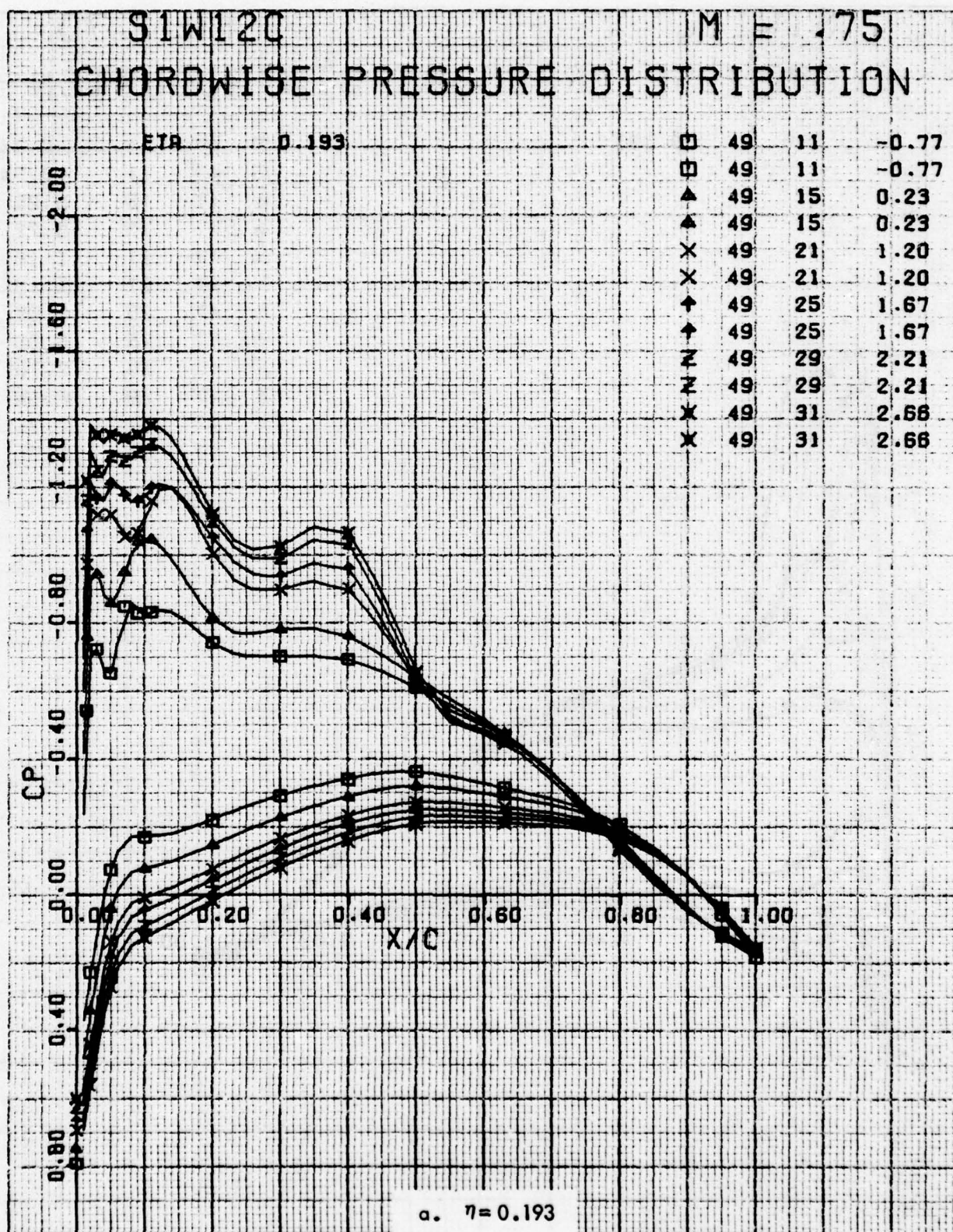


Figure 35. Chordwise Pressure Distributions for Various Angles of Attack. Baseline Leading Edge, Fixed Transition, Grit Code C, $M = 0.75$.

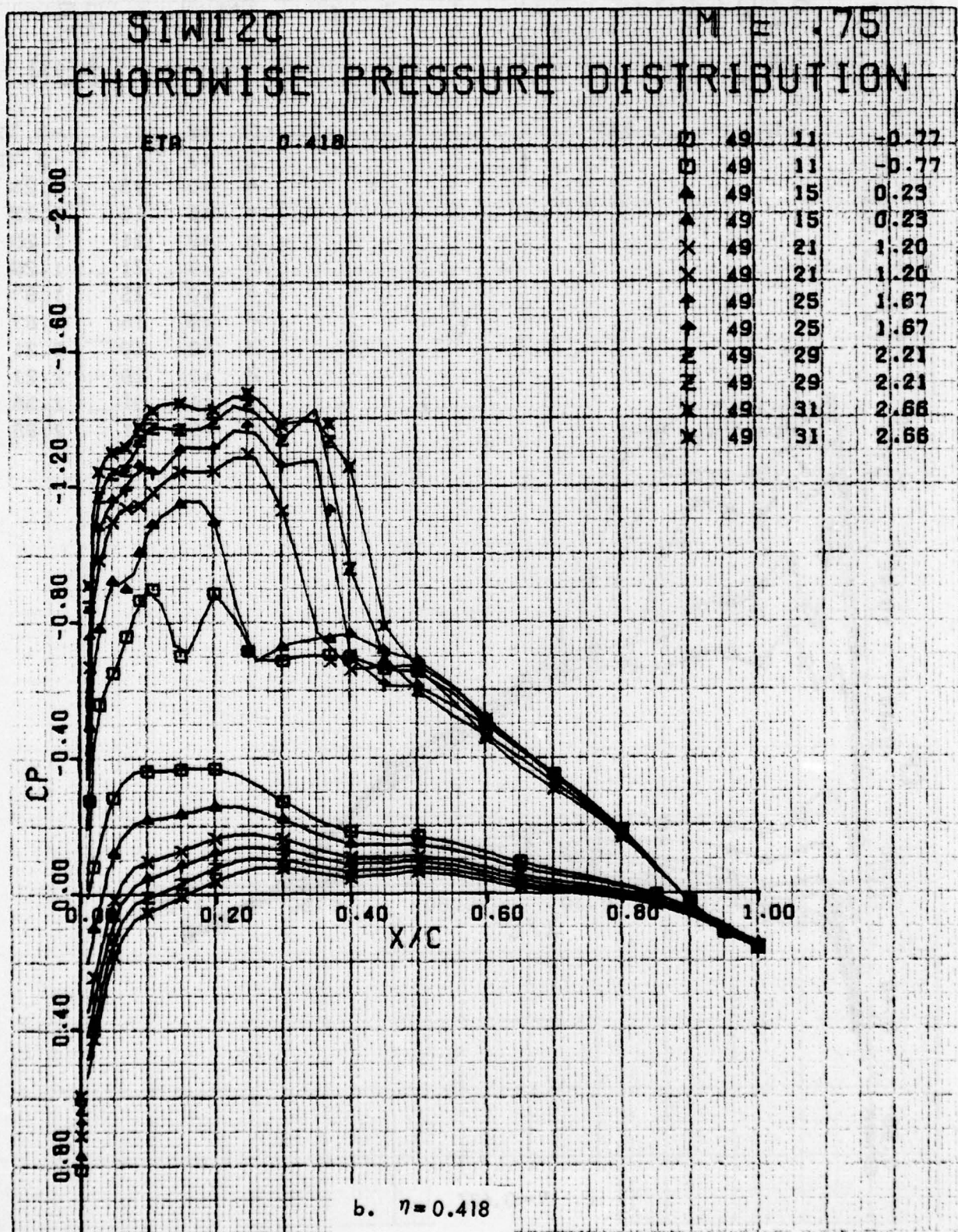


Figure 35. Continued

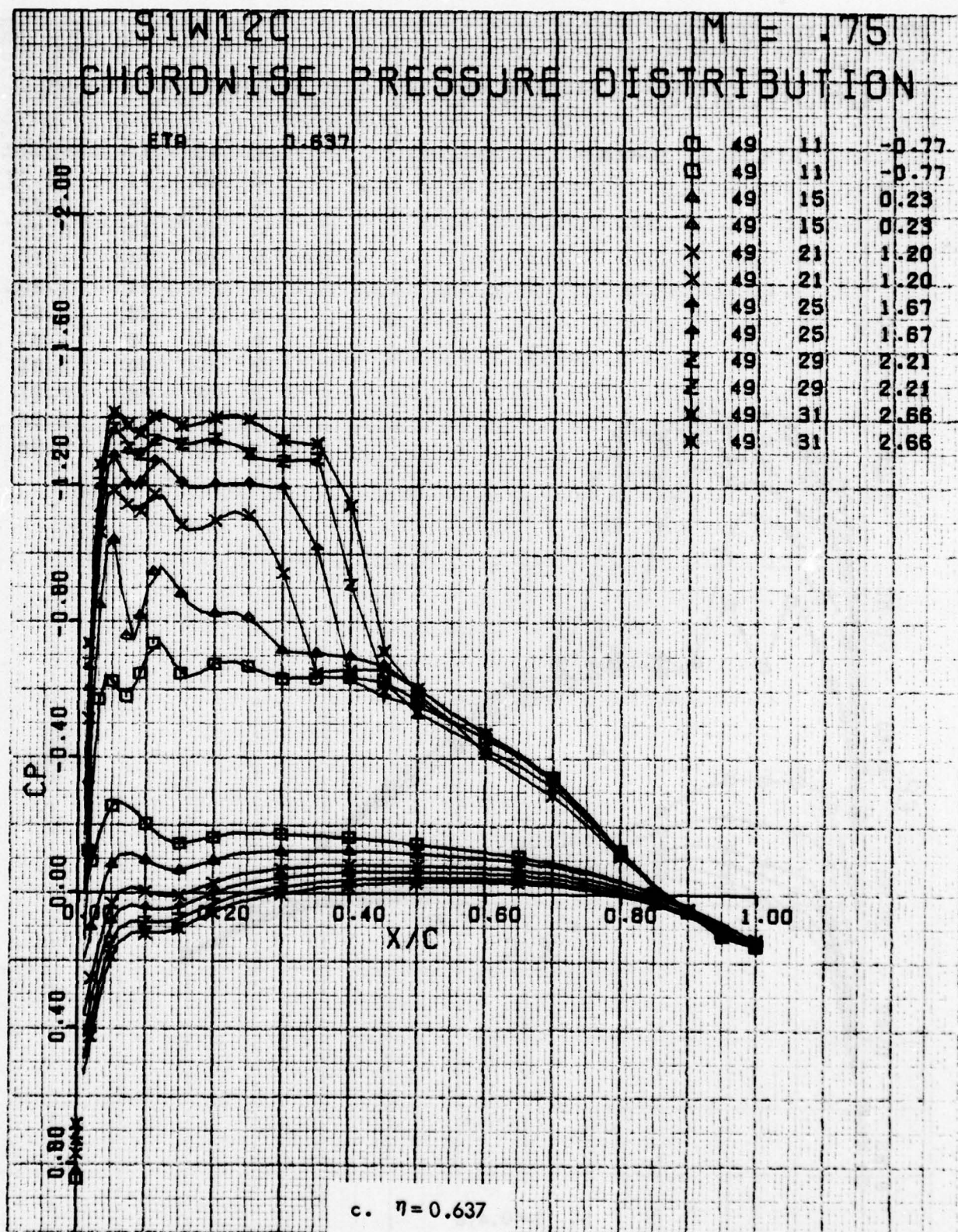


Figure 35. Continued

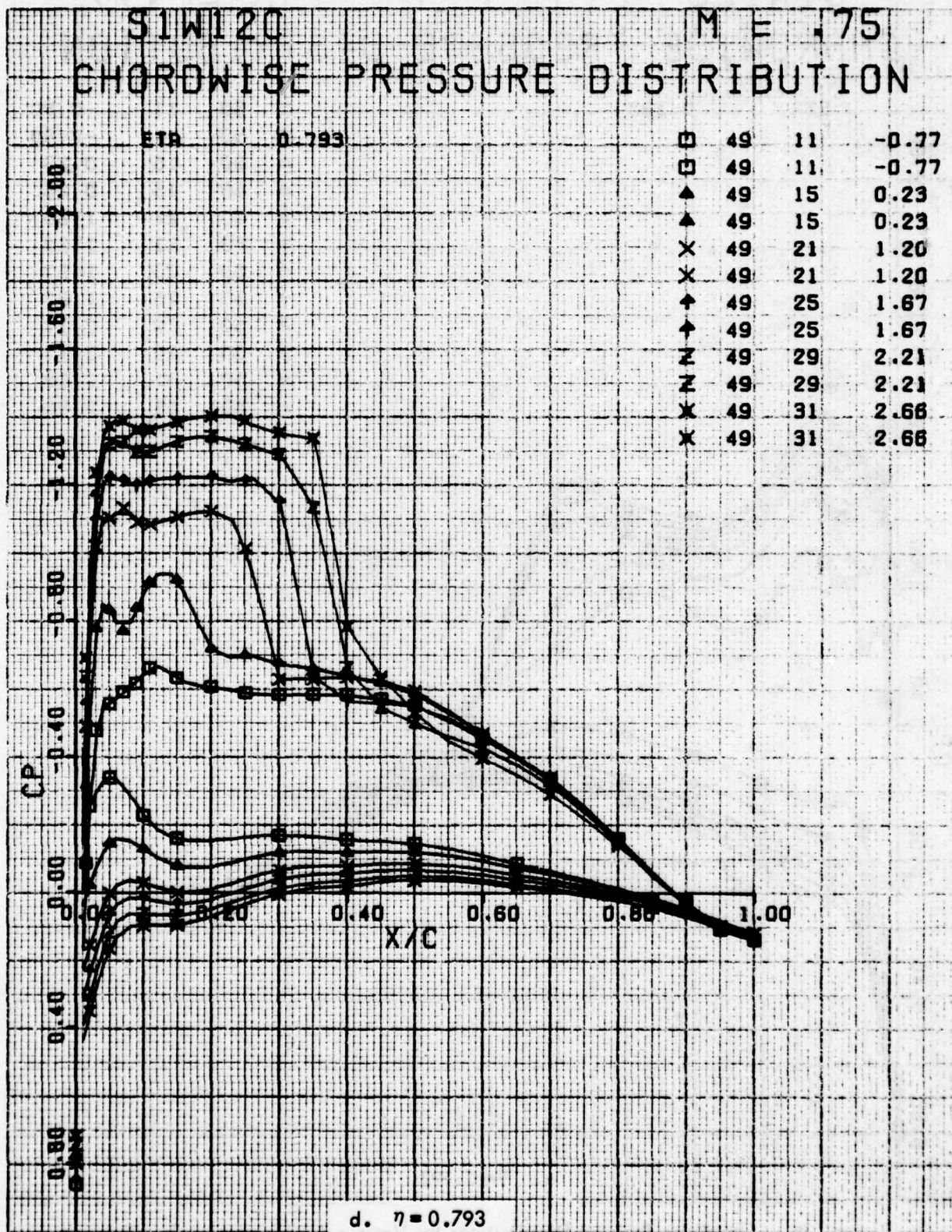


Figure 35. Concluded

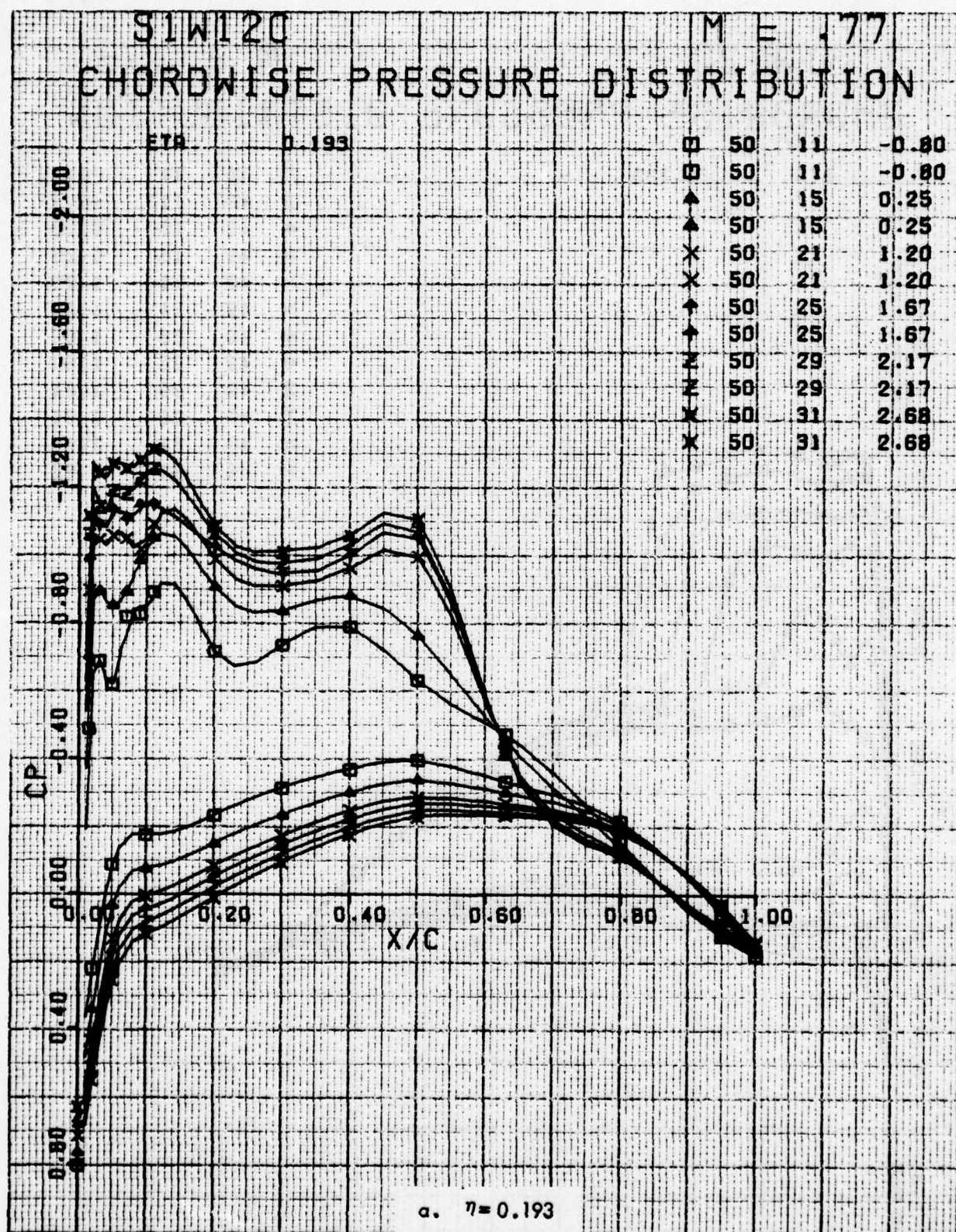


Figure 36. Chordwise Pressure Distributions for Various Angles of Attack. Baseline Leading Edge, Fixed Transition, Grit Code C, $M = 0.77$.

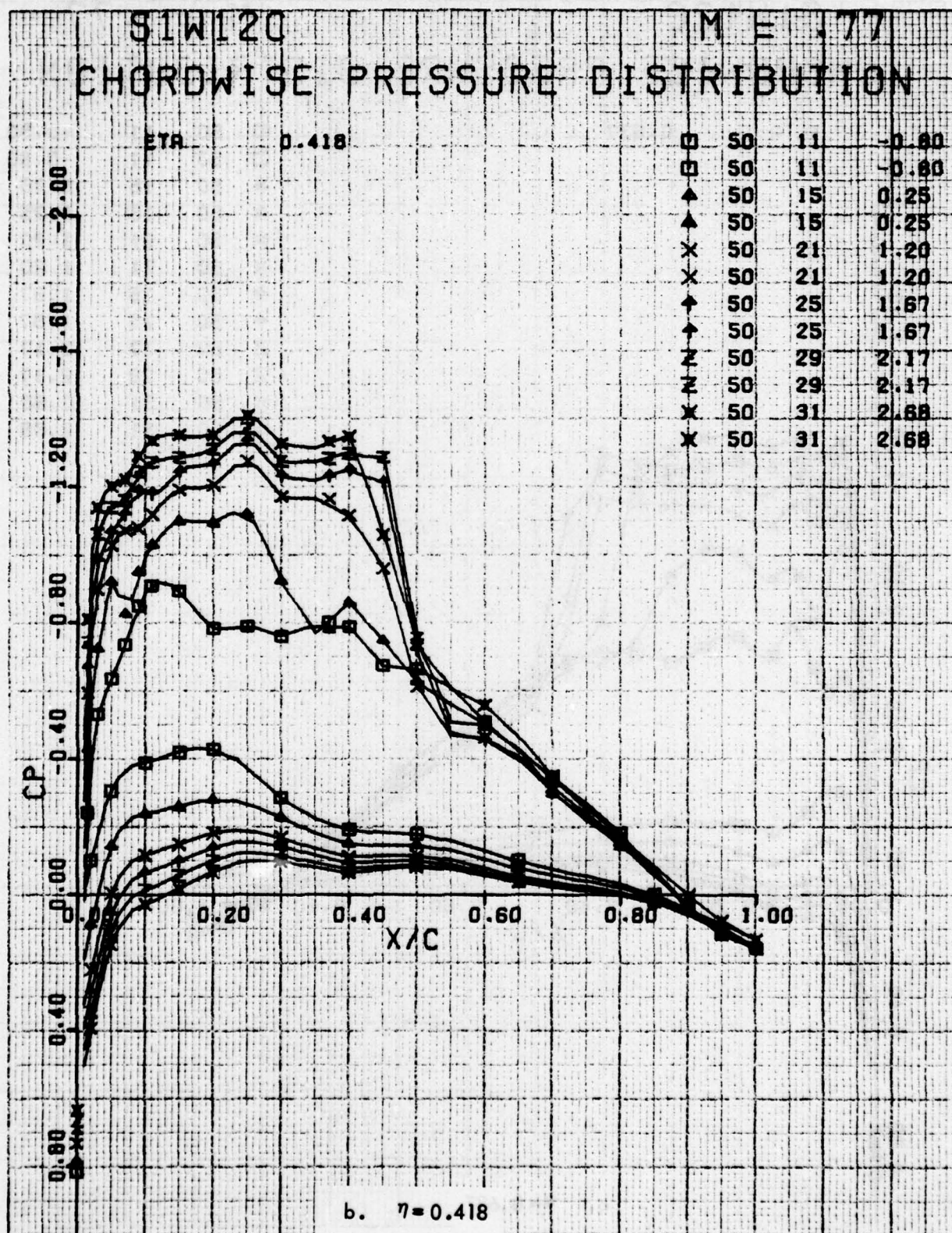


Figure 36. Continued

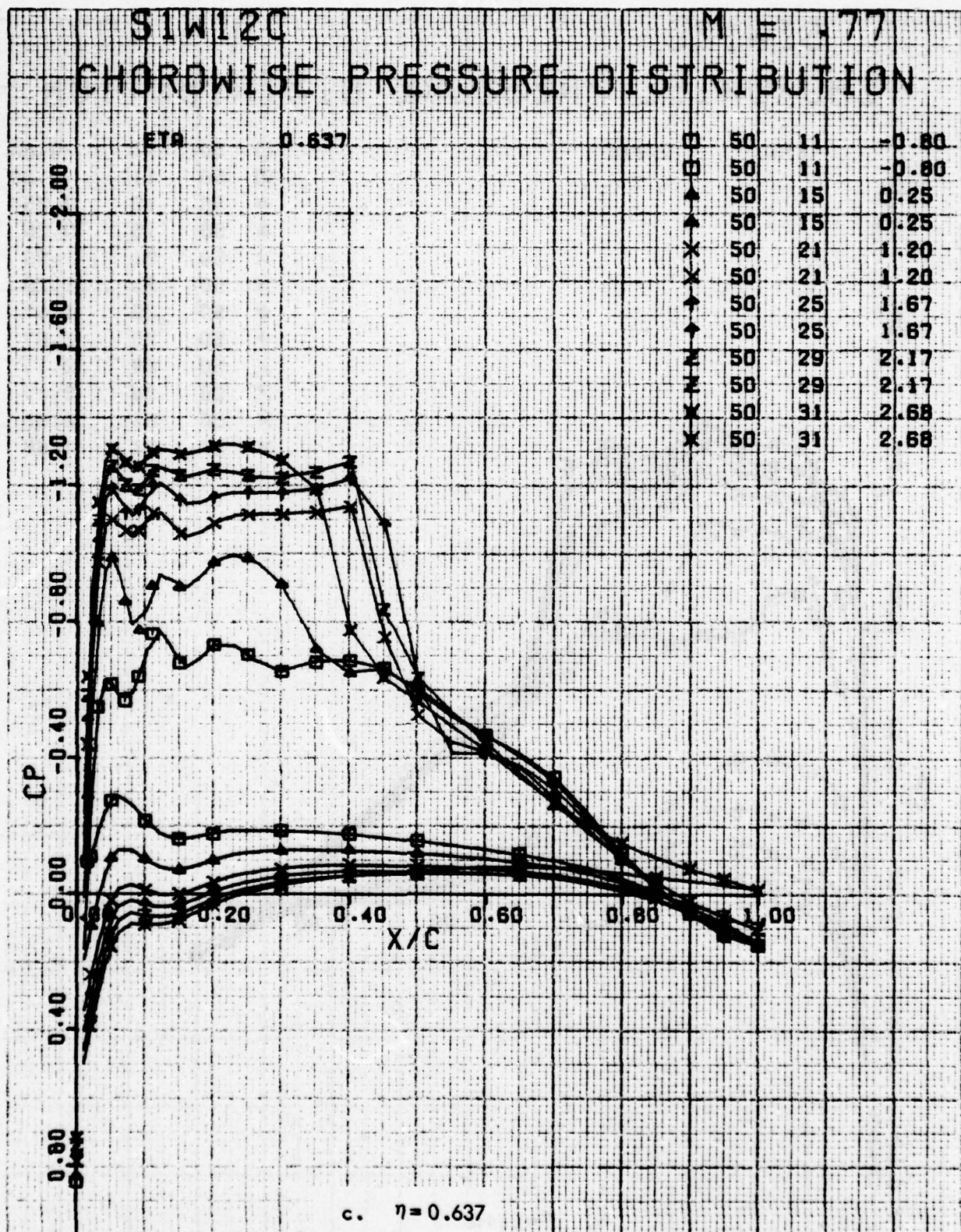


Figure 36. Continued

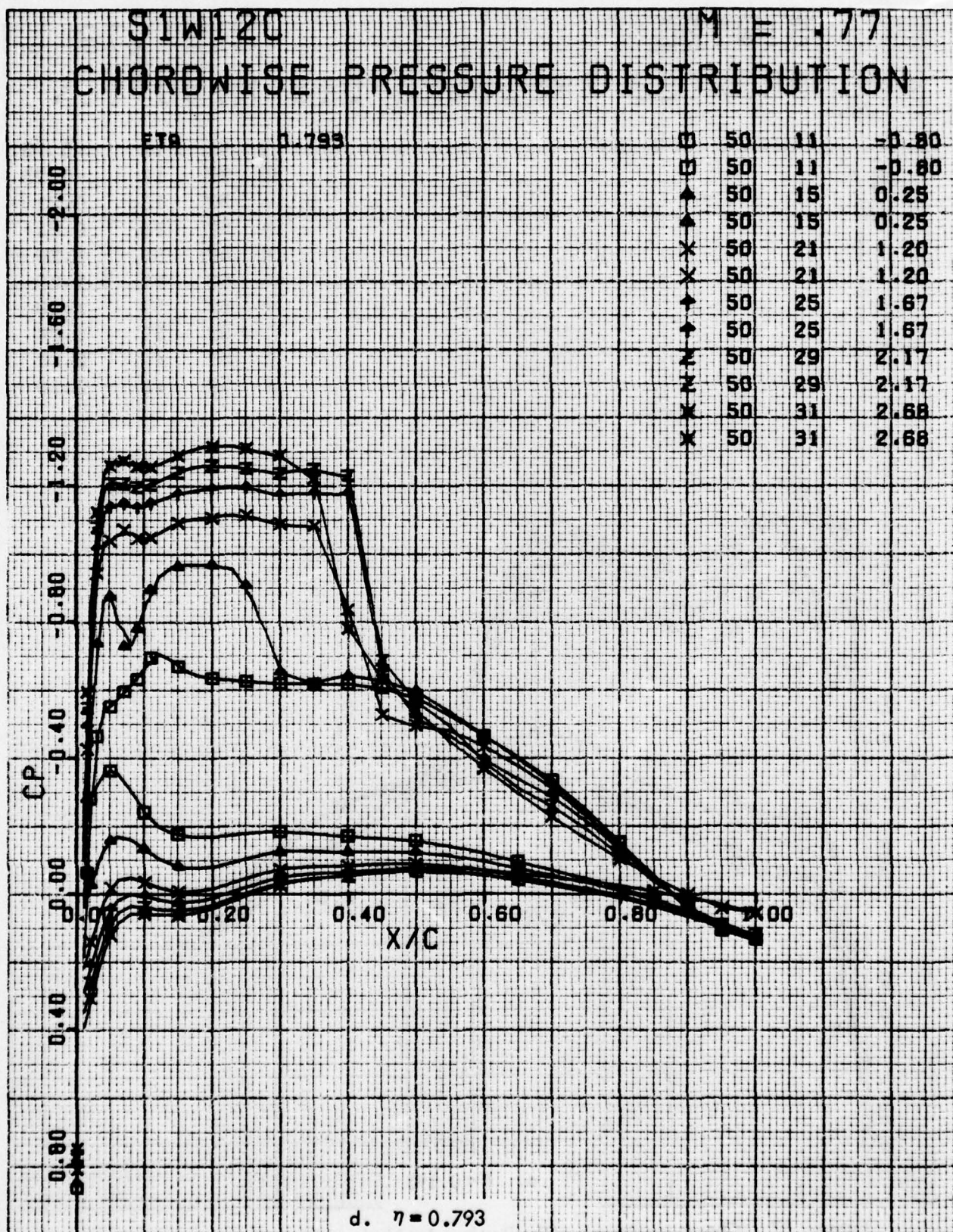


Figure 36. Concluded

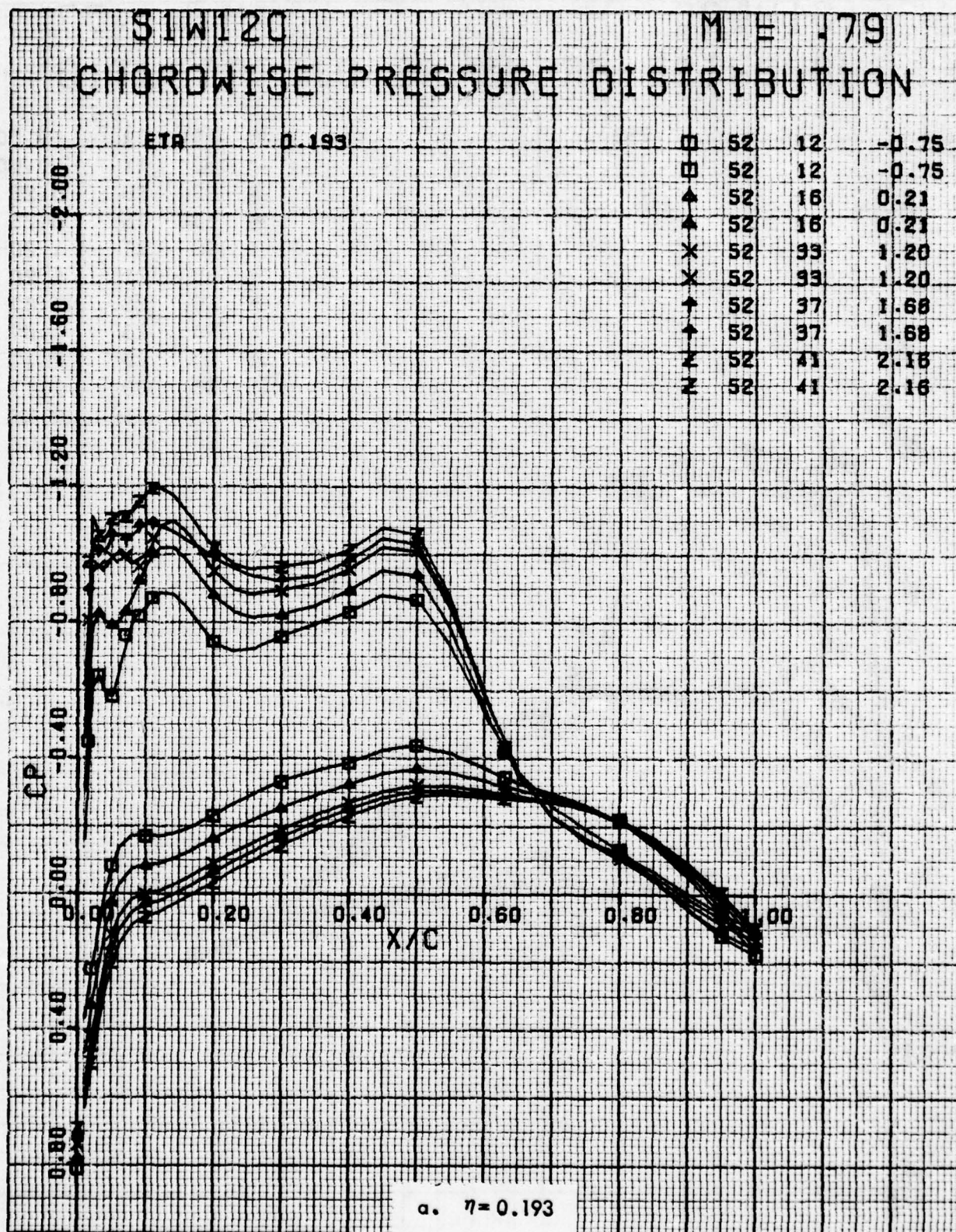


Figure 37. Chordwise Pressure Distributions for Various Angles of Attack. Baseline Leading Edge, Fixed Transition, Grit Code C, $M = 0.79$.

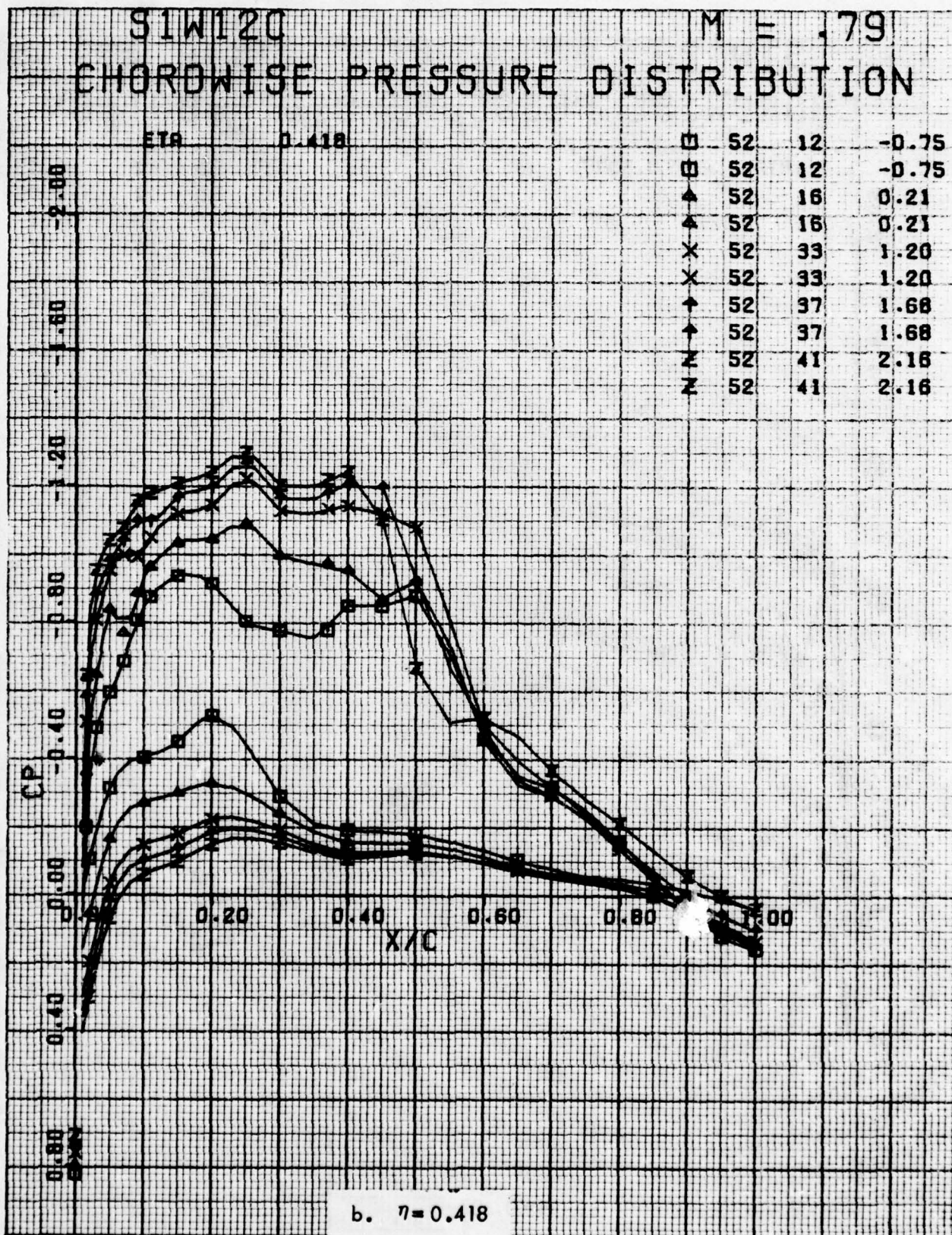


Figure 37. Continued

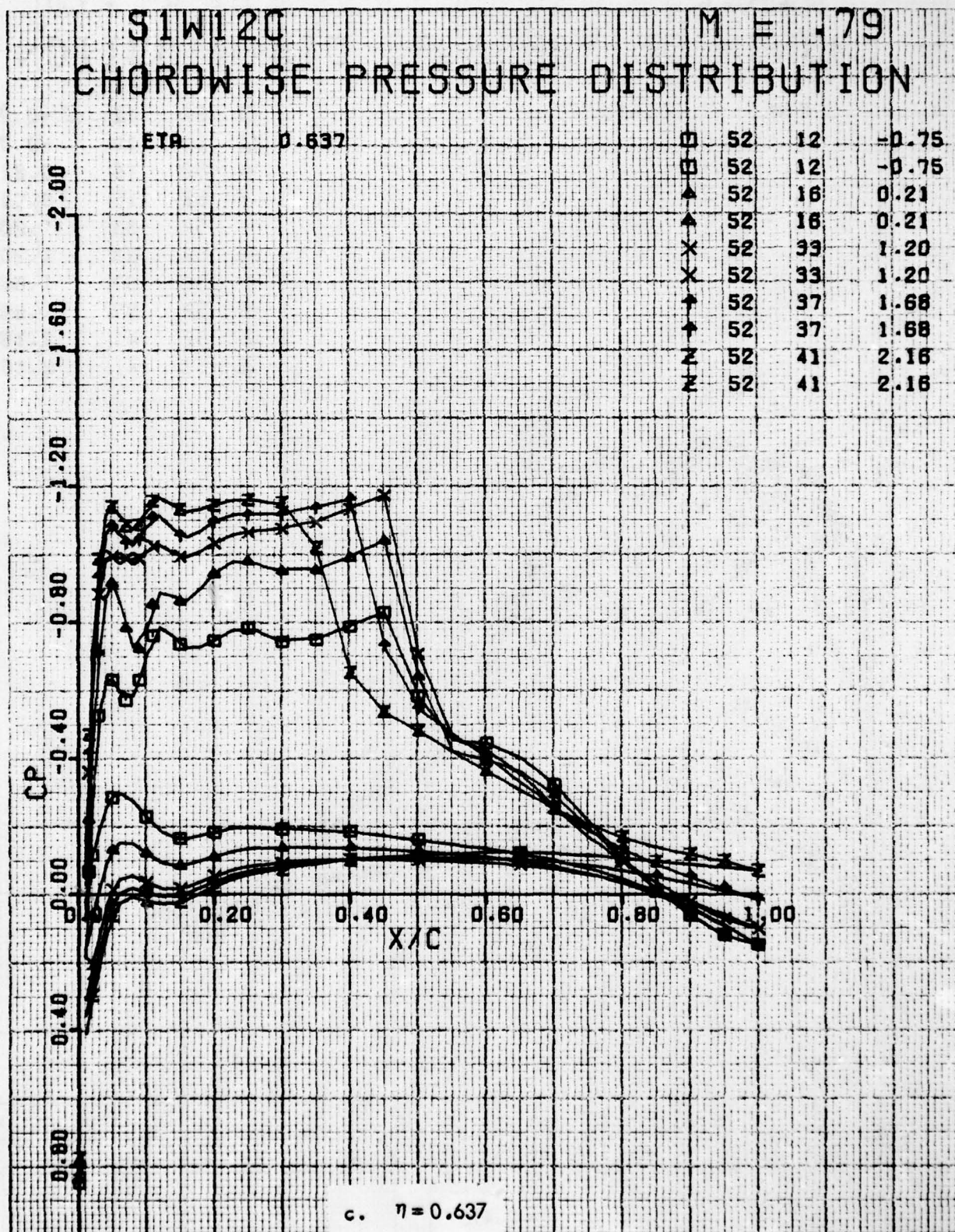


Figure 37. Continued

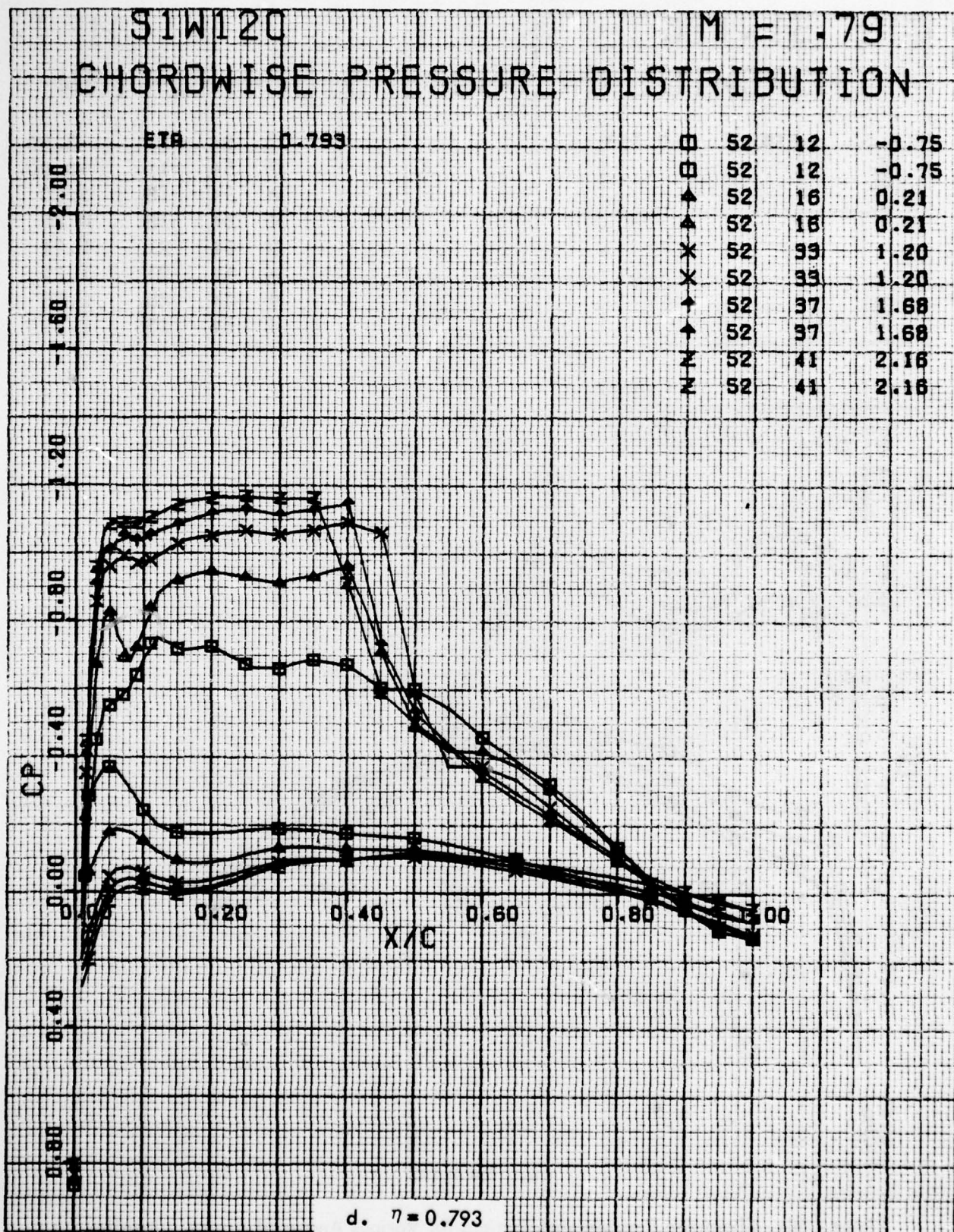


Figure 37. Concluded

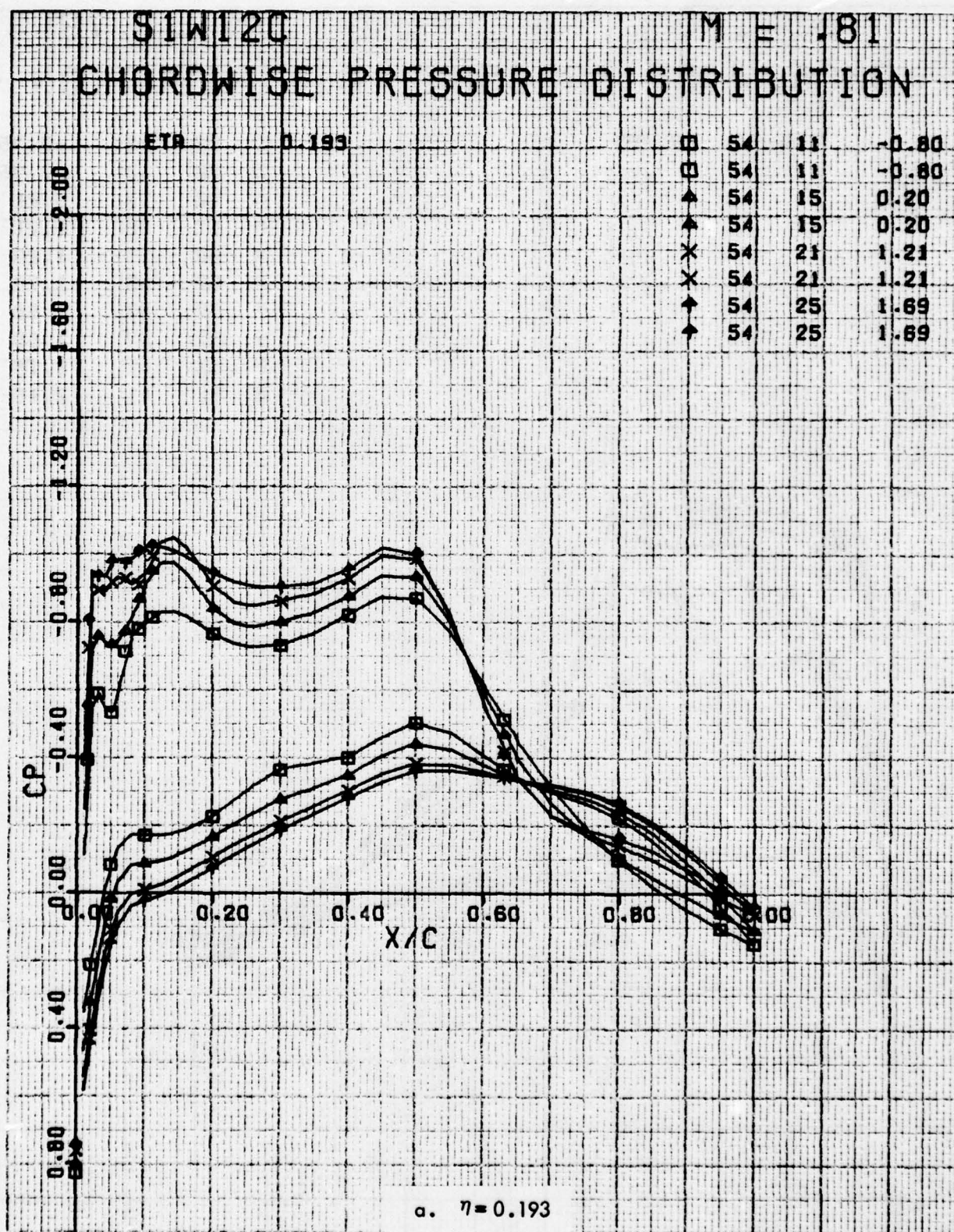


Figure 38. Chordwise Pressure Distributions for Various Angles of Attack. Baseline Leading Edge, Fixed Transition, Grit Code C, $M = 0.81$.

S1W120 M E .81
CHORDWISE PRESSURE DISTRIBUTION

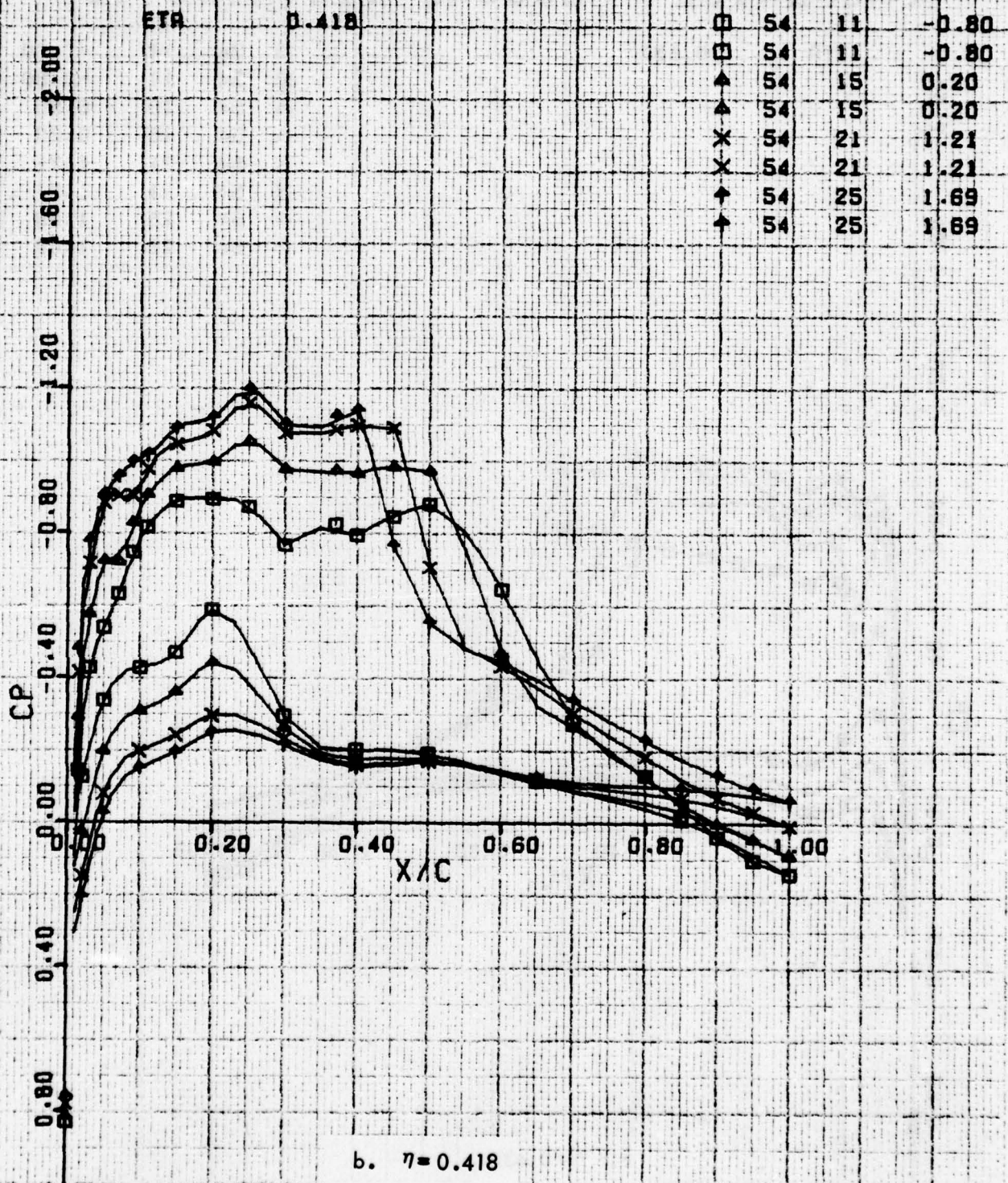


Figure 38. Continued

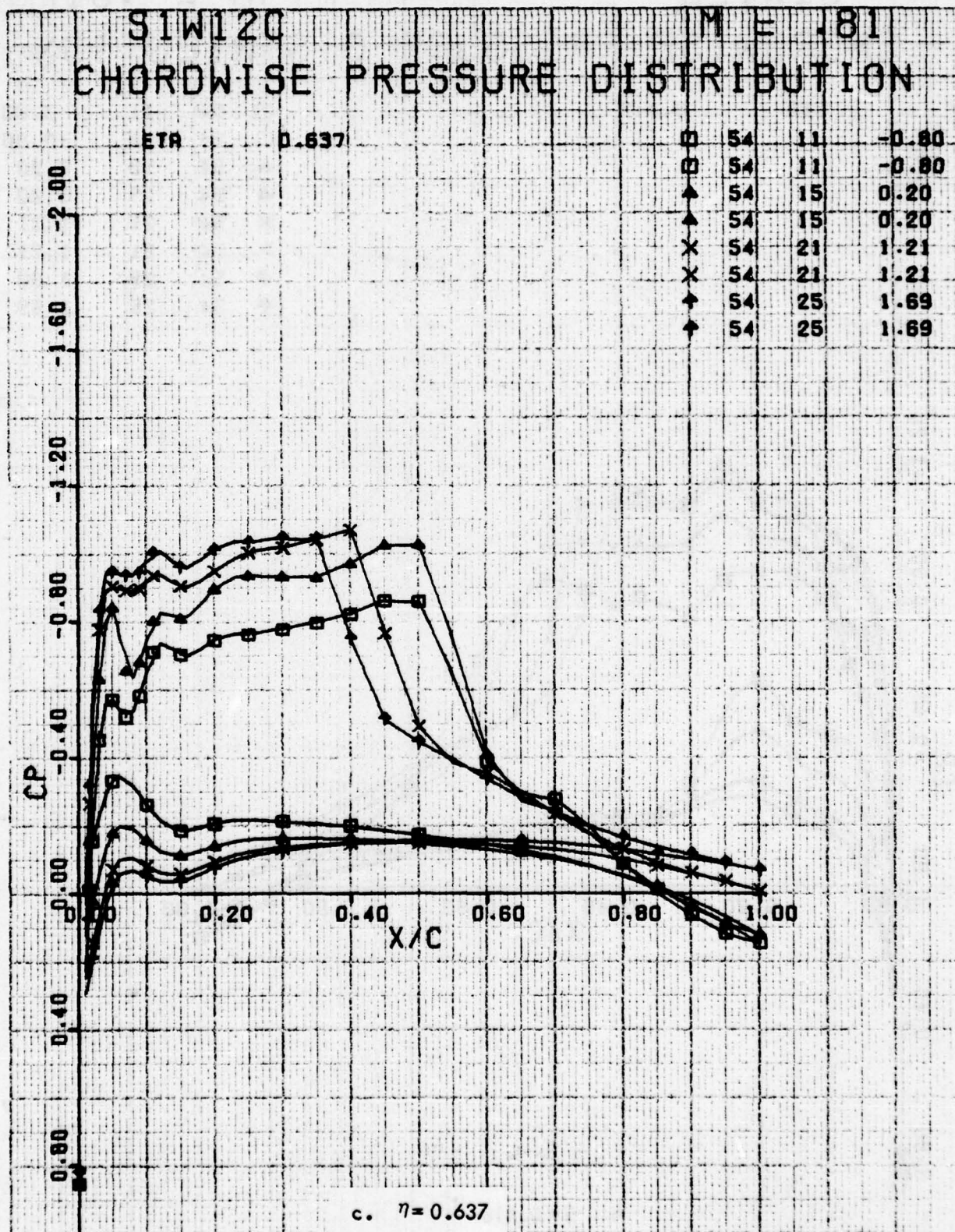


Figure 38. Continued

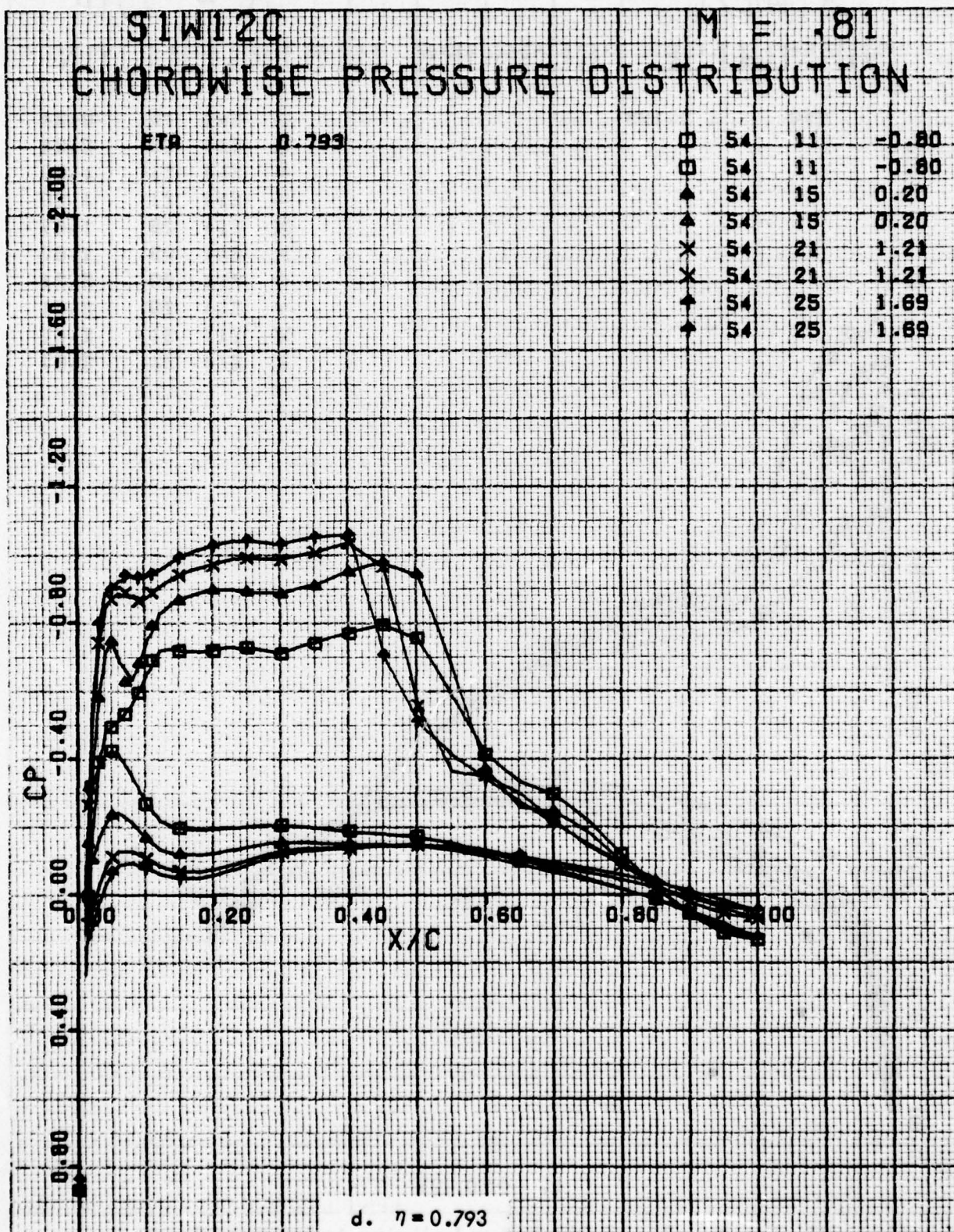


Figure 38. Concluded

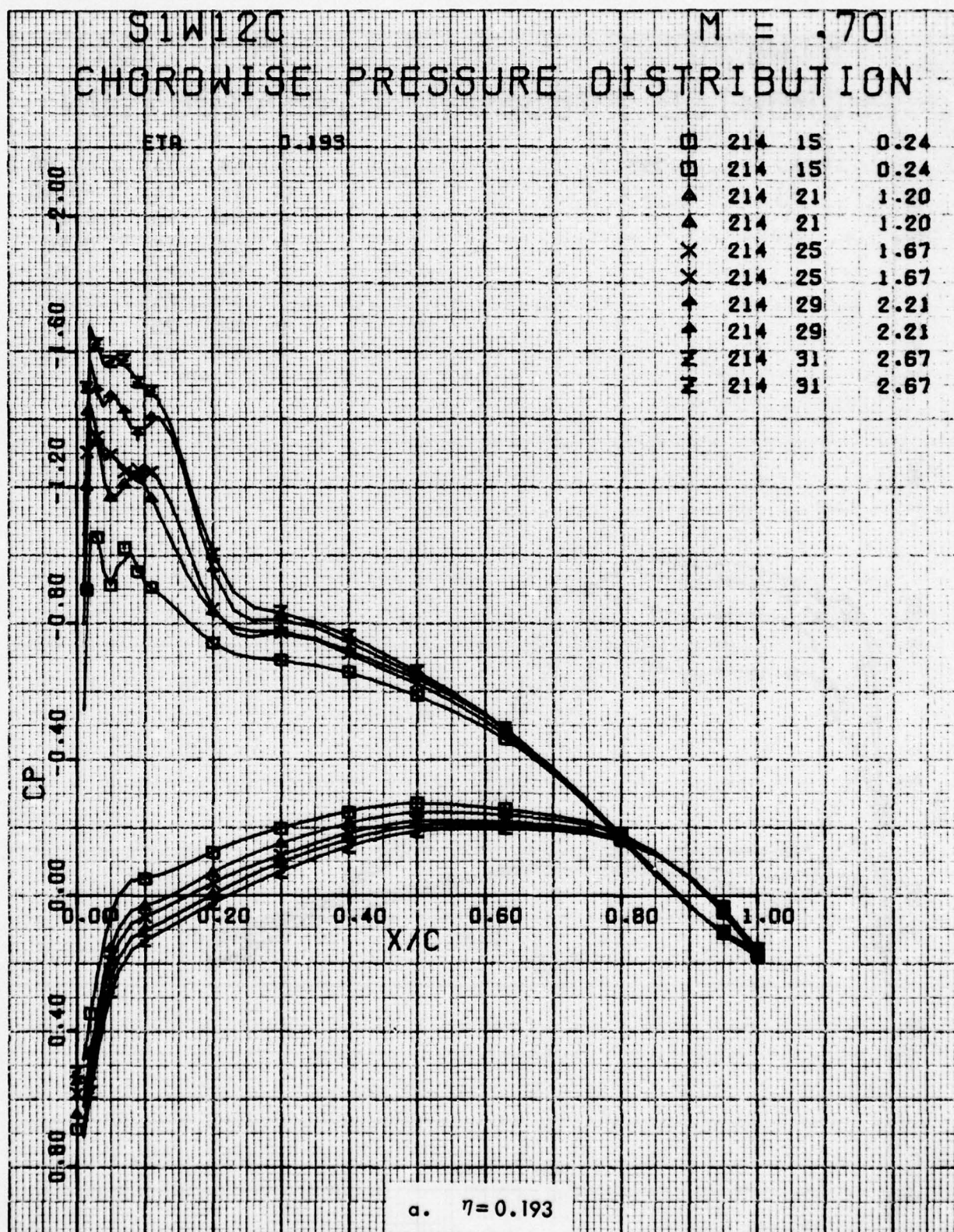


Figure 39. Chordwise Pressure Distributions for Various Angles of Attack. Baseline Leading Edge, Fixed Transition, Grit Code D, $M = 0.7$.

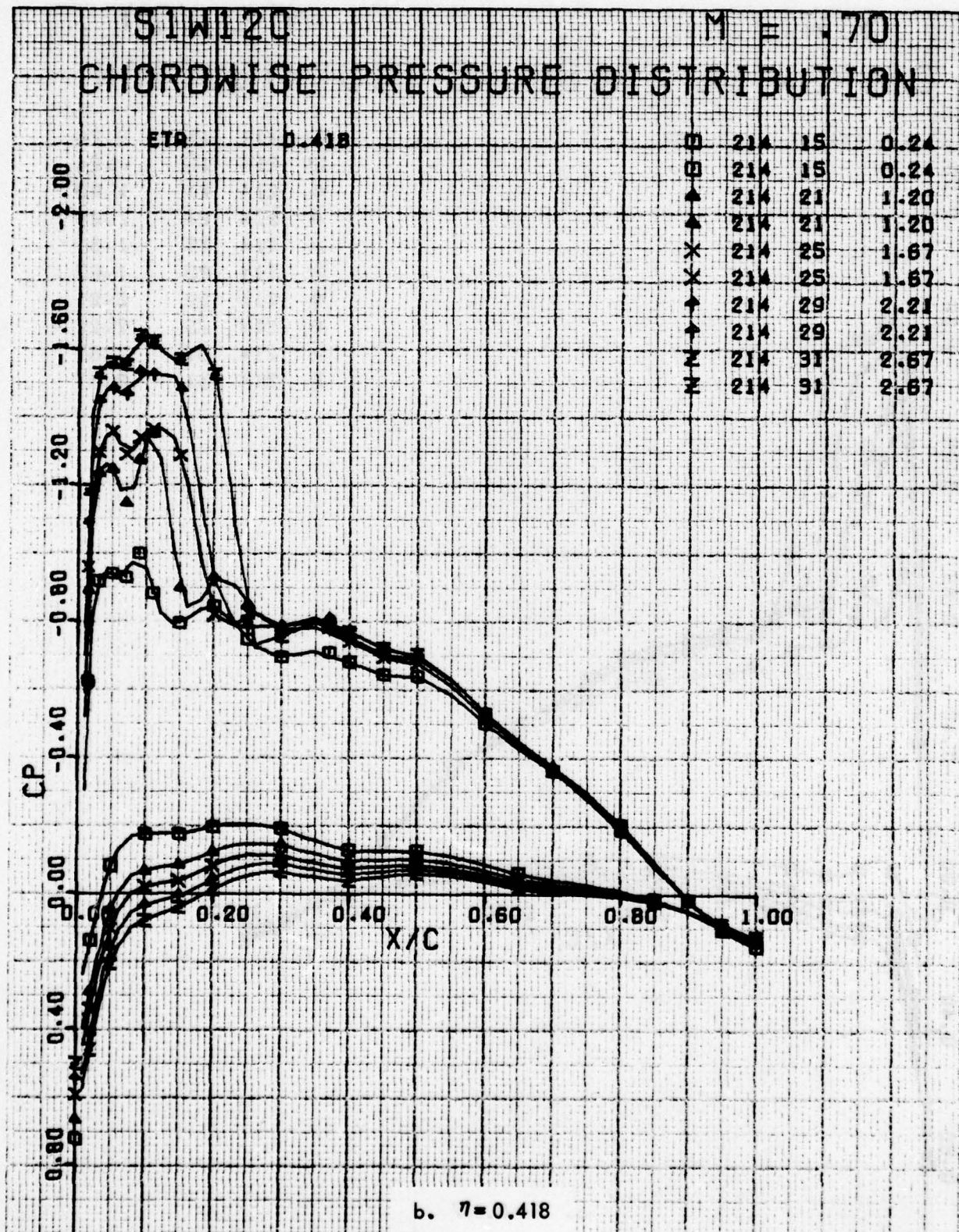


Figure 39. Continued

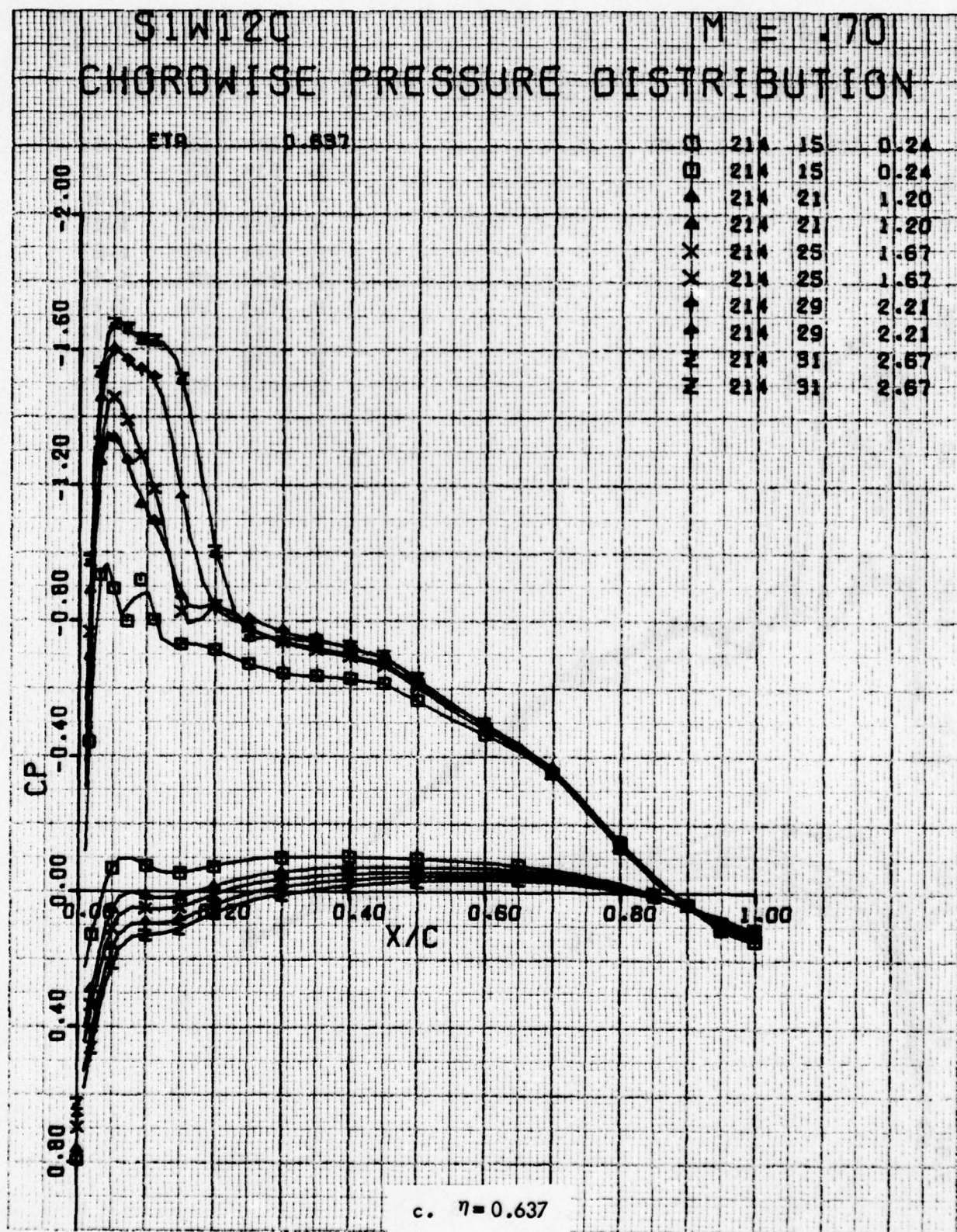


Figure 39. Continued

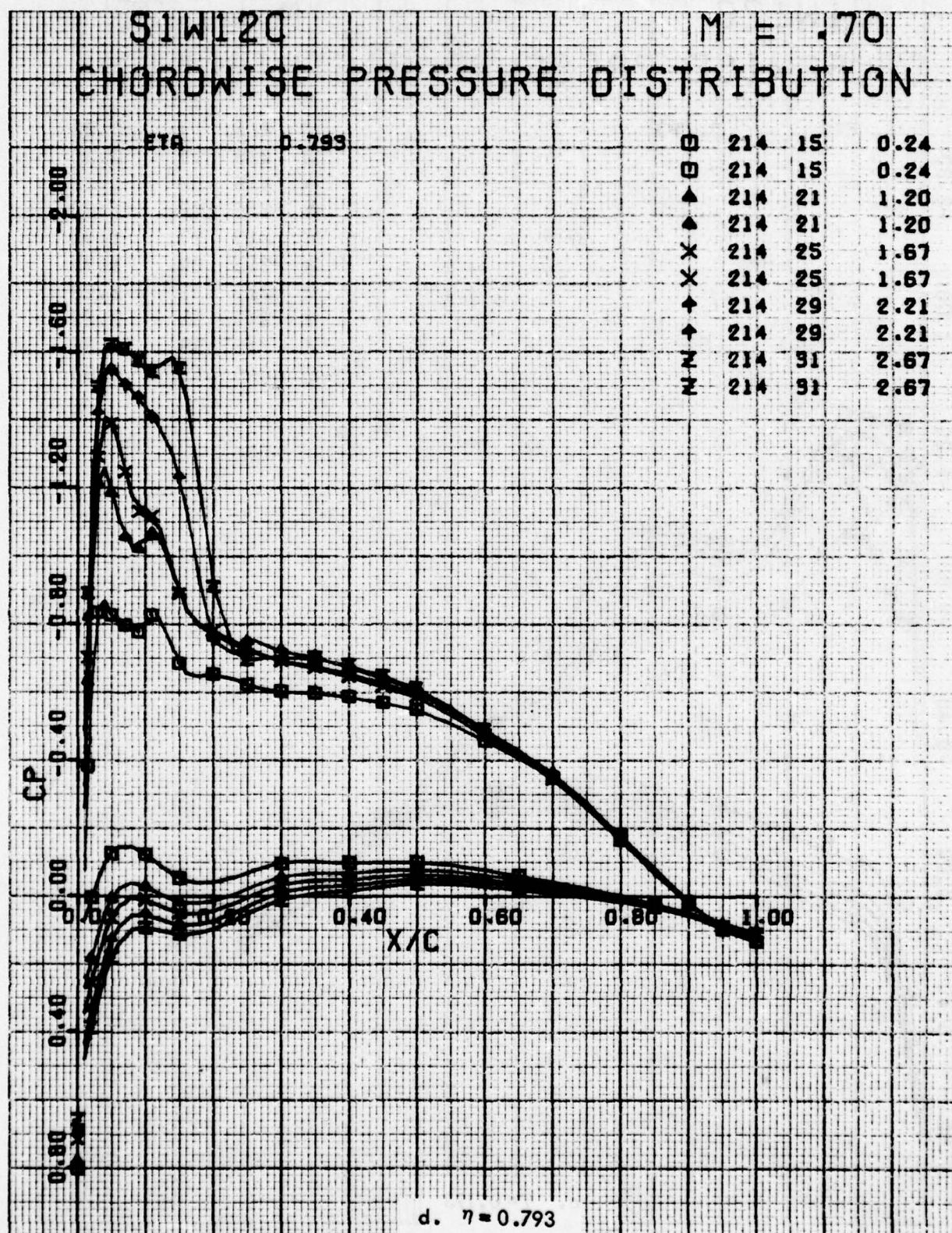


Figure 39. Concluded

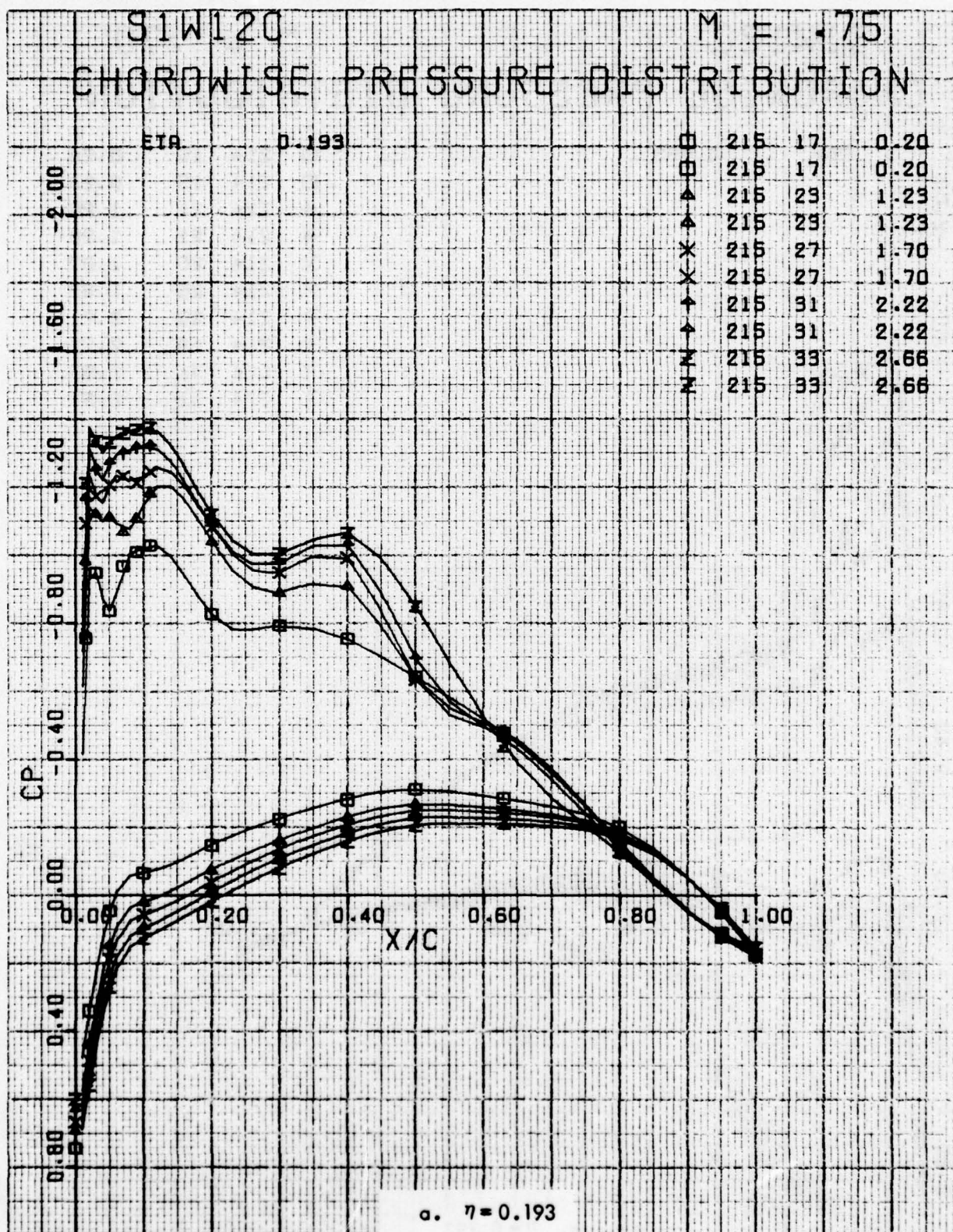


Figure 40. Chordwise Pressure Distributions for Various Angles of Attack. Baseline Leading Edge, Fixed Transition, Grit Code D, $M = 0.75$.

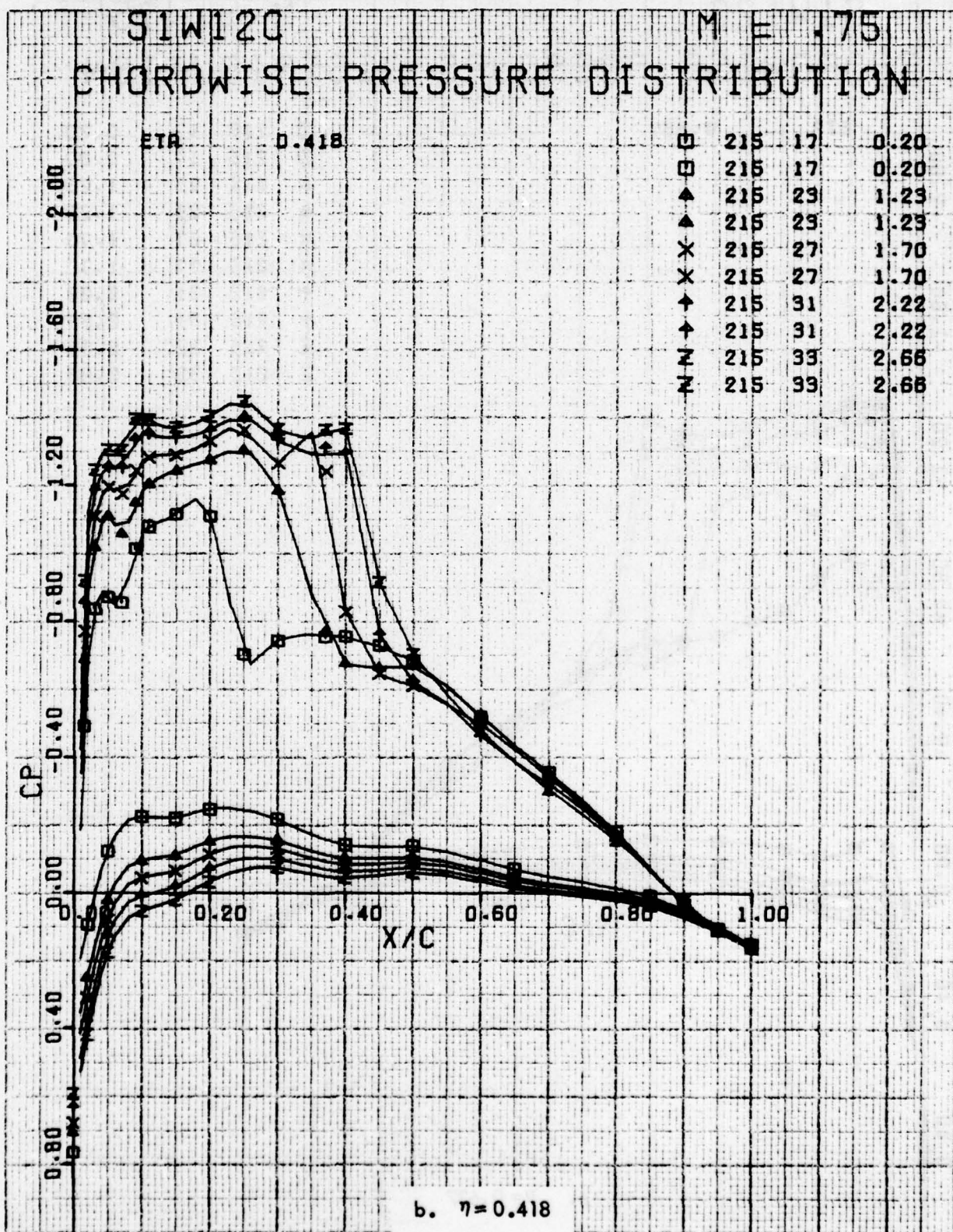


Figure 40. Continued

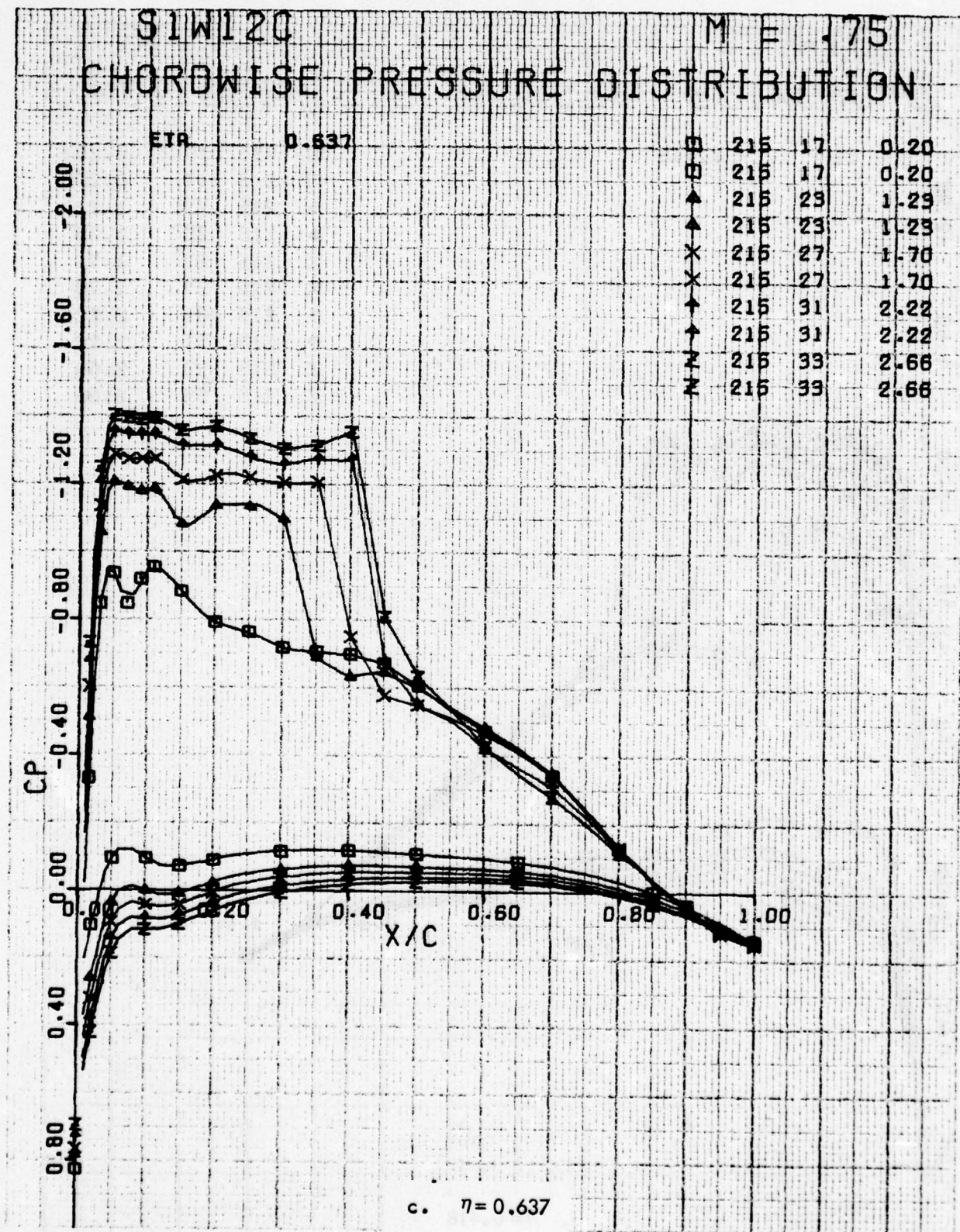


Figure 40. Continued

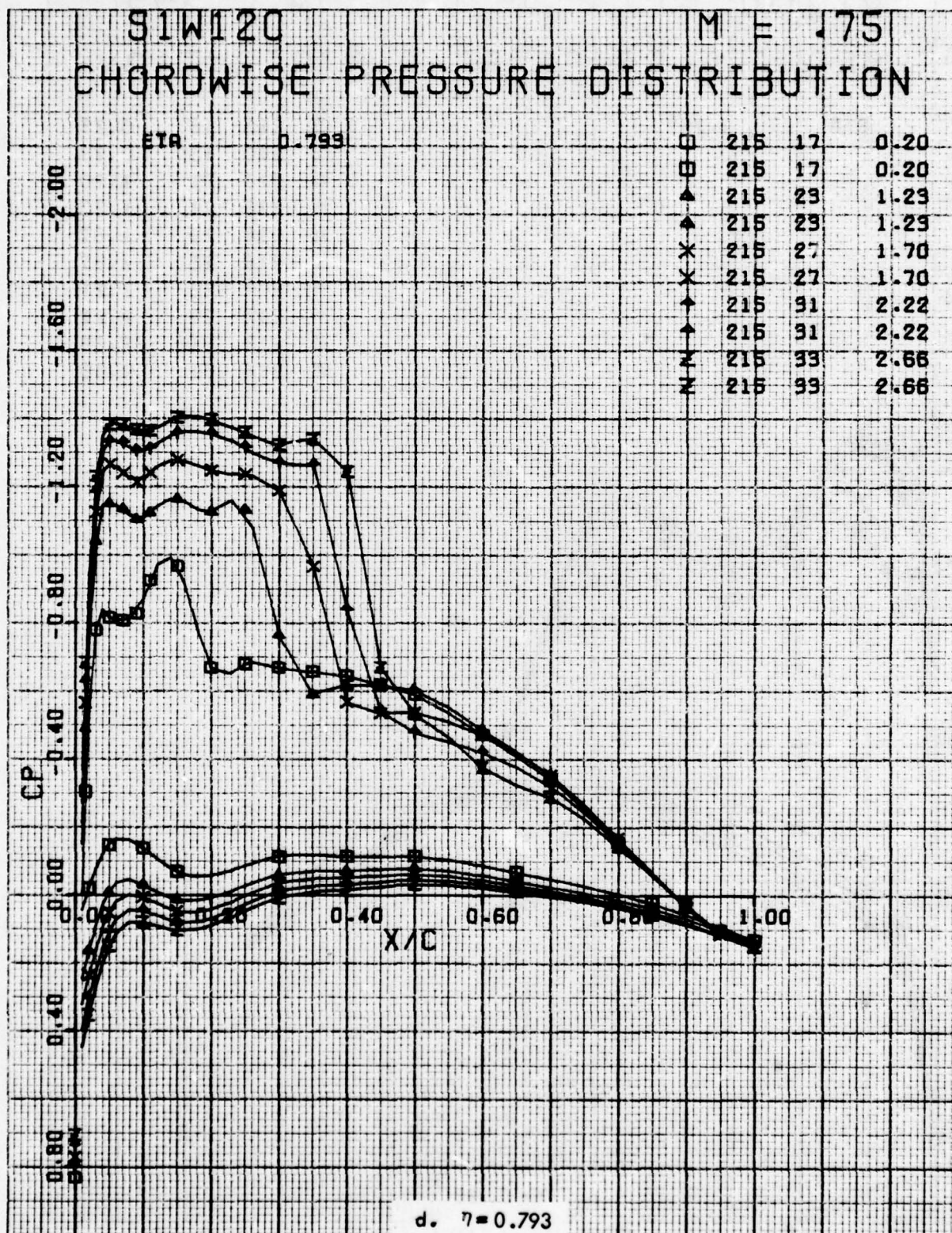


Figure 40. Concluded

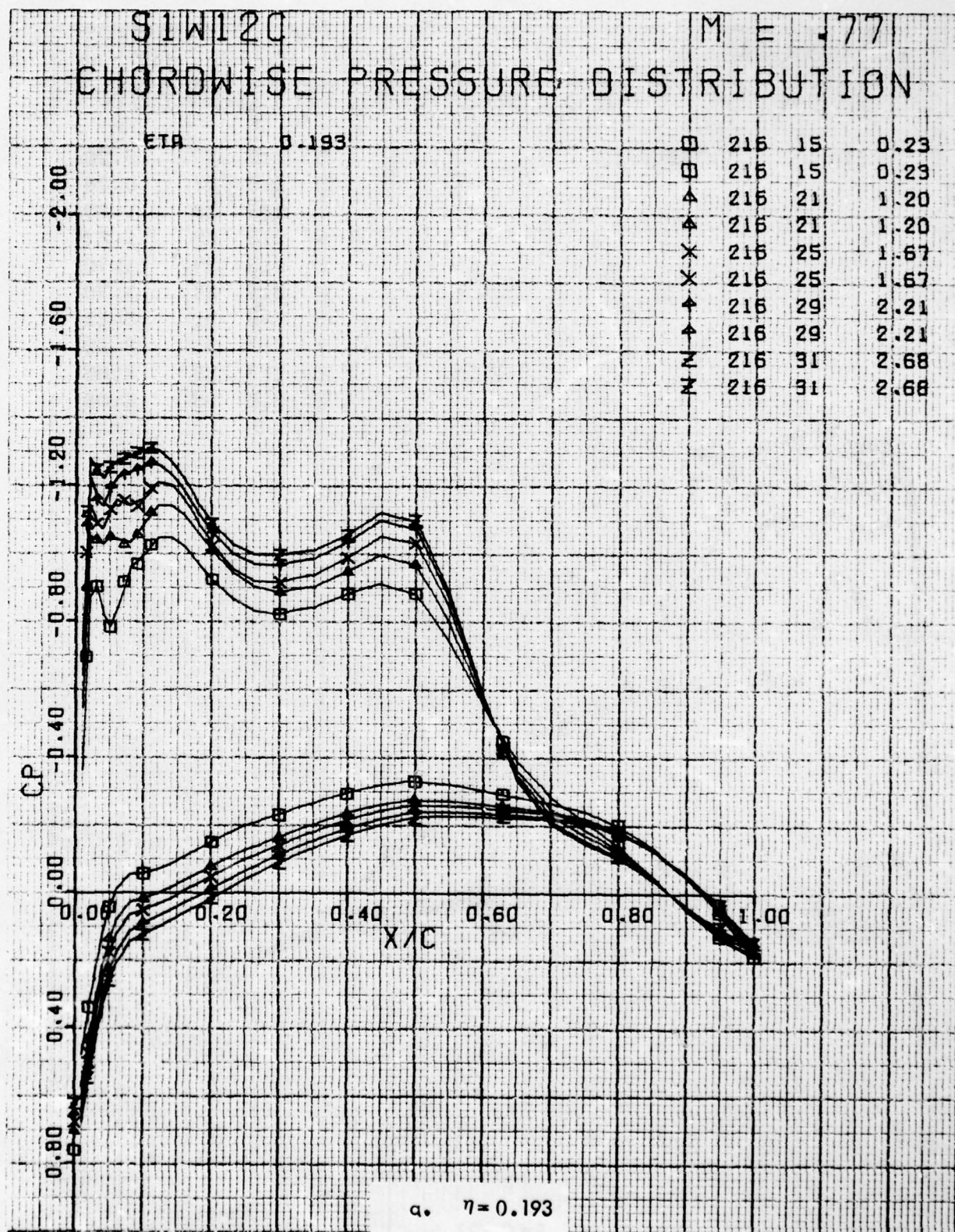


Figure 41. Chordwise Pressure Distributions for Various Angles of Attack. Baseline Leading Edge, Fixed Transition, Grit Code D, M = 0.77.

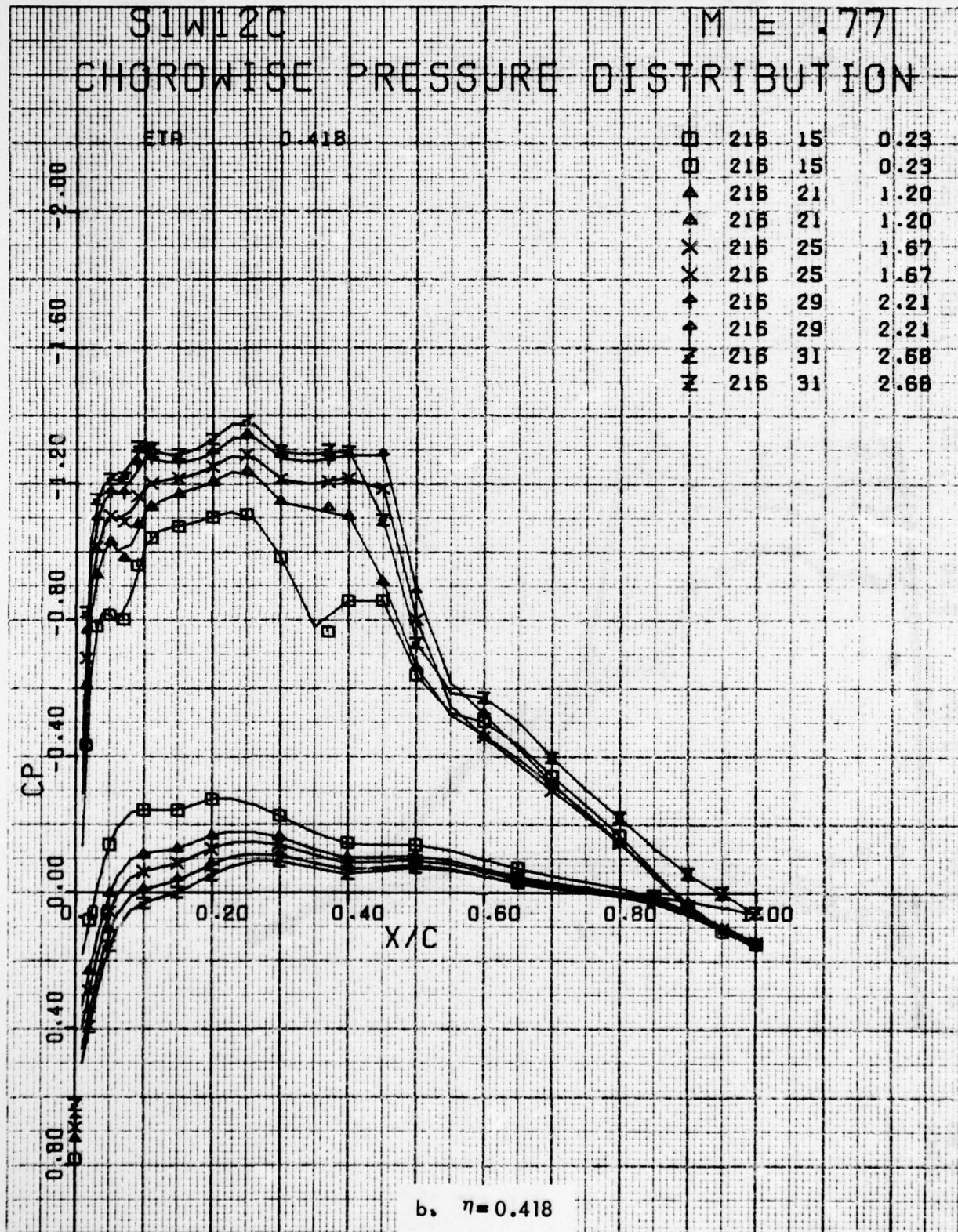


Figure 41. Continued

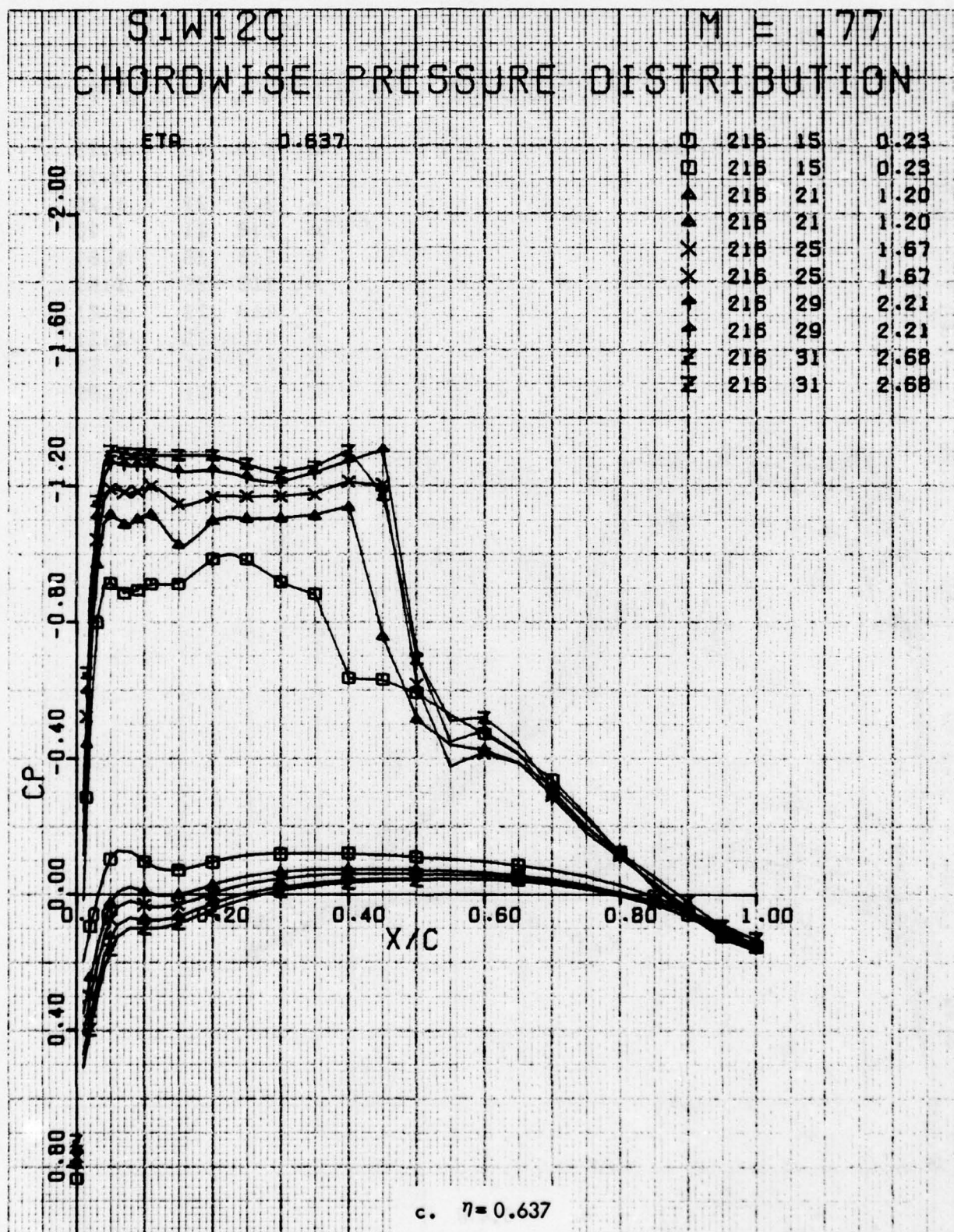


Figure 41. Continued

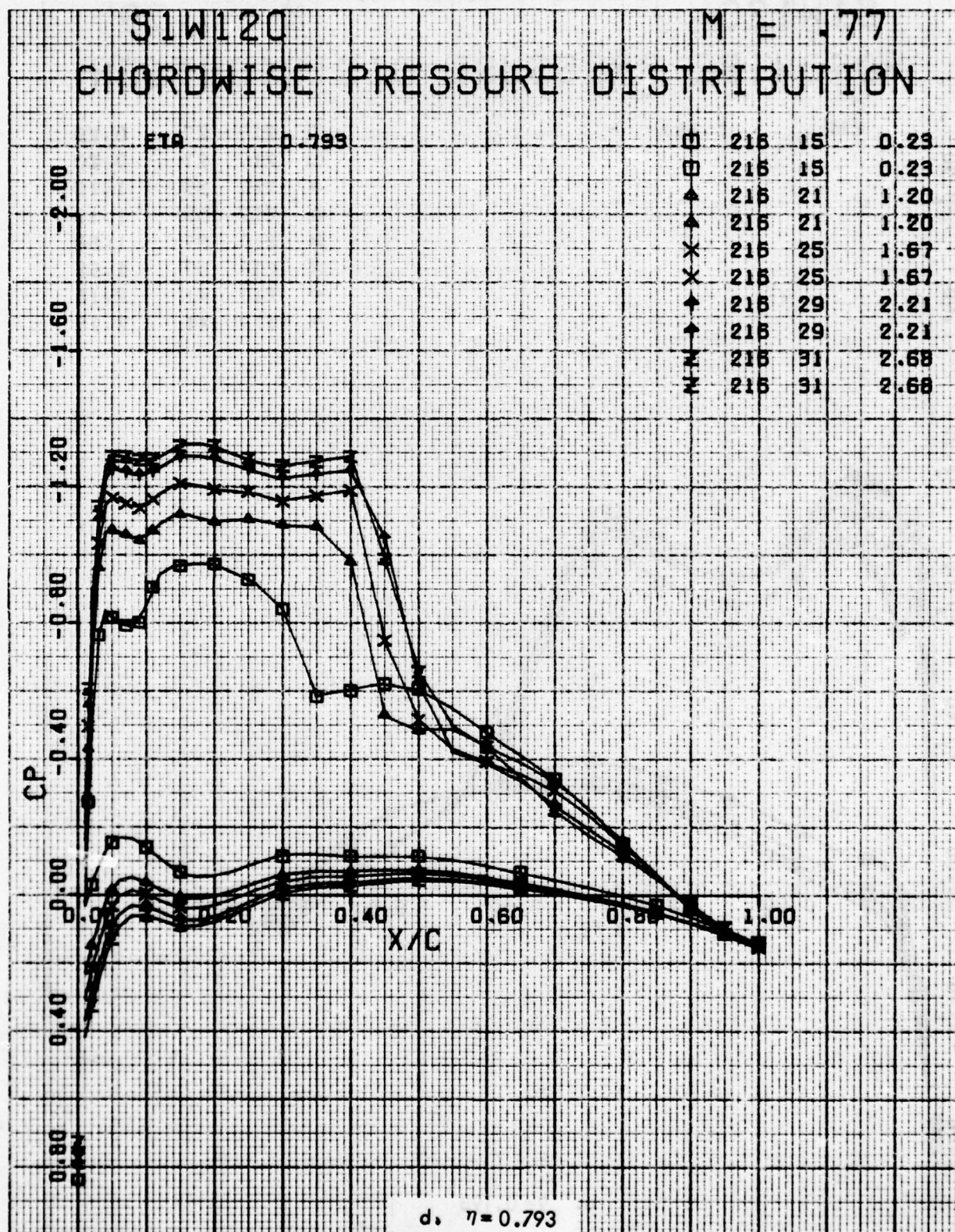


Figure 41. Concluded

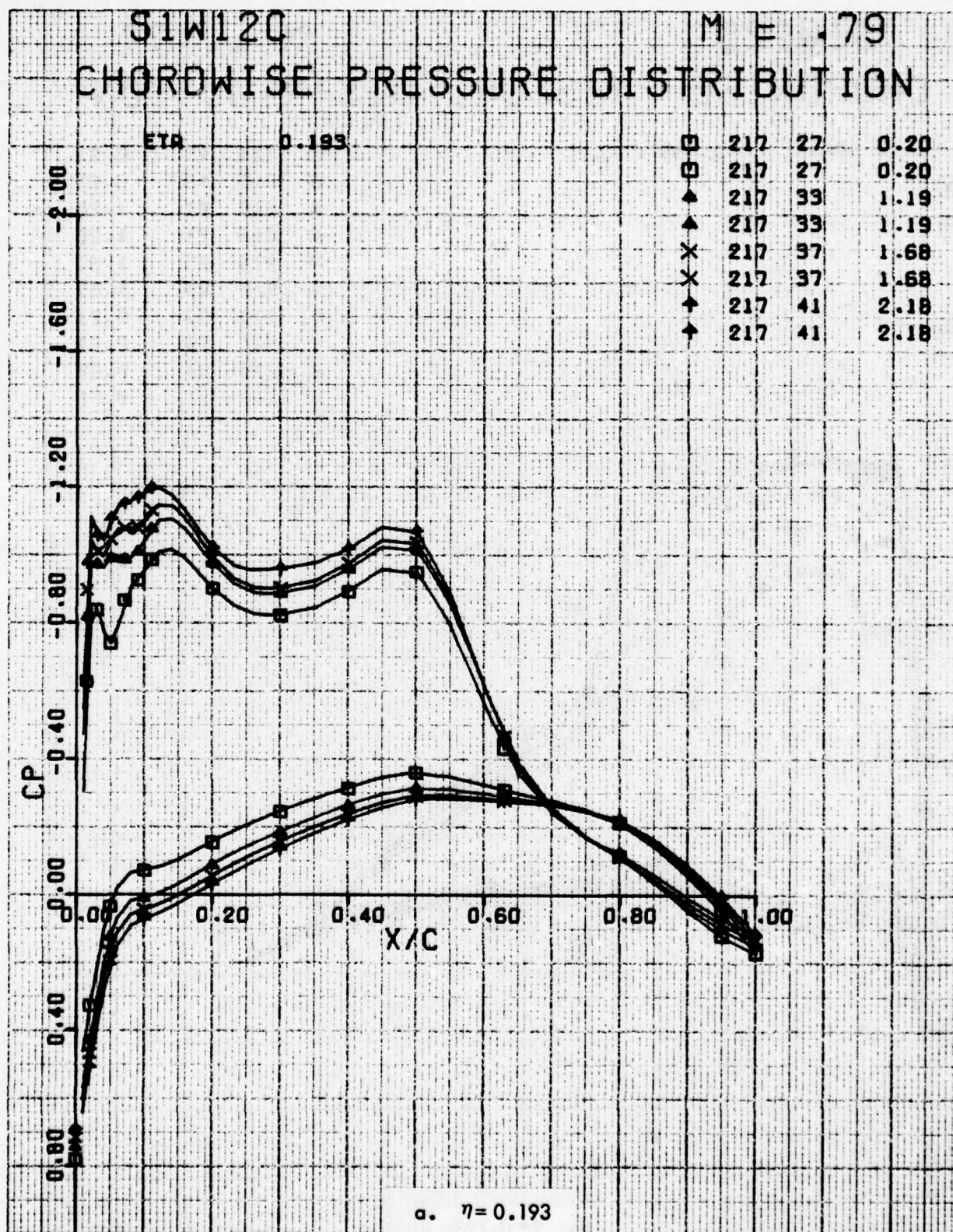


Figure 42. Chordwise Pressure Distributions for Various Angles of Attack. Baseline Leading Edge, Fixed Transition, Grit Code D, $M = 0.79$.

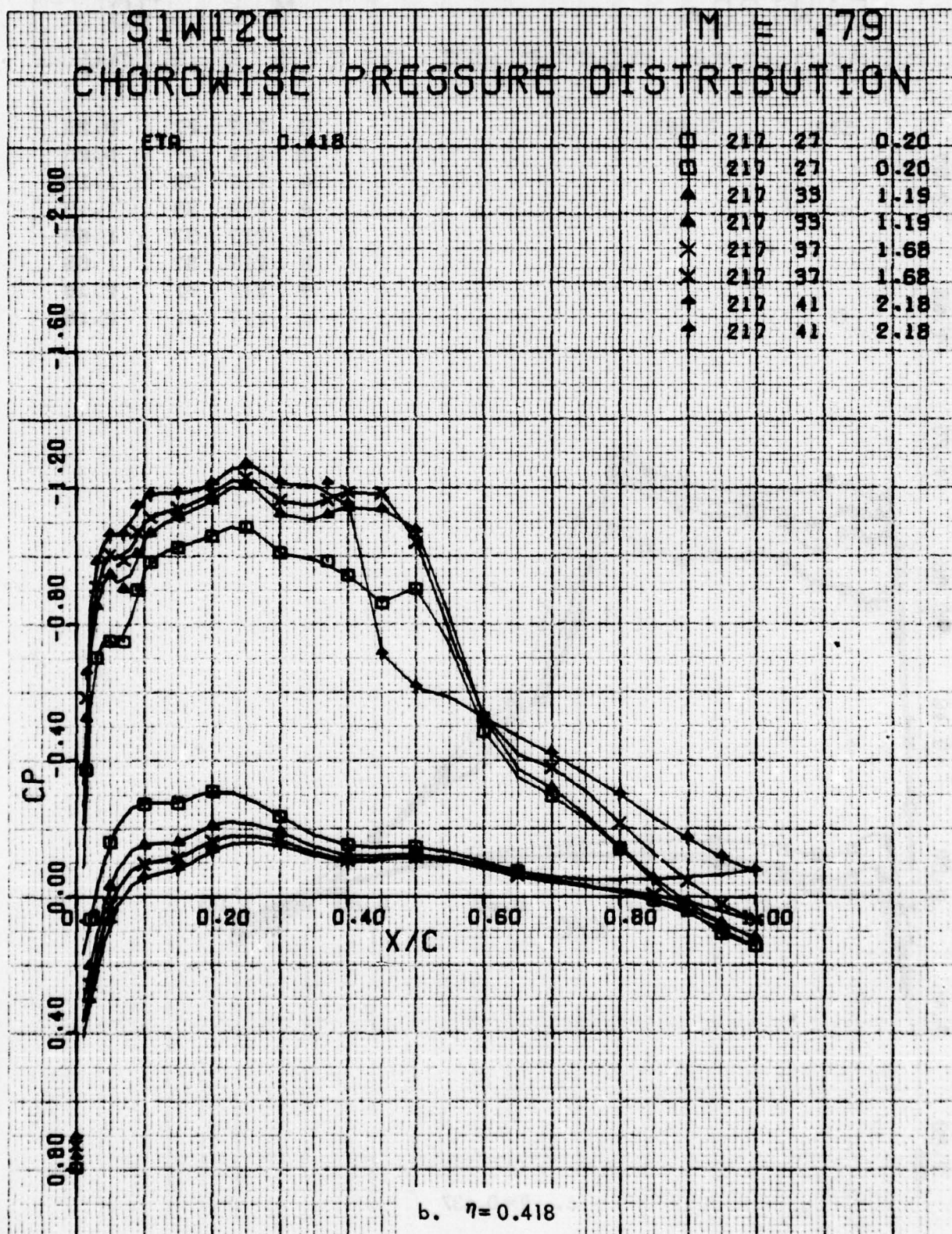


Figure 42. Continued

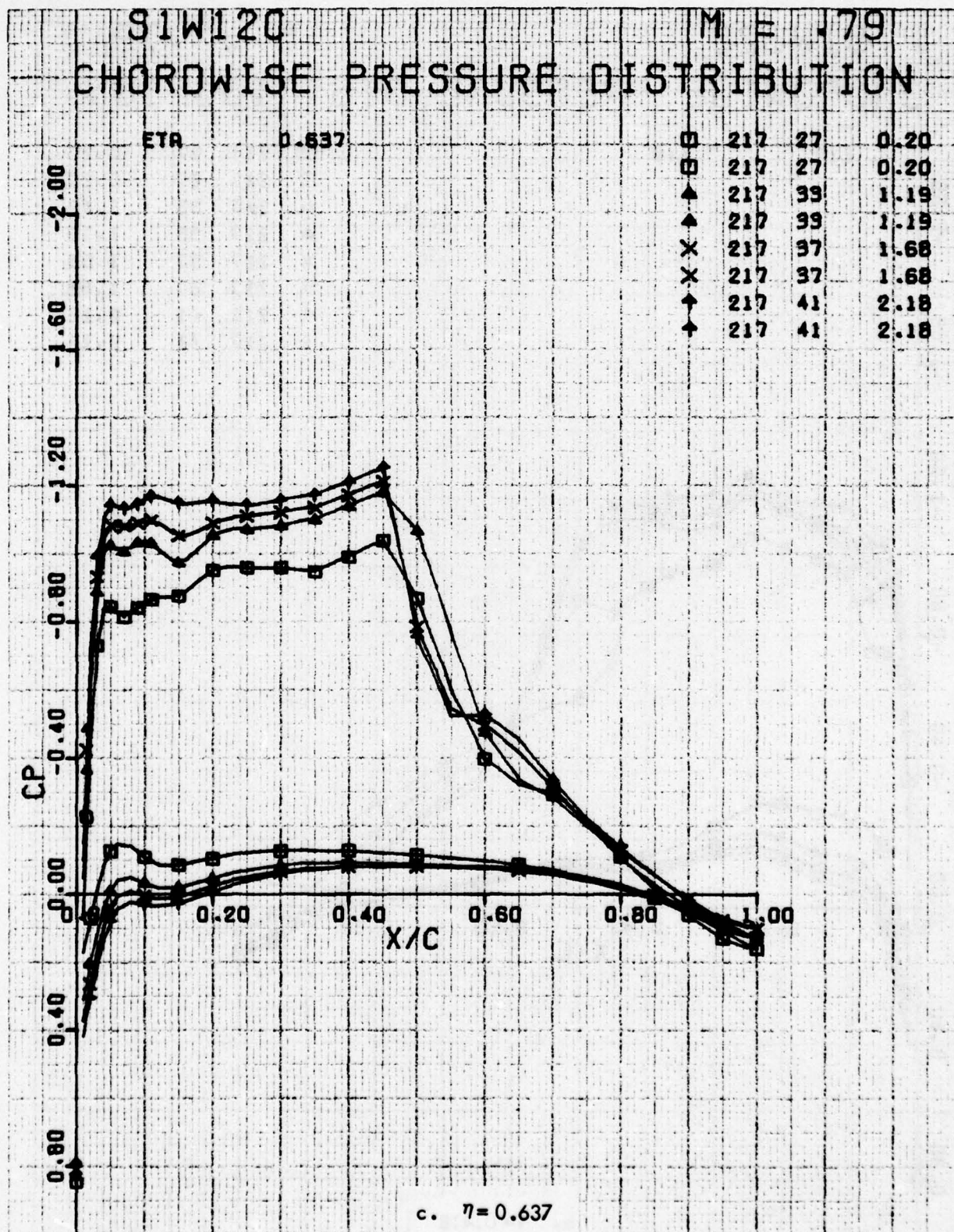
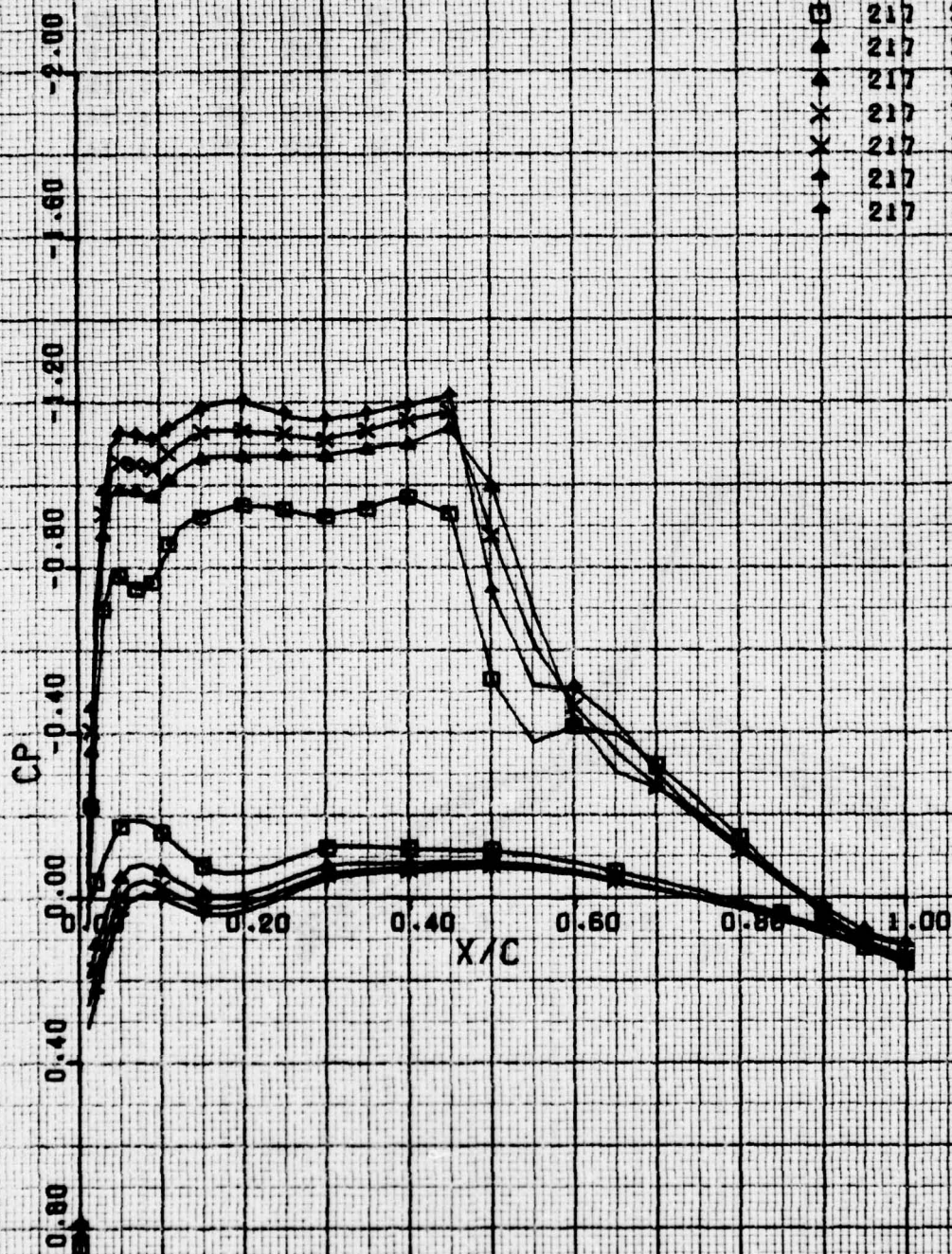


Figure 42. Continued

S1W12C M = .79 CHORDWISE PRESSURE DISTRIBUTION

ETA 0.793

□	217	27	0.20
□	217	27	0.20
▲	217	39	1.19
▲	217	39	1.19
×	217	37	1.68
×	217	37	1.68
♦	217	41	2.18
♦	217	41	2.18



d. $\eta = 0.793$

Figure 42. Concluded

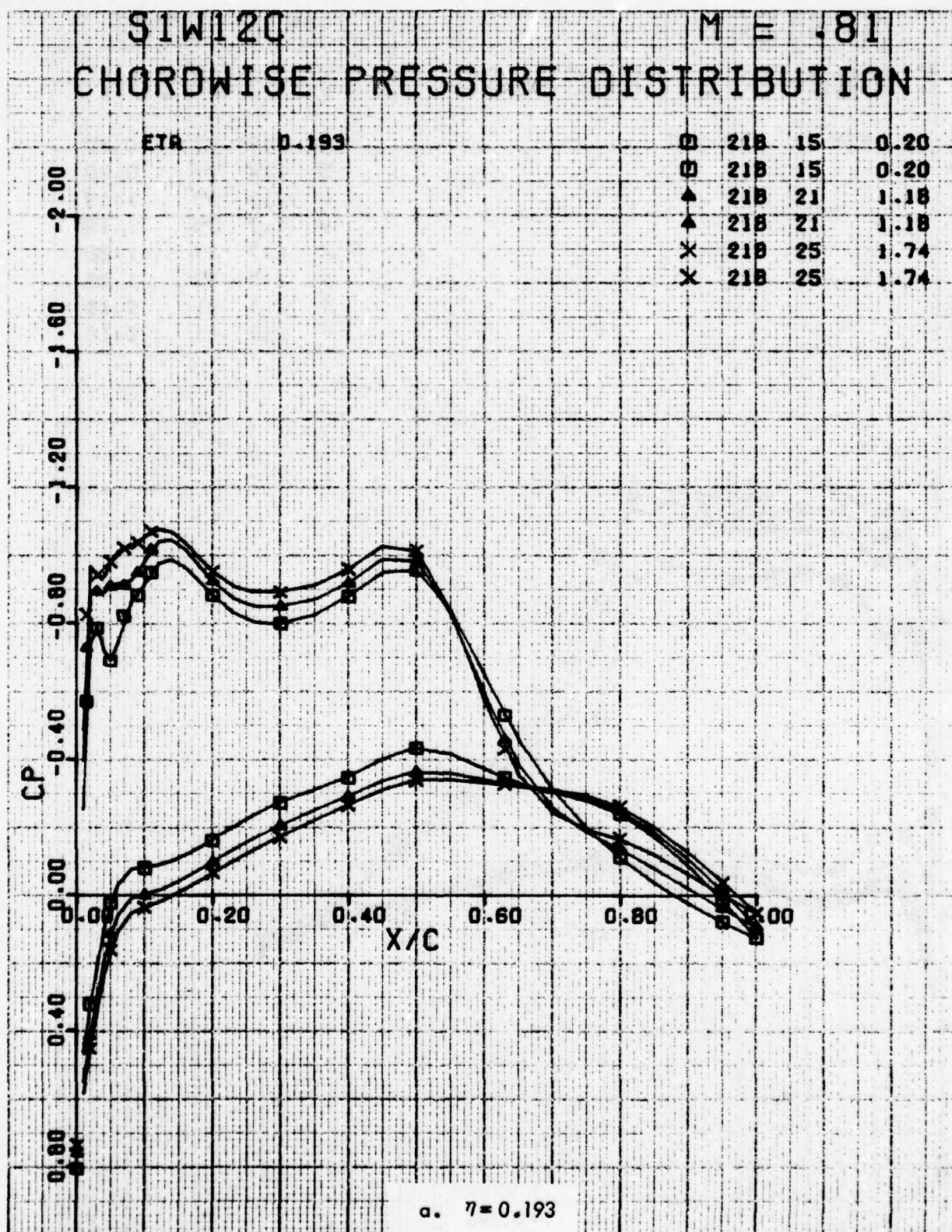


Figure 43. Chordwise Pressure Distributions for Various Angles of Attack. Baseline Leading Edge, Fixed Transition, Grit Code D, $M = 0.81$.

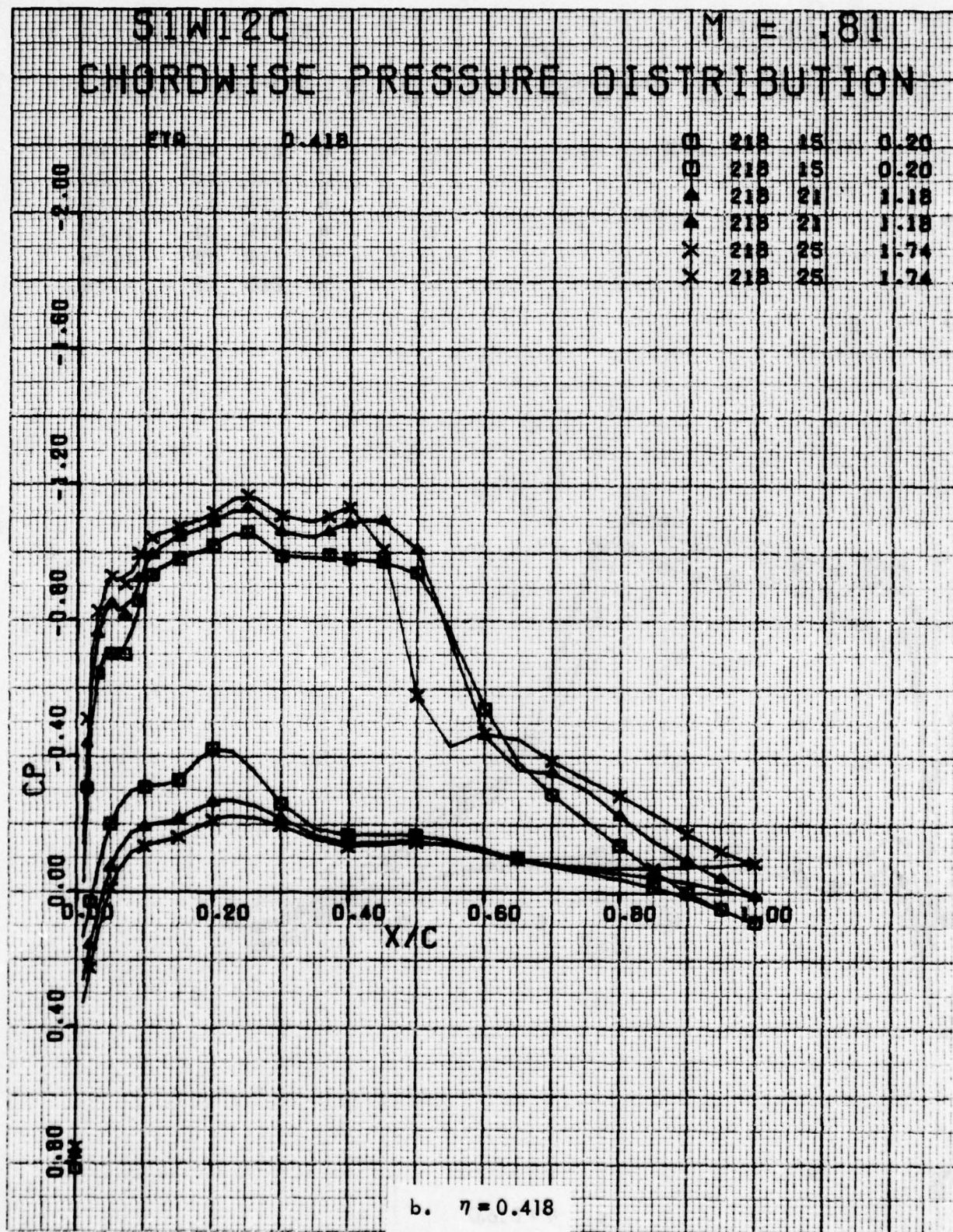


Figure 43. Continued

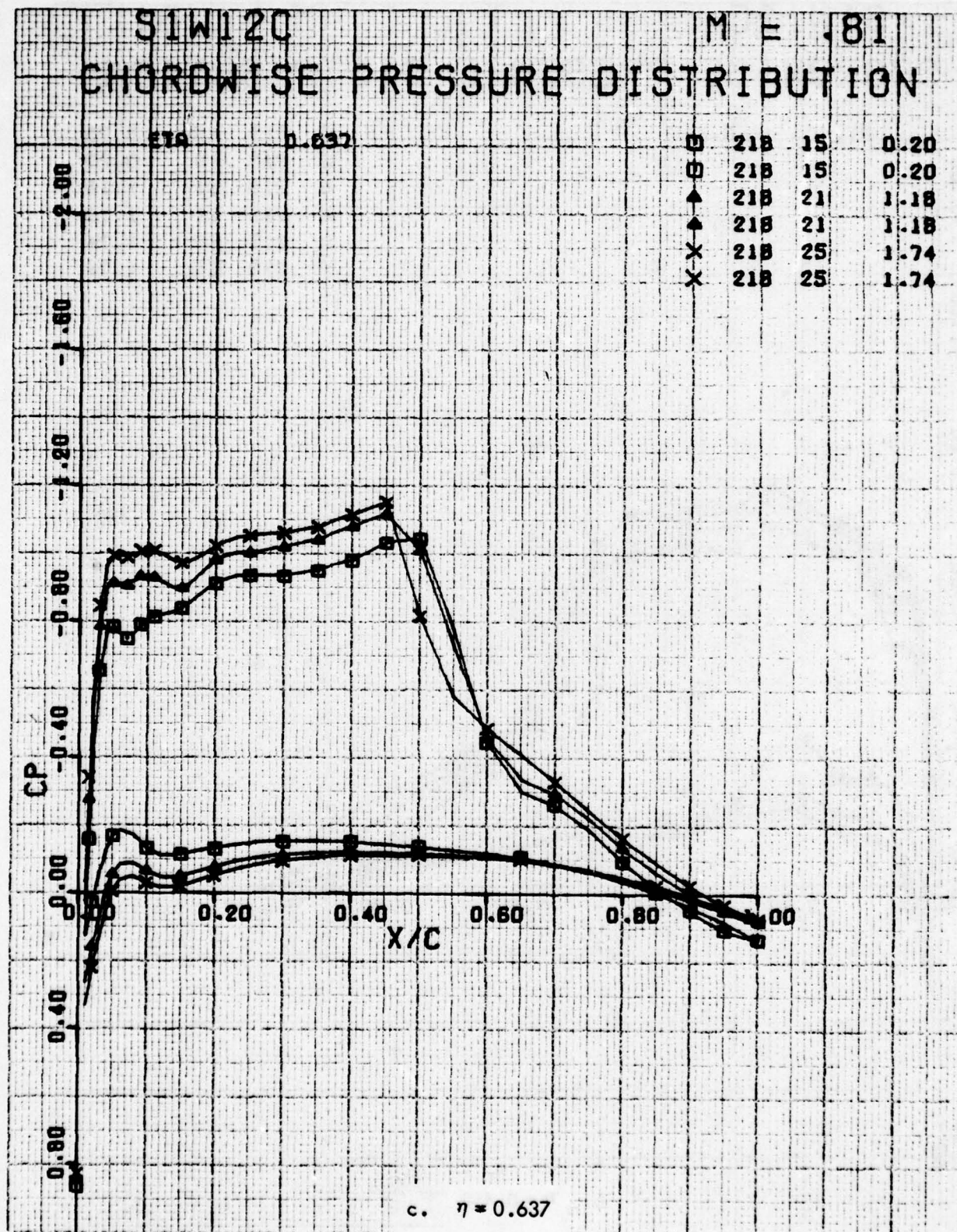


Figure 43. Continued

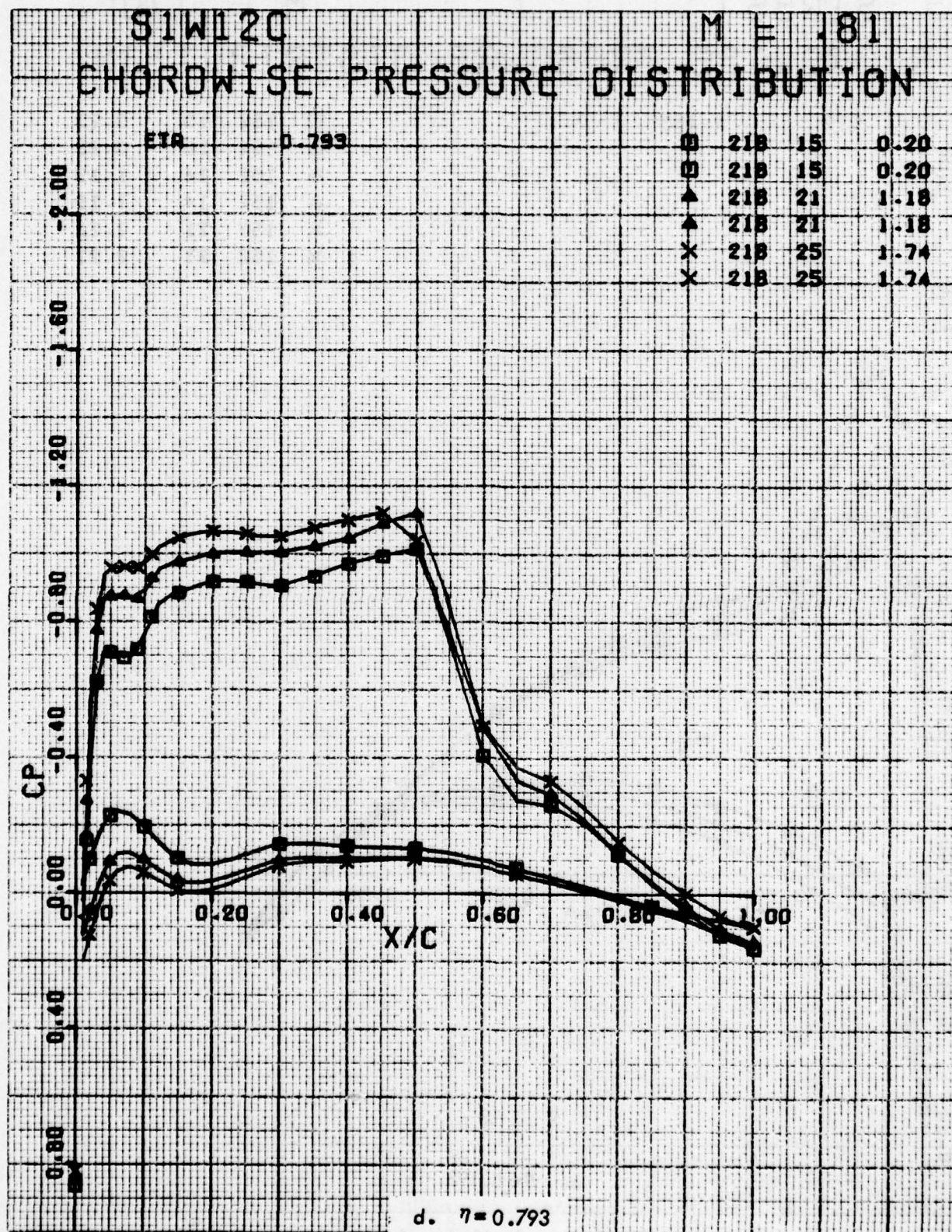


Figure 43. Concluded

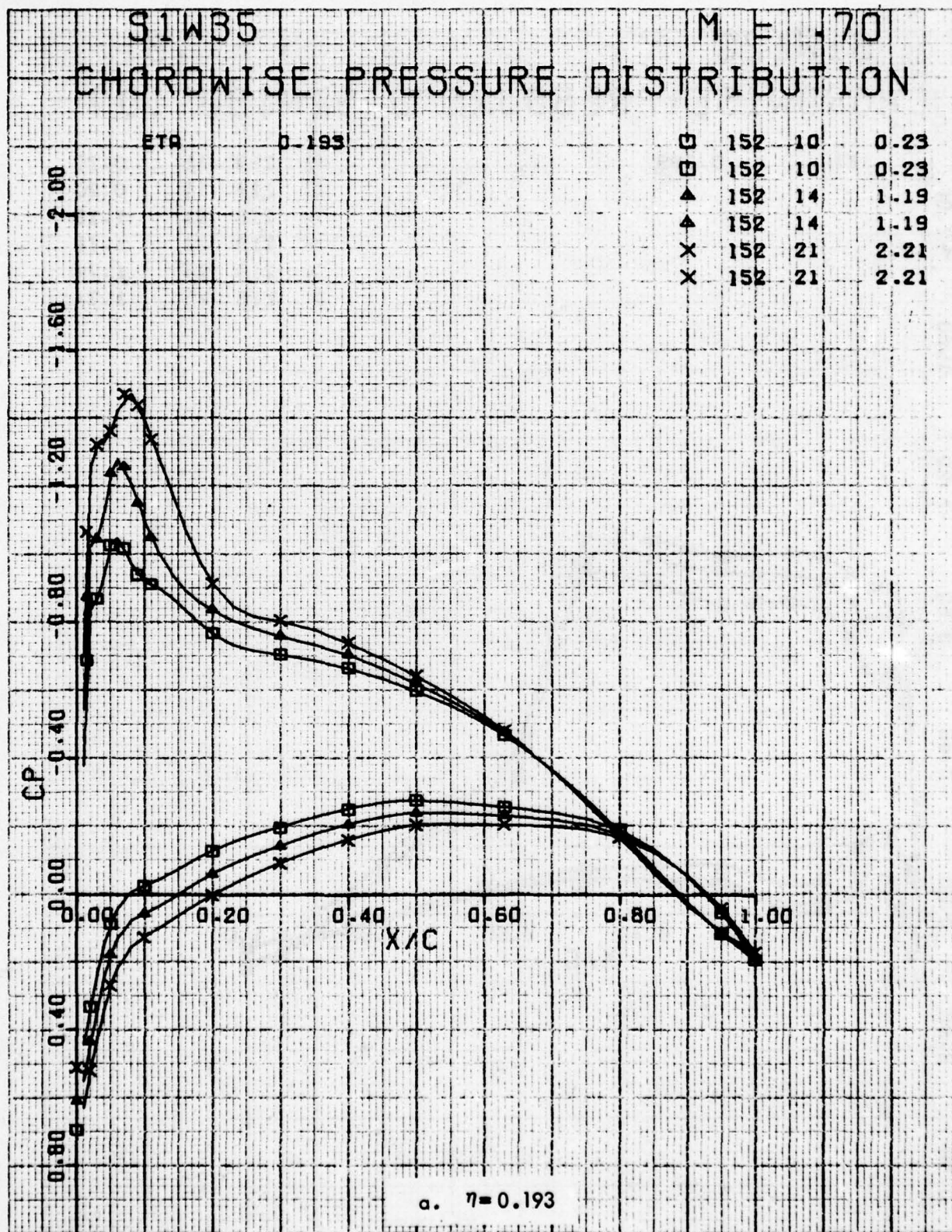


Figure 44. Chordwise Pressure Distributions for Various Angles of Attack. W³⁵ Leading Edge Modification, Free Transition, M = 0.7.

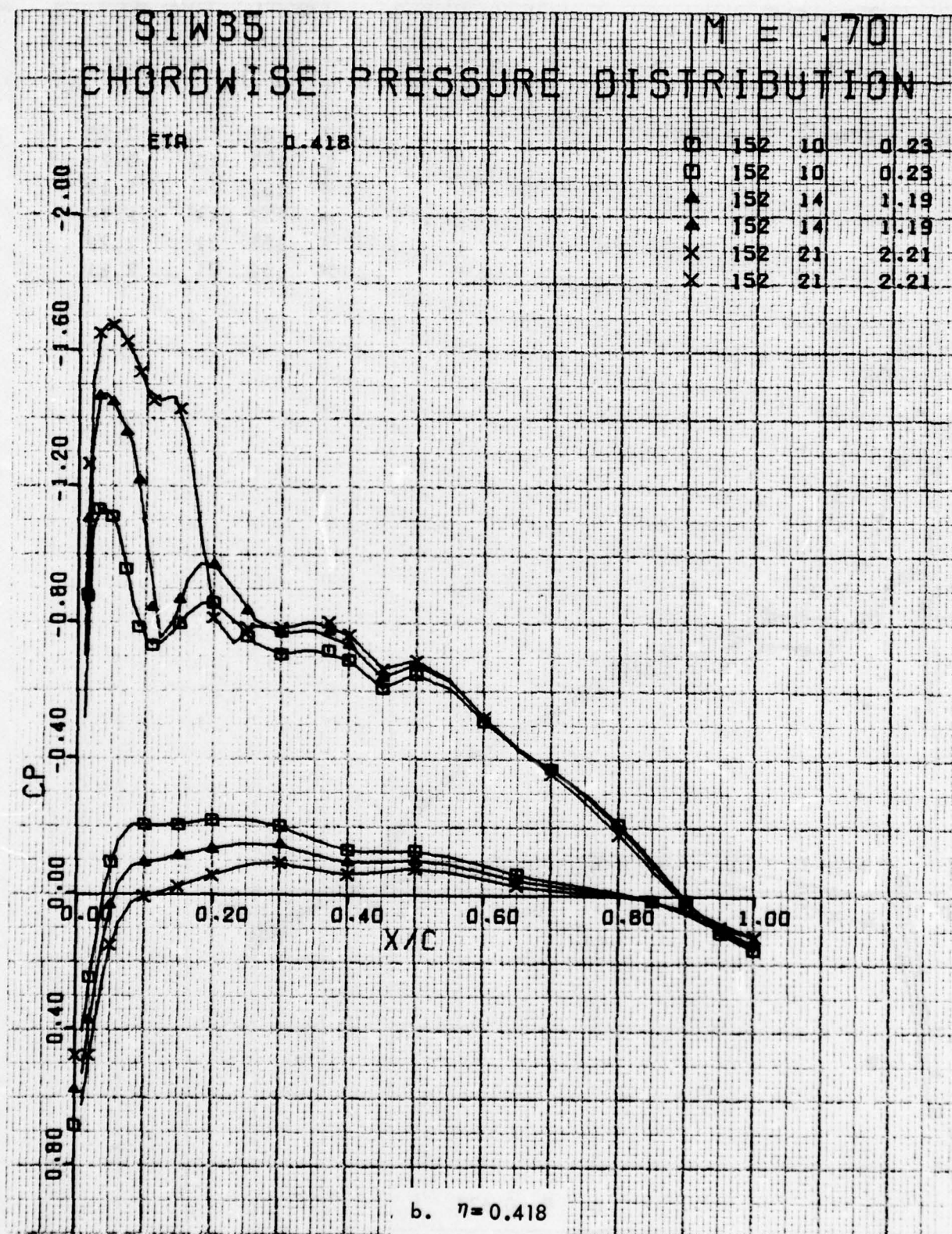


Figure 44. Continued

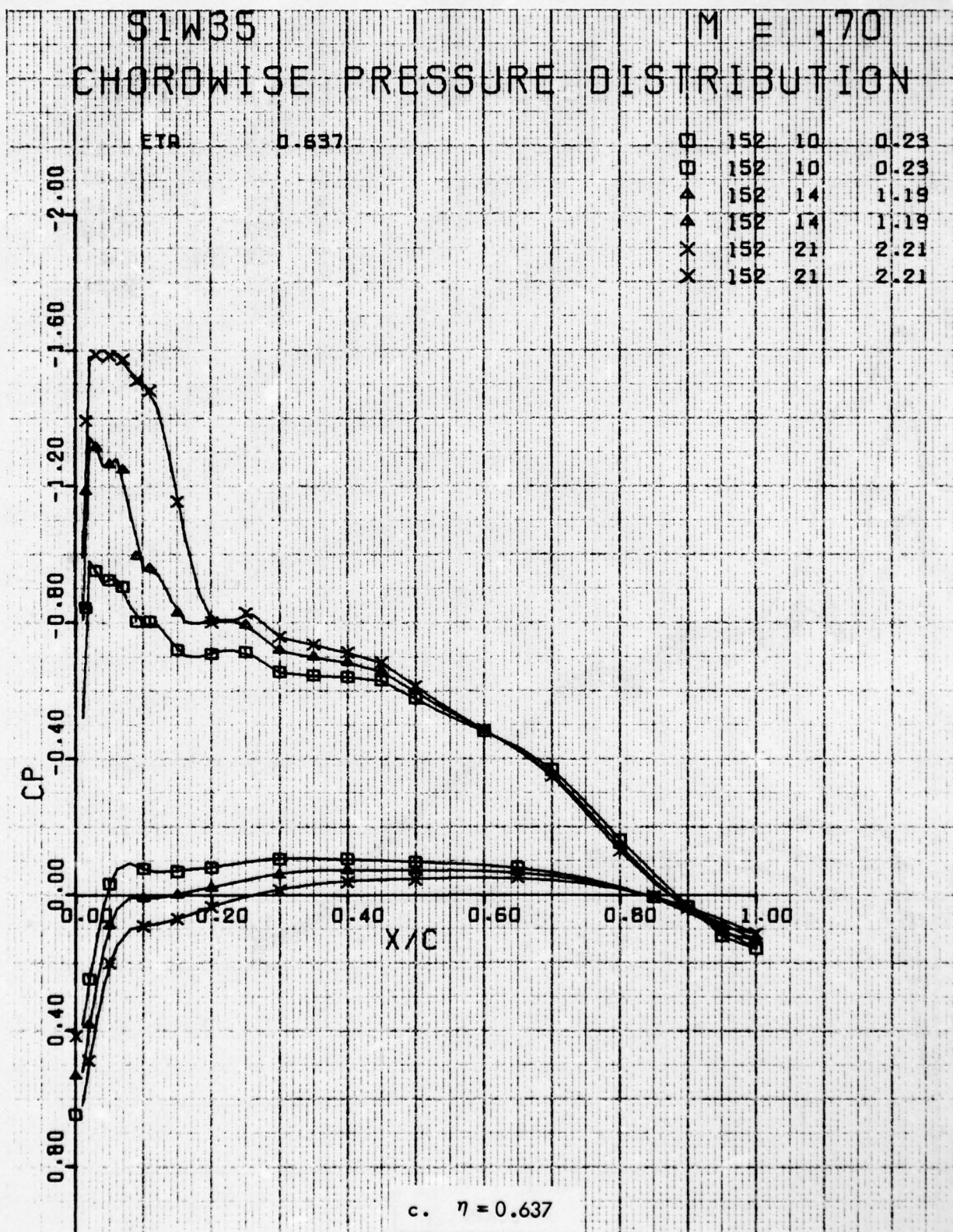


Figure 44. Continued

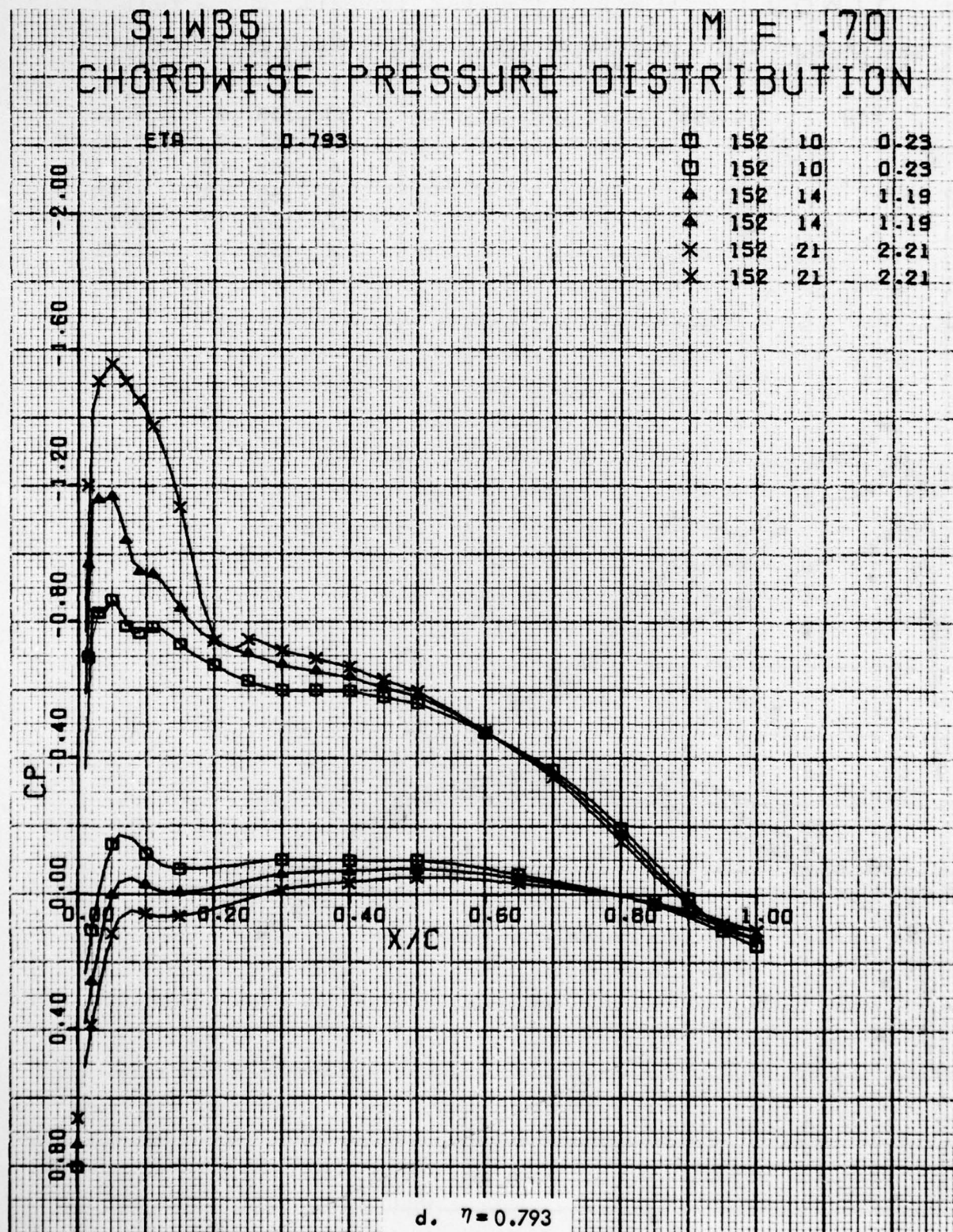


Figure 44. Concluded

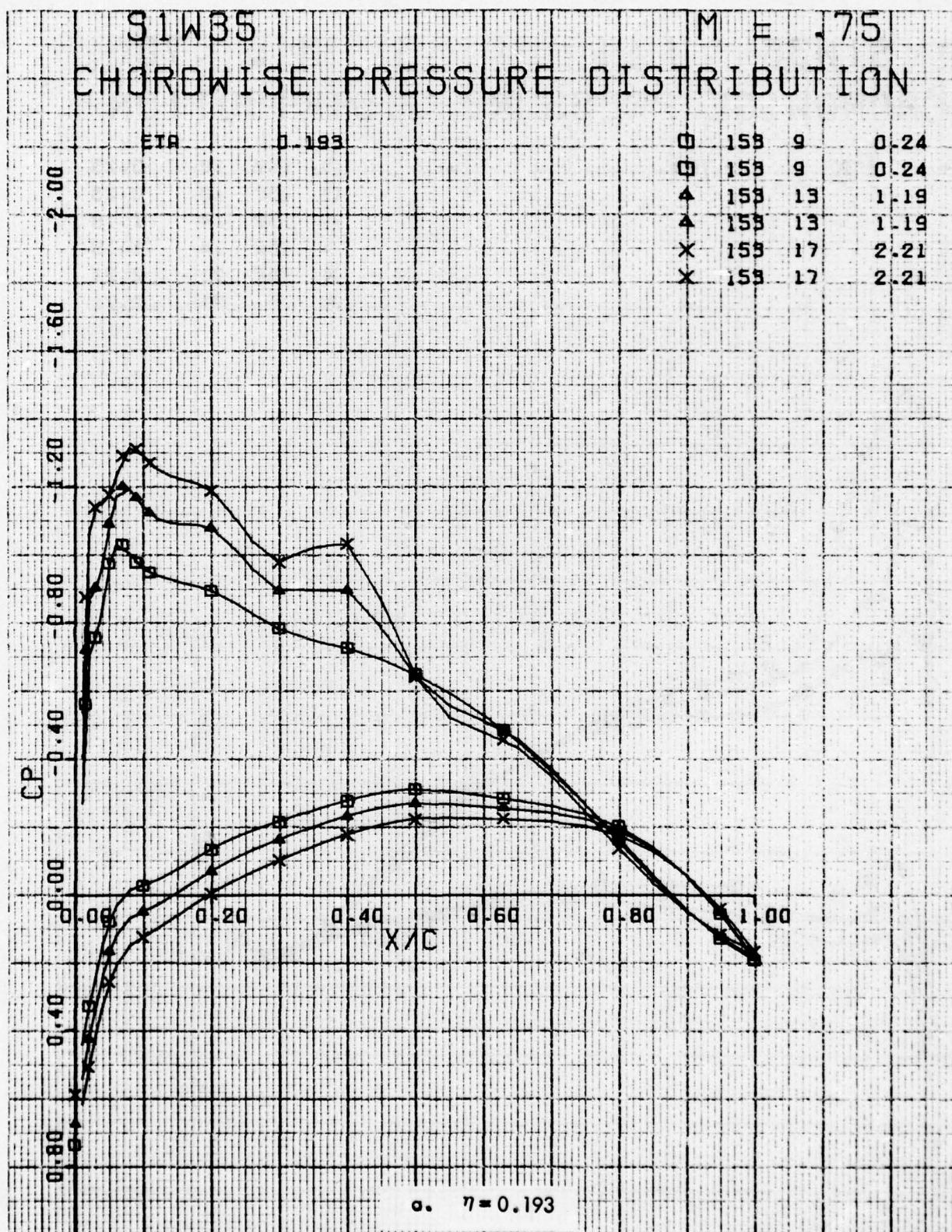


Figure 45. Chordwise Pressure Distributions for Various Angles of Attack. W^{35} Leading Edge Modification, Free Transition, $M = 0.75$.

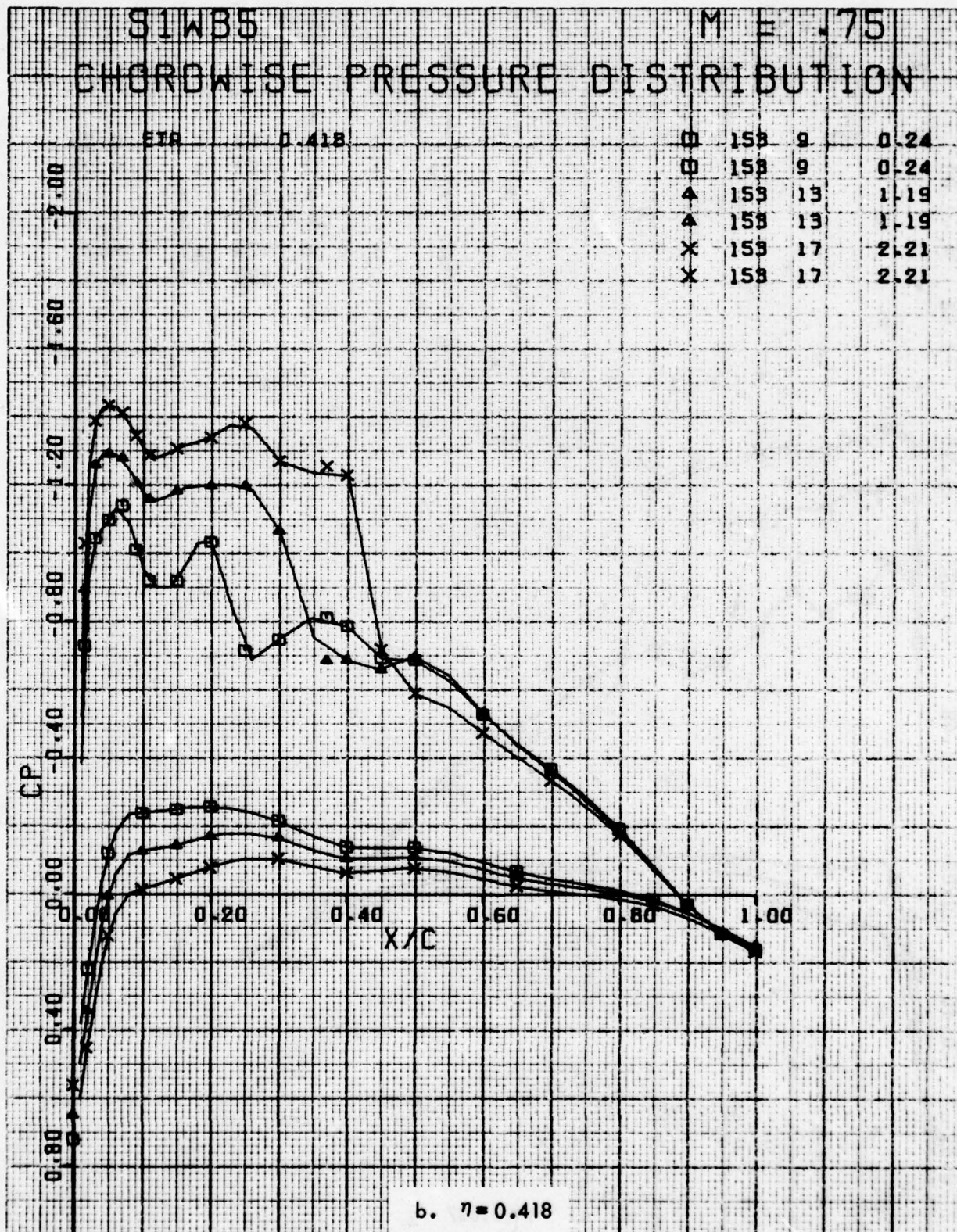


Figure 45. Continued

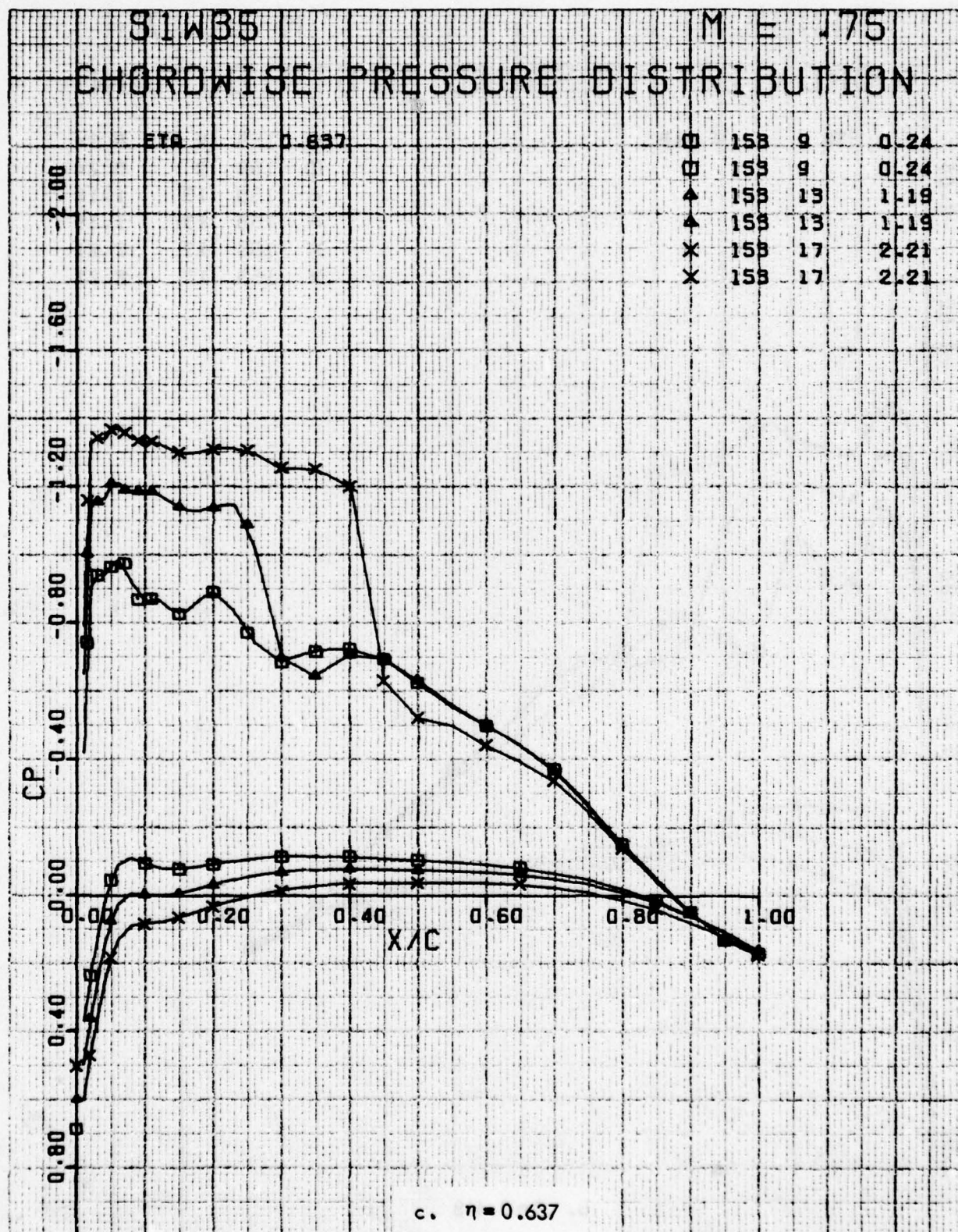


Figure 45. Continued

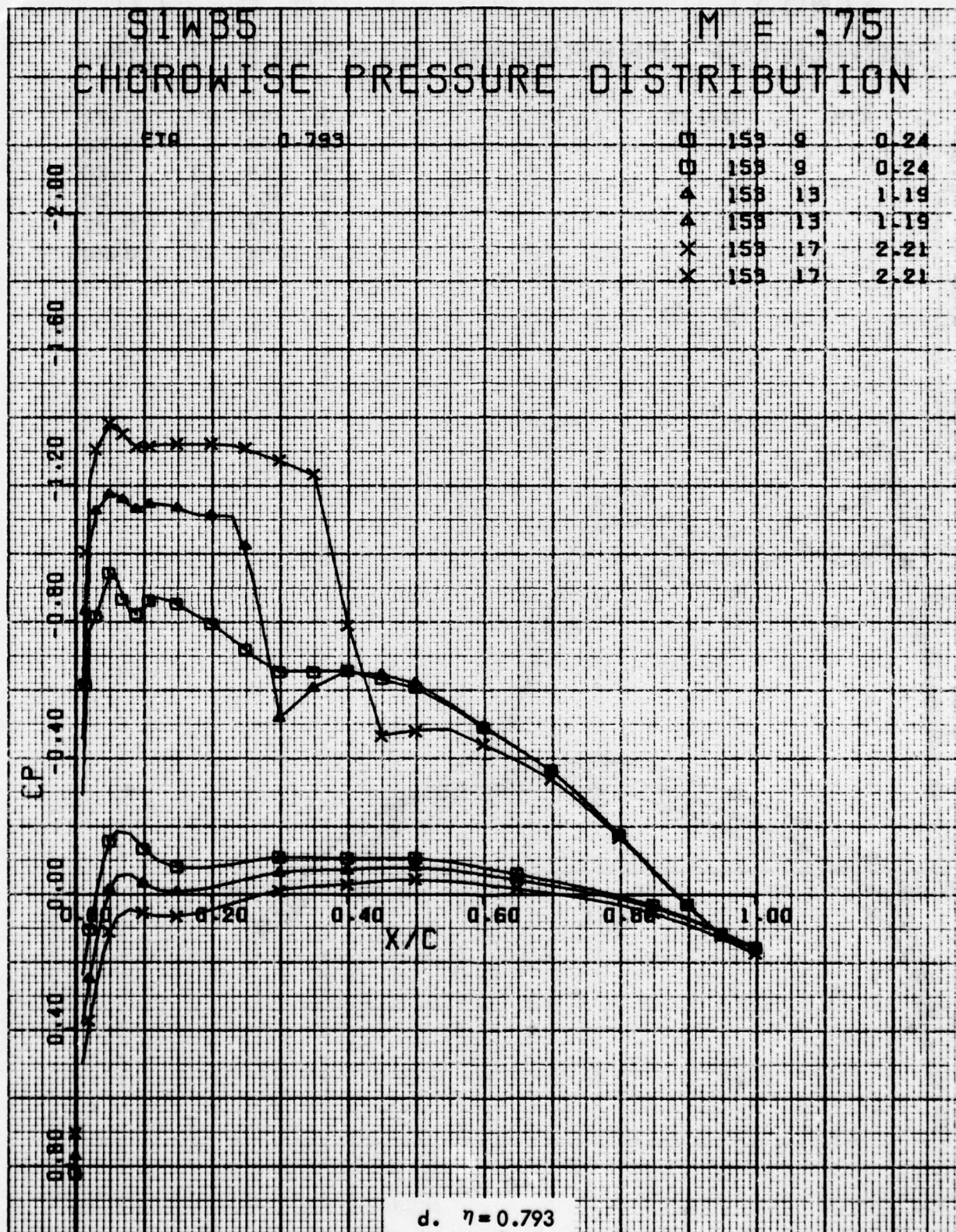


Figure 45. Concluded

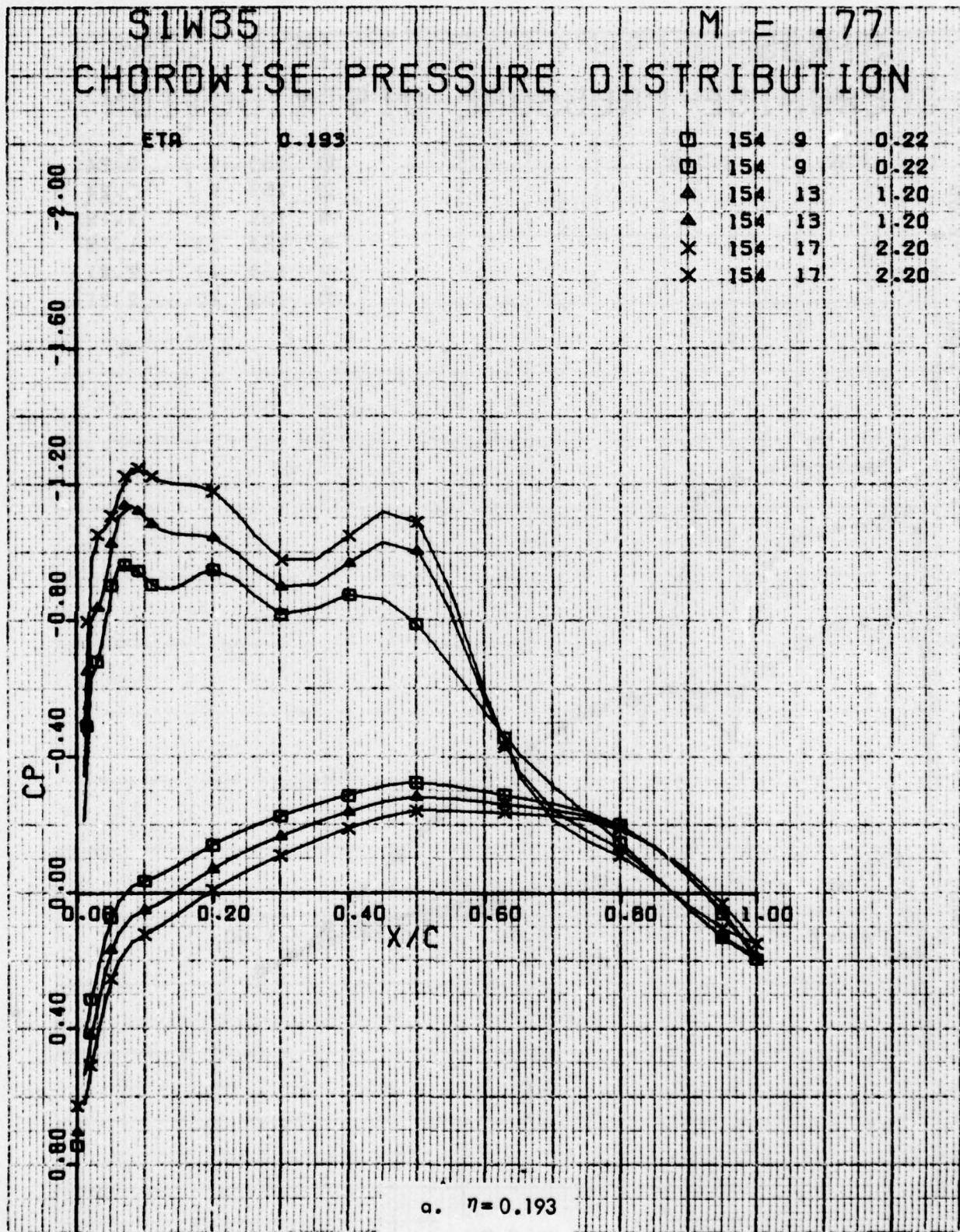


Figure 46. Chordwise Pressure Distributions for Various Angles of Attack. W³⁵ Leading Edge Modification, Free Transition, M = 0.77.

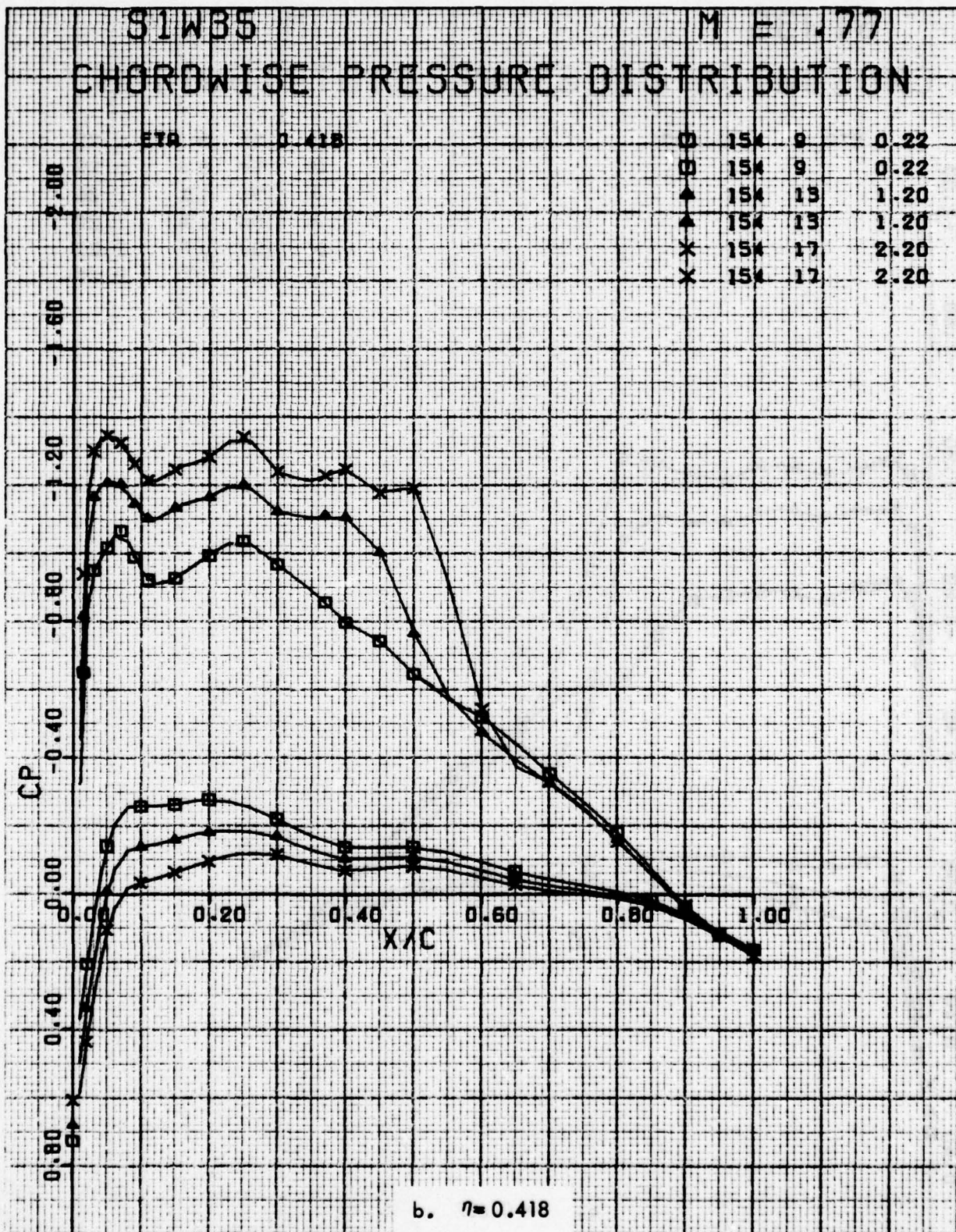


Figure 46. Continued

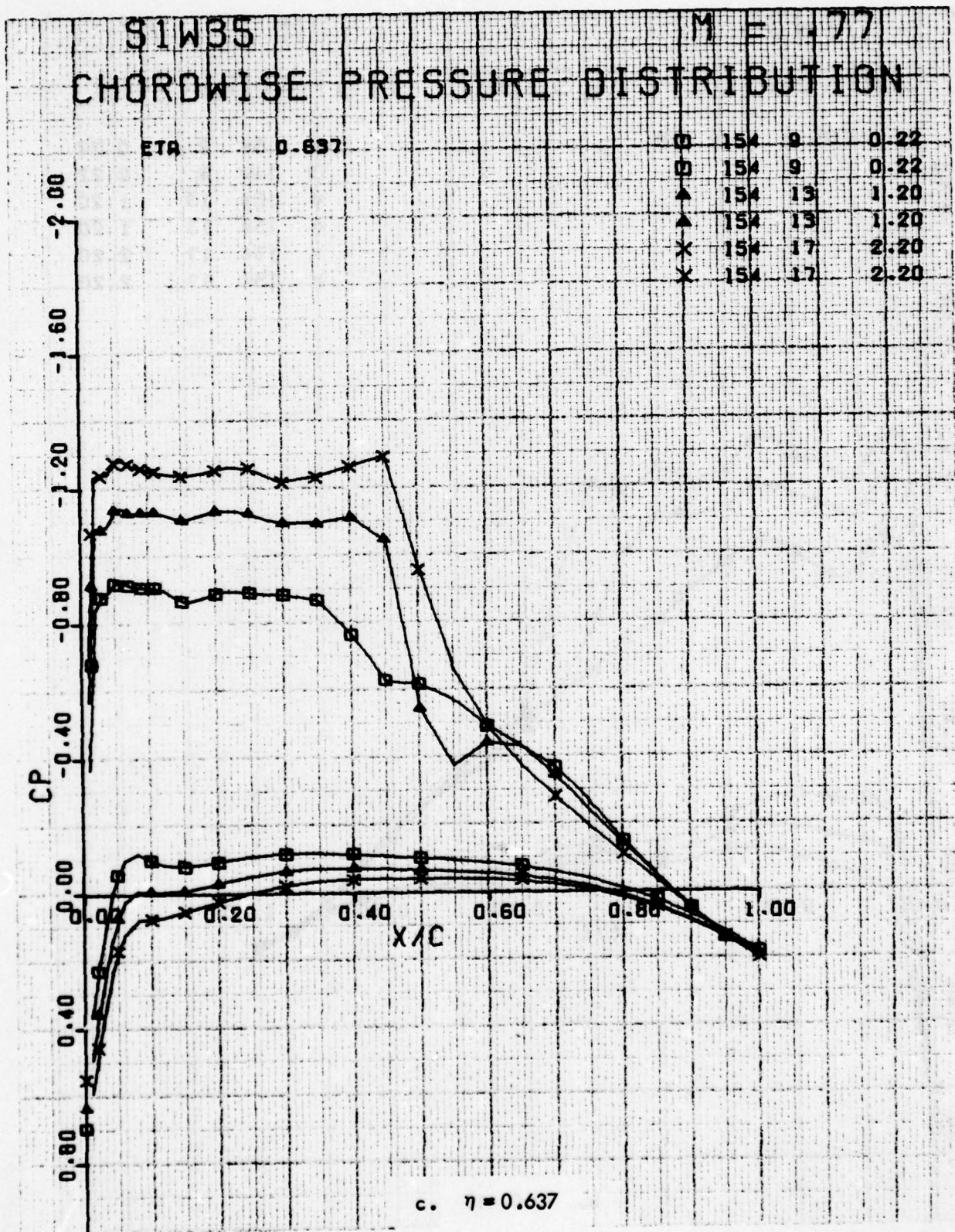


Figure 46. Continued

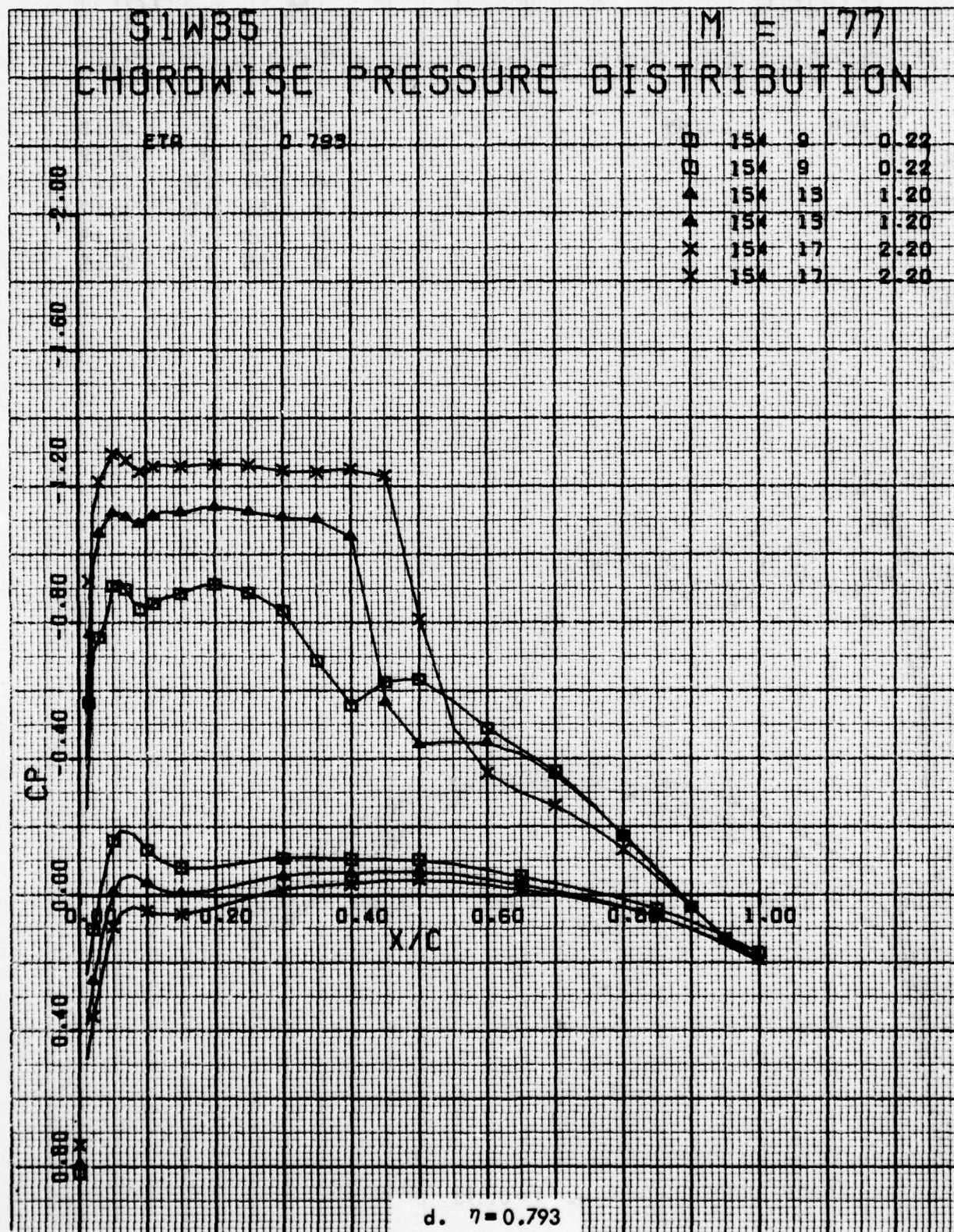


Figure 46. Concluded

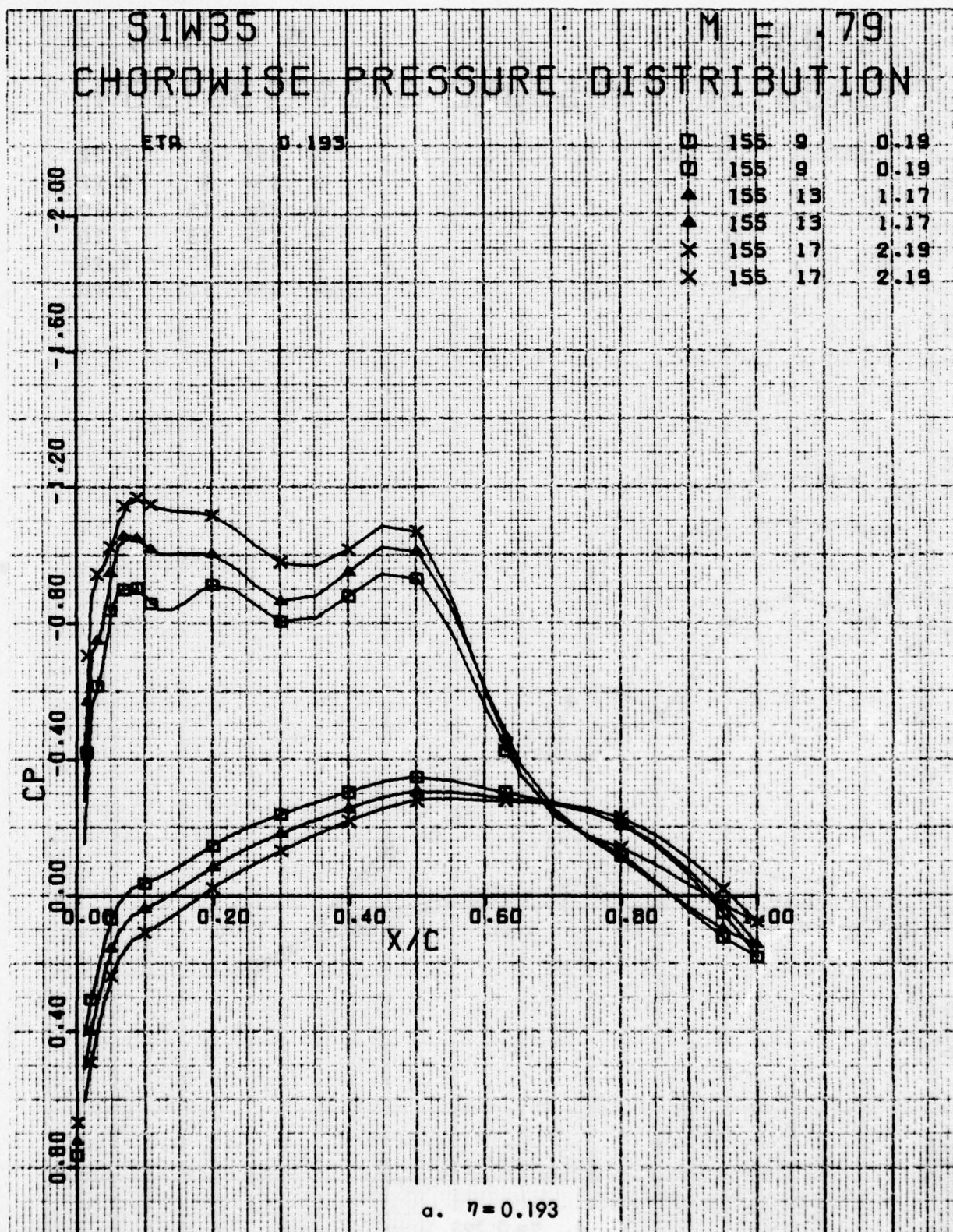


Figure 47 . Chordwise Pressure Distributions for Various Angles of Attack. W³⁵ Leading Edge Modification, Free Transition, M = 0.79.

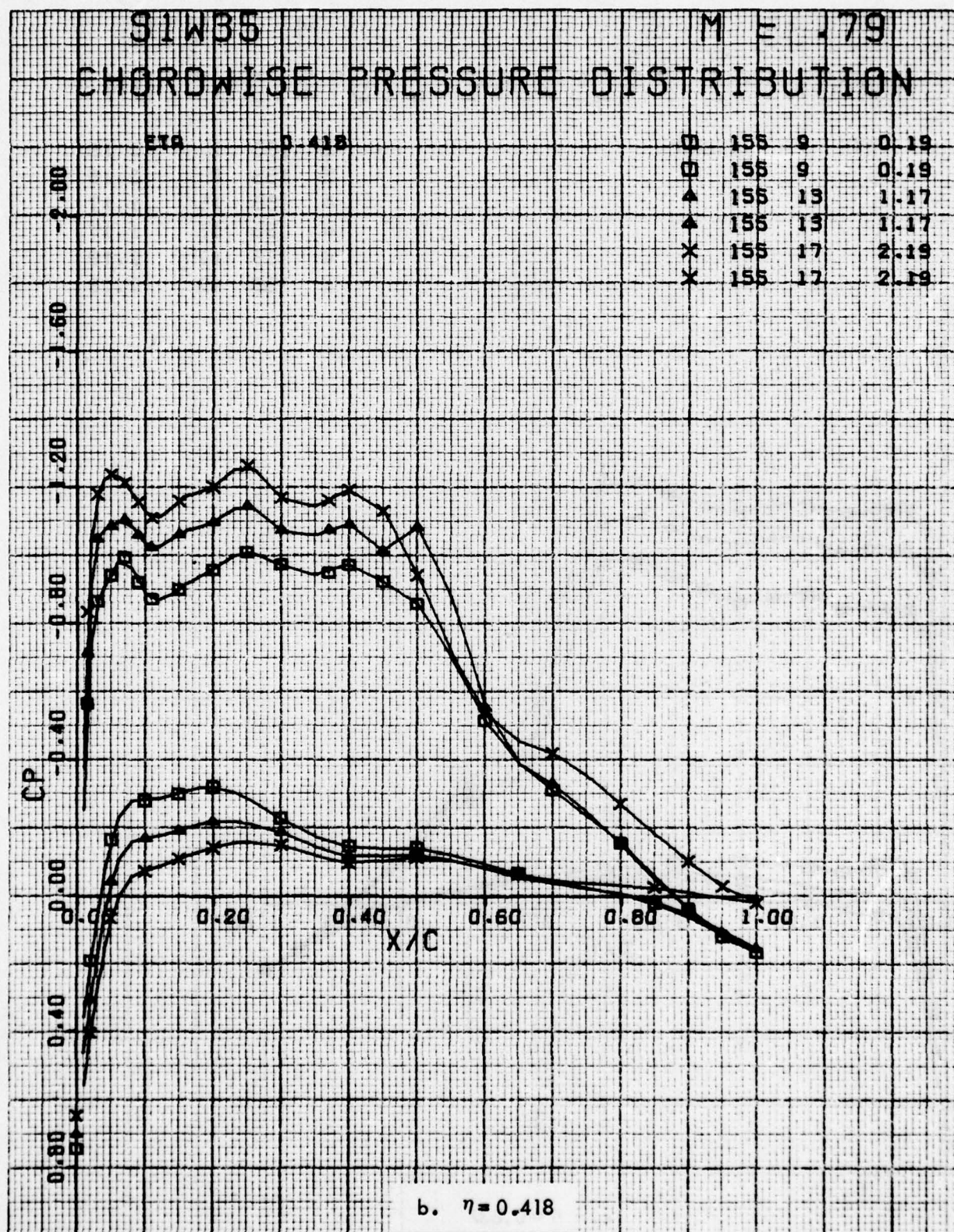


Figure 47. Continued

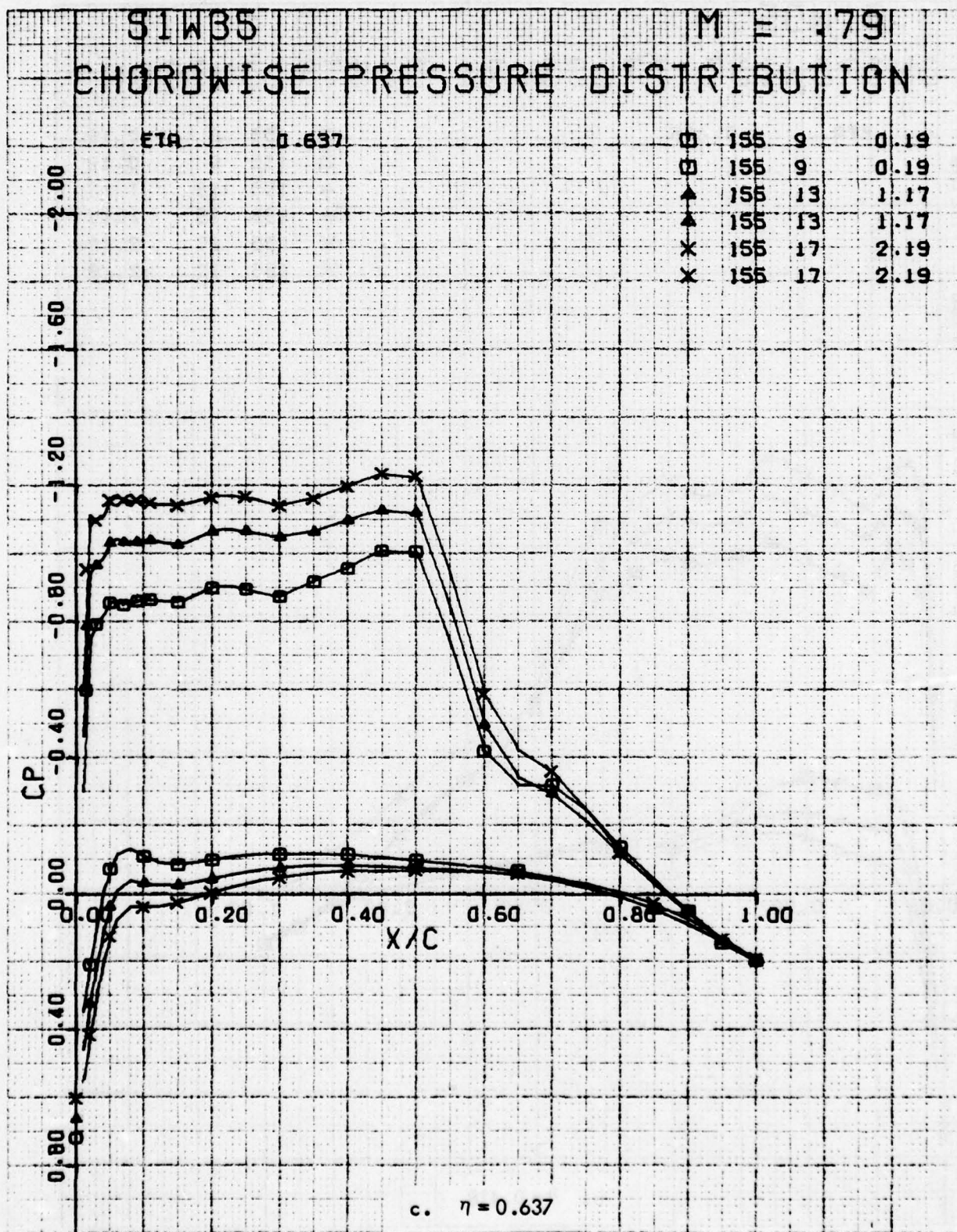


Figure 47. Continued

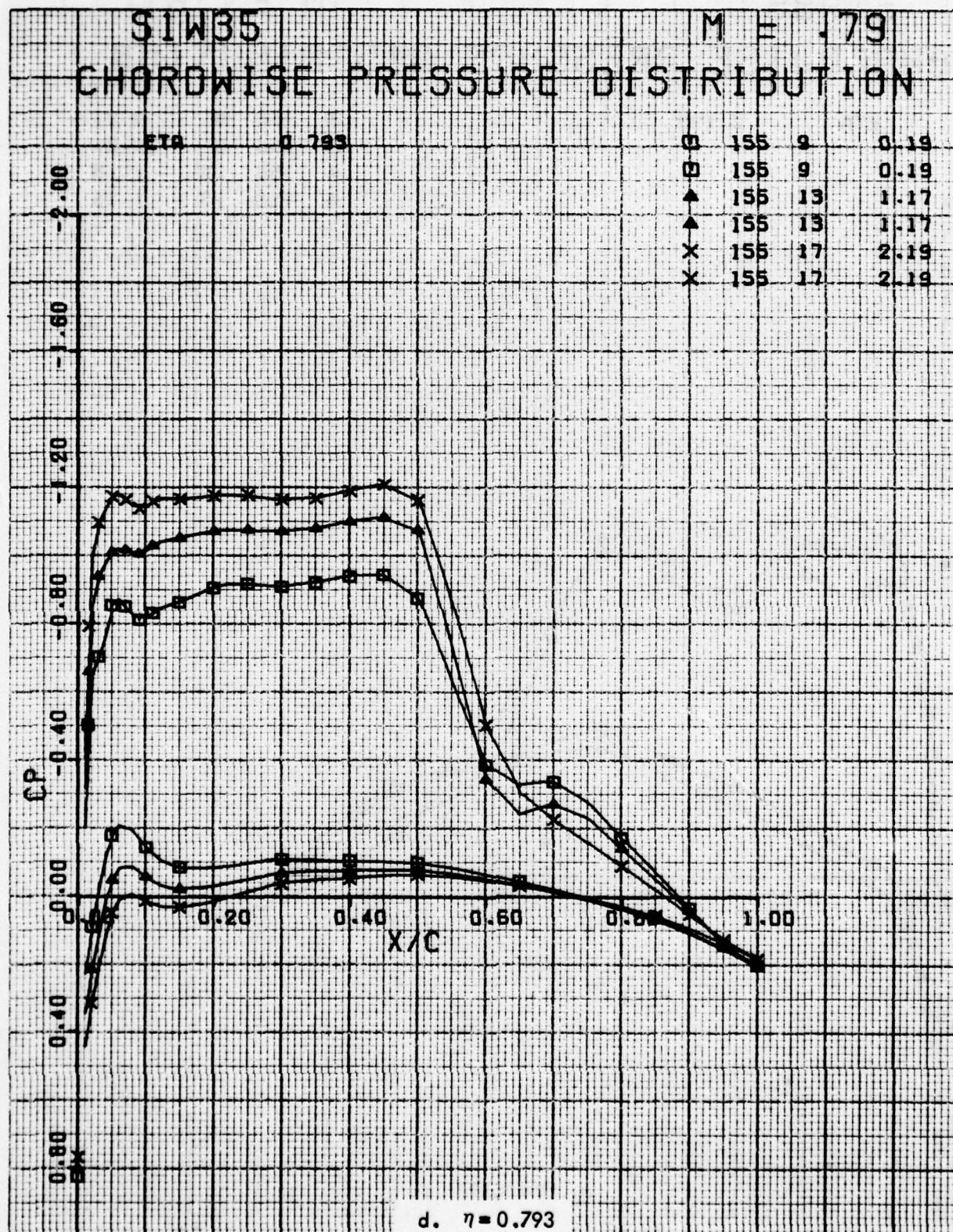


Figure 47. Concluded

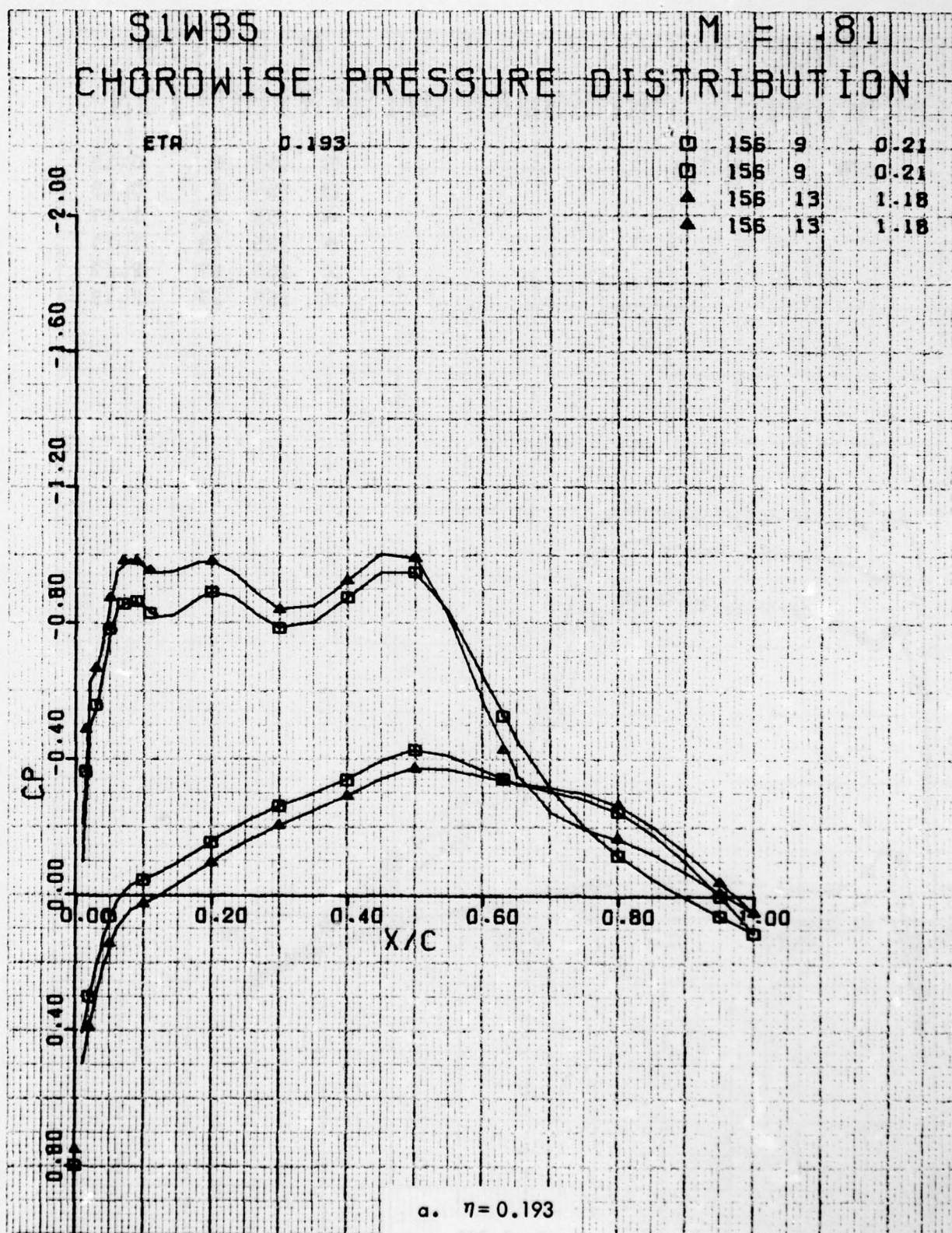


Figure 48 . Chordwise Pressure Distributions for Various Angles of Attack. W³⁵ Leading Edge Modification, Free Transition, M = 0.81.

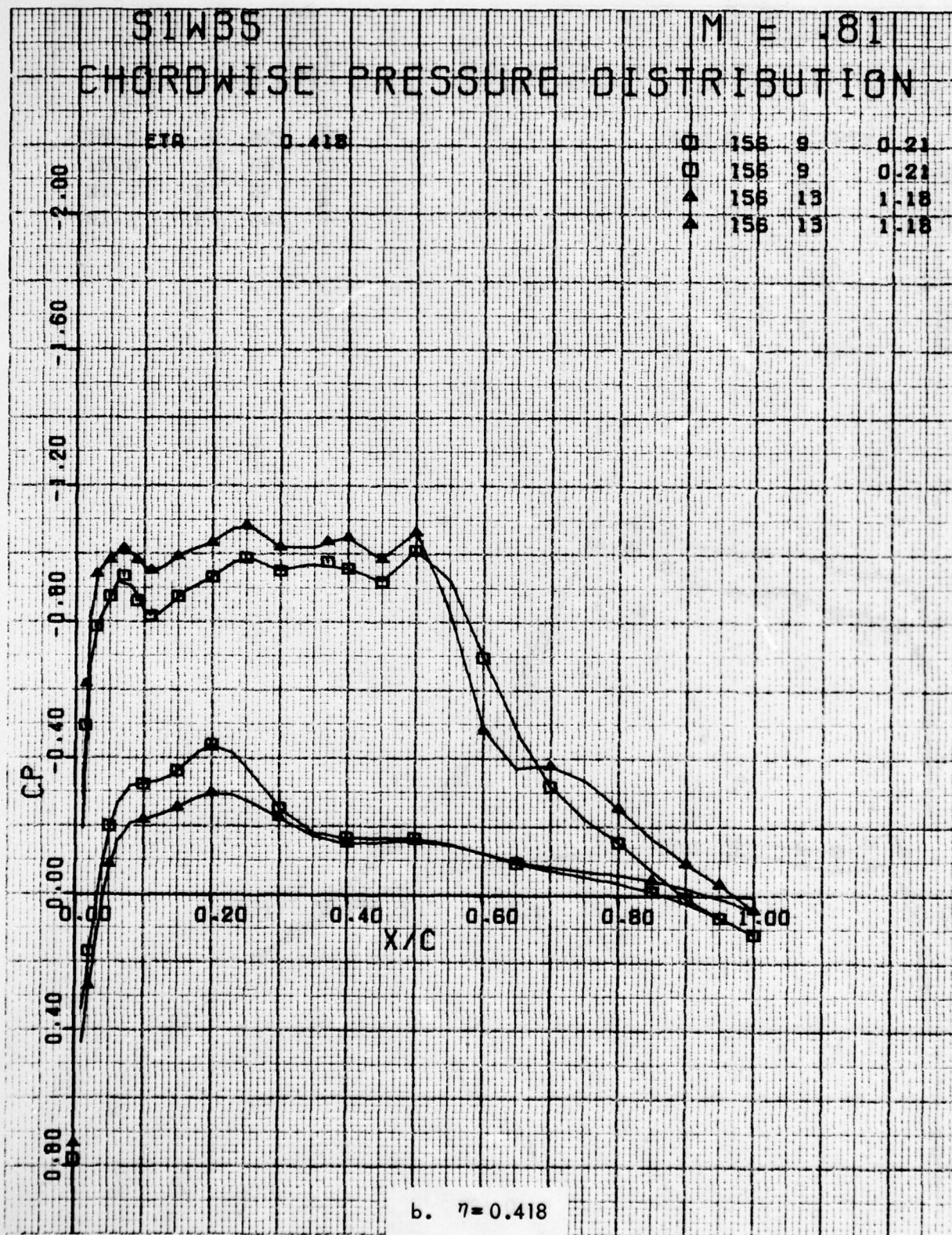


Figure 48. Continued

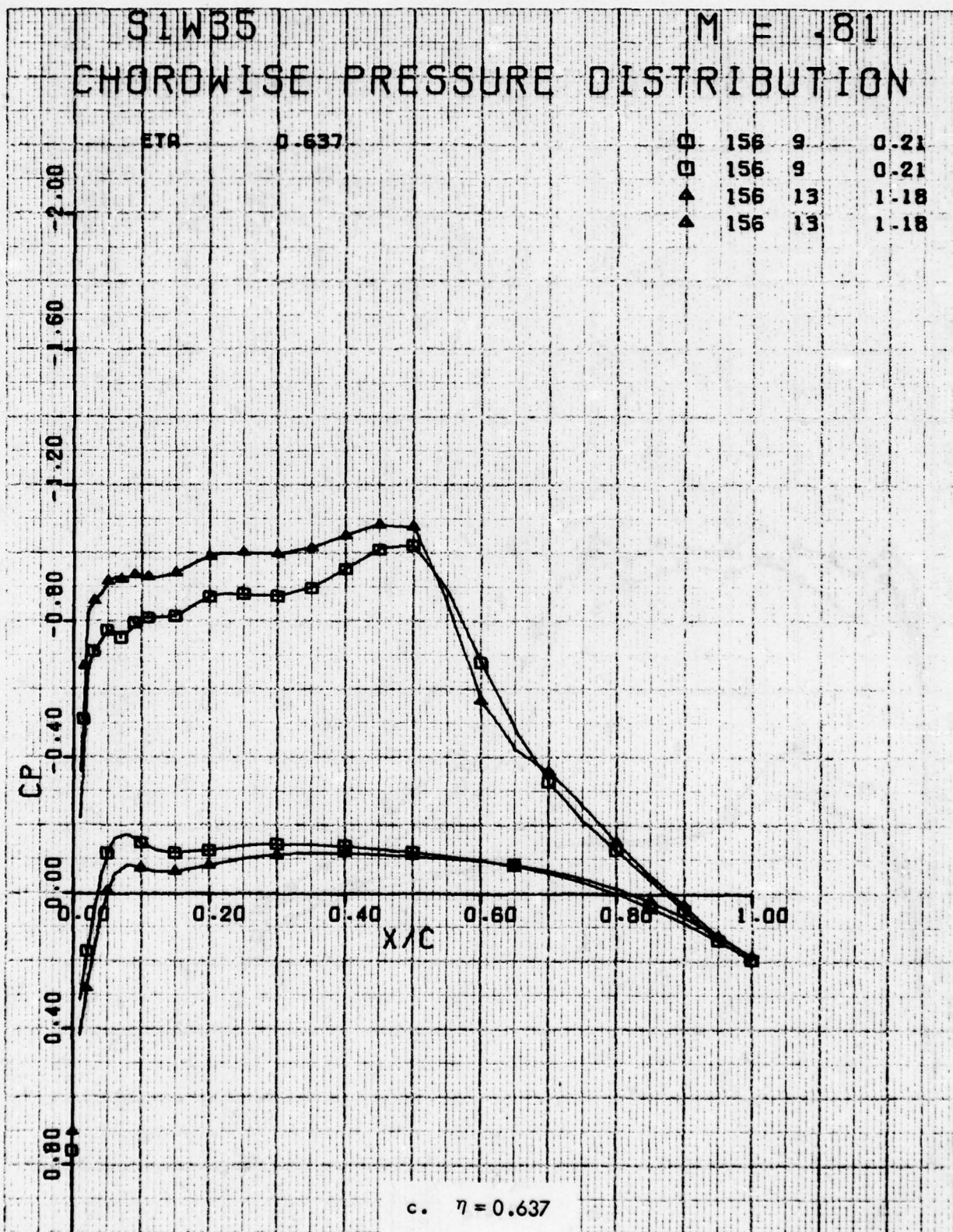


Figure 48. Continued

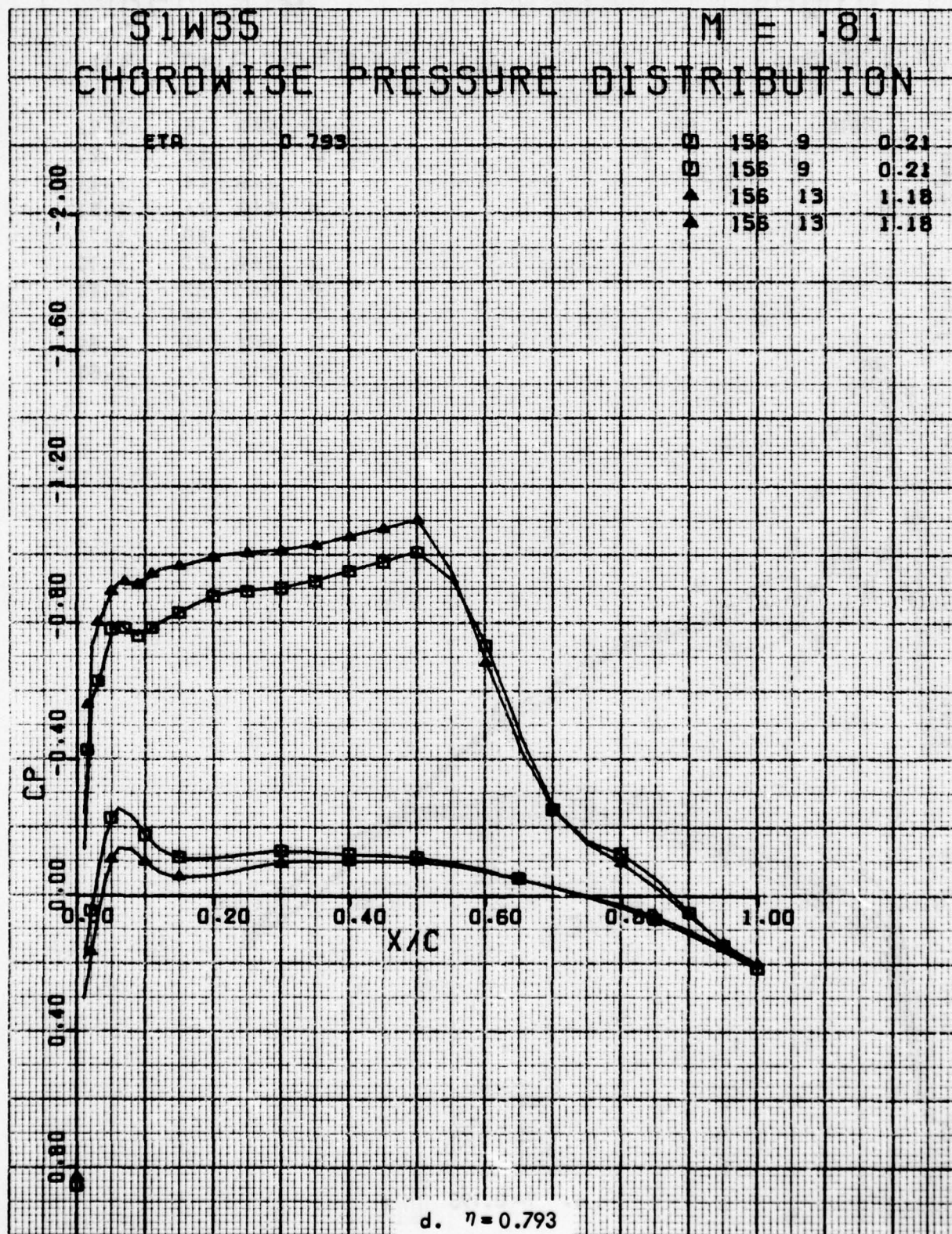


Figure 48. Concluded

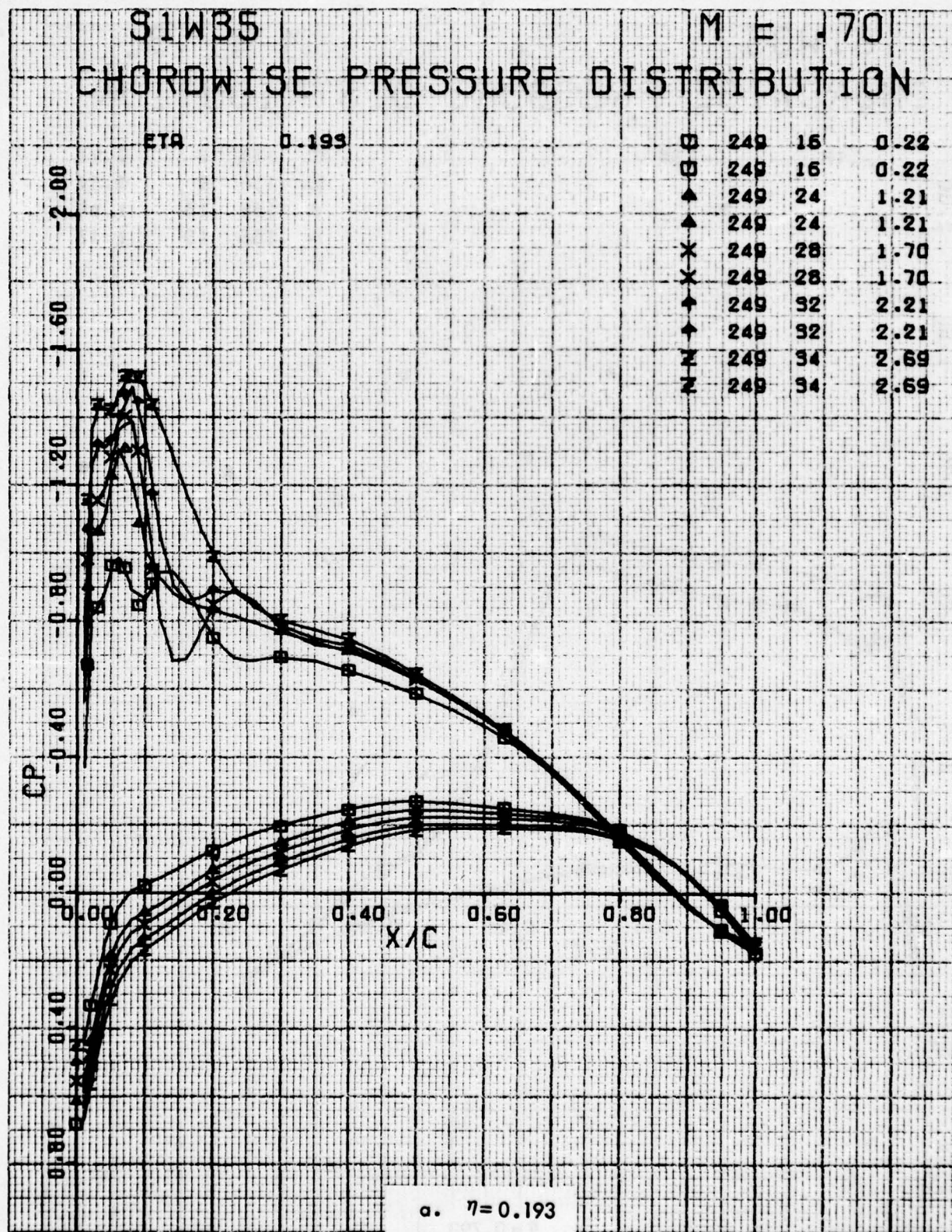


Figure 49. Chordwise Pressure Distributions for Various Angles of Attack. W^{35} Leading Edge Modification, Fixed Transition, Grit Code D. $M = 0.7$.

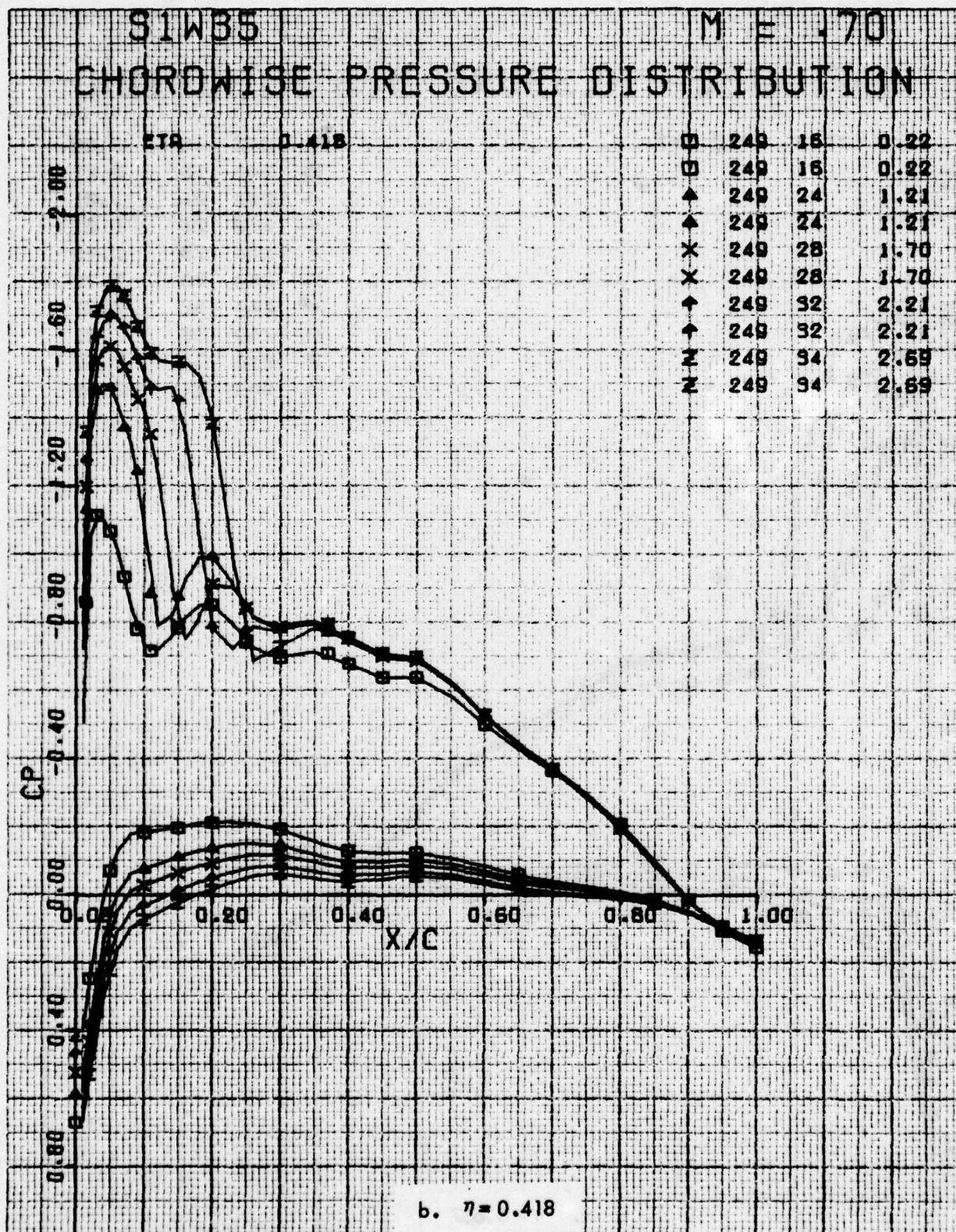


Figure 49. Continued

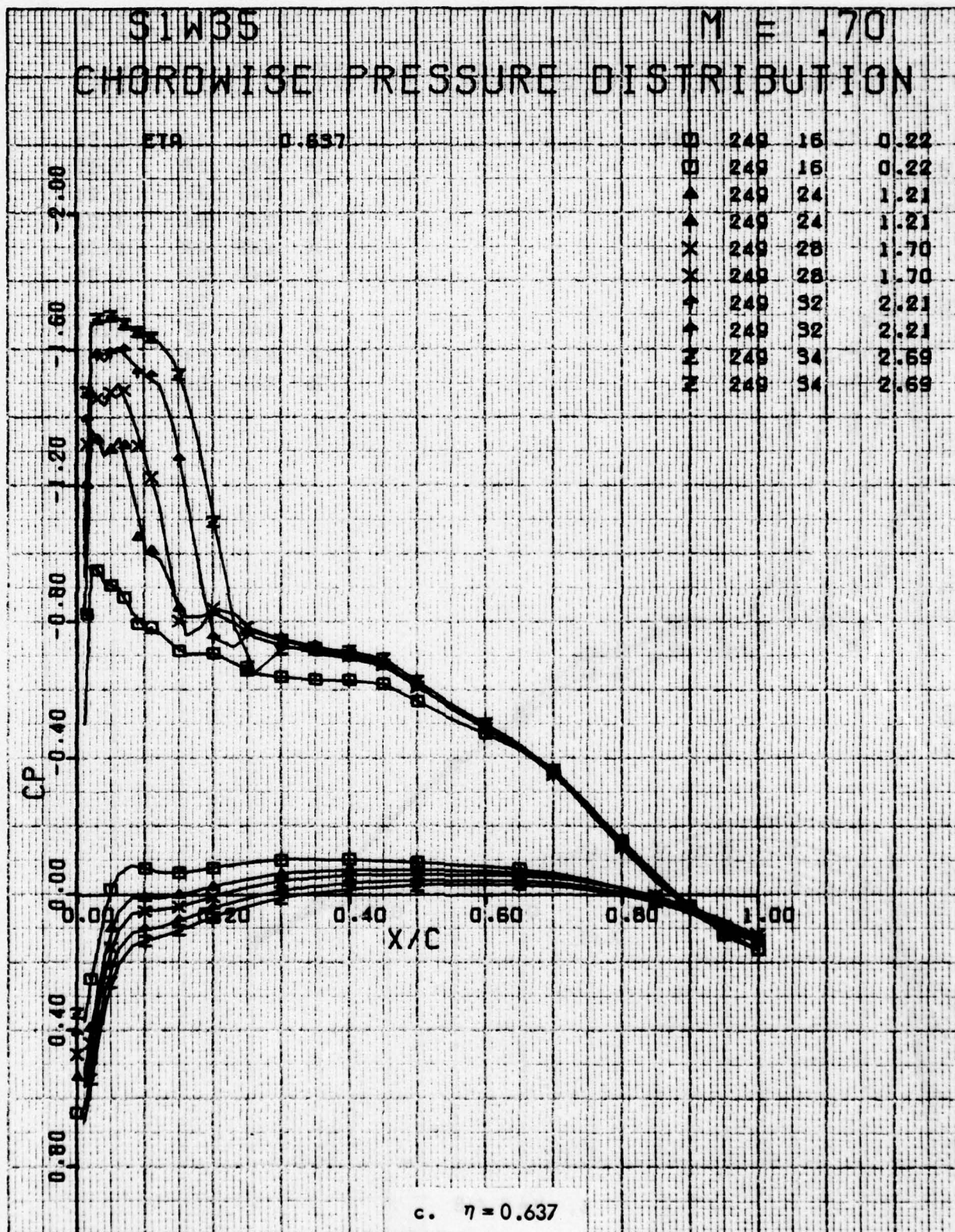


Figure 49. Continued

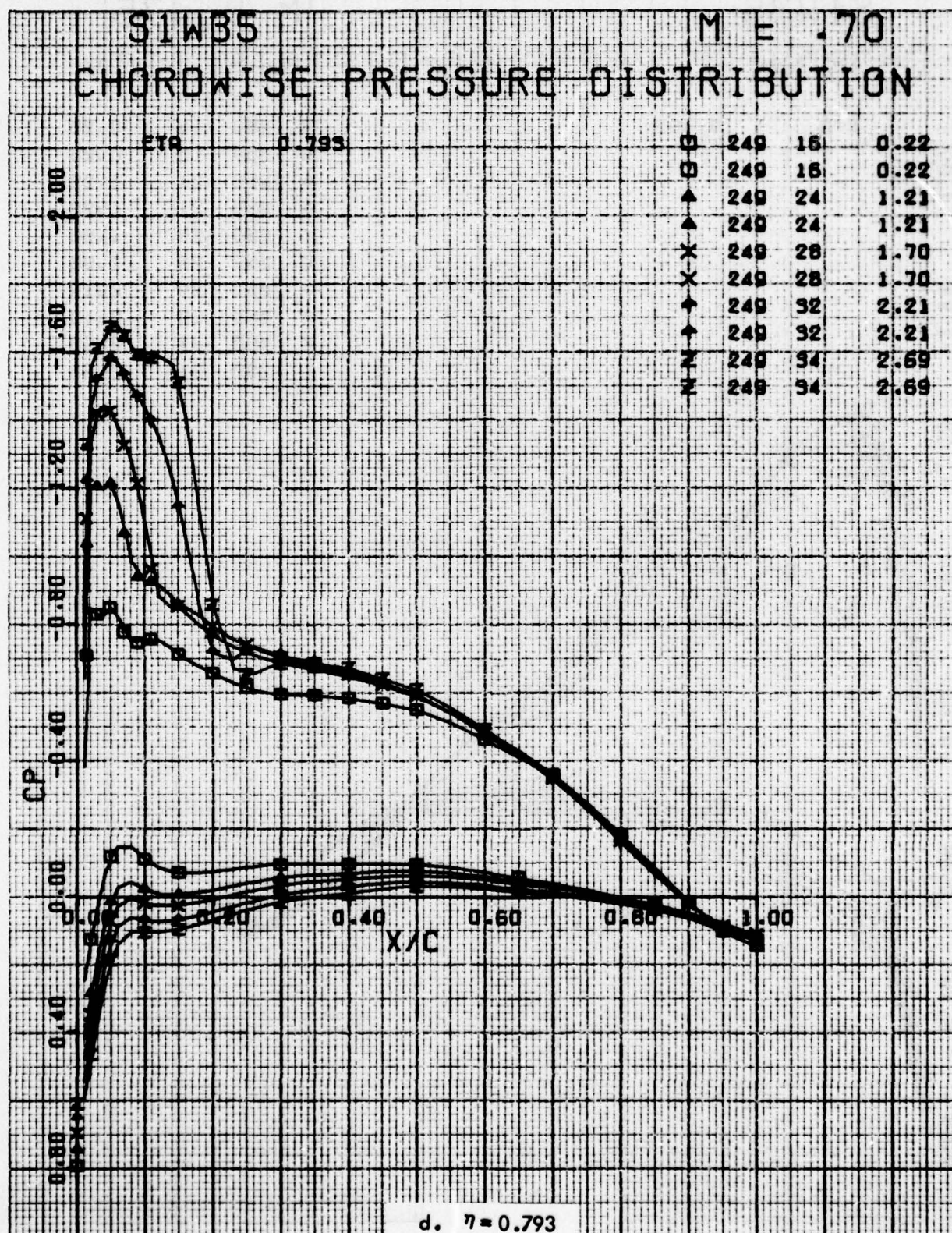


Figure 49. Concluded

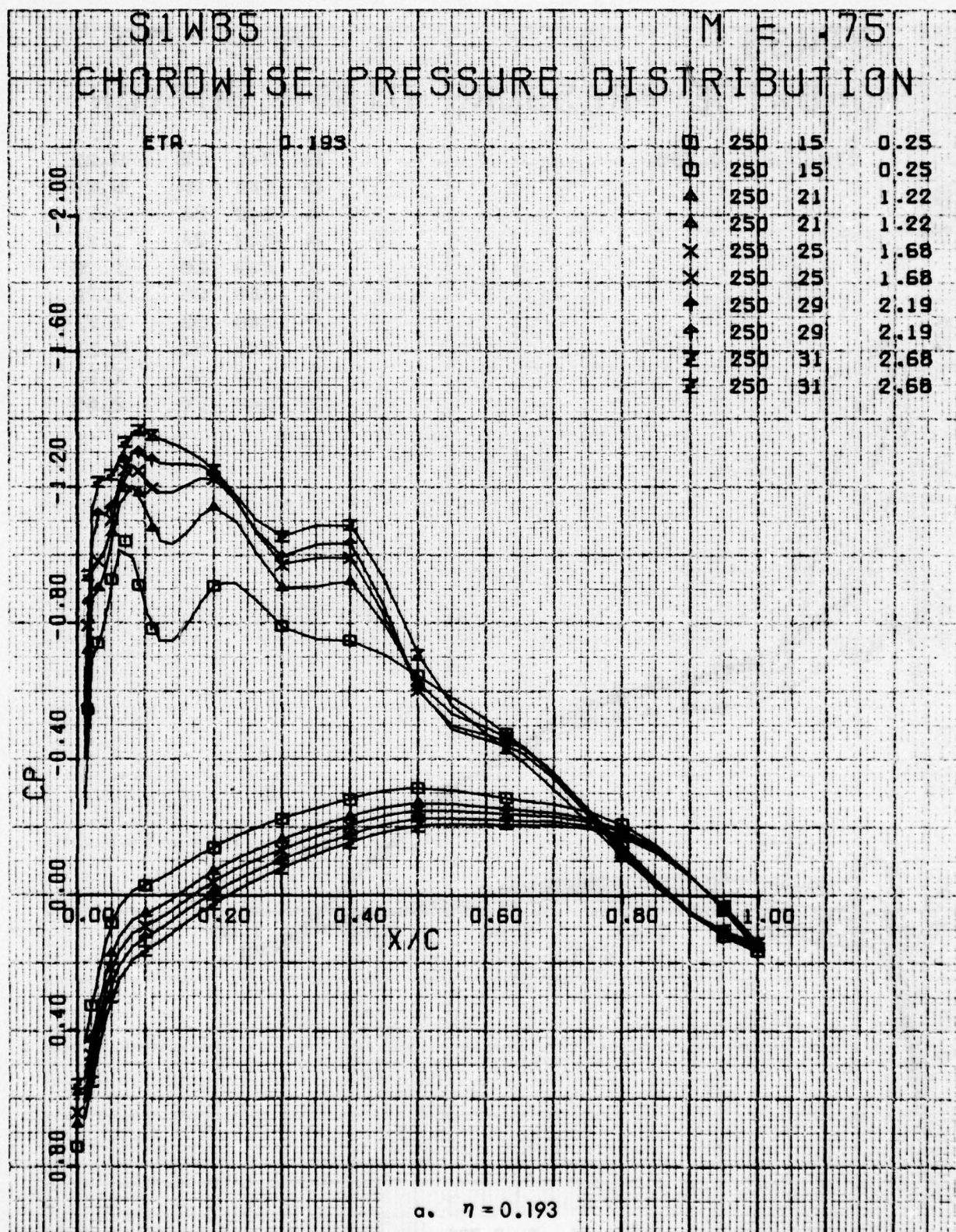


Figure 50 . Chordwise Pressure Distributions for Various Angles of Attack. W³⁵ Leading Edge Modification, Fixed Transition, Grit Code D, M = 0.75.

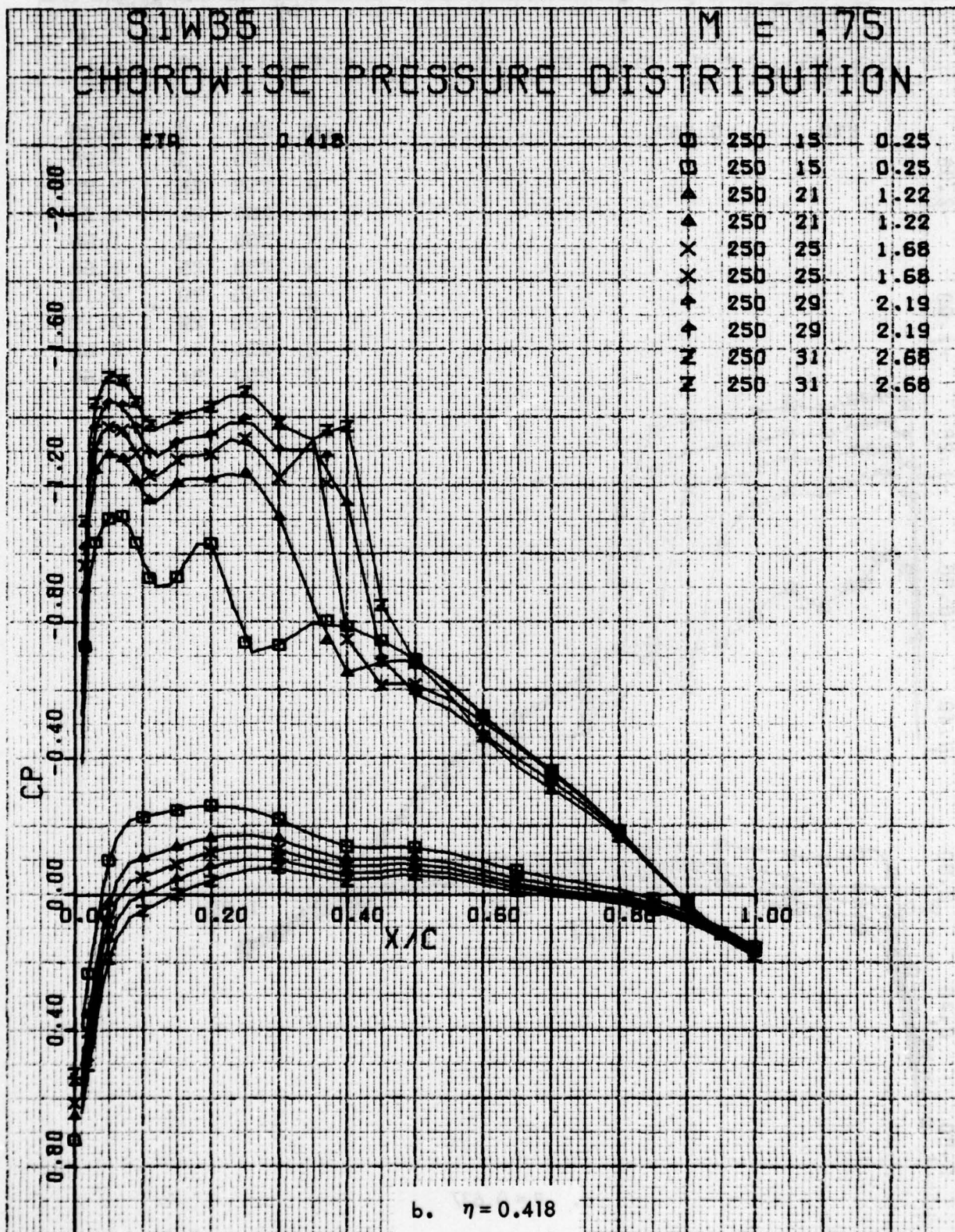


Figure 50. Continued

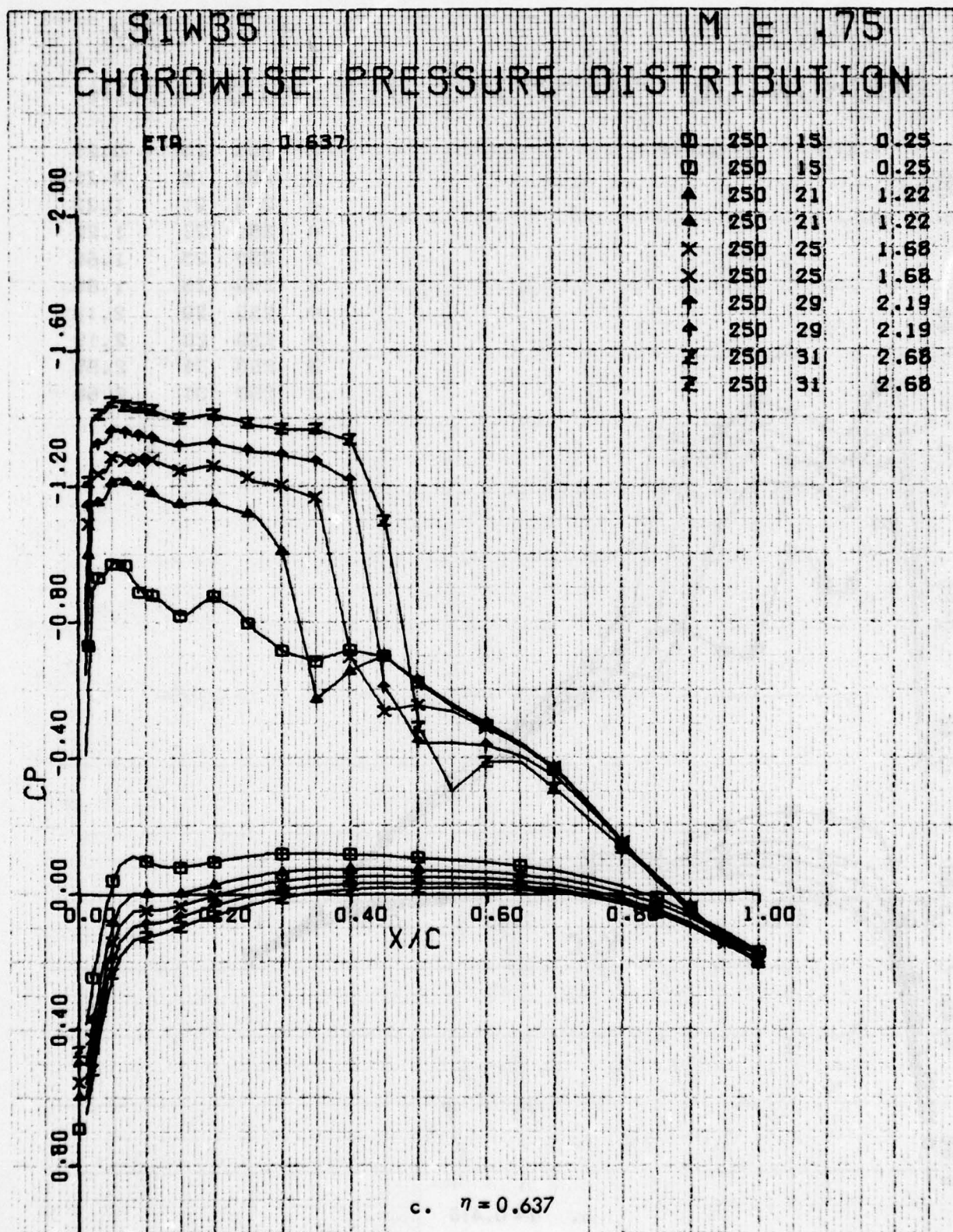


Figure 50. Continued

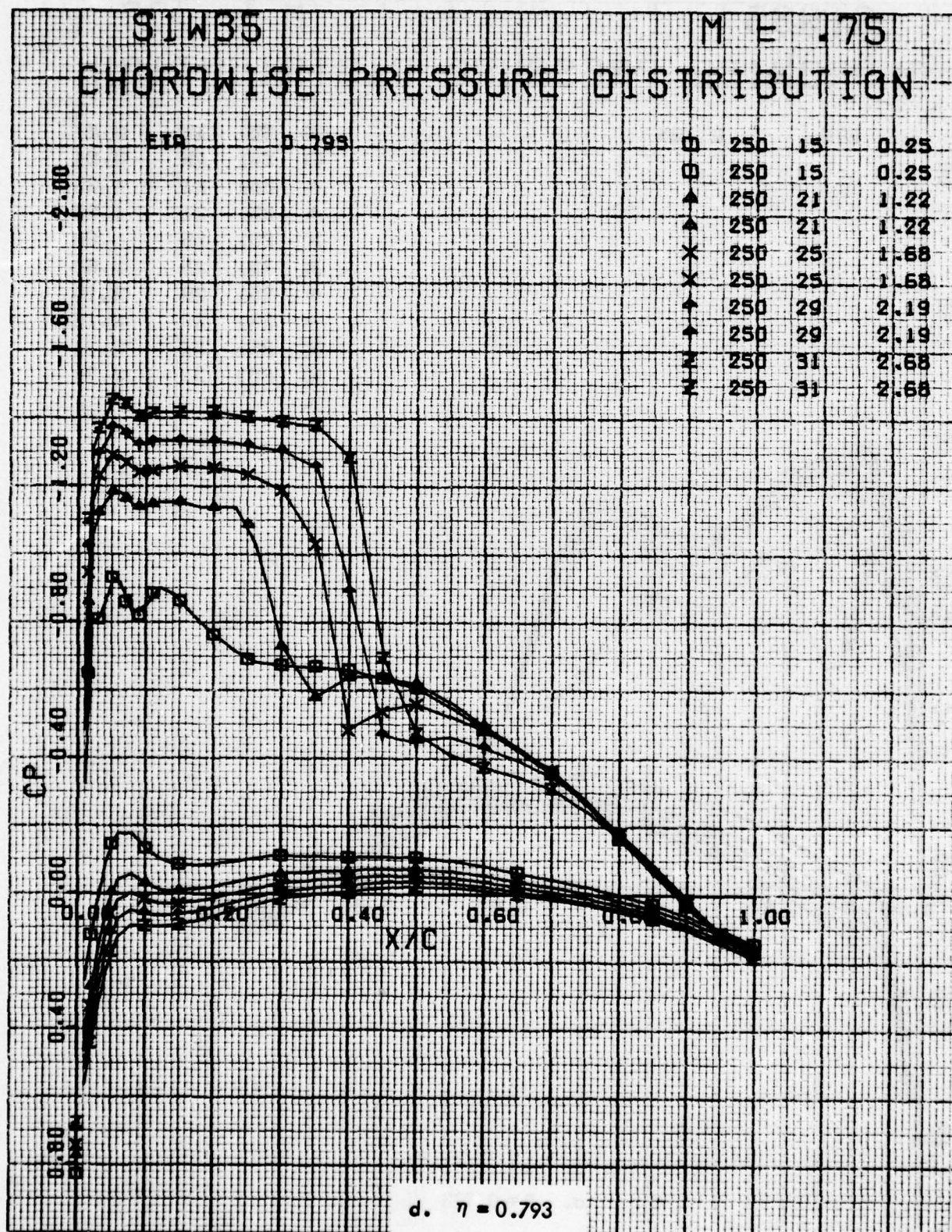


Figure 50. Concluded

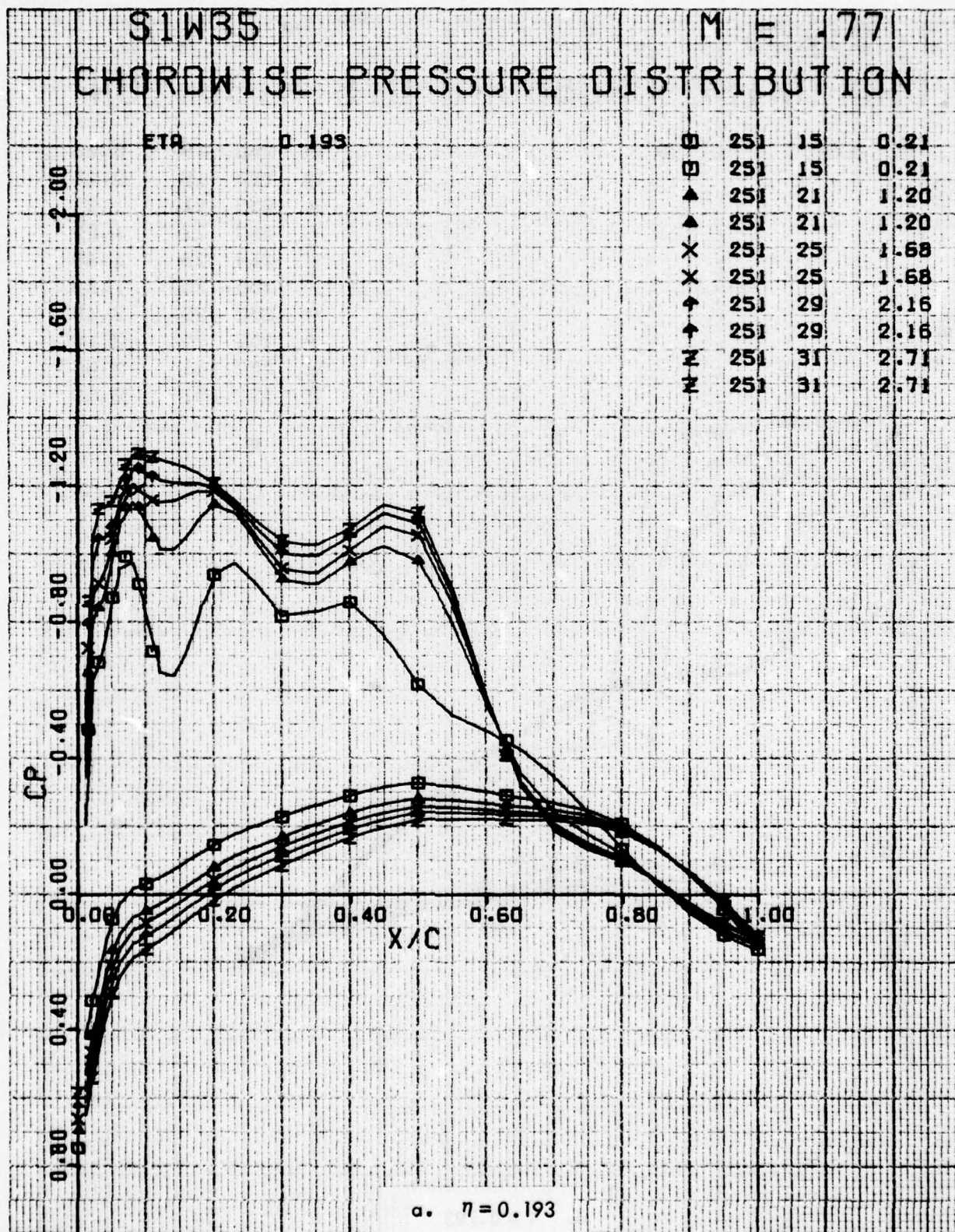


Figure 51 . Chordwise Pressure Distributions for Various Angles of Attack. W³⁵ Leading Edge Modification, Fixed Transition, Grit Code D, M = 0.77.

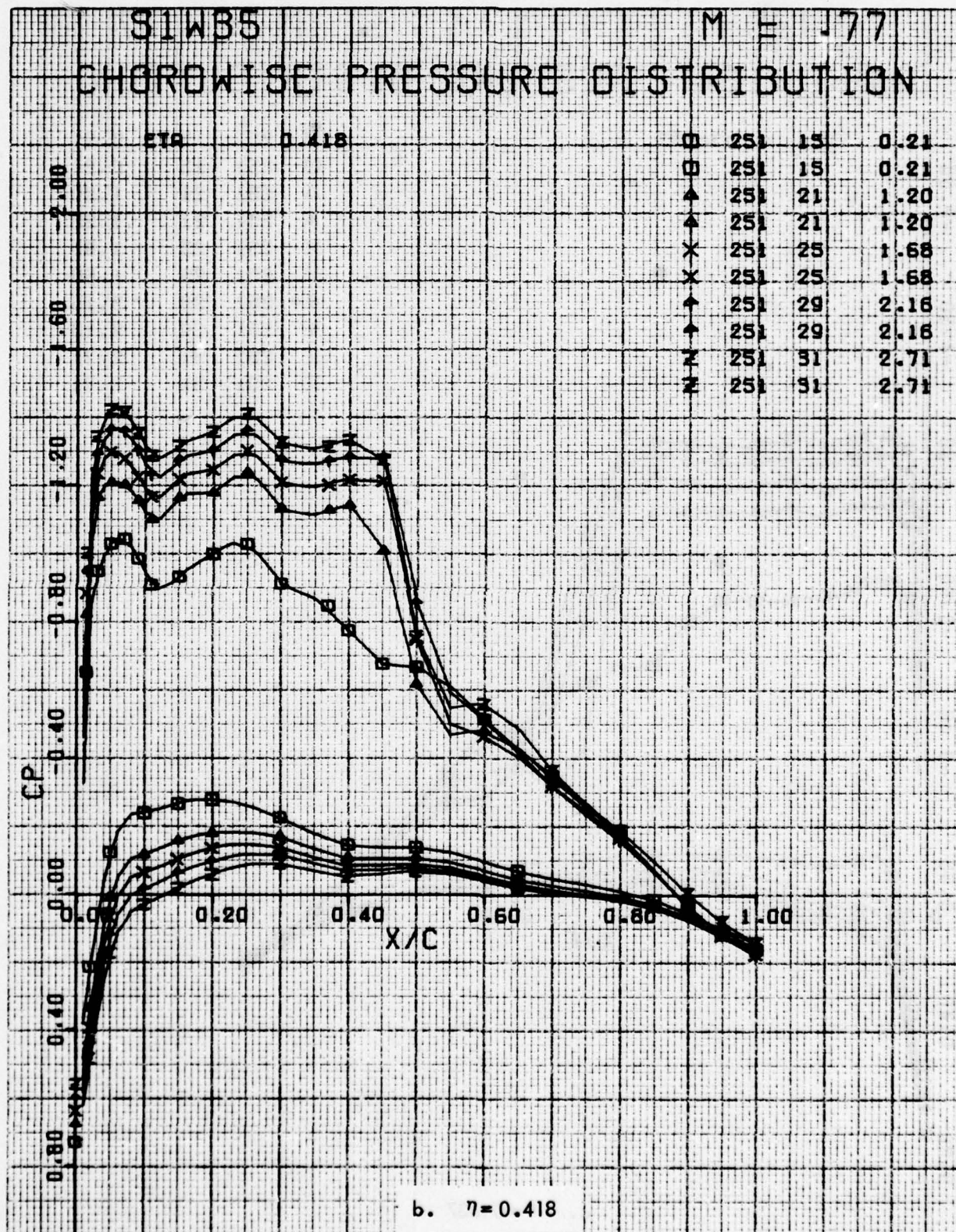


Figure 51. Continued

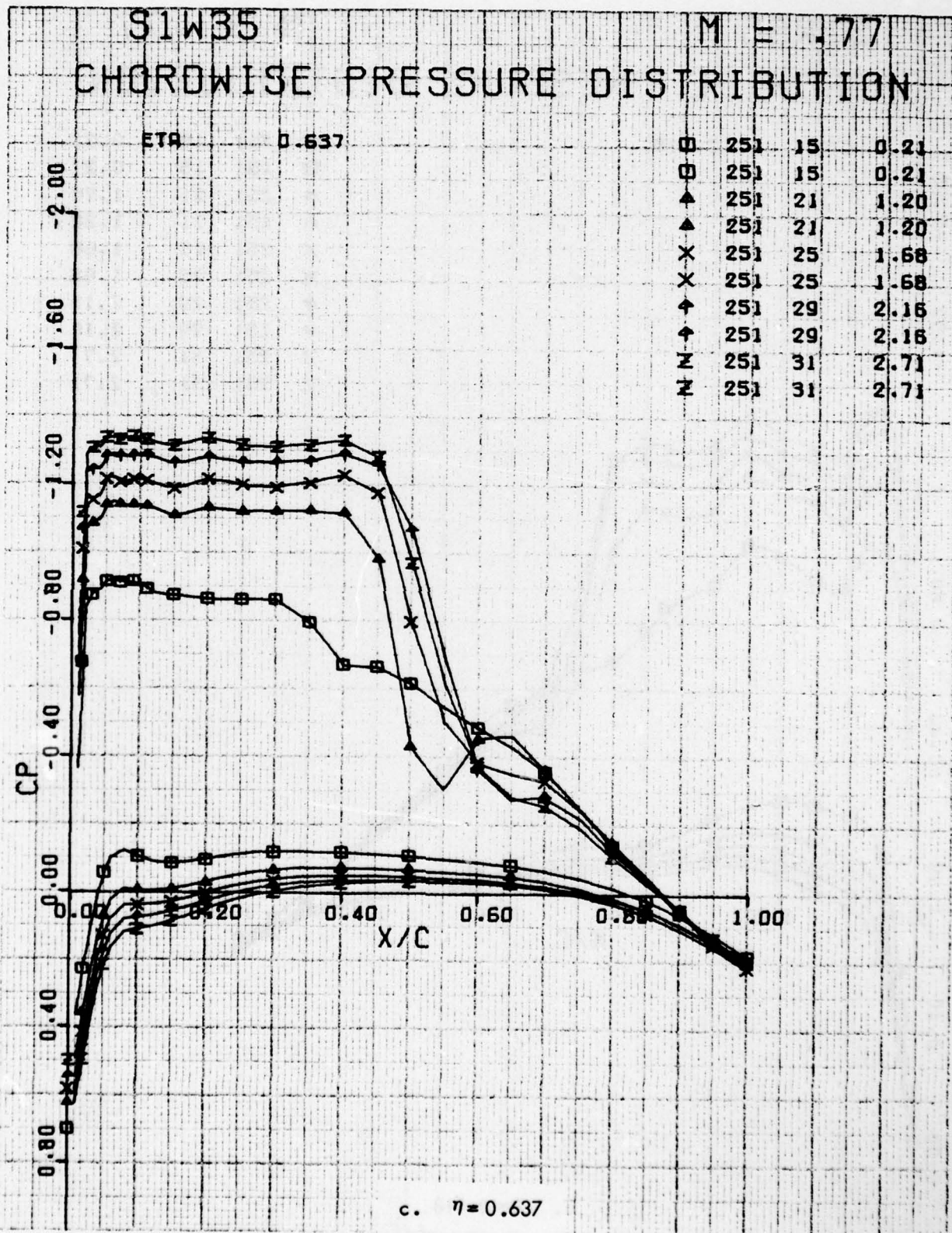


Figure 51. Continued

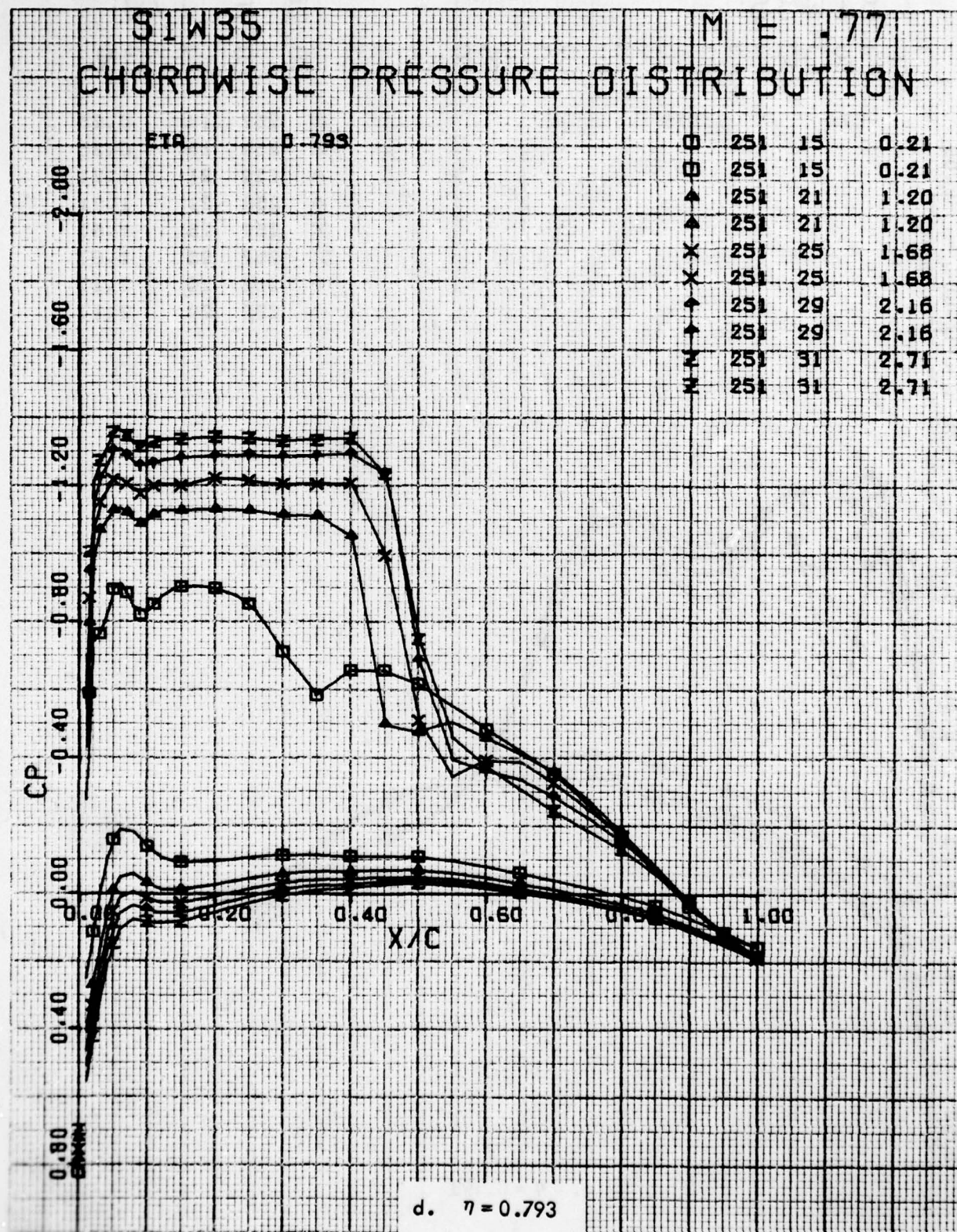


Figure 51. Concluded

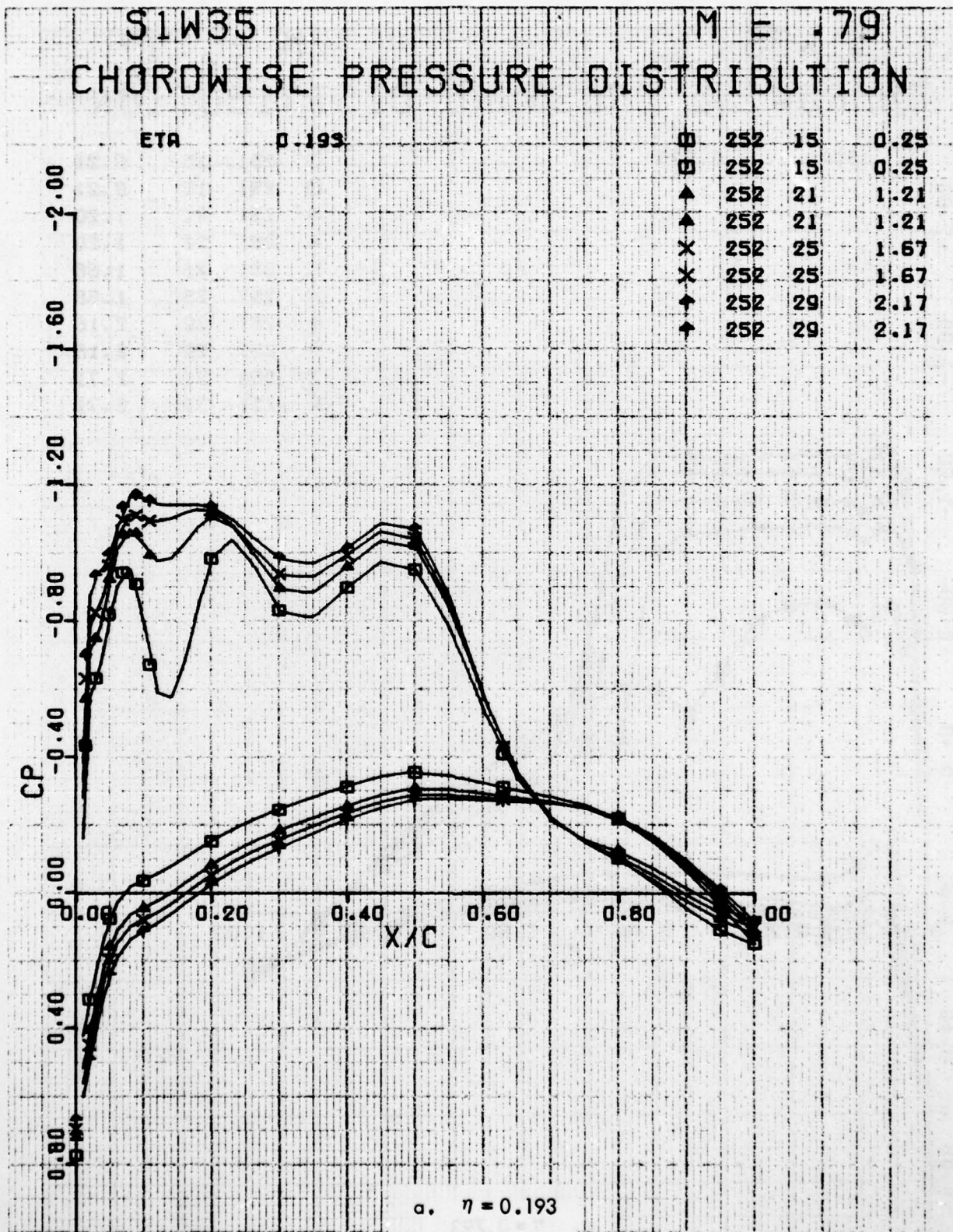


Figure 52 . Chordwise Pressure Distributions for Various Angles of Attack. W³⁵ Leading Edge Modification, Fixed Transition, Grit Code D, M = 0.79.

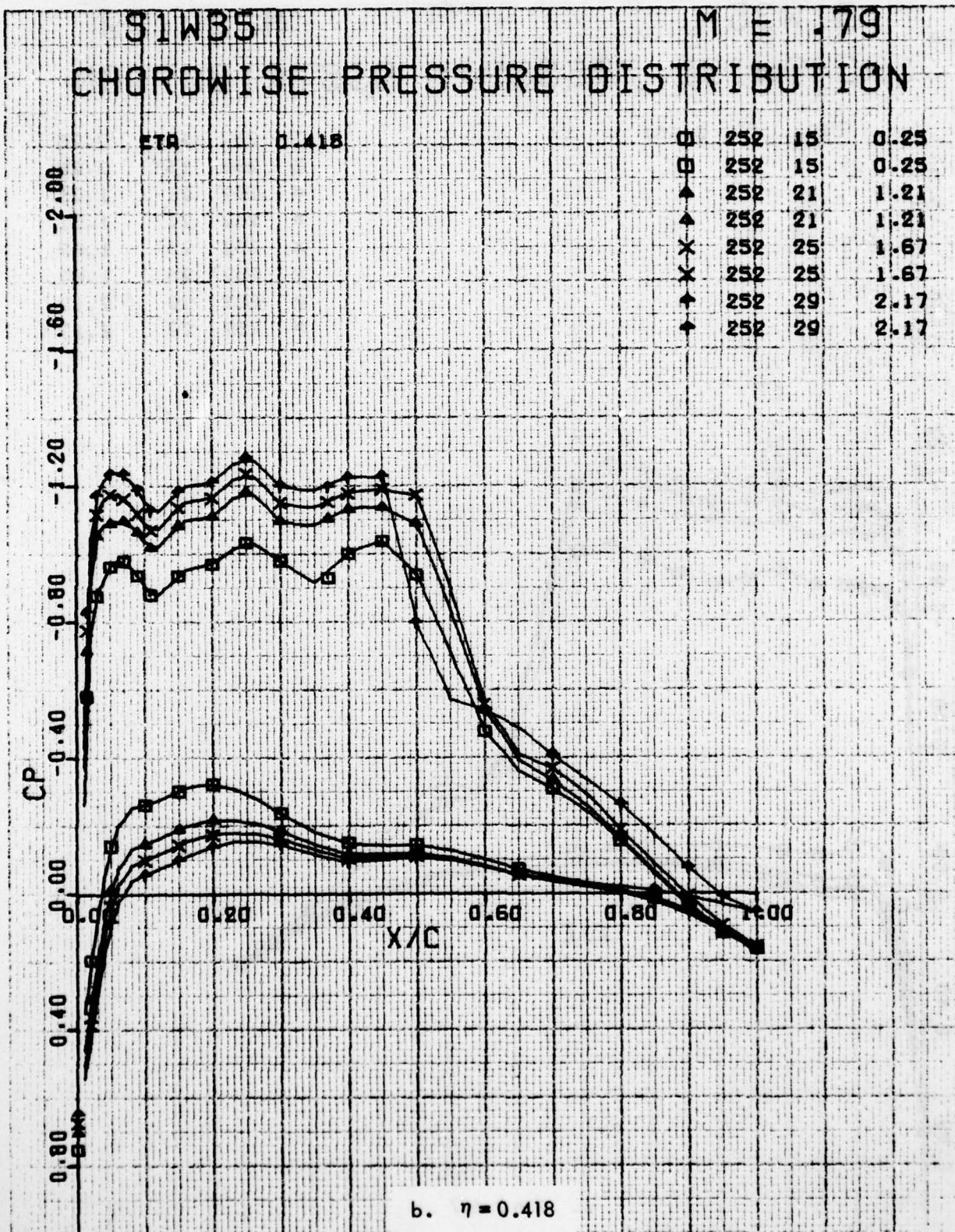


Figure 52. Continued

S1W35 M = .79 CHORDWISE PRESSURE DISTRIBUTION

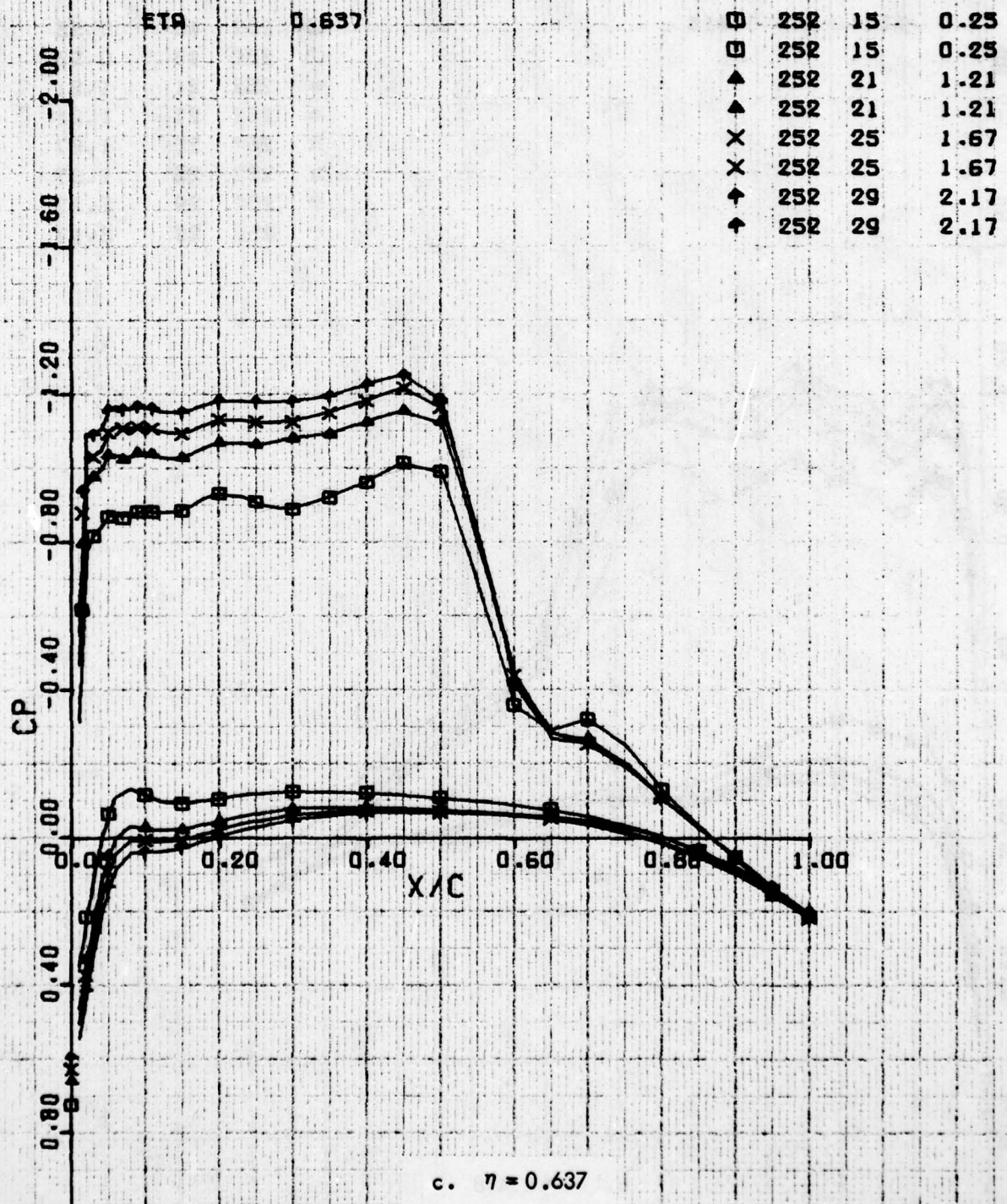


Figure 52. Continued

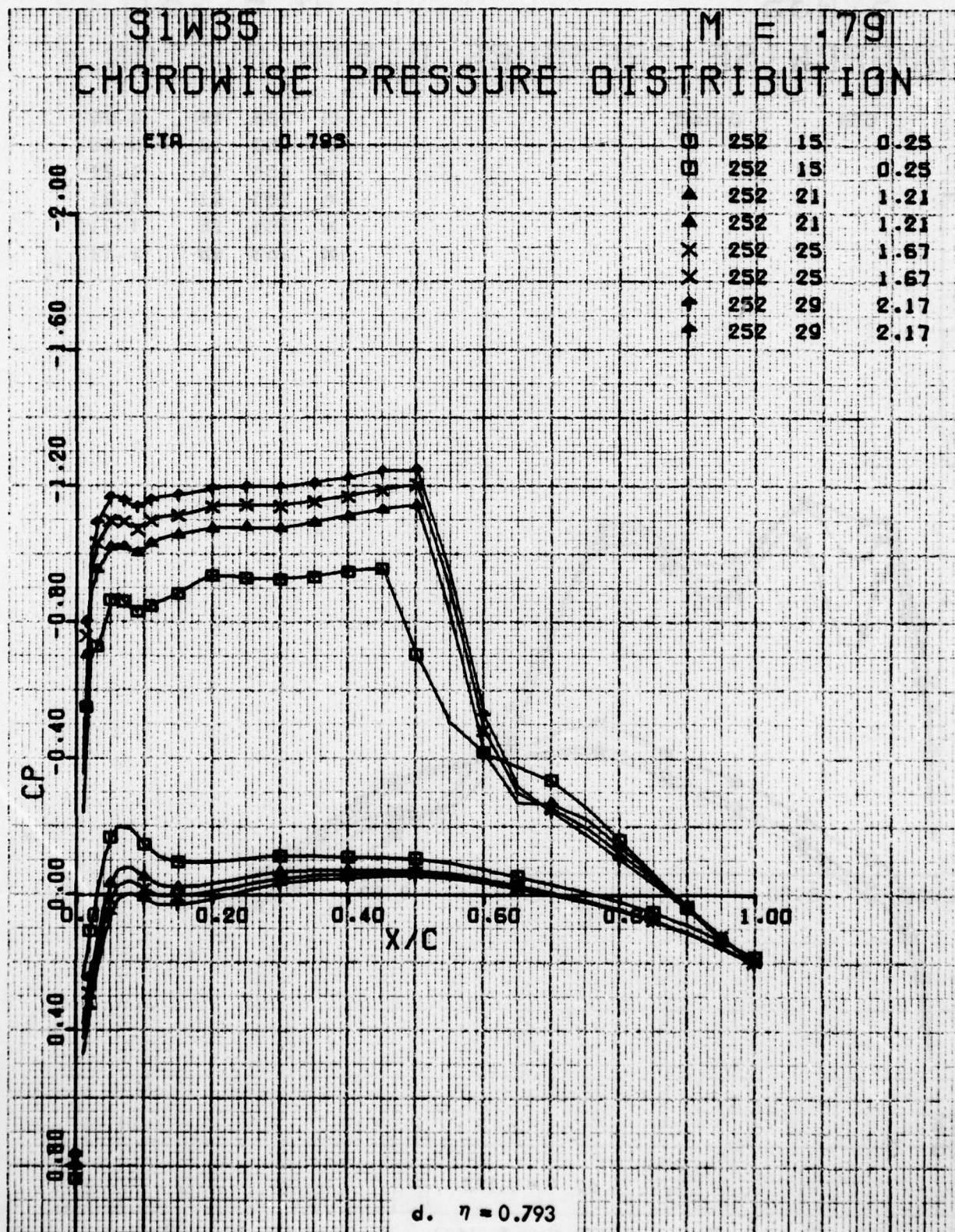


Figure 52. Concluded

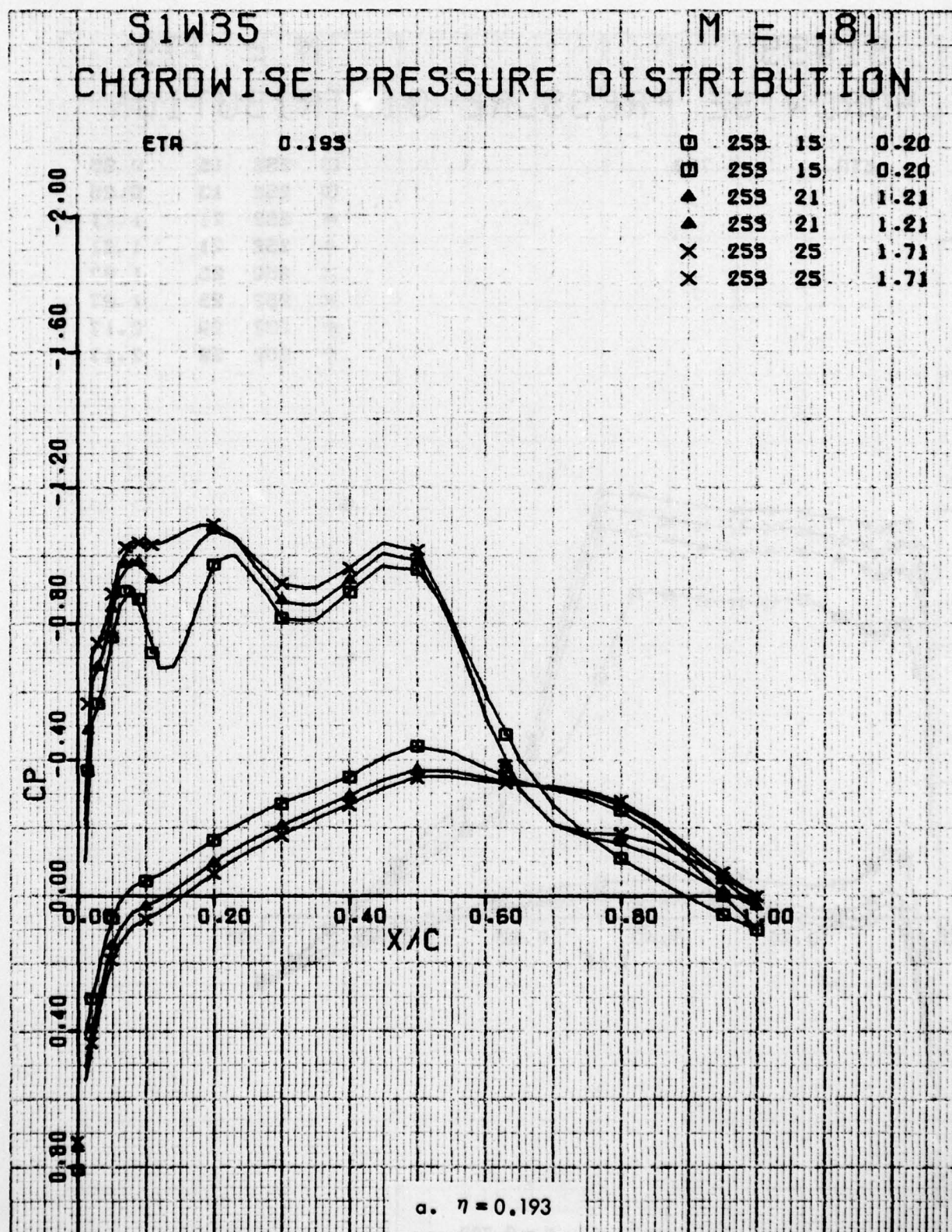


Figure 53. Chordwise Pressure Distributions for Various Angles of Attack. W³⁵ Leading Edge Modification, Fixed Transition, Grit Code D, M = 0.81.

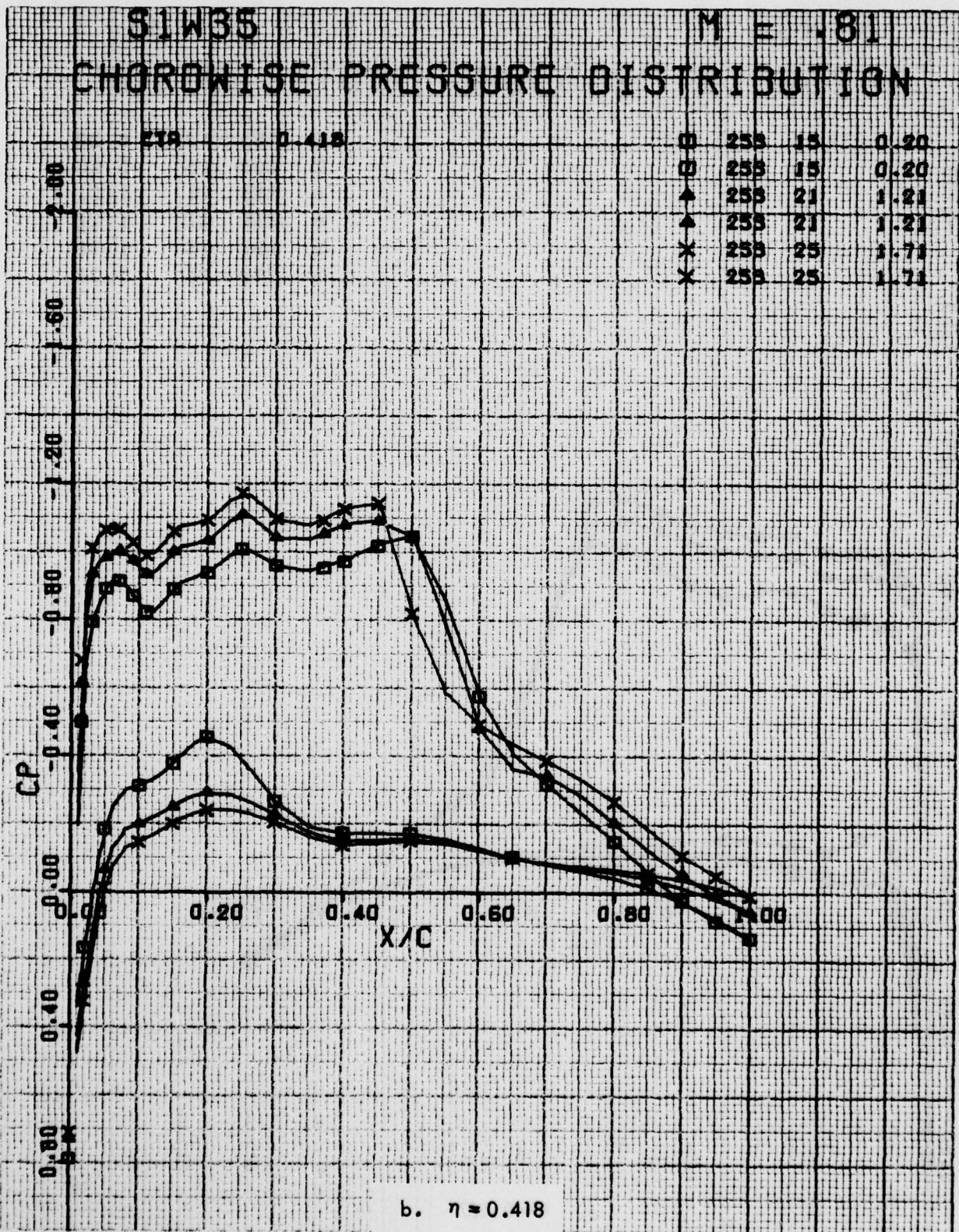


Figure 53. Continued

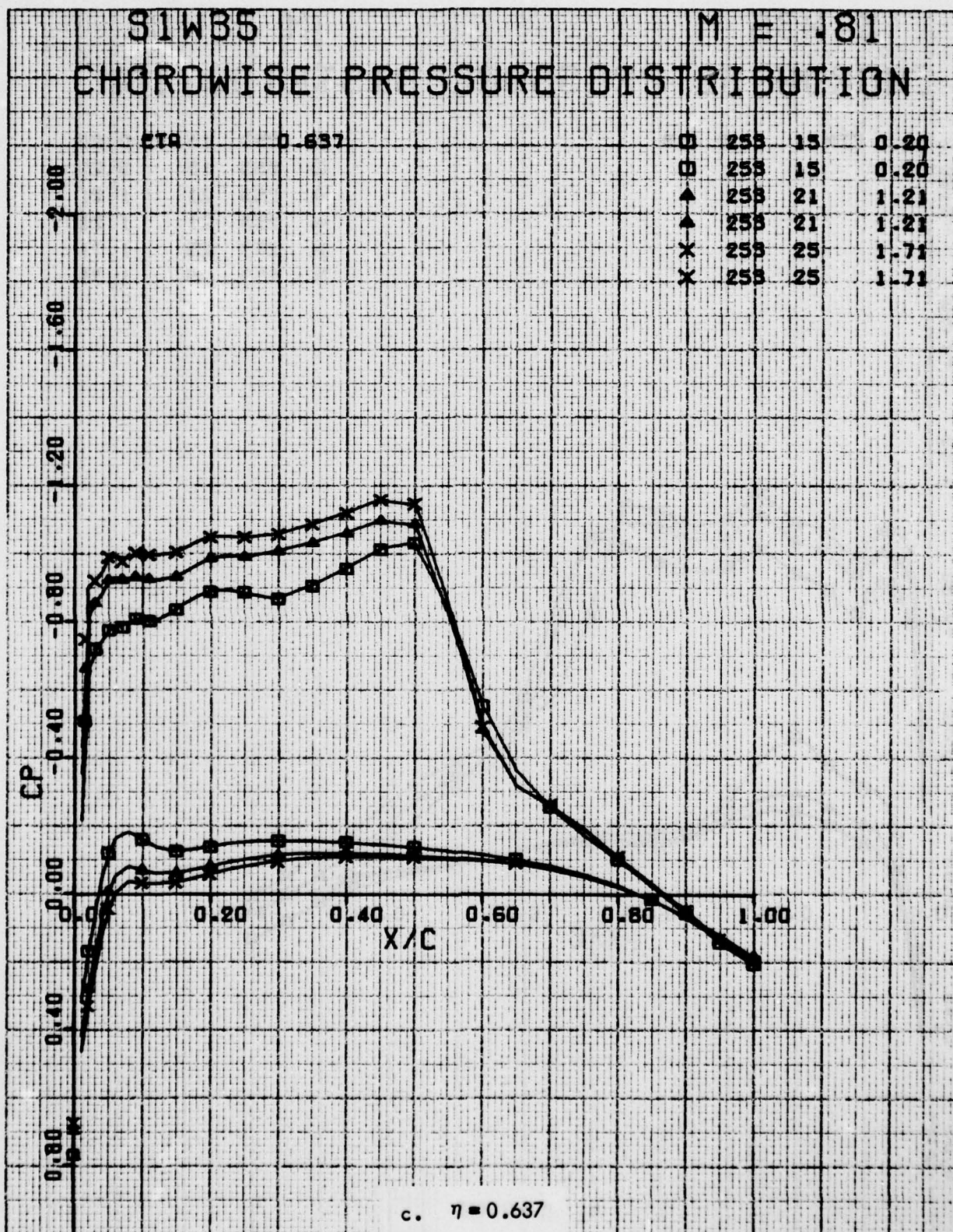


Figure 53. Continued

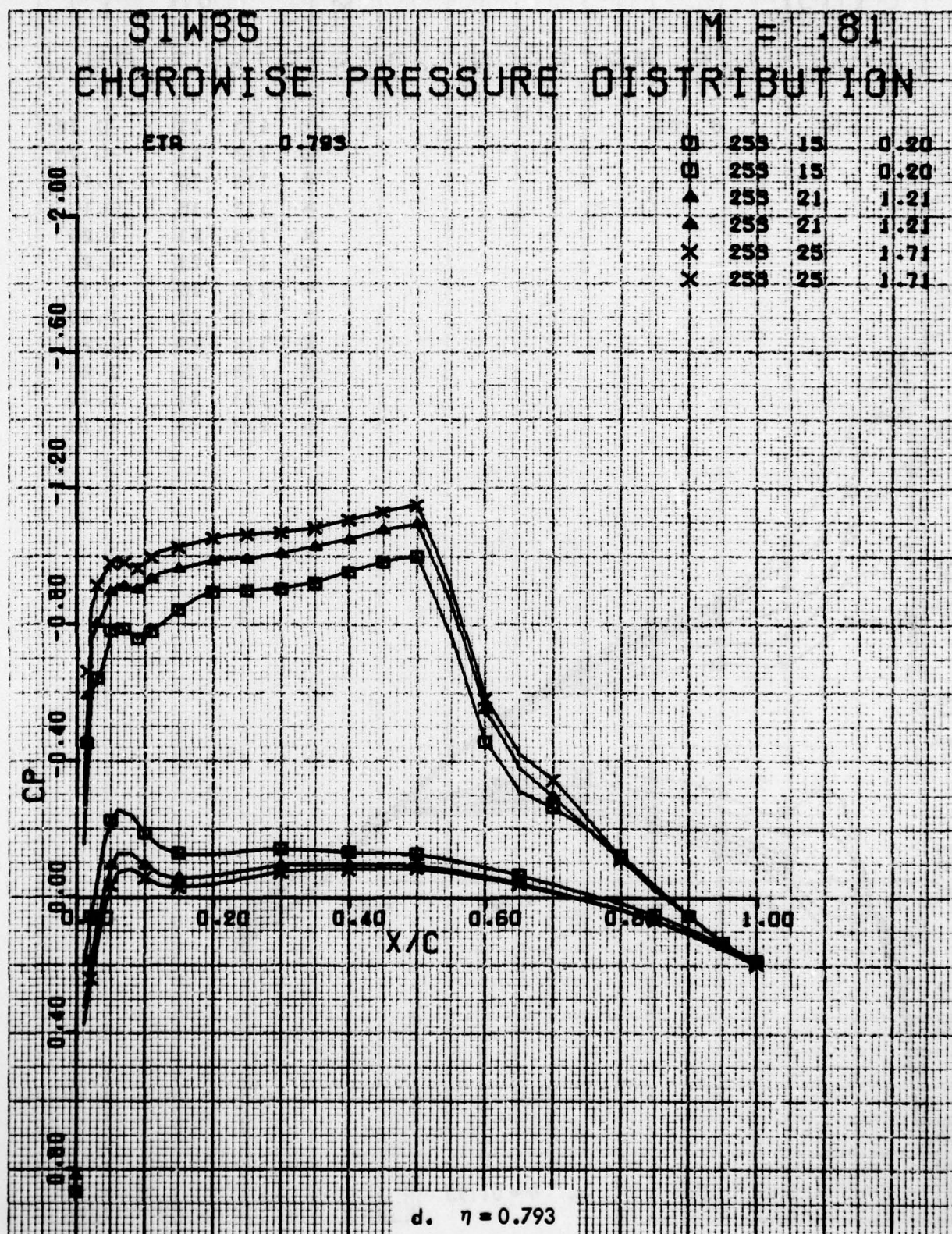


Figure 53. Concluded

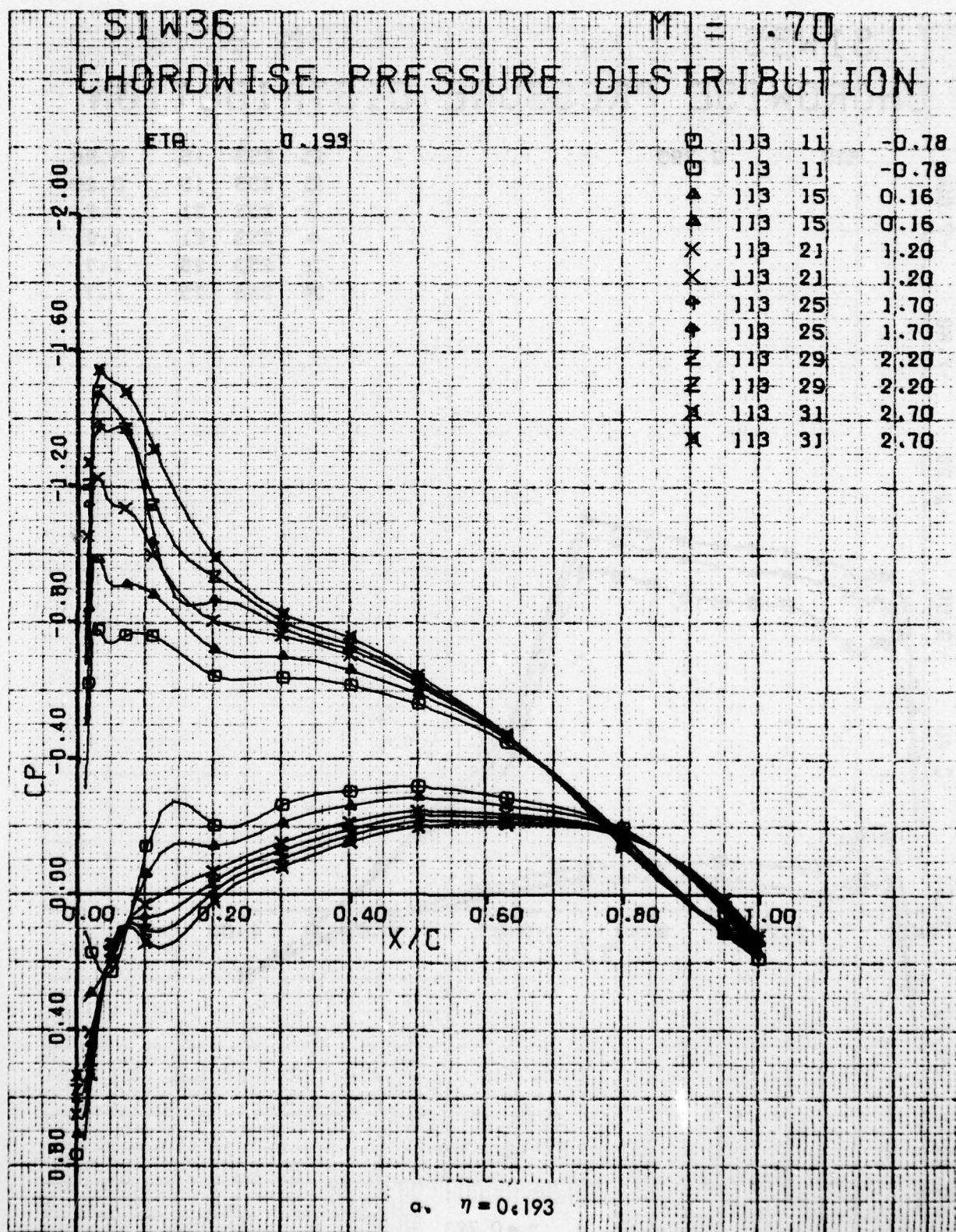


Figure 54. Chordwise Pressure Distributions for Various Angles of Attack. W^{36} Leading Edge Modification, Fixed Transition, Grit Code B, $M = 0.7$.

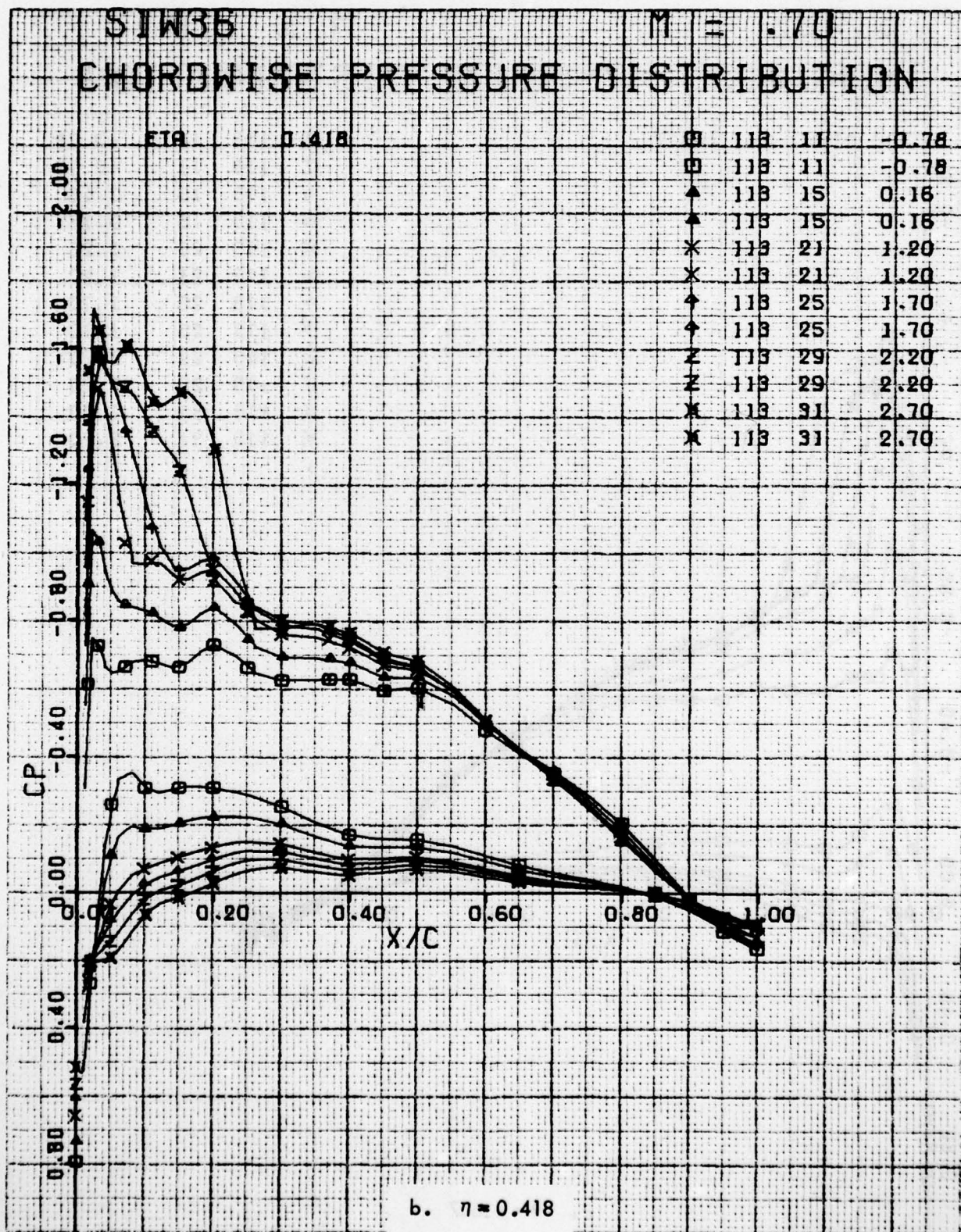


Figure 54. Continued

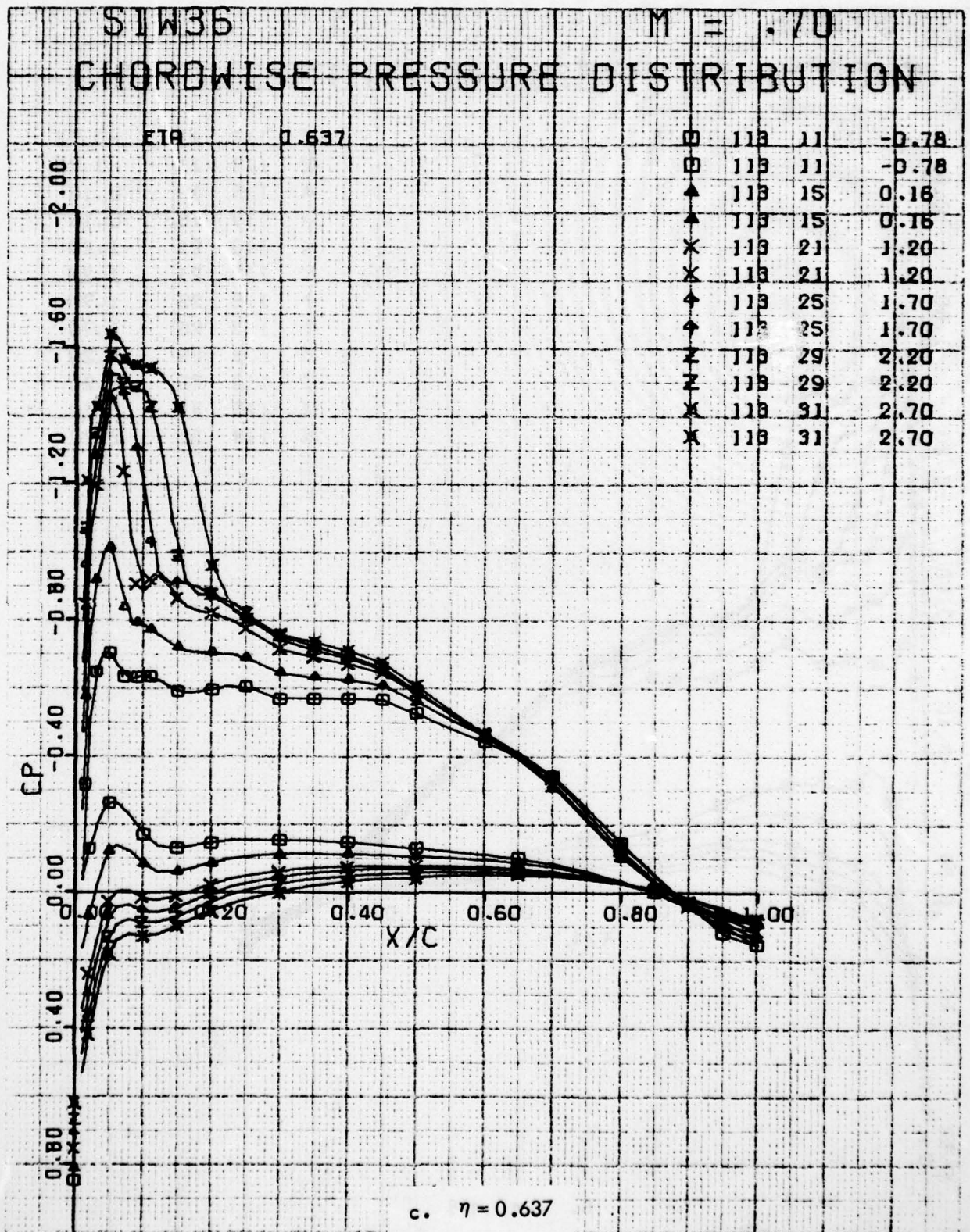


Figure 54. Continued

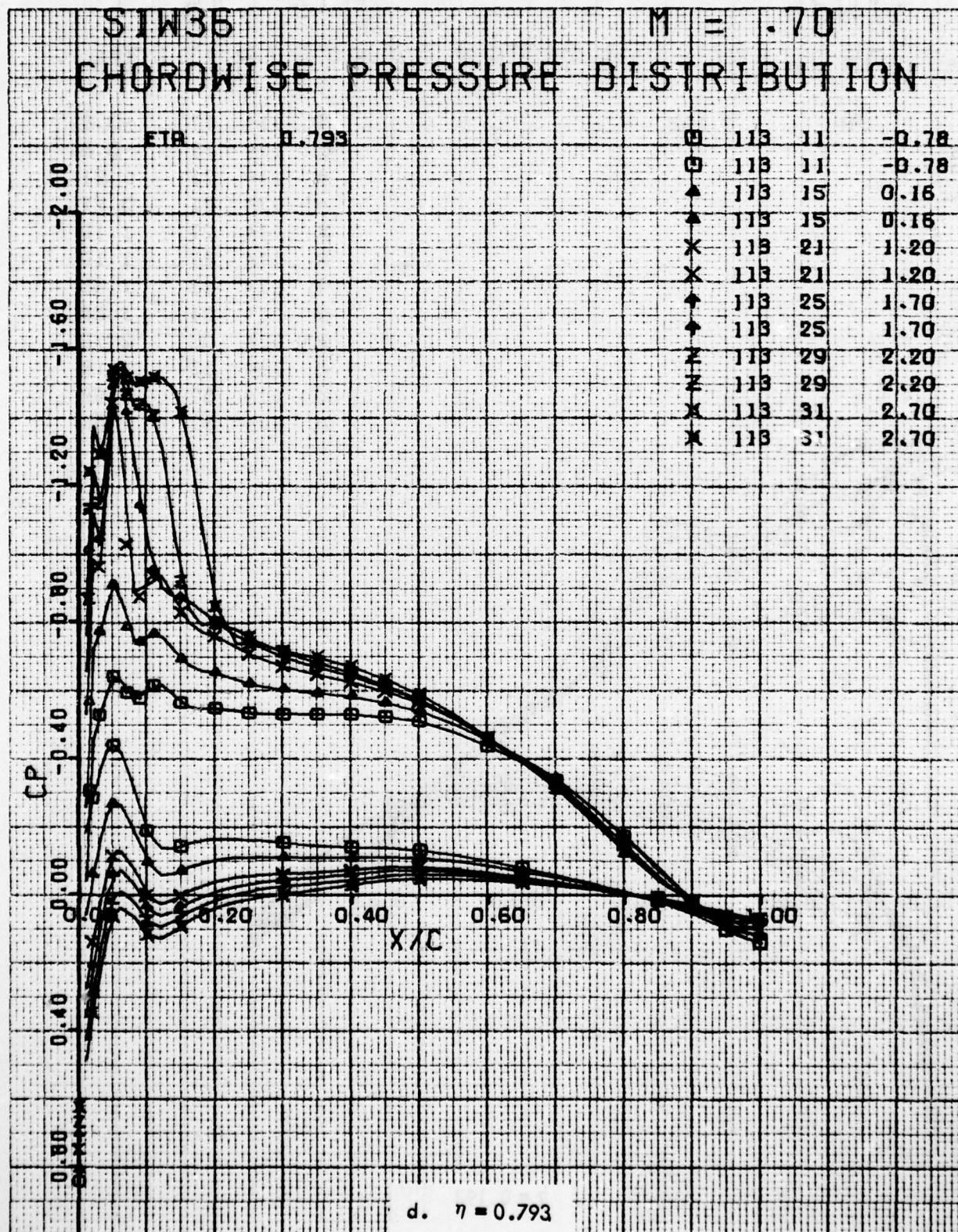


Figure 54. Concluded

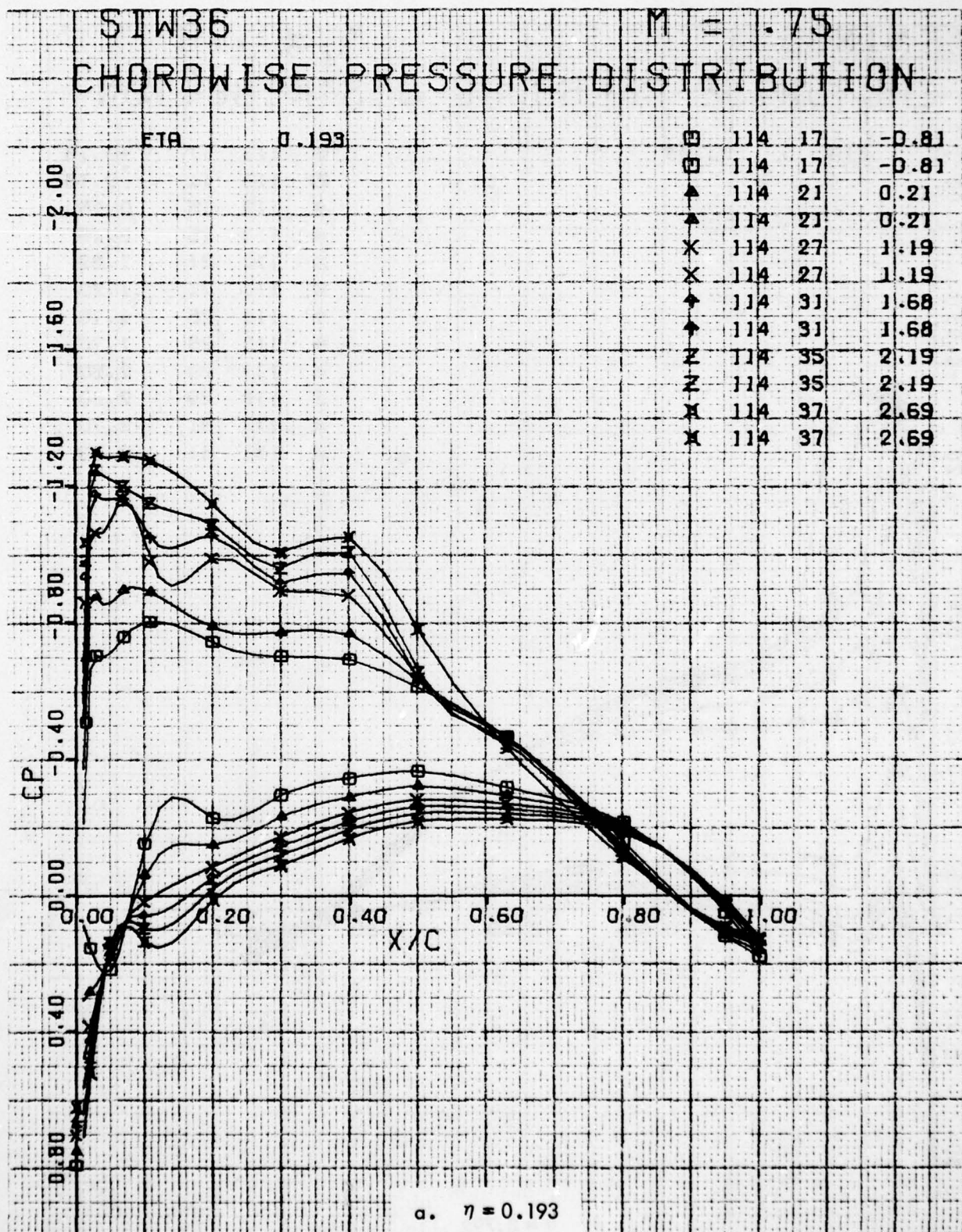


Figure 55 . Chordwise Pressure Distributions for Various Angles of Attack. W³⁶ Leading Edge Modification, Fixed Transition, Grit Code B, $M = 0.75$.

AD-A077 688

LOCKHEED-GEORGIA CO MARIETTA

F/G 1/3

AERODYNAMIC INVESTIGATION OF C-141 LEADING EDGE MODIFICATION FO--ETC(U)

JUN 79 W T BLACKERBY , P R SMITH

F09603-77-A-0204

UNCLASSIFIED

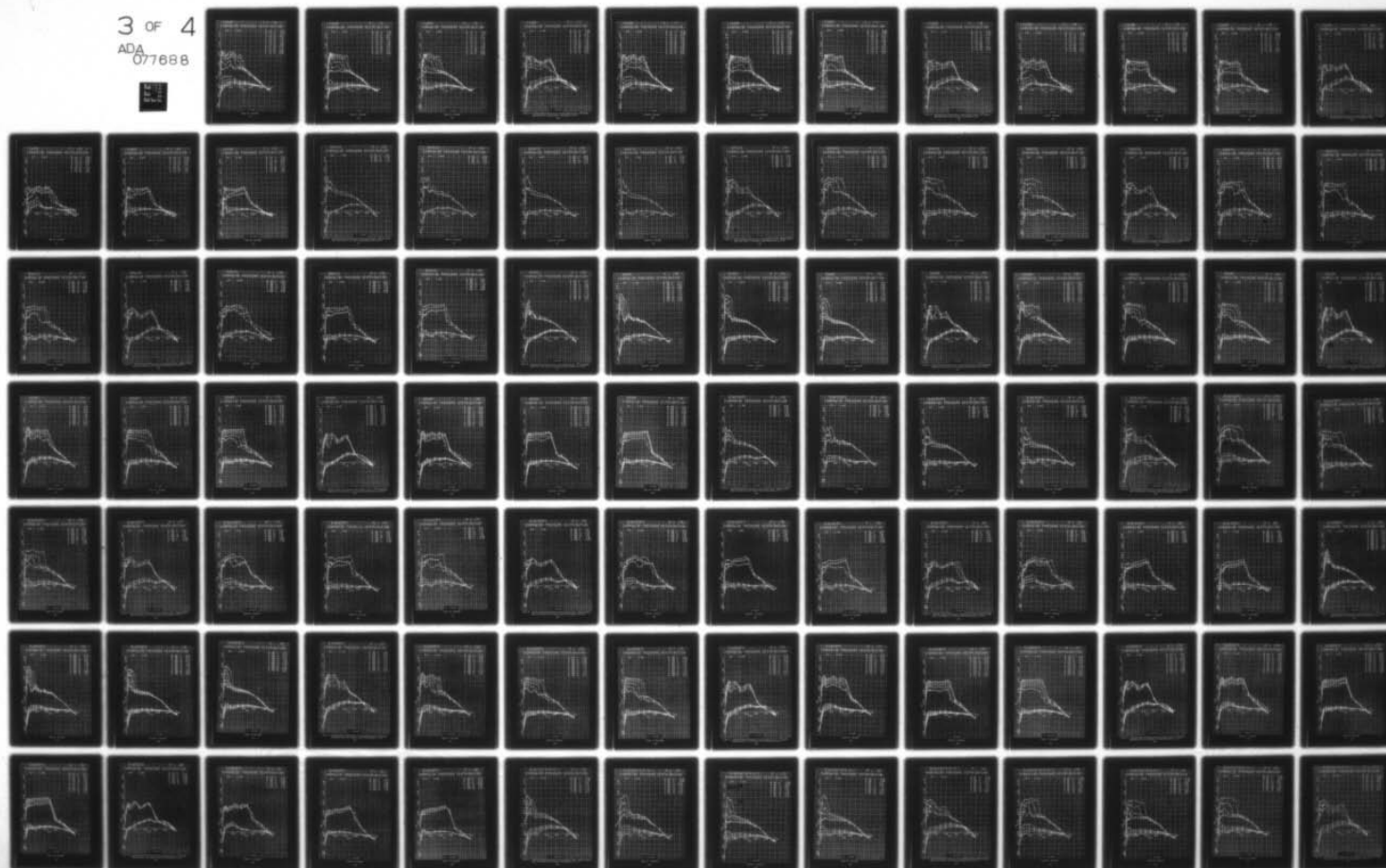
LG78ER0233-VOL-2

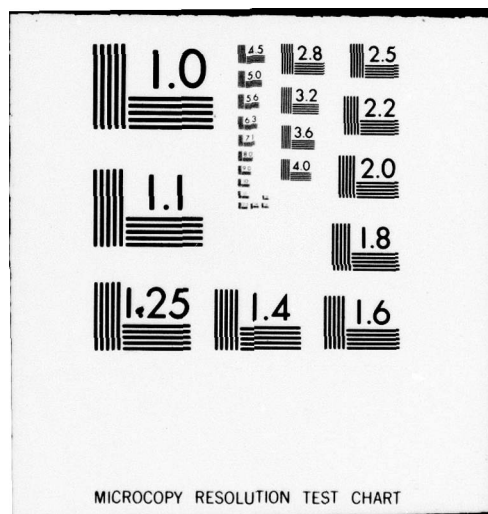
AFFDL-TR-79-3059-VOL-2

NL

3 OF 4

ADA
077688





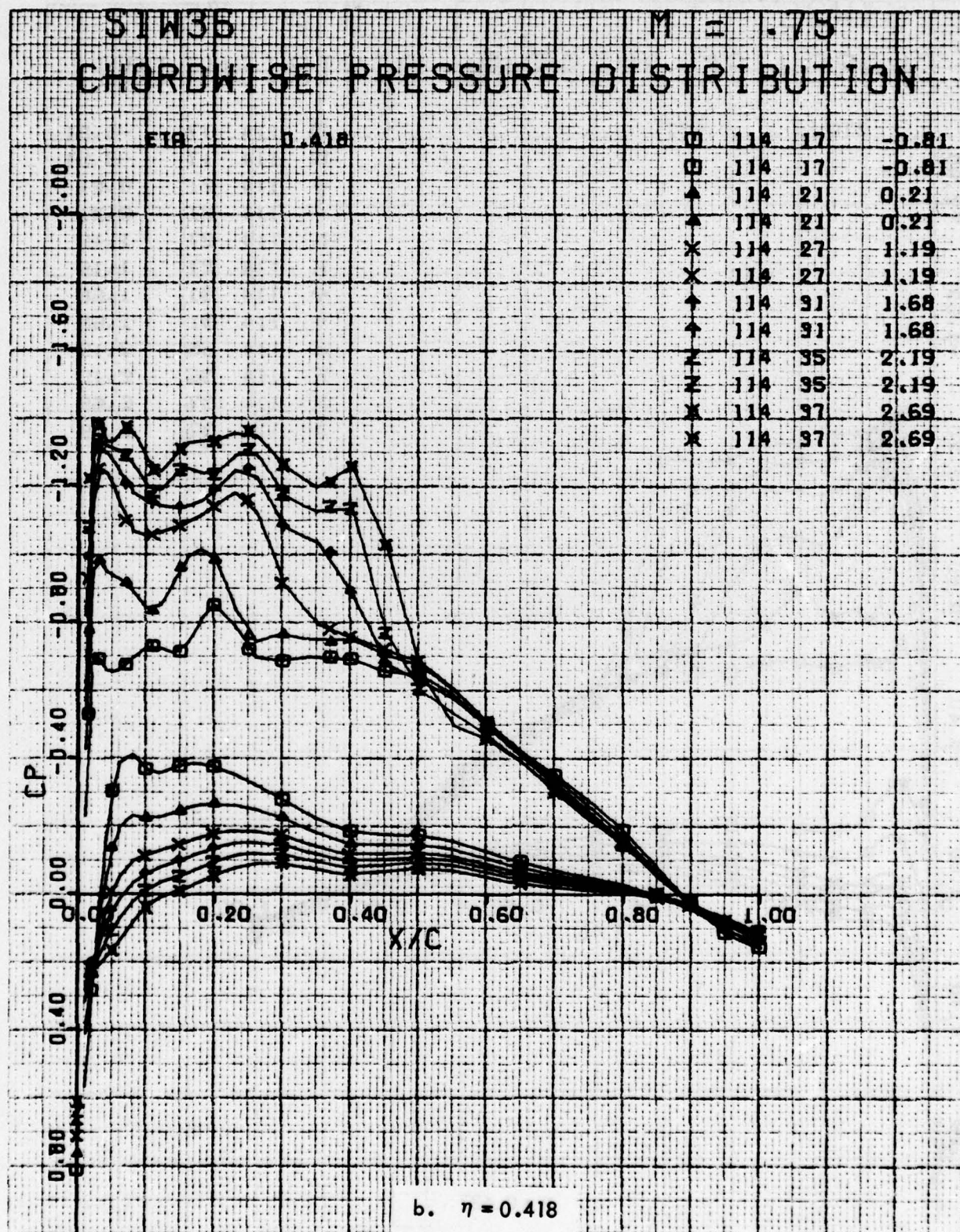


Figure 55. Continued

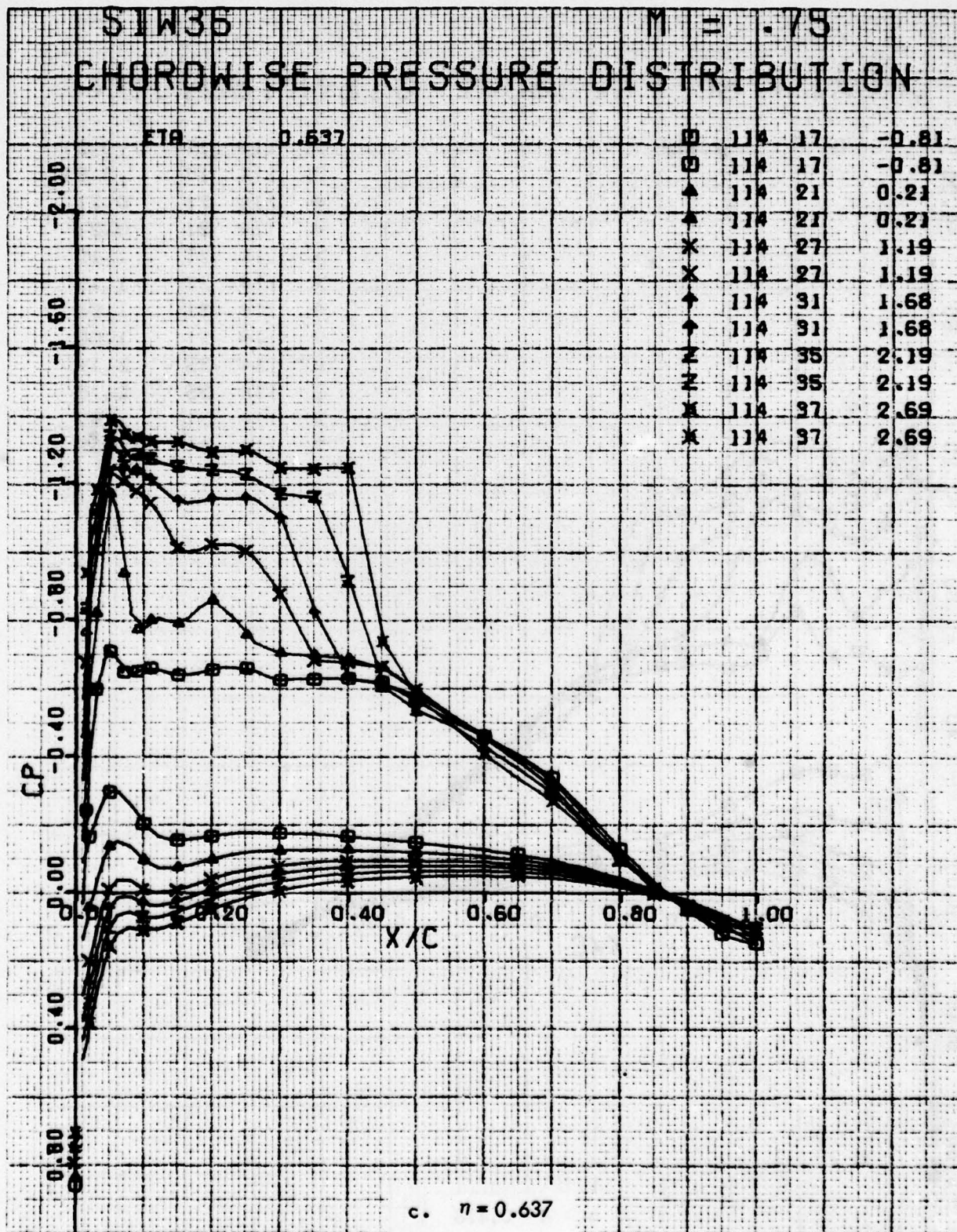


Figure 55. Continued

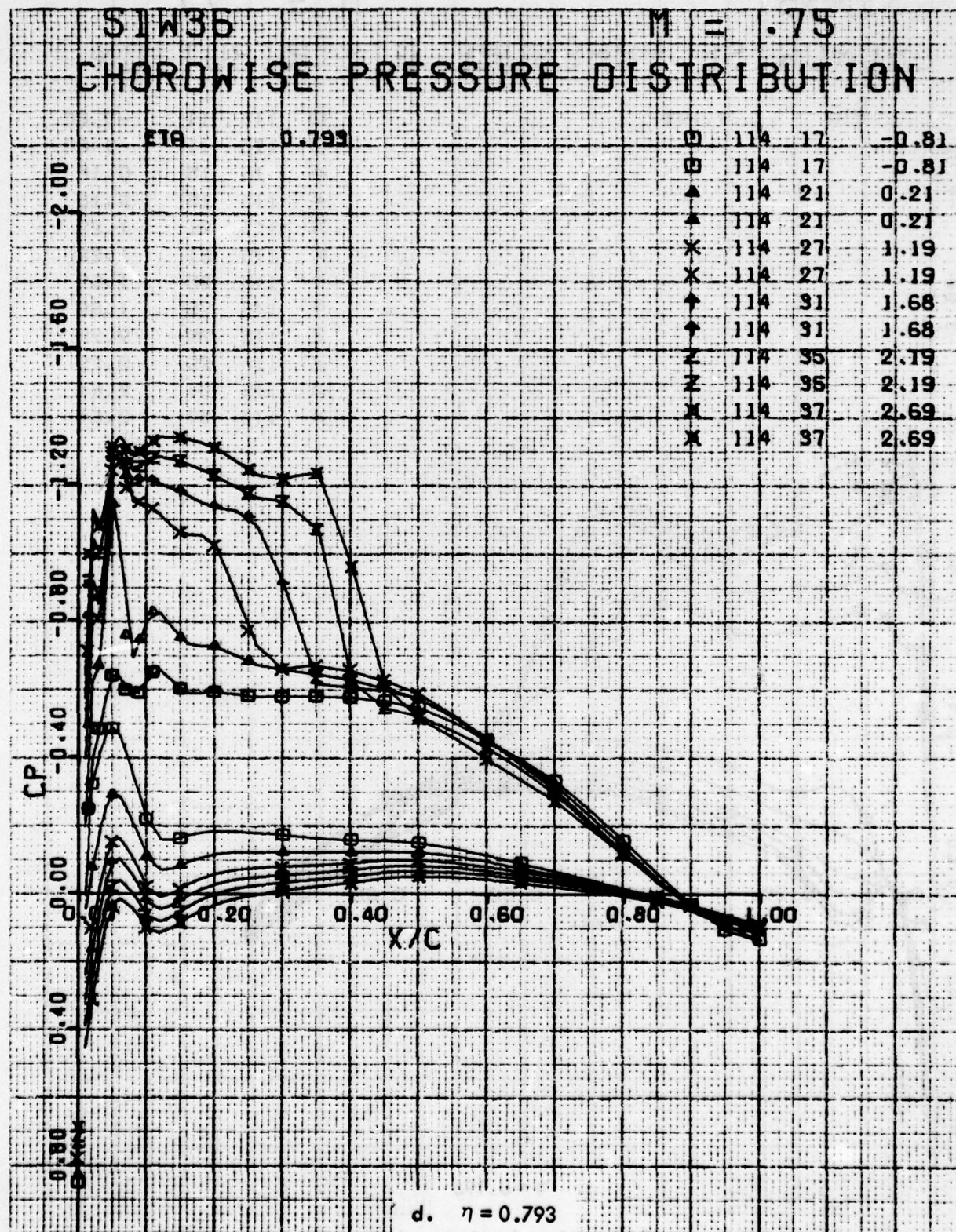


Figure 55. Concluded

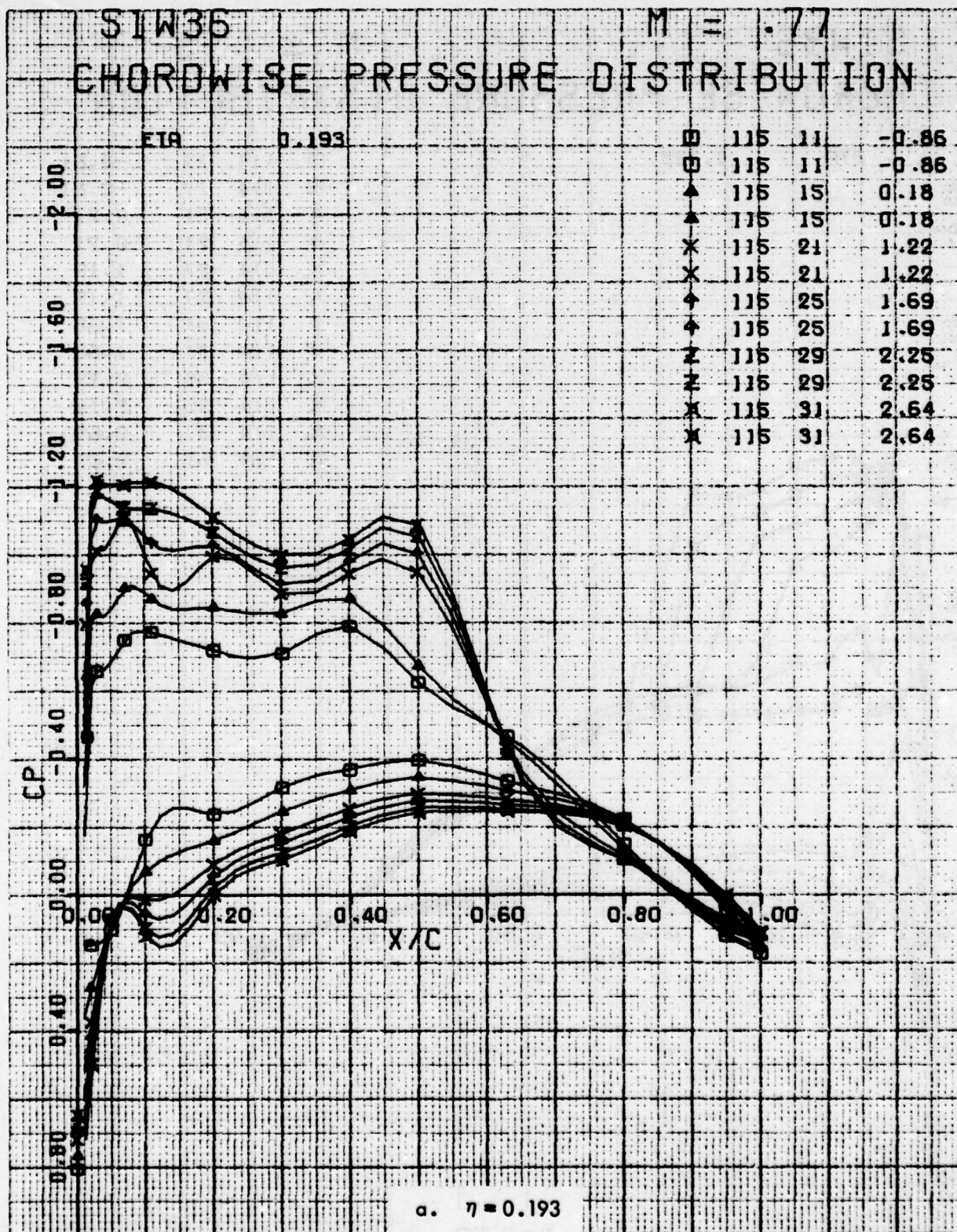


Figure 56. Chordwise Pressure Distributions for Various Angles of Attack. W³⁶ Leading Edge Modification, Fixed Transition, Grit Code B, M = 0.77.

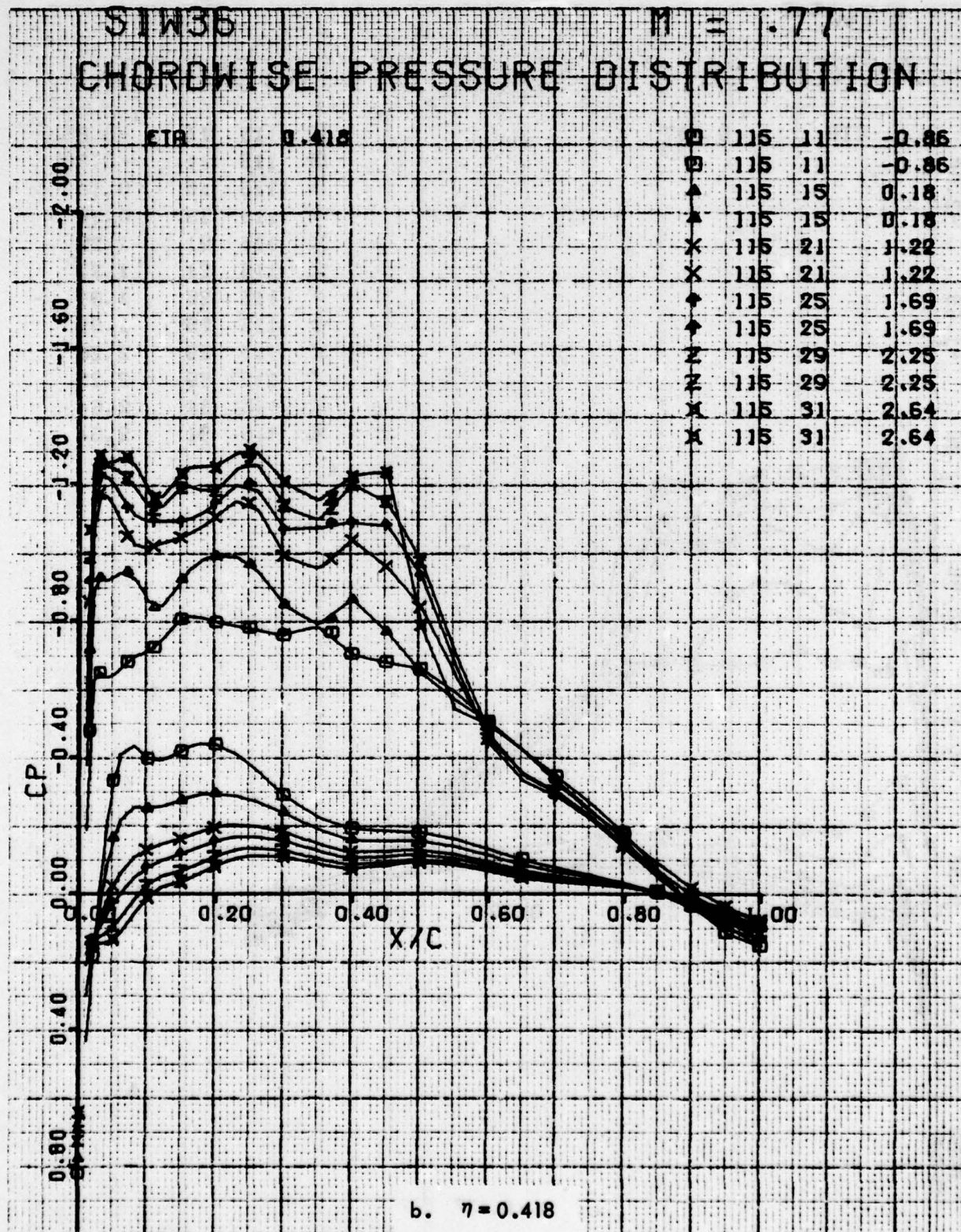


Figure 56. Continued

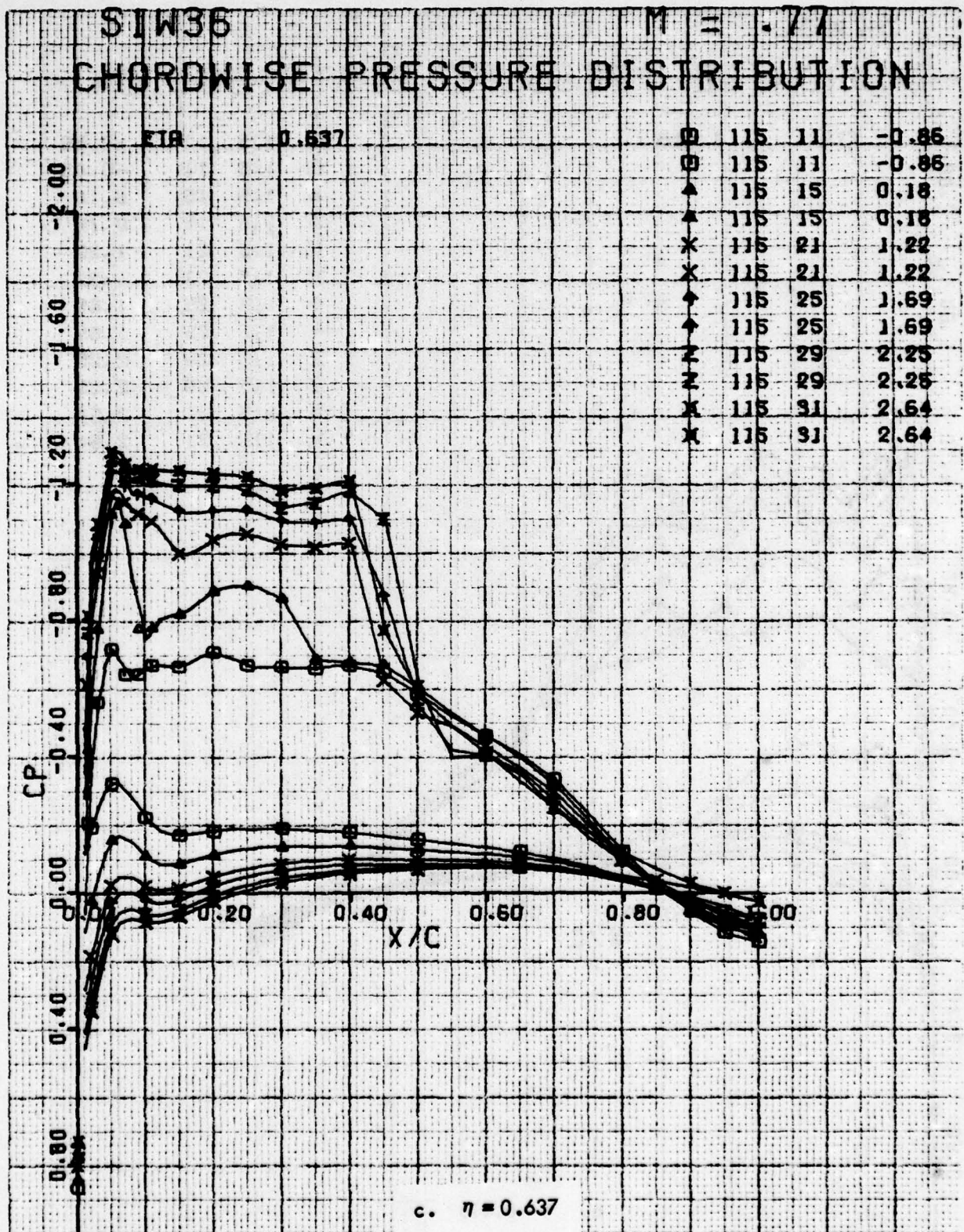


Figure 56. Continued

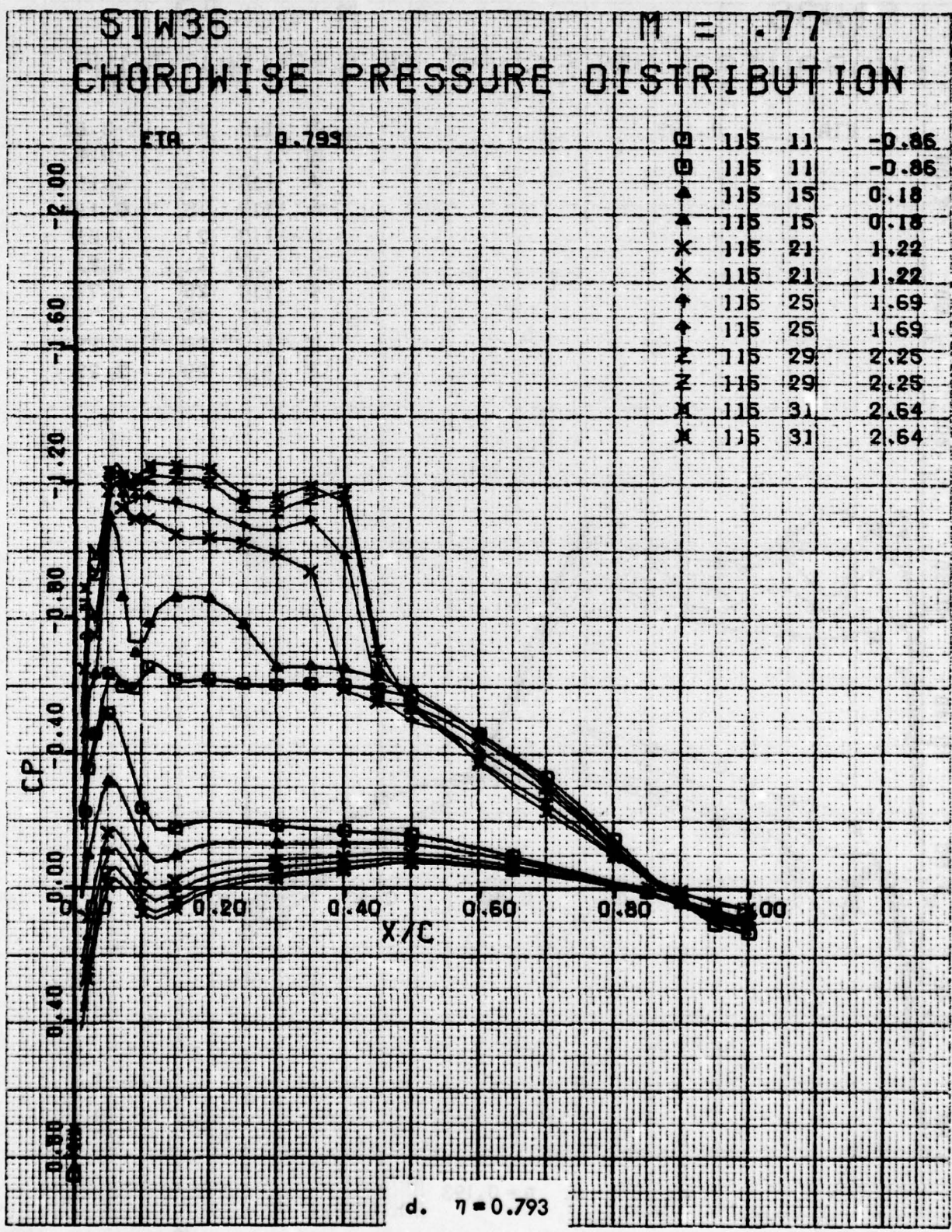


Figure 56. Concluded

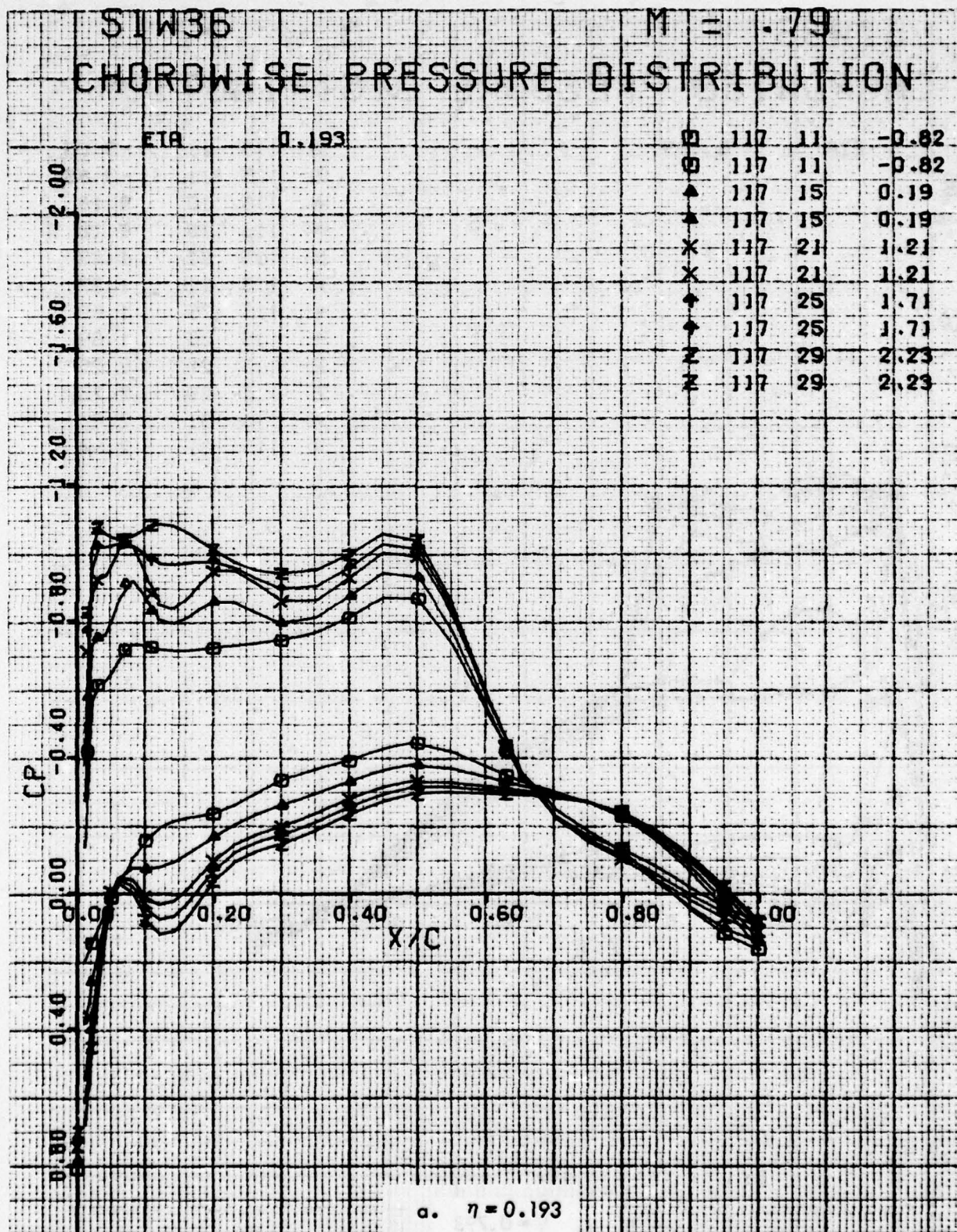


Figure 57. Chordwise Pressure Distributions for Various Angles of Attack. W³⁶ Leading Edge Modification, Fixed Transition, Grit Code B, M = 0.79.

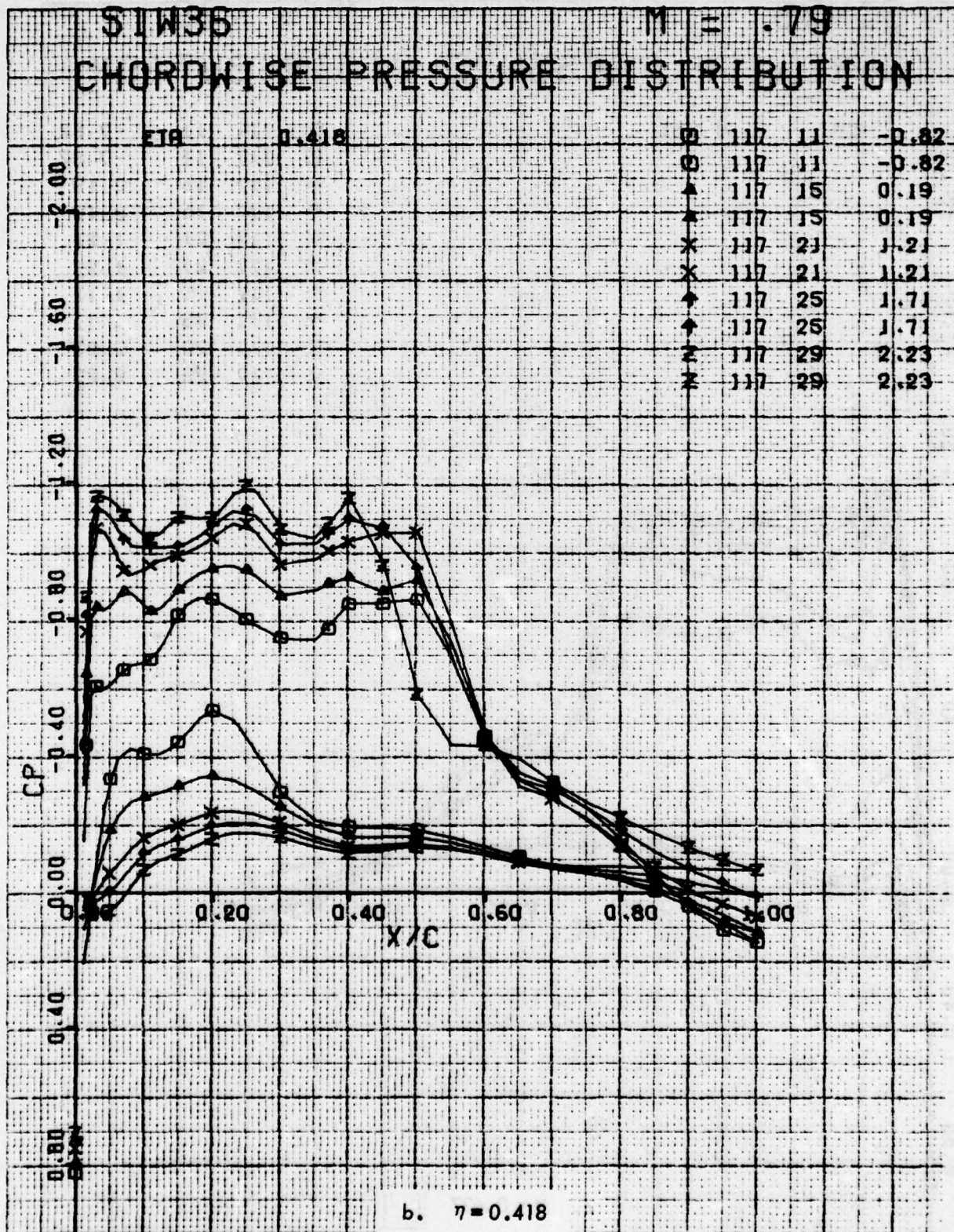


Figure 57. Continued

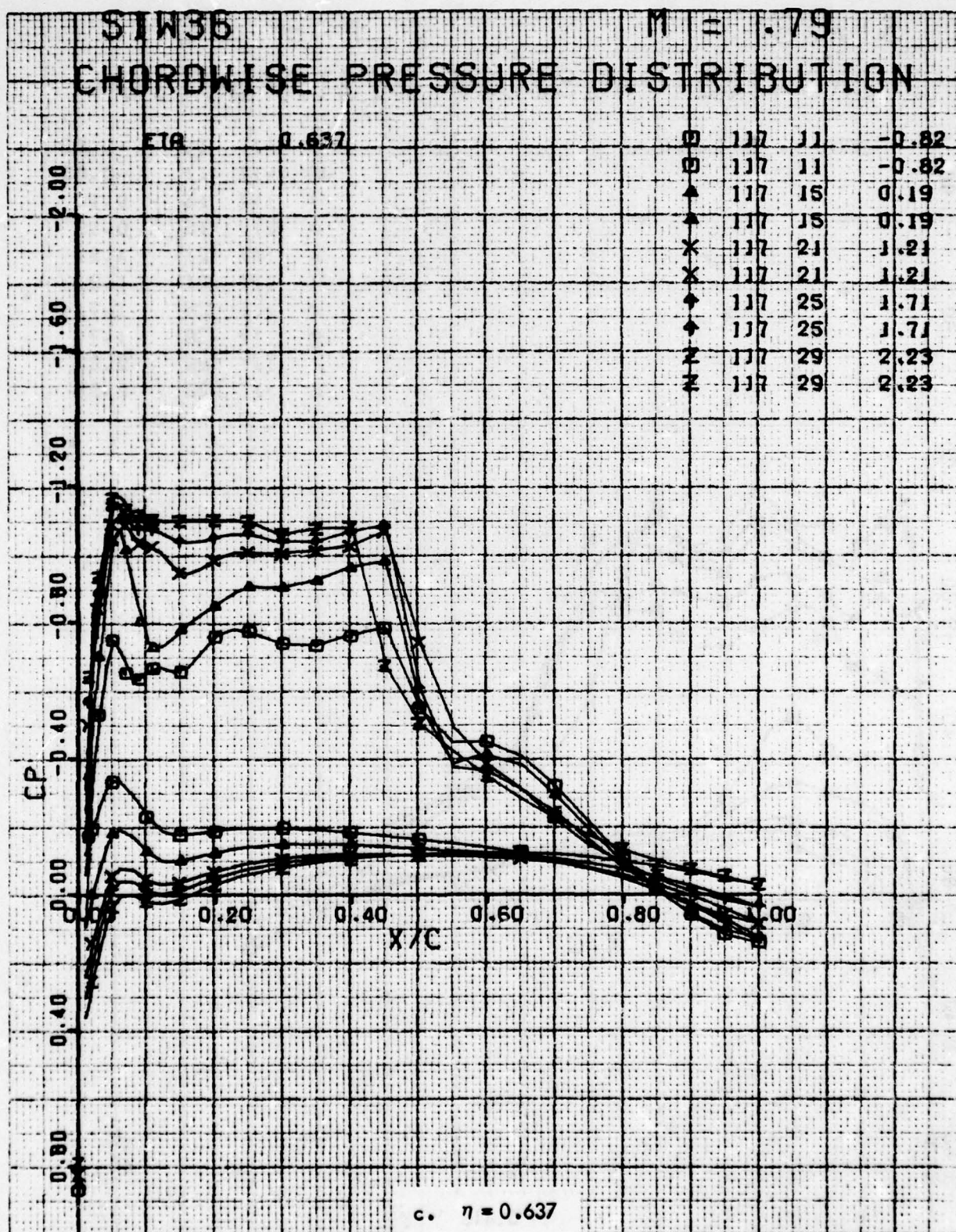


Figure 57. Continued

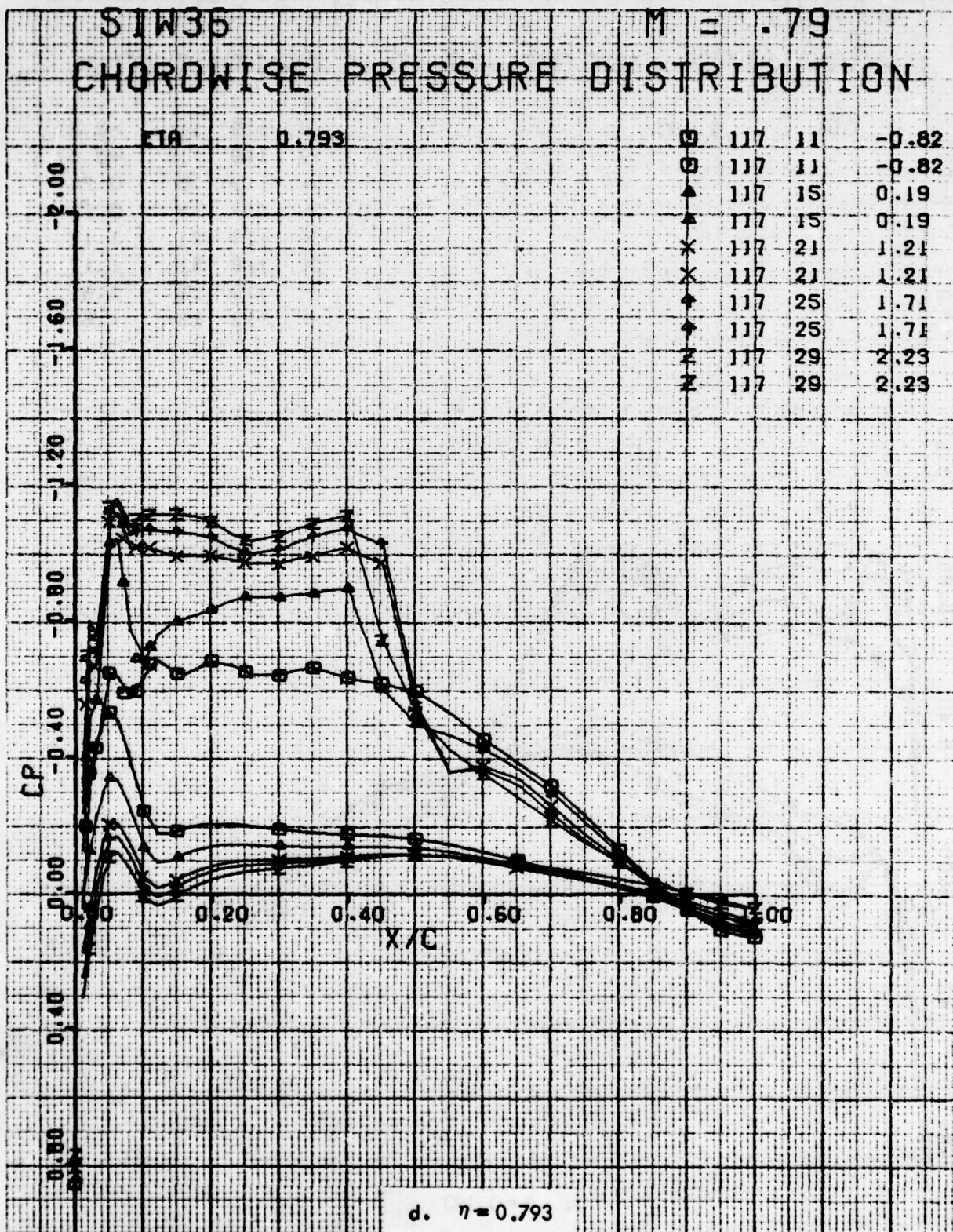


Figure 57. Concluded

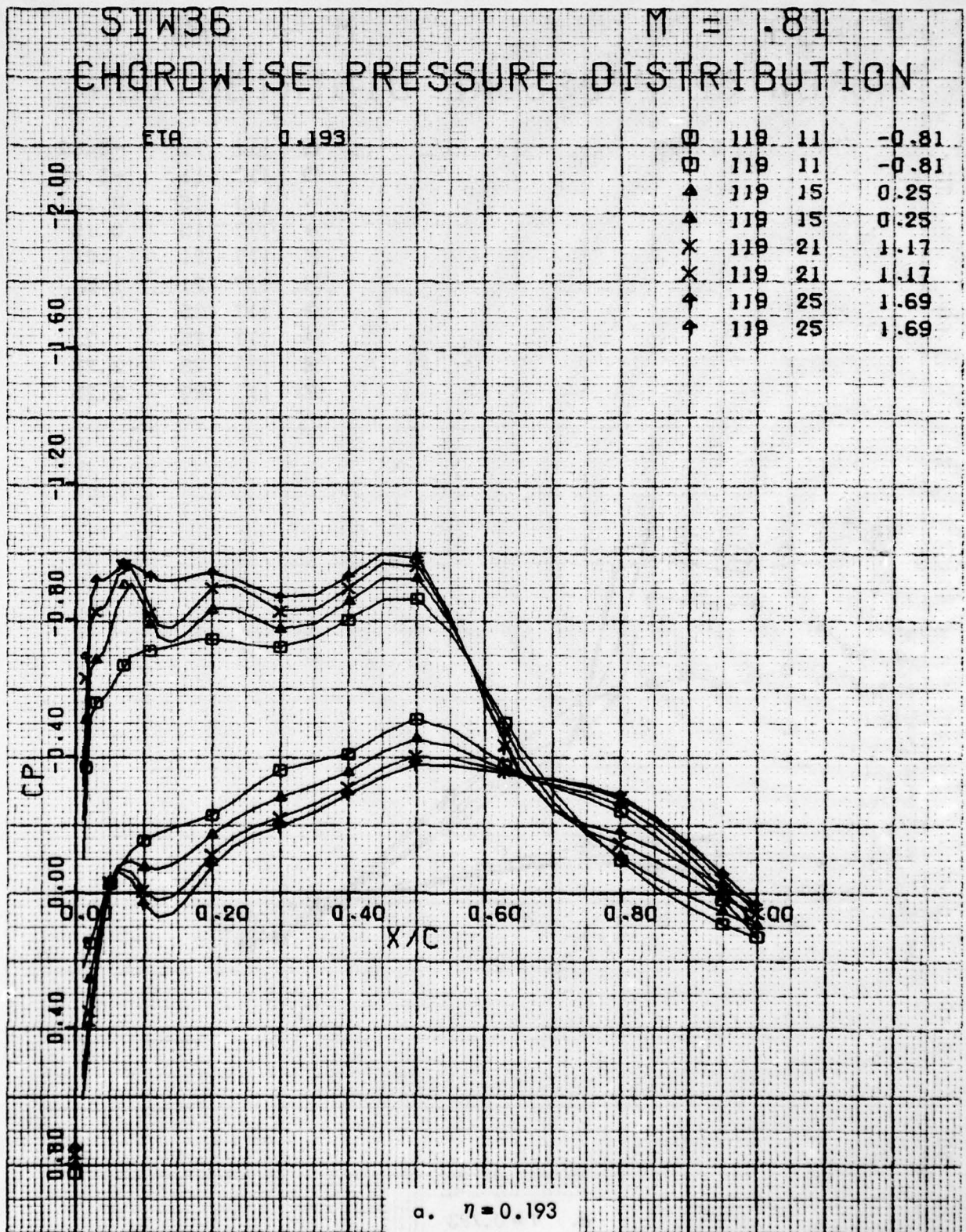


Figure 58. Chordwise Pressure Distributions for Various Angles of Attack. W³⁶ Leading Edge Modification, Fixed Transition, Grit Code B, M = 0.81.

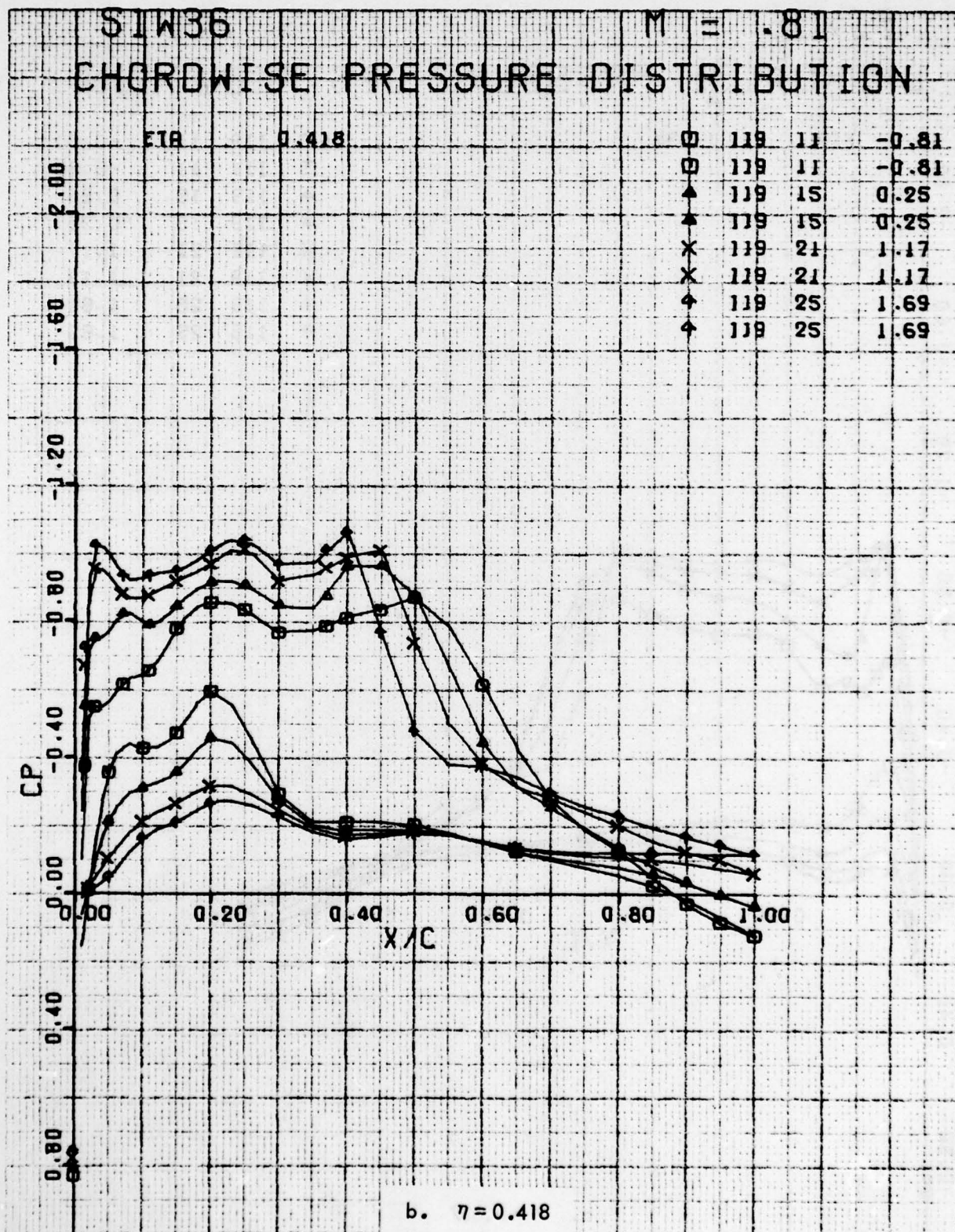


Figure 58. Continued

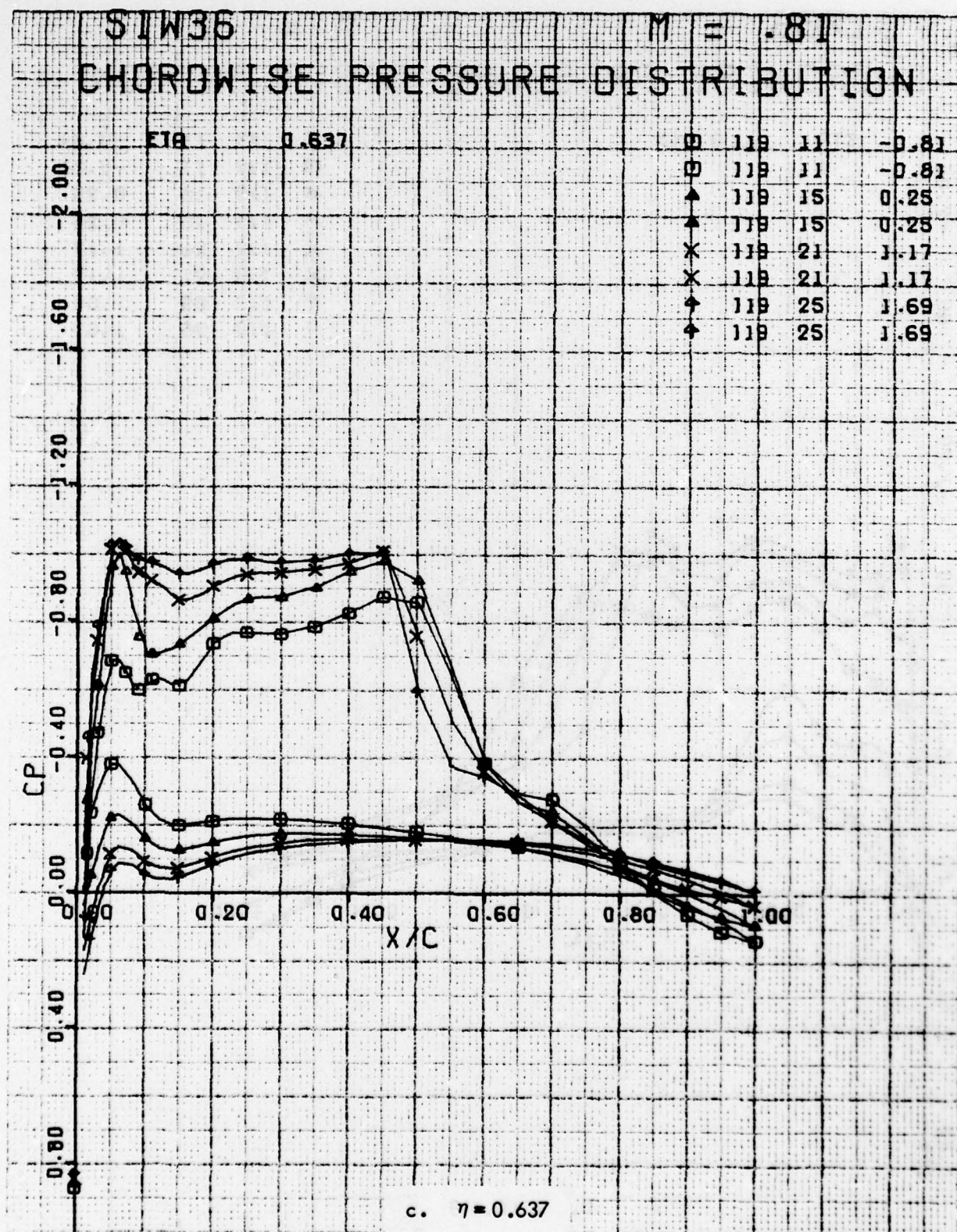


Figure 58. Continued

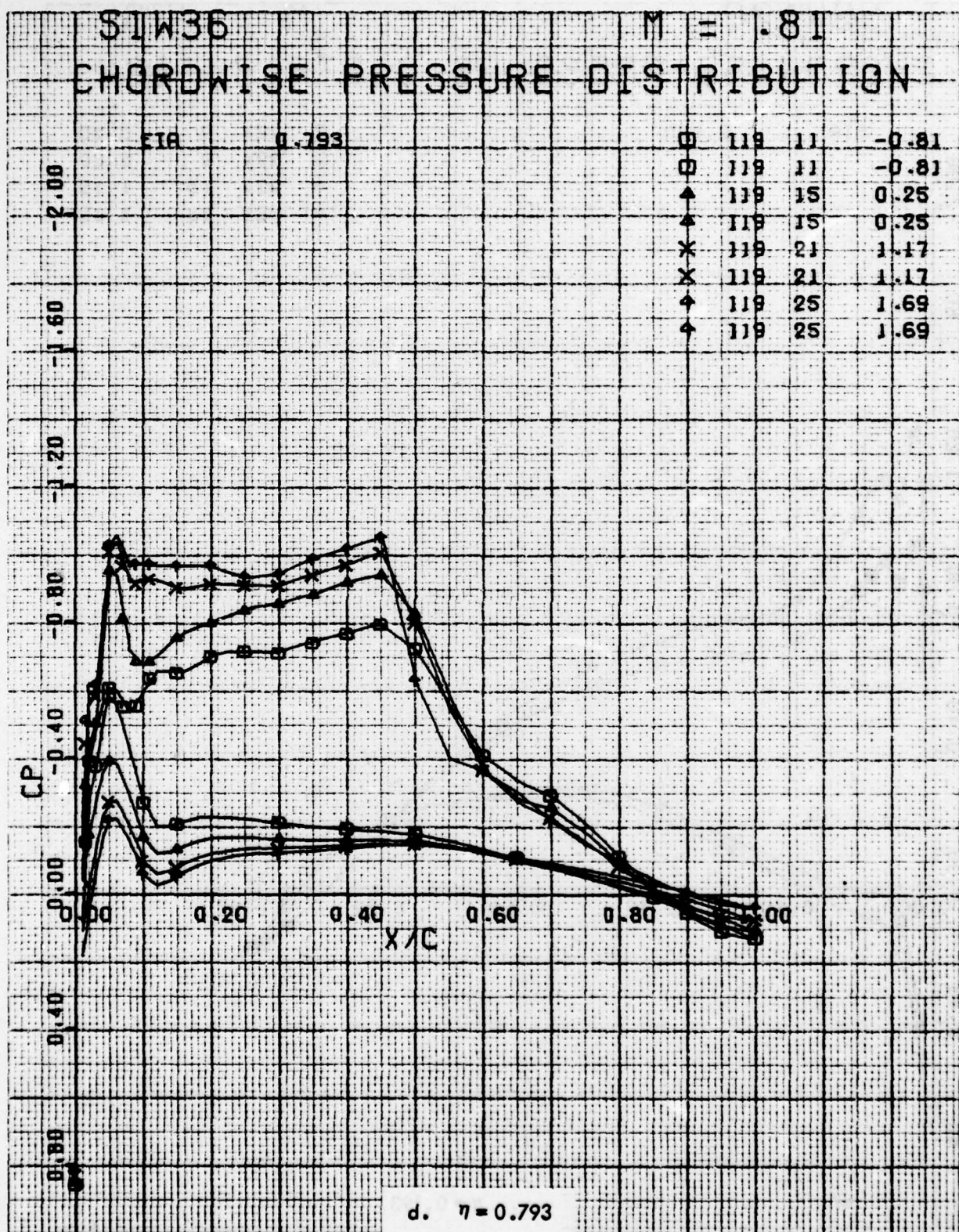


Figure 58. Concluded

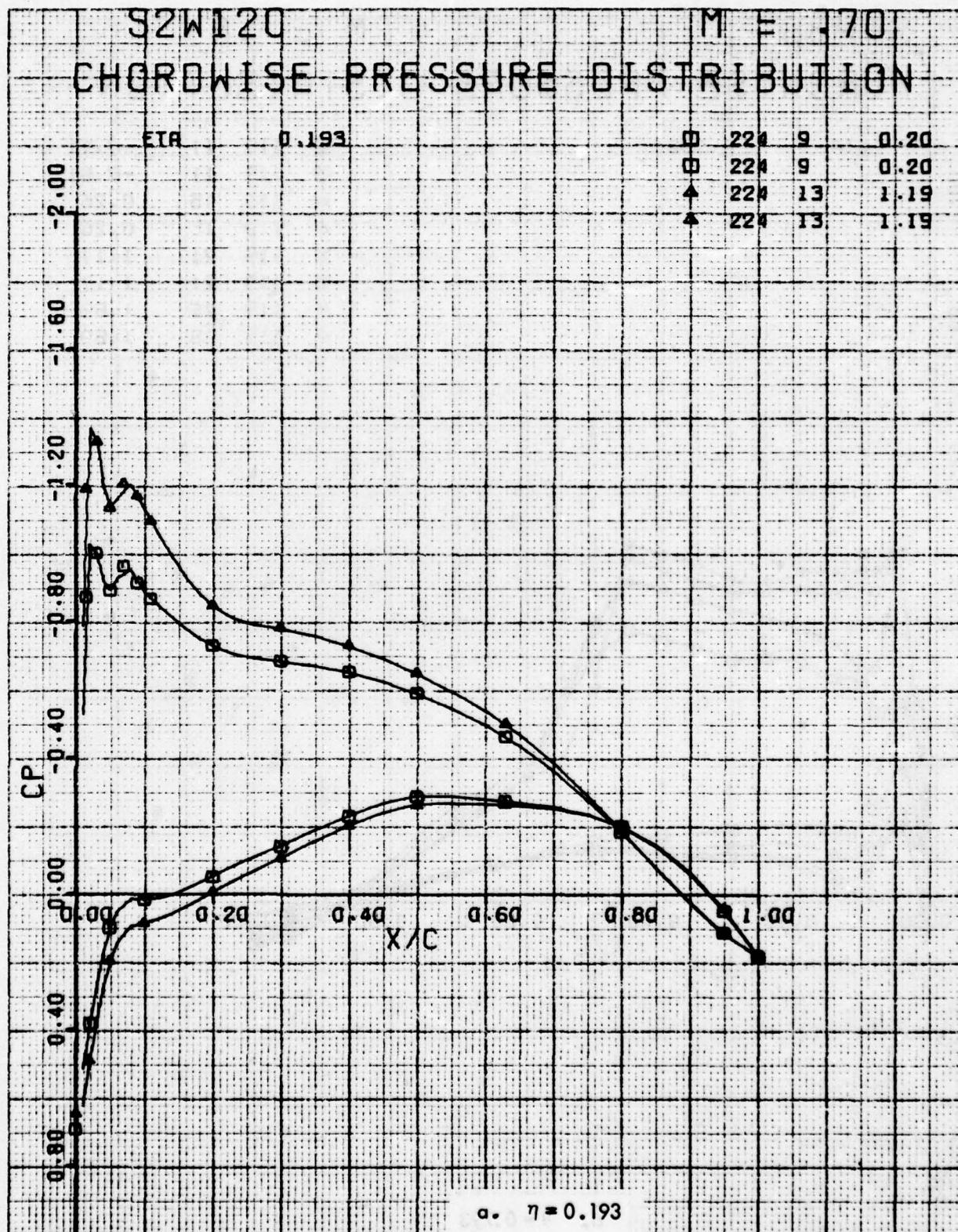


Figure 59. Chordwise Pressure Distributions for Various Angles of Attack. Baseline Leading Edge, Fixed Transition, Grit Code D, Pylon/Nacelles Off, $M = 0.7$.

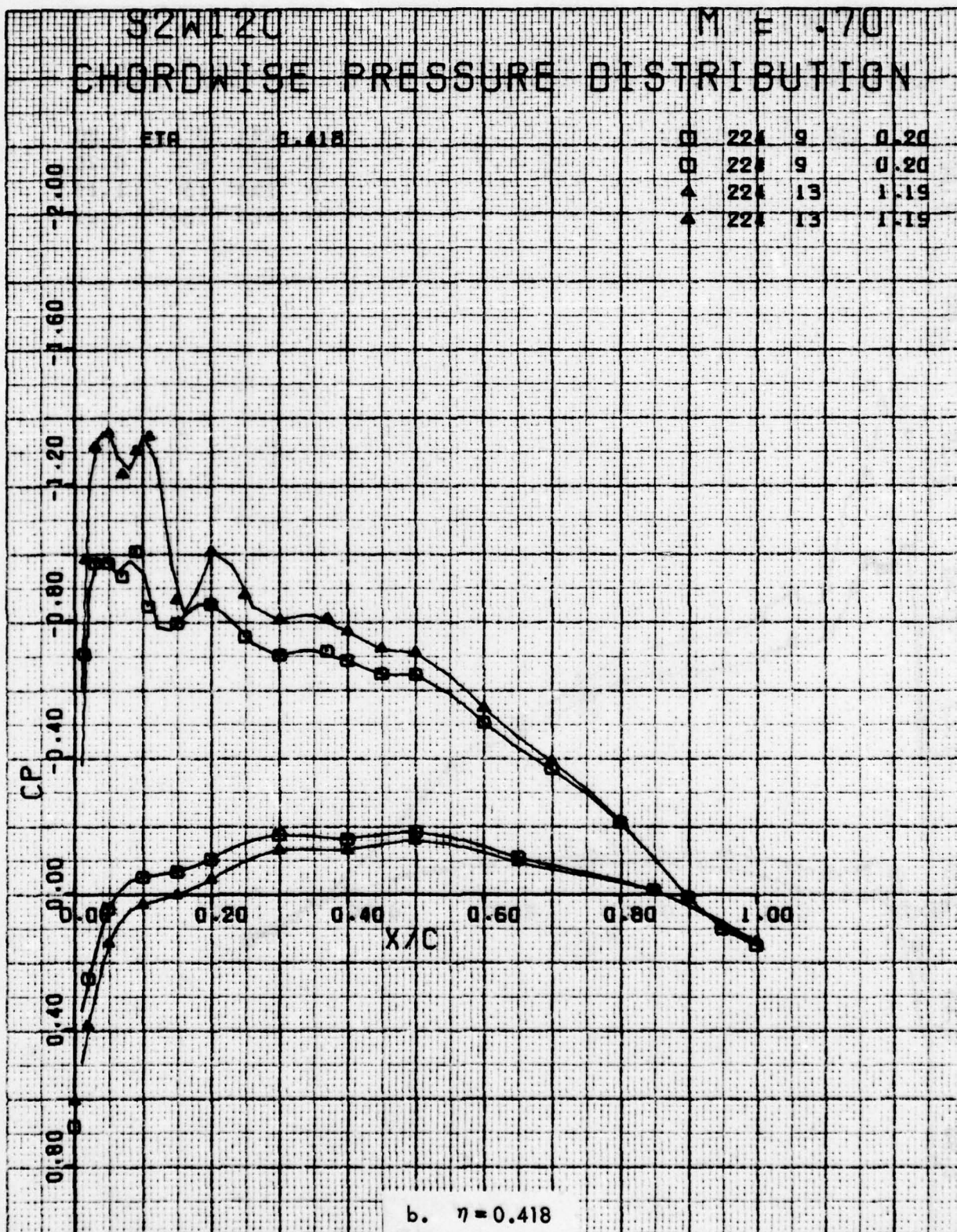


Figure 59. Continued

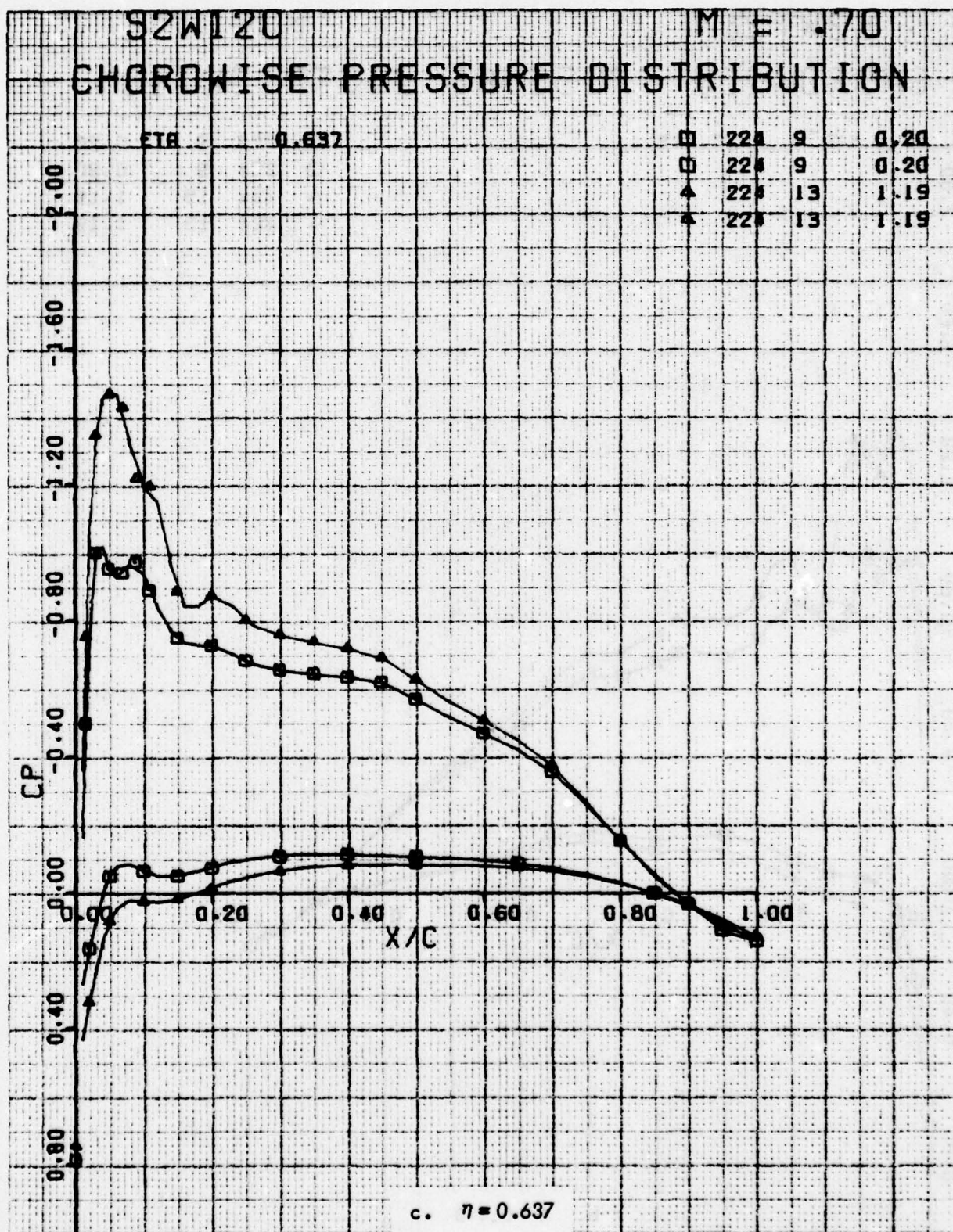


Figure 59. Continued

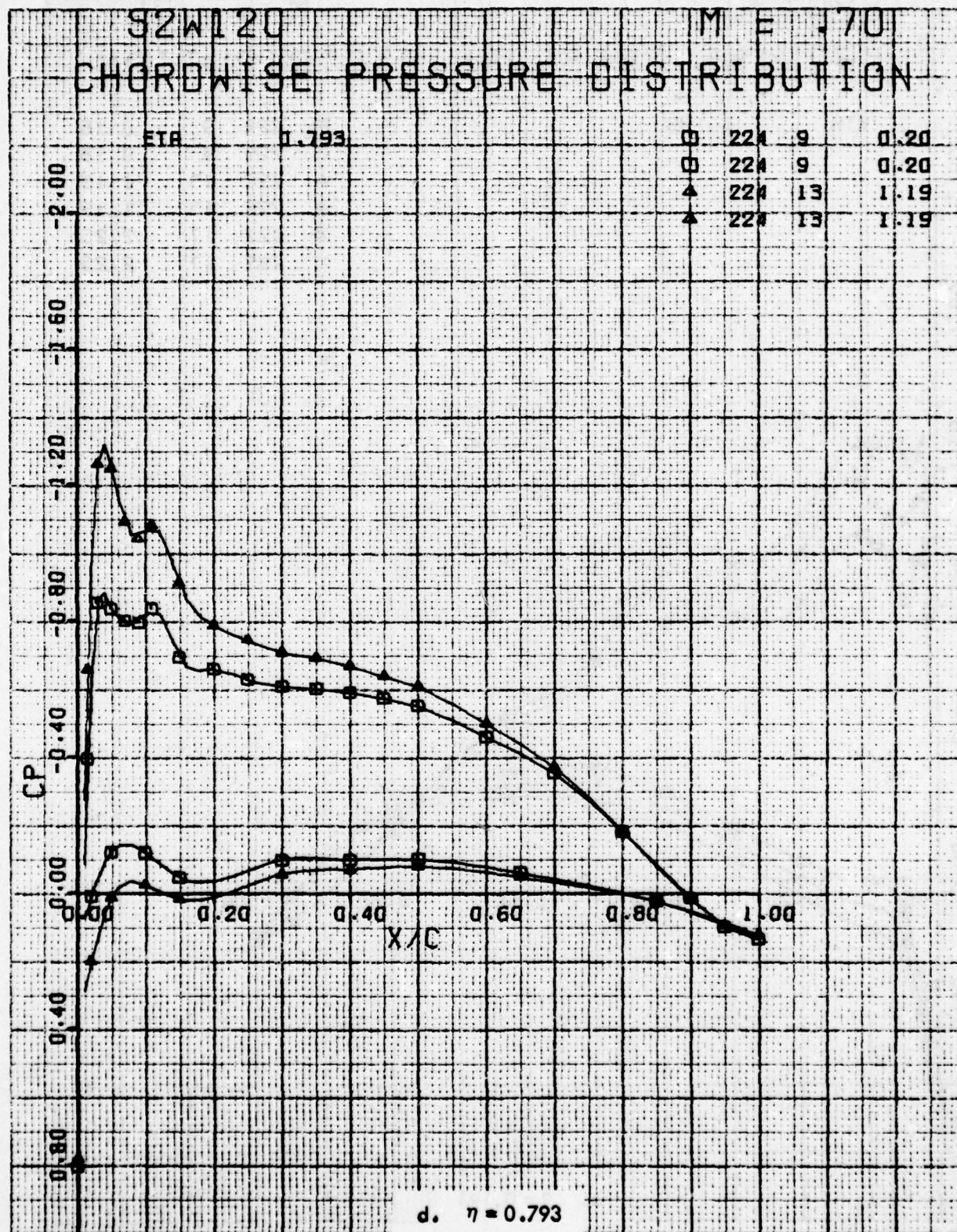


Figure 59. Concluded

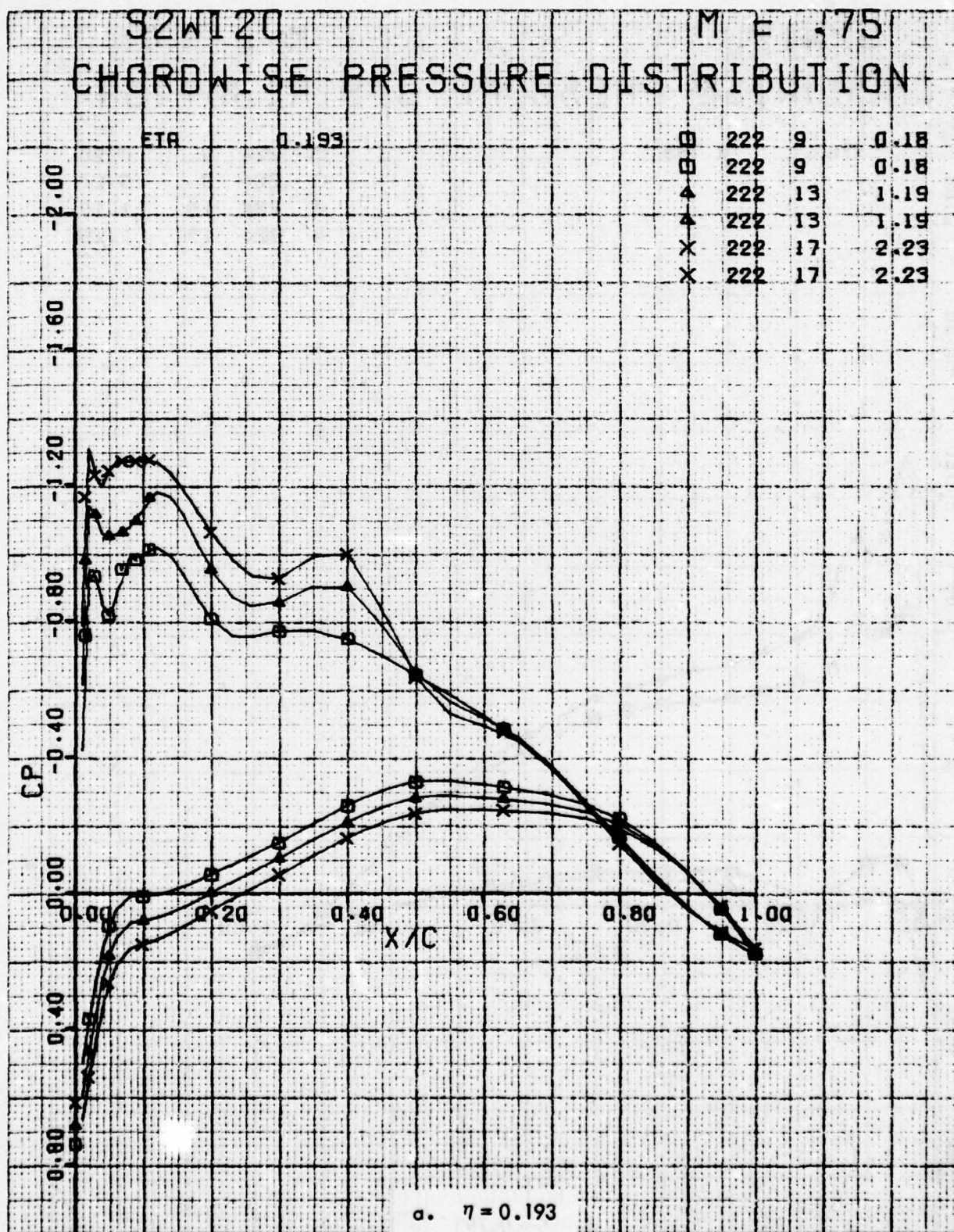


Figure 60 . Chordwise Pressure Distributions for Various Angles of Attack. Baseline Leading Edge, Fixed Transition, Grit Code D, Pylon/Nacelles Off, $M = 0.75$.

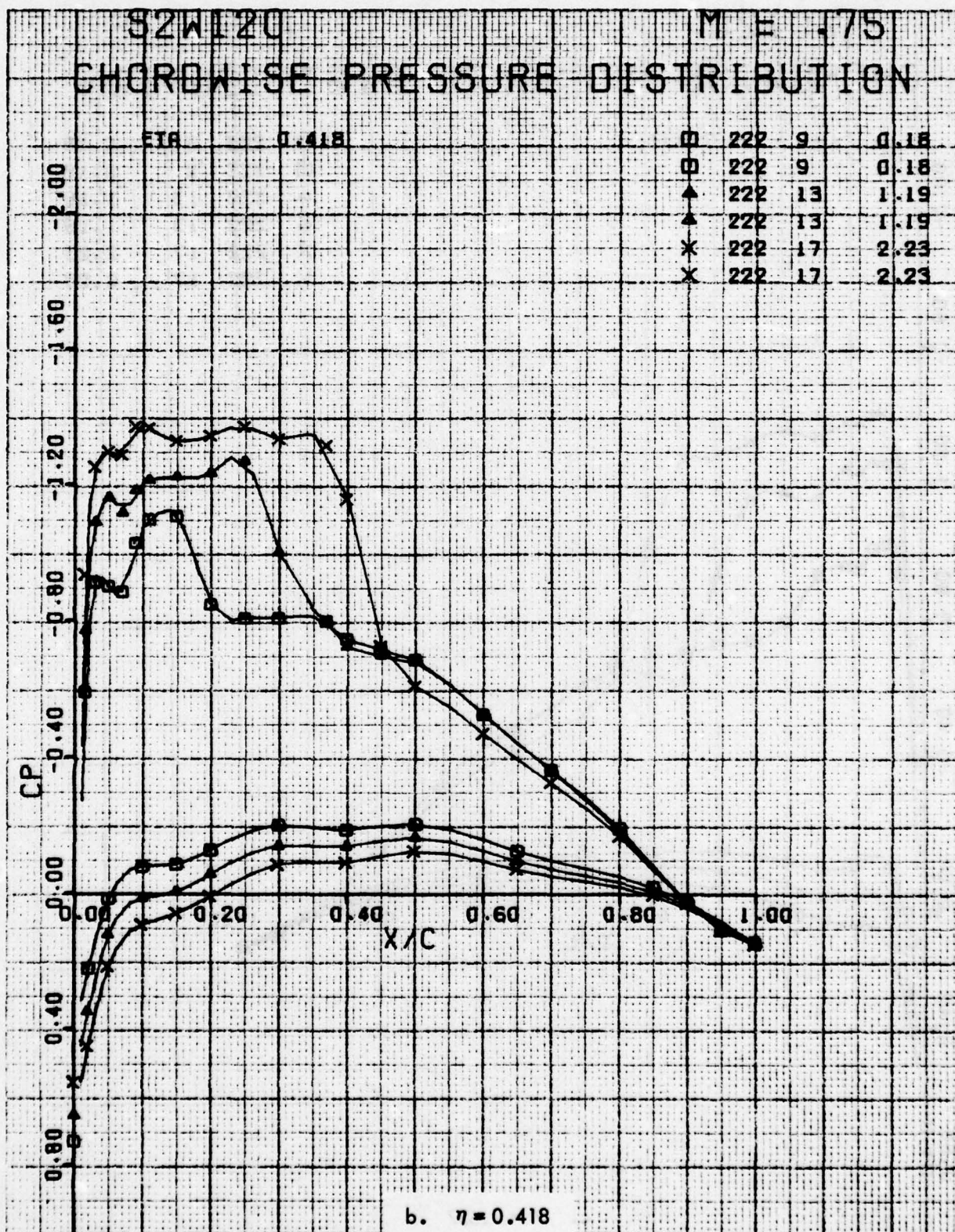


Figure 60. Continued

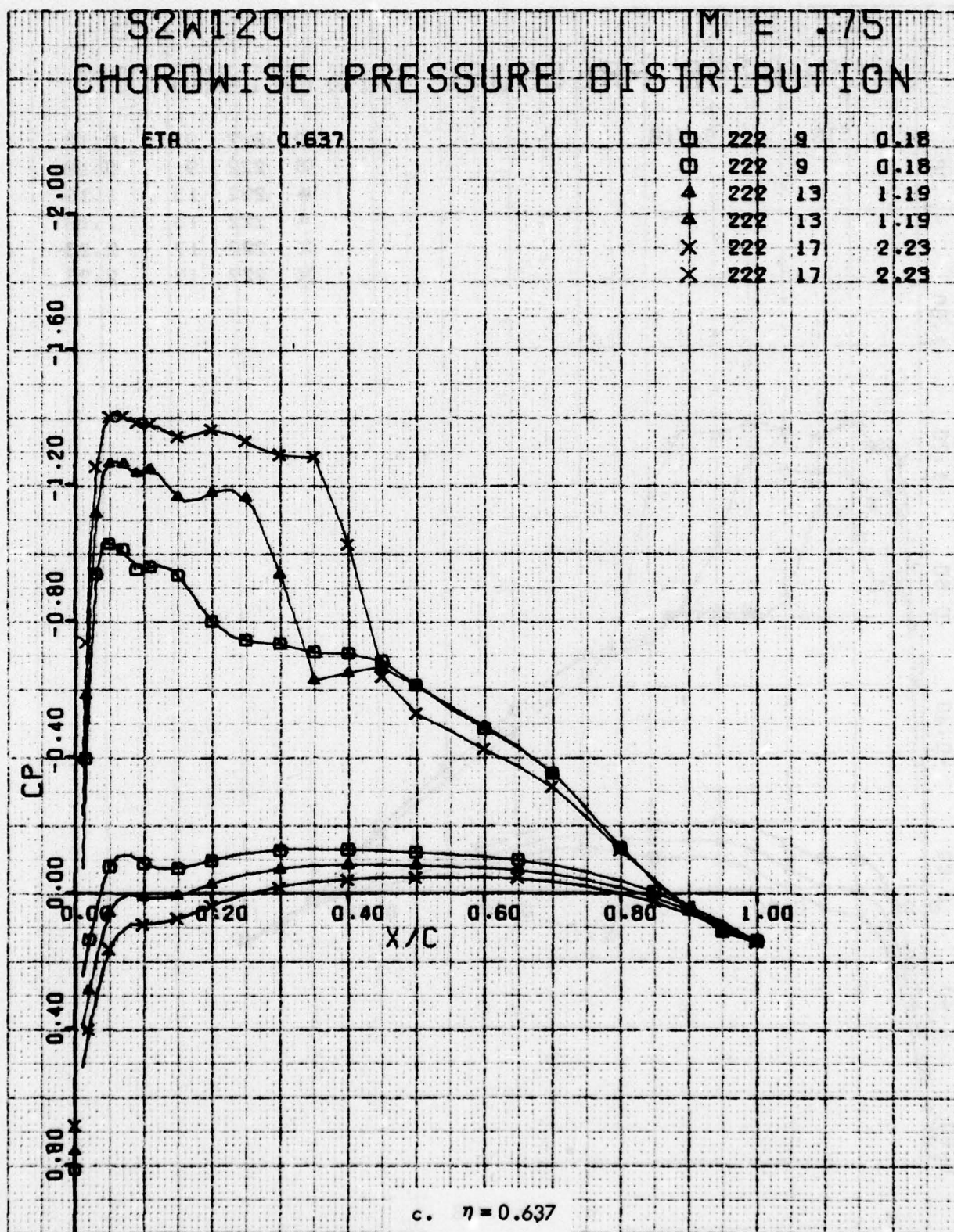


Figure 60. Continued

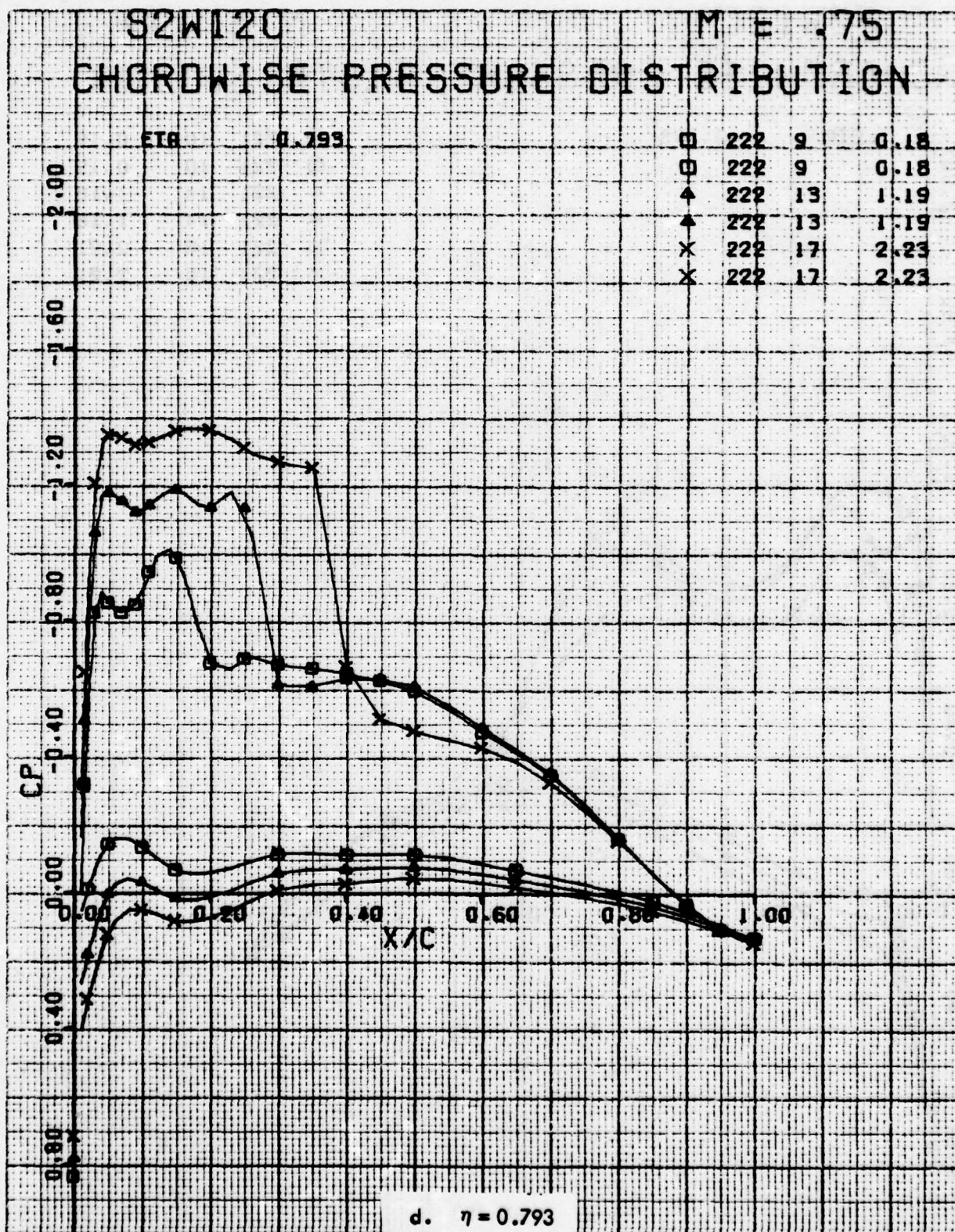


Figure 60. Concluded

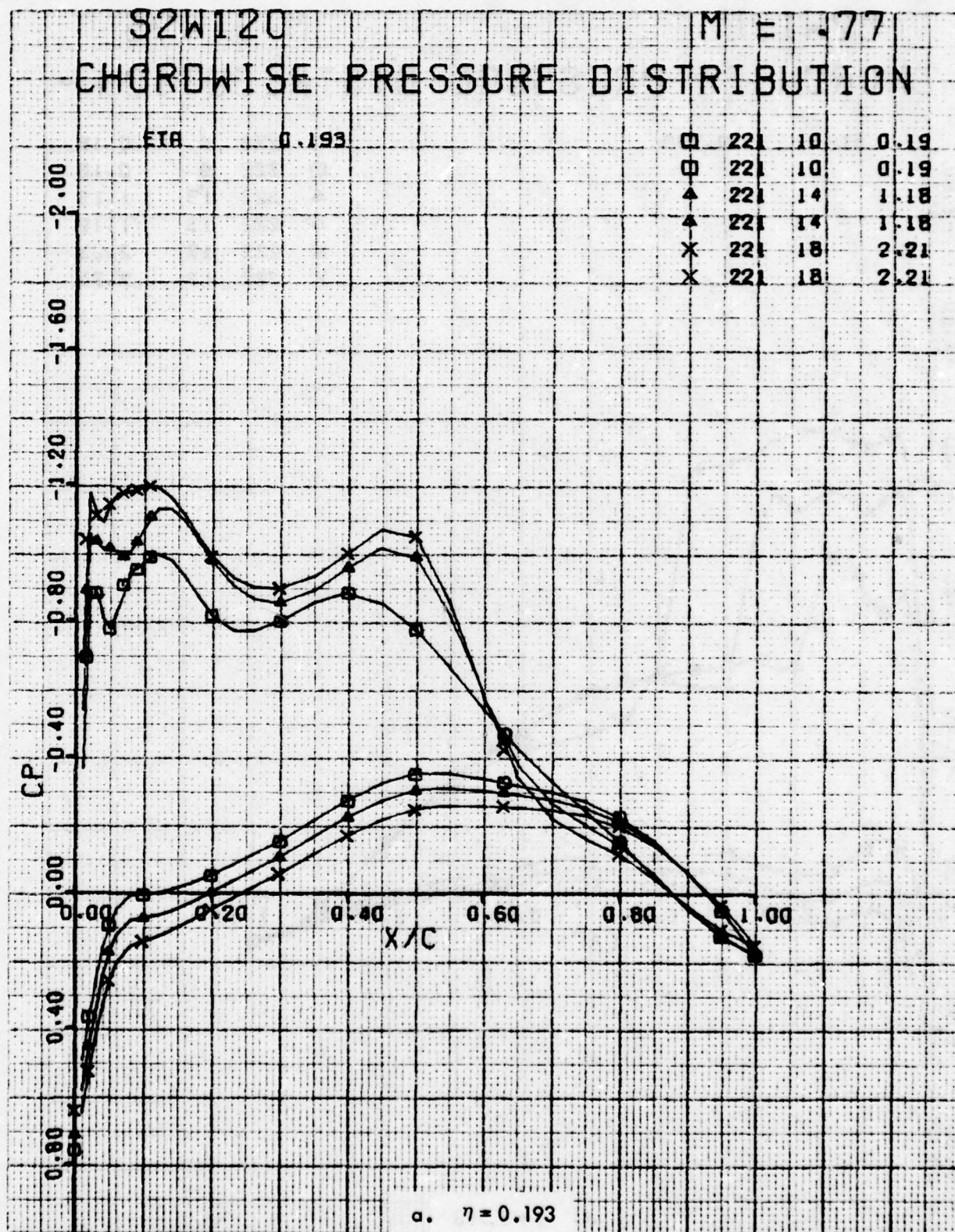


Figure 61. Chordwise Pressure Distributions for Various Angles of Attack. Baseline Leading Edge, Fixed Transition, Grit Code D, Pylon/Nacelles Off, M = 0.77.

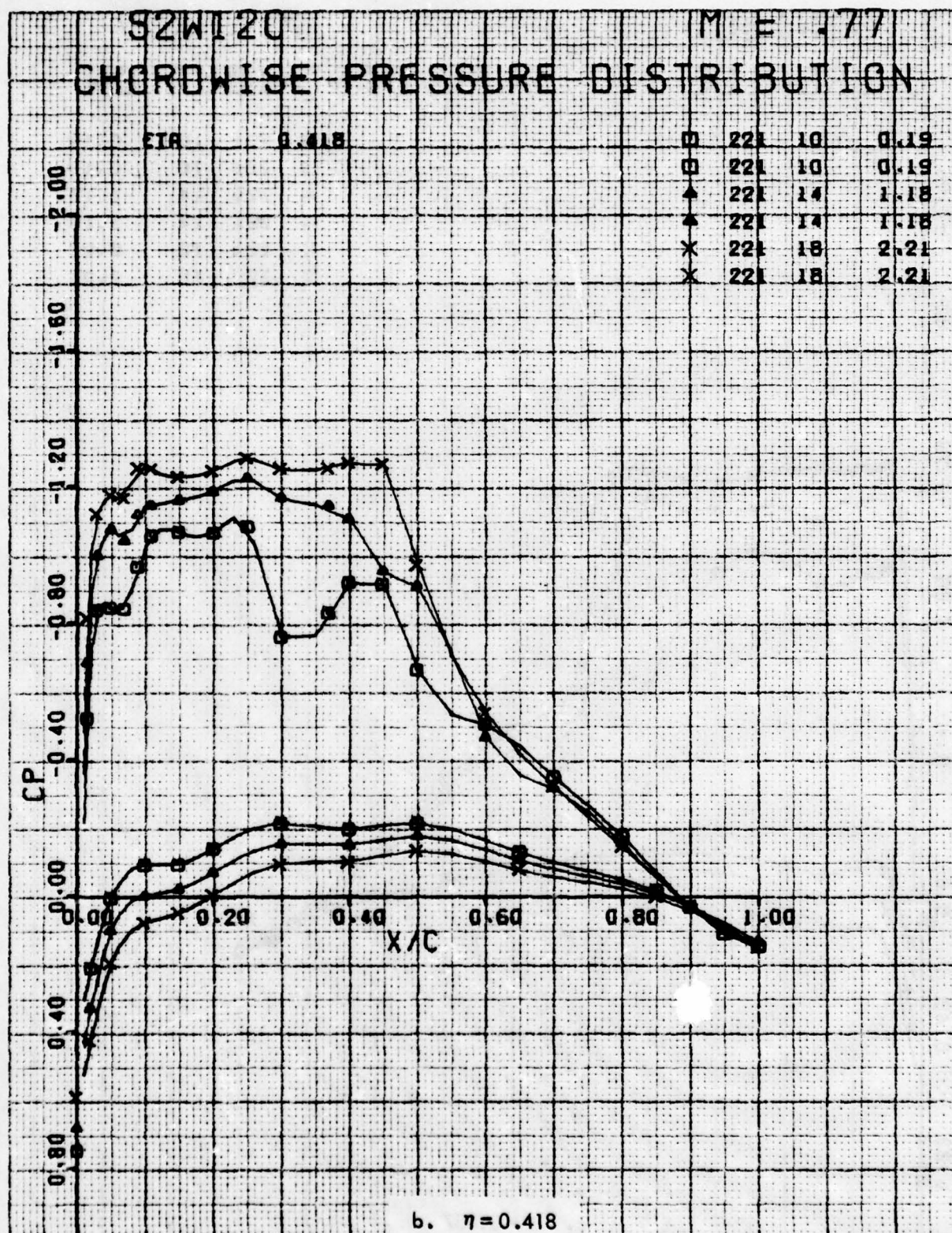


Figure 61 . Continued

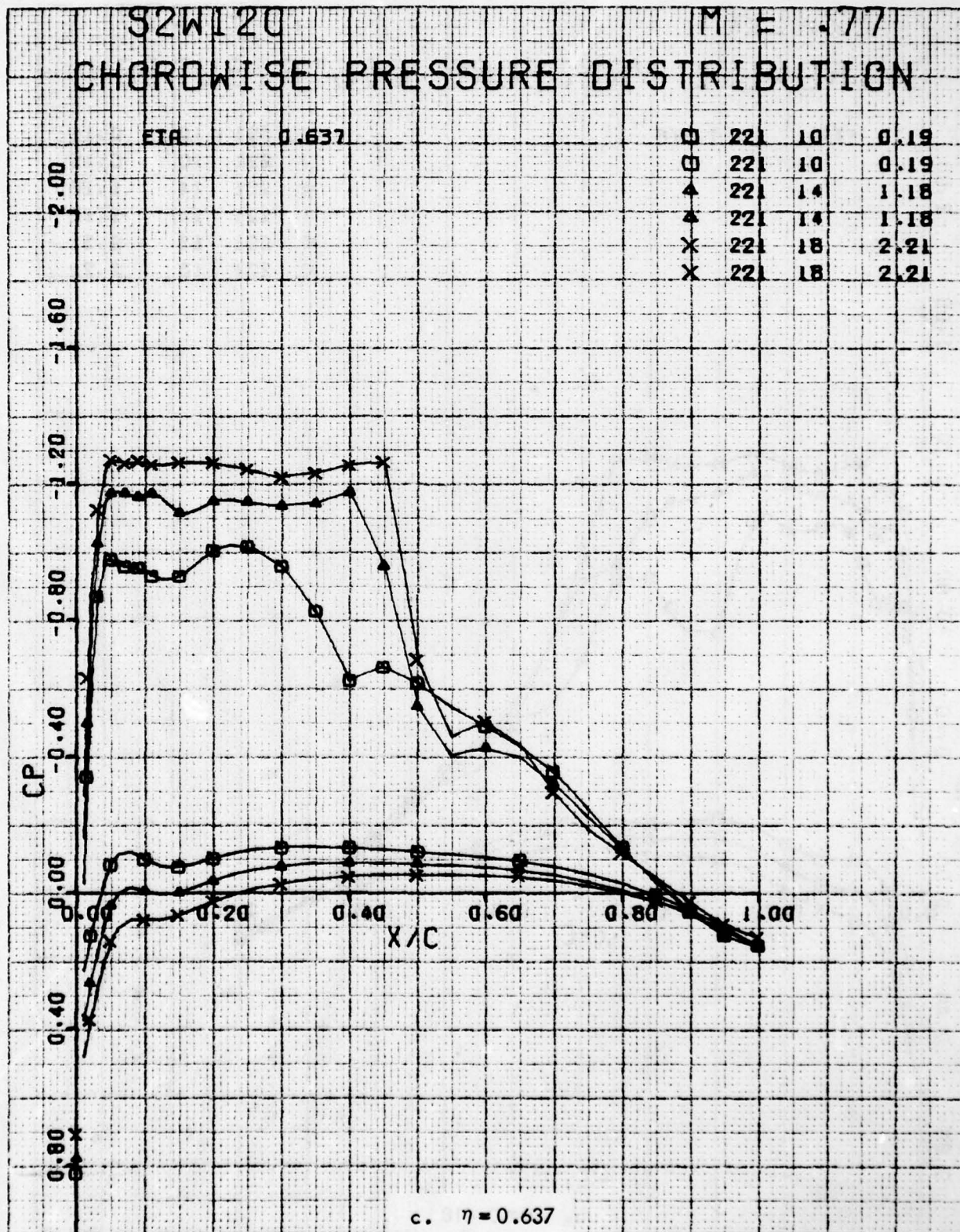


Figure 61. Continued

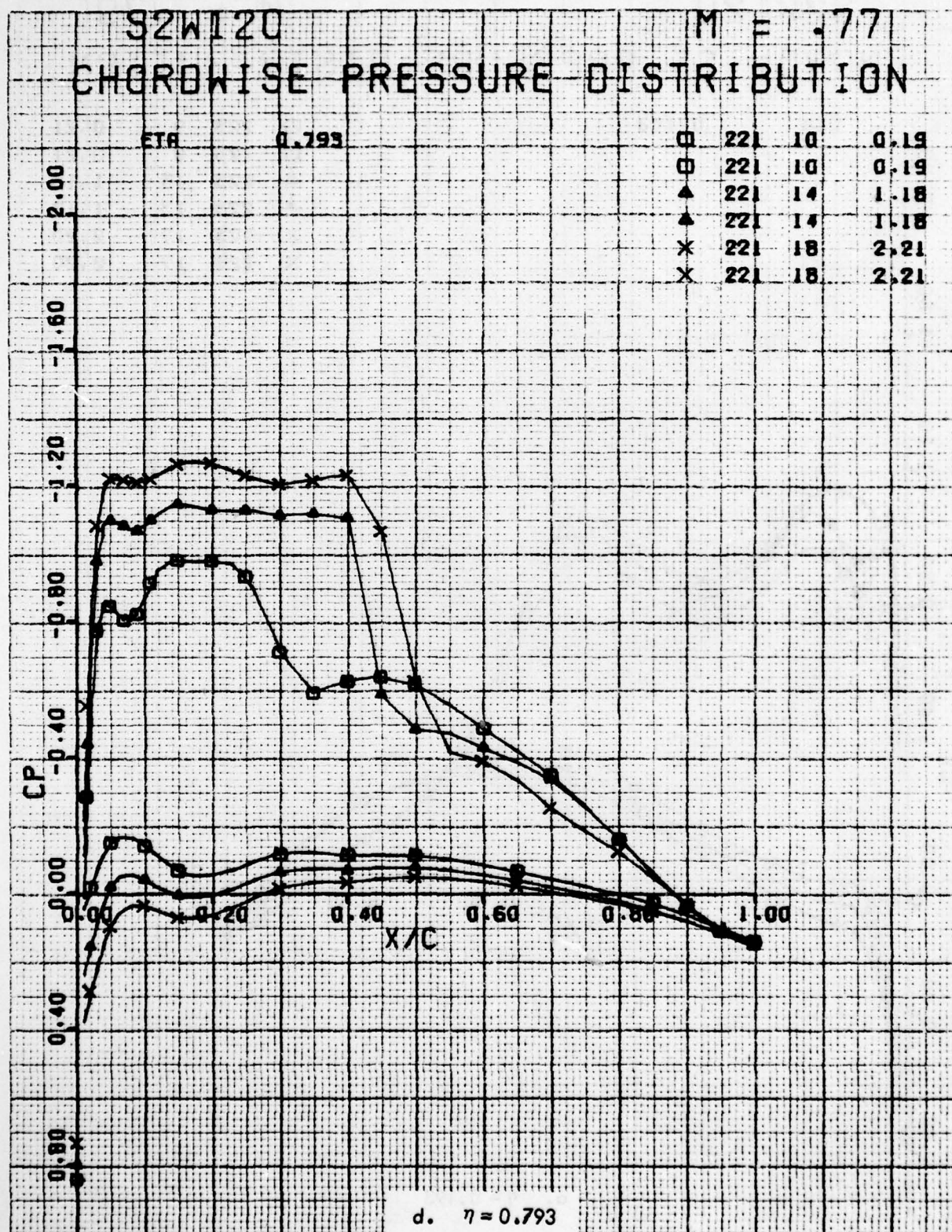


Figure 61. Concluded

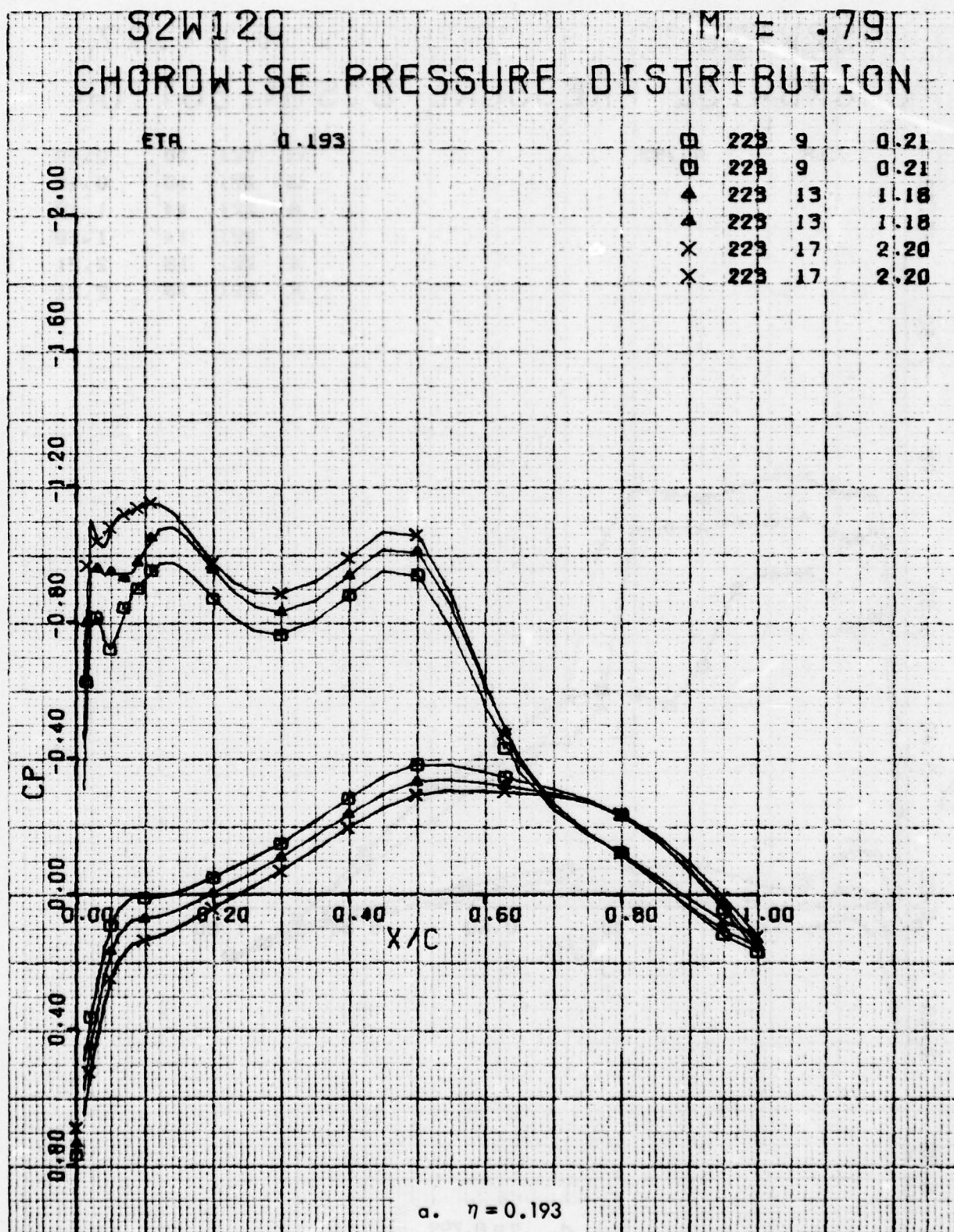


Figure 62. Chordwise Pressure Distributions for Various Angles of Attack. Baseline Leading Edge, Fixed Transition, Grit Code D, Pylon/Nacelles Off, $M = 0.79$.

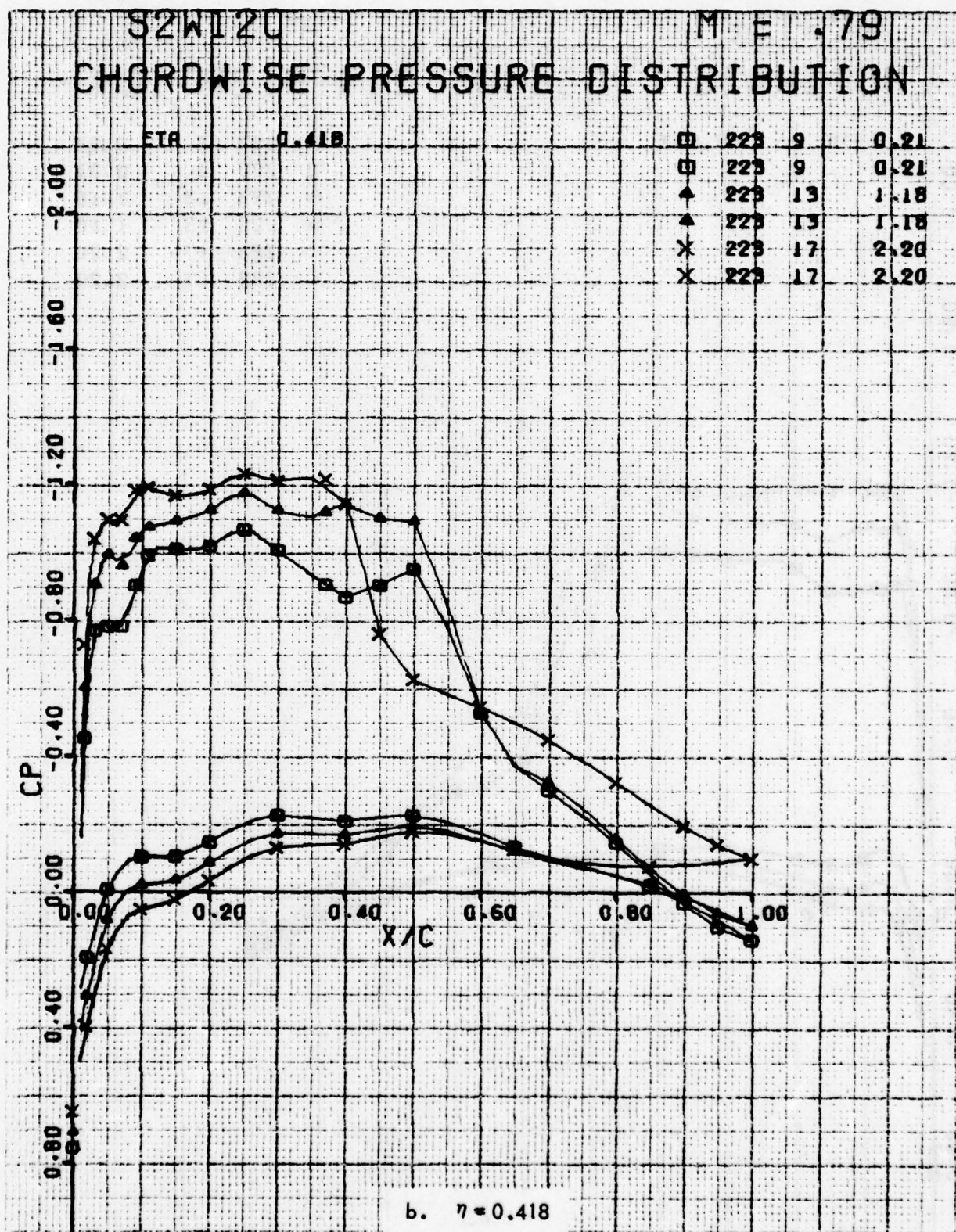


Figure 62 . Continued

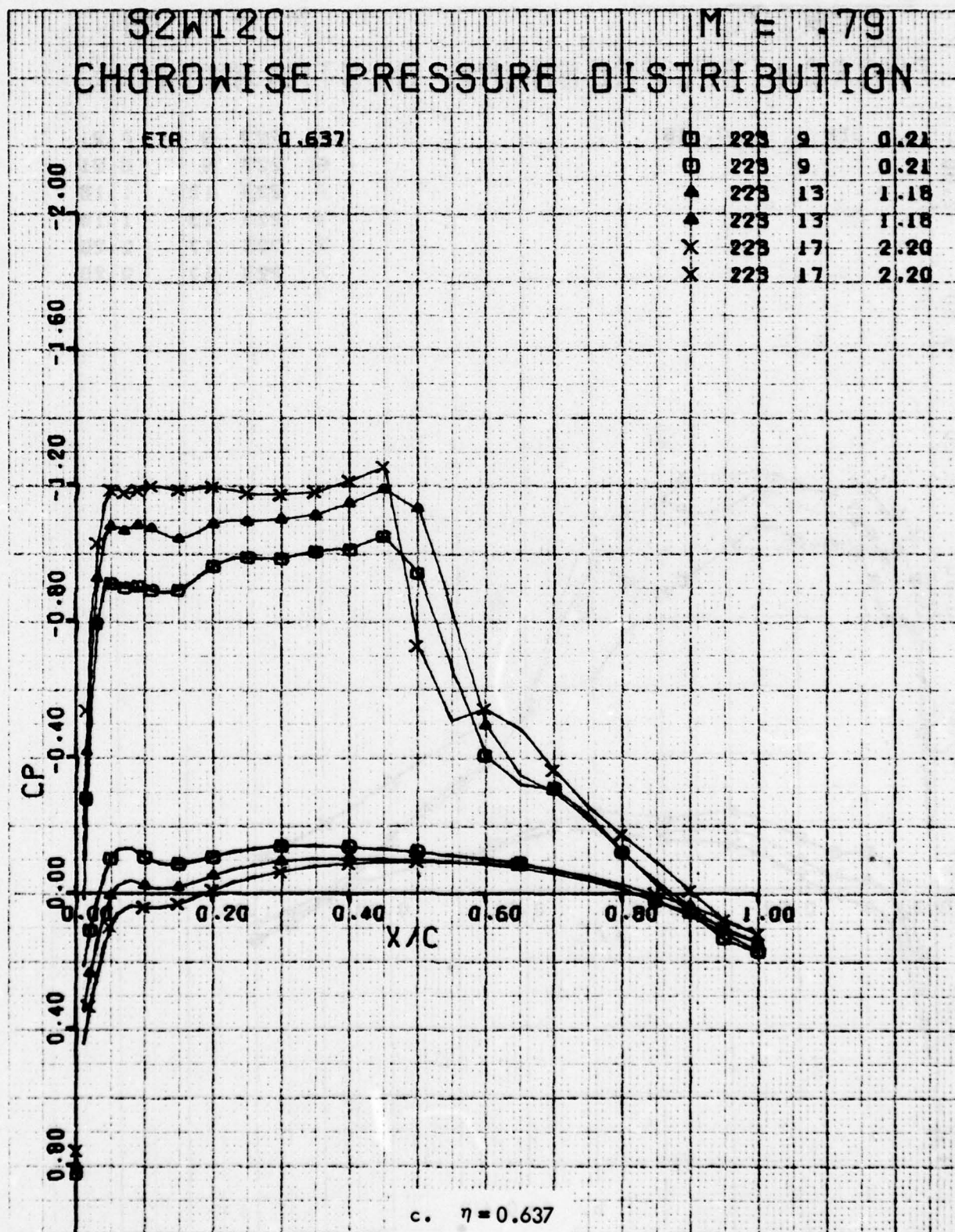


Figure 62. Continued

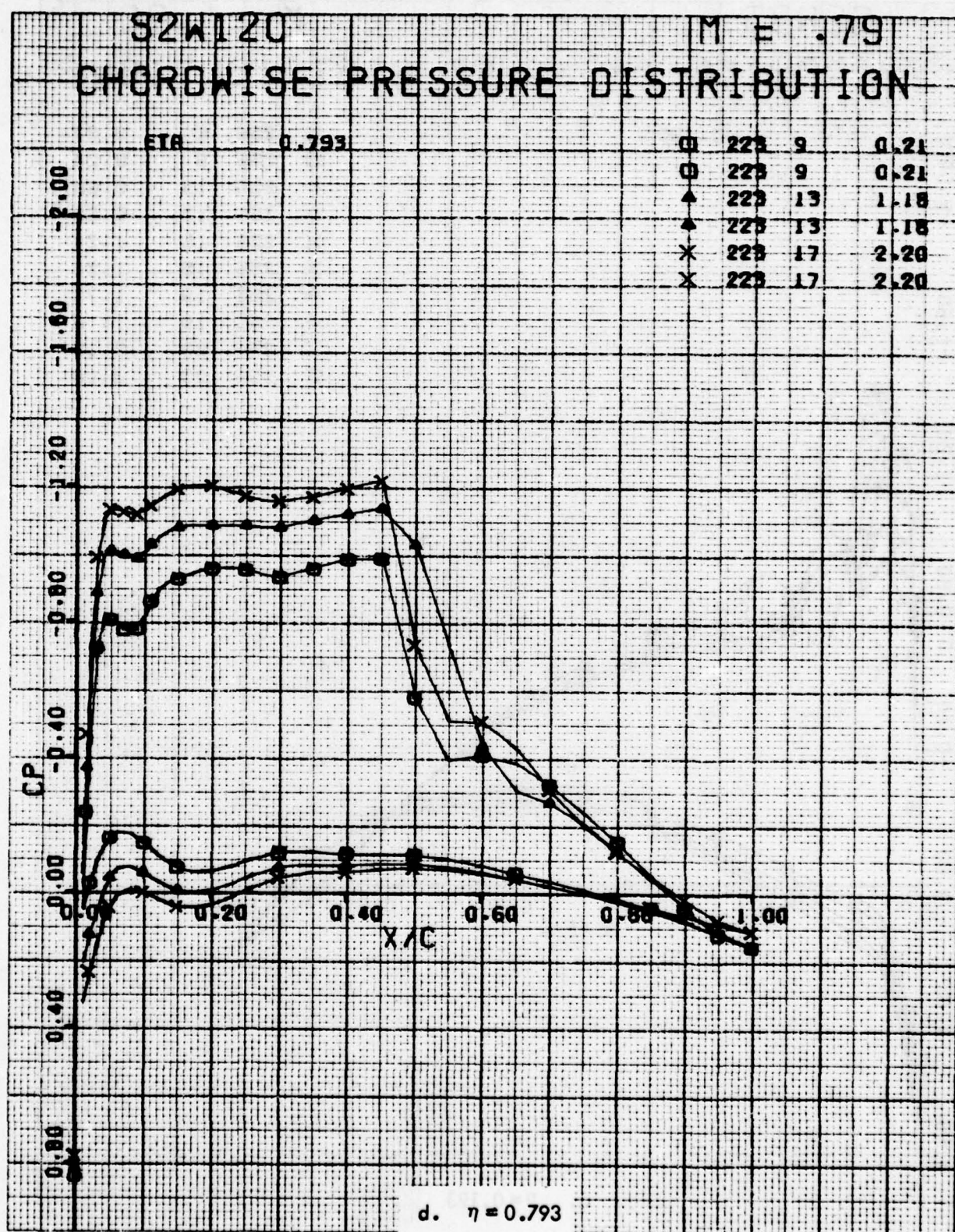


Figure 62. Concluded

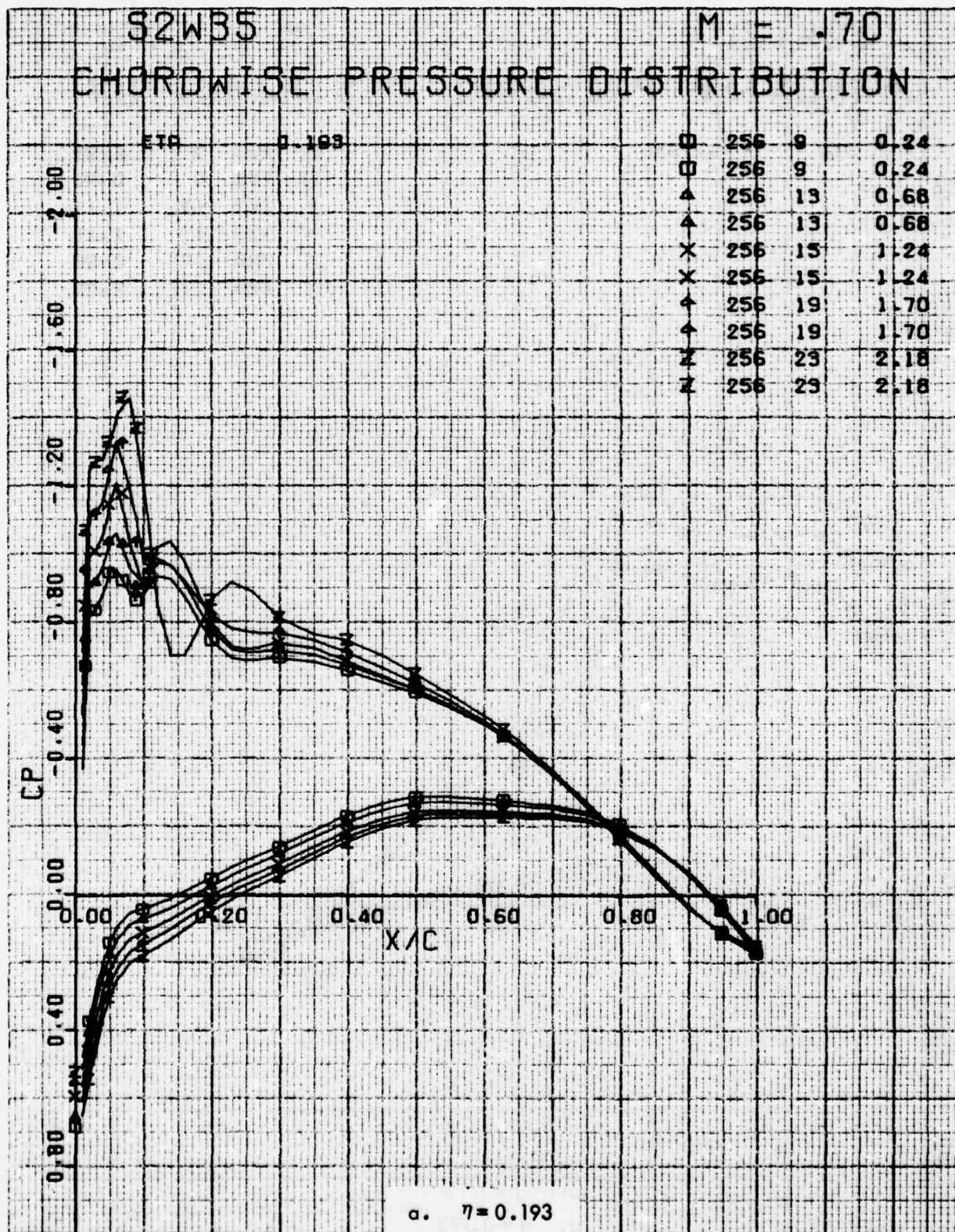


Figure 63. Chordwise Pressure Distributions for Various Angles of Attack. W³⁵ Leading Edge Modification, Fixed Transition, Grit Code D, Pylon/Nacelles Off, M = 0.7.

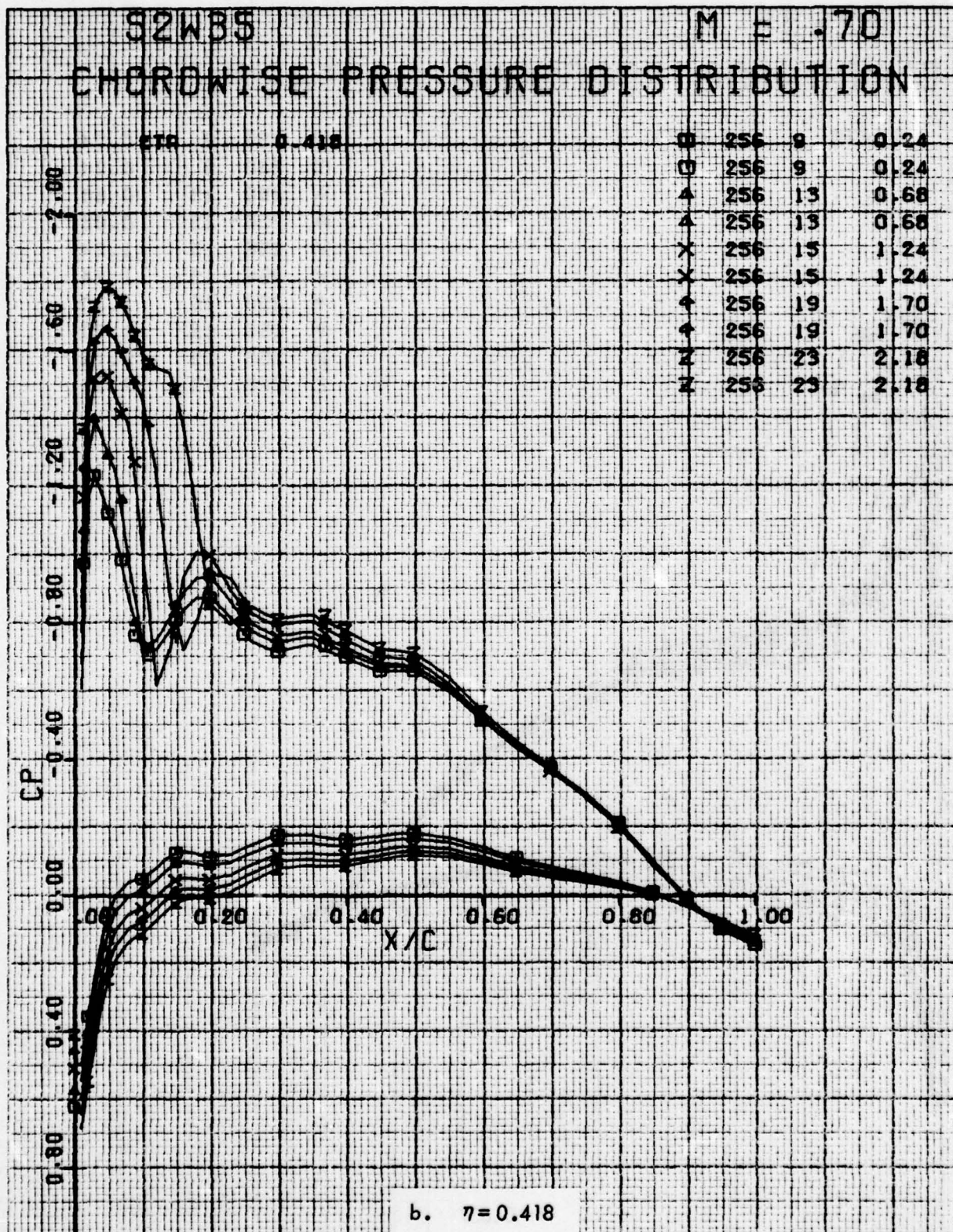


Figure 63 . Continued

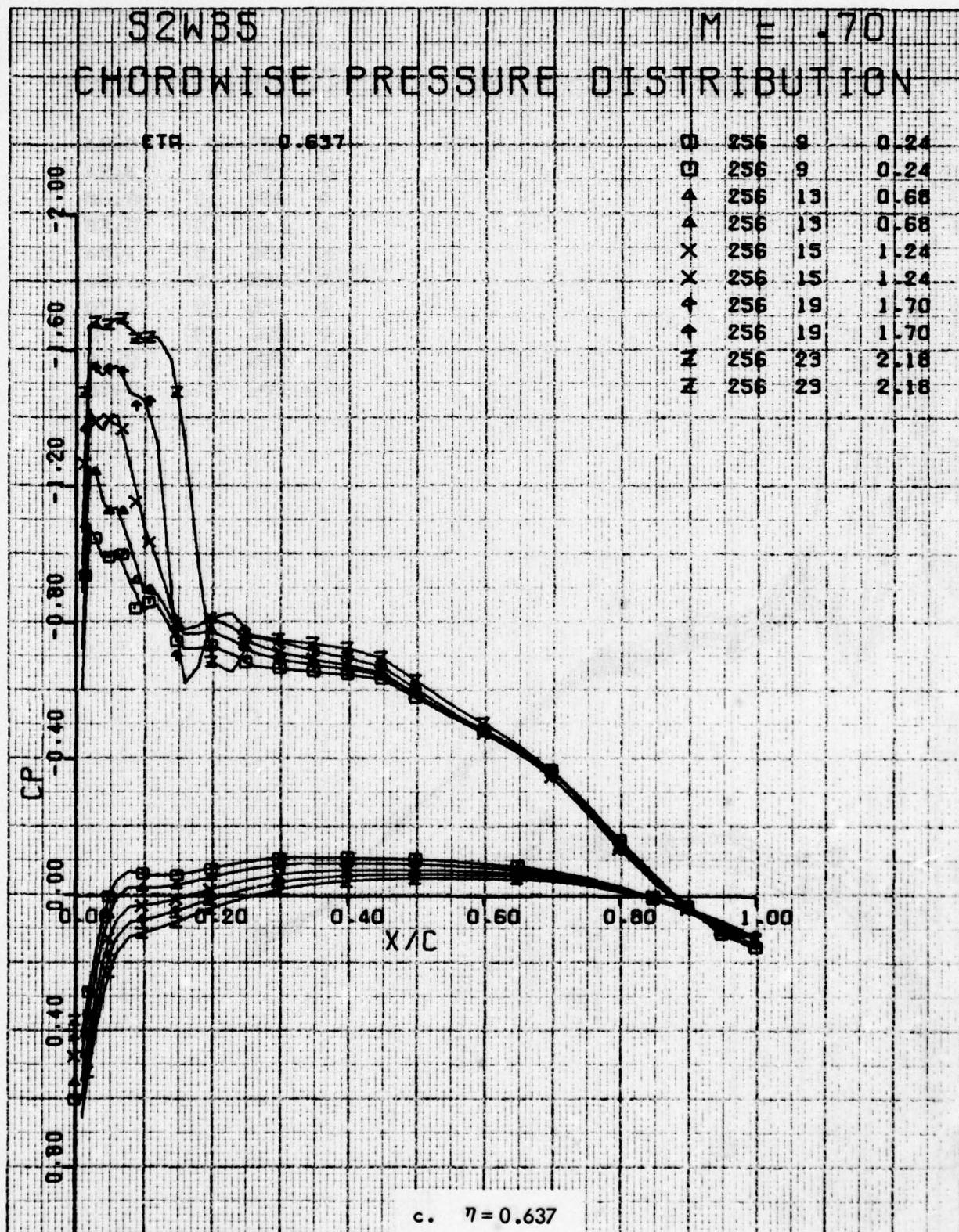


Figure 63. Continued

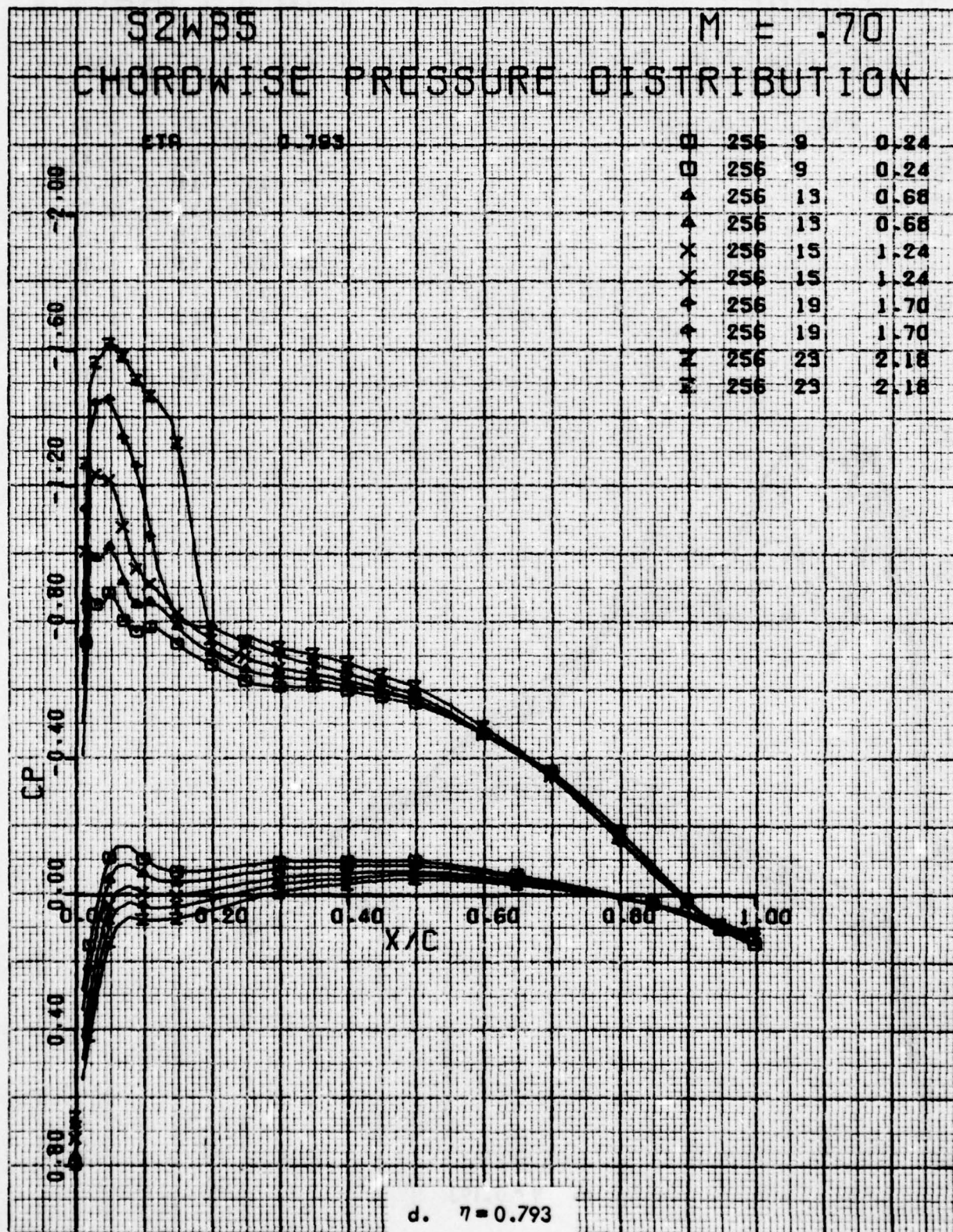


Figure 63. Concluded

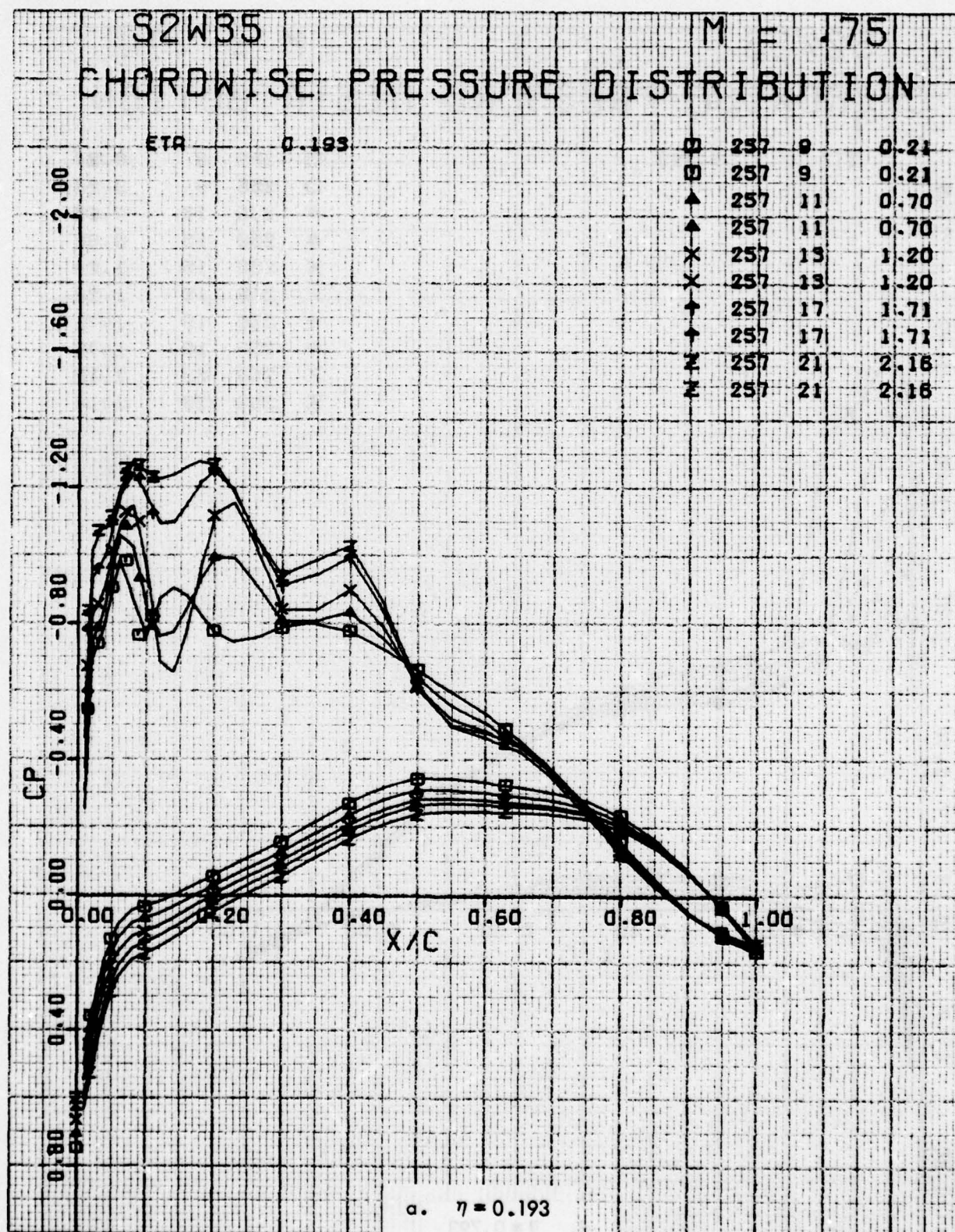


Figure 64. Chordwise Pressure Distributions for Various Angles of Attack. W35 Leading Edge Modification, Fixed Transition, Grit Code D, Pylon/Nacelles Off, M = 0.75.

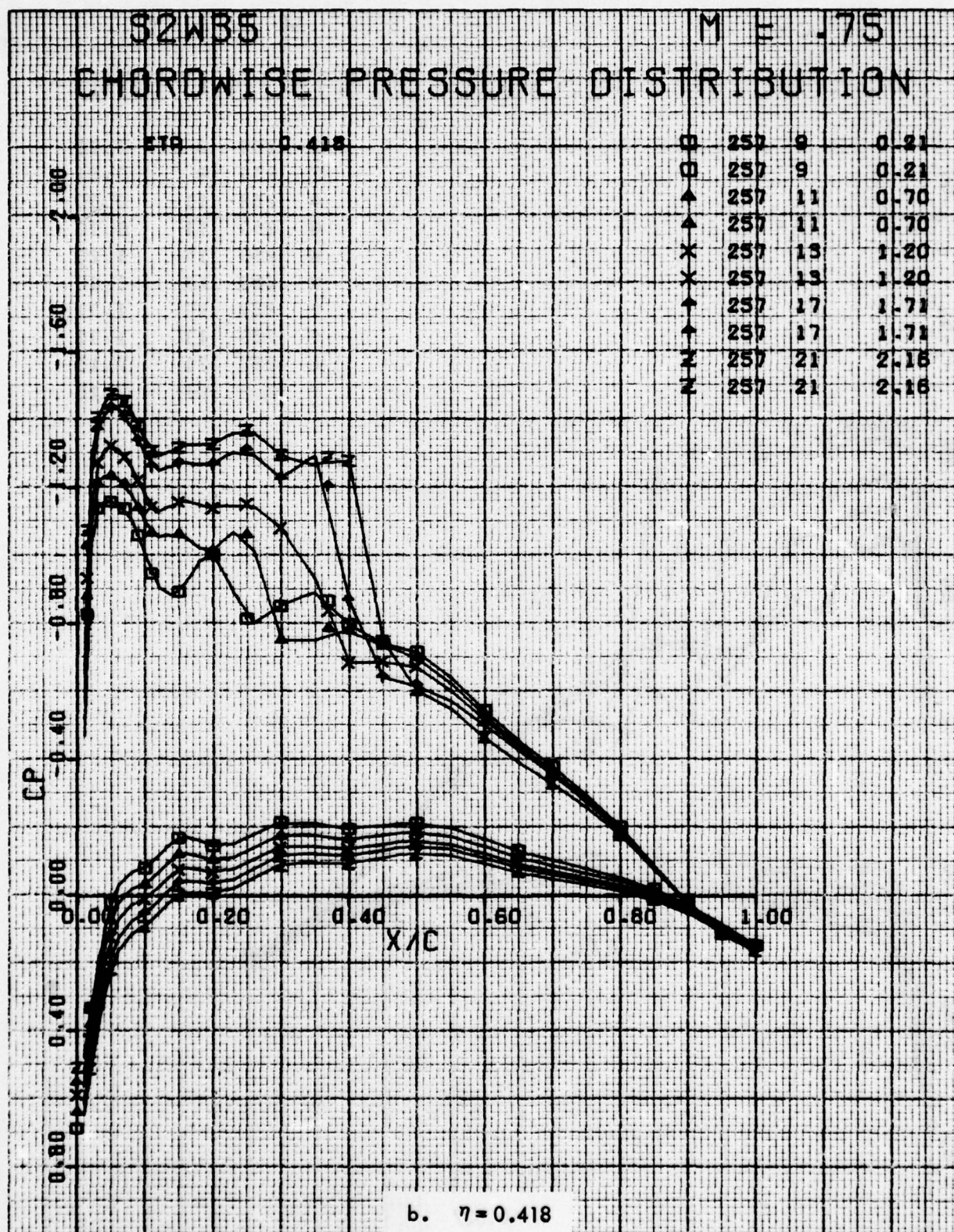


Figure 64. Continued

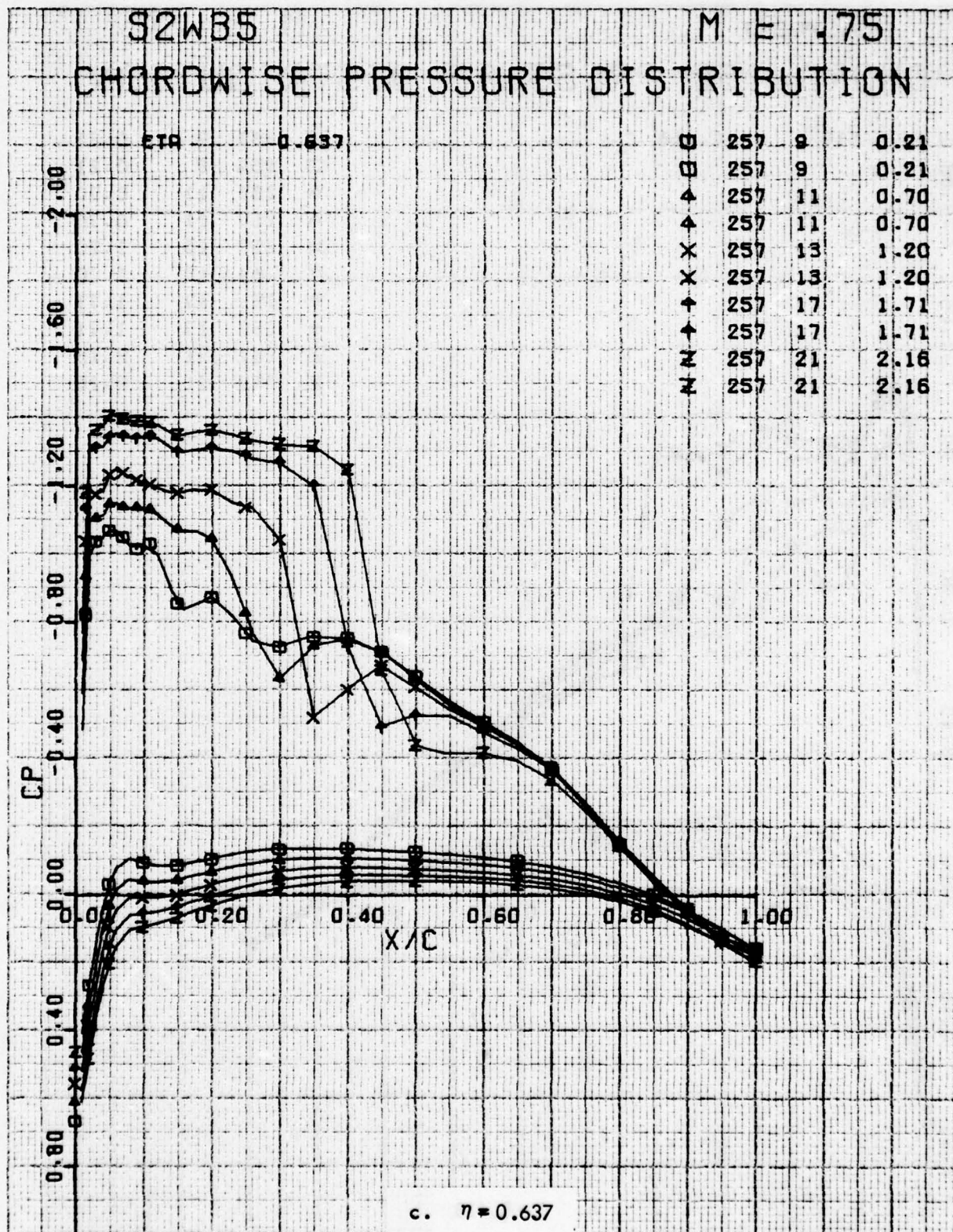


Figure 64 . Continued

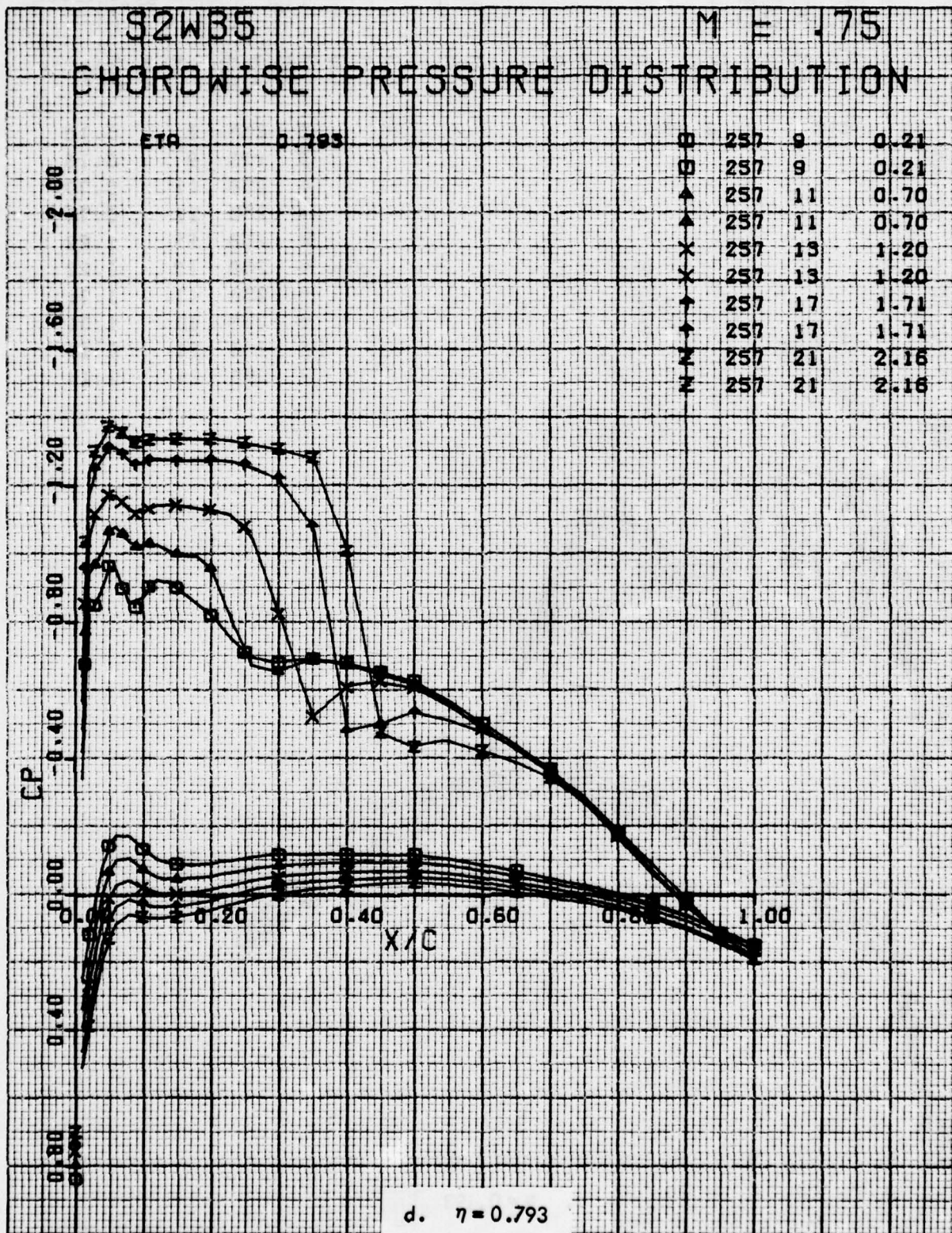


Figure 64. Concluded

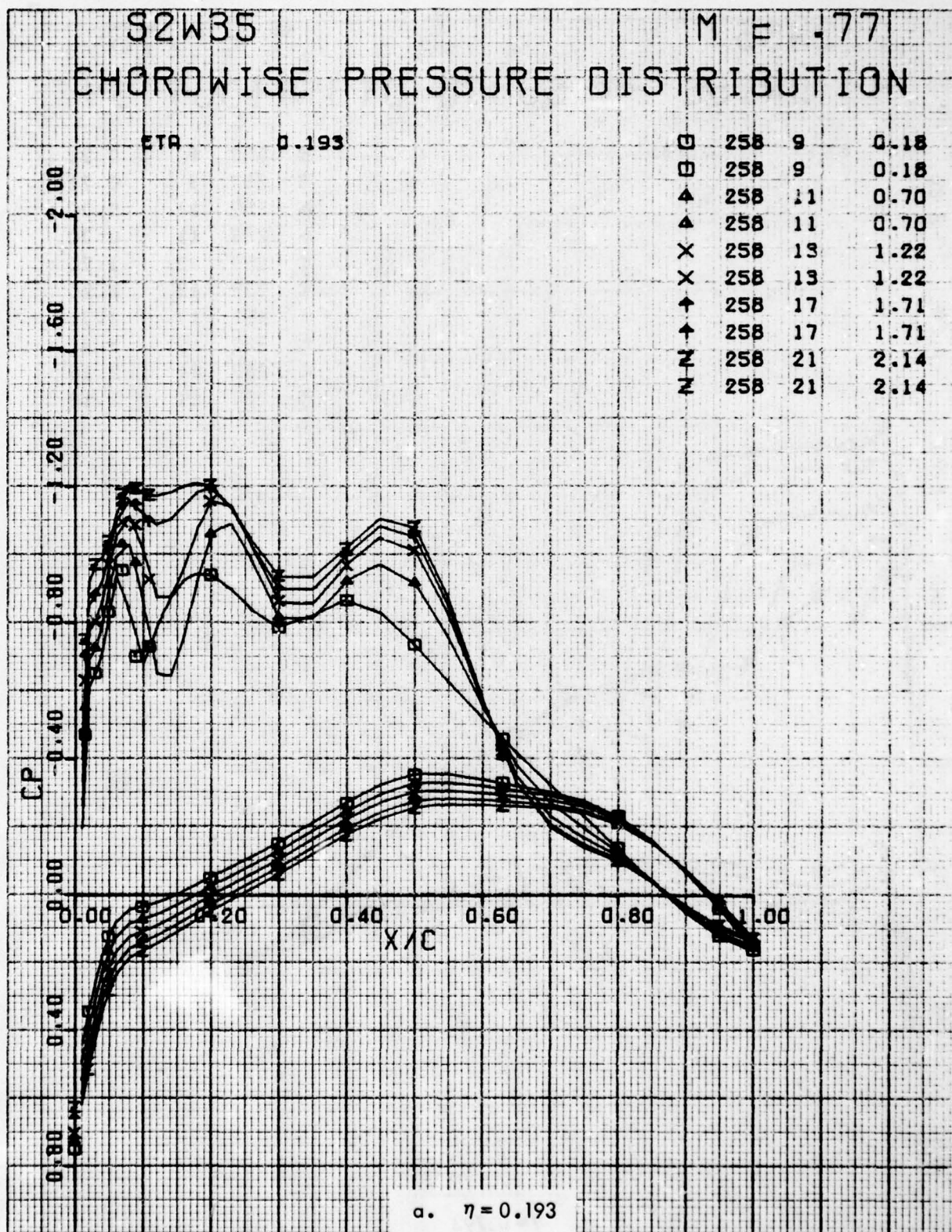


Figure 65. Chordwise Pressure Distributions for Various Angles of Attack. W³⁵ Leading Edge Modification, Fixed Transition, Grit Code D, Pylon/Nacelles Off, M = 0.77.

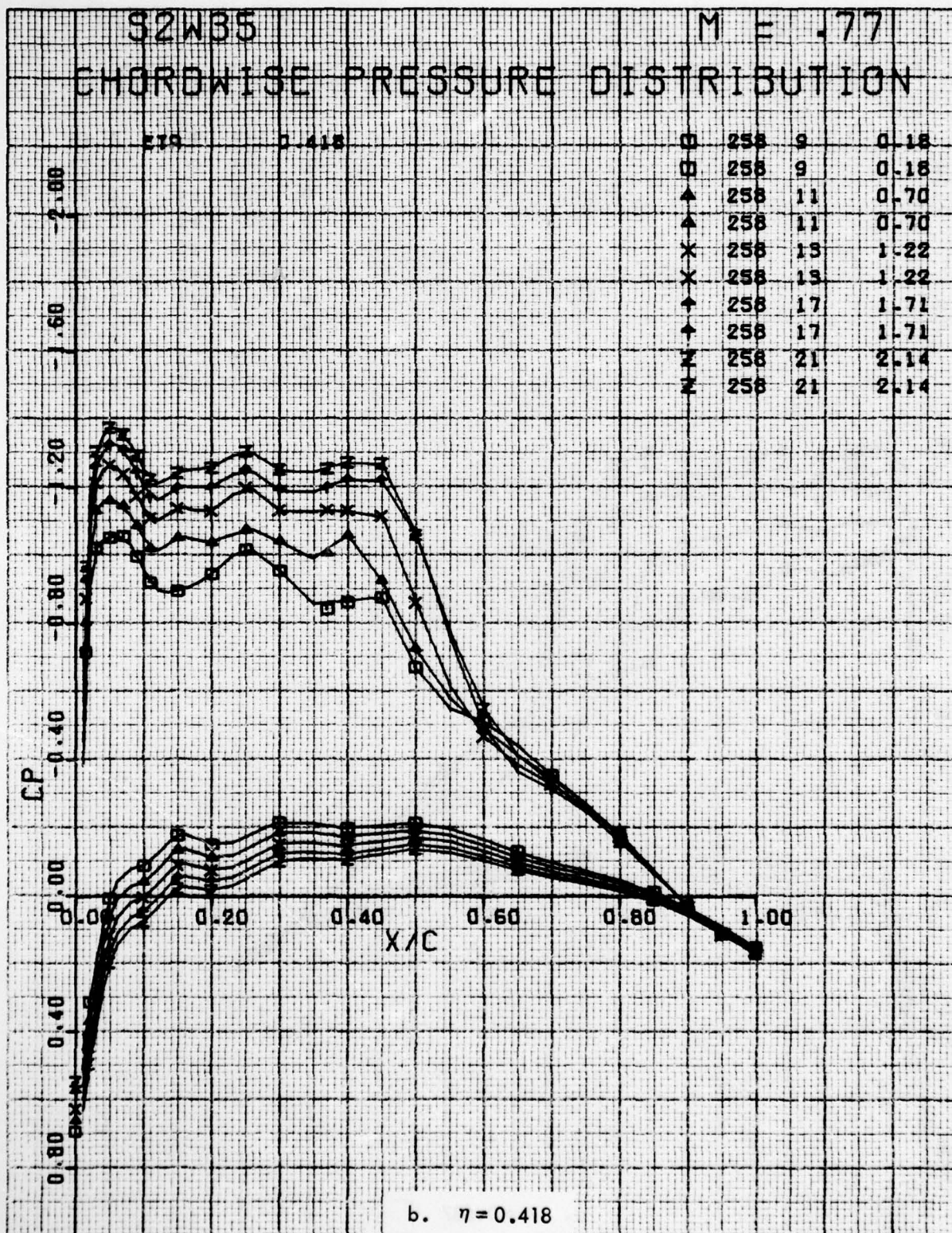


Figure 65. Continued

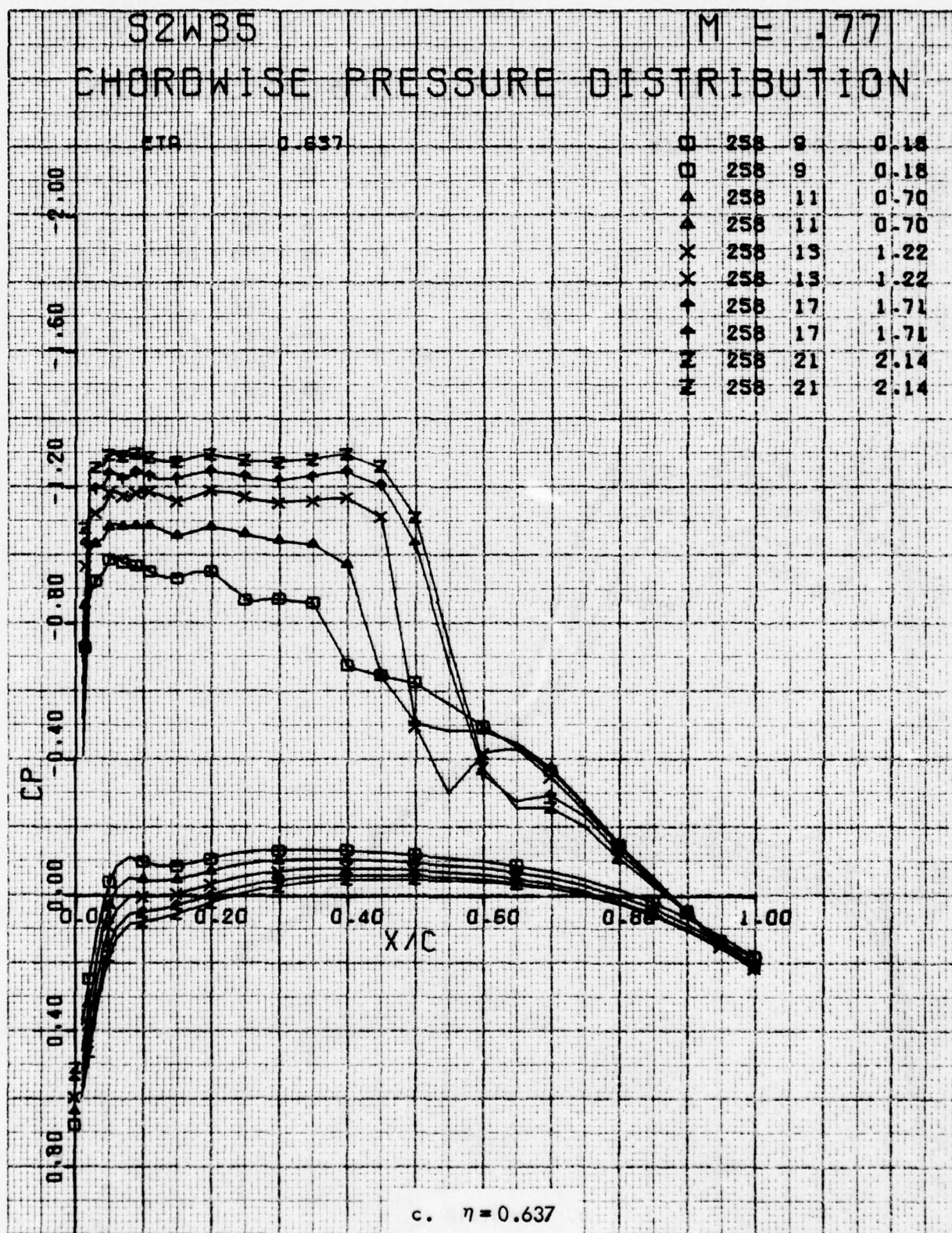


Figure 65 . Continued

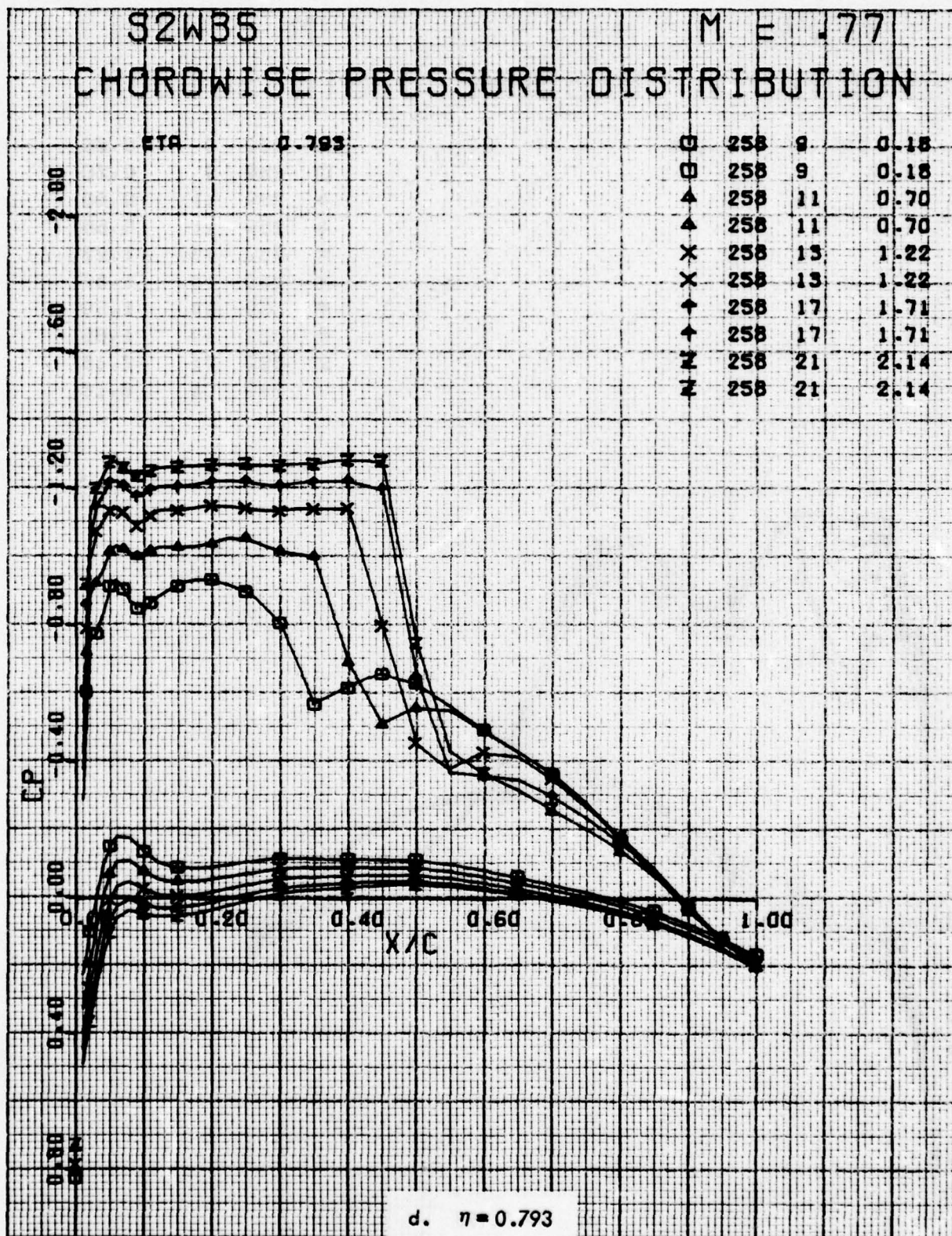


Figure 65. Concluded

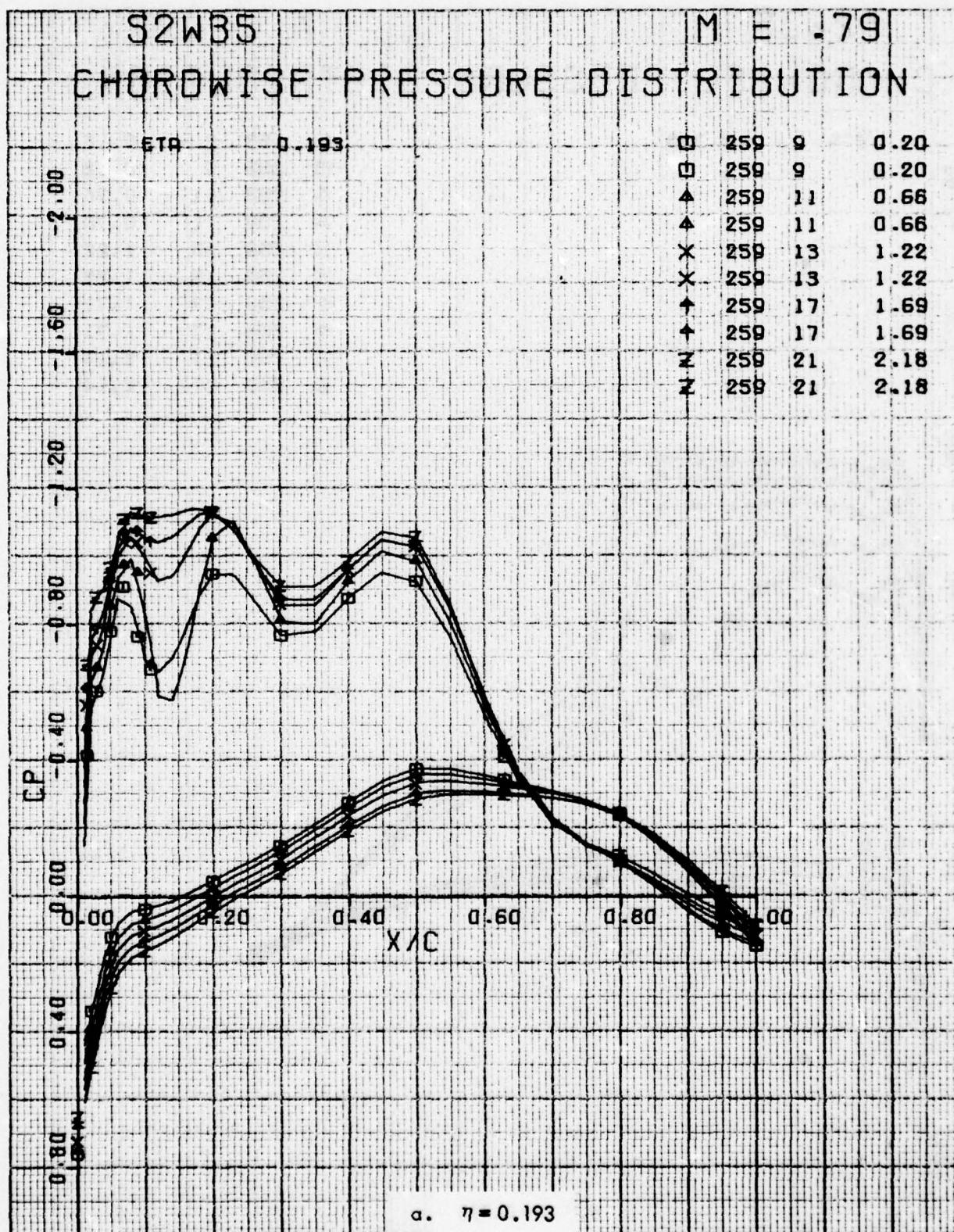


Figure 66 . Chordwise Pressure Distributions for Various Angles of Attack. W³⁵ Leading Edge Modification, Fixed Transition, Grit Code D, Pylon/Nacelles Off, M = 0.79.

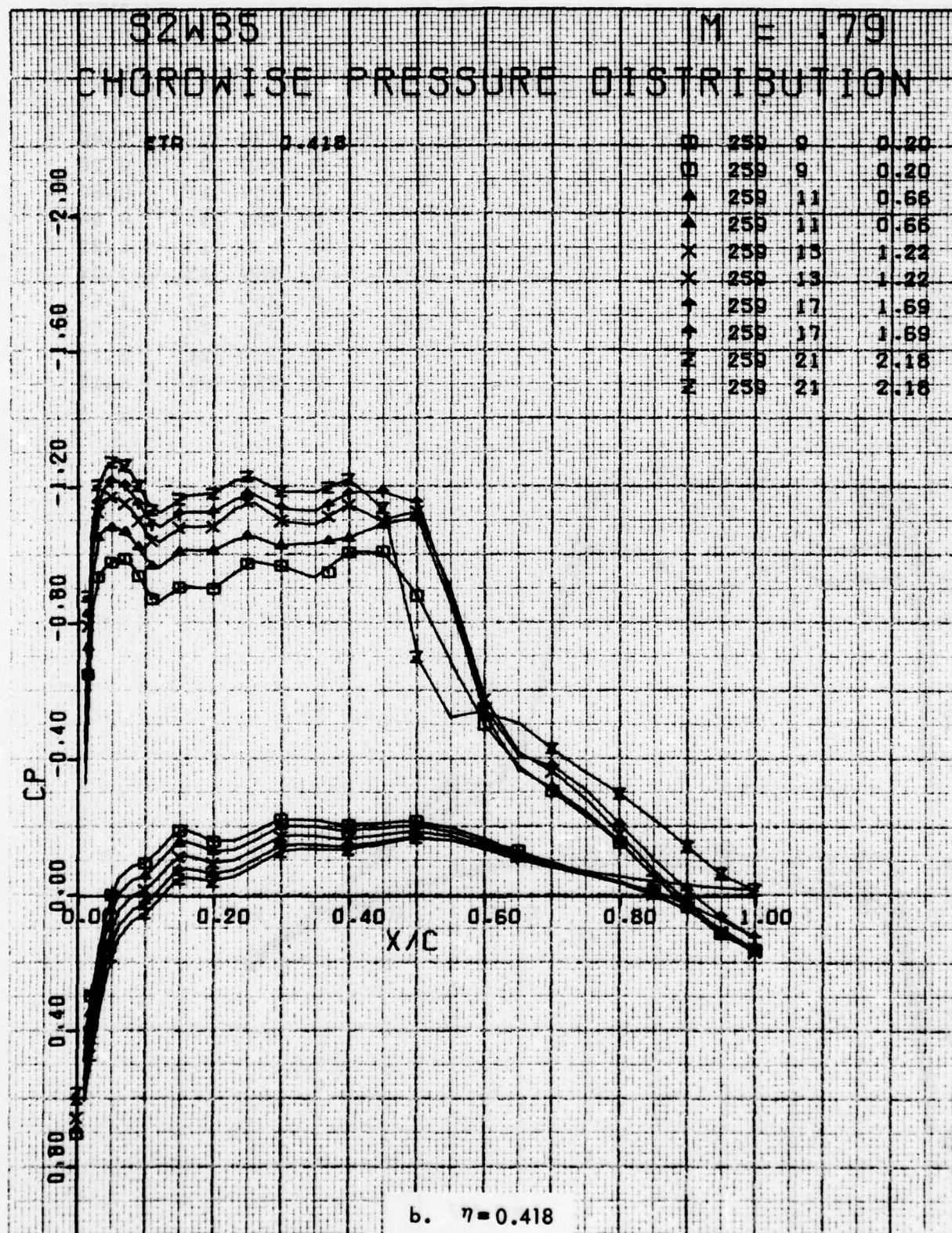


Figure 66. Continued

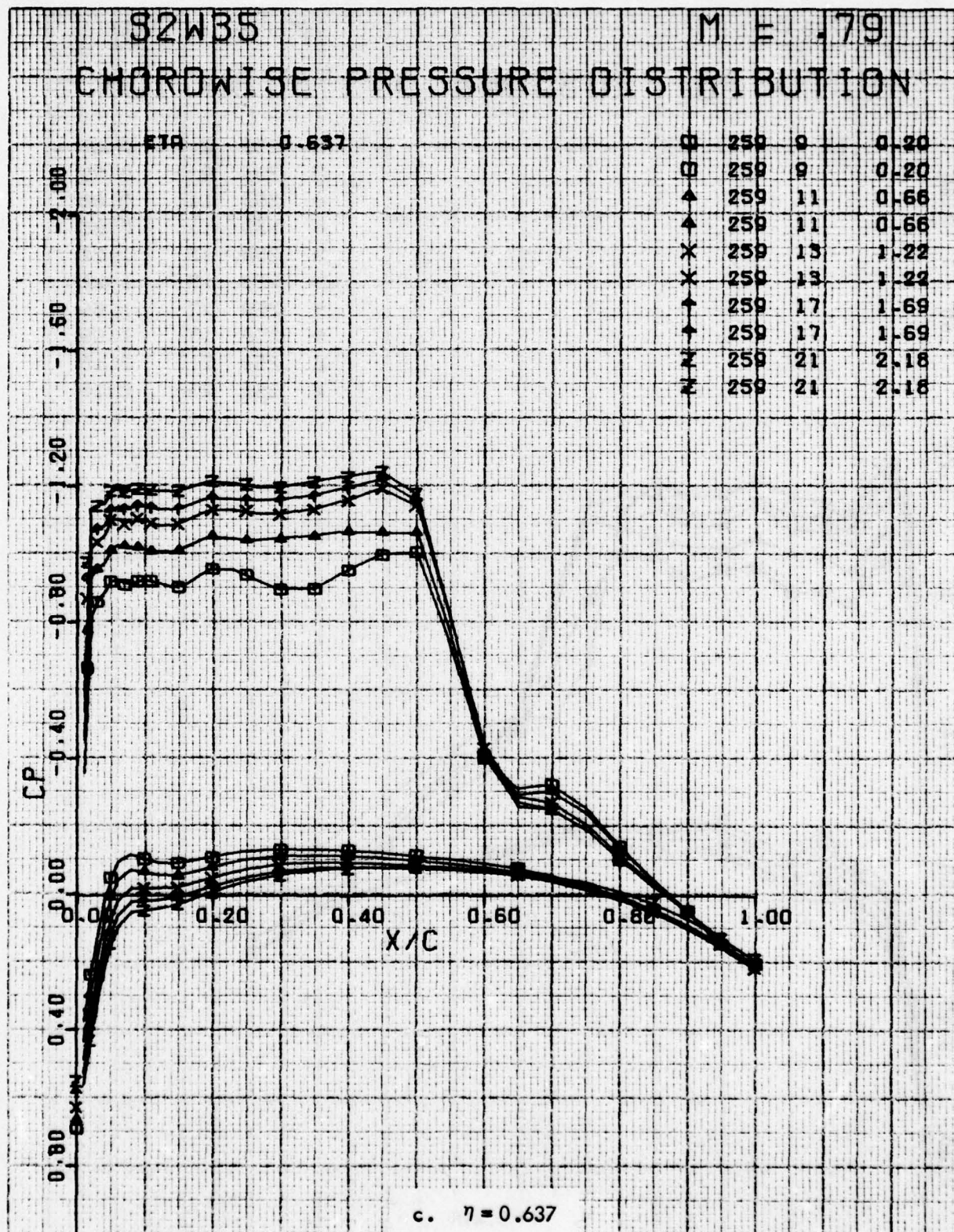


Figure 66 . Continued

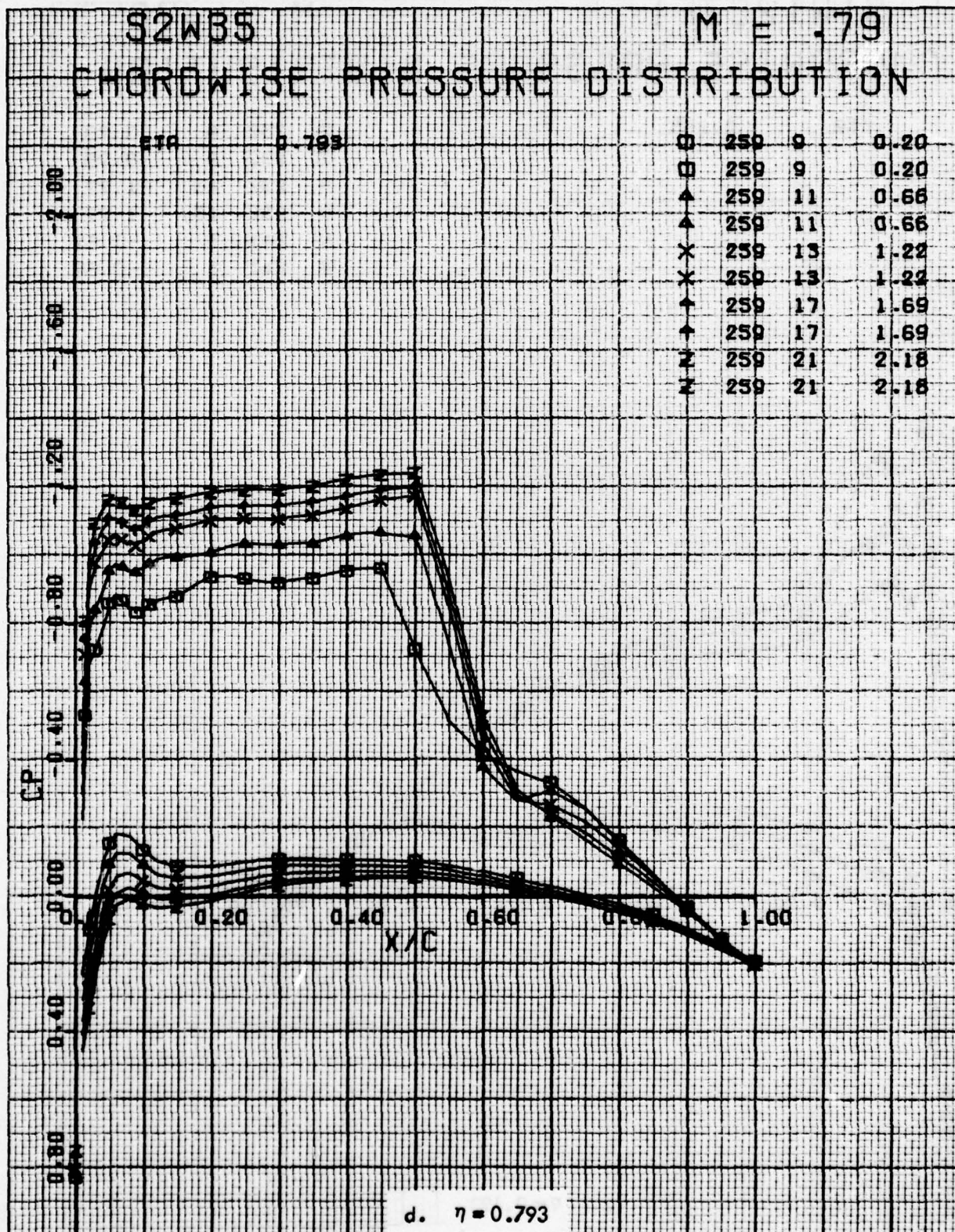


Figure 66. Concluded

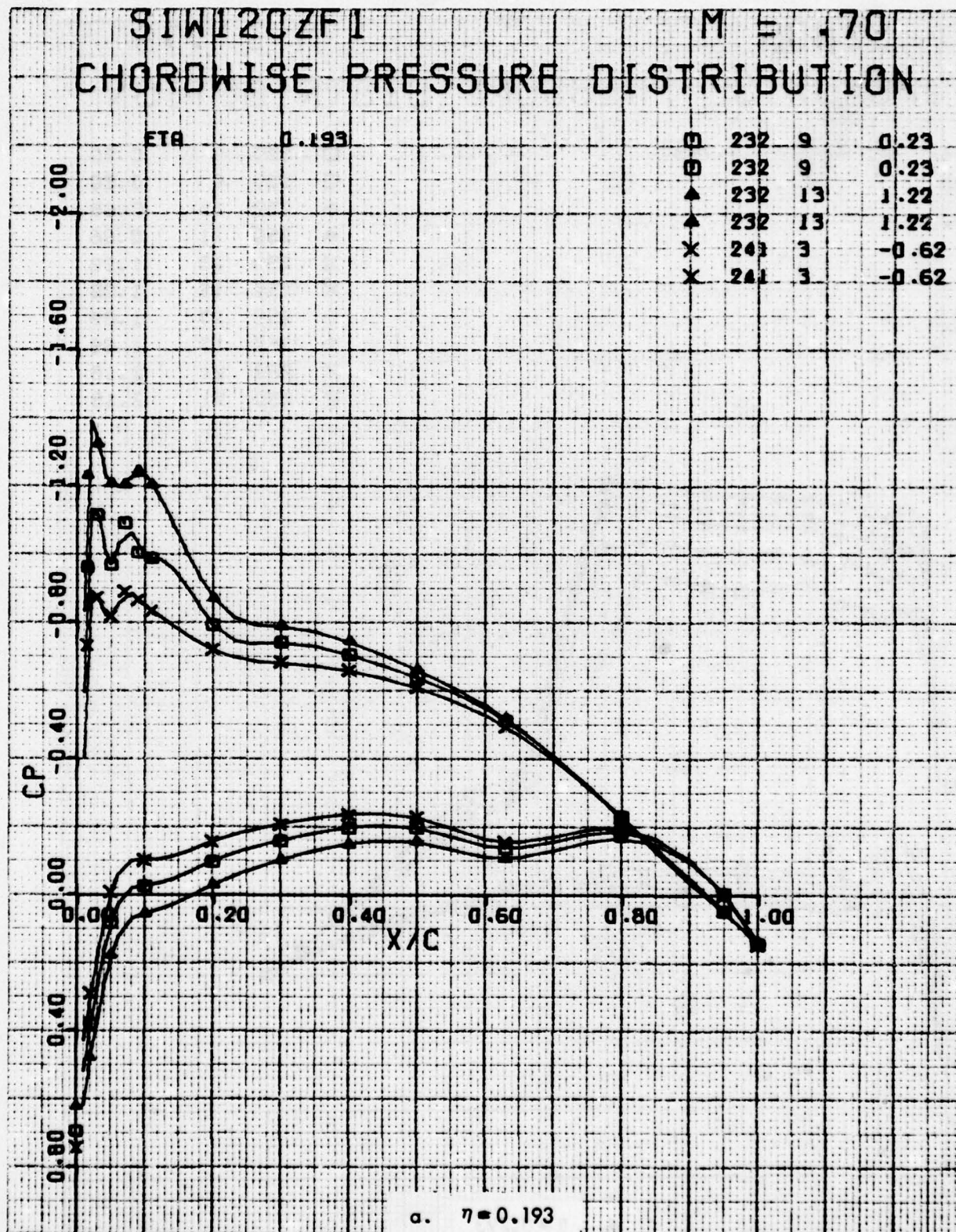


Figure 67. Chordwise Pressure Distributions for Various Angles of Attack. Baseline Leading Edge, Fixed Transition, Grit Code D, Eight Anti-Drag Bodies, $M = 0.7$.

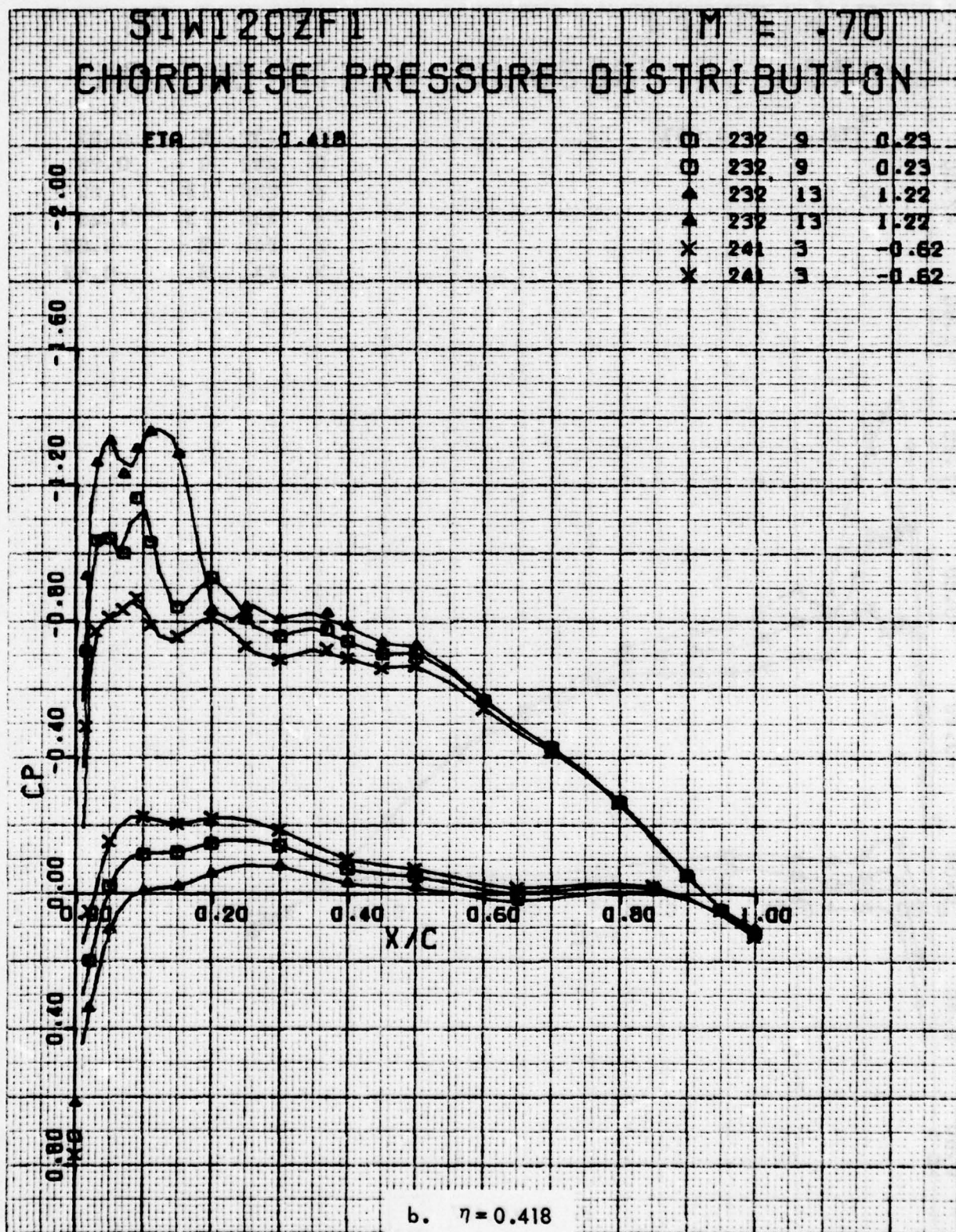


Figure 67. Continued

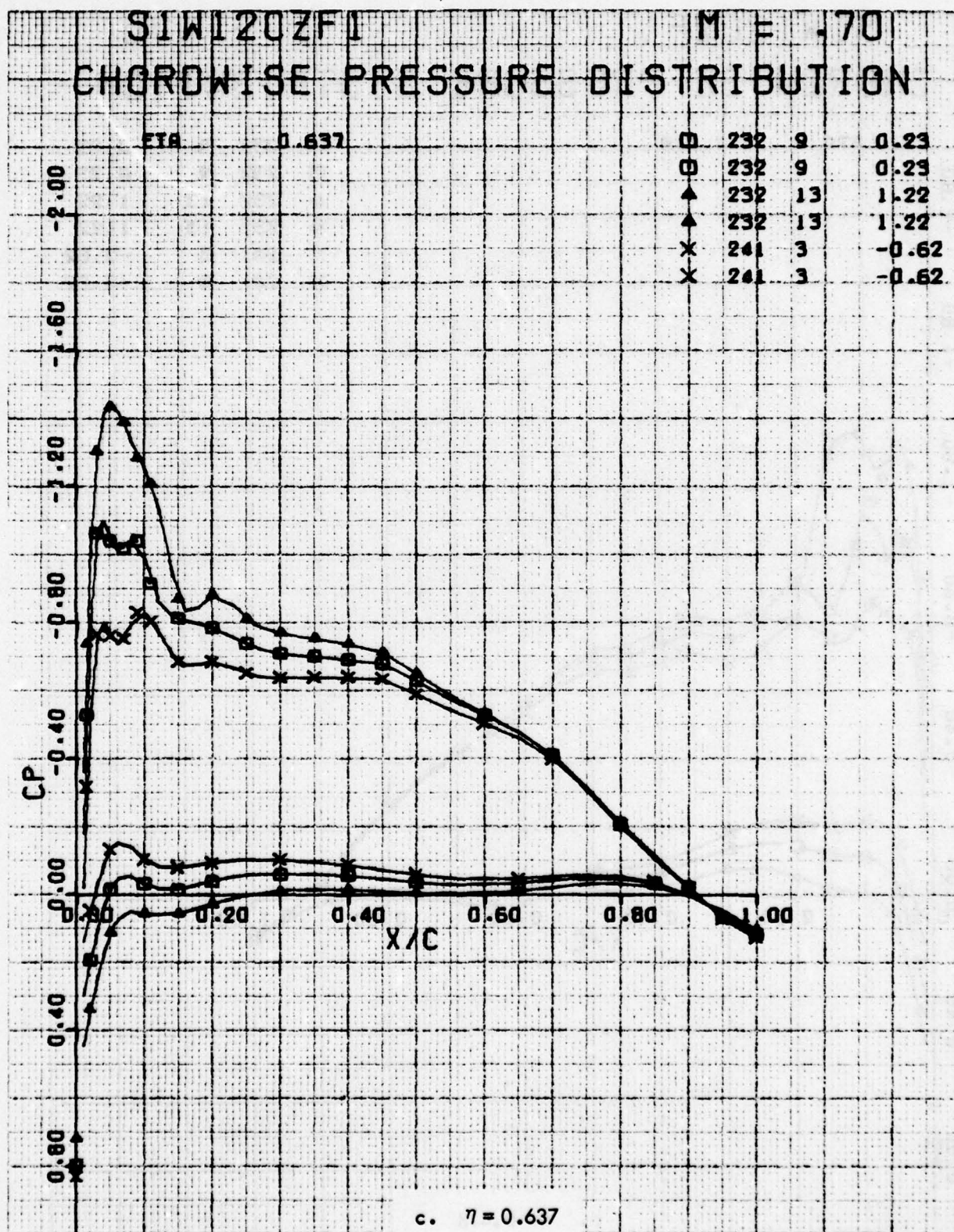


Figure 67 . Continued

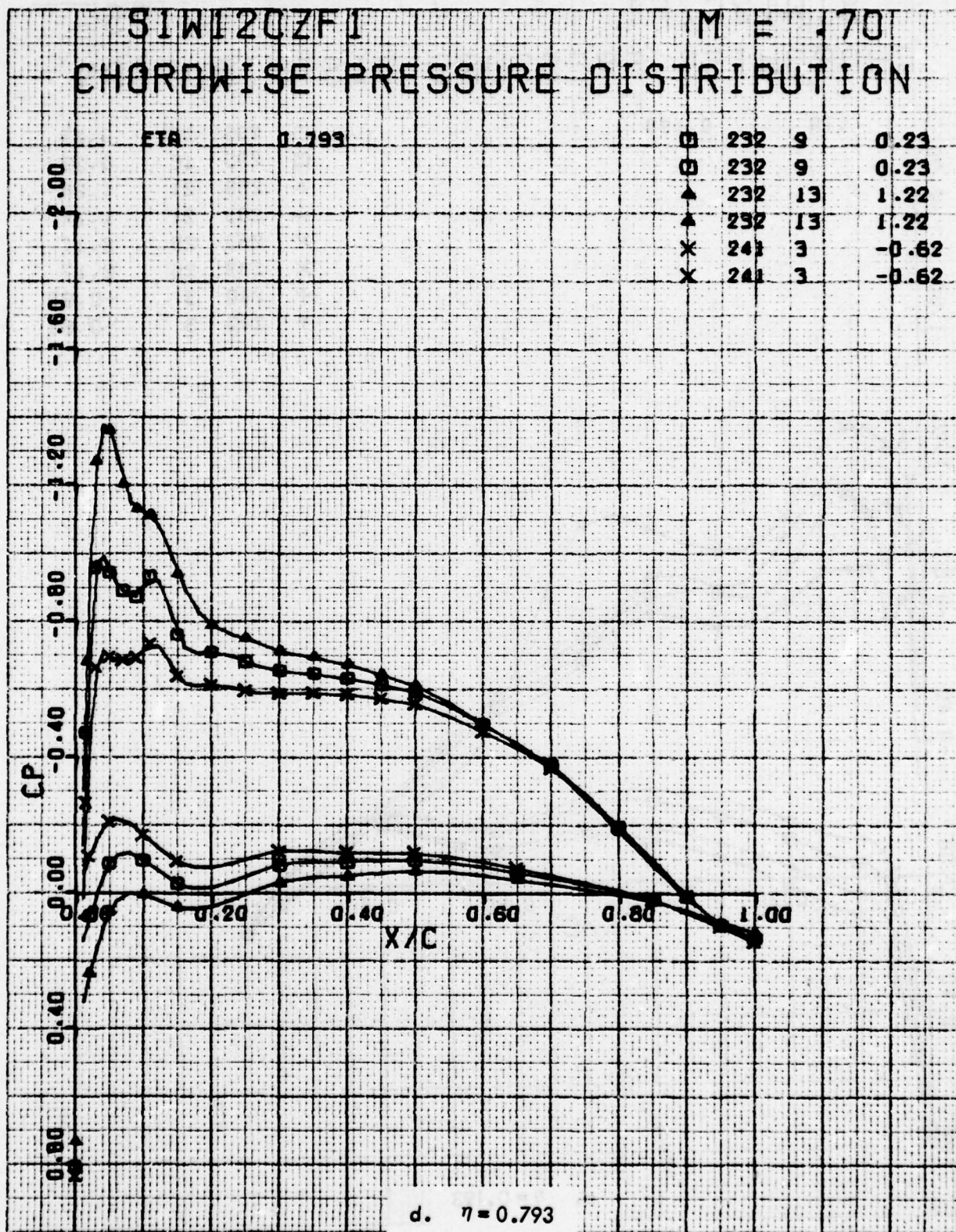


Figure 67. Concluded

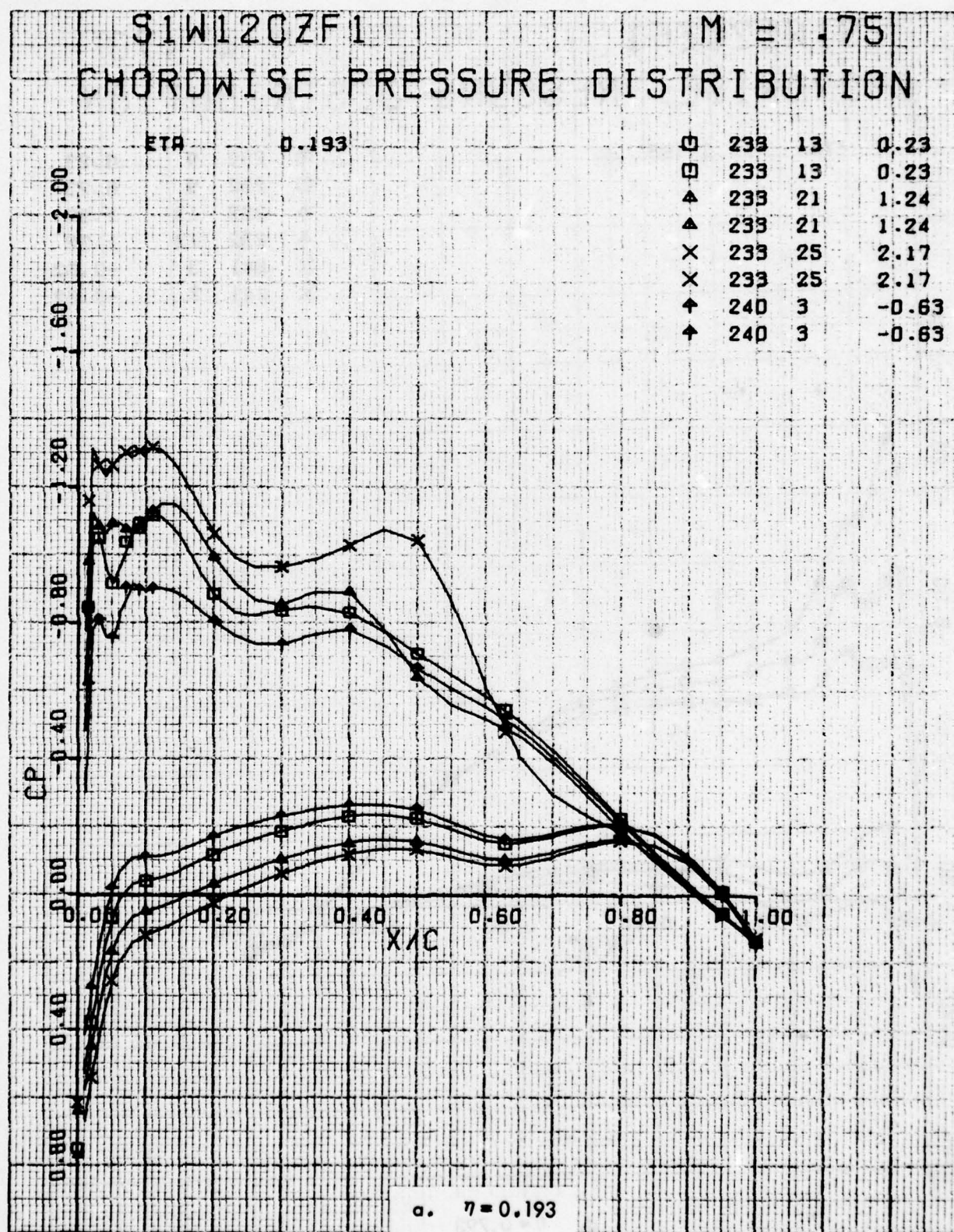


Figure 68. Chordwise Pressure Distributions for Various Angles of Attack. Baseline Leading Edge, Fixed Transition, Grit Code D, Eight Anti-Drag Bodies, $M = 0.75$.

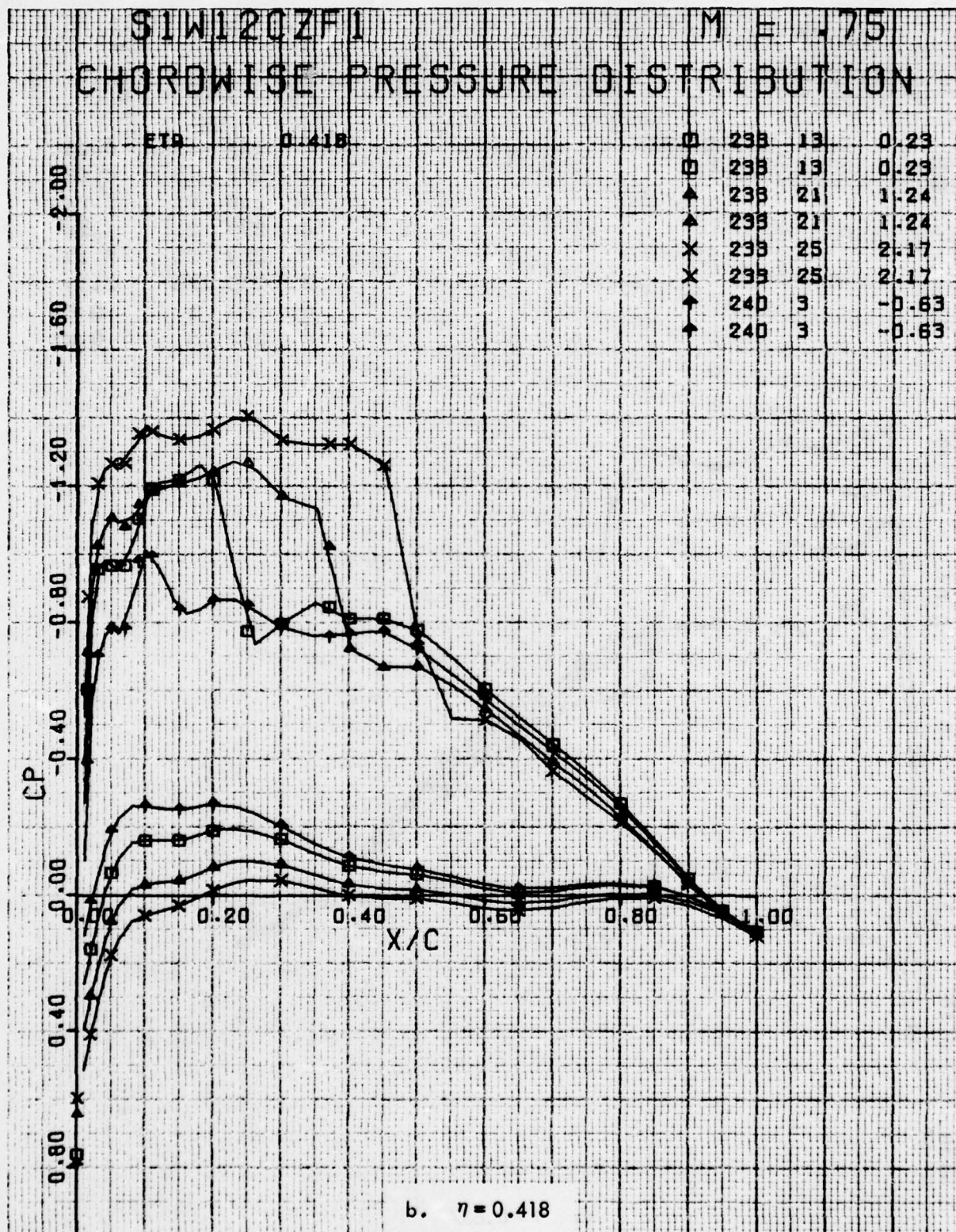


Figure 68. Continued

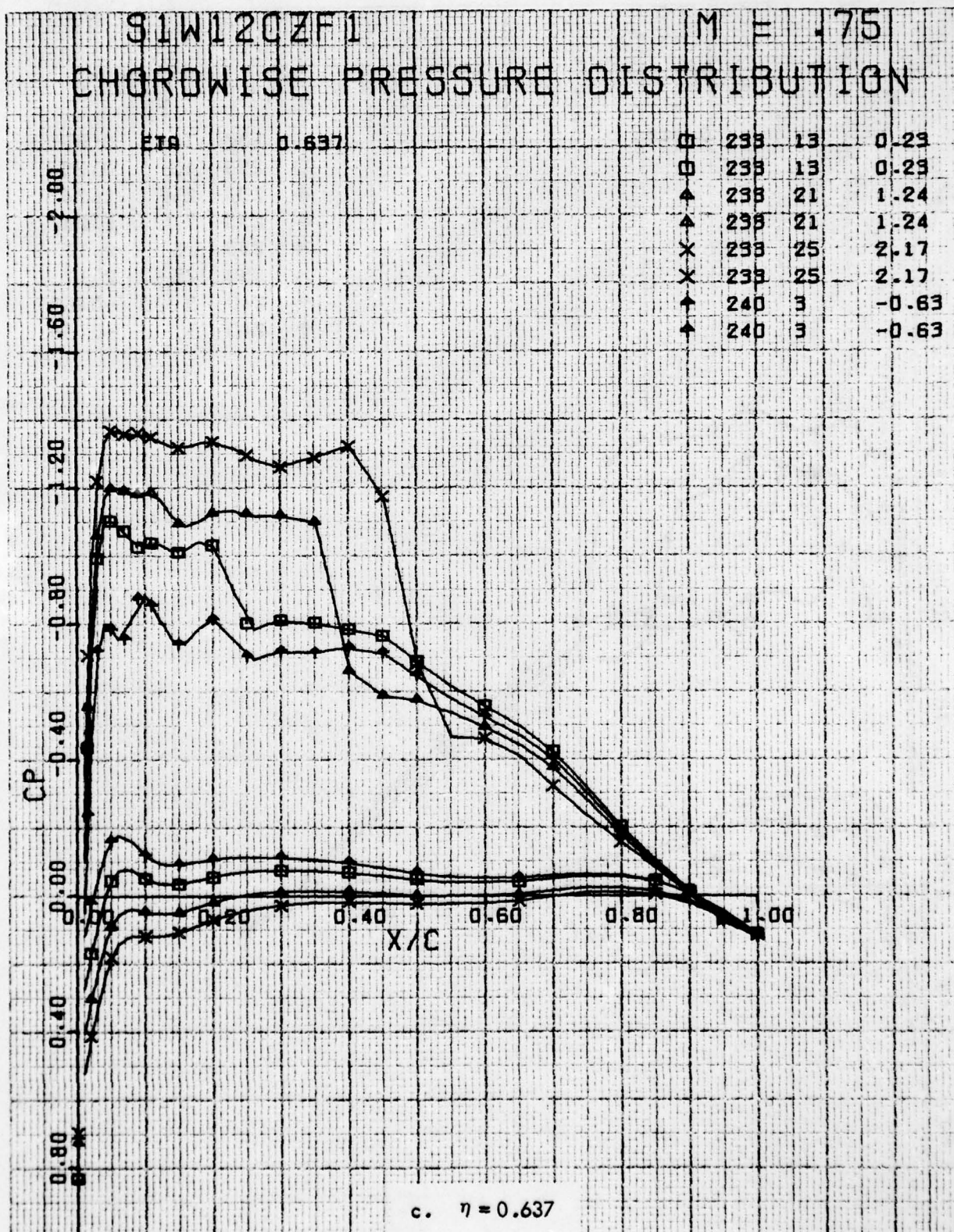


Figure 68 . Continued

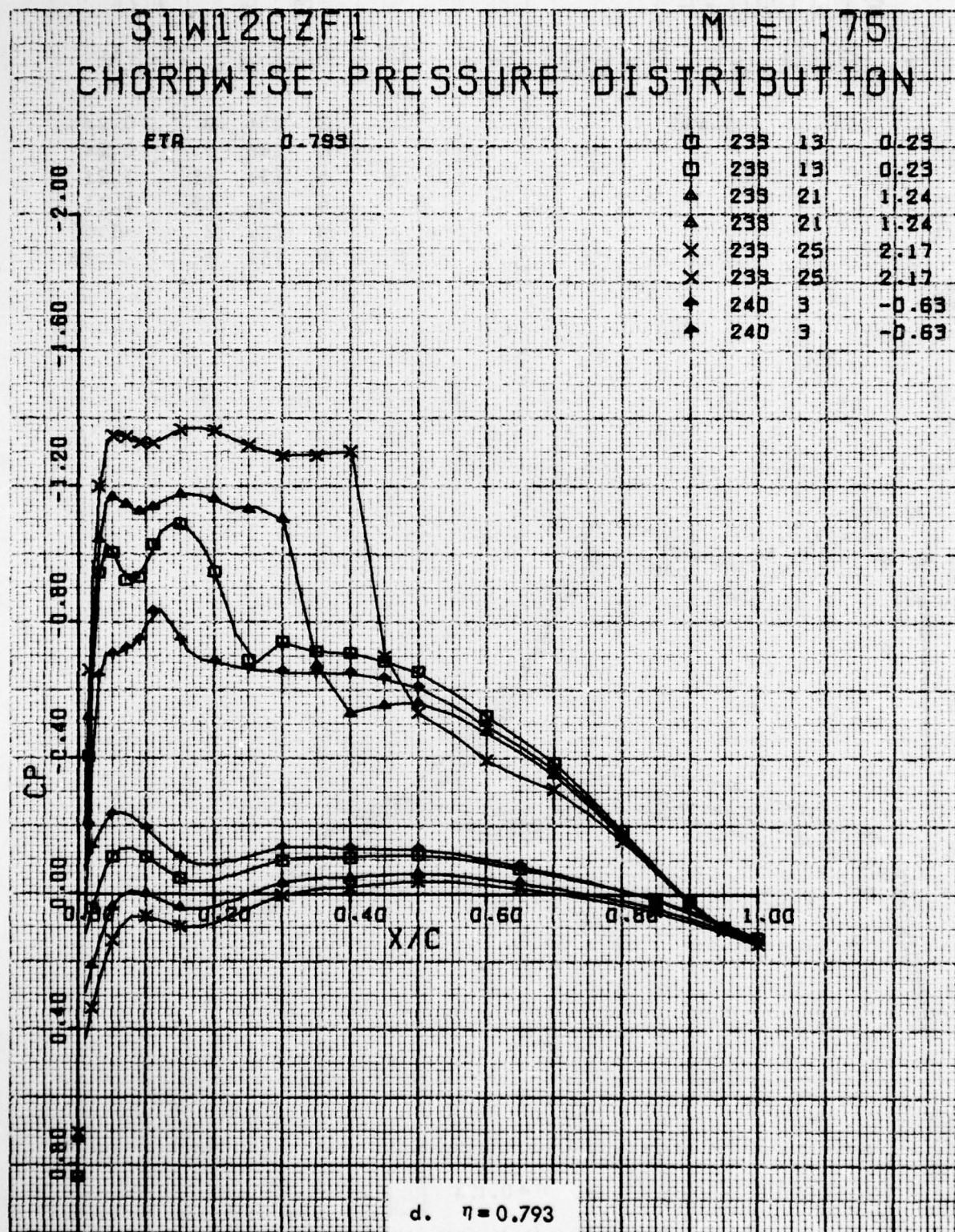


Figure 68. Concluded

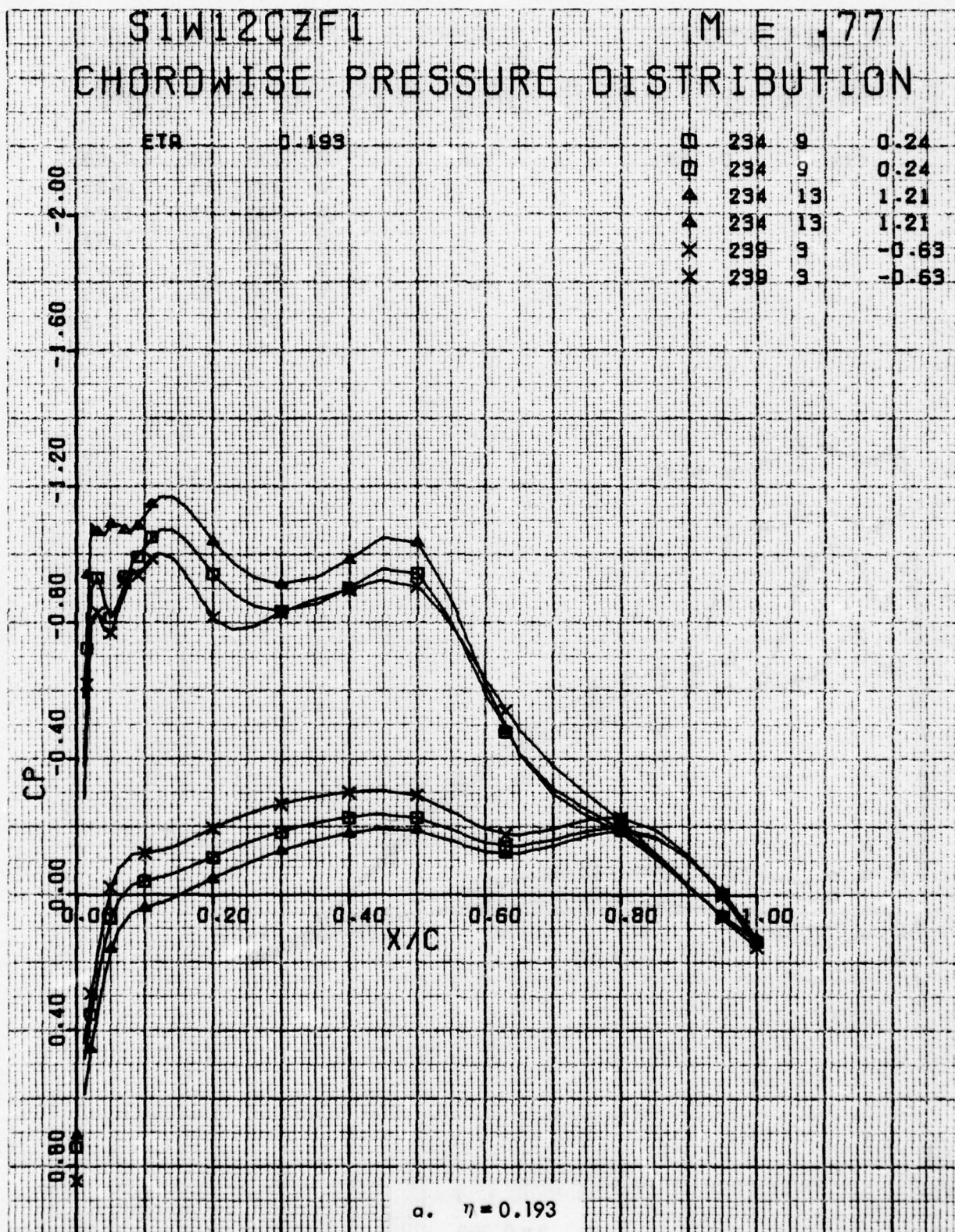


Figure 69. Chordwise Pressure Distributions for Various Angles of Attack. Baseline Leading Edge, Fixed Transition, Grit Code D, Eight Anti-Drag Bodies, $M = 0.77$.

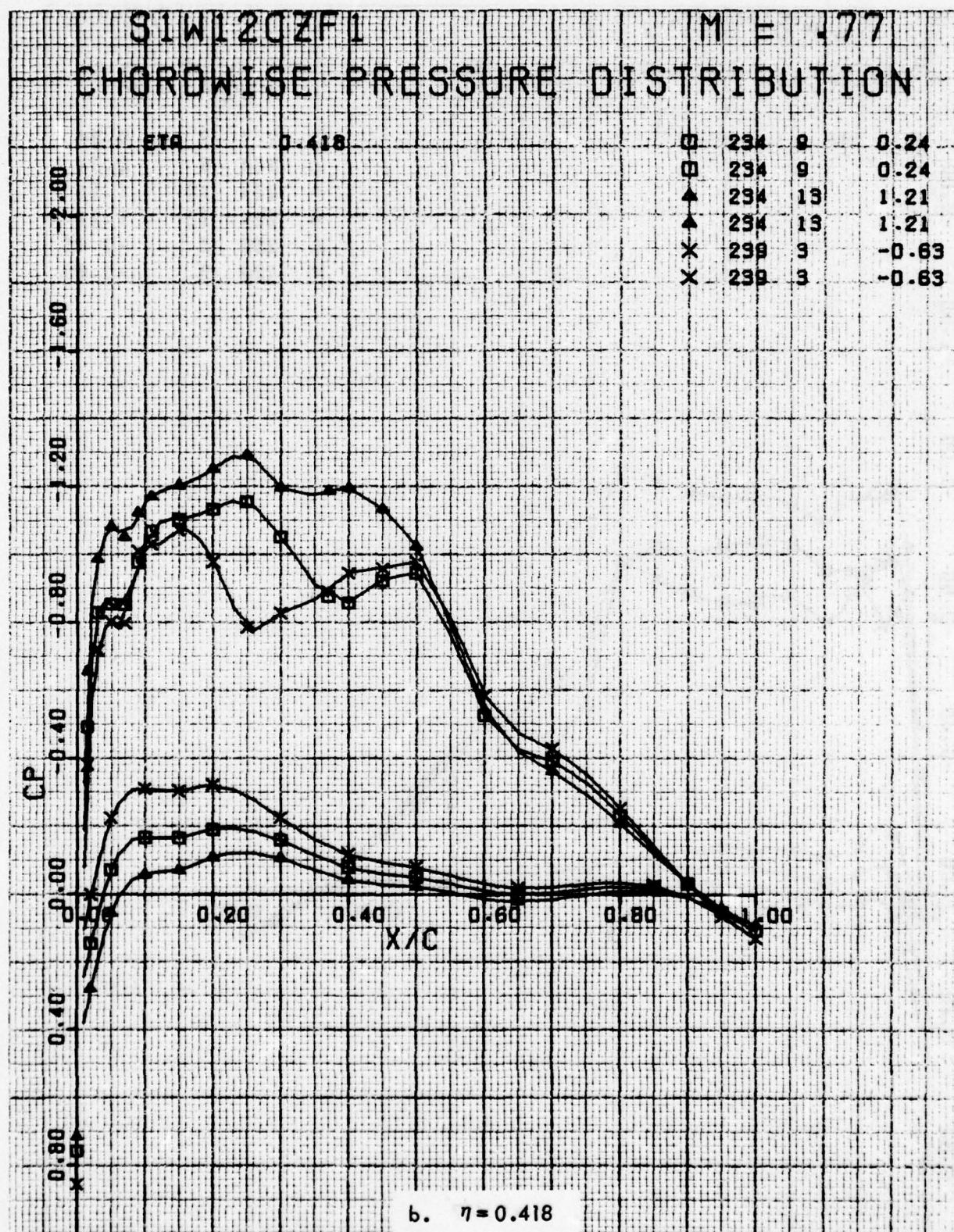


Figure 69. Continued

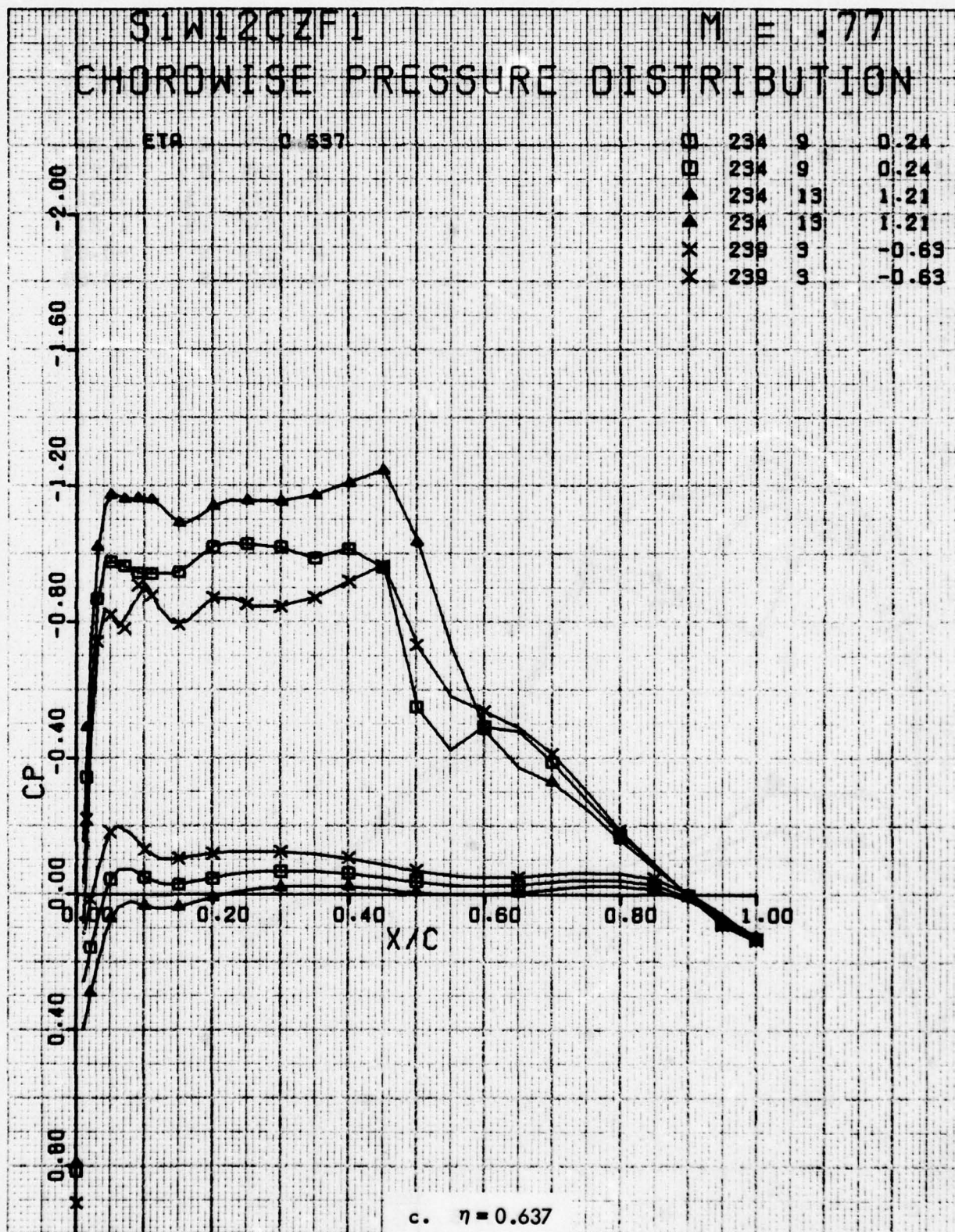


Figure 69 . Continued

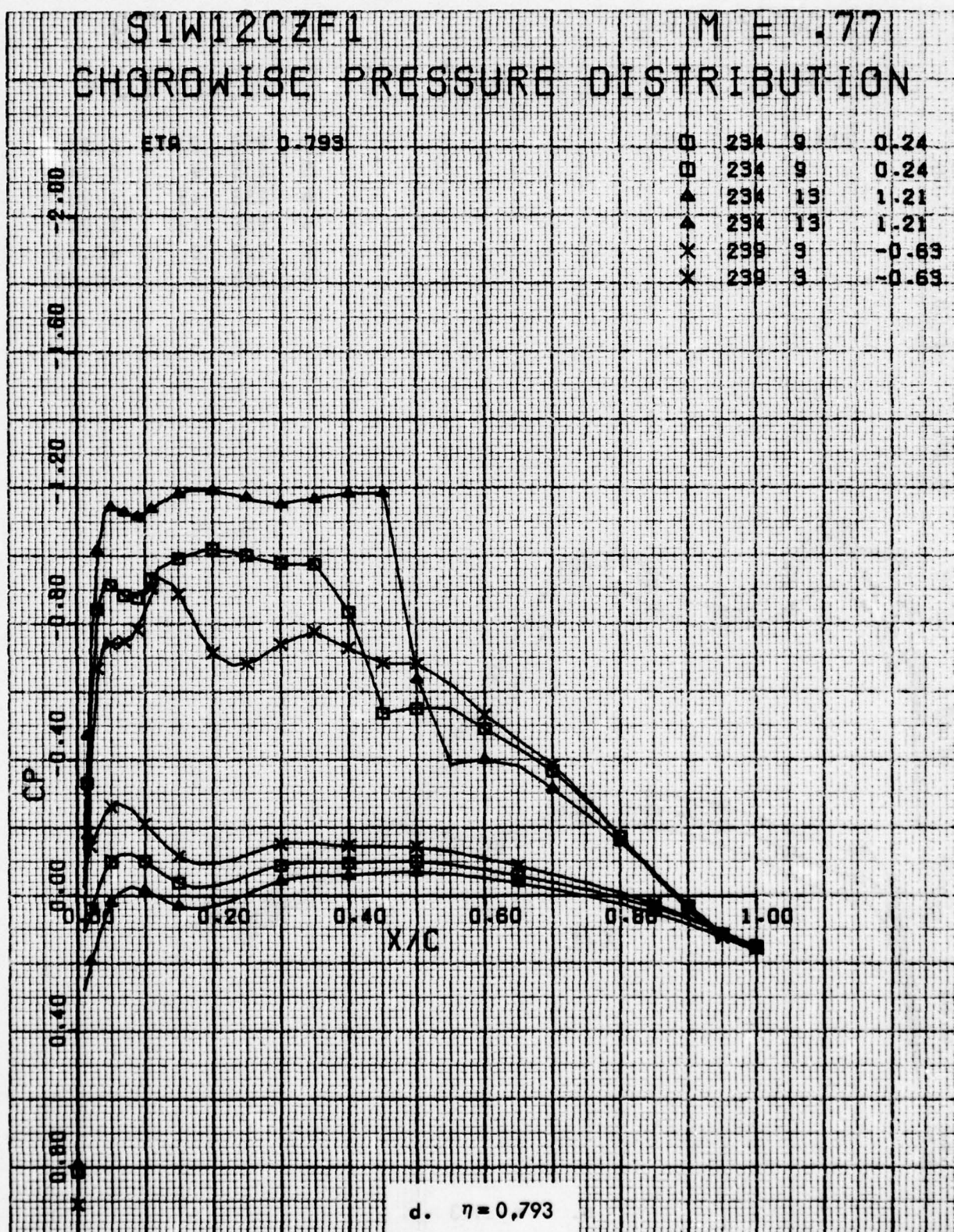


Figure 69. Concluded

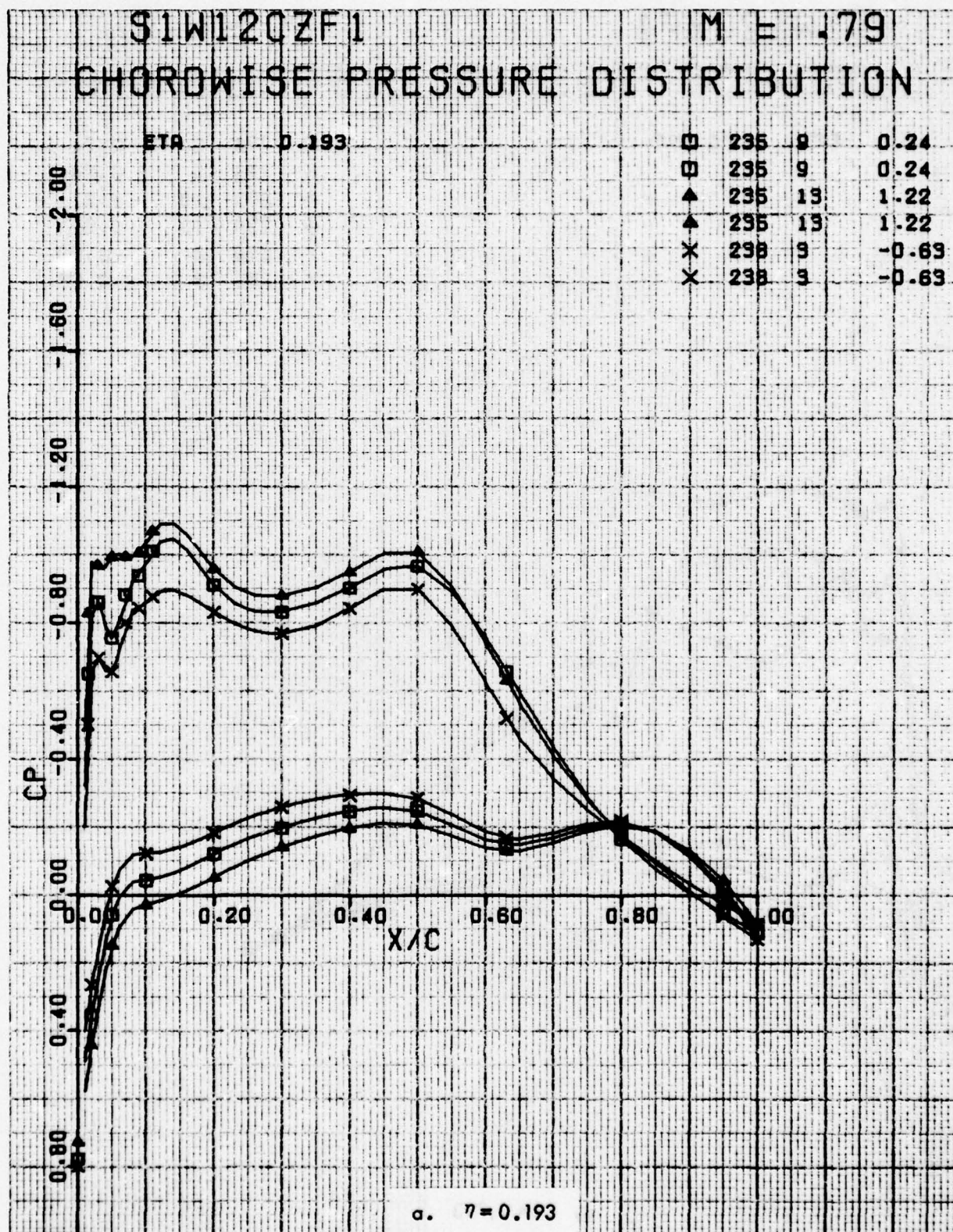


Figure 70. Chordwise Pressure Distributions for Various Angles of Attack. Baseline Leading Edge, Fixed Transition, Grit Code D, Eight Anti-Drag Bodies, $M = 0.79$.

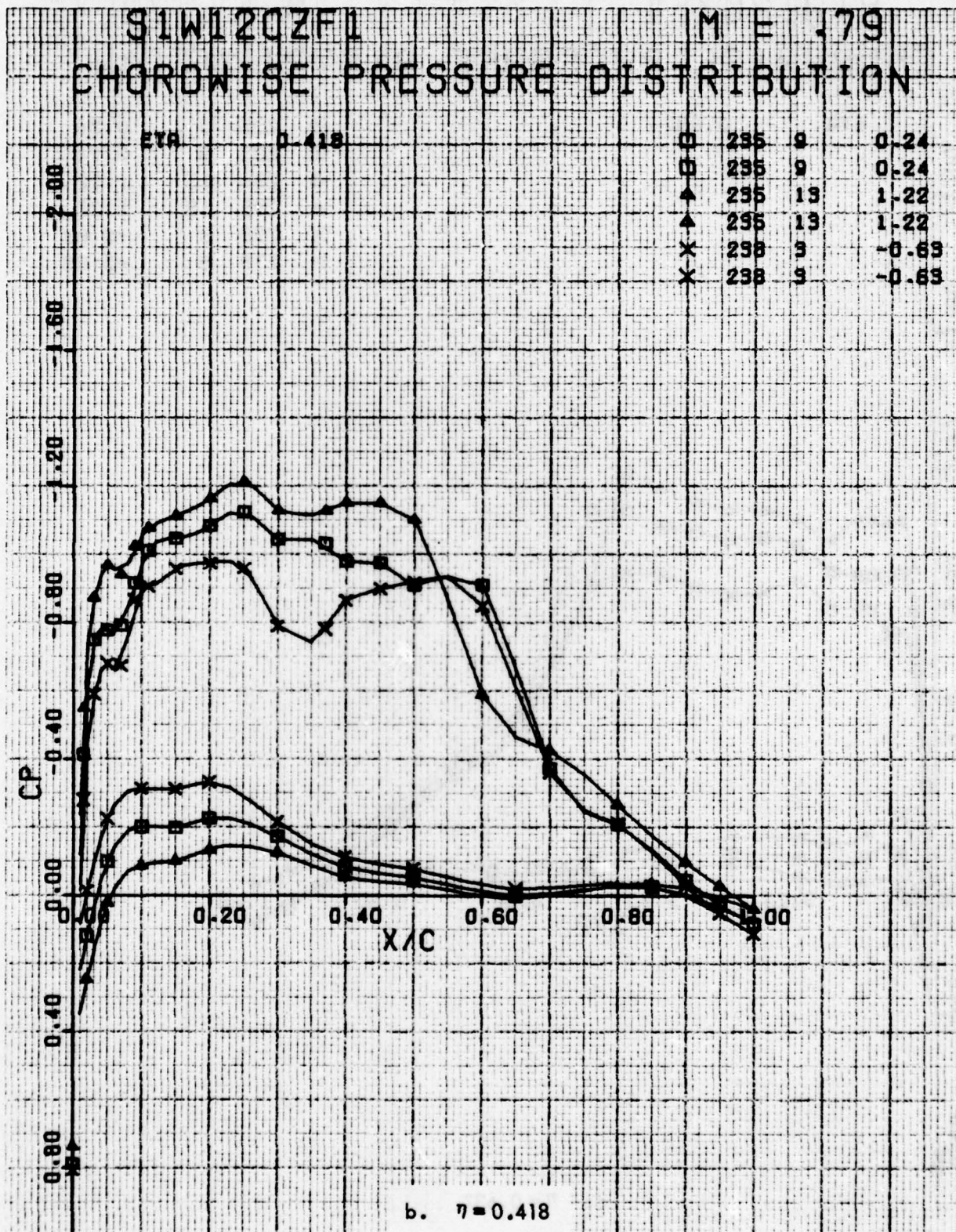


Figure 70. Continued

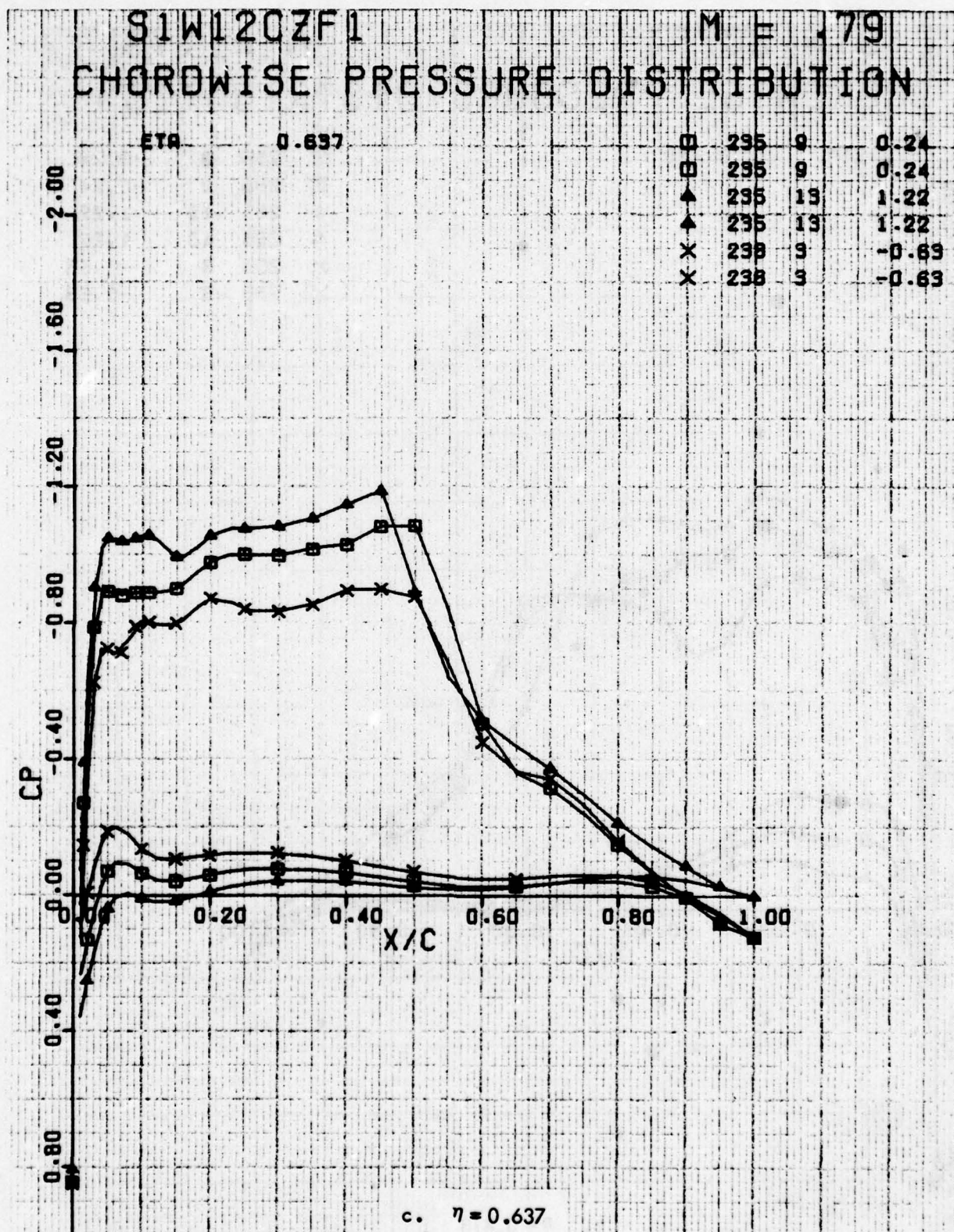


Figure 70 . Continued

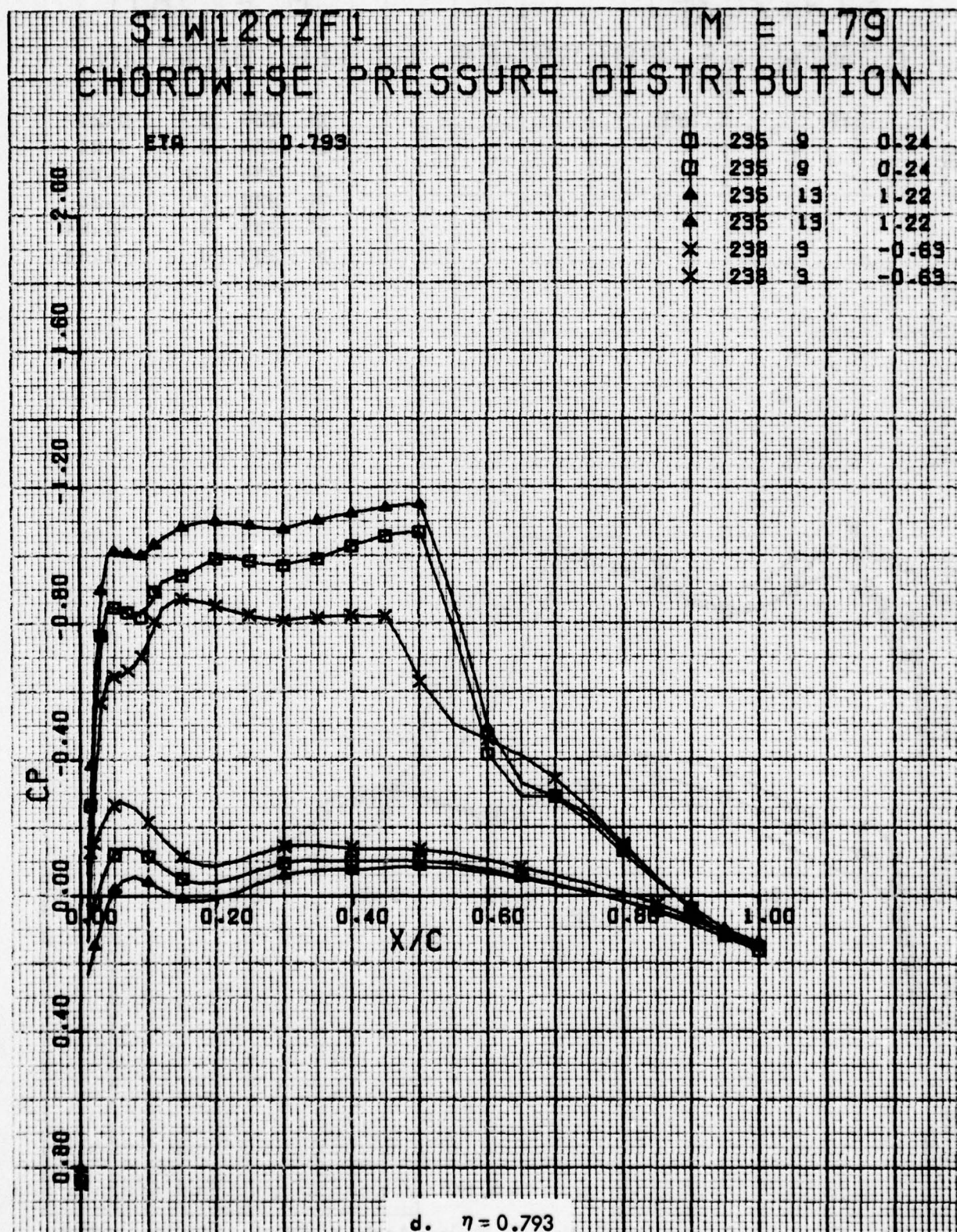


Figure 70. Concluded

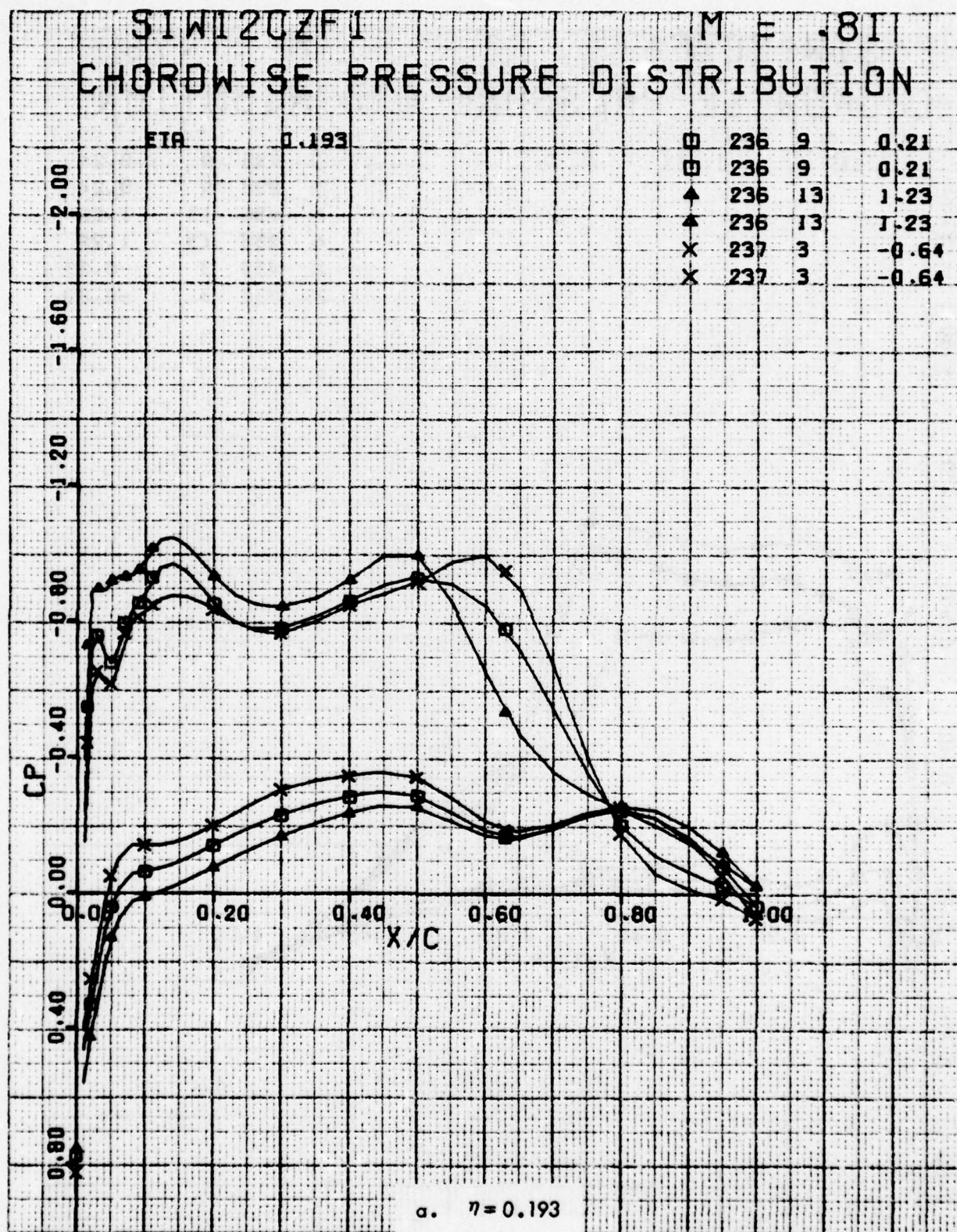


Figure 71. Chordwise Pressure Distributions for Various Angles of Attack. Baseline Leading Edge, Fixed Transition, Grit Code D, Eight Anti-Drag Bodies, $M = 0.81$.

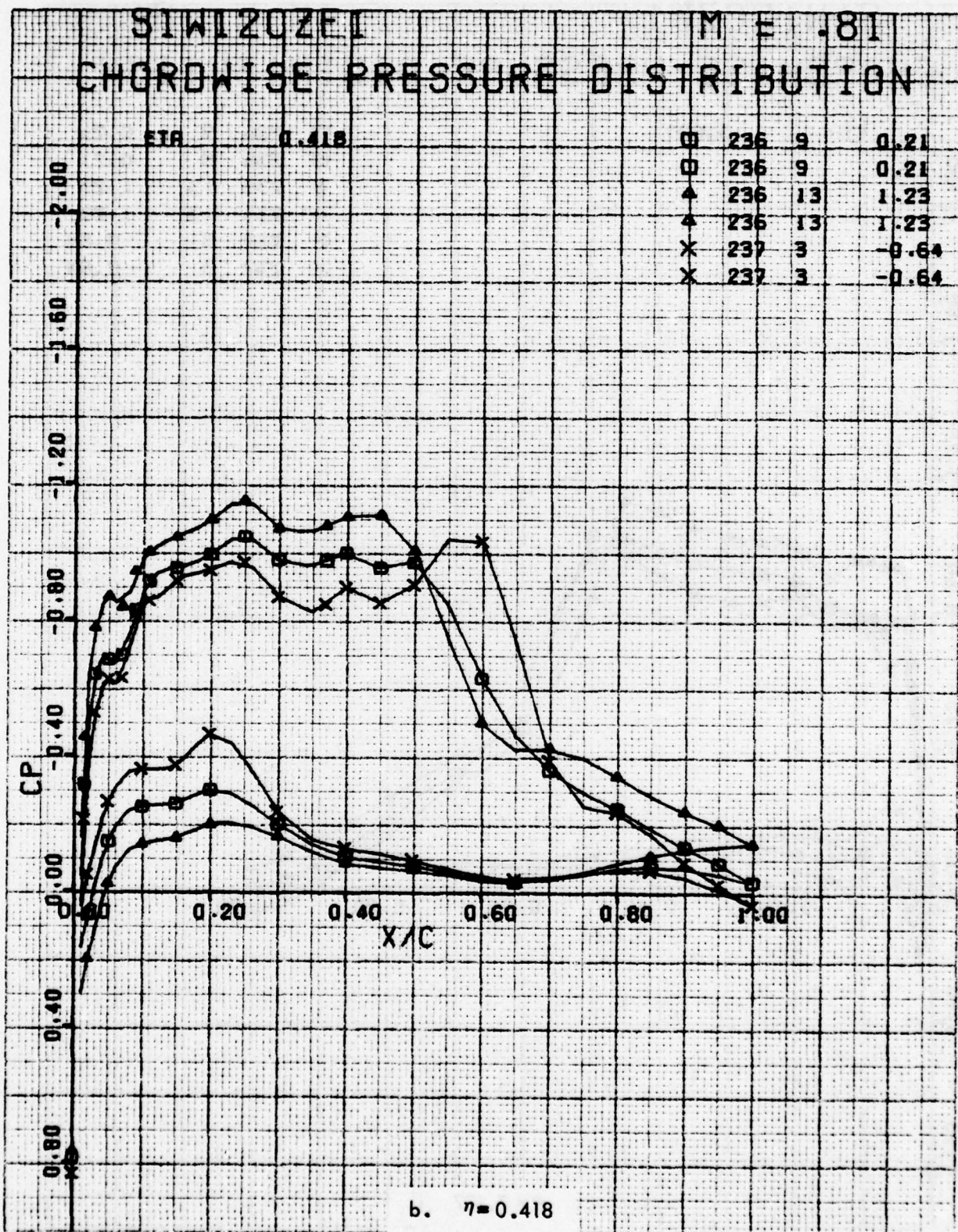


Figure 71. Continued

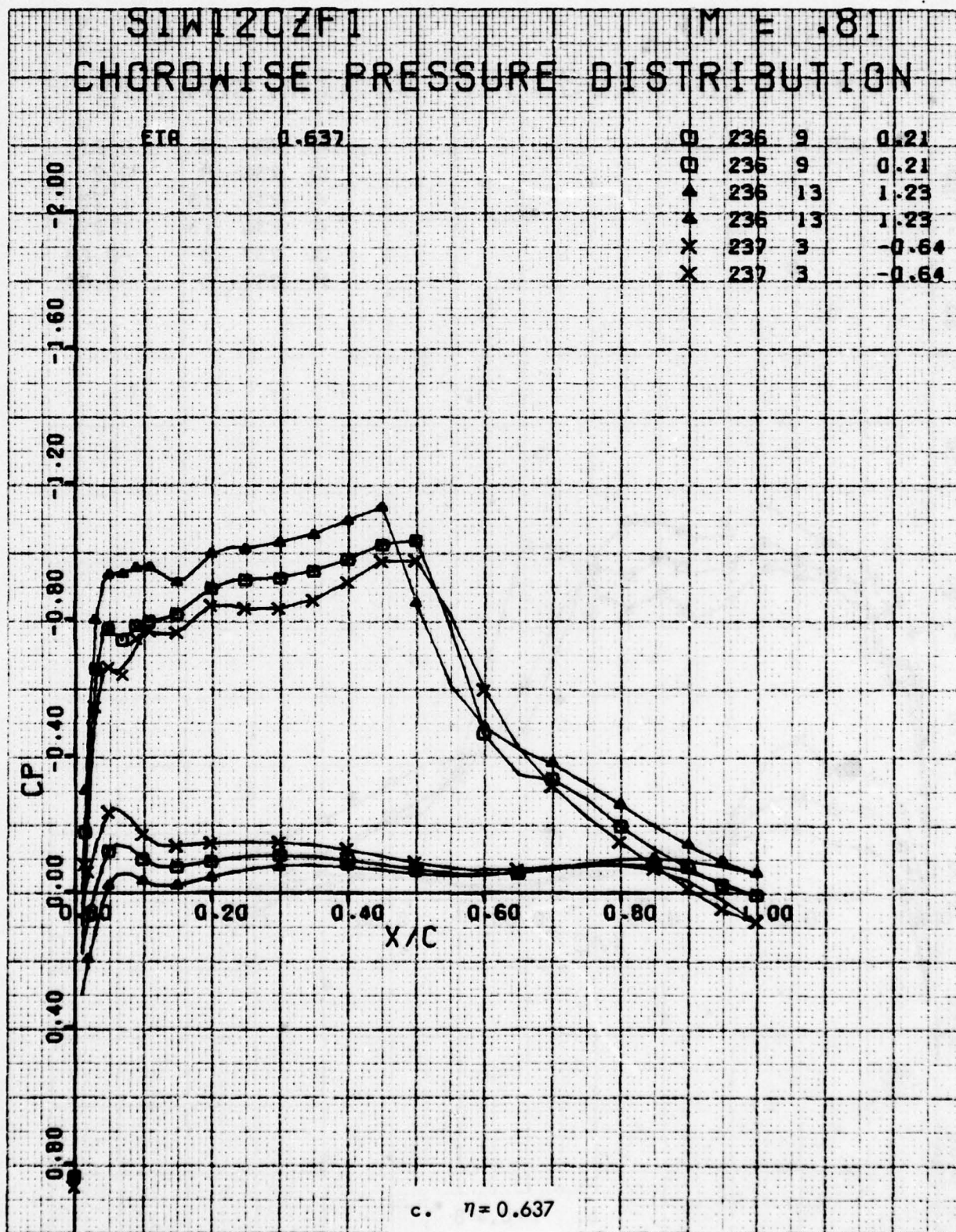


Figure 71 . Continued

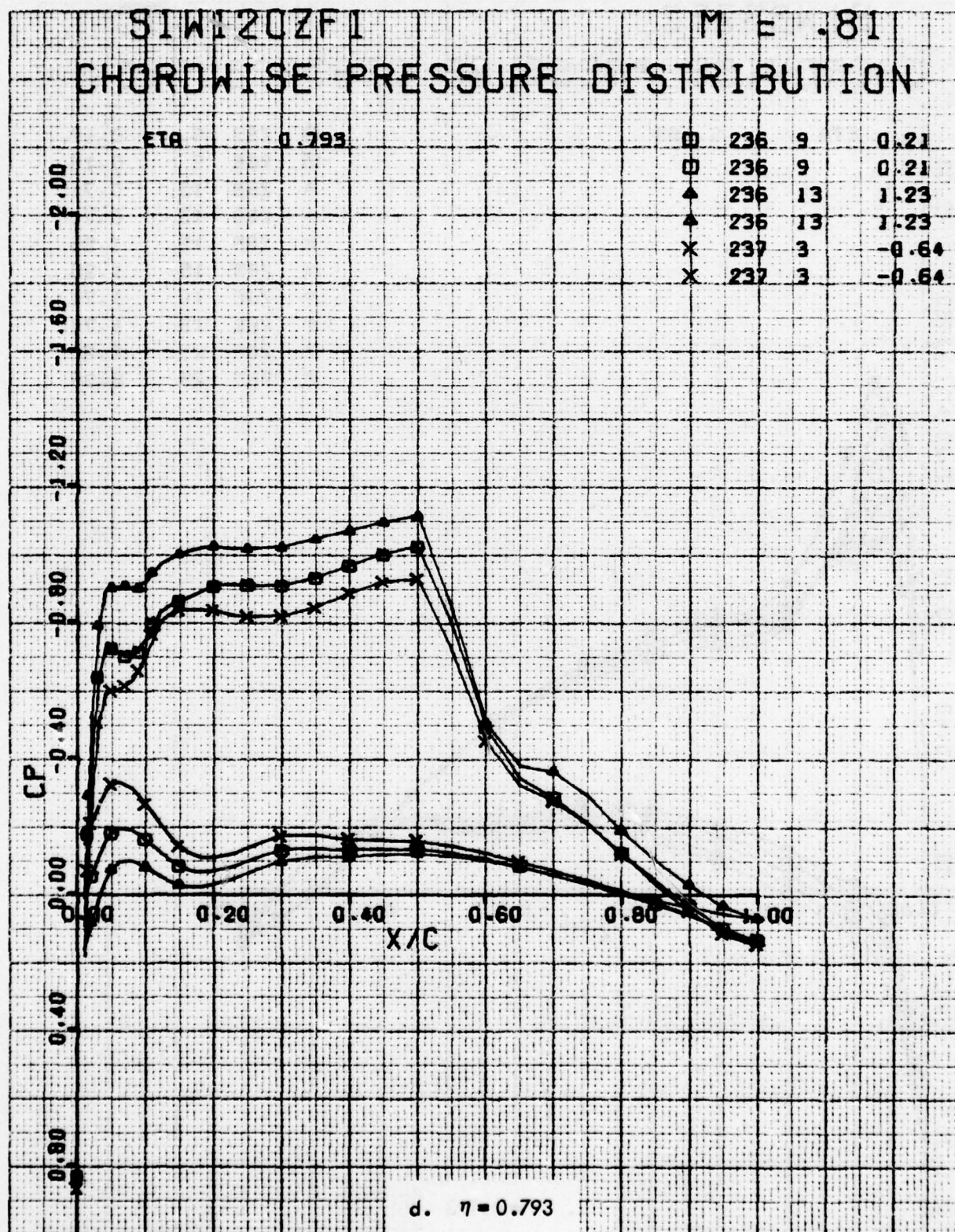


Figure 71. Concluded

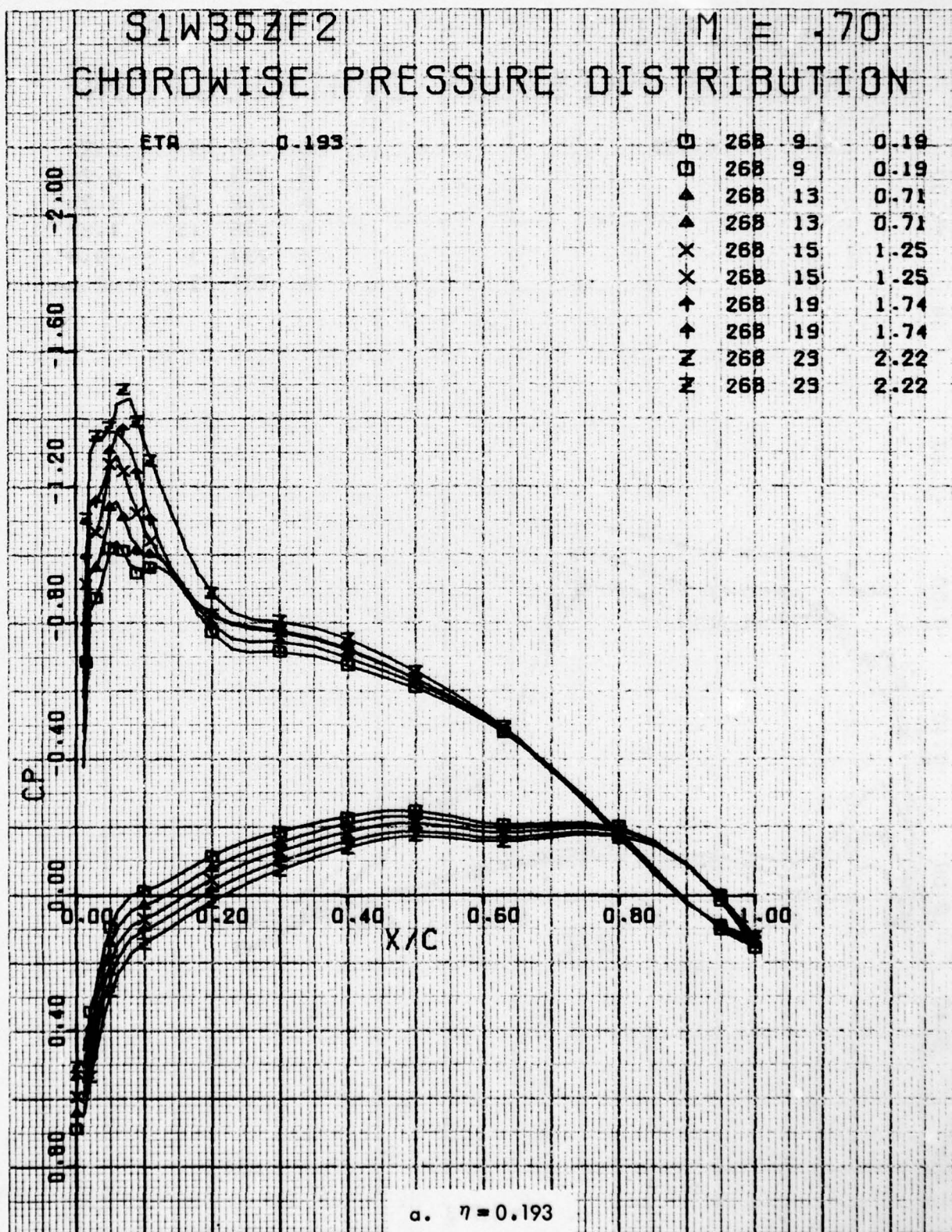


Figure 72. Chordwise Pressure Distributions for Various Angles of Attack. W^{35} Leading Edge Modification, Free Transition, Four Anti-Drag Bodies, $M = 0.7$.

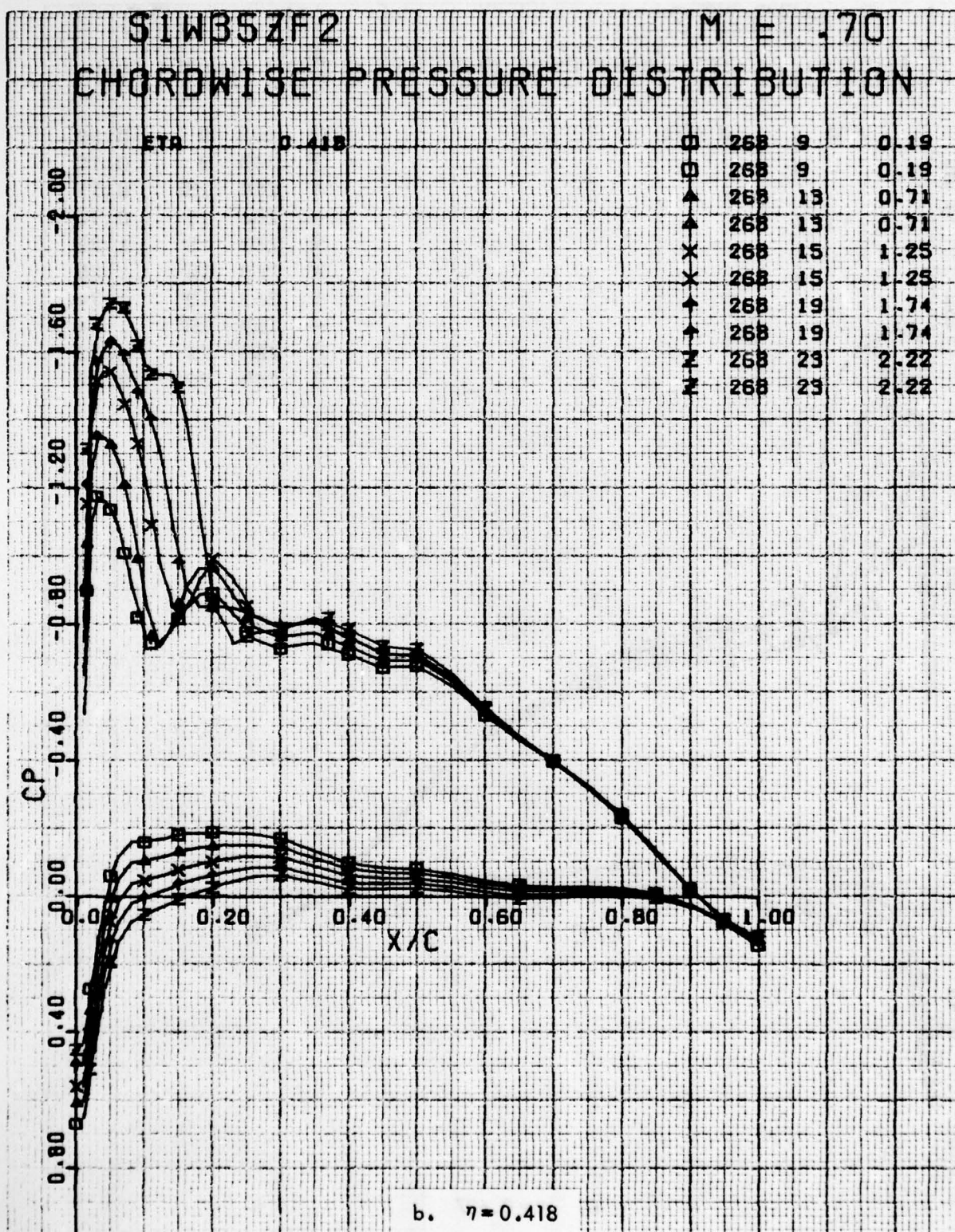


Figure 72. Continued

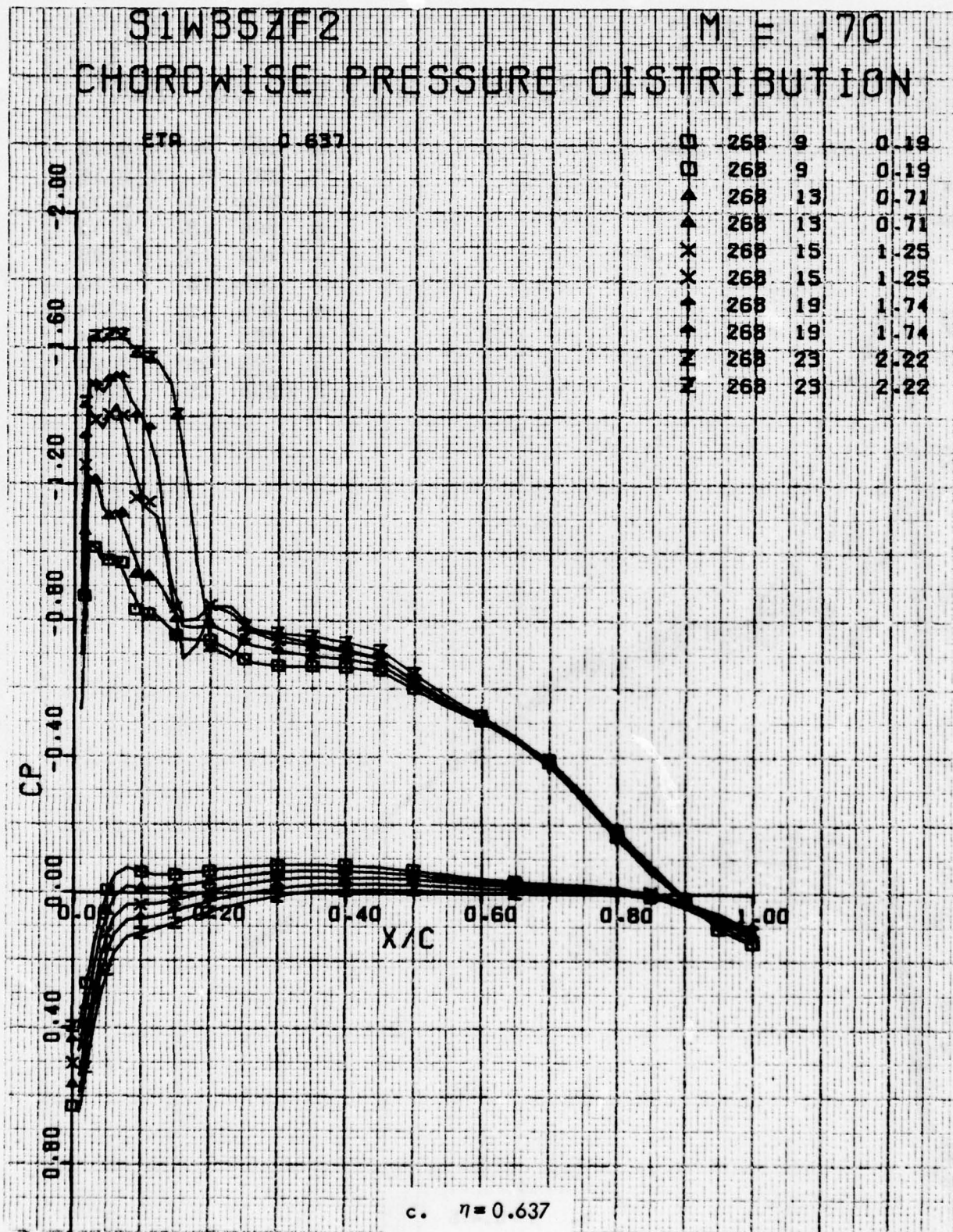


Figure 72 . Continued

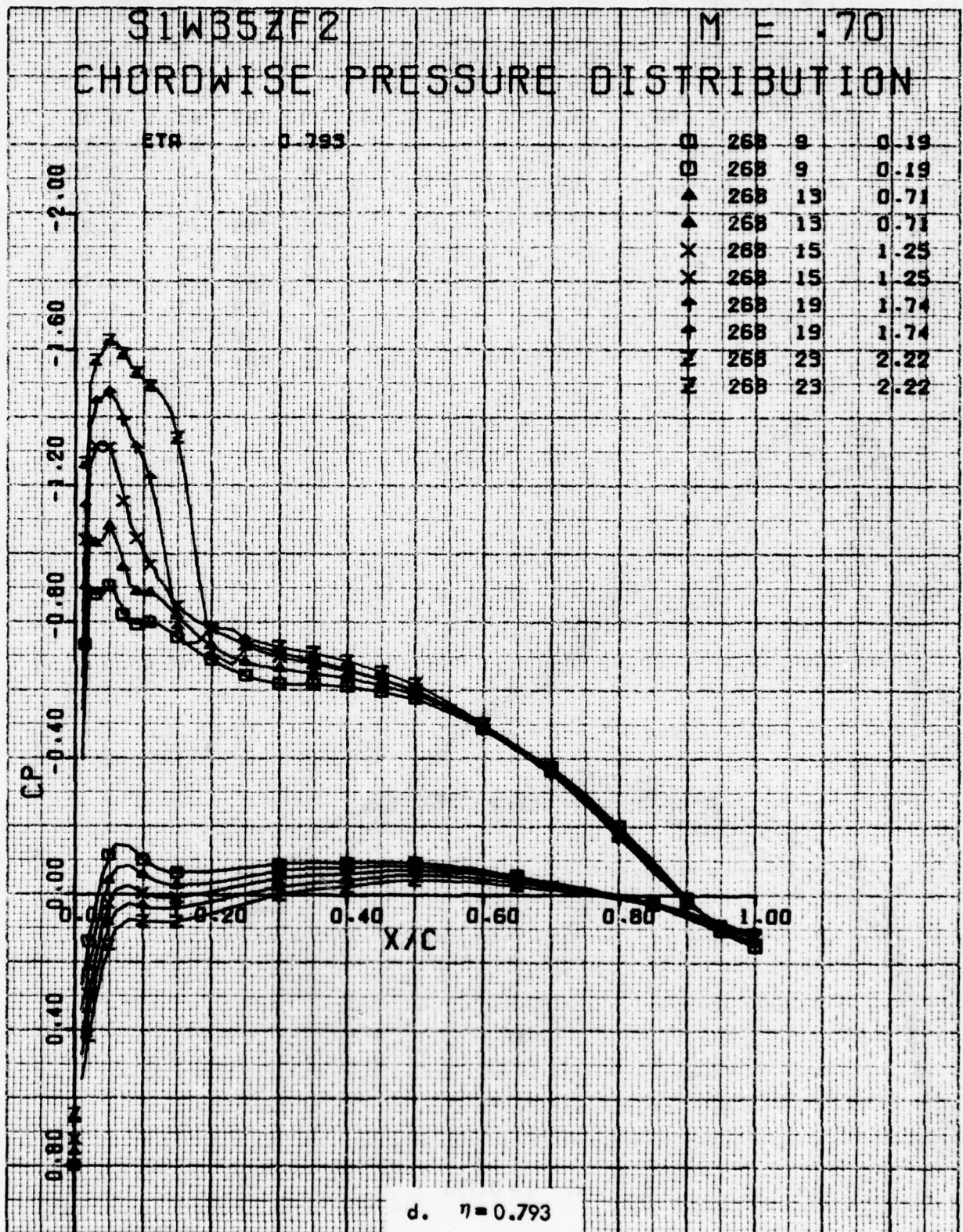


Figure 72. Concluded

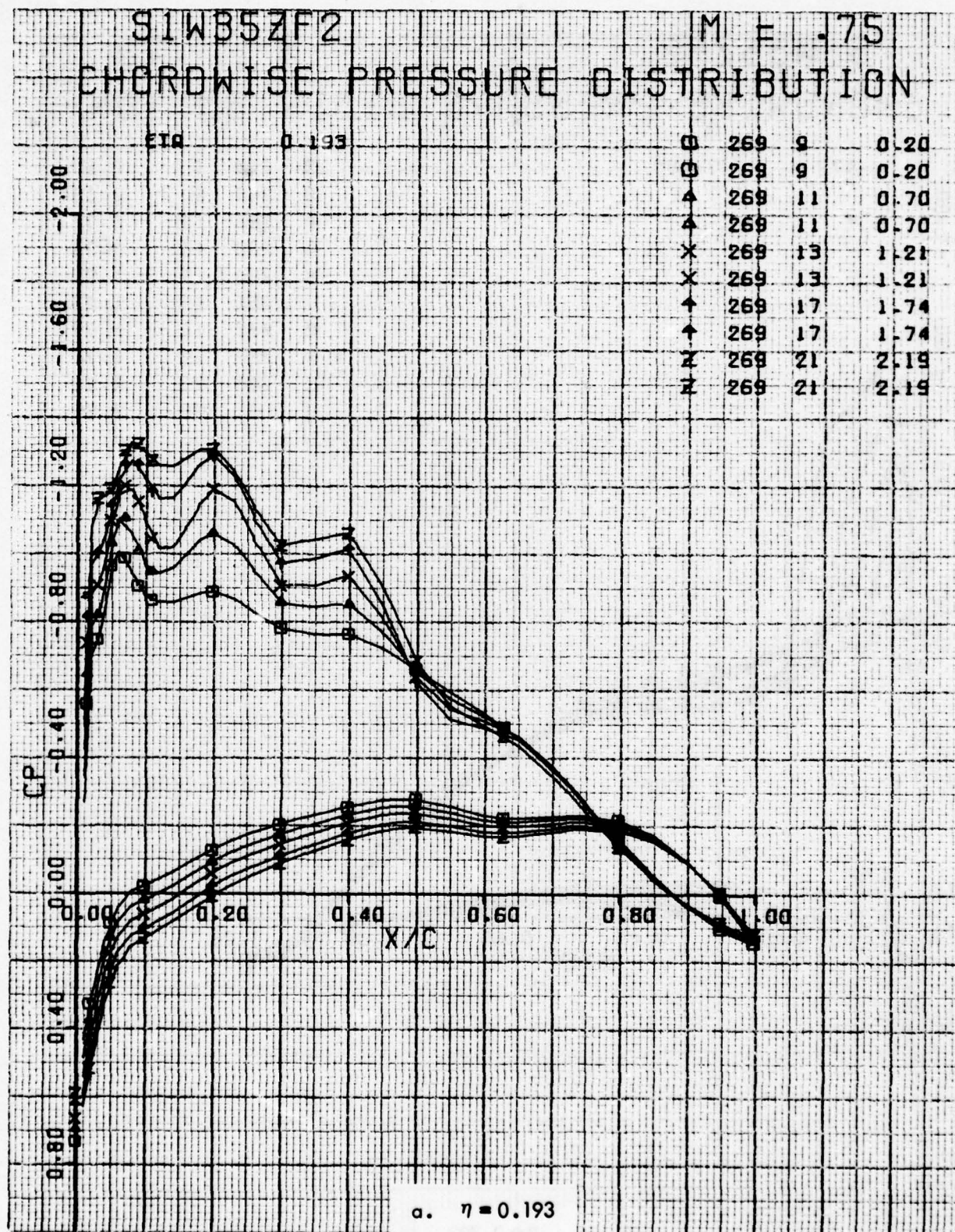


Figure 73. Chordwise Pressure Distributions for Various Angles of Attack. W³⁵ Leading Edge Modification, Free Transition, Four Anti-Drag Bodies, M = 0.75.

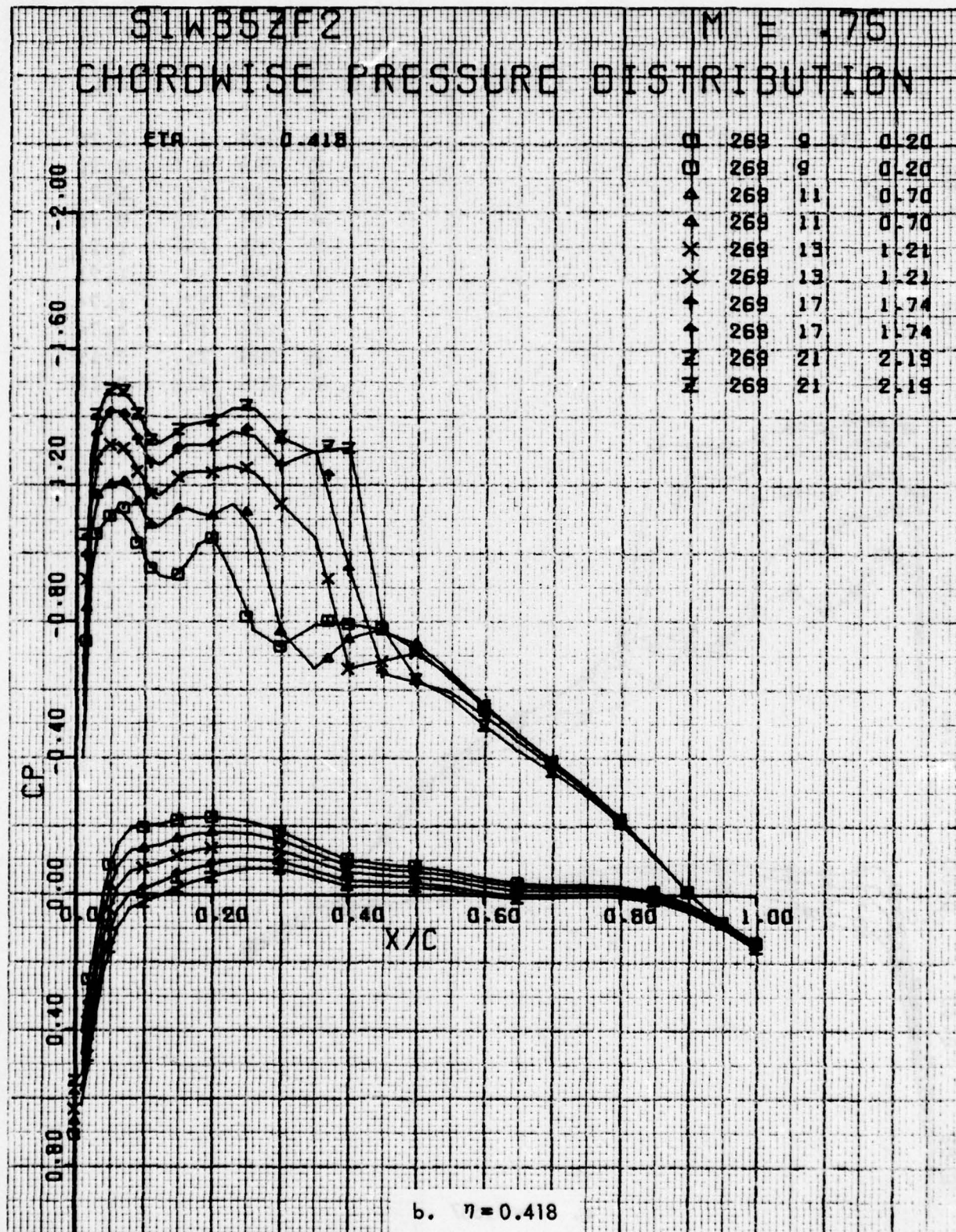


Figure 73 . Continued

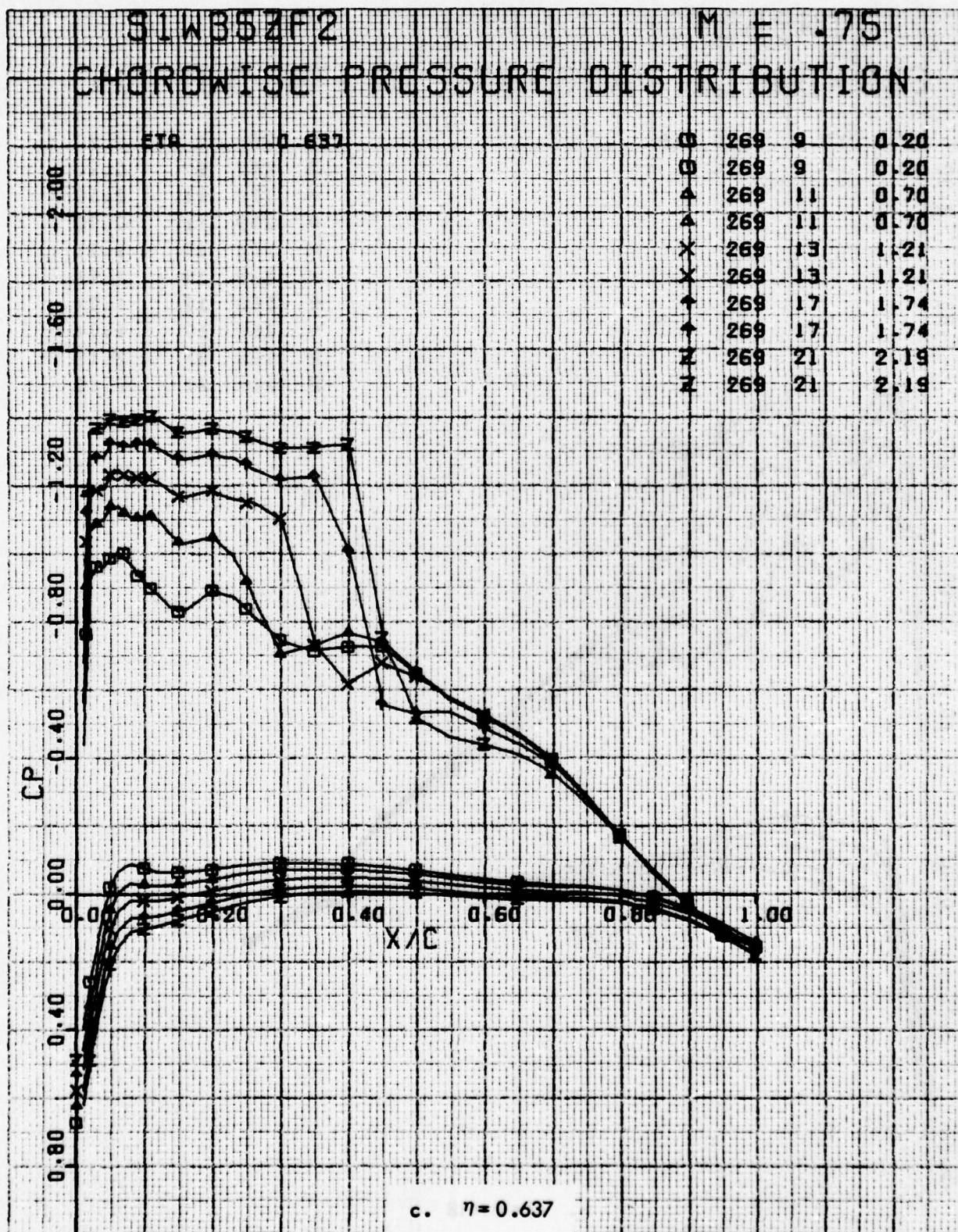


Figure 73. Continued

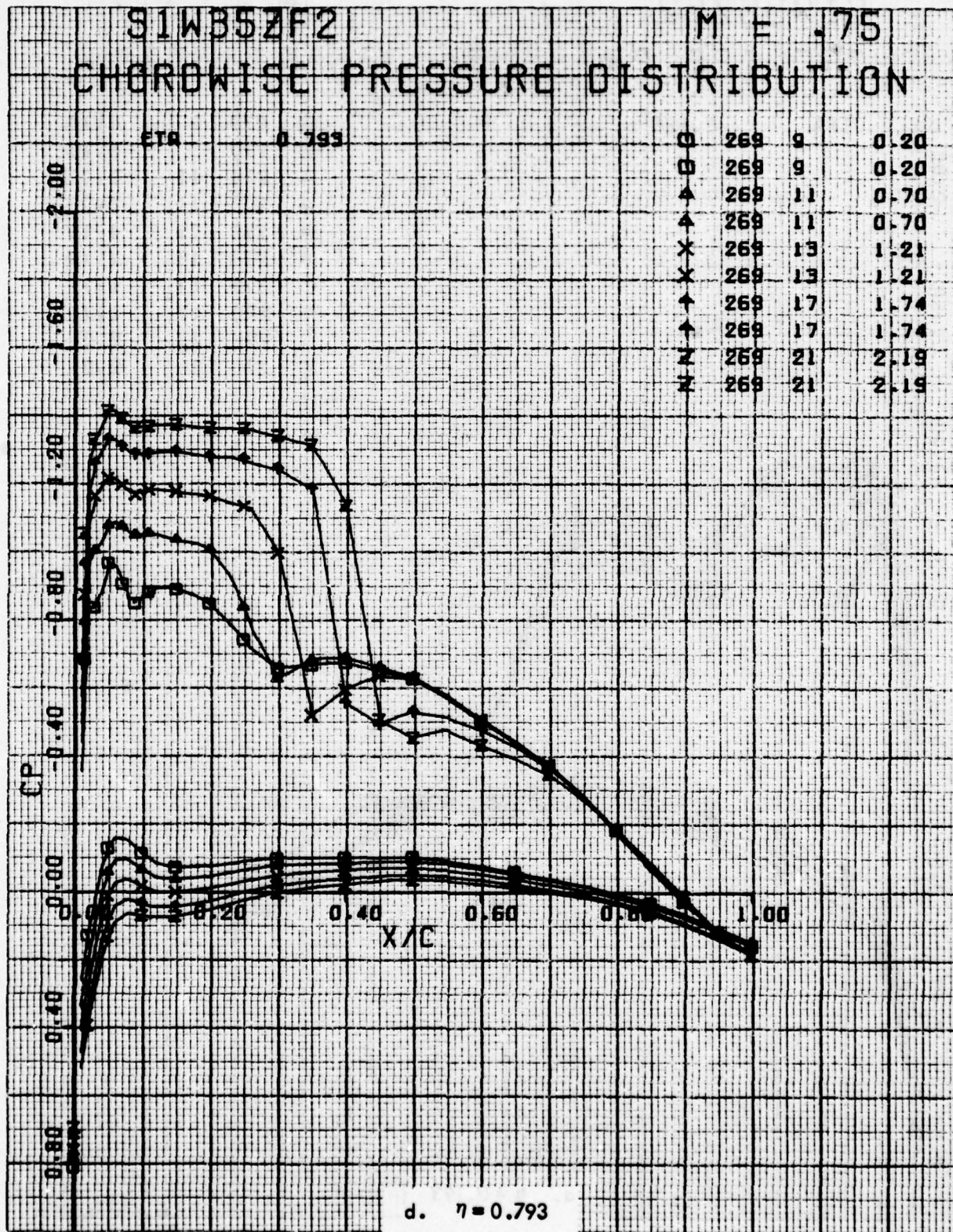


Figure 73. Concluded

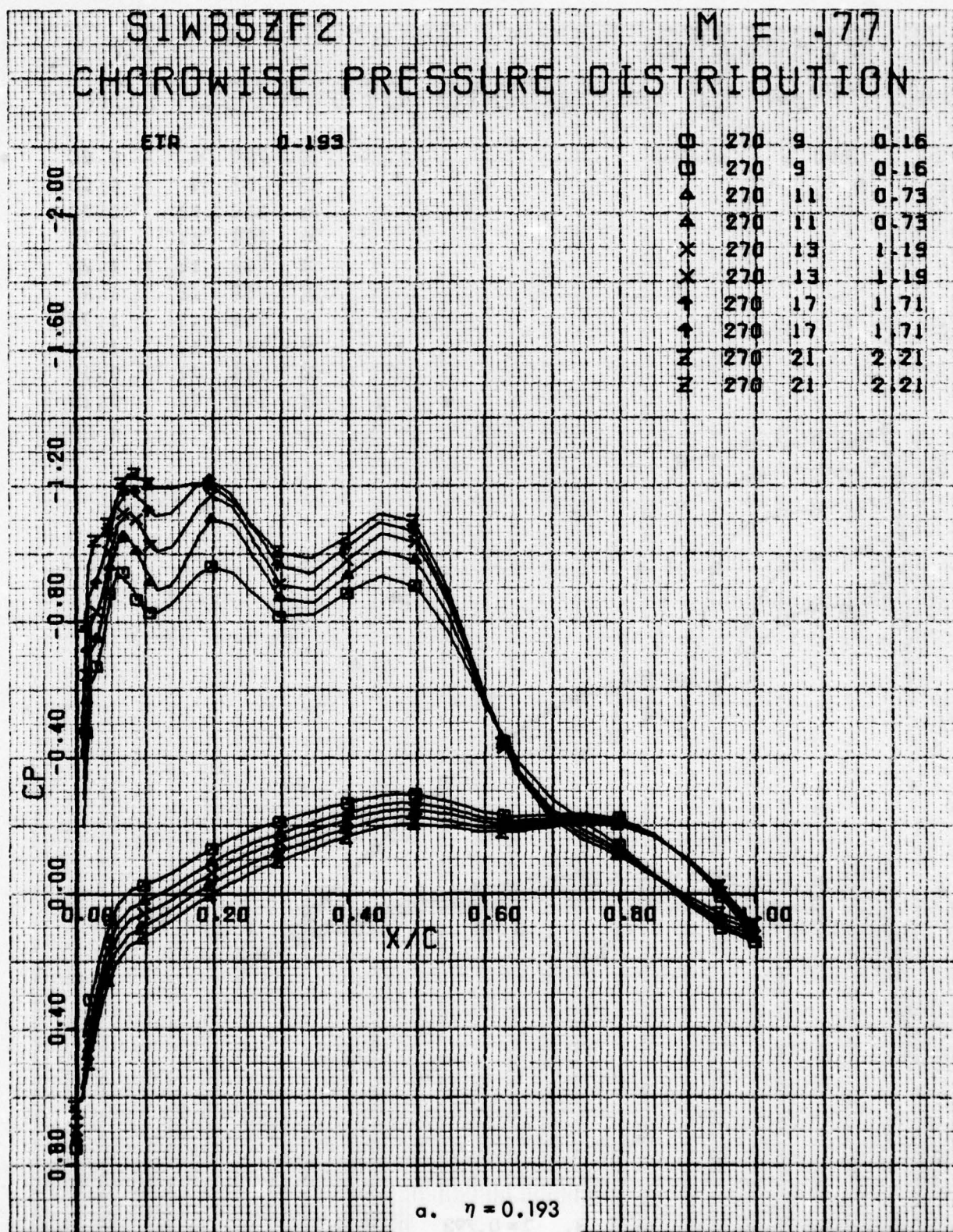


Figure 74. Chordwise Pressure Distributions for Various Angles of Attack. W³⁵ Leading Edge Modification, Free Transition, Four Anti-Drag Bodies, M = 0.77.

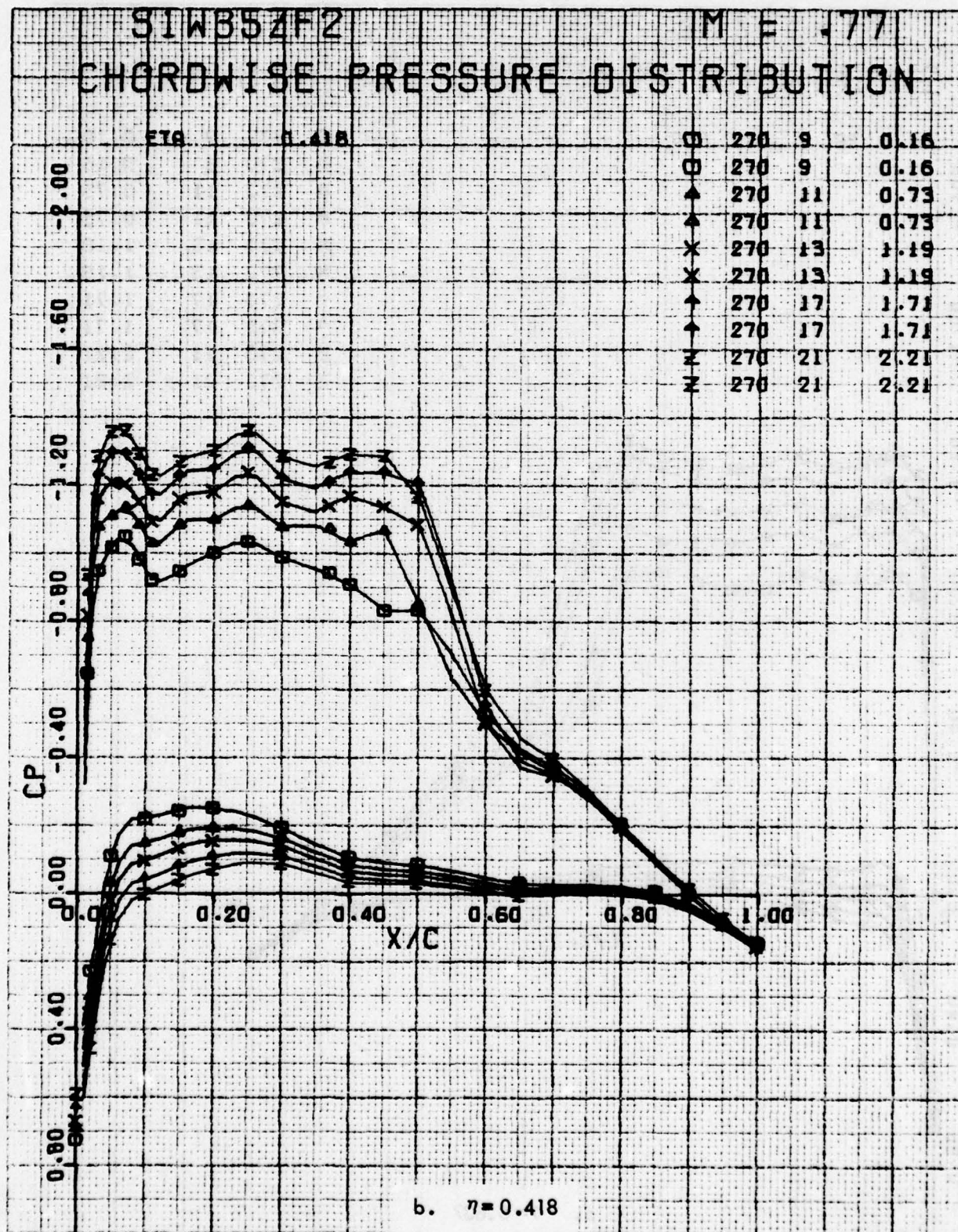


Figure 74 . Continued

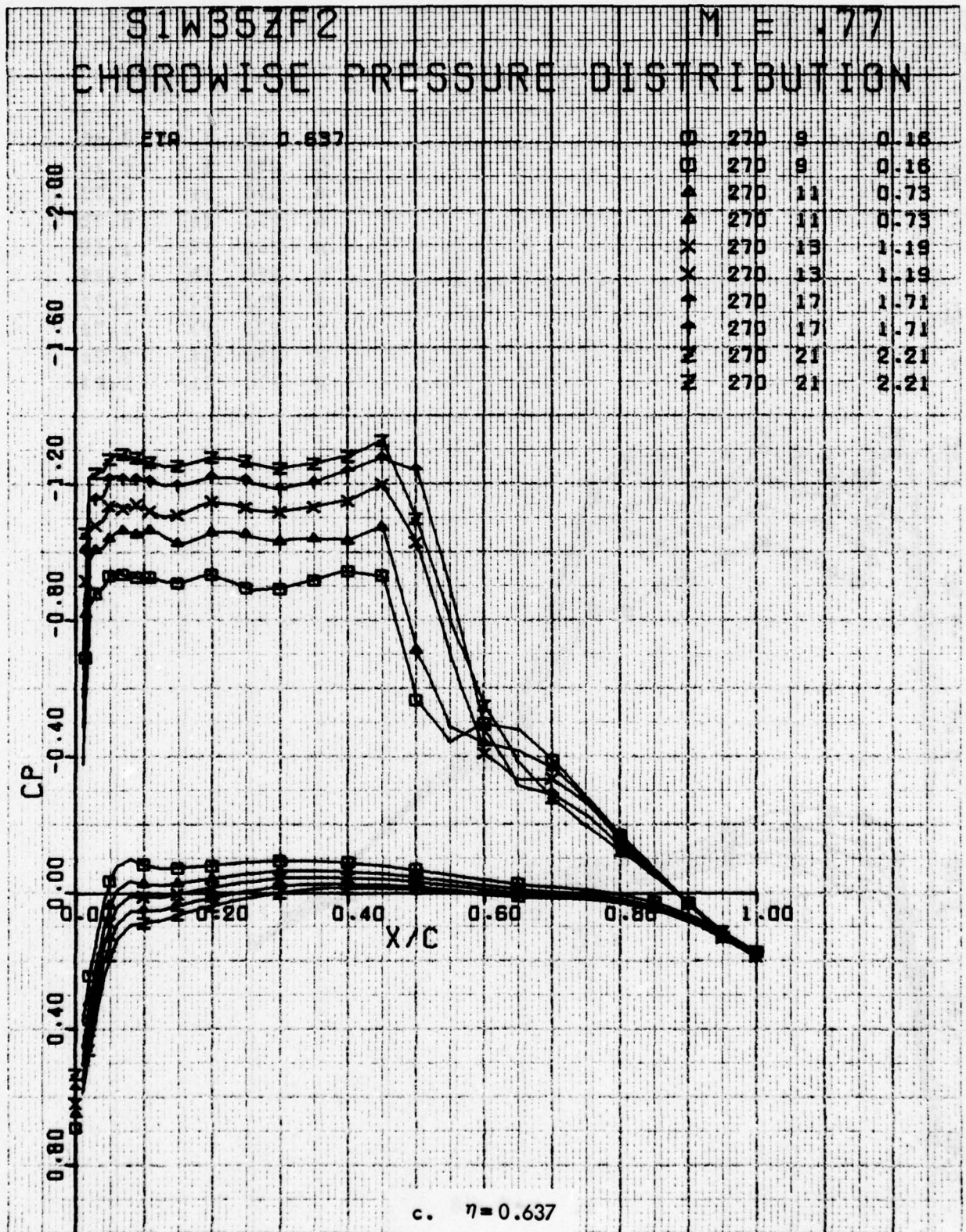


Figure 74. Continued

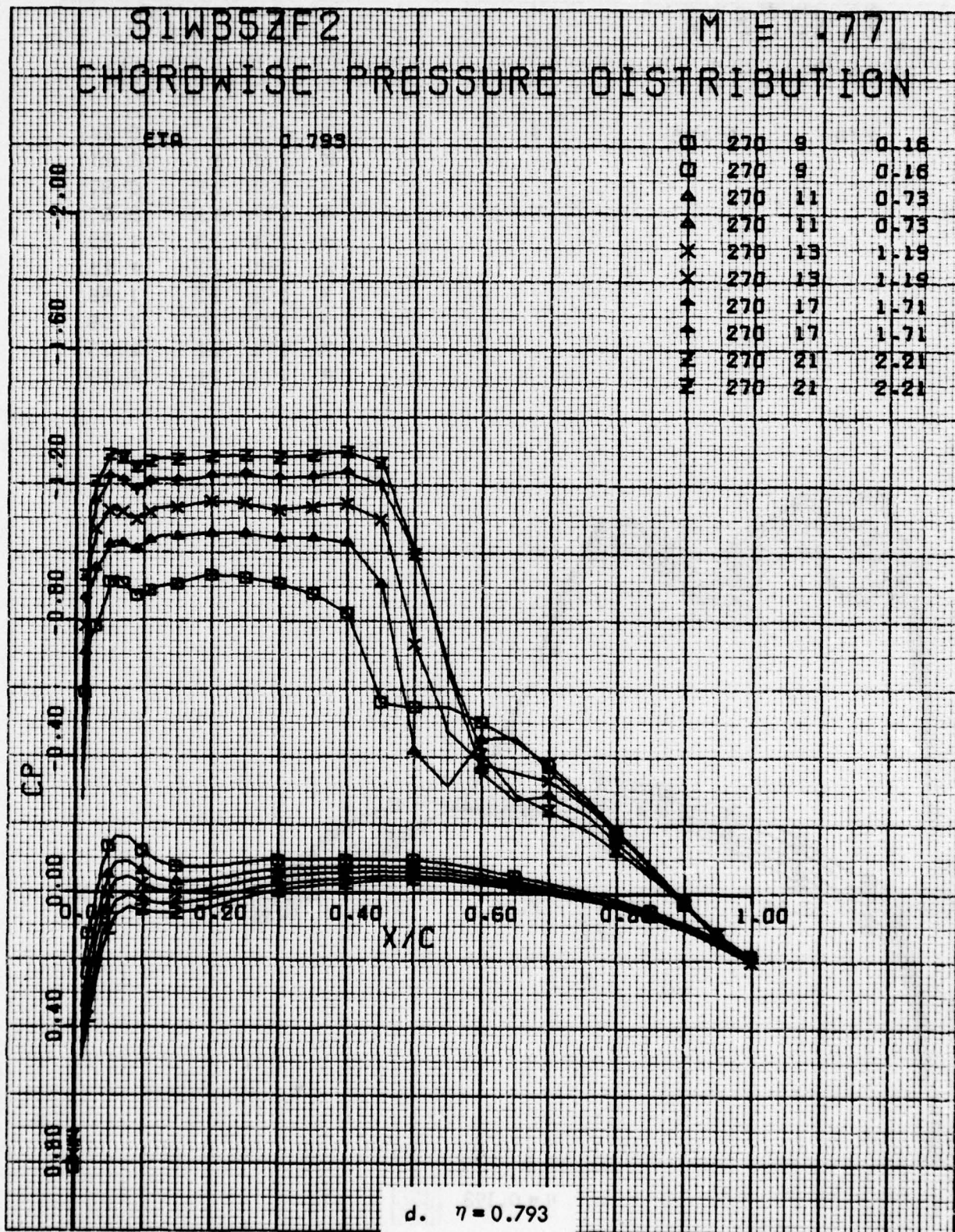


Figure 74. Concluded

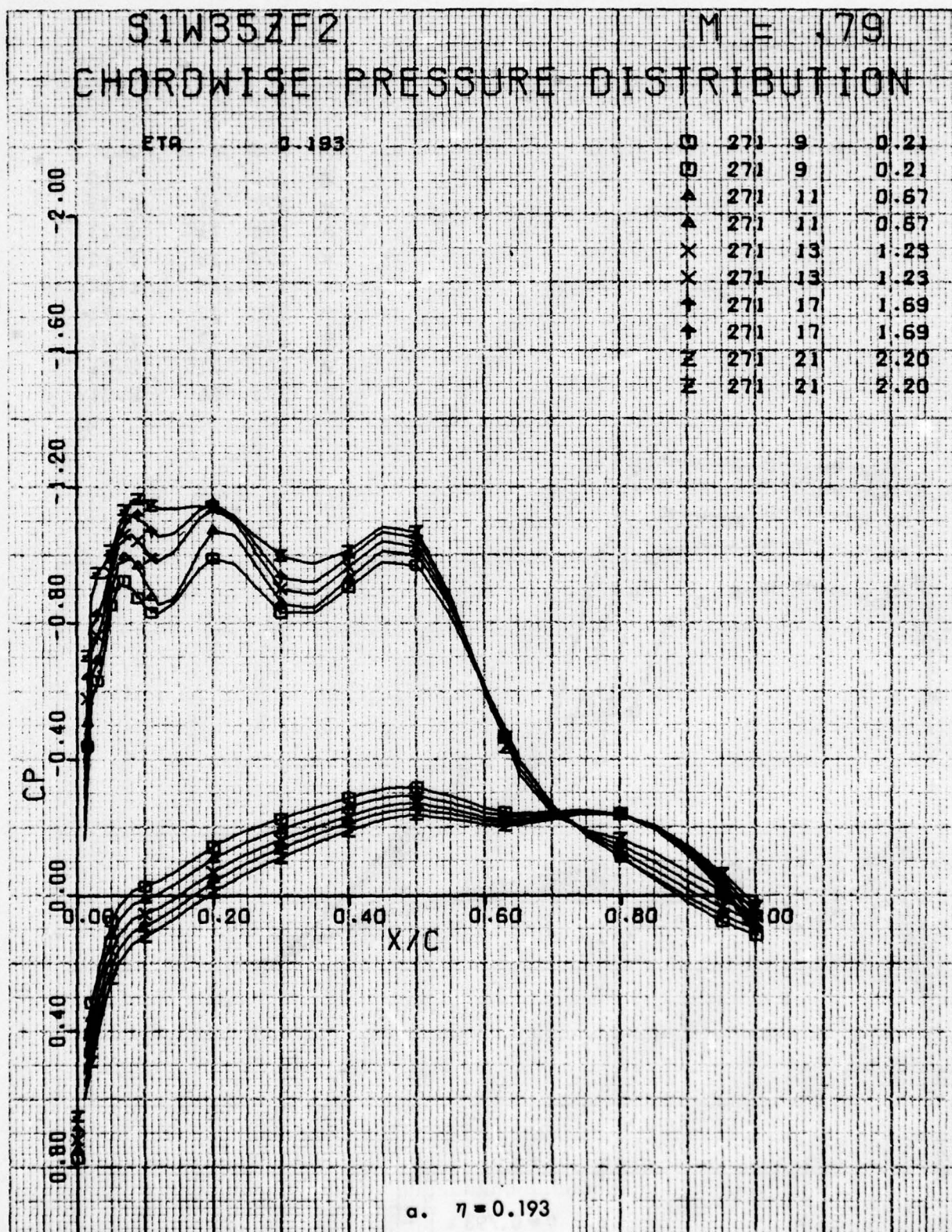


Figure 75. Chordwise Pressure Distributions for Various Angles of Attack. W³⁵ Leading Edge Modification, Free Transition, Four Anti-Drag Bodies, M = 0.79.

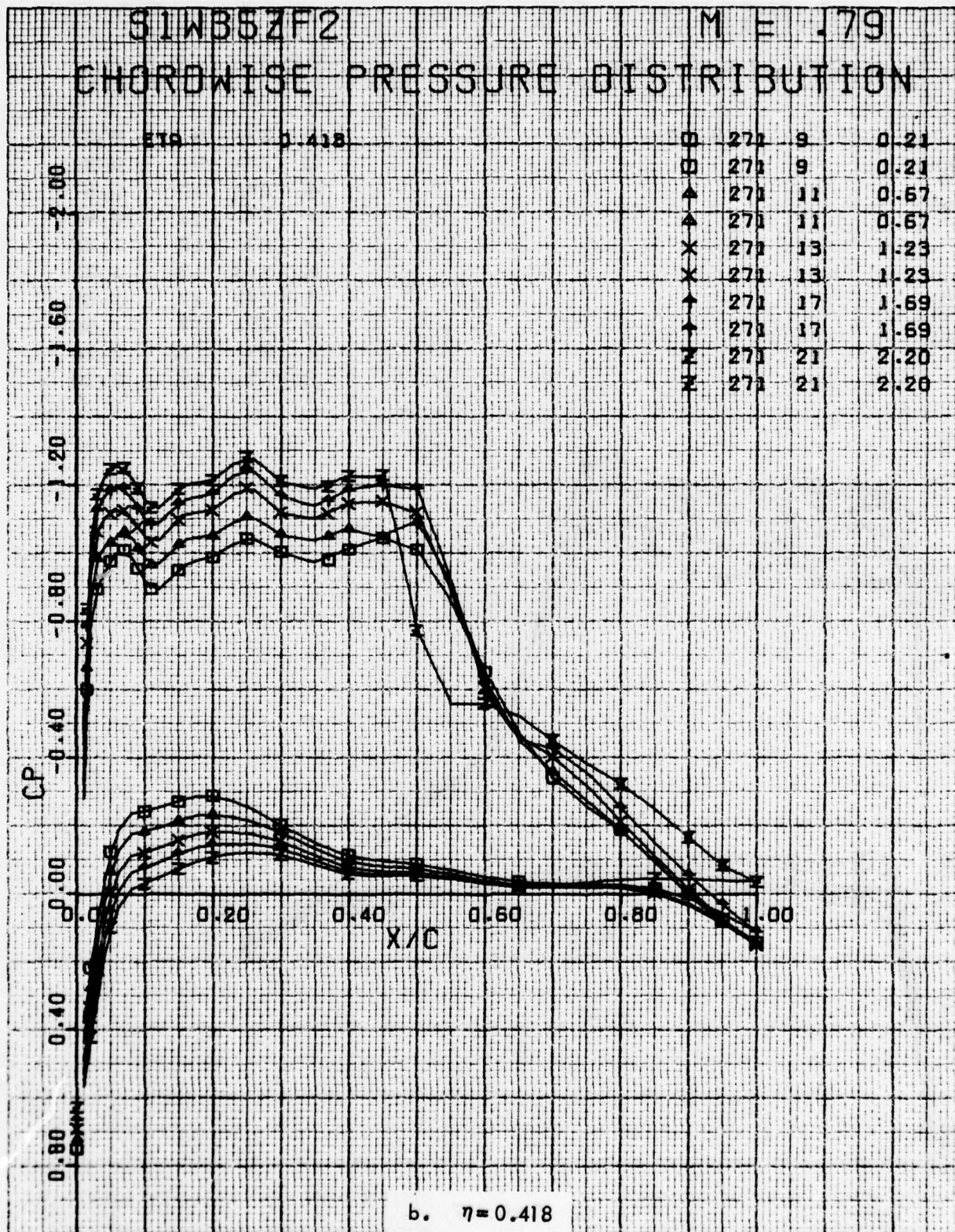


Figure 75 . Continued

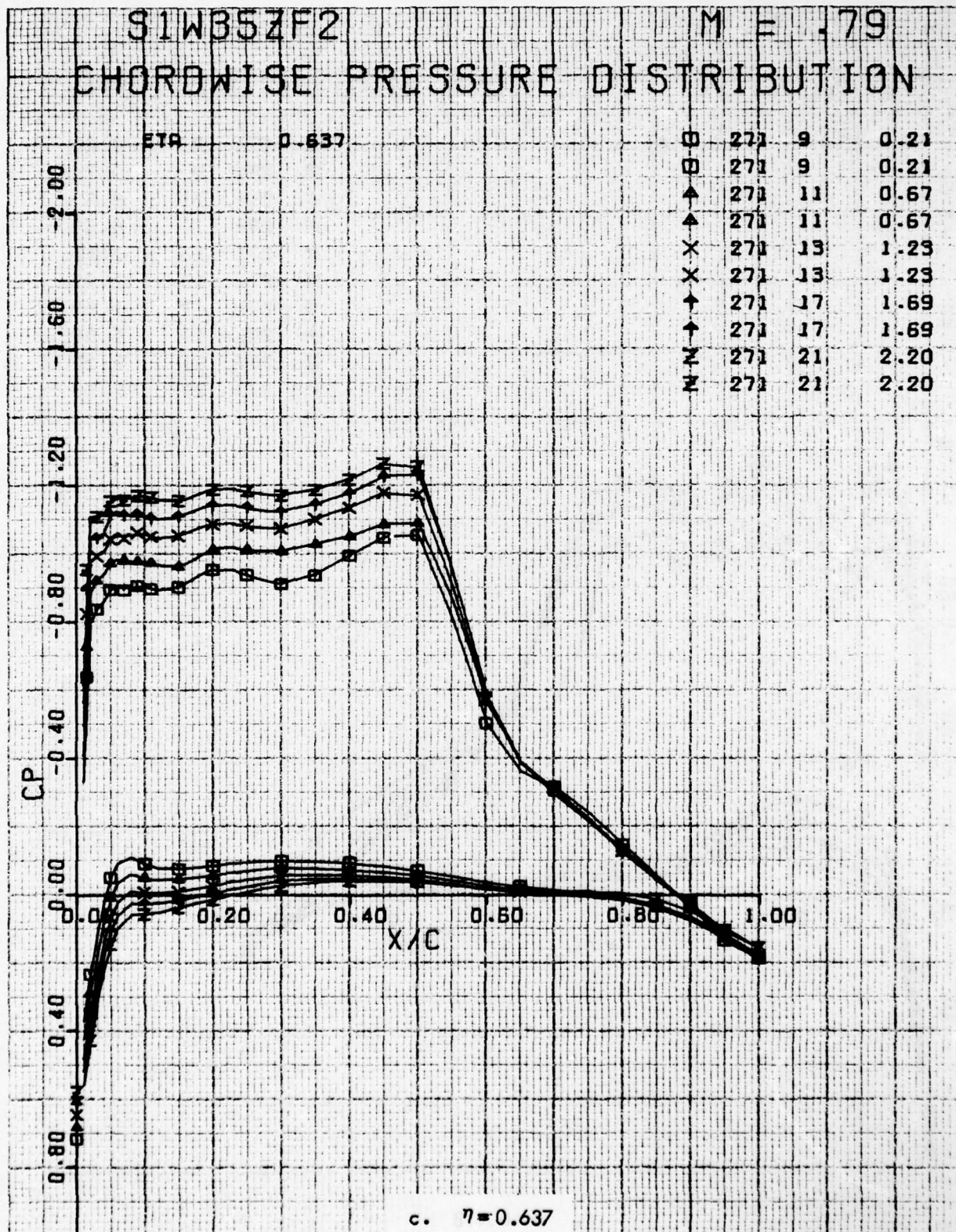


Figure 75. Continued

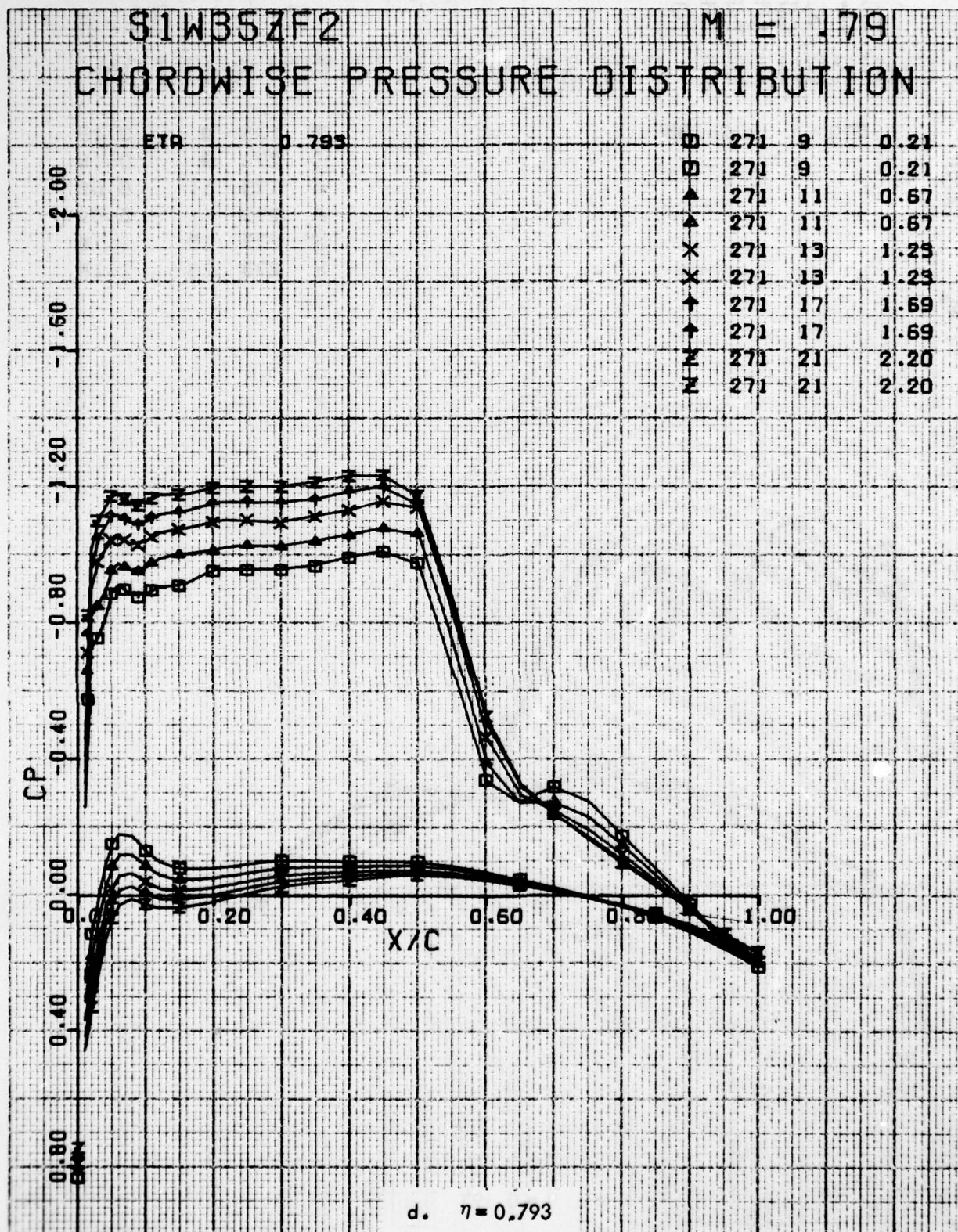


Figure 75. Concluded

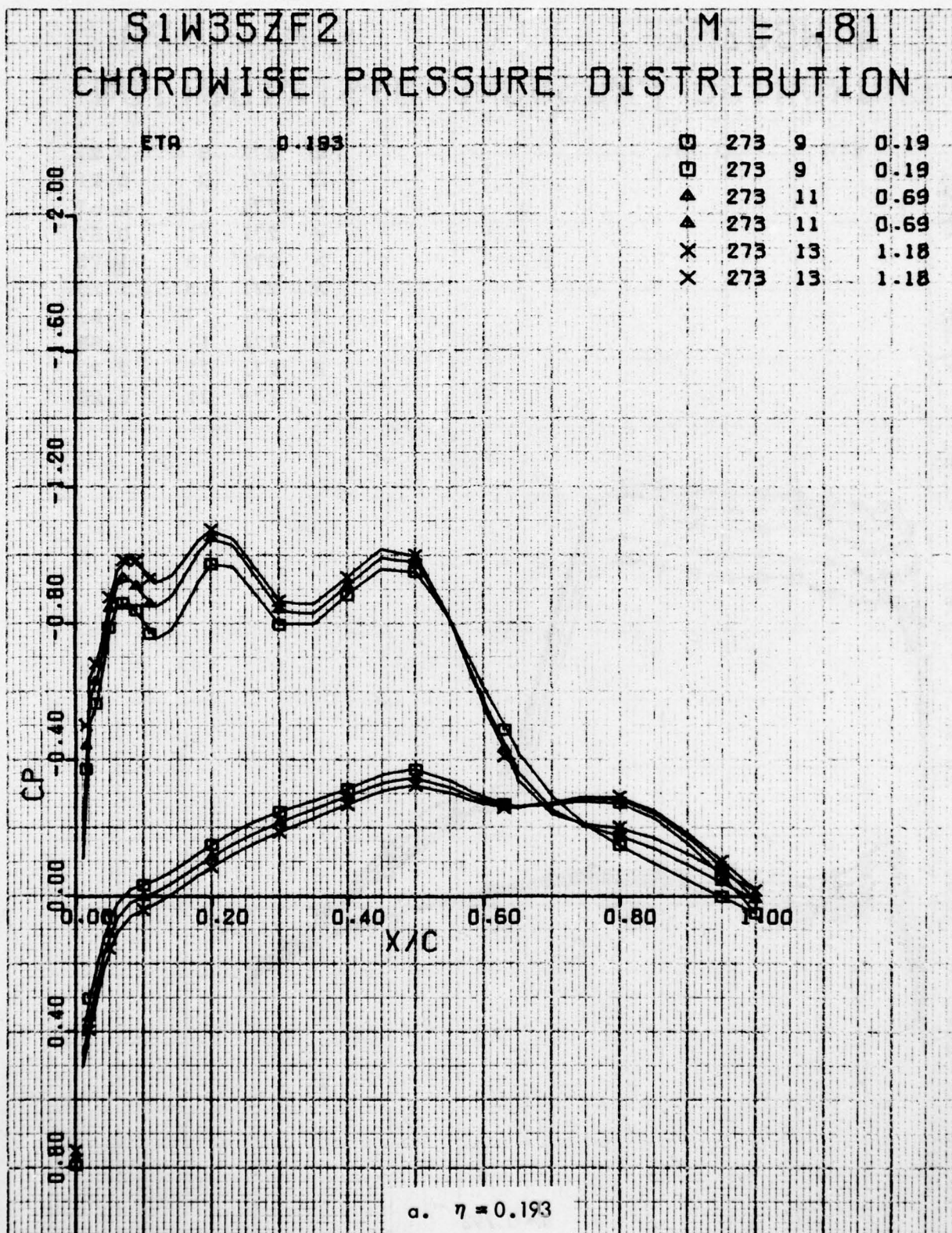


Figure 76 . Chordwise Pressure Distributions for Various Angles of Attack. W³⁵ Leading Edge Modification, Free Transition, Four Anti-Drag Bodies, M = 0.81.

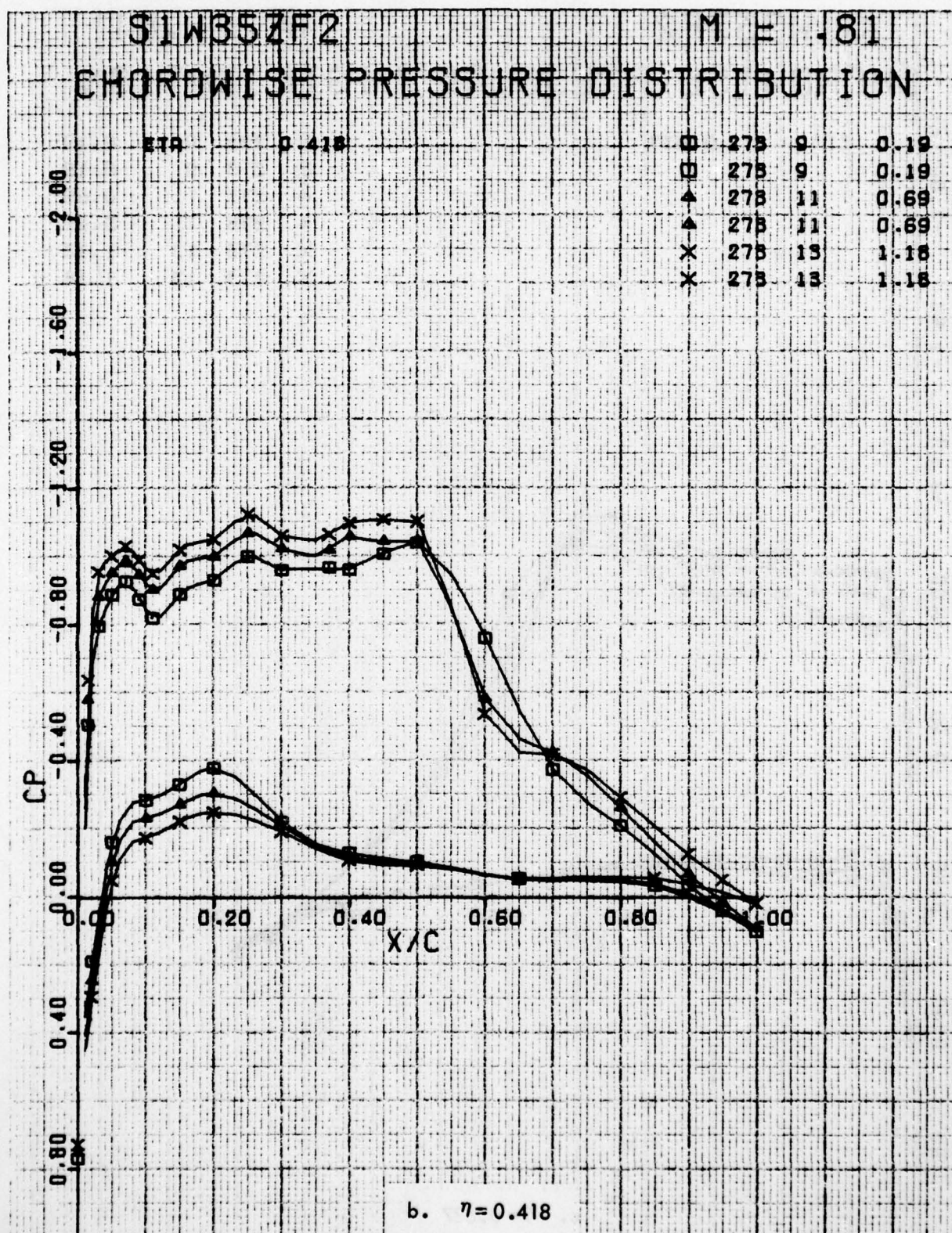


Figure 76 . Continued

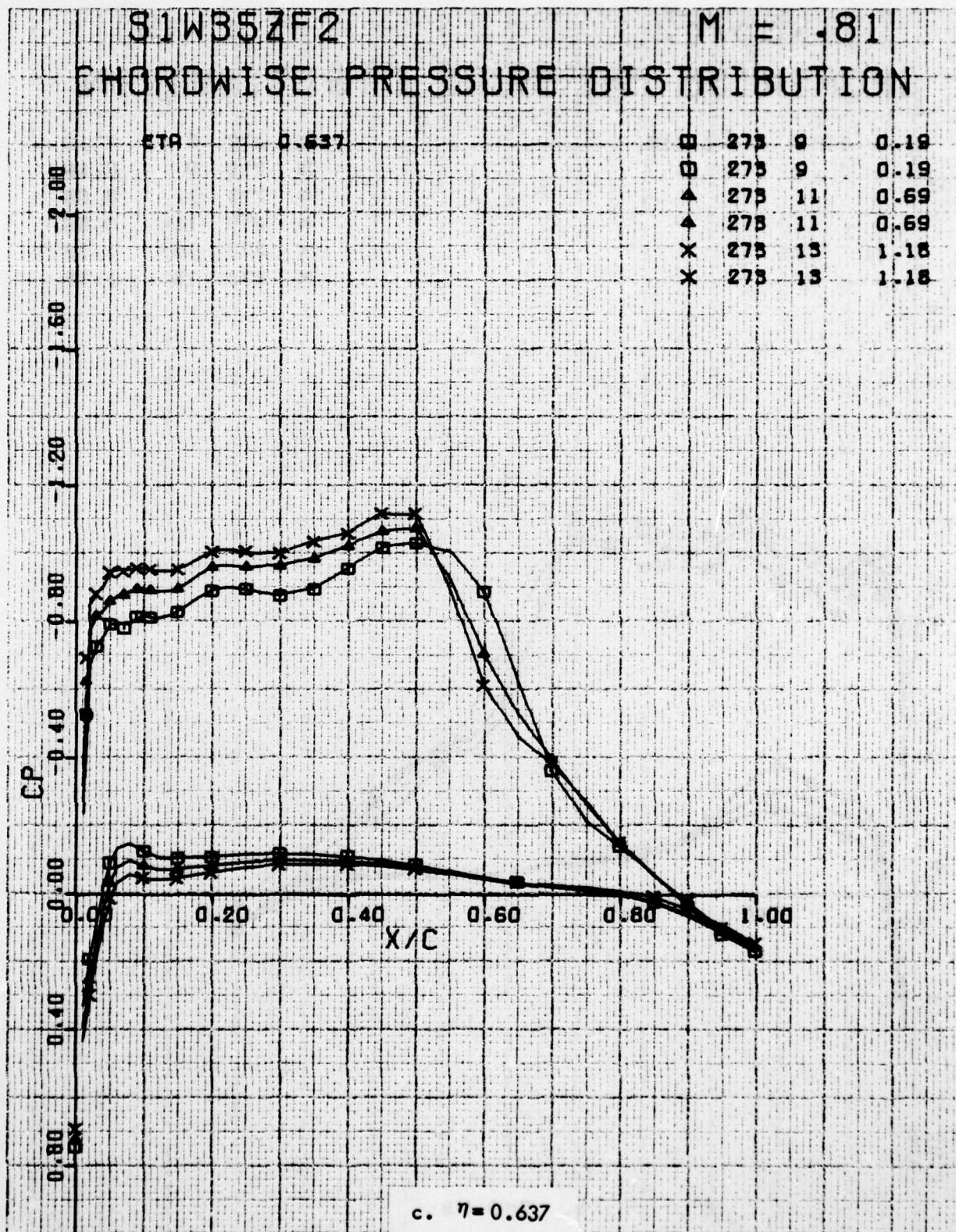


Figure 76. Continued

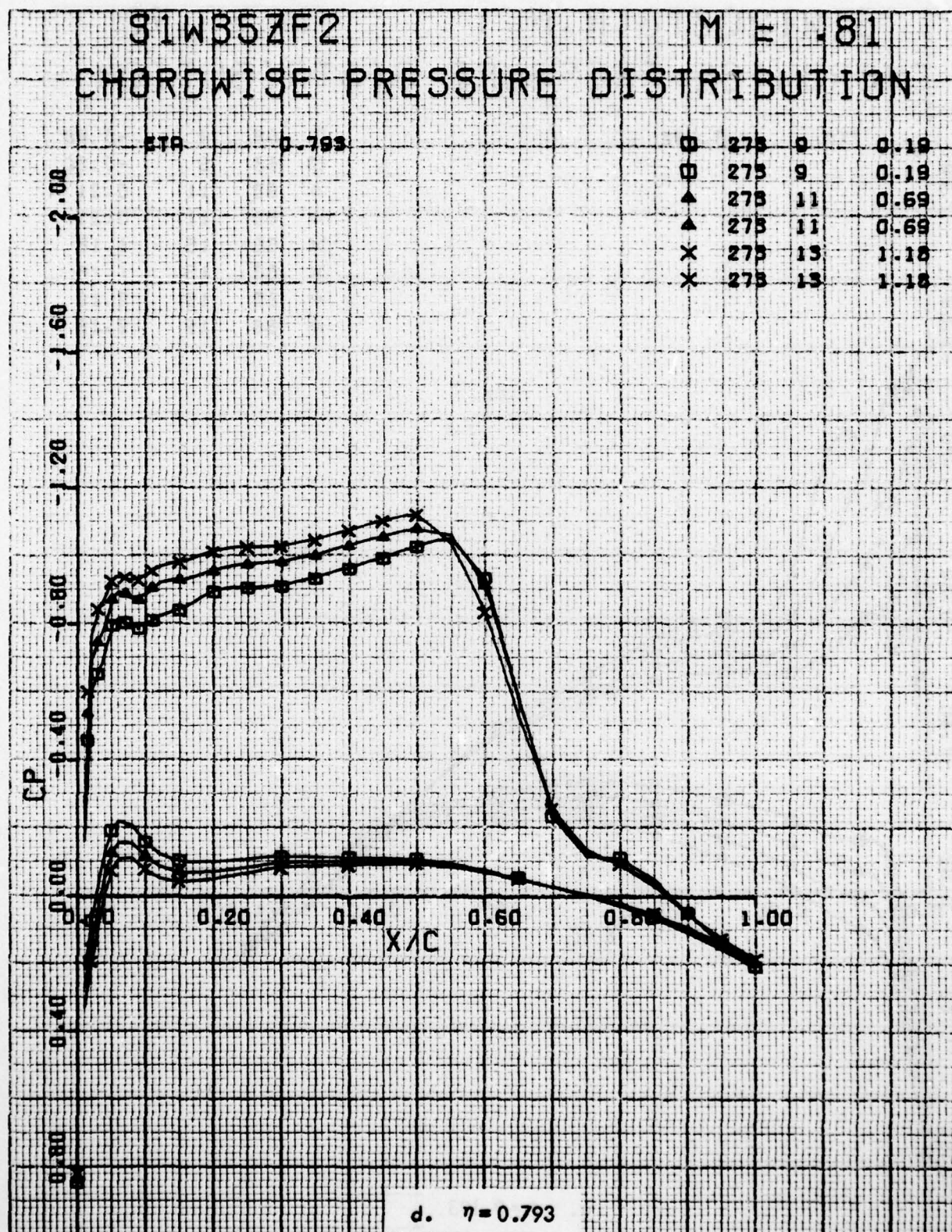


Figure 76. Concluded

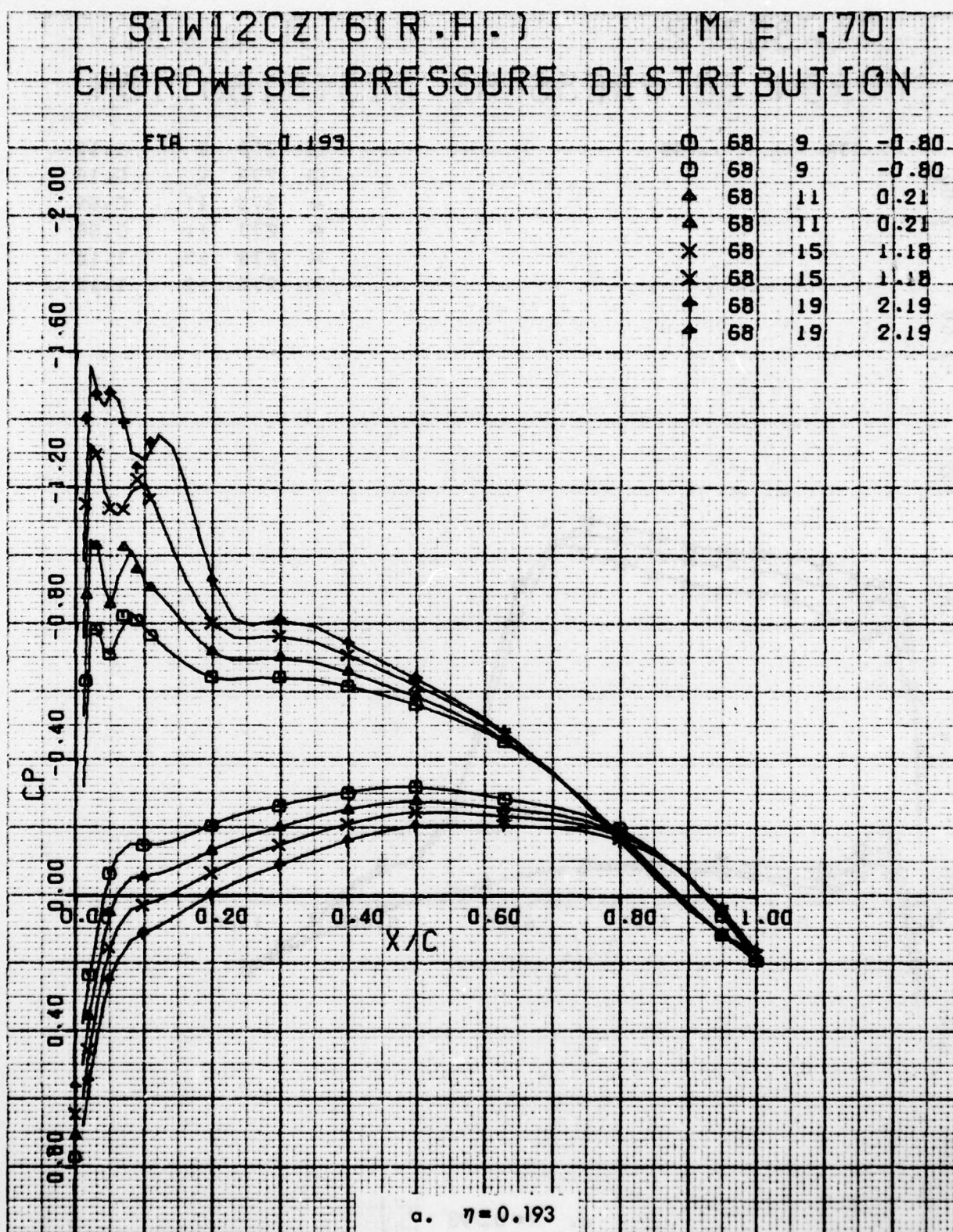


Figure 77. Chordwise Pressure Distributions for Various Angles of Attack. Baseline Leading Edge, Fixed Transition, Grit Code C, One Swept Tip, $M = 0.7$.

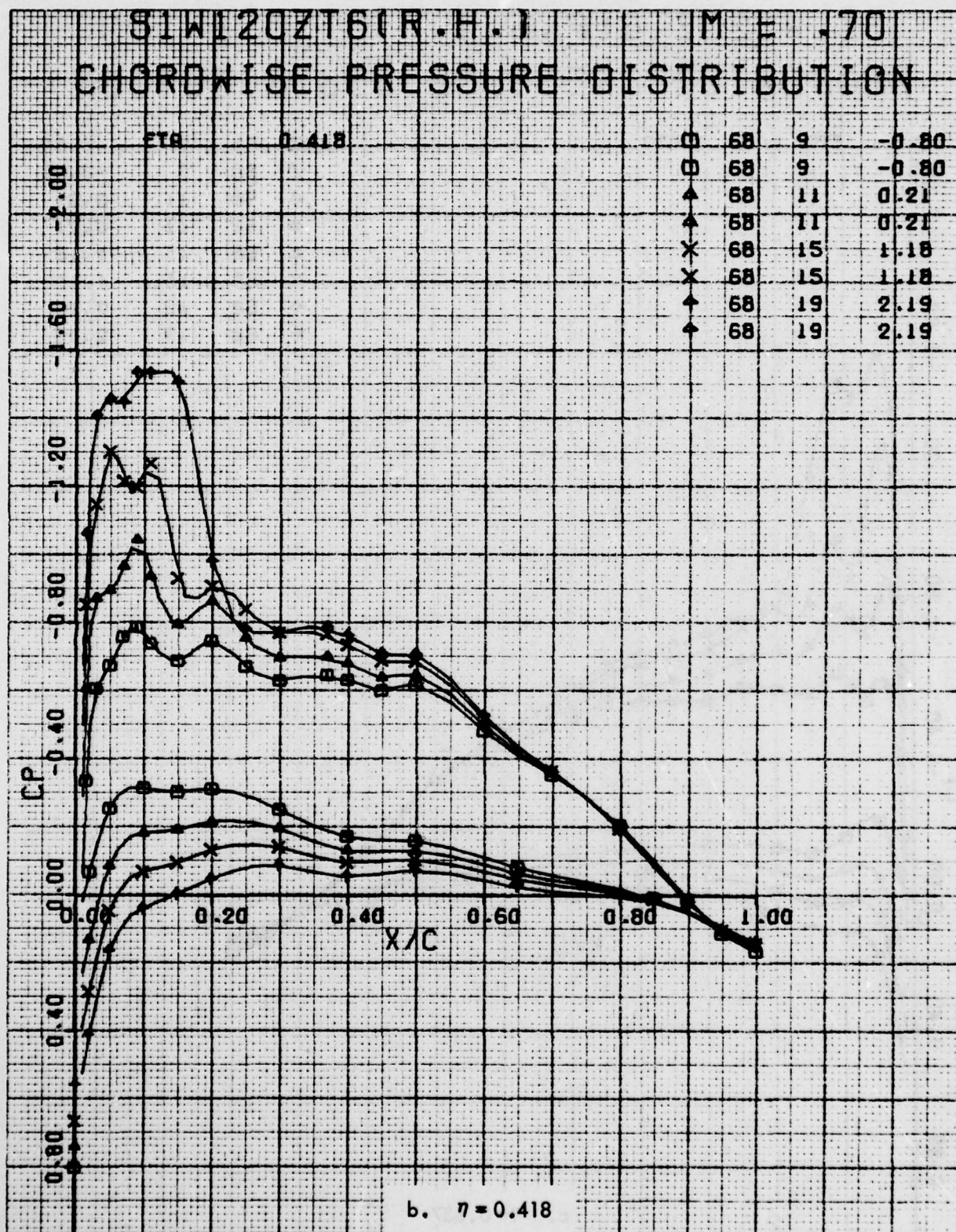


Figure 77 . Continued

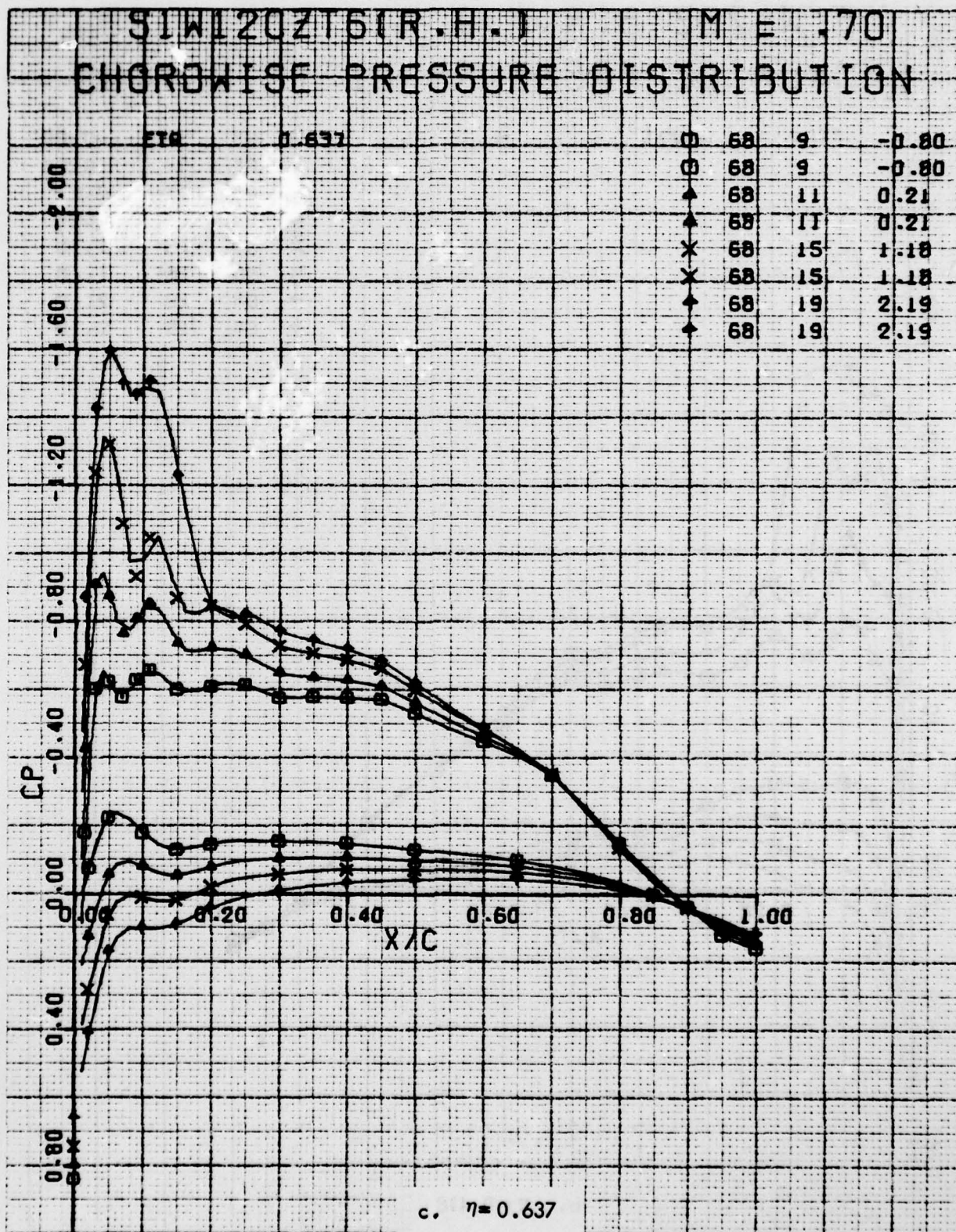


Figure 77. Continued

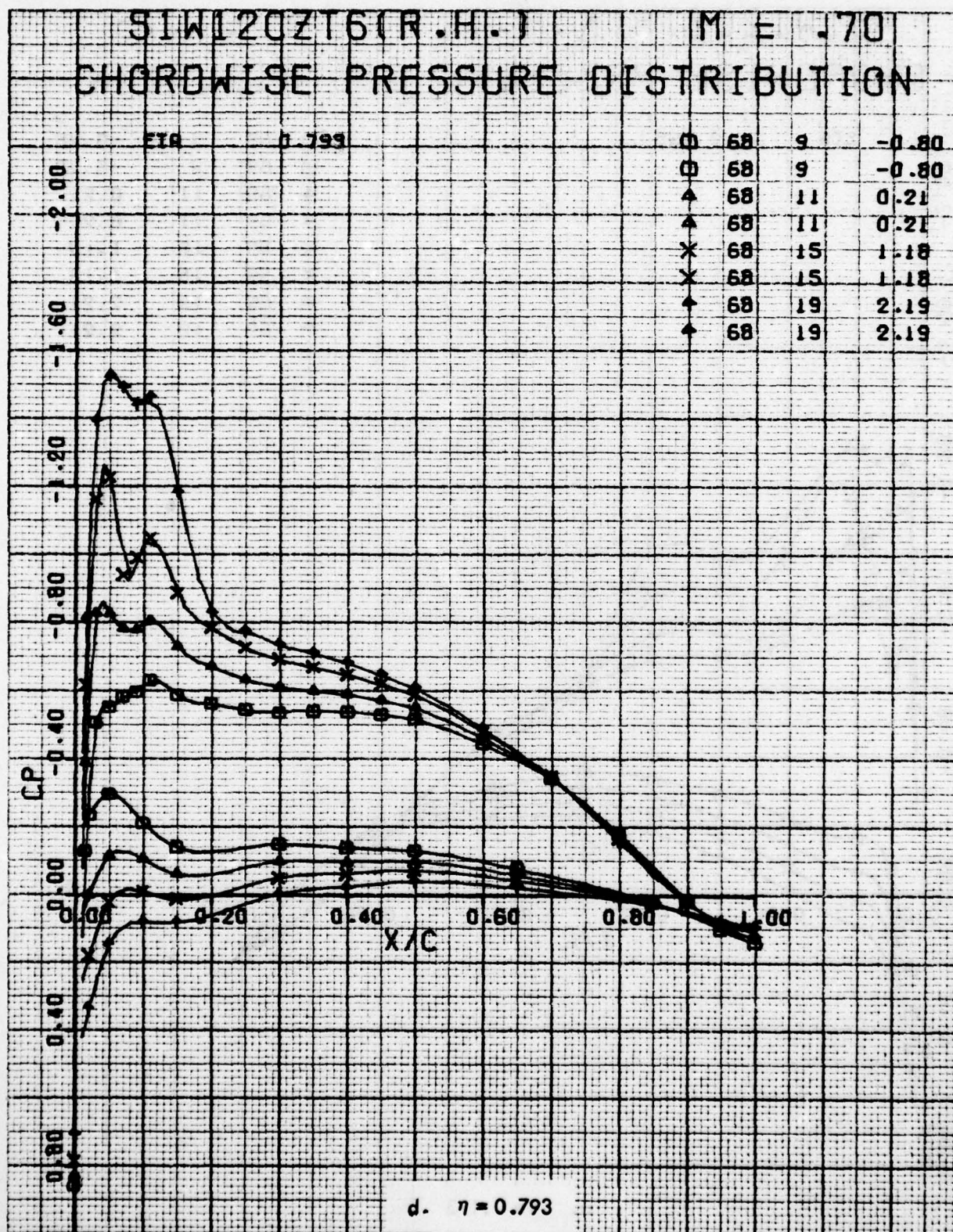


Figure 77. Concluded

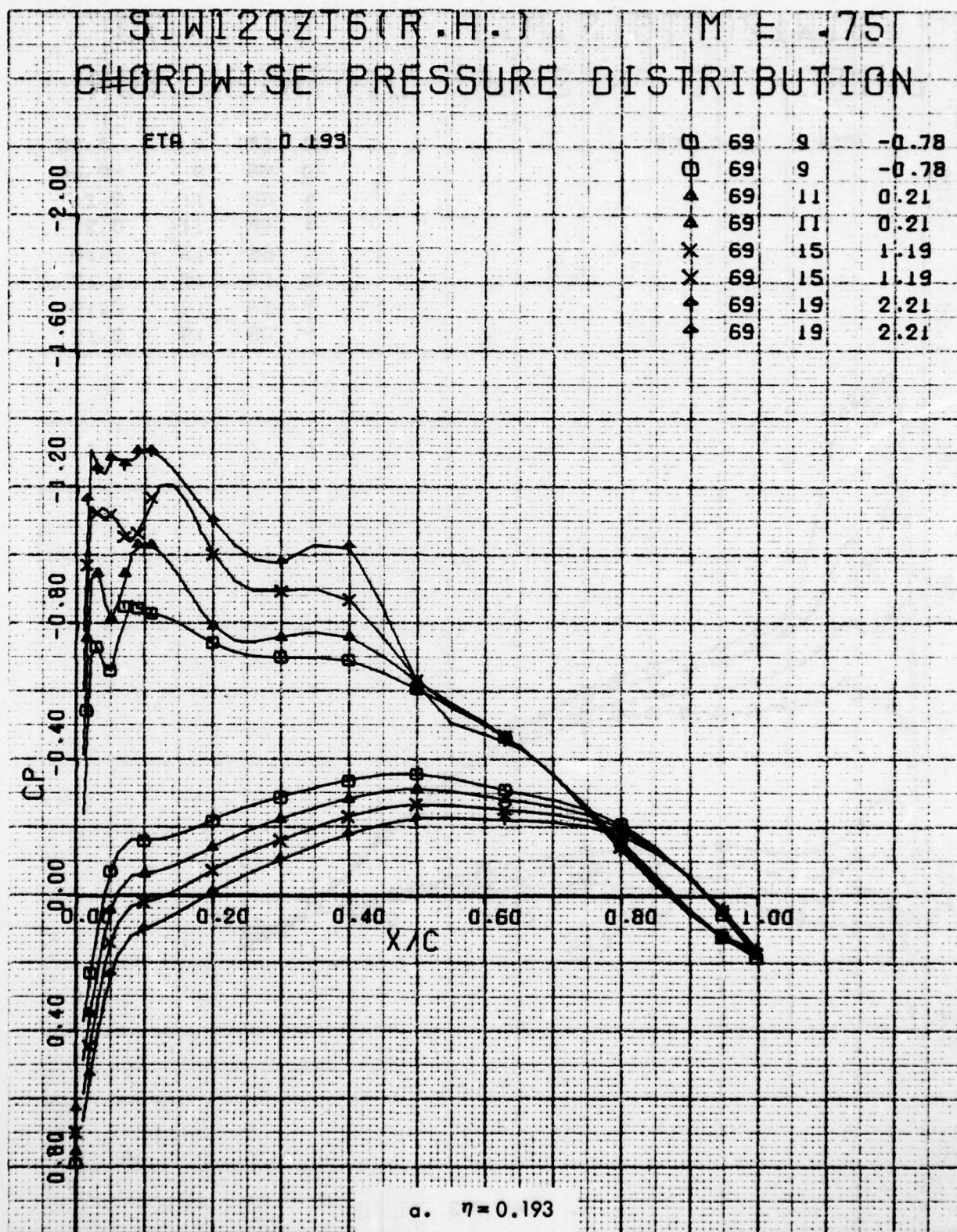


Figure 78. Chordwise Pressure Distributions for Various Angles of Attack. Baseline Leading Edge, Fixed Transition, Grit Code C, One Swept Tip, $M = 0.75$.

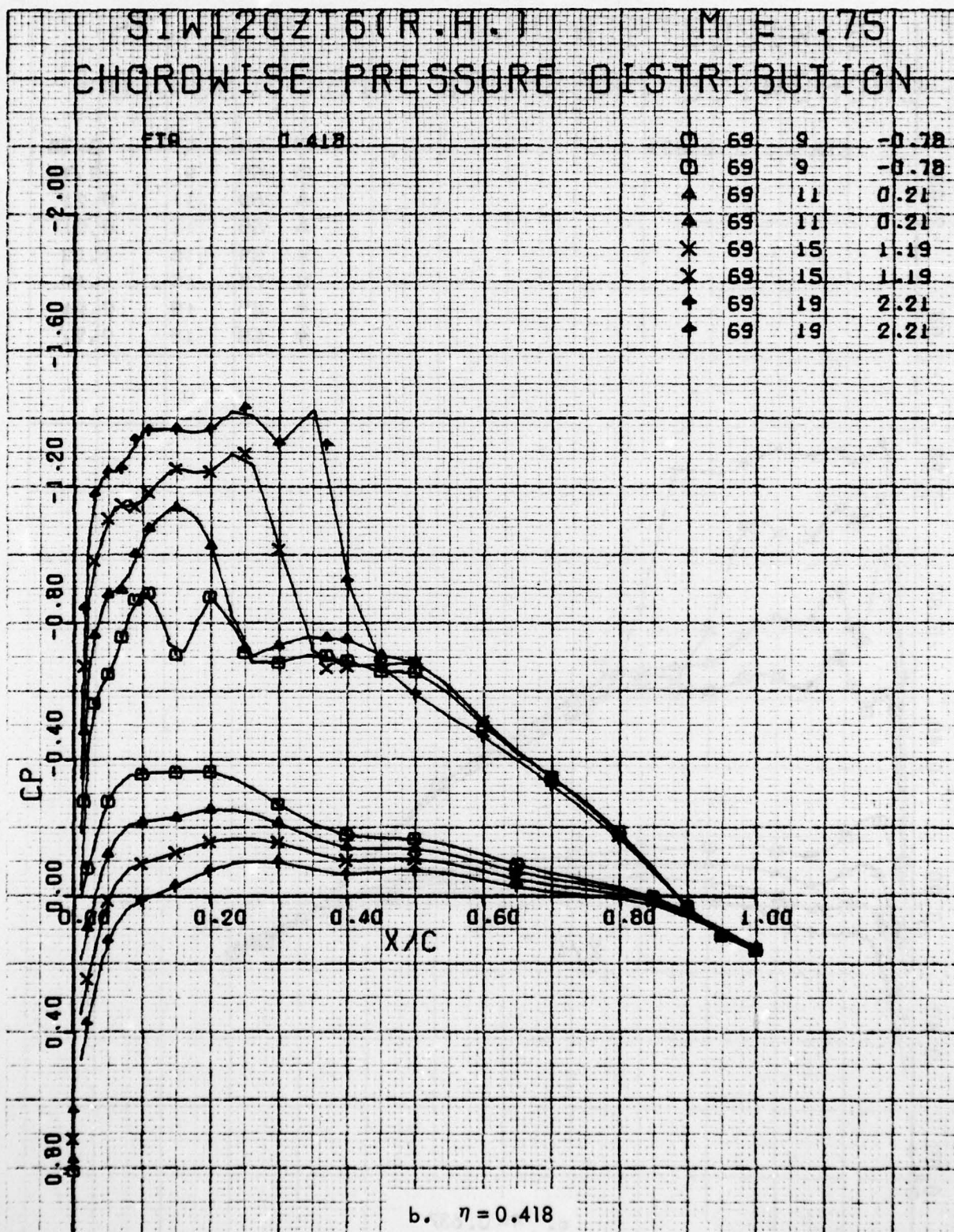


Figure 78 . Continued

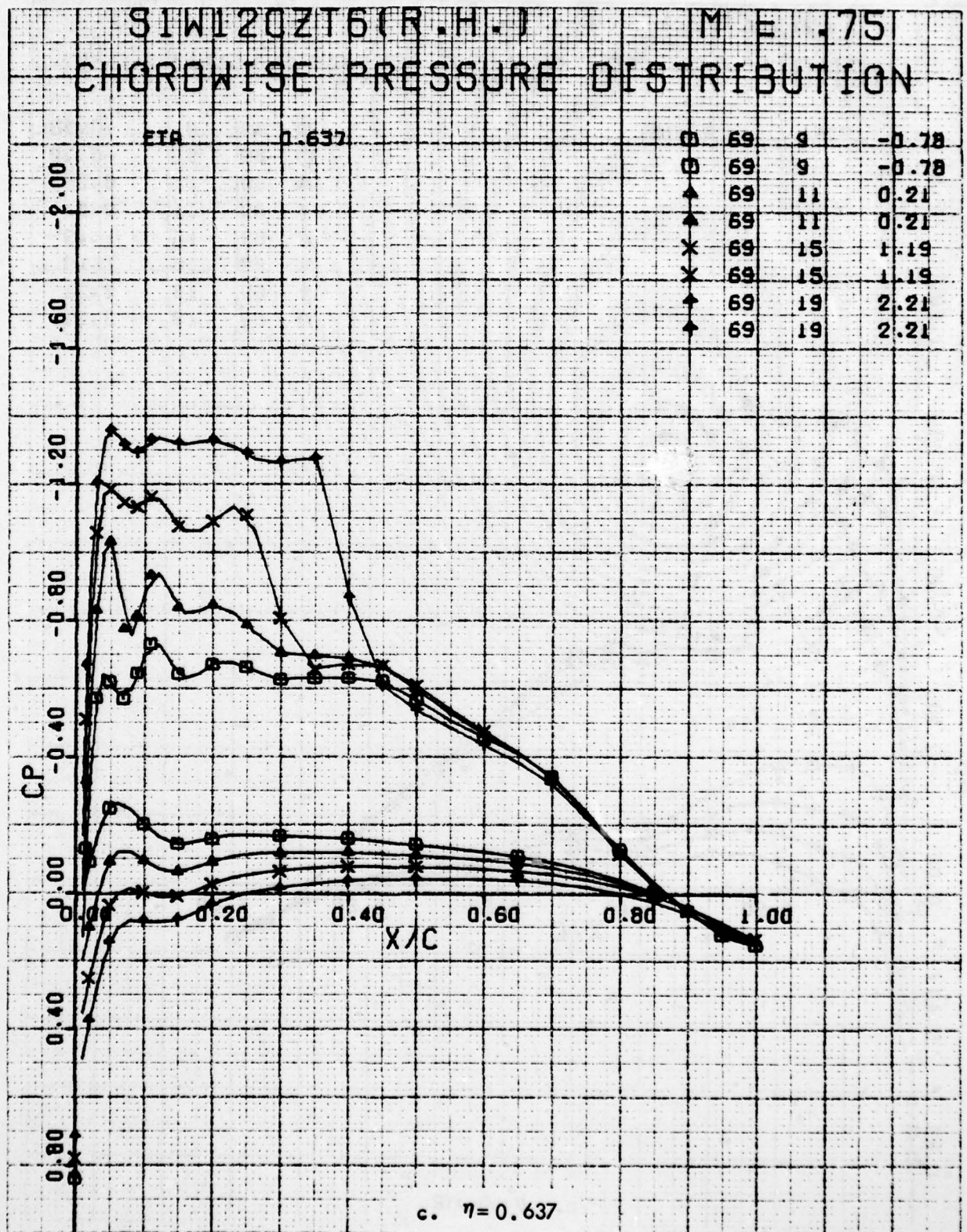


Figure 78. Continued

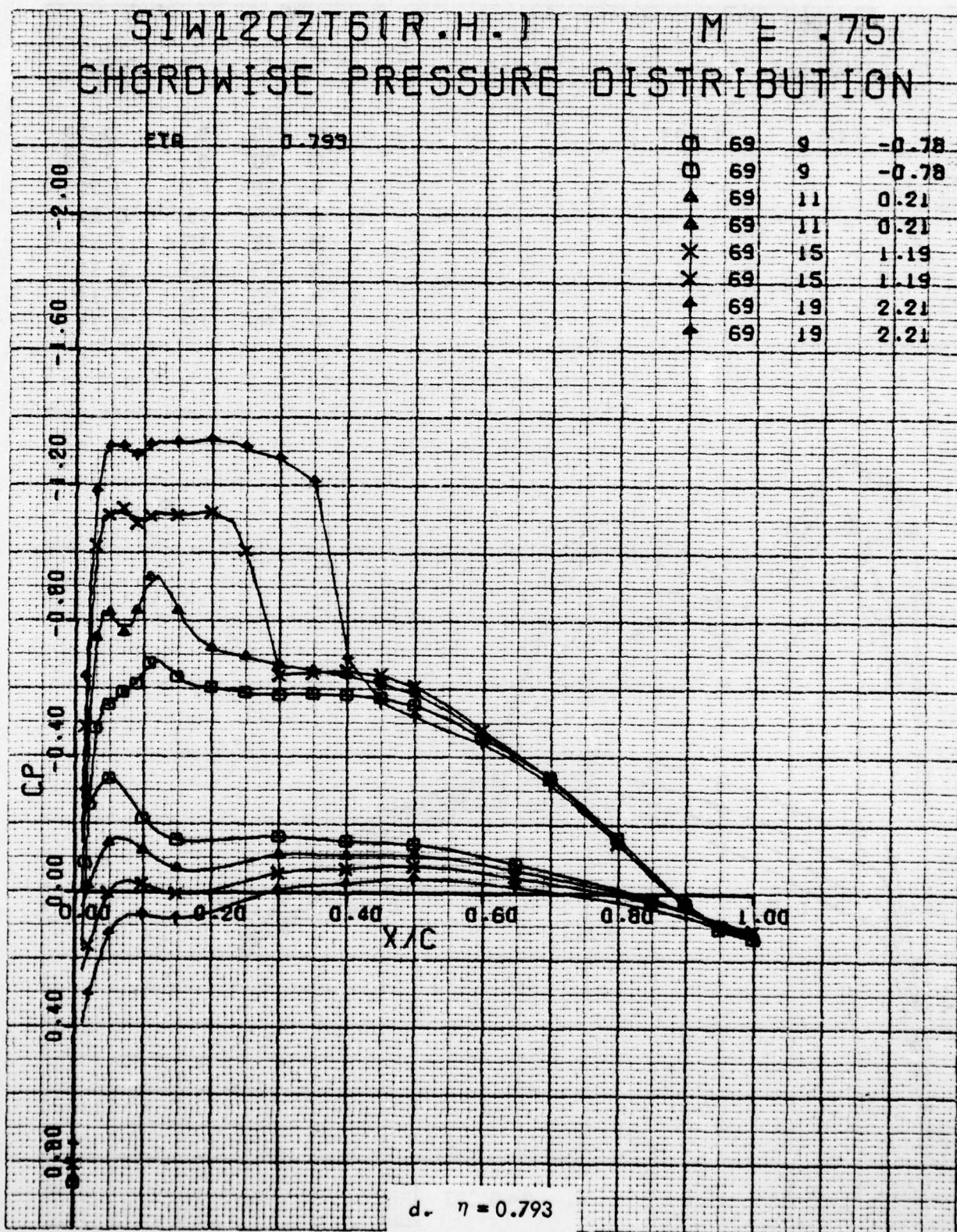


Figure 78. Concluded

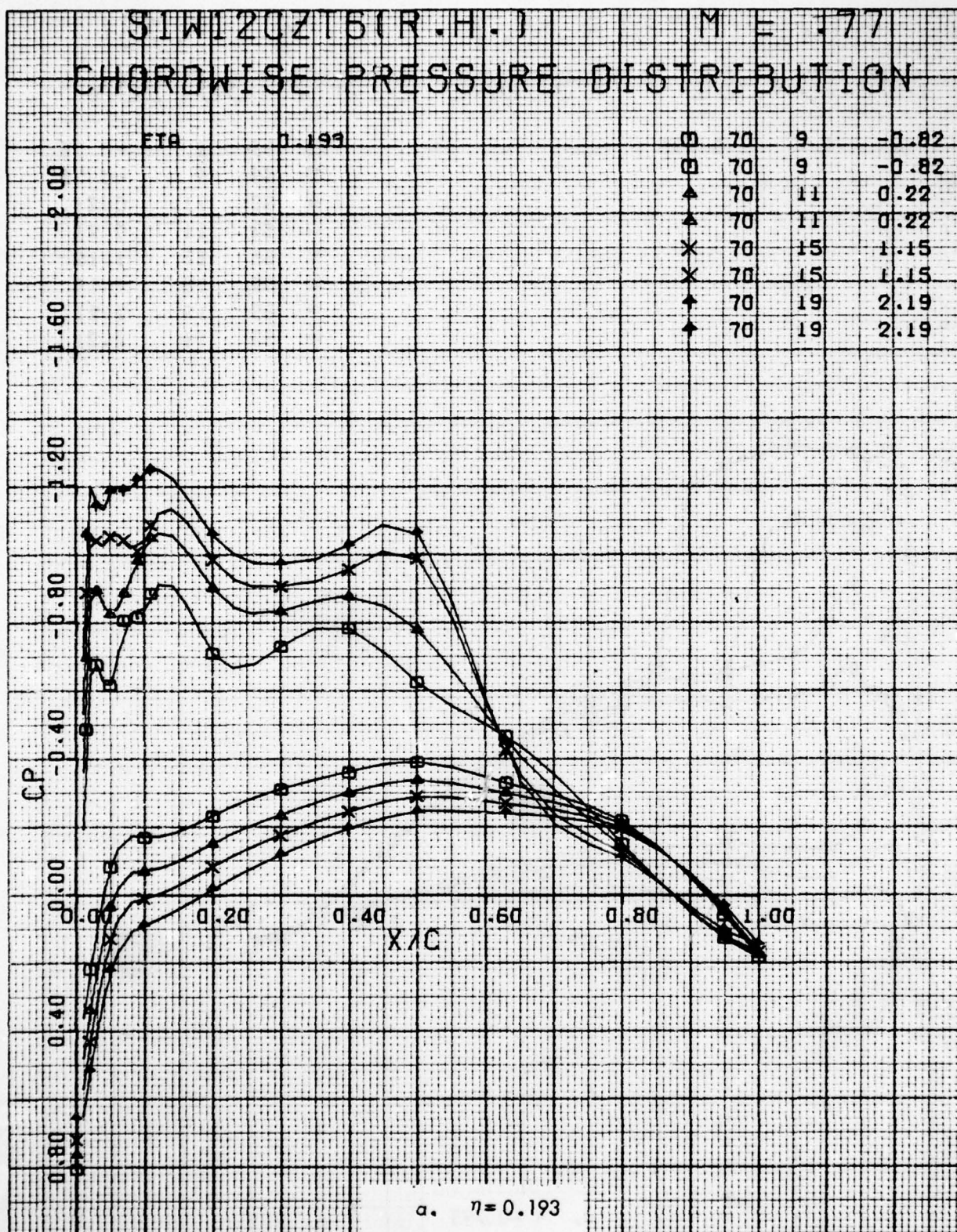


Figure 79. Chordwise Pressure Distributions for Various Angles of Attack. Baseline Leading Edge, Fixed Transition, Grit Code C, One Swept Tip, $M = 0.77$.

AD-A077 688

LOCKHEED-GEORGIA CO MARIETTA

F/G 1/3

AERODYNAMIC INVESTIGATION OF C-141 LEADING EDGE MODIFICATION FO--ETC(U)

JUN 79 W T BLACKERBY , P R SMITH

F09603-77-A-0204

UNCLASSIFIED

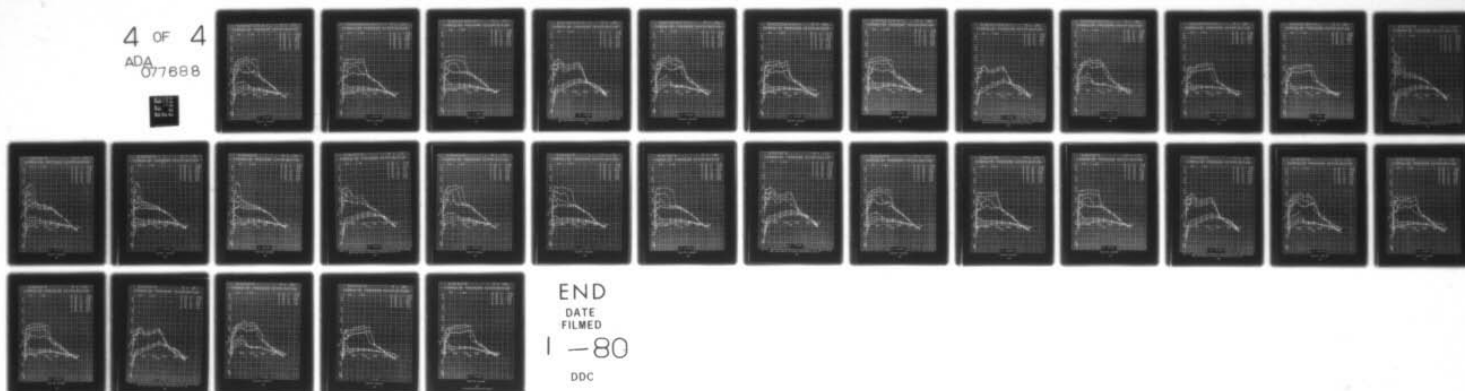
LG78ER0233-VOL-2

AFFDL-TR-79-3059-VOL-2

NL

4 OF 4

ADA
077688



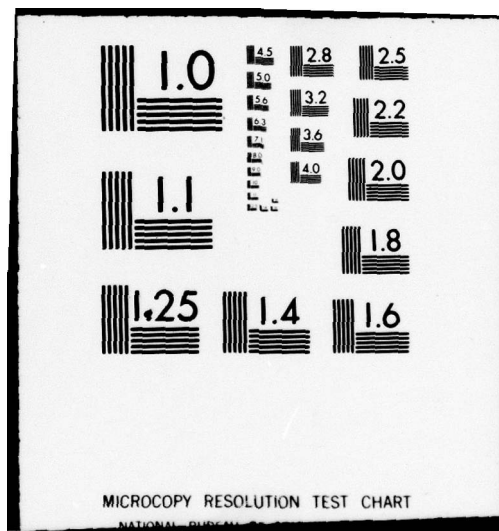
END

DATE

FILMED

1-80

DDC



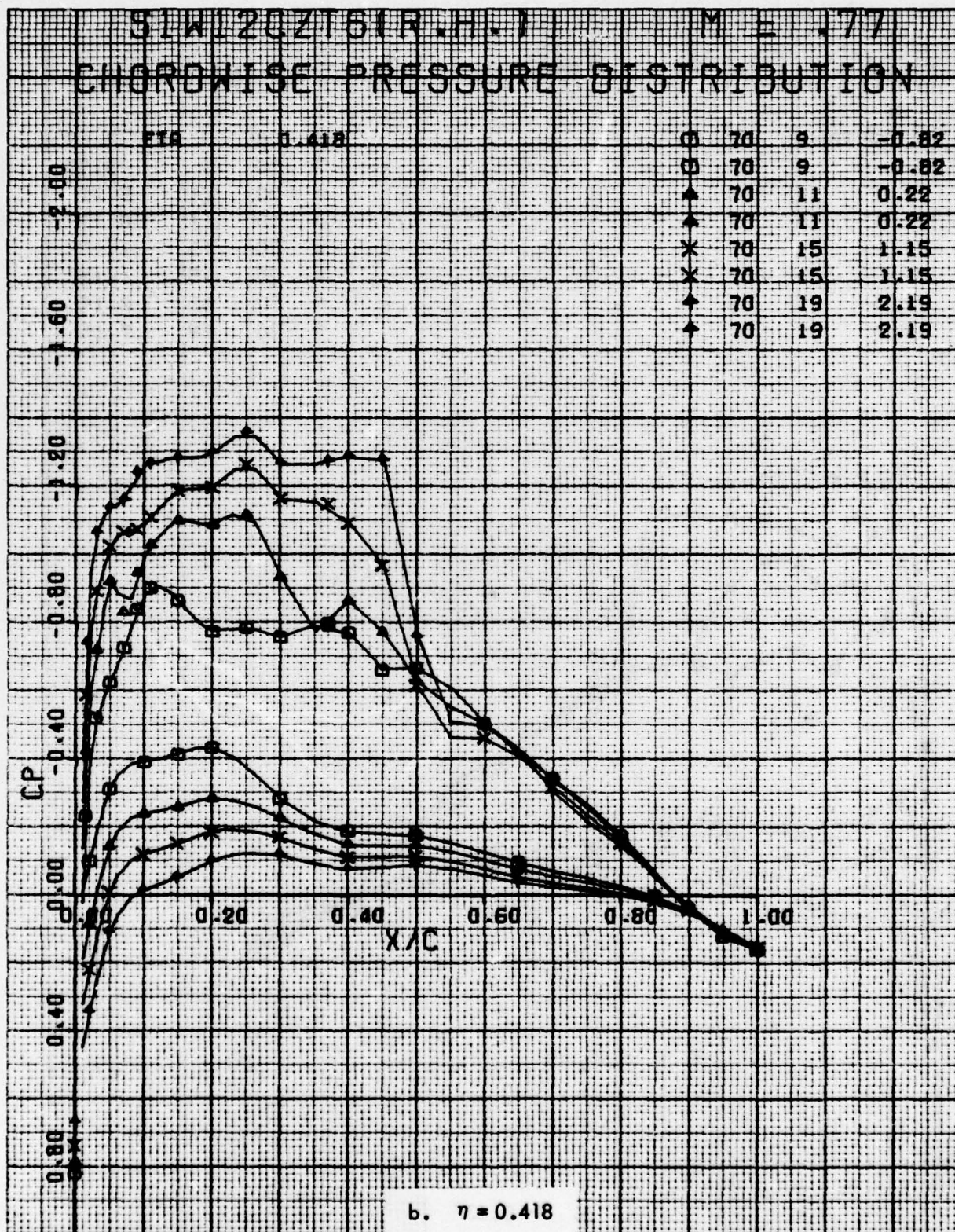


Figure 79 . Continued

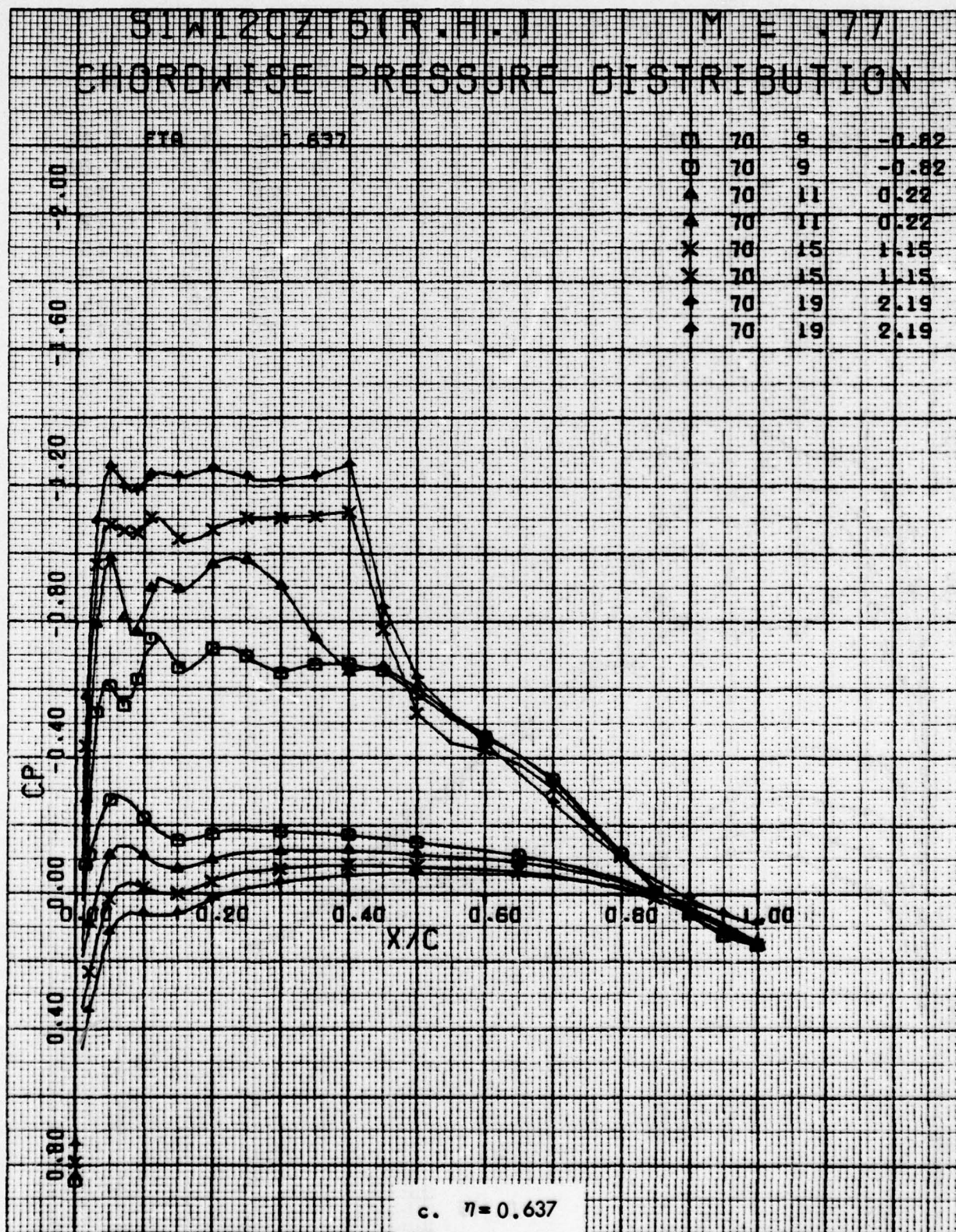


Figure 79. Continued

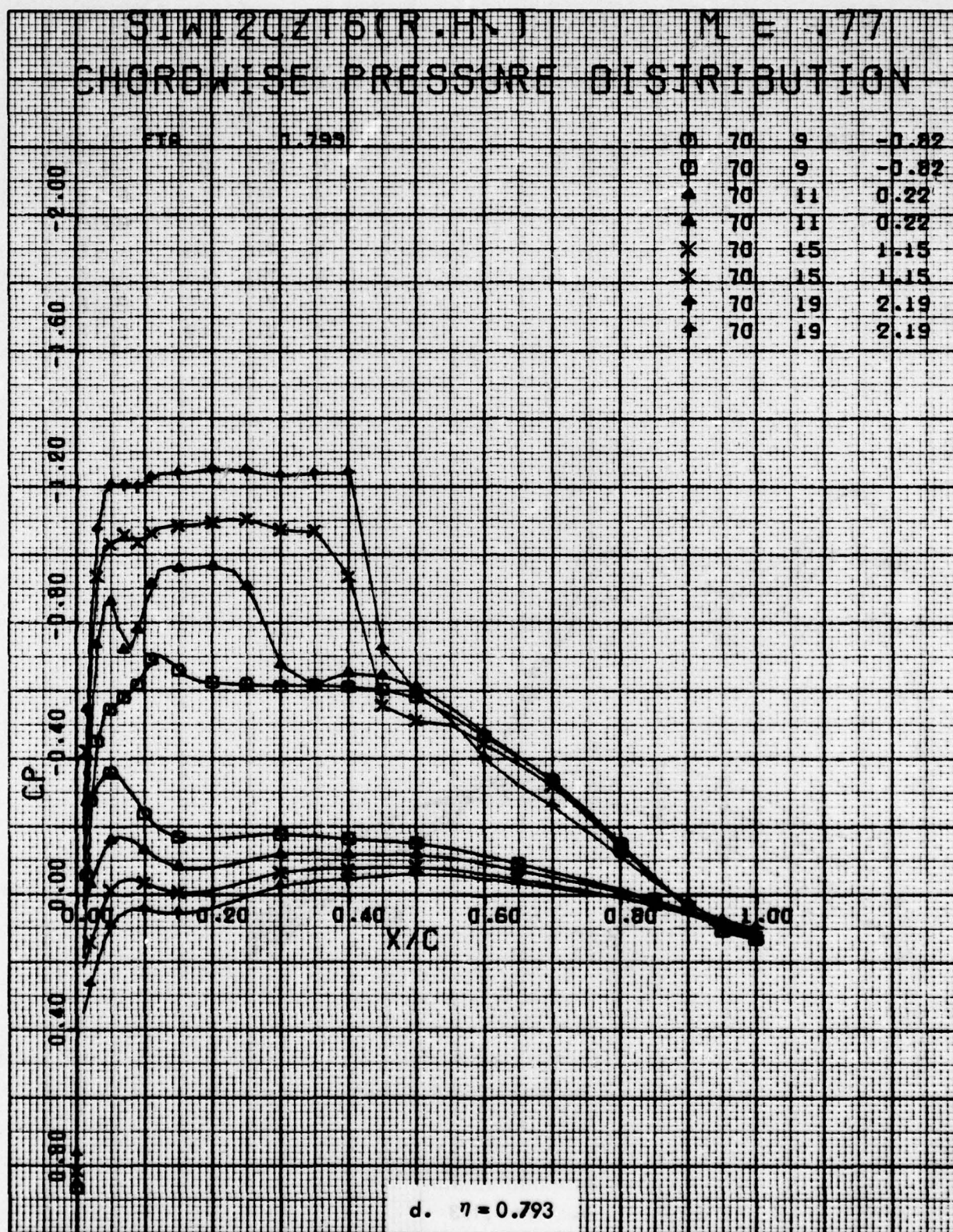


Figure 79. Concluded

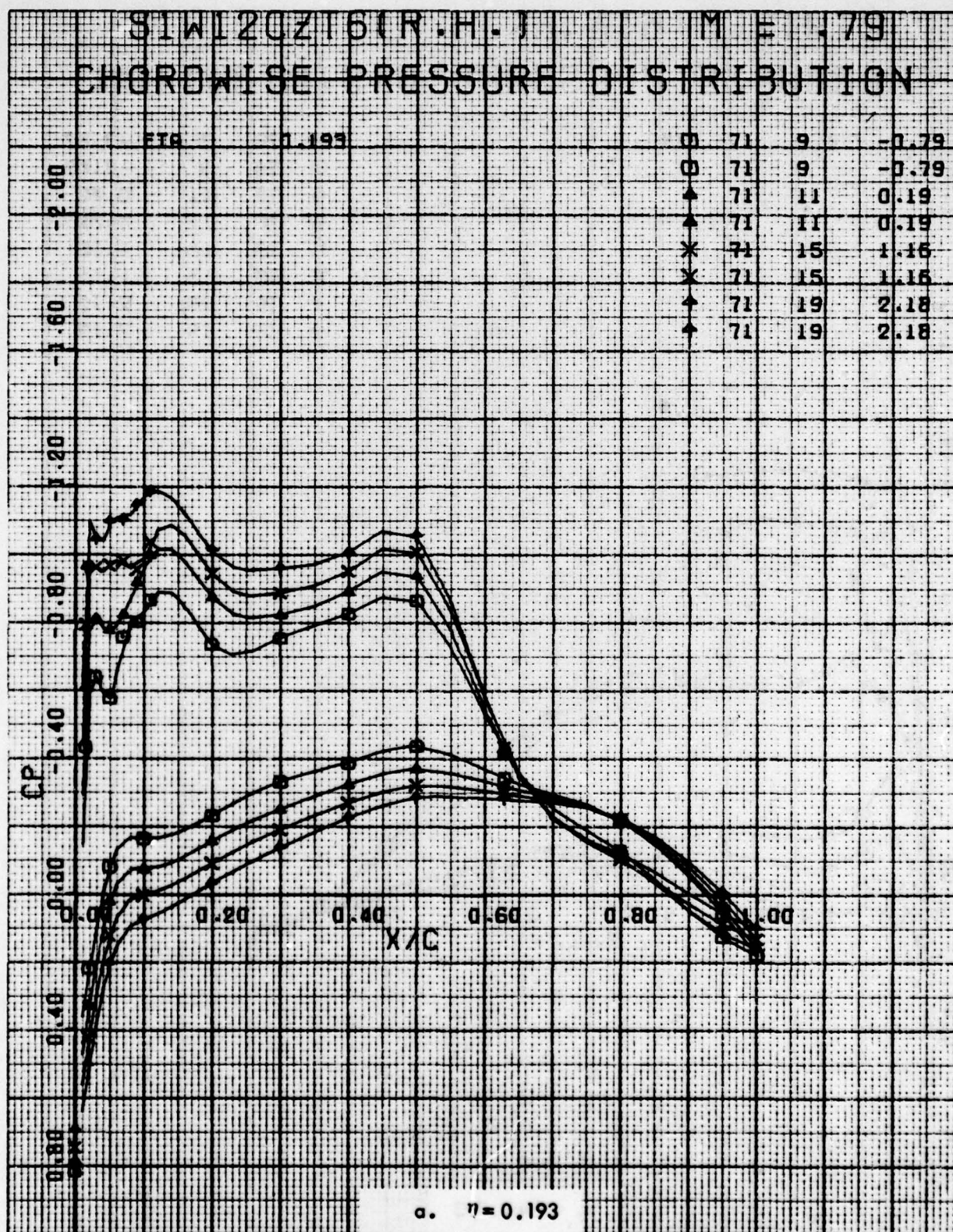


Figure 80. Chordwise Pressure Distributions for Various Angles of Attack. Baseline Leading Edge, Fixed Transition, Grit Code C, One Swept Tip, $M = 0.79$.

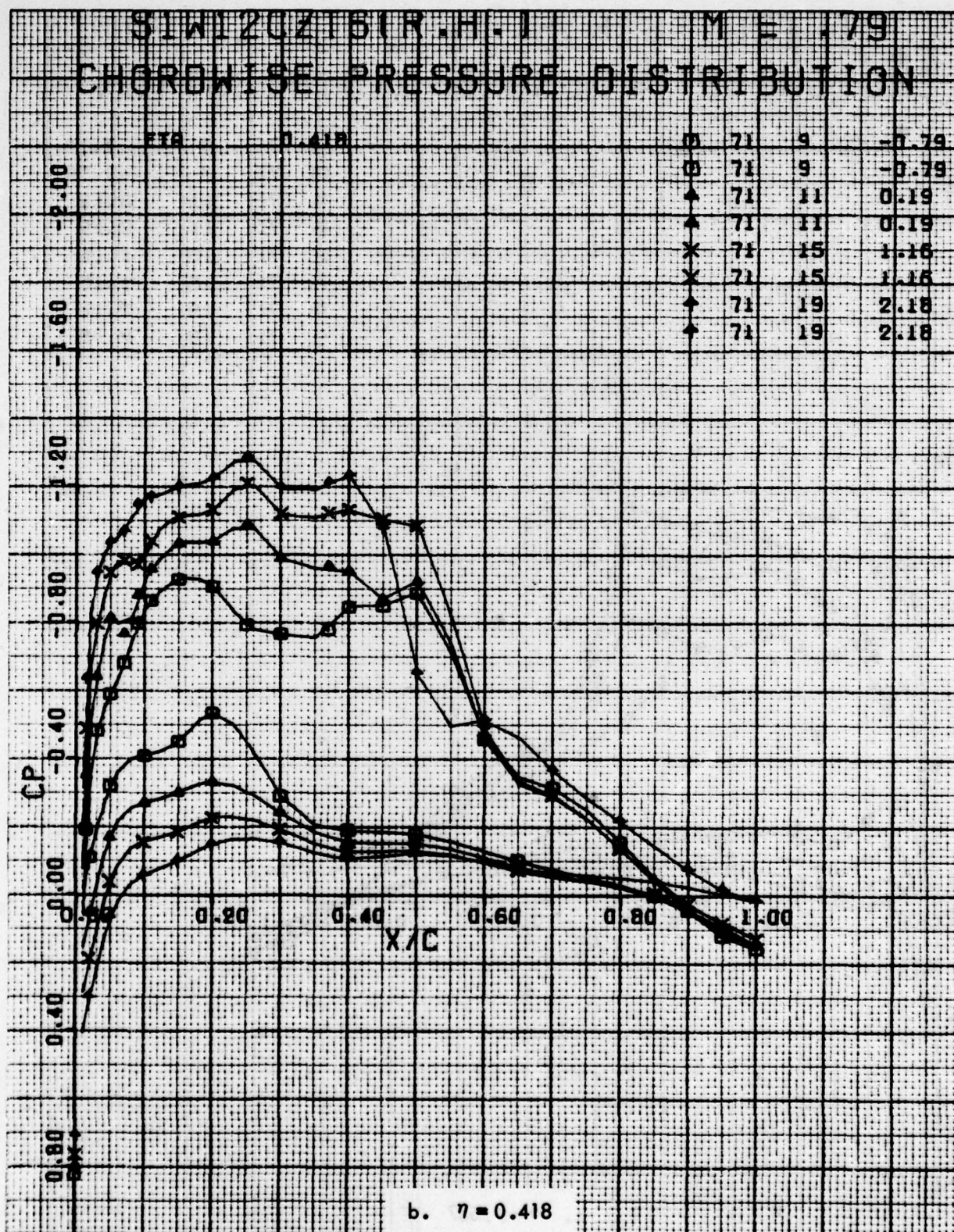


Figure 80 . Continued

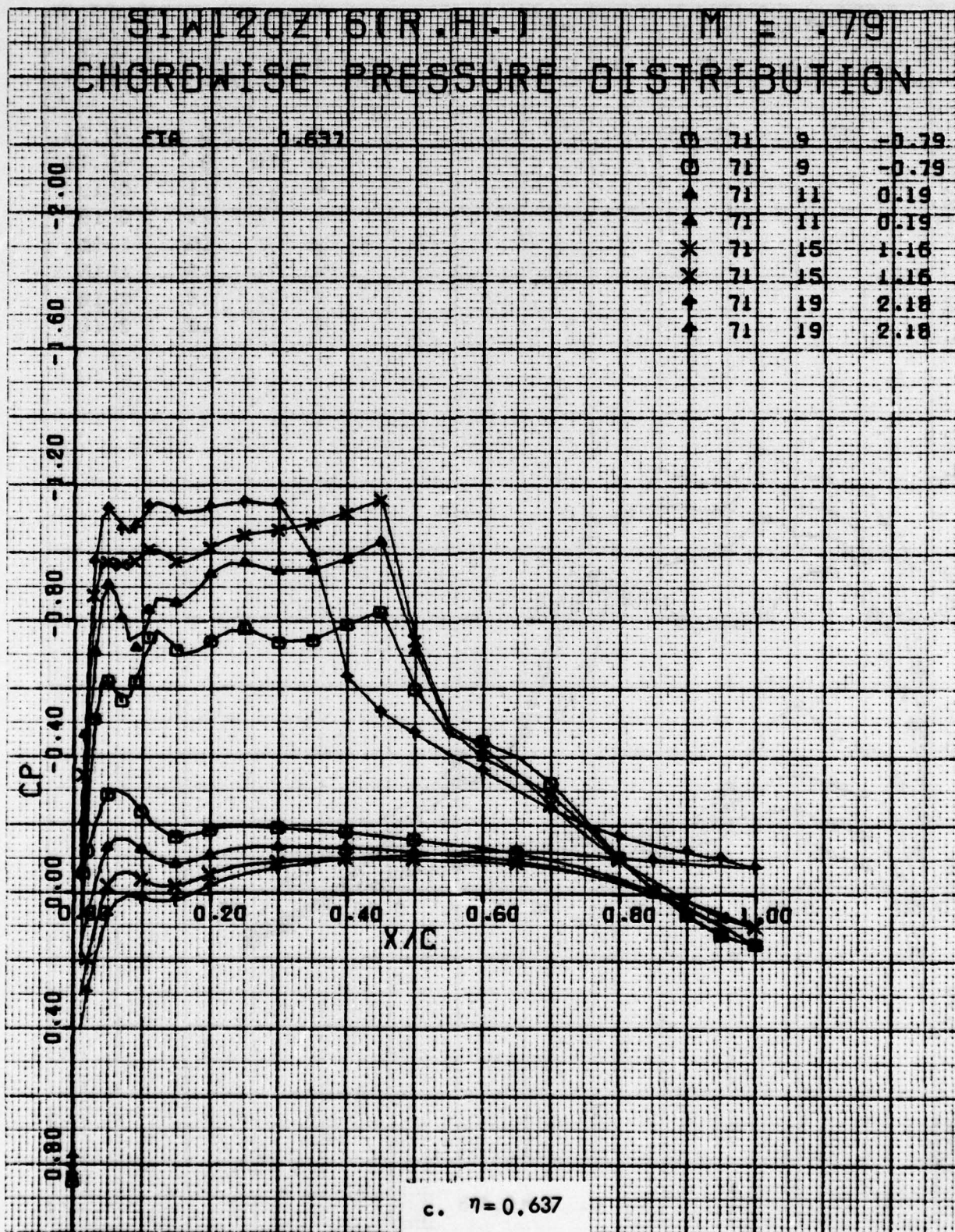


Figure 80. Continued

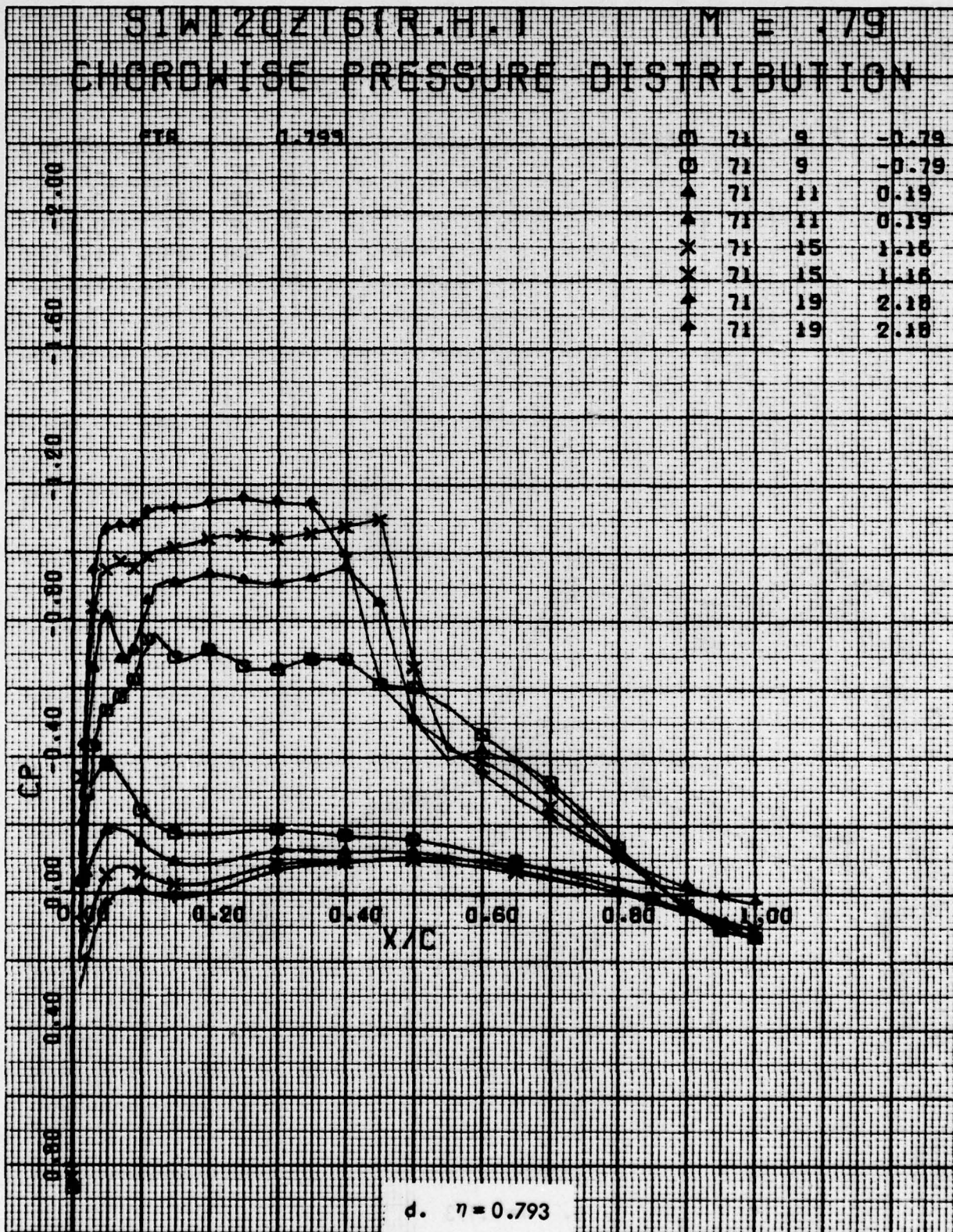


Figure 80. Concluded

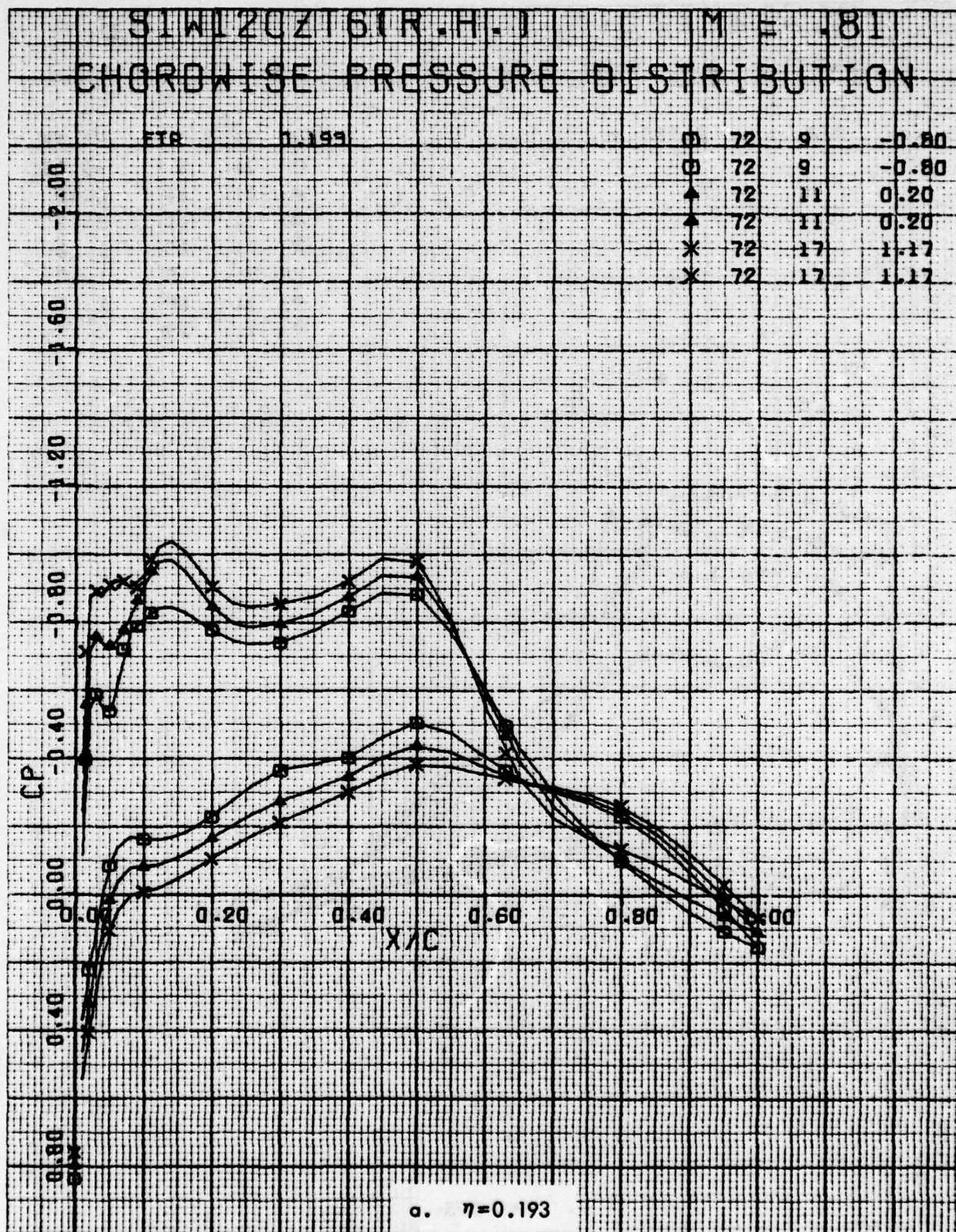


Figure 81 . Chordwise Pressure Distributions for Various Angles of Attack. Baseline Leading Edge, Fixed Transition, Grit Code C, One Swept Tip, $M = 0.81$.

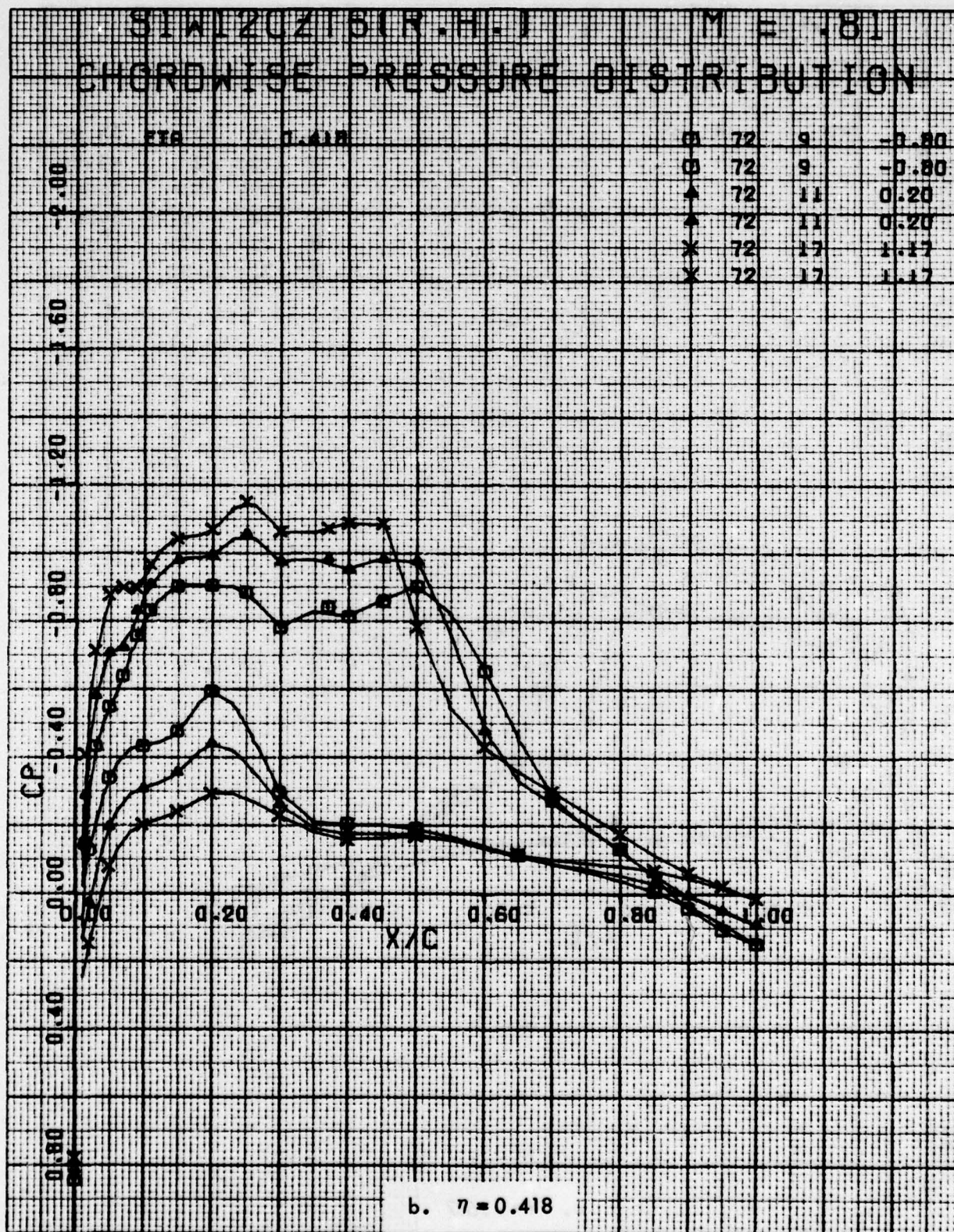


Figure 81 . Continued

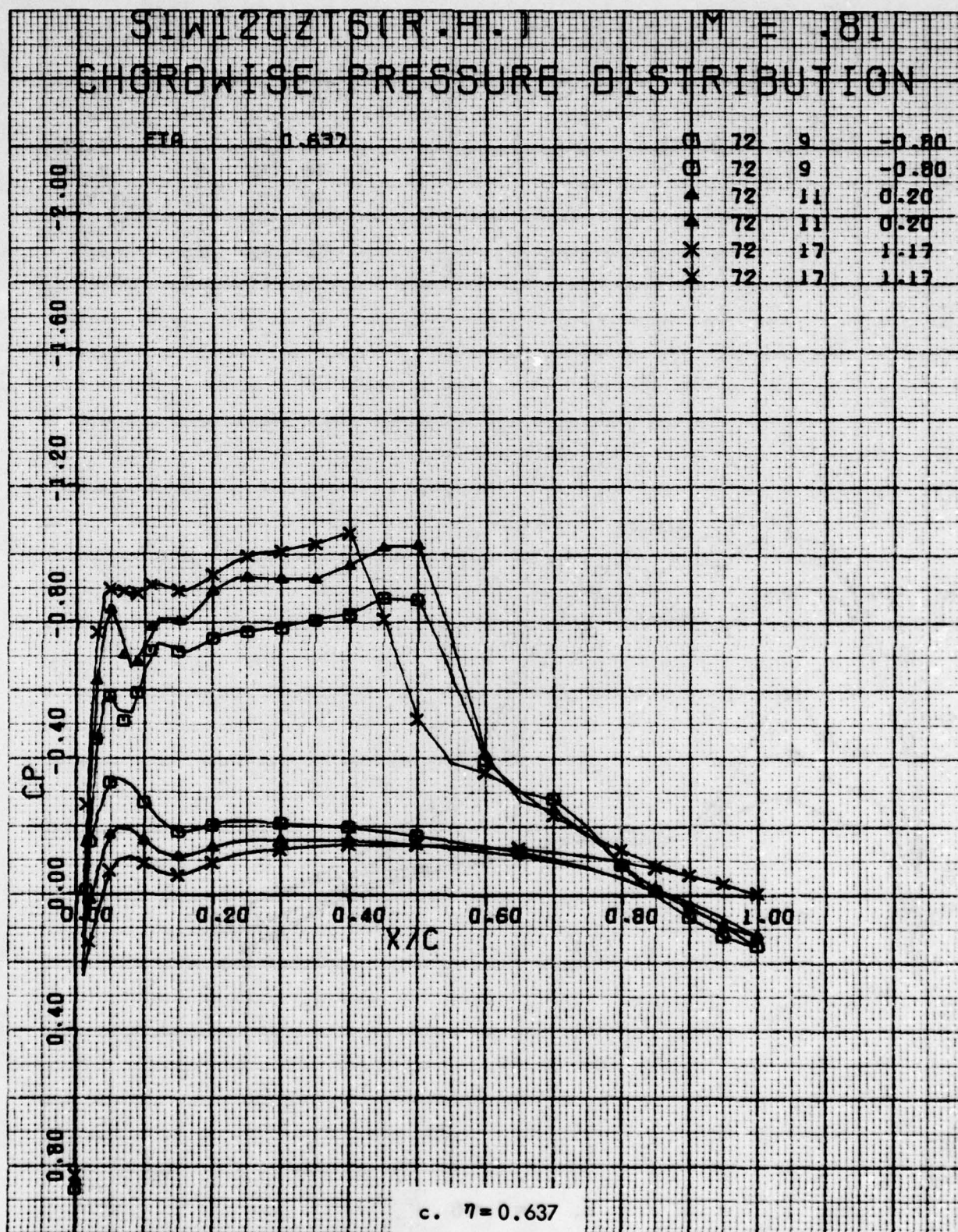


Figure 81. Continued

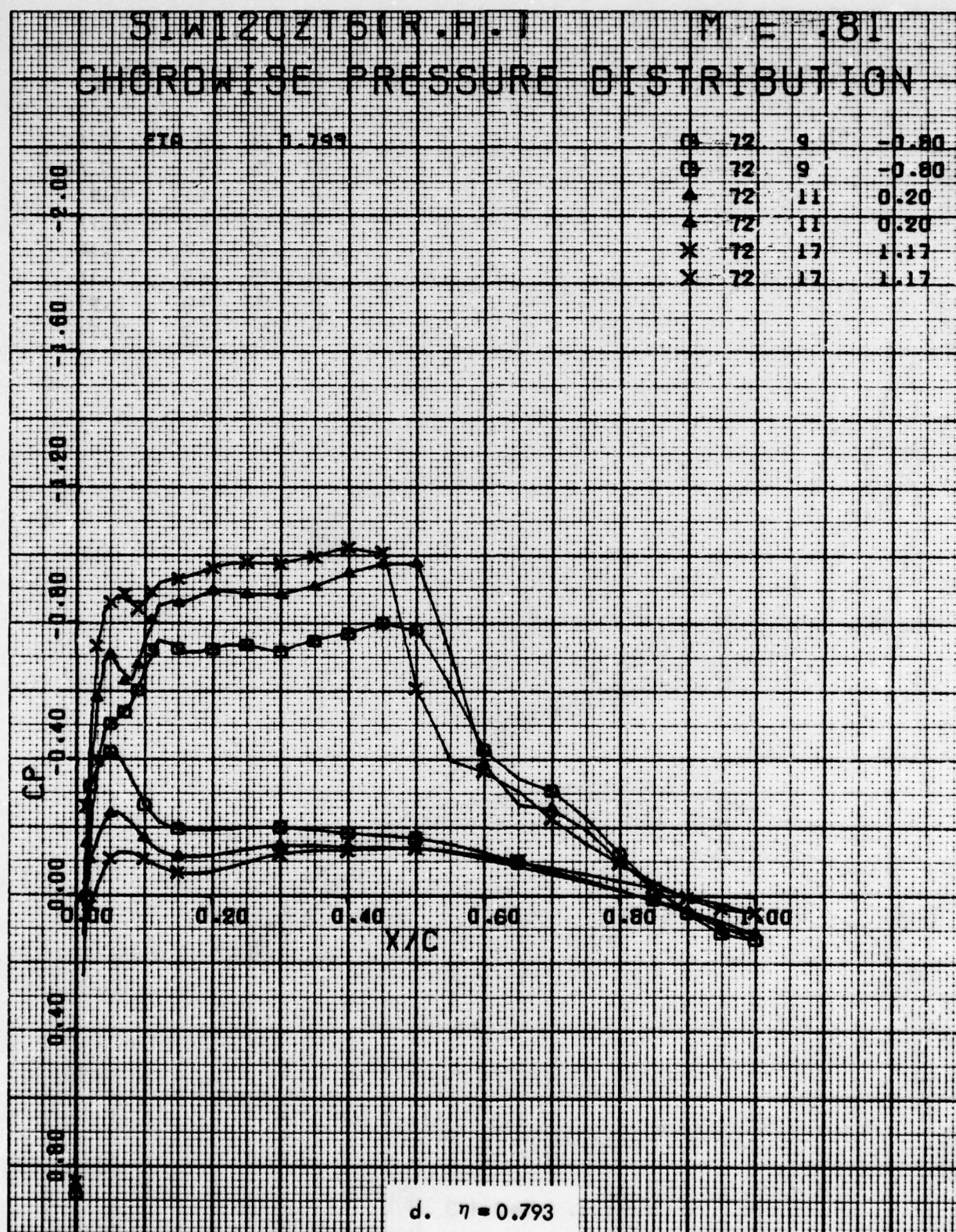


Figure 81. Concluded

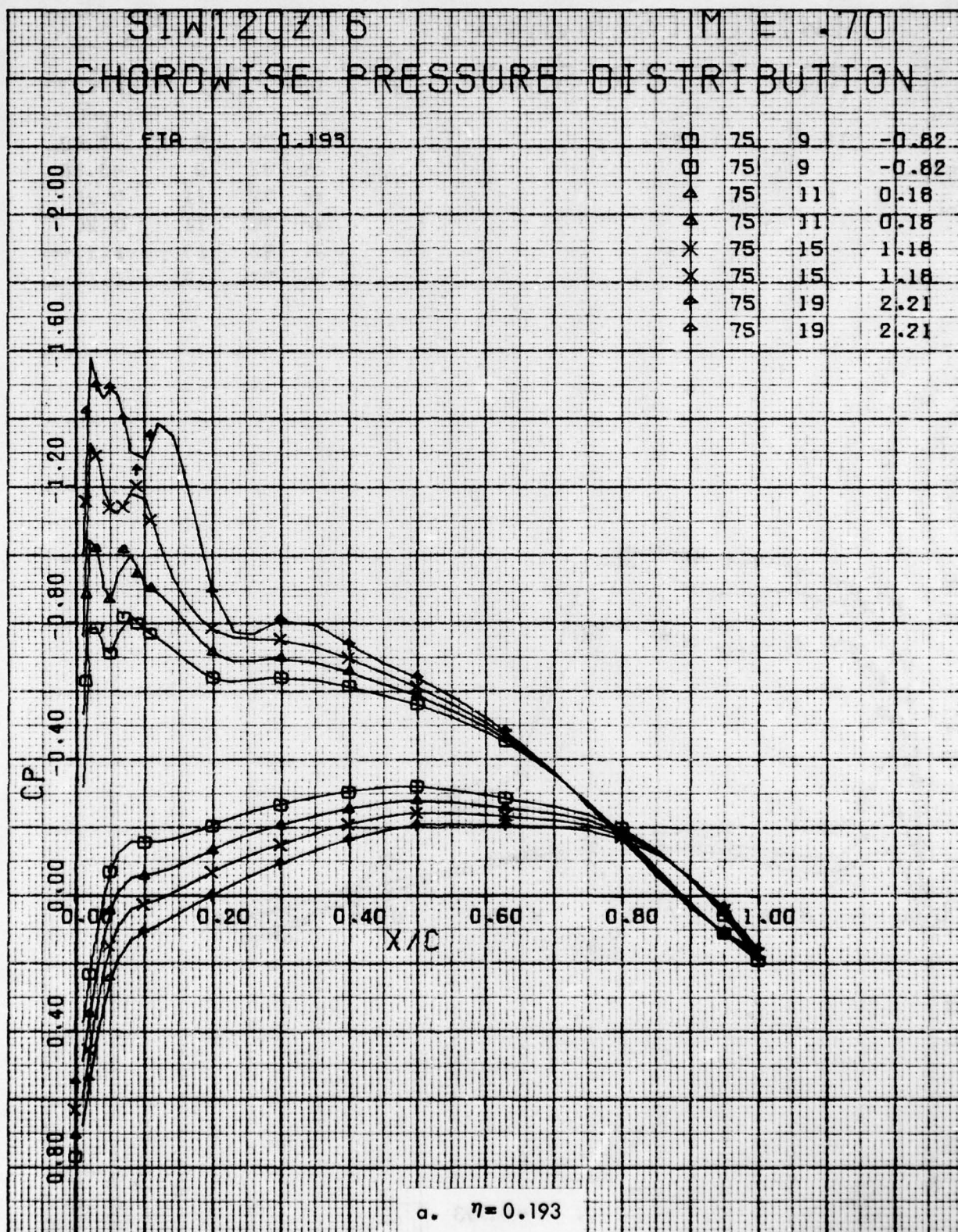


Figure 82. Chordwise Pressure Distributions for Various Angles of Attack. Baseline Leading Edge, Fixed Transition, Grit Code C, Both Swept Tips, $M = 0.7$.

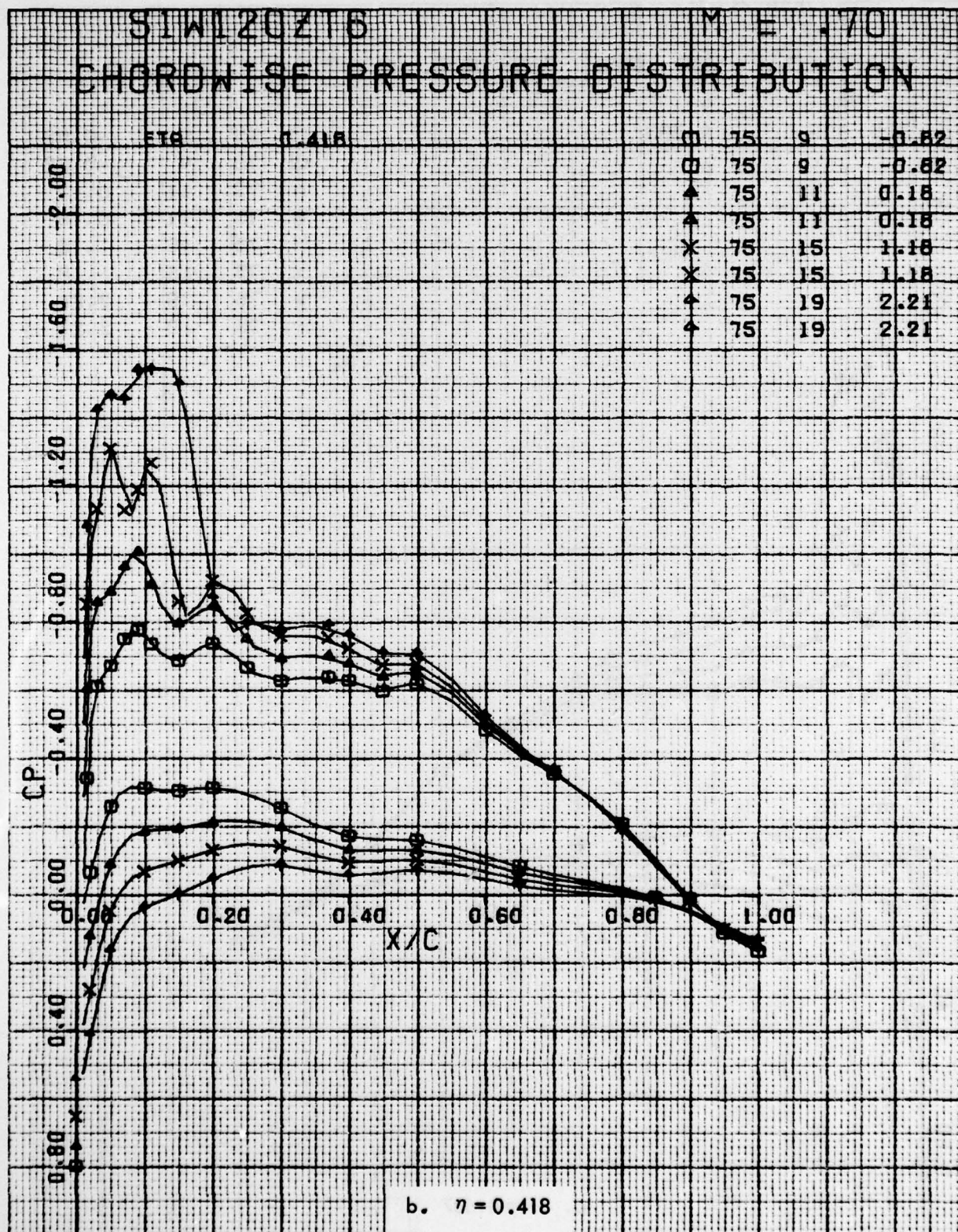


Figure 82. Continued

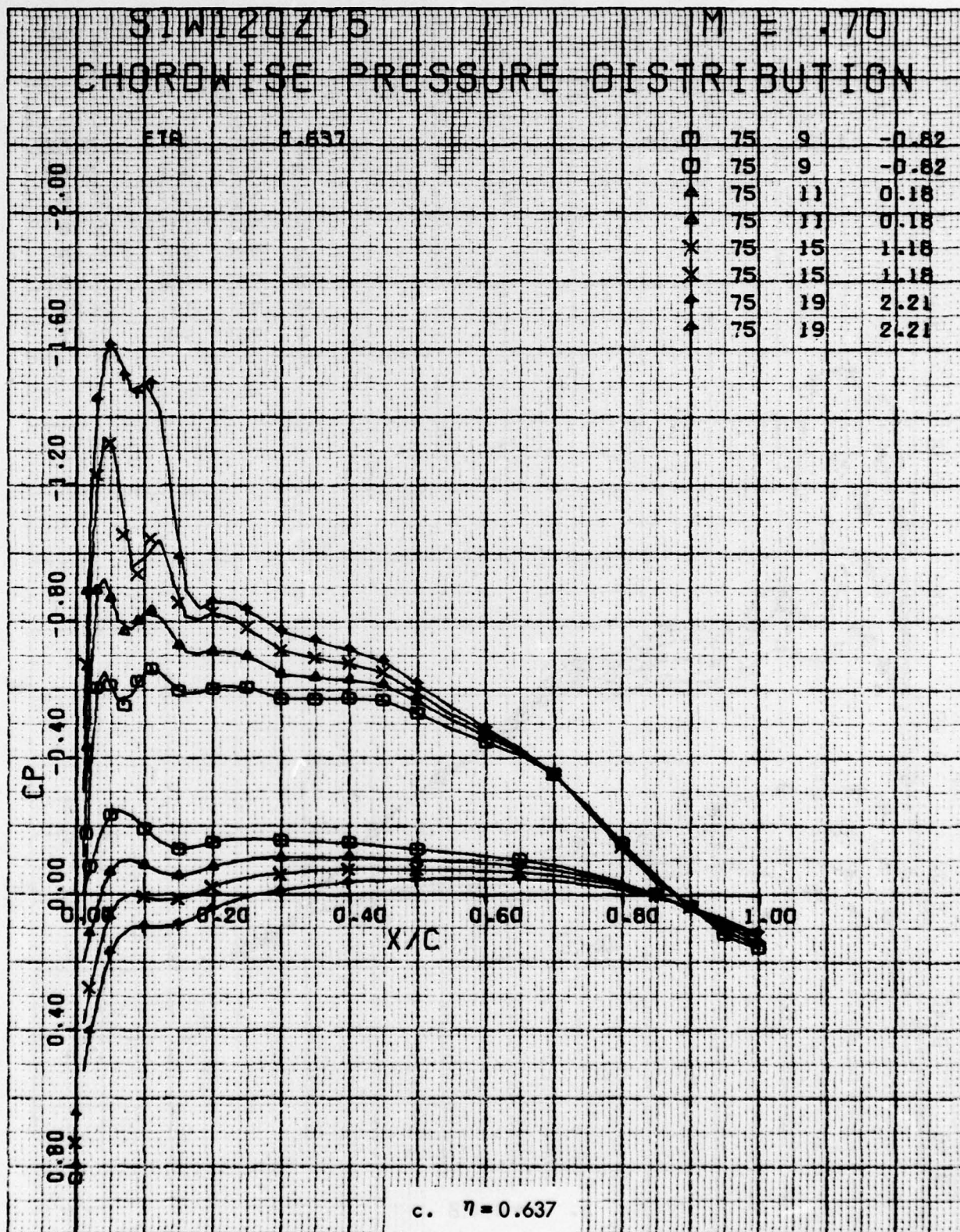


Figure 82 . Continued

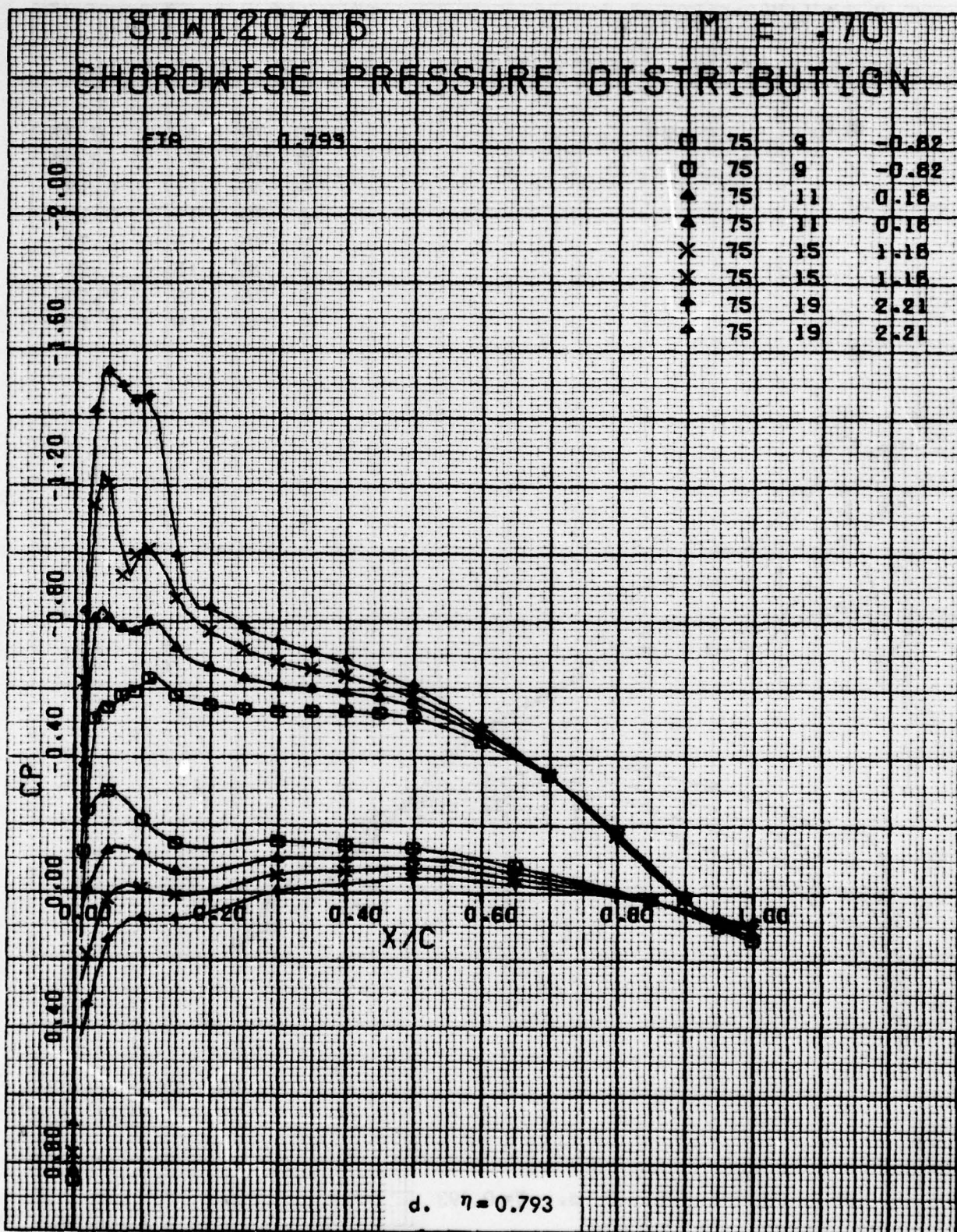


Figure 82. Concluded

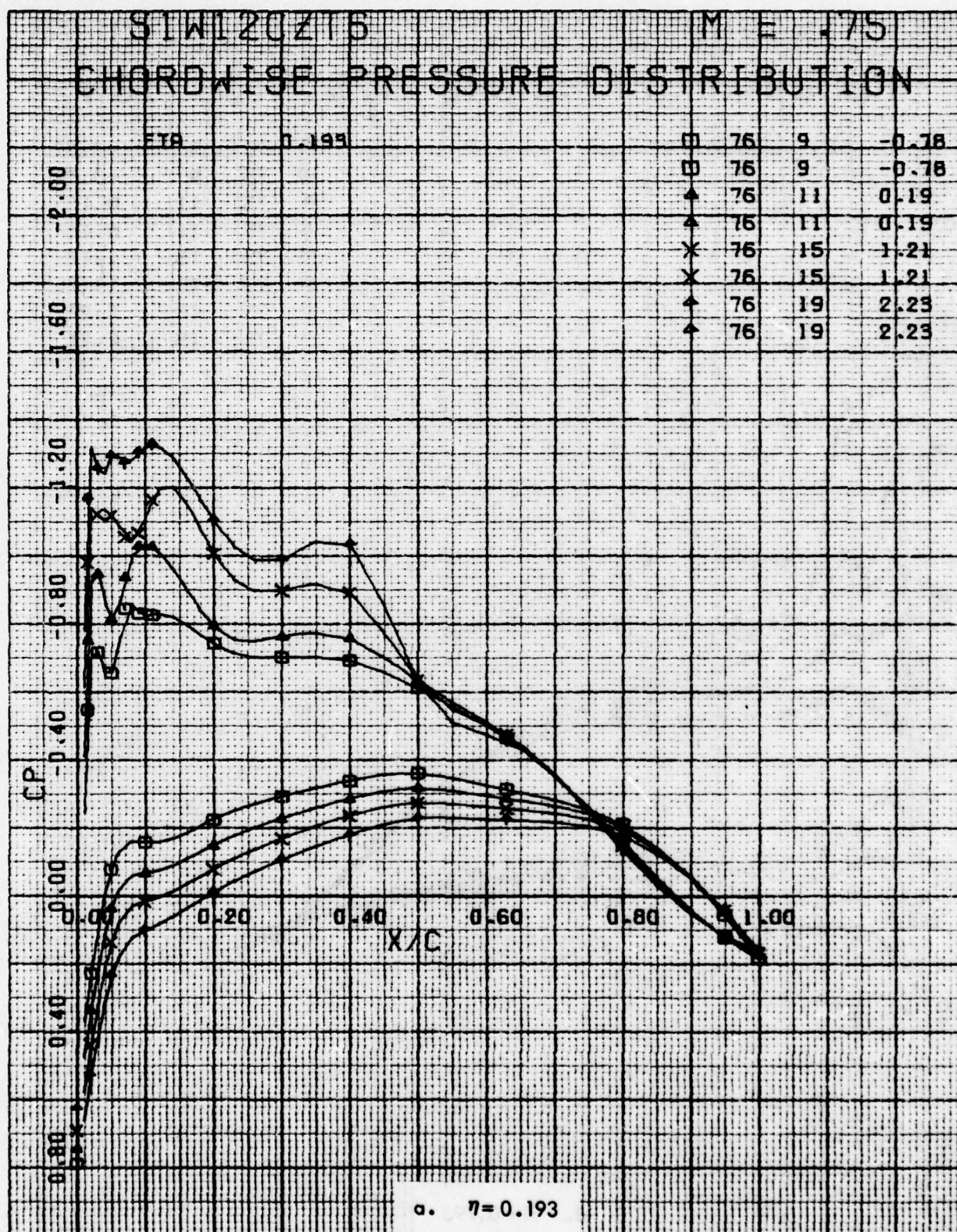


Figure 83. Chordwise Pressure Distributions for Various Angles of Attack. Baseline Leading Edge, Fixed Transition, Grit Code C, Both Swept Tips, $M = 0.75$.

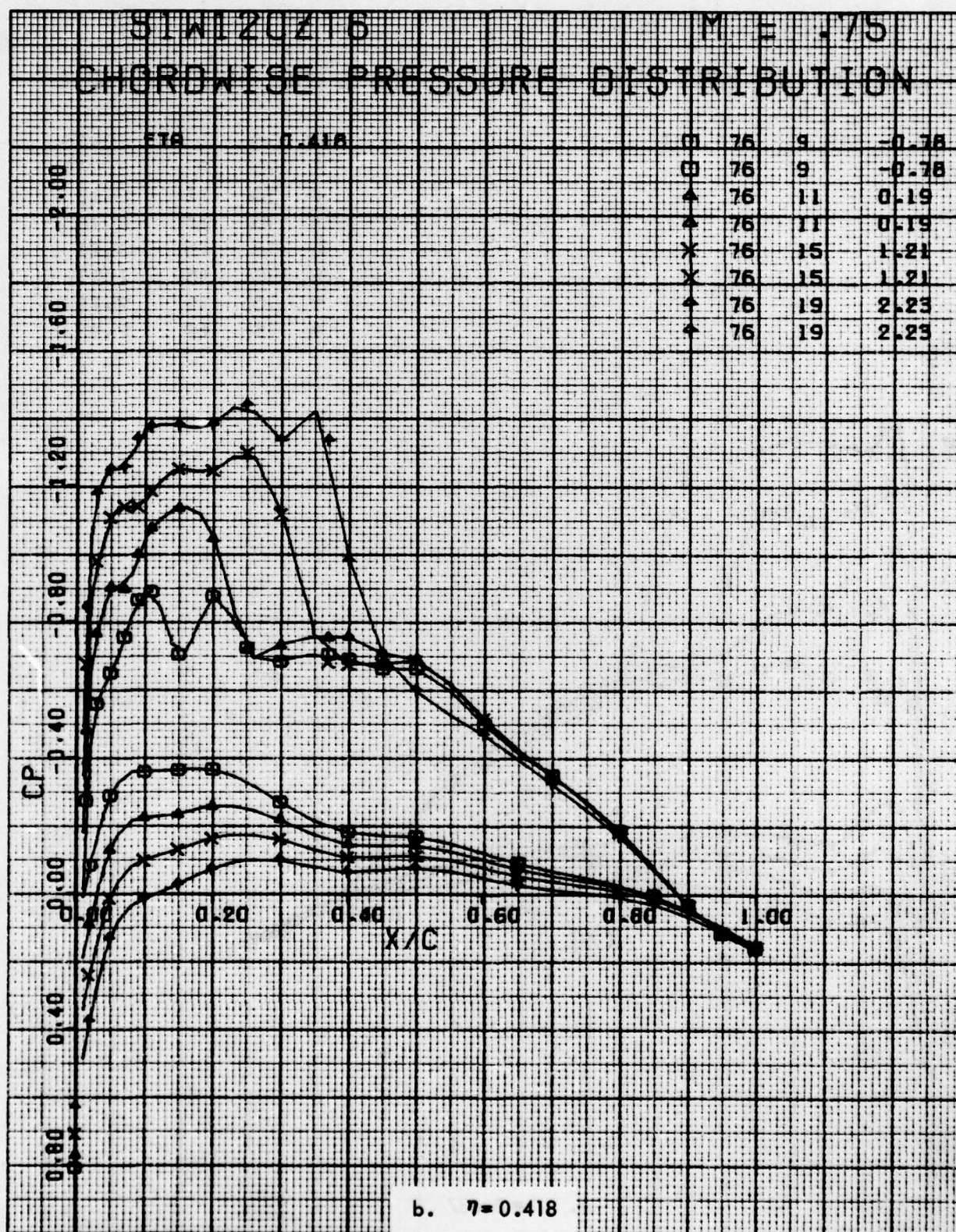


Figure 83. Continued

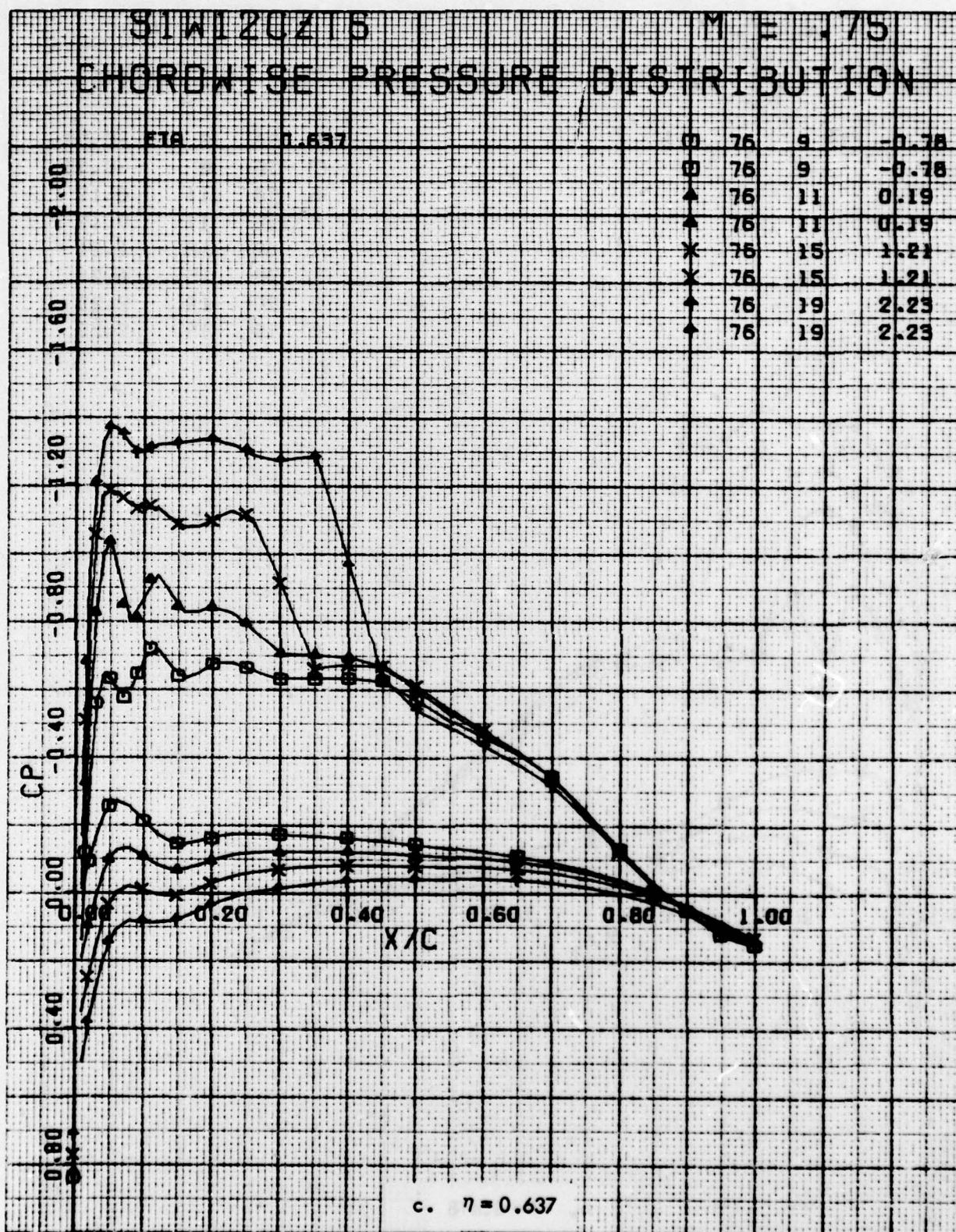


Figure 83 . Continued

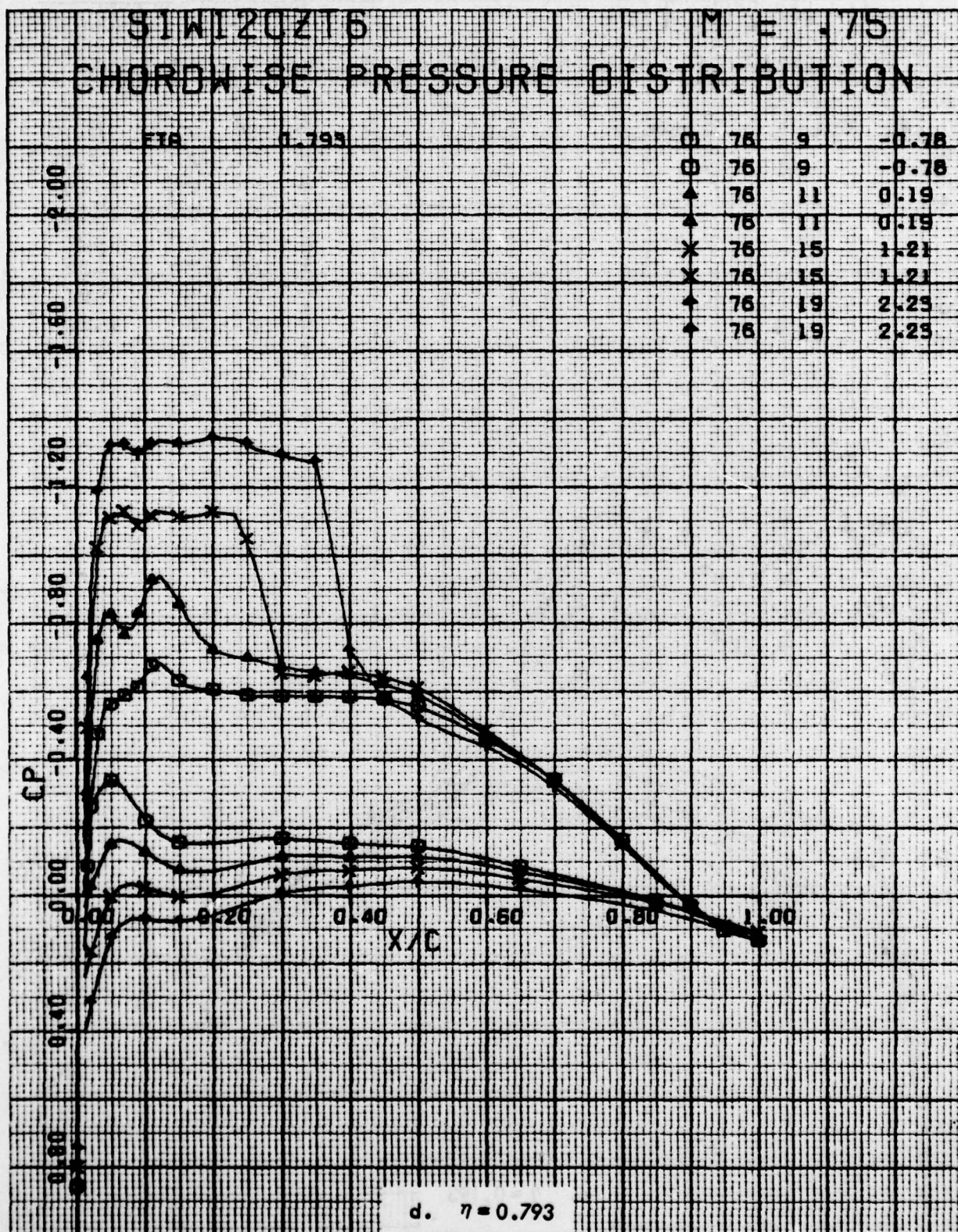


Figure 83. Concluded

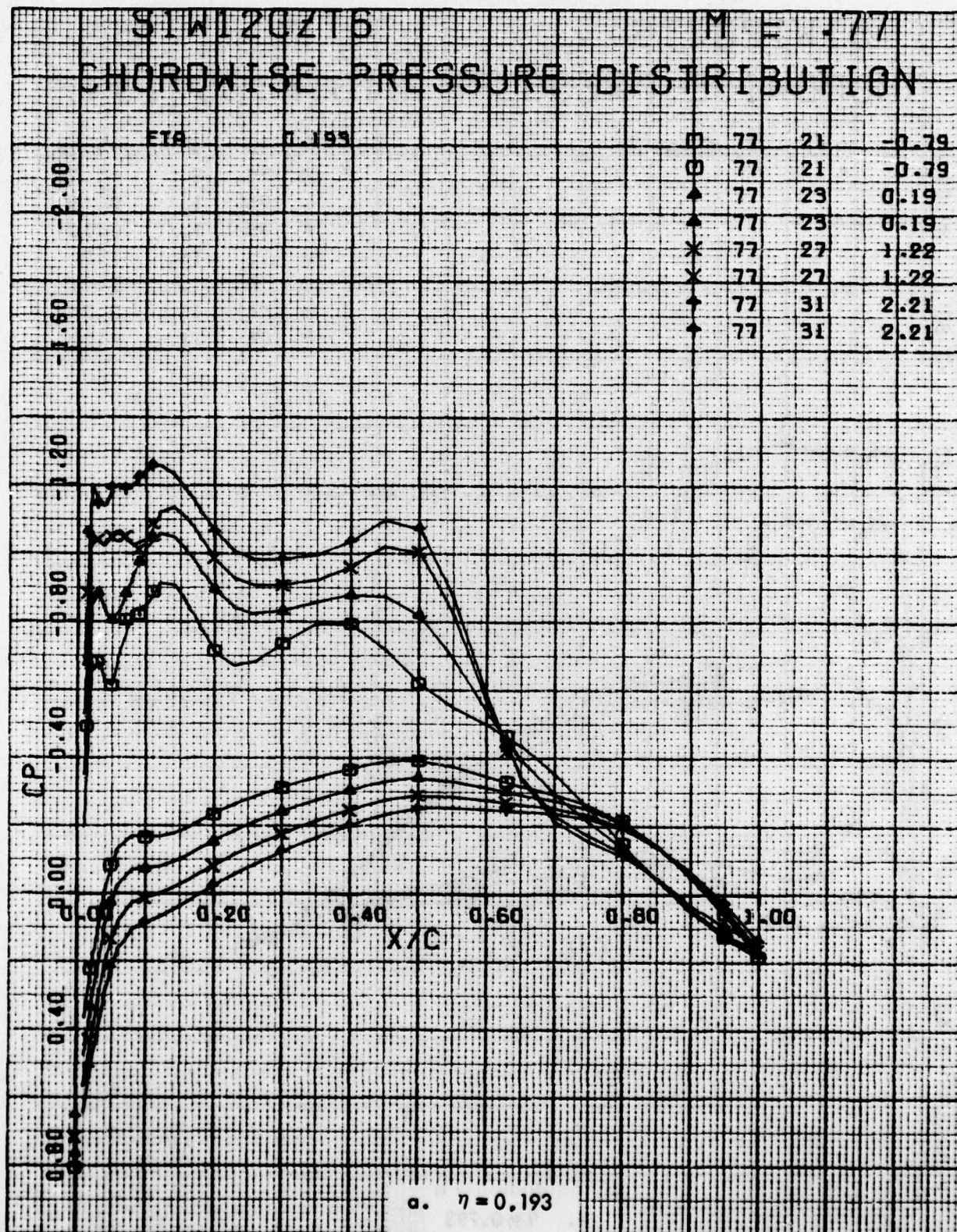


Figure 84. Chordwise Pressure Distributions for Various Angles of Attack. Baseline Leading Edge, Fixed Transition, Grit Code C, Both Swept Tips, $M = 0.77$.

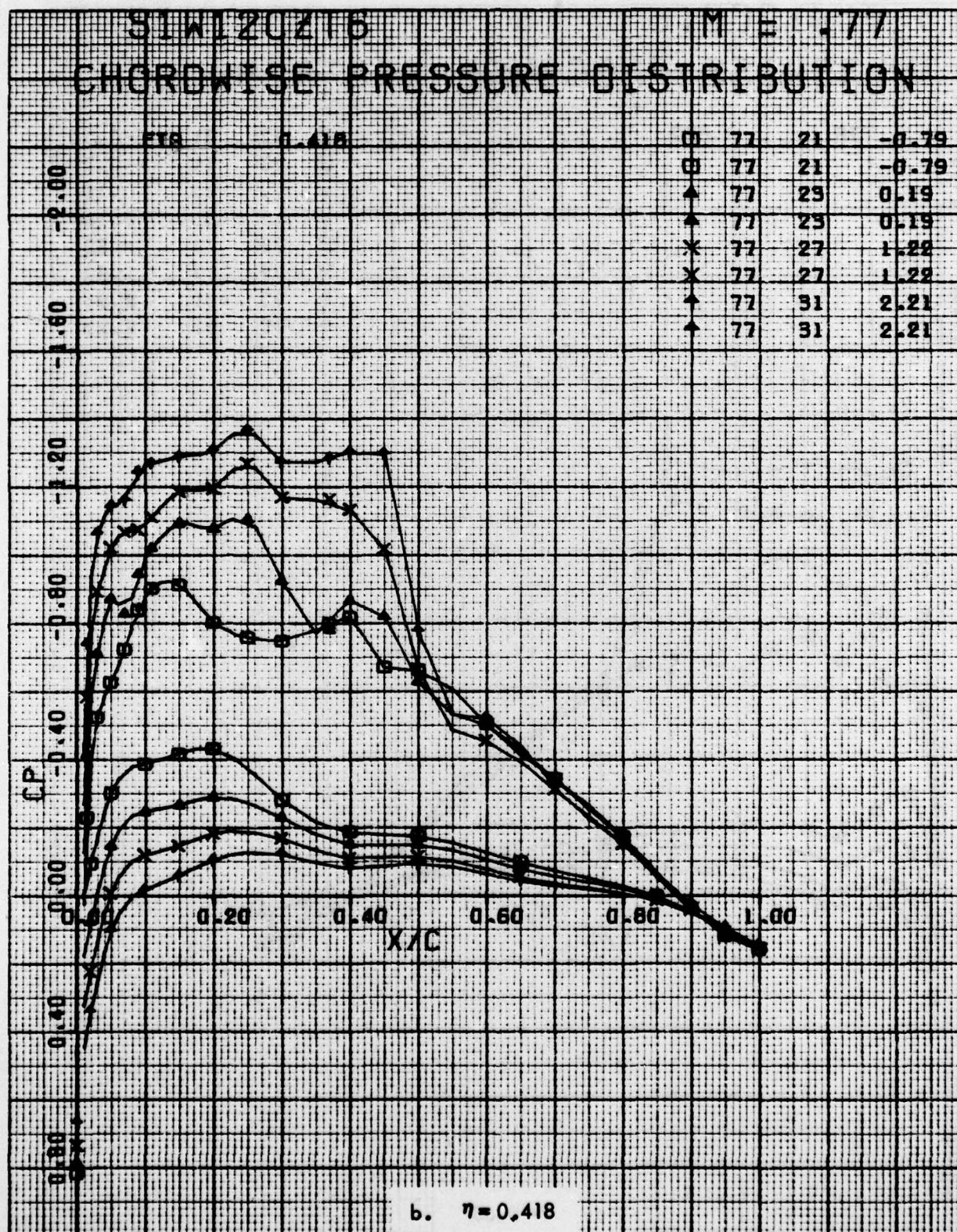


Figure 84 . Continued

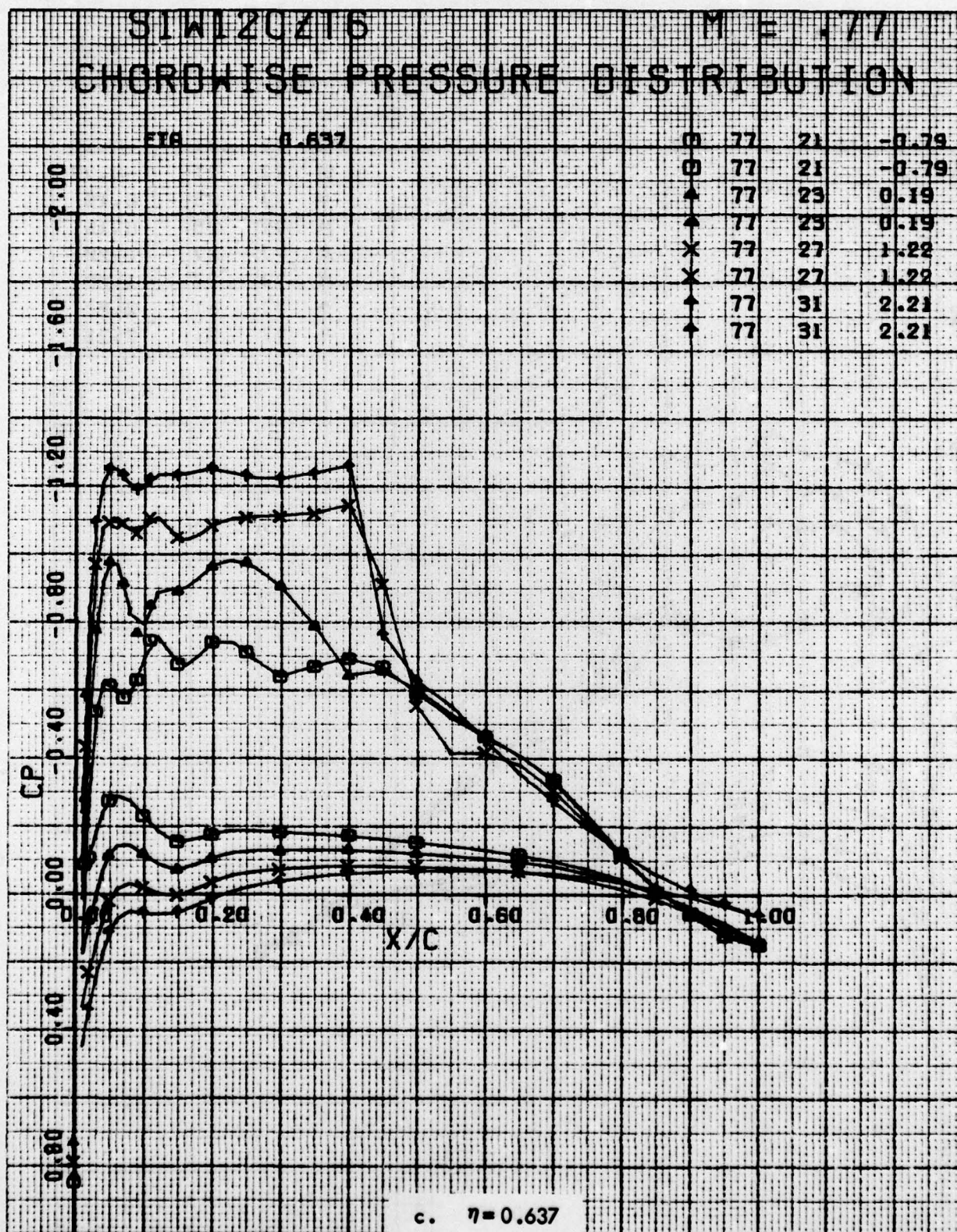


Figure 84. Continued

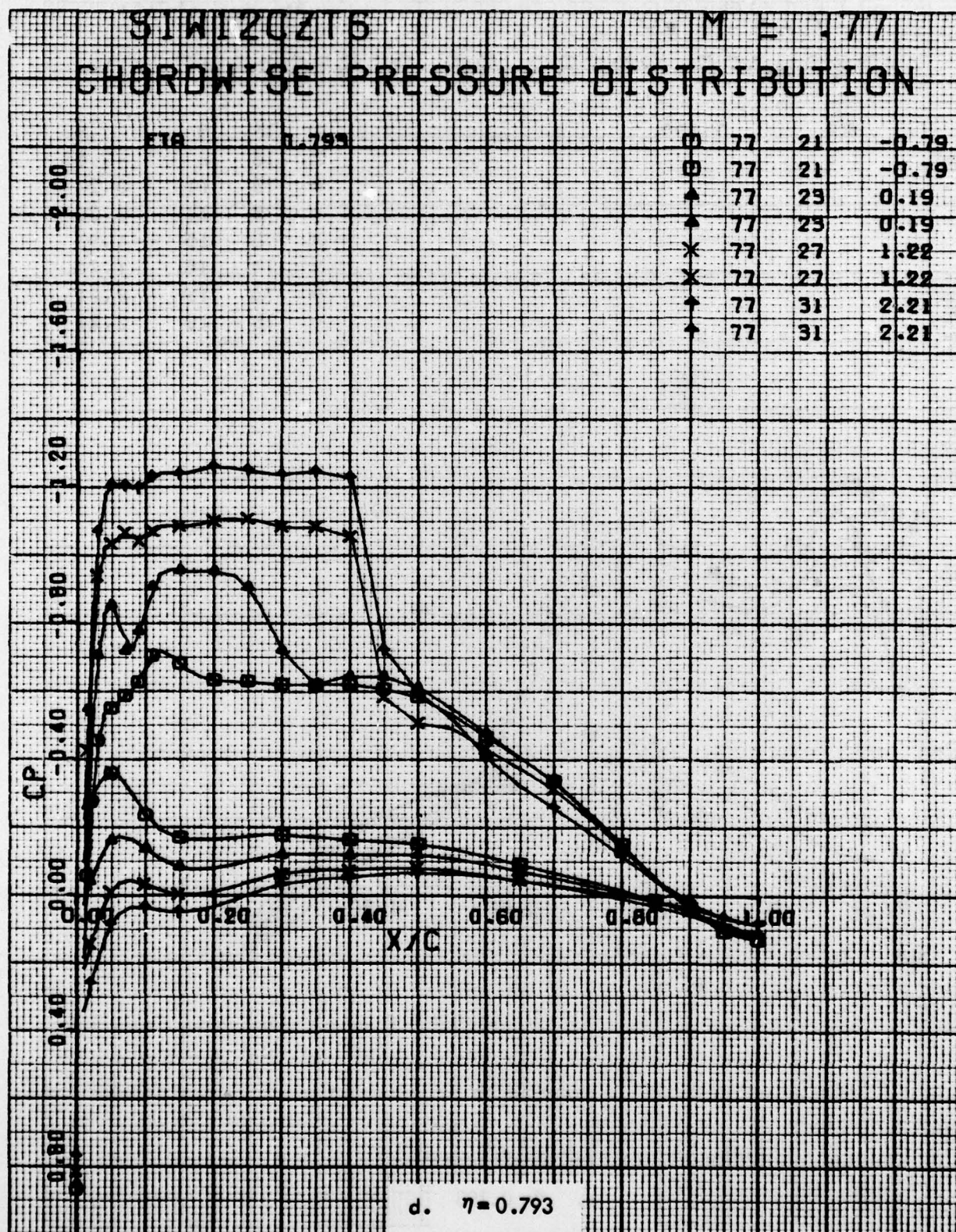


Figure 84. Concluded

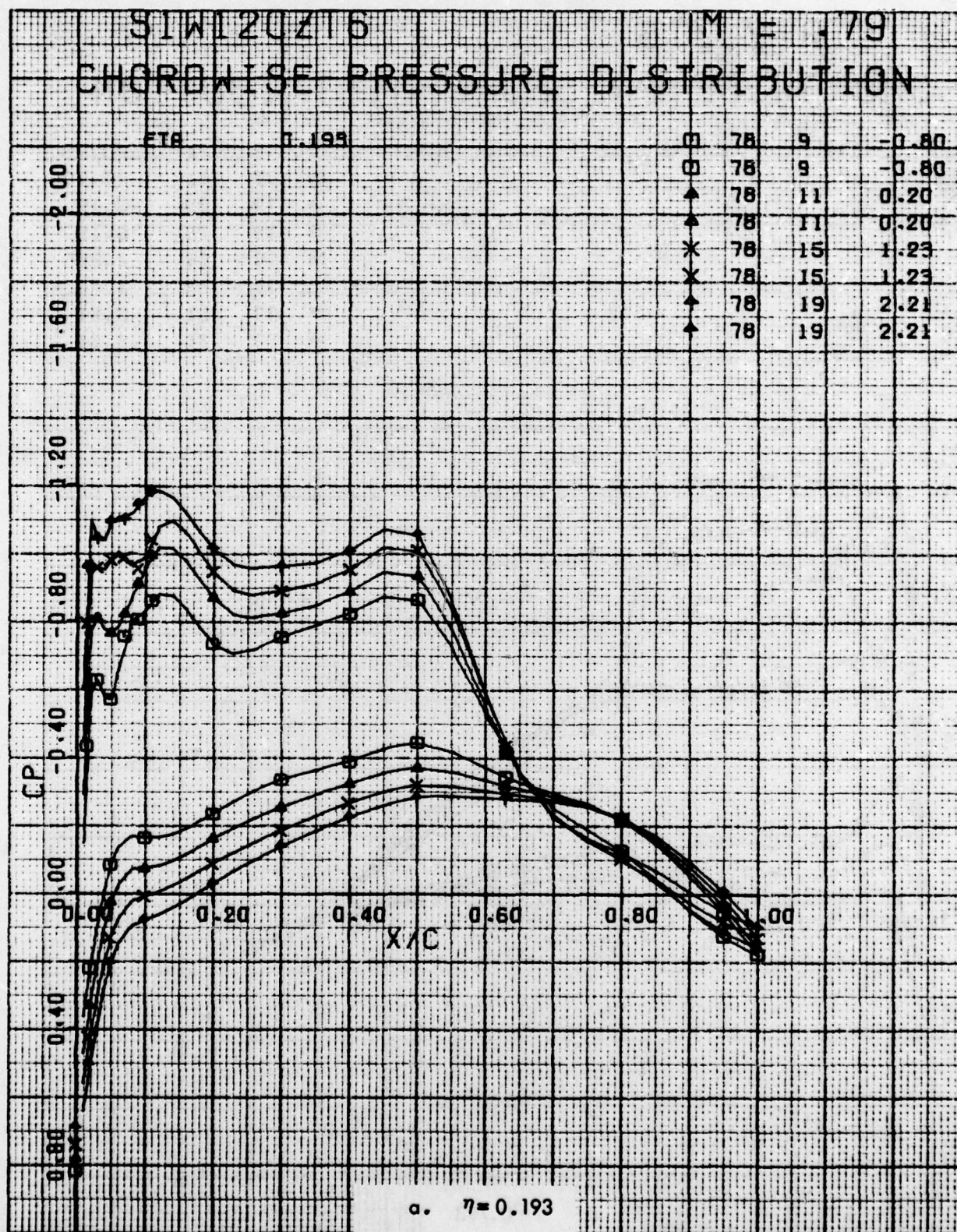


Figure 85. Chordwise Pressure Distributions for Various Angles of Attack. Baseline Leading Edge, Fixed Transition, Grit Code C, Both Swept Tips, $M = 0.79$.

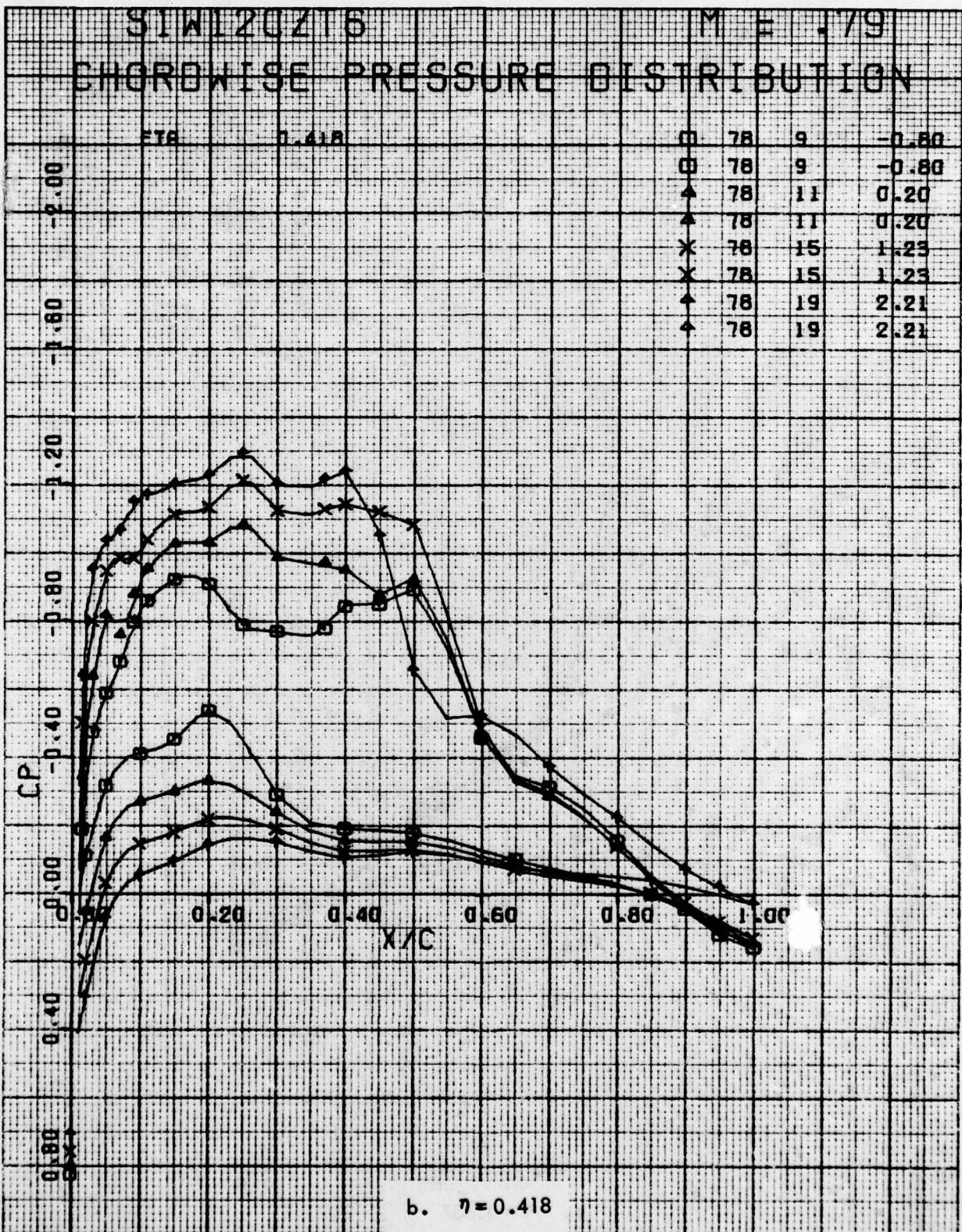


Figure 85 . Continued

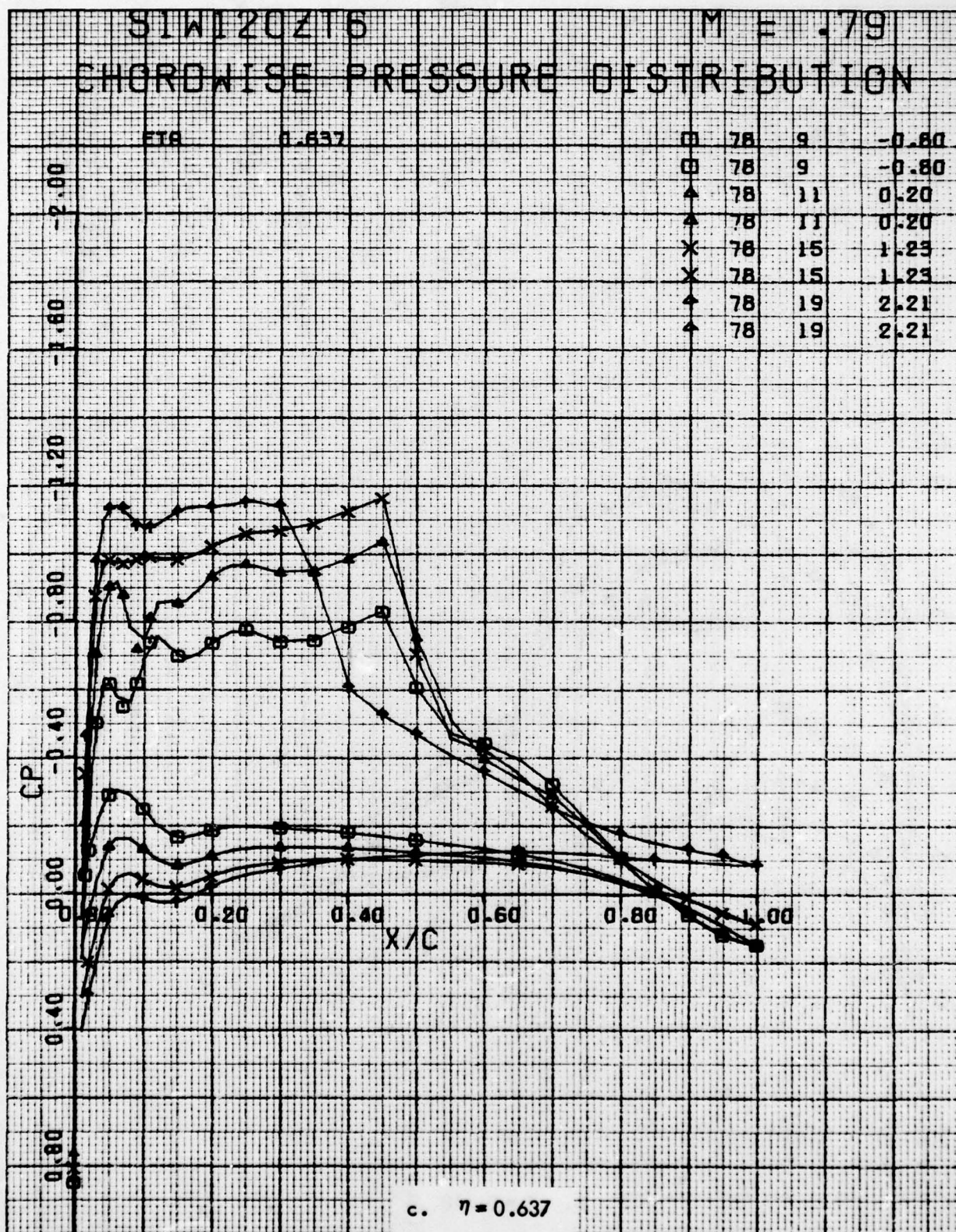


Figure 85. Continued

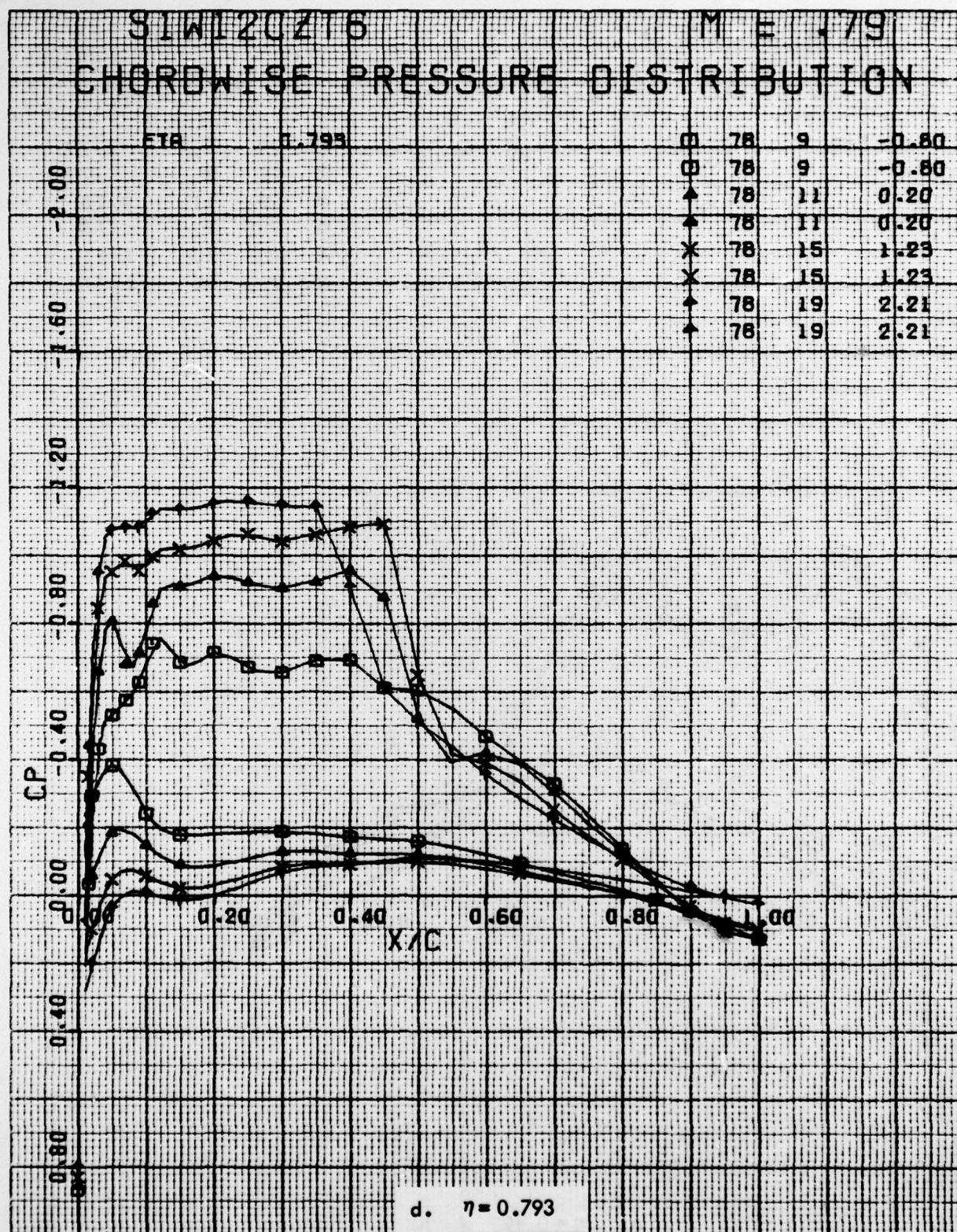


Figure 85. Concluded

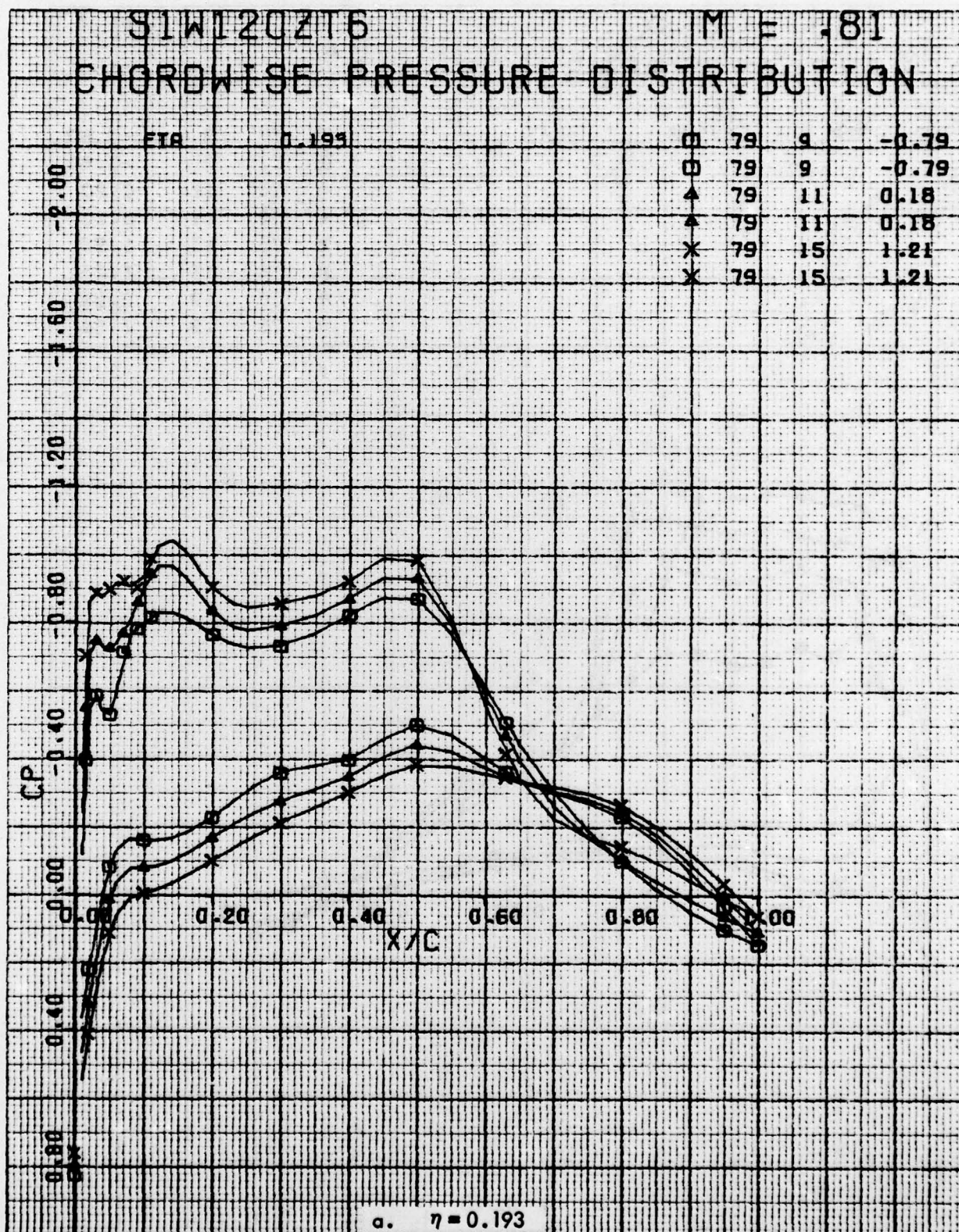


Figure 86. Chordwise Pressure Distributions for Various Angles of Attack. Baseline Leading Edge, Fixed Transition, Grit Code C, Both Swept Tips, $M = 0.81$.

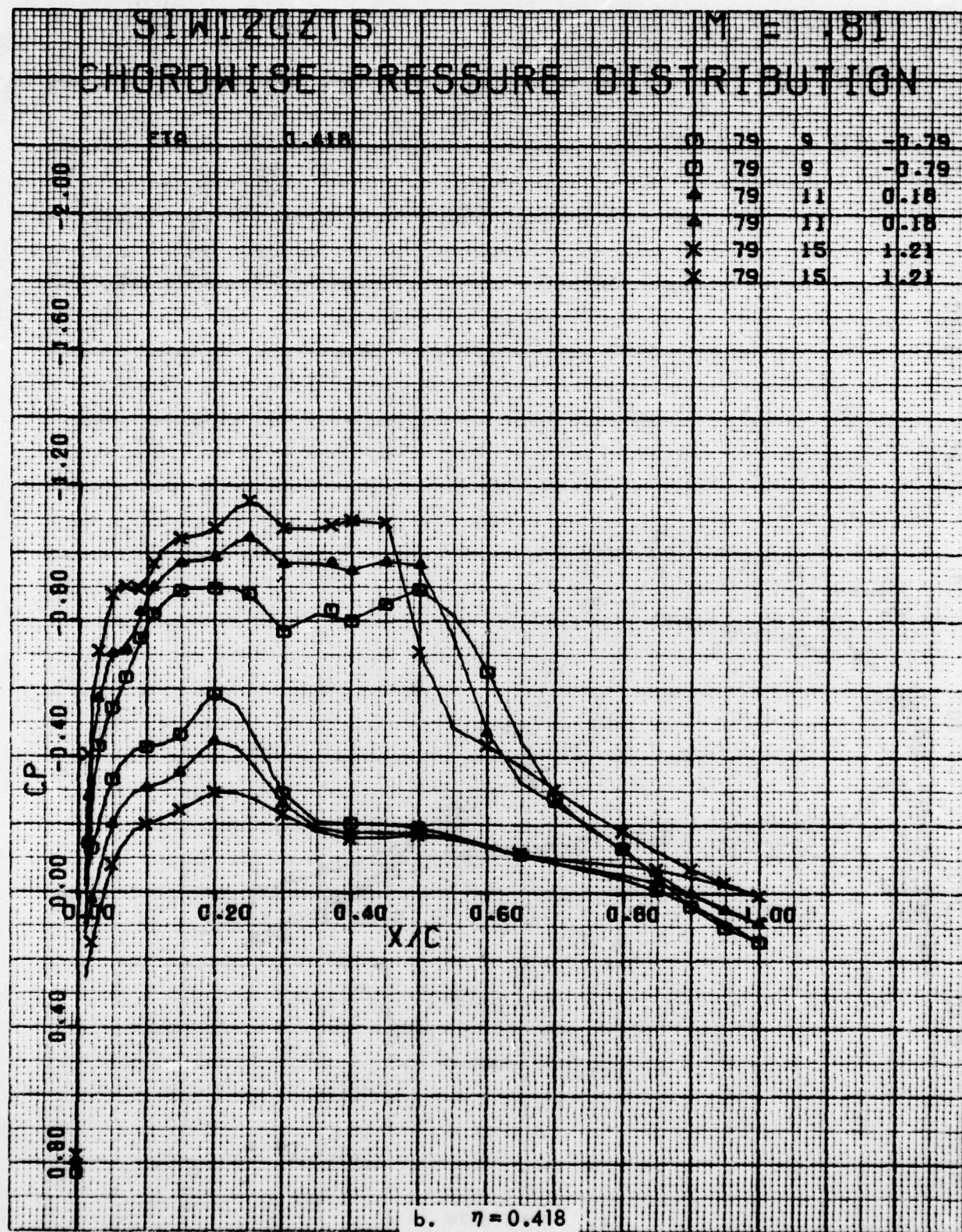


Figure 86 . Continued

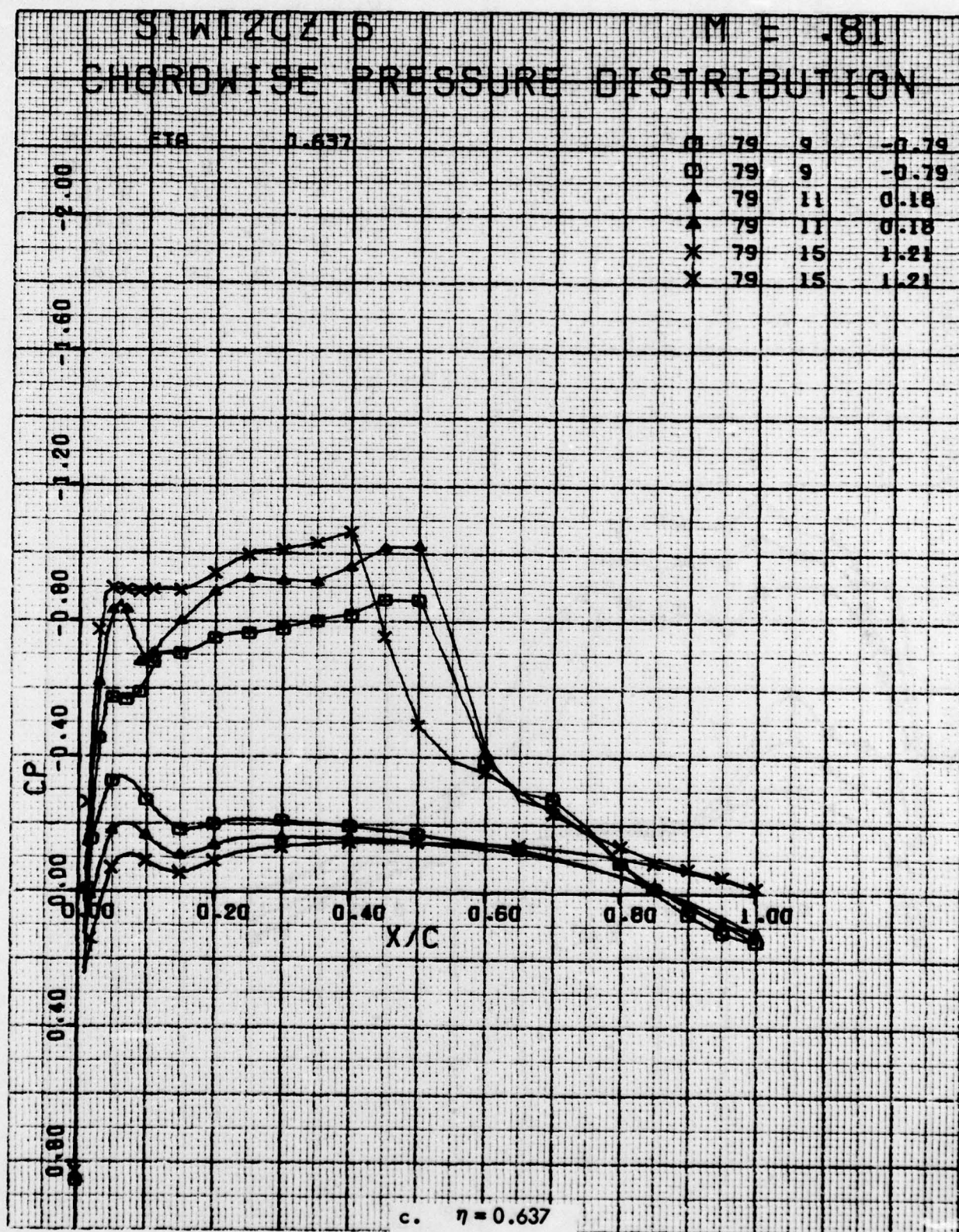


Figure 86. Continued

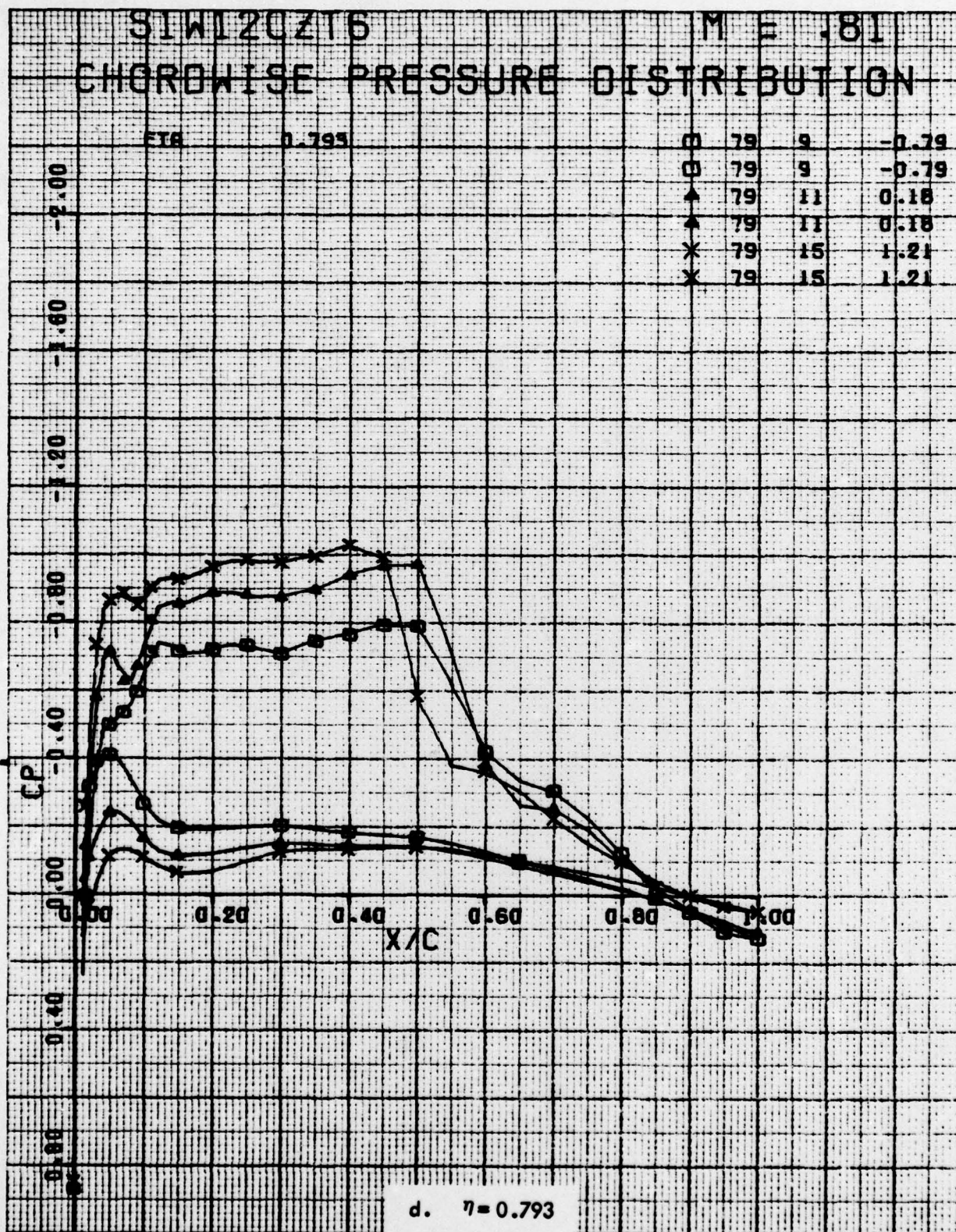


Figure 86. Concluded